Rapporter och meddelanden nr 91

Petrogenesis of some Proterozoic granitoid suites and associated basic rocks in Sweden (geochemistry and isotope geology)



Ulf B. Andersson

SGU
Sveriges Geologiska Undersökning

Uppsala 1997

Rapporter och meddelanden nr 91

Petrogenesis of some Proterozoic granitoid suites and associated basic rocks in Sweden (geochemistry and isotope geology)

Ulf B. Andersson

SGU
Sveriges Geologiska Undersökning

Uppsala 1997

ISSN 0349-2176
ISBN 91-7158-596-6

Dissertation for the degree of Doctor of Philosophy
in Mineralogy, Petrology and Tectonics
presented at Uppsala University in 1997

Address

Ulf B. Andersson
Institutionen för geovetenskap
Uppsala universitet
Norbyvägen 18 B
SE-752 36 UPPSALA

Layout: Agneta Ek, SGU

Printed by Wikströms Tryckeri AB, Uppsala 1997

Table of contents

Abstract 5

1. Introduction: background and scope of study 6

2. Regional geology of the Fennoscandian shield 7

3. The Transscandinavian igneous belt (TIB) 11

4. The geology of TIB in northern Östergötland-southern Närke 15
4.1. Field relations in the studied areas 15
4.1.1. The Tjällmo-Vättern zone (TVZ) 15
4.1.2. The Kårtorp area 18
4.1.3. The Tiveden area 18
4.2. Petrography-mineralogy 19
4.3. Geochemistry 23
4.3.1. Major element characteristics 23
4.3.2. Trace element discrimination, granitoids 24
4.3.3. Spider diagrams, granitoids 24
4.3.4. Trace element discrimination, basic rocks 27
4.3.5. Spider diagrams, basic rocks 31
4.3.6. Harker variation diagrams 33
4.3.7. REE patterns 39
4.4. Isotope geology 40
4.4.1. U-Pb zircon geochronology 40
4.4.2. Nd isotopes 40
4.4.3. Sr isotopes 45
4.5. Discussion 46
4.5.1. Isotopes 46
4.5.1.1. Geochronology 46
4.5.1.2. Nd isotopic interpretations 47
4.5.1.3. Sr isotopic interpretations 50
4.5.2. Geochemistry 53
4.5.2.1. Kårtorp area: correlation with magnetic characteristics 53
4.5.2.2. Granites 53
4.5.2.2.1. General 53
4.5.2.2.2. Major element modelling, partial melting 55
4.5.2.2.3. Trace element modelling, partial melting 56
4.5.2.2.4. Haplogranite system relations 58
4.5.2.3. The basic suite 59
4.5.2.3.1. General 59
4.5.2.3.2. Enclaves 61
4.5.2.3.3. Partial melting modelling, major elements 62
4.5.2.3.4. Partial melting modelling, trace elements 65
4.5.2.3.5. Fractional crystallization, major elements 66
4.5.2.3.6. Fractional crystallization, trace elements 68
4.5.2.3.7. Summary interpretations of the basic suite 70
4.5.2.4. The hybrids 70
4.5.3. Concluding discussion on the genesis of the Småland–Värmland rocks 71

5. The Fennoscandian rapakivi complexes 73

6. The Subjotnian Rödö rapakivi complex 77
6.1. Field relations 77
6.2. Petrography-mineralogy 83
6.3. Geochemistry 88
6.3.1. Silicic rocks 90
6.3.2. Basic-intermediate rocks 94
6.3.3. Variation diagrams 98
6.3.4. REE patterns 105

6.4. Isotope geology 109
6.4.1. U-Pb zircon geochronology 109
6.4.2. Nd isotopes 110
6.4.3. Sr isotopes 115
6.4.4. Pb whole rock isotopes 117
6.5. Discussion 118
6.5.1. Geochemistry 118
6.5.1.1. General 118
6.5.1.2. Major element modelling of the silicic suite 118
6.5.1.3. Trace element modelling of the Rödö silicic suite 121
6.5.1.4. Fluids and fluorocarbonates 123
6.5.1.5. Origin of the silicic parental magma 127
6.5.1.6. Relation to the haplogranite system 127
6.5.1.7. Rödö (and Postjotnian) dolerites 128
6.5.1.8. Hybrid porphyries and enclaves 131
6.5.2. Notes on the composite dykes 132
6.5.3. Isotopes 133
6.5.3.1. Age 133
6.5.3.2. Nd isotopic relations 134
6.5.3.3. Sr isotopic relations 140
6.5.3.4. Pb-WR isotopic relations 142

7. The minor Subjotnian (rapakivi) complexes in Jämtland and Ångermanlan 142
7.1. Field relations 142
7.1.1. The Mårdsjö complex 142
7.1.2. The Mullnäset complex 144
7.1.3. The Strömsund complex 144
7.1.4. The Nordsjö complex 144
7.2. Petrography-mineralogy 144
7.3. Geochemistry 147
7.3.1. Major element characteristics 147
7.3.2. Trace element discrimination 147
7.3.3. Harker variation diagrams 150
7.3.4. REE patterns and spider diagrams 155
7.4. Isotope geology 161
7.4.1. U-Pb zircon geochronology 161
7.4.2. Nd isotopes 163
7.4.3. Sr isotopes 163
7.4.4. Pb feldspar isotopes 165
7.5. Discussion 167
7.5.1. Isotopes 167
7.5.1.1. Ages 167
7.5.1.2. Nd isotopic relations 167
7.5.1.3. Sr isotopic relations 168
7.5.1.4. Pb feldspar isotopic relations 168
7.5.2. Geochemistry 170
7.5.2.1. The Härnö and Revsund suites 170
7.5.2.2. The Subjotnian complexes 171
7.5.2.3. Major element modelling 173
7.5.2.4. Trace element modelling 175

8. Discussion on the genesis of the central Swedish rapakivi complexes 178

9. Summary of main results 182

10. Acknowledgements 184

11. References 185

Appendices 202

Abstract

Two rock suites of the Fennoscandian shield have been studied: i. rocks belonging to the Transscandinavian igneous belt (TIB, 1.85–1.65 Ga), and ii. rocks belonging to the Subjotnian (1.65–1.50 Ga) rapakivi complexes. The former rocks of this study are located in the southern part of TIB, in the Småland-Värmland belt (SVB) of central southern Sweden (northern Östergötland and southern Närke). Of the Subjotnian rocks, the study has focussed on five small complexes in central Sweden, previously little studied. These are, from north to south, Strömsund, Mullnäset, Nordsjö, Mårdsjö, and Rödön.

Both geochemical and isotopic evidence favour a generation of the SVB-granites from the preexisting early Svecofennian crust, with no measurable involvement of Archaean material. 25–40 % melting of tonalitic to granodioritic protoliths in the lower crust is suggested from geochemical modelling and comparison with experimental data. Interaction with coeval basic magmas has resulted in extensive hybridization in certain areas. Most of the geochemical variation in the range 52–70 % SiO_2 can be explained in terms of mixing. The basic SVB-suite shows considerable evolutionary variation. The spinel-plagioclase-phlogopite lherzolites occurring in a few places are interpreted as representing a possible mantle source for the basic suite. The most primitive basites can be derived by c. 25–30 % melting of this source material. Further evolution in the suite is consistent with c. 30 % fractionation of dominantly, clinopyroxene from the primitive magmas. A suite of mafic magmatic enclaves show strongly evolved character, and are geochemically similar to lamprophyres. Some of the hybrid systems have such basic endmembers. This evolved composition is tentatively interpreted as resulting from extended (>80 %) fractionation from the gabbros of dominantly clinopyroxene and plagioclase. The SVB-granitoids were generated in response to the heat input from extensive underplating of the lower crust by the mantle-derived basic magmas. During buoyant rise of the crustal magmas entrainment and mixing with the underlying basic magmas was extensive, as shown by the widespread occurrence in SVB of quartz monzonitic to monzodioritic high-magnetic hybrid rocks.

Four U-Pb zircon ages in the range 1.53–1.50 Ga are reported from the Subjotnian (rapakivi) complexes in central Sweden. These are the youngest Subjotnian ages recorded so far. Excluding the 1.56–1.53 Ga Salmi batholith in the east, a trend of general younging westwards is evident for the Fennoscandian rapakivi complexes. A major Archaean component is indicated in the central Swedish rapakivi magmatism by low initial Nd (average -7.0 at 1.52 Ga) and Pb ($^{207}Pb/^{204}Pb$ lower than 15.220 in feldspars) isotopic compositions. A group of zircons recovered from the 1.52 Ga Nordsjö syenite give an age of 2.70±0.04 Ga (ion-probe data). These data strongly suggest that a significant part of the lower crust in central Sweden is Archaean in age.

The complexes in Jämtland–Ångermanland (the northernmost four) usually consist of three units: i. a basic, ii. a syenitic-peralkaline silicic unit, and iii. a met- to peraluminous silicic unit, which are coeval but not comagmatic. The basic mantle-derived magma intruded the lower crust, where the syenitic and granitic magmas were generated from different protoliths. The granitic rapakivi magmas derive from felsic undepleted sources of tonalitic-granodioritic composition, while the syenites may be derived from a combination of mafic undepleted (monzodioritic) sources and sources depleted after granitic extraction. The three magmas followed the same channelways simultaneously to their upper crustal emplacement levels. The peralkaline silicic rocks can be derived from a syenitic parental magma by 55–70 % fractionation of dominantly one feldspar (anorthoclase), with minor Fe-Ti-oxides, clinopyroxene and fayalite. This model is supported by the composition and phenocryst assemblage of trachyte dykes. The Rödö complex consists of a granite pluton and associated silicic, basic and intermediate dyke rocks. Strong fractionation in the silicic system (up to >90 %) of dominantly quartz, K-feldspar, and plagioclase has resulted in some extremely evolved residual magmas (very high contents of incompatible elements, especially Rb, U, Th, Nb, Ga, Zr, Hf, and the HREEs) emplaced as quartz-feldspar porphyry dykes. In addition, a fluid phase precipitating, e.g. Ca-LREE-fluorocarbonates, was an important controlling factor in this evolution. Two generations of hybrid porphyries (intermediate dykes) are formed by magma mixing of primitive and evolved endmembers, respectively, of the Rödö silicic and basic suites.

1. Introduction: background and scope of study

Detailed modern studies of the origin and petrogenesis of granitoids within the Fennoscandian shield are not numerous (e.g. Huhma 1986, Nurmi & Haapala 1986, Martin 1987, Öhlander et al. 1987, 1993, Wilson et al. 1987a, b, Skiöld et al. 1988, Öhlander & Zuber 1988b, Nironen 1989, Claesson & Lundqvist 1995), the rapakivi complexes perhaps being the most well-studied (e.g. Vorma 1975, 1976, Kornfält 1976, Haapala 1977, Rämö 1991, Eklund 1993, Neymark et al. 1994, Lindh & Johansson 1996, Amelin et al. 1997). The present study aims at contributing to this end by deciphering the magmatic evolution of some Proterozoic granitoids and associated rocks belonging to, 1) the Transscandinavian igneous belt (1.85–1.65 Ga) in southern Sweden and, 2) the Subjotnian (rapakivi) complexes (1.65–1.50 Ga) of central Sweden.

In assessing the problem of granitoid genesis and evolution it became clear that basic and intermediate rocks are intimately related to the granites and play an important role in their genesis (cf. e.g. Huppert & Sparks 1988, Pitcher 1993, Wiebe 1993, 1994, 1996). Associated basic, intermediate and silicic rocks in the studied areas are therefore treated in their context, where the interrelations of their respective evolutions are discussed. The evolution of the basic and silicic rock suites in each respective complex can be modelled in terms of partial melting and fractional crystallization processes. The origin of the intermediate rocks is highlighted in the different areas. In addition to geochemical variations due to fractional crystallization and partial melting, hybridization through magma mixing is considered to be a process of major importance. The basic magmas underplating and intruding the continental crust not only provide the heat necessary for crustal melting but are also actively interacting with the newly formed crustal melts, to produce a range of chemically intermediate rocks. This process is highly dependent on the physical states of the interacting magmas, which determine the nature of the resulting products (e.g. Sparks & Marshall 1986, Frost & Mahood 1987, Fernandez & Barbarin 1991, Weinberg 1992, Cruden et al. 1995). Magma mingling refers to a process where the interacting magmas retain their initial chemical identities and produces essentially structural evidence for contemporaneity such as mafic microgranular enclaves, pillowed contacts, synplutonic dykes, and net-veined complexes, while mixing refers to a process of chemical homogenization of the magmas (e.g. Blake et al. 1965, Walker & Skelhorn 1966, Yoder 1973, Wiebe 1974, 1988, 1991, Didier 1973, Gamble 1979, Taylor et al. 1980, Vernon 1983, Didier & Barbarin 1991, Barbarin & Didier 1992, Blundy & Sparks 1992, Pitcher 1993, Hibbard 1995). The importance of the latter process has only recently received proper attention as a major process in the geochemical evolution of plutonic magmas (e.g. Goldie 1978, Wiebe 1980, Brown & Becker 1986, Reid & Hamilton 1987, Ayrton 1988, Zorpi et al. 1989, Smith et al. 1990, Debon 1991, Bateman 1995, Metcalf et al. 1995, Moreno-Ventas et al. 1995, Collins 1996, Sisson et al. 1996), and even prompted revisions of the genetic nomenclature of granitoid rocks to include hybrid granitoids (Barbarin 1990, Castro et al. 1991), although strongly disputed by some workers (e.g. Chappell 1996).

In Fennoscandia, plutonic hybridization as a cause of geochemical variation has been recognized only sporadically (Lindberg & Eklund 1988, Andersson 1989, 1991, Branigan 1989, Nironen 1989, Ehlers & Lindroos 1990, Eklund et al. 1991, 1994), and the present work attempts to constrain this process somewhat more rigorously for the Småland–Värmland (SVB) belt in the southern part of the Transscandinavian igneous belt (TIB). The geochemical model, including suites of mixed rocks, outlined for the SVB below, is considered also to be more generally applicable, especially within the TIB, but also in other Fennoscandian granitoid generations (cf. Andersson 1991).

In contrast to the TIB, the importance of plutonic mixing for the geochemical evolution in the Subjotnian (rapakivi) complexes in Sweden appears to be very limited, and magma interaction restricted to dykes and local mingling and mixing (below, and Persson 1996a). The nature of the intermediate rocks is also different and mainly syenitic, compared with the dominantly monzonitic rocks in the TIB. This calls for a mode of origin other than mixing for the Subjotnian syenites, probably related to lower crustal melting of mafic and/or depleted crustal sources, as discussed below. In the Subjotnian complexes a fluid phase is suggested to be of considerable importance for the geochemical evolution. This is especially convincing in the Rödö complex, where numerous miarolitic cavities in all rock types and their specific mineralogy can be related to the magma evolution.

The tectonic settings and implications of the magmatism is discussed only briefly. The TIB is tentatively related to a changeover from compressional forces, related to Svecofennian collisional thick-

ening, to an environment of extensional collapse of the overthickened crust where mantle upwelling and basic underplating were prevalent (cf. e.g. Korja et al. 1993, Korja & Heikkinen 1995, Stephens & Wahlgren 1996). This orogeny-related extensional environment may have been active in the shield continuously or intermittently from the TIB magmatism to the intrusion of the rapakivi (Subjotnian) complexes, as there is a continuous range in ages, where the youngest TIB rocks (c. 1.66 Ga) and the oldest rapakivi rocks (1.65 Ga, in dyke swarms 1.67 Ga) are close in time. In this way the "anorogenic" rapakivi complexes may actually be related to the Svecofennian collisional event (Korja & Heikkinen 1995, Stephens & Wahlgren 1996).

This thesis was originally initiated by Anders Wikström, who suggested a study on the nature of the highly magnetic rocks at Kårtorp in the SVB. From this starting point (Andersson 1989) the studies expanded to cover the relationships between basic, intermediate, and silicic plutonics in this part of the SVB, as it was realized that the Kårtorp rocks were part of bigger picture relating to plutonic hybridization (Andersson 1991). Because the structural and mineralogical evidence for magma mixing is largely erased in the relatively deep-seated plutonic level of the SVB (c. 15–25 km, Andersson et al. 1992, Andersson 1997b, and below), I turned to the shallow crustal rapakivi complexes (c. 1–3 km, Väisänen et al. 1994, Väisänen & Hölttä 1996, Eklund et al. 1996b, Shebanov et al. 1996) to find better preserved mingling and mixing occurrences to compare with the SVB rocks (cf. Andersson & Eklund 1994). This, however, led to a deeper involvement in the geology of the rapakivi complexes and a project concerning the little known small Swedish Subjotnian complexes was launched (financed by the Geological Survey of Sweden; Andersson 1994). The thesis combines the results from these two lines of research.

2. Regional geology of the Fennoscandian shield

The Fennoscandian shield consists of several amalgamated rock domains (subdivided into provinces, cf. Gaál & Gorbatschev 1987), generally younging southwestwards (Fig. 1). The northeastern parts comprise an Archaean nucleus. Rocks in the Archaean domain span the age range 3.1–2.6 Ga and are subdivided into three provinces: the Kola peninsula, the Belomorian and the Karelian provinces. At least two crust-forming orogenies have been identified. The earliest, the Saamian (3.1–2.9 Ga) consists mainly of tonalite-trondhjemite-granodiorite (TTG) suites scattered throughout the domain, whereas the main late Archaean event, the Lopian orogeny (2.9–2.6 Ga), comprises generally low-grade granite-greenstone terrains in the Karelian province but high-grade metasedimentary and metaplutonic rocks in the Belomorian and Kola provinces (e.g. Gaál & Gorbatschev 1987).

After the Lopian orogeny the domain was cratonized. In the latest Archaean and earliest Proterozoic (2.6–2.1 Ga), dominantly mafic volcanics and sedimentary rocks of the Lapponian, Sumi-Sariolan, and Jatulian groups were deposited. This deposition mostly occurred in elongated basins bounded by faulting. The 2.0–1.9 Ga Lapland granulite belt forms a major younger unit within the Archaean craton, thrust onto the Karelian rocks to the south, presumably during continental collision (e.g. Gorbatschev & Gaál 1987)

The central parts of the shield are occupied by the Svecofennian domain, i.e. southern and western Finland, northern and eastern Sweden. This domain comprises several relatively discrete episodes of rock formation. The earliest is the early orogenic (previously often referred to as primorogenic) Svecofennian episode with the time span of c. 2.00–1.86 Ga, where most of the activity occurred 1.90–1.86 Ga. This is a major crustforming orogenic period in the Fennoscandian shield (e.g. Patchett et al. 1987, Patchett & Kouvo 1986), and is the time when the first Svecofennian crust accreted to the Archaean nucleus in the northeast (e.g. Hietanen 1975, Patchett & Arndt 1986, Gaál 1990). These early rocks comprise both large amounts of supracrustals, different types of often highly migmatitic metasediments and dominantly silicic volcanics, and plutonics. The latter form a calc-alkaline I-type suite with dominantly granodiorites and tonalites (Patchett & Arndt 1986, Huhma 1986, Nurmi & Haapala 1986, Gaal & Gorbatschev 1987, Front & Nurmi 1987). Gabbros and other mafic rocks are also common, whereas granites are subordinate. The traditional view has been that after the cessation of the early Svecofennian magmatism the crust was stabilized and a period of relative quiescence followed (c. 1.86 –1.83 Ga), and that the crust was sufficiently consolidated to allow rifting and the injection of dyke swarms, the s.c. intraorogenic dykes (cf. e.g. Magnusson et al. 1940, 1963, Gorbatschev et al. 1987,

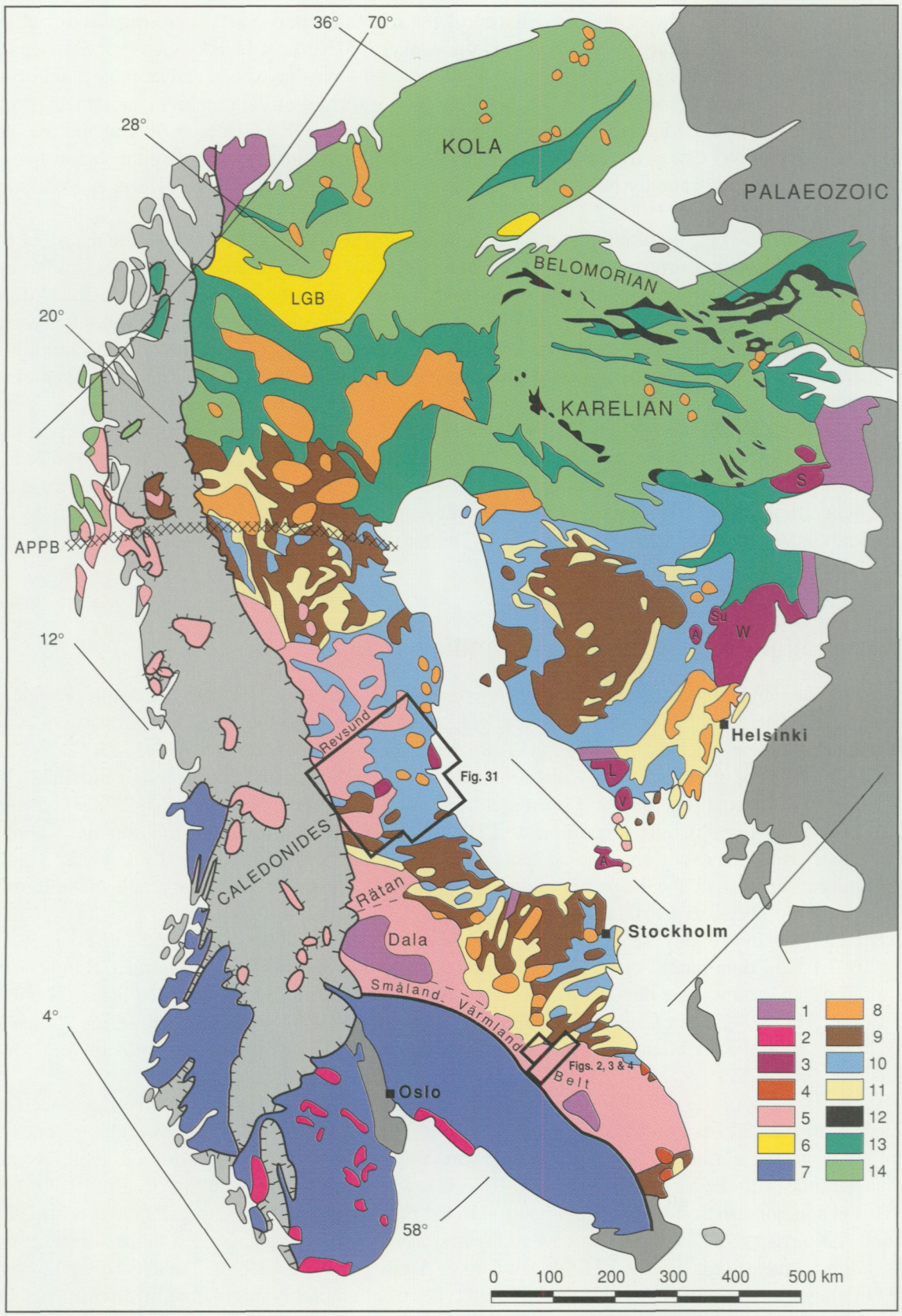

Fig. 1. Lithological subdivision of the Fennoscandian shield. 1. Jotnian sedimentary rocks, <1.50, >1.26 Ga. 2. Late Sveconorwegian intrusions, c. 1.00–0.85 Ga. 3. The Fennoscandian rapakivi complexes, c. 1.65–1.50 Ga. 4. Younger anorogenic intrusives in SE Sweden, c. 1.40–1.35 Ga. 5. The Transscandinavian Igneous Belt, c. 1.85–1.65 Ga. 6. The Lapland Granulite Belt, c. 2.0–1.9 Ga. 7. The Southwest Scandinavian Domain, c. 1.76–0.90 Ga. 8. "Late orogenic" Svecofennian intrusives, c. 1.84–1.77 Ga. 9. Early orogenic Svecofennian intrusives, c. 1.95–1.86 Ga. 10. Early Svecofennian sedimentary supracrustals, pre-1.86 Ga. 11. Early Svecofennian volcanics, c. 1.90–1.87 Ga. 12. Archaean greenstone belts and basins, c. 2.9–2.7 Ga. 13. Earliest Proterozoic cover of the Archaean craton, c. 2.5–2.0 Ga. 14. Archaean crust, c. 3.1–2.6 Ga. Frames outline areas of subsequent maps. Modified from Gaál & Gorbatschev (1987). APPB is the Archean-Proterozoic palaeoboundary of Öhlander et al. (1987, 1993).

Stålhös 1991). However, numerous synplutonic dykes within the early Svecofennian granitoids suggest that a substantial part of this dyke generation is closely related to the plutonism, genetically and in time (A.Wikström 1992, and pers. comm. 1996). Most of the regional metamorphism and formation of migmatitic gneisses observed in the Svecofennian was produced during or shortly before the late orogenic period (1.83-1.77 Ga; e.g. Magnusson et al. 1962, Gaal & Gorbatschev 1987, Stålhös 1991, Andersson 1997b). Metamorphism of early orogenic age has, however, been identified in central southern and eastern Finland (cf. e.g. Hopgood et al. 1983, Korsman et al. 1984, Vaasjoki & Sakko 1988, Hölttä 1988, 1995, Korja et al. 1994).

A second generation of extensive magmatism followed within the Svecofennian domain c. 1.83–1.77 Ga (cf. e.g. Gaál & Gorbatschev 1987, Öhlander & Romer 1996). This late Svecofennian magmatism (previously often referred to as serorogenic) is represented almost exclusively by granitoid intrusions, essentially granites s.s. with a high and restricted range in SiO_2-content, and generally S-type and syn-collision characteristics (Nurmi & Haapala 1986, Claesson & Lundqvist 1995). However, larger massifs of this generation in central southern Sweden tend to have within-plate geochemical characteristics, similar to those in the TIB (Öhlander & Zuber 1988, Zuber & Öhlander 1990, 1991). No supracrustal rocks associated with these granitoids have been recognized, and very few intermediate to basic rocks. The late orogenic period is a period of extensive reworking of the early Svecofennian crust, giving rise to smaller and larger crustal magma batches, and associated metamorphism and migmatization. Numerous pegmatites occur in conjunction with this metamorphism and magmatism, some of which contain rare elements (e.g. Smeds 1994, Romer & Smeds 1994, Lindroos et al. 1996). Thus the early orogenic period (ca 2.00–1.86 Ga) is essentially the time of crust formation in the Svecofennian domain, whereas this crust was most extensively reworked 1.83–1.77 Ga ago (e.g. Patchett & Kouvo 1986, Patchett et al. 1987, Huhma 1986).

On the western margin of the Svecofennian domain several vast belts of large batholiths have intruded, collectively referred to as the Transscandinavian igneous belt (TIB, e.g. Gorbatschev & Bogdanova 1993). TIB stretches from southeasternmost Sweden NNW to the Caledonian front in central Norway. It is also exposed in windows in the Caledonian cover rocks, and west of the Caledonian rocks (e.g. Gorbatschev 1985, Romer et al. 1992). The total length of TIB is about 1400 km. It is overwhelmingly dominated by magmatic rocks, comprising granitoids and minor basic plutonics as well as substantial volumes of silicic volcanics. Sedimentary rocks are only found in the central parts, associated with the Dala granitoids and volcanics (see Hjelmqvist 1966). The TIB granitoid suite is dominantly alkali-calcic and less aluminous compared with the early and late Svecofennian groups, and shows dominantly I- and volcanic-arc characteristics (Lindh & Gorbatschev 1984, Lindh & Persson 1990). The age range for TIB rocks has recently been proven to be large, ca 1.85–1.65 Ga (e.g. Jarl & Johansson 1987, Patchett et al. 1987, Persson & Wikström 1993, Jarl 1992, Mansfeld 1995, Larson & Berglund 1992, Wikström 1996, Heim et al. 1996, Jarl et al. 1993, Stephens et al. 1993). The ages thus completely overlap those of the late orogenic rocks within the Svecofennian domain, suggesting that coeval tectonic process is responsible for both these magmatic suites (cf. Andersson 1991, Gorbatschev & Bogdanova 1993).

The TIB rocks have traditionally been described as postorogenic since they can be observed to crosscut the Svecofennian structures (e.g. Magnusson et al. 1963, Lundqvist 1979). Recent studies (Wikström 1984, 1991) have, however, shown that the TIB granitoids in certain areas are conformably folded together with the adjoining Svecofennian rocks. This is consistent with their overlapping ages with the late orogenic granites (e.g. this study, Persson & Wikström 1993, Wikström 1996). A more detailed discussion is given in chapters 3 and 4.

The Svecofennian domain can be subdivided into three separate provinces; the southern, central, and northern (e.g. Gaál & Gorbatschev 1987). The southern province stretches from eastern southern Sweden to southern Finland. It comprises the Bergslagen volcano-metallogenetic district and its extension into Finland (Orijärvi district; e.g. Gaál 1990), dominated by silicic volcanics and granitoids, with minor metasediments. Another major part within this province is the dominantly metasedimentary, highly migmatitic Sörmland basin, southeast of Bergslagen (cf. Stålhös 1991, Romer & Öhlander 1995). The early orogenic plutonic suite dominates in NE part of the province north of the Sörmland basin area. The late orogenic suite intrudes all parts of the southern province, but is most voluminous in the volcanic-dominated Bergslagen area and southern Finland (e.g. Sederholm 1926, Nurmi & Haapala 1986, Öhlander & Zuber 1988).

The central Svecofennian province in central Sweden and west-central Finland is largely dominated by a basin of metasedimentary rocks, the Bothnian basin (e.g. Hietanen 1975). The sedimentary sequences are dominated by metagraywackes and the stratigraphic thickness may reach 10 000 m (Lundqvist 1987). In Finland, major parts of the central province are occupied by granitoids of the central Finnish batholith (e.g. Hietanen 1975, Simonen 1980, Front & Nurmi 1987). Only minor amounts of early orogenic plutonics occur on the Swedish side (Lundegårdh et al. 1984, Lundqvist et al. 1990). The metasediments are often strongly migmatized, although areas of lower grade are intercalated. A specific suite of granitoids has intruded the sediments. These, the so-called Härnö-type granites, are granites (s.s.) with typical S- and syn-collision characteristics (e.g. Claesson & Lundqvist 1995). They form generally relatively small, usually rather locally formed bodies, which sometimes grade into migmatite granites. The western parts are dominated by the 1.80–1.77 Ga Revsund granitoid suite (Lundegårdh et al. 1984, Patchett et al. 1987, Skiöld 1988, Claesson & Lundqvist 1995).

The northern Svecofennian province consists in the south of the Skellefte ore district, which is a marine volcano-sedimentary area with major complex sulphide ores (e.g. Lundberg 1980, Claesson 1985, Rickard 1986, Weihed et al. 1992). This area has been interpreted as having (rifted) island arc affinity (e.g. Claesson 1985, Rickard 1986, Vivallo 1987), and juvenile isotopic characteristics (Wilson et al. 1985, 1987). Northwards, the Skellefte district is succeeded by generally silicic terrestrial volcanics of the Kiruna–Arvidsjaur group (e.g. Perdahl 1995) and several generations of granitoids. Both early and late orogenic plutonism is widespread, and have ages in the intervals 1.93–1.87 and ca 1.81–1.77 Ga, respectively (Huhma 1986, Wilson et al. 1987, Vaasjoki & Sakko 1988, Skiöld 1988, Skiöld et al. 1993). In the Kiruna area also mafic volcanics are abundant. Major apatite iron ores are associated with the Kiruna volcanics (Parák 1975).

Recently, Nd-isotopic mapping in the northern Svecofennian province has revealed that the Svecofennian crust north of a line approximately from Luleå on the coast to Jokkmokk in the northwest is underlain by major Archaean components (e.g. Öhlander et al. 1987, 1993, Mellqvist 1996; Fig.1), as shown by the negative initial ε_{Nd} values in Svecofennian volcanics and plutonics. South of this line down to the Skellefte district, initial ε_{Nd} values are generally positive for all rocks, suggesting little involvement of older crust in the genesis of the Svecofennian rocks. Recently, Archaean rocks have been found outcropping as far south as in the Luleå area (Wikström et al. 1996, Lundqvist et al. 1996).

Several views concerning plate tectonic scenarios for the Svecofennian have been put forward (the most recent by Ruotoistenmäki 1996). Most researchers, however, agree that the Svecofennian was amalgamated by 1.86 Ga, by the accretion of island arcs (the Skellefte–Vihanti–Pyhäsalmi districts in the north and Bergslagen–Orijärvi in the south) and an intervening (back-arc) sedimentary basin (the Bothnian basin) to the Archaean nucleus in the northeast (e.g. Hietanen 1975, Patchett & Arndt 1986, Gaál 1986, 1990, Gaál & Gorbatschev 1987). Several authors stress bimodality as an indication of rift environments and preexistence of continental crust in the volcanic belts (e.g. Rickard 1986, Lagerblad 1988, Vivallo & Willdén 1988, Gaál 1990). Both the northern and southern Svecofennian volcanic belts can thus be interpreted as rifted continental island arcs (e.g. Claesson 1985, Vivallo & Claesson 1987, Baker et al. 1988, Gaál 1990). However, no Archaean influence has been traced in these volcanic belts (Wilson et al. 1985, 1987, Huhma 1986, Patchett & Kouvo 1986, Patchett et al. 1987), so the continental material in the volcanic arcs must have formed only shortly before the arcs in early Proterozoic times. Recently, deep crustal seismic reflectors dipping north below the Skellefte area (BABEL-group 1990, Öhlander et al. 1993), have been interpreted as remnants of an early Svecofennian subduction zone. The importance of collisional tectonics has been stressed by some authors recently. Nurmi & Haapala (1986), Romer & Smeds (1994) and Romer & Öhlander (1995) invoke continent collision and crustal thickening after the early orogenic accretion of arcs to account for the late orogenic plutonism, whereas Gaál (1990) relates this magmatism to subduction-related magmatic underplating and accompanied thickening. Öhlander & Zuber (1988a, b) and Zuber & Öhlander (1990, 1991) have suggested an intracontinental tensional environment for the intrusion of late orogenic Svecofennian granitoids, associated with major gravity lows, in central southern Sweden. Korja & Heikkinen (1995) stress the importance of postcollisional extensional collapse along major crustal detachment zones and accompanied mafic underplating in the evolution of the late to post kinematic Svecofennian. Korja (1995) further suggests that the early orogenic granitoids may have formed in a postcollisional setting, as a result of the collisional thickening of the volcanic arcs. Baker et al. (1988) suggest formation of Presvecofennian continental material and collisional tectonics already 2.6–1.9 Ga.

West of the TIB, the Southwest Scandinavian Domain (SSD) begins (Gaál & Gorbatschev 1987). The so-called Protogine zone has traditionally been regarded as the western limit of TIB and the Svecofennian. This "zone" essentially coincides with the onstart of penetrative Sveconorwegian deformation (Wahlgren et al. 1994). Semipenetrative to nonpenetrative Sveconorwegian deformation occurs frequently also further east, so the area affected by Sveconorwegian deformation extends at least 40 km into the TIB and Svecofennian (Wahlgren et al. 1994, Page et al. 1996). The strong tectonic overprinting, however, does not seem to coincide with a lithological boundary. Highly deformed TIB-rocks are found further west in the Southwest Scandinavian Domain (Lindh & Gorbatschev 1984, Larson et al. 1986, Lindh & Persson 1990, Wahlgren et al. 1994), especially in Värmland county. Another major deformation zone separates the SSD in southwest Sweden into two blocks: the eastern and western Gneiss segment (the Mylonite zone, e.g. Stephens et al. 1996). The southern parts of the eastern Gneiss segment have been subjected to granulite facies metamorphism of around 700°C and 10 kbar at ca 900 Ga (Johansson et al. 1991), suggesting substantial uplift in relation to the Svecofennian in the east (4–6 kbar 650–800°C; Andersson et al. 1992, Wikström & Larsson 1993, Andersson 1997b). The earliest magmatism in the SSD was calc-alkaline (mainly tonalites and granodiorites and associated volcanics) in character and ca 1.75–1.65 Ga in age (the Gothian; e.g. Gaál & Gorbatschev 1987, Connelly & Åhäll 1996, and ref. therein). Other episodes of magmatism occurred intermittently until the latest phases of postkinematic (Sveconorwegian) magmatism (1.10–0.90 Ga, which includes the major batholiths of the Östfold–Bohus granite, the Rogaland anorthosite complex and Sveconorwegian pegmatites (Romer & Smeds 1996, and ref. therein), and marks the culmination of the Sveconorwegian period.

3. The Transscandinavian Igneous Belt

The Transscandinavian Igneous Belt (TIB) is a huge belt of granitoid batholiths trending across the Scandinavian peninsula from its southeasternmost corner NNE- and N-wards ca 1400 km (Fig. 1). Some authors have preferred to call it the Transscandinavian Granite-Porphyry Belt (e.g. Lindh & Persson 1990), but as mafic to intermediate rocks constitute an essential part of it, the former name is preferred here. This term was coined by Patchett et al. (1987). It has also been called the Postsvecokarelian belt (e.g. Nyström 1982, Wilson et al. 1986). Rocks with similar age ranges, petrography, and geochemistry have thus been lumped together, suggesting also a similar way of generation (e.g. Gorbatschev 1980, Nyström 1982, Wilson 1980, 1982, Lindh & Persson 1990). Recently, also the Revsund granitoid suite in central Sweden has been included in the TIB (Gorbatschev & Bogdanova 1993), based on age and geochemical character. The TIB is dominated by plutonic granitoid magmatism with lesser amounts of volcanics. The plutonic rocks have generally an alkali-calcic geochemical trend, from granites over quartz monzonites, monzonites, to monzodiorites with the majority being granites and quartz monzonites (e.g. Persson 1978, Nyström 1982, Lindh & Gorbatschev 1984, Wilson et al. 1986, Lindh & Persson 1990, Ahl & Sundblad 1994). Mafic plutonic rocks are generally associated with the granitoids in lesser amounts. The small postorogenic intrusions occurring in the archipelago of SW Finland, in SE Finland and Russian Karelia (e.g. Eklund et al. 1996b, Konopelko & Ivanikov 1996) with ages in the range 1815–1770 Ma (Suominen 1991, Konopelko & Ivanikov 1996), may be related to the TIB-group. They are small composite intrusions with rocks trending from granite, over quartz monzonites (syenites) to monzodiorites (Nurmi & Haapala 1986). Some of them have intruded as ring intrusions (Bergman 1986), and mixing and mingling relations are common (Lindberg & Eklund 1988, Konopelko & Ivanikov 1996), as well as associated lamprophyric dykes (Eklund et al. 1996b), and other mafic rocks sometimes of extreme composition (Konopelko & Ivanikov 1996).

The TIB can be subdivided into three main areas with specific lithological characteristics, namely:

a) The *Småland–Värmland belt (SVB)* constitutes the southernmost parts of the TIB, occupying most of Småland, tapering to a narrow belt in northern Östergötland and continuing northwards through SW Närke, eastern Västergötland and eastern Värmland and finally disappearing beneath the Caledonides in Norway (Fig. 1). Voluminous associated silicic volcanic rocks are found in the southern parts (e.g. Persson 1974, 1985, 1989, Persson & Wikman 1986, Lundqvist et al. 1994), whereas associated basic to intermediate rocks are fairly abundant in all parts of the SVB (e.g. Wikström et al. 1985, Vinnefors 1985, Wilson et al. 1986, Persson 1985, 1989, Wikström 1987, Andersson 1989, 1991, Wikström

& Karis 1991, this study). The granitoids are of two main types traditionally referred to as the Filipstad and Växjö types. The first is a coarse K-feldspar porphyritic rock where the irregularly rounded megacrysts often display plagioclase mantles, whereas the second is a medium to coarse, but even-grained type. Field relations usually indicate a younger relative age for the Växjö type granites, and a common interpretation is that they represent the last, most evolved members of the SVB-suite (e.g. Gorbatschev 1971, Persson et al. 1981). The composition of the Filipstad type granitoids shows an intermediate trend from granites to monzodiorites with a dominance for quartz monzonites and granites, whereas the Växjö granitoids generally have more a restricted silicic composition. The mafic to intermediate rocks are usually associated with the Filipstad type granitoids (e.g. Wilson et al. 1986, Andersson 1989, 1991, this study). The age range in the SVB is 1.85–1.65 Ga. The oldest rocks occur in the central parts (the area of the rocks of this study, Chapter 4), and the youngest have been found in a narrow zone along the western (tectonic) margin towards the Sveconorwegian province. The distinction in the field between these youngest rocks and the older TIB granitoids with geochronological age differences of 100–200 Ma presently appears to be somewhat unclear. Recently, Larson & Berglund (1992) have subdivided TIB into three age groupings according to new geochronological data. These are TIB I (1.81–1.76 Ga), TIB II (1.70–1.69 Ga), and TIB III (1.67–1.65 Ga). The Småland-–Värmland belt is the type area for TIB I, which until the recent data appeared was thought to have an age span of 1.81–1.76 Ga (e.g. Patchett et al. 1987, Jarl & Johansson 1988, Wikström 1993, Mansfeld 1995, Persson 1995). The recent work of Persson & Wikström (1993), and Wikström (1996) have extended the upper age limit of TIB I to 1.85 Ga. TIB III rocks so far have been recognized only along the western margin of the Småland–Värmland belt (Jarl 1992, Jarl et al. 1993, Larson & Berglund 1992, Wikman 1993, Heim et al. 1996, Lundqvist & Persson 1996). Stephens et al. (1993) have obtained the age 1699±7 Ma for a

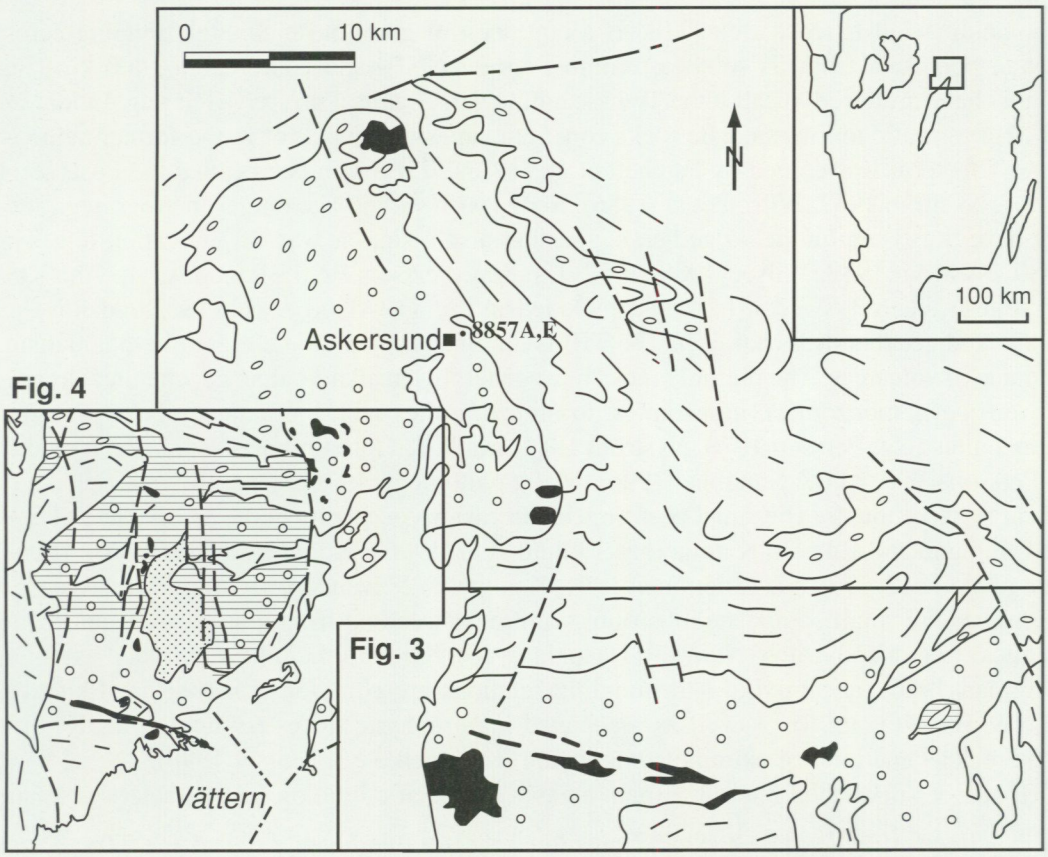

Fig. 2. Sketch map to show an overview and regional setting of Figs. 3 and 4. It shows the general outline of the contact area between the Svecofennian Domain in north and east (shown with lines tracing the structural pattern), and the Småland-Värmland belt (SVB) in the west and south (rings and ovals). Areas with ovals mark deformed varieties of the SVB granitoids (augen gneisses). Black areas are SVB basic rocks. Horizontal ruling outlines areas with extensive hybridization. Stippled area west of Lake Vättern (Tiveden) marks a greyish granitoid of unclear age position, probably of SVB age. Areas of Figs. 3 and 4 are marked. The position of sample locality 8857 is marked. Modified after Wikström (1987), Wikström & Karis (1991), and Wikström (1995).

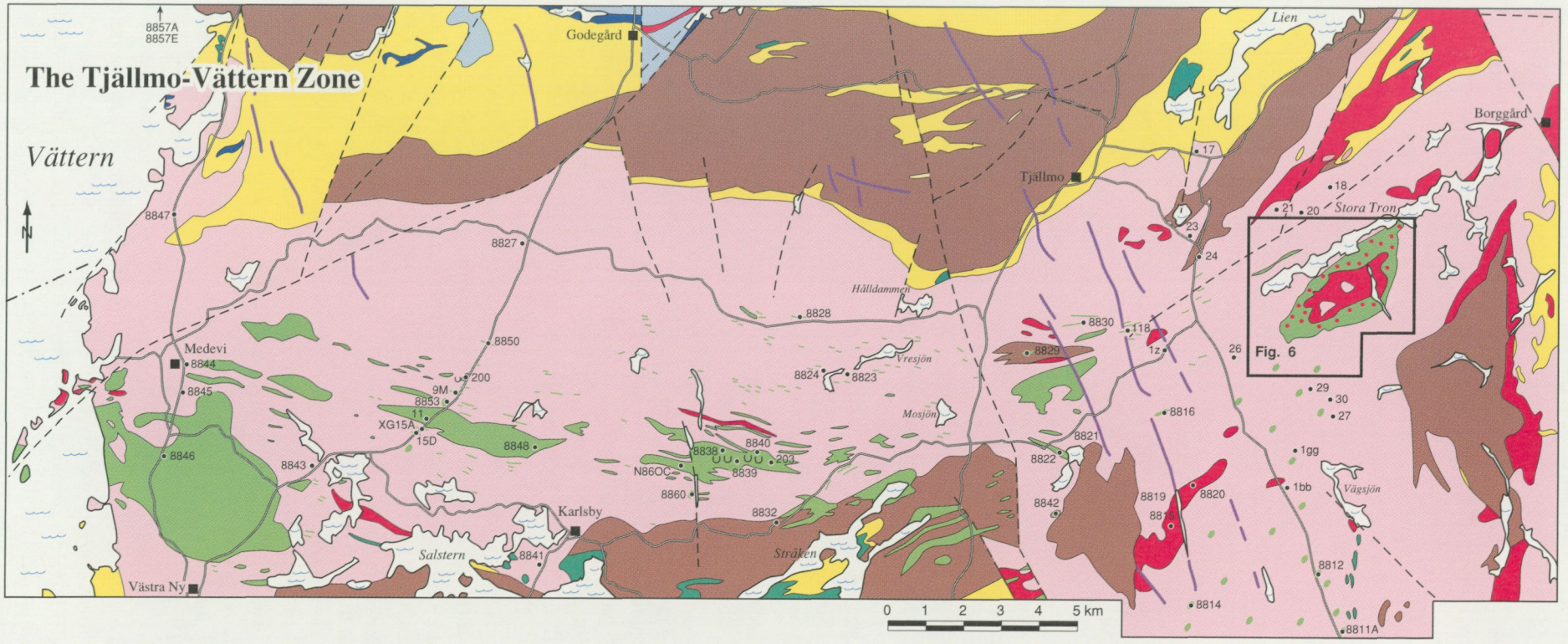

Fig. 3. Geology of the Tjällmo–Vättern zone (TVZ). The legend is found in Fig. 4. Numbers refer to analyzed samples. The frame outlines the area of Fig. 6. Modified after Wikström & Karis (1991). The TVZ is the northern contact zone of SVB rocks towards the Svecofennian in northern Östergötland (cf. Fig. 1). The SVB granitoids (pink and red) contains a conspicuous suite of basic rocks (light green) often in elongated bodies east–west, showing a variety of contact relations to the granitoids, including a transition from slightly older, contemporaneous (mingling and local mixing), and younger (dykes). See text for discussion.

mafic intrusion close to the front of Sveconorwegian deformation in SE Värmland. There is, thus, an age overlap of TIB II (below) and III, and the scheme of Larson & Berglund (1992) needs revision.

b) The *Dala–Rätan province*. This central area of TIB consists of TIB I and TIB II rocks. Three different types of granitoids have traditionally been separated in the southern (Dala) parts of the area, the Järna, Siljan, and Garberg granites (e.g. Hjelmqvist 1966). The TIB I (c. 1.79 Ga; Åberg & Bollmark 1985, Persson & Ripa 1993) Järna granitoid suite resembles the Filipstad type Småland–Värmland granitoids. It is usually reddish, coarse grained, and Kfsp porphyritic (however, usually lacking the rapakivi texture), and trend towards intermediate compositions, showing I-type characteristics (Kresten 1986, Ahl 1991). The Järna granite is also frequently associated with basic intrusive rocks (Hjelmqvist 1966). Geochronology in the area suggests a second generation of magmatism (TIB II) at 1.71– 1.66 Ga (Wilson et al. 1985, Patchett et al. 1987, Lundqvist & Persson 1996, Delin 1996, Ahl et al. in prep.) comprising the Siljan and Garberg granitoid suites, which are generally more silicic in composition and are dominated by granites (s.s.) usually coarse porphyritic and occasionally showing plagioclase mantling (Hjelmqvist 1966, Ahl & Sundblad 1994). These suites are more evolved showing elevated concentrations of elements which are commonly high also in rapakivi granites, such as e.g. F, Rb, Sn, and Nb, as well as contain greisen veins with high abundances of, e.g., also Pb, Zn, Cu, Mo, W, As, Li, Be, Ag, and Au (Ahl 1994). North and west of the granitoid areas extensive silicic and intermediate volcanics occur (the Dala porphyries), as well as associated sediments mainly quartzites and conglomerates (Hjelmqvist 1966). According to recent geochronology (Lundqvist & Persson 1993, 1996), these are largely of TIB II ages. TIB I porphyries, however, also exist.

North of the Dala porphyries the Rätan batholith occurs (Lundegårdh et al. 1984), belonging to the TIB II generation (1.70–1.66 Ga; Wilson et al. 1985, Patchett et al. 1987, Delin 1996, Ahl et al. in prep.). It is dominated by granitoid rocks of less silicic composition compared with the Dala granites of TIB II, generally showing a granitic to quartz monzonitic trend (Delin & Aaro 1992, Ahl & Sundblad 1994). The rocks are generally coarse and mostly porphyritic with occasional rapakivi mantling (Delin & Aaro 1992, Ahl & Sundblad 1994). Associated gabbroic rocks have a very limited extent (Delin & Aaro 1992). No supracrustal rocks have been identified as associated with this suite.

c) The Rätan batholith is separated in the north from the *Revsund granitoid suite* by a major crustal shear zone (e.g. Sjöström & Bergman 1996). The Revsund area is a vast belt of batholiths trending northwards in central Sweden, up to the Skellefte ore district in Västerbotten county (Lundegårdh et al. 1984, Lundqvist et al. 1990, Gavelin 1955). It is partly overlain by Caledonian rocks in the west and passes into the vast areas of metasedimentary dominated rocks of the Bothnian basin to the east. It has been known for some time to have age ranges in the same interval (1.80–1.77 Ga; Wilson et al. 1985, Patchett et al. 1987, Sköld 1988, Claesson & Lundqvist 1995) as the late-orogenic and TIB I granites further south, and has recently also been considered as a northern extension of TIB (Gorbatschev & Bogdanova 1993). The Revsund suite of rocks is dominated by (reddish) grey coarse porphyritic varieties, with rounded to rectangular Kfsp megacrysts up to 10 cm in size (Lundegårdh et al. 1984, Lundqvist et al. 1990). The composition of the suite spans the range from granite to monzodiorite (Persson 1978, Fig. 56), but granites are voluminously dominating (Lundqvist et al. 1990). Red, more evolved, types also exist (e.g. the Grötingen batholith in southern Jämtland; Lundegårdh et al. 1984, Smeds 1994) as well as dark, partly even-grained types (Persson 1978, Lundegårdh et al. 1984). Gabbroic rocks occur subordinately, but no supracrustal rocks have been identified as belonging to this suite. Associated pegmatites are very rare (Lundqvist et al. 1990, Claesson & Lundqvist 1995). Geochemically they are alkali-calcic, with I- to A-type affinities, and in many respects similar to the SVB-granitoids (Gorbatschev 1990, Lundqvist et al. 1990, Claesson & Lundqvist 1995). S-type affinities have been suggested by, e.g. Armands & Xefteris (1987).

The coarse porphyritic *Sorsele granitoids* in western Västerbotten (Gavelin 1955) was already earlier interpreted as a part of TIB, based on magnetic and geochemical characteristics (e.g. Wilson 1980, Berthelsen & Marker 1986). Rocks of TIB-age and petrographical and geochemical affinity are encountered within and to the west of the Caledonian rocks in the Lofoten area, as the northernmost extension of the belt (e.g. Andresen 1980, Gorbatschev 1985, Romer et al. 1992).

The western limit of the TIB proper is demarkated by the geographical extension eastwards of penetrative Sveconorwegian deformation. This deformational boundary occurs in a zone that separates the Southwest Scandinavian Domain from the TIB and the Svecofennian Domain sometimes referred to as

the Protogine zone (cf. Rodhe 1992). It has recently been subjected to a detailed structural study in the northern part of the Småland–Värmland belt (Wahlgren et al. 1994). These authors have suggested that the term Protogine zone (PZ) should be abandoned, and be replaced by the Sveconorwegian Frontal Deformation Zone (SFDZ), which is placed far east (c. 40 km) of the PZ and marks the easternmost extension of known major Sveconorwegian tectonic influence (albeit not penetrative).

4. The geology of TIB in northern Östergötland – southern Närke

This part of the TIB has been described by, e.g. Blomberg (1901), Carlsson (1880), Erdmann (1889), Gorbatschev (1971), Gorbatschev et al. (1976), Jönsson (1887), Karlsson (1887), Linnarsson & Tullberg (1882), Persson et al. (1985), Stolpe (1881a, b), Westergård et al. (1926), Wikman et al. (1980), Wikström (1976, 1984, 1987, 1991, 1992), Wikström & Aaro (1986), Wikström et al. (1980, 1985), Wikström & Karis (1991), and several descriptions are under way (Wikström in prep., Wahlgren in prep). It is an area central in the Småland–Värmland belt (SVB) part of TIB (Fig. 1), on the margin to the early Svecofennian domain in the north and east, where the SVB tapers to a narrow zone continuing northwards. Along the winding contact towards the Svecofennian the forces during the intrusion of the batholith seem to have played a major role in the development of the large-scale structures in the adjoining country rocks, where lobes of SVB rocks have deformed conformably with the Svecofennian rocks (Wikström 1984, 1991). Numerous mafic bodies and dykes occur in the granitoids (Wikström & Karis 1991). These were previously mostly believed to be of early Svecofennian origin and present in the younger granites of the SVB as large xenoliths or older intrusive phases of the SVB (e.g. Magnusson et al. 1963, Gorbatschev 1971, Gorbatschev et al. 1976, Wikman et al. 1980). In recent years it has, however, become evident that a majority of them are actually synplutonic with the granitoid suite (e.g. Wikström et al. 1985, Wilson et al. 1986), showing abundant signs of magma mixing and mingling, and areas of extensive hybridization (Andersson 1989, 1991). This is explored in some detail below.

4.1. FIELD RELATIONS IN THE STUDIED AREAS

The field areas in the SVB studied in this investigation are outlined in Fig. 2, and shown in more detail in Figs. 3 and 4. Figs. 3 and 4 have the legend in common shown on Fig. 4.

4.1.1. The Tjällmo–Vättern zone (TVZ)

TVZ is a zone of associated mafic rocks in coarse porphyritic Filipstad-type granitoids, stretching east–west about 40 km, from around Tjällmo in the east to Lake Vättern in the west on the southern Finspång map-sheets (Fig. 3; Wikström & Karis 1991). It can be followed uninterrupted across the lake to its western side on aeromagnetic anomaly maps (Wikström 1995), where it finally disappears (or curves into the Sveconorwegian structural pattern), just south of the Tiveden area described below. No lateral movements have thus affected this zone of basic magmatism in the SVB due to tectonics associated with the Vättern graben (Wikström 1995).

The mafic bodies within the granite in this zone tend to be elongated east–west (Fig. 3), parallel with the outer intrusion contact of the granite batholith (Wikström 1987, 1991), and this feature may be related to the magmatic intrusion tectonics of the batholith (Wikström 1987). The mafic rocks themselves are diverse in nature. Both large gabbro bodies (e.g. the large massif in the west) down to dm- to m-sized dykes occur. It is generally difficult to interpret the field geological age relations, except with the dykes (Fig. 5a). Magma mingling and local mixing structures are often observed, indicating coeval mafic-felsic magmatism in the TVZ (Andersson 1991, Wikström & Karis 1991). Within the basic suite, three occurrences of ultrabasic rocks have been identified (Fig. 3). These are spinel- and plagioclase-bearing lherzolites/olivine websterites, also containing phlogopite. The host rocks to the basic suite are generally the "normal" coarse porphyritic Filipstad type granitoids with relatively abundant mafic minerals (Fig. 5f), but more felsic varieties are common (Fig. 7b) usually without sharp contacts to the more "mafic", normal Filipstad granitoids.

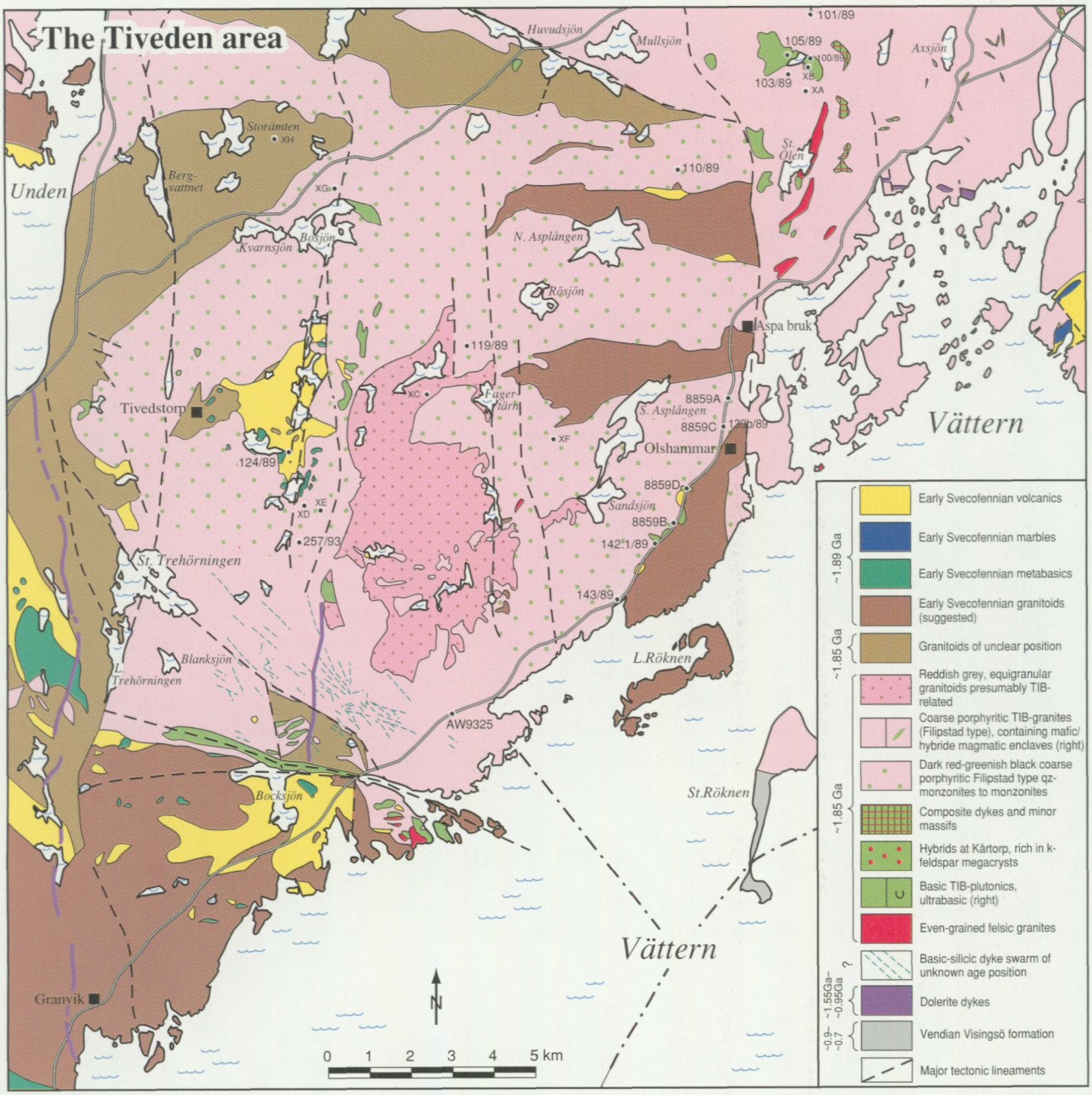

Fig. 4. Geology of the Tiveden area of southern Närke and northern Västergötland. Modified after Wikström (1995, and in prep.). Numbers refer to analyzed samples. The area is dominated by hybridized SVB granitoids (quartz monzonites and monzonites; pink with green dots). The age position of several of the foliated granitoids in the area (greenish brown) is presently unclear due to the geochronological age overlap recently recorded (Wikström 1996). A major tectonic lineament (the Aspa fault; Wikström 1995) separates the central Tiveden block from an eastern block with relatively silicic SVB granites. In the central parts of the area a reddish grey equigranular (sometimes with scattered megacrysts of K-feldspar) granitoid occur. This rock type has diffuse and unclear contacts to the regular SVB granitoids and is here regarded as belonging to the SVB suite. In the southern parts of the area, a suite of numerous silicic-intermediate-basic dykes cross-cut the SVB granitoids sharply. This dyke generation is presumably significantly younger than the SVB, although its age is presently unknown. See text for discussion.

Fig. 5. a) Example of a basic dyke cutting the Filipstad granitoid in the TVZ. This dyke generation is regarded as closely related to the basic intrusives and the SVB granitoids (SVB dykes). Often these dykes are among the most primitive basic rocks in the suite chemically (see chapter on geochemistry). b) Rounded xenocryst-free mafic magmatic enclave (MME) in Filipstad granitoid (c. 2 km south of Kårtorp, close to loc. 29; Fig. 3). c) Xenocryst-rich MME (hybrid). Crystals incorporated in the enclave from the surrounding granitic crystal mush during dynamic magma mixing. C. 1 km south of Kårtorp (locality 35; Fig. 6). d) Specimen containing a zoned MME. Slightly more fine-grained (and mafic) margin may represent chilling of mafic magma drop in the cooler granitic crystal mush. The central part is slightly hybridized. Both margin and core have been analyzed (8812M and 8812L, respectively; Appendix 2a). C. 6.5 km south of Kårtorp (loc. 8812; Fig. 3). e) Zoned enclave in the Kårtorp hybrid zone (loc. 132b; Fig. 6). This enclave has a hybridized zone following the outer margin, as well as joining the margins together in the middle. Xenocrysts in the marginal zone show alignment parallel to the outer contact. Two areas of apparently little hybridization occur in each half of the enclave. This enclave has been cited as an example of internal circulation of material inside an enclave as the result of relative flow to the surrounding magma (Weinberg 1992). f) Typical Filipstad type granitoid, with abundant plagioclase-mantled K-feldspar phenocrysts (Kårtorp area). g) Hybrid SVB rock. Phenocrysts have generally diminished in size and become more scattered due to a larger component of mafic minerals (Kårtorp hybrid zone; loc. 33-131a, Fig. 6). h) More mafic type of hybrid. Most of the felsic phenocrysts have dissolved, as they were not stable in the hotter more basic composition of the hybrid magma. They grew originally in the coarse porphyritic Filipstad granitoid crystal mush, before the mixing event (Kårtorp hybrid zone; loc. 132b, Fig. 6).



5a



5b



5c

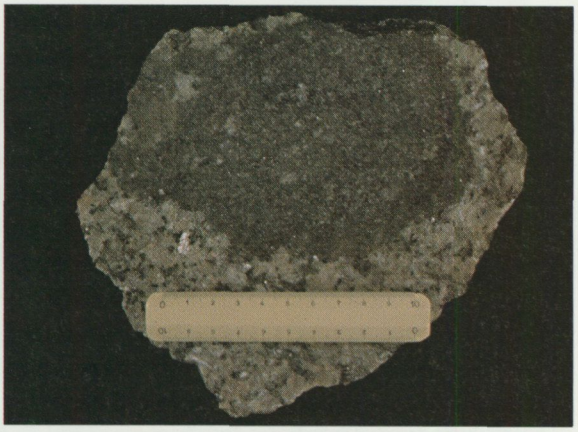

5d



5e



5f



5g



5h

Mafic and hybrid magmatic enclaves occur all over the TVZ, but unevenly distributed, e.g. abundant in the area south of Kårtorp, but more sparse further west. They are generally rounded, ideally oval, but often irregular. Different degrees of hybridization are evident from their mineralogy, from essentially primary mafic to almost granitic, often containing xenocrysts of K-feldspar and quartz almost identical to those of the surrounding granite (Fig. 5c). In some cases they are zoned with dark (chilled) margins and lighter centres (more felsic) (Fig. 5d).

4.1.2. The Kårtorp area

The Kårtorp area is situated in the easternmost part of the TVZ, southeast of Tjällmo (Fig. 3), and is associated with a major positive magnetic anomaly (cf. Wikström & Karis 1991). It consists of a peripheral most basic zone of monzodiorites, which grade inwards without any sharp contacts to quartz monzodiorites, quartz monzonites and granites (Fig. 6). All intermediate rocks are interpreted to be hybrids (see chapter 4.5.2.4. below). The central parts consist of an even-grained, coarse, felsic granite. The latter shows sharp contacts to its surroundings, and appears to be magmatically unrelated to the surrounding hybrids. Similar granites elsewhere in the SVB (the so-called Växjö type) usually display field evidence of being younger, and have generally been interpreted to represent the most evolved stage in the SVB-suite (e.g. Gorbatschev 1971, Persson et al. 1981). In the hybrid zone all gradations between the "normal" coarse porphyritic Filipstad type granite and even- and medium-grained monzodiorite occur, displayed in the density of K-feldspar megacrysts and amount of mafic minerals. These macroscopic variations can be correlated with the whole rock chemistry. The more mafic the hybrid the more corroded the felsic megacrysts become, decreasing in size (Fig. 5f–h). The outer contact of the hybrid zone towards the Filipstad type granites is generally relatively sharp.

Smaller areas with somewhat hybridized granite occur south of the Kårtorp area, which is also seen in the distribution of outcrop susceptibility (Fig. 23b). Scattered mafic-hybrid enclaves occur in the hybrid zone, and are relatively abundant in the granites south of the Kårtorp area. A few of these show internal compositional zoning, and alignment of xenocrysts (Fig. 5e), suggesting dynamical magmatic exchange with the surrounding magma (Andersson 1991, Weinberg 1992).

4.1.3. The Tiveden area

A large area with a strong positive magnetic anomaly occurs in the Tiveden area (unpubl. aeromagnetic map, SGU 1986, Eriksson & Henkel 1994), west of Lake Vättern and TVZ. This area is composed of coarse porphyritic SVB-granitoids and associated basic rocks together with inliers of older Svecofennian rocks (Fig. 4). The associated mafic rocks occur as separate massifs with hybridic margins towards the granites, and as rare dykes. Recent geochronology (Wikström 1996) indicates that the Tiveden area belongs to the oldest rocks of the SVB-suite, around 1.85 Ga. Similar ages have been obtained also in the Askersund area just northeast of Tiveden (Persson & Wikström 1993), while the Kårtorp monzodiorite some 50 km to the east gives c. 1.81 Ga (chapter 4.4.1.). Further complications have arisen by the fact that also some grey tonalitic gneisses in Tiveden give the same ages as the coarse porphyritic Filipstad granitoids (Wikström 1996). The tonalites were previously regarded as part of the early Svecofennian sequence, but may in light of these new age data perhaps be part of the SVB-suite, in similarity with the "grey Växjö granites" in Småland (Wikström 1996).

In detail, most of the positive magnetic anomalies can be correlated with outcropping mafic rocks or, in particular, dark (redbrown-violet-dark green-black, Fig. 7a) coarse to coarse K-feldspar porphyritic hybrid SVB-rocks. These are macroscopically very similar to the Filipstad type and all gradations of intermediate rocks occur, trending from granites to quartz monzodiorites and quartz monzonites. The transitions between the rock types are generally very gradational over large distances, in the scale of hundreds of meters to kilometers. The most basic hybrid varieties have generally lost all K-feldspar megacrysts, and are grey even-grained rocks, but still relatively coarse (quartz monzodiorites). The internal lows in the huge magnetic anomaly can generally be correlated with the Svecofennian (?) inliers of metagranitoids and metasupracrustal rocks (Fig. 4). A major N–S trending tectonic zone (the Aspa fault, Wikström 1995) divides the area in an eastern and western part (Fig. 4). East of this tecton-

ic break the SVB-granitoids are much more felsic and dominated by granites s.s, as well as being low magnetic. In this eastern part, and further to the north, numerous mixed and mingled dykes have intruded more or less synplutonically (Wikström 1992). The lithologies indicate that major vertical movements have taken place along the fault zone, whereby the western side has moved upwards relative to the eastern. The highly magnetic intermediate rocks of central Tiveden have thus been brought up to the present erosional levels partly by tectonic processes. A similar relation between the Kårtorp area and the western areas of the TVZ may also be at hand since a major NNW–SSE trending fault zone is present west of Tjällmo (Fig. 3). The displacement directions, however, have not been established in the field, nor have any quantitative estimates of displacement along these fault zones been attempted. The latest movements have taken place in Postcambrian times. A suite of numerous small dykes (dm to a few m) of dominantly intermediate compositions cuts sharply through the southern parts of the Tiveden SVB-granitoid area in Fig. 4, and thus appears to be younger than the SVB-magmatism. The age of this suite is not known.

4.2. PETROGRAPHY/MINERALOGY

The Filipstad type granitoids typically contain K-feldspar (microcline) megacrysts (up to c. 3–4 cm), now and then irregularly mantled by plagioclase. The megacrysts are generally irregularly rounded and the mantles usually consist of several small grains of plagioclase. Plagioclase is also a major free phase forming relatively large grains (up to c. 1 cm). Quartz is variably abundant, generally smaller in size ($\leq$ 0.5 cm) compared with the feldspars. Quartz contents, of course, decrease significantly when the rocks grade towards monzonites/monzodiorites. Biotite is ubiquitous, and is the only Fe-Mg-silicate in the most silicic types. Biotite is normally well-preserved, but may occasionally be partly altered to chlorite. Hornblende is the other major Fe-Mg silicate, occurring abundantly in the less silicic "normal" Filipstad granites. Biotite and hornblende are often intimately intergrown, where in many instances biotite appears to replace hornblende. Ilmenite and magnetite are relatively common, and usually associated with the ferromagnesian silicates. Ilmenite may occur as free grains but commonly forms exsolution-oxidation lamellae in magnetite. Titanite is typical of the Filipstad type granitoids, at least in the areas investigated here. It is almost always anhedral and secondary in nature. Commonly it forms a mantle around magnetite or ilmenite grains, or has totally replaced the oxide phases, being intimately associated with biotite+hornblende. Apatite is a ubiquitous accessory phase forming stubby or slightly elongated grains. Zircon is also a common accessory phase.

The scanty mineral chemical data available is summarized in Table 1. It contains almost only analyses of the ferromagnesian silicates, especially from the hybrid rocks. Analyses of ilmenite and magnetite have not been included in the table, but the MnO content of ilmenite varies between 1.7 and 5.9 wt%.

In the Kårtorp area, as the hybrid rocks become more basic in composition, the K-feldspar megacrysts become corroded and diminish in size and finally disappear. Only some interstitial microcline remains. Similarly, quartz gradually decreases in abundance, while plagioclase increases accordingly. The Fe-Mg silicates also increase in amount, especially amphibole. Minor amounts of clinopyroxene occur in the most basic hybrids, usually strongly altered to amphibole and quartz. Amphibole-quartz pseudomorphs after clinopyroxene is a characteristic feature in these rocks (Fig. 7c). The first amphibole to form from the pyroxenes is a colourless actinolite (Table 1), which occurs in the centre of the pseudomorphs close to any remaining pyroxene. Further away towards the margin the amphibole becomes a bluish green hornblende. The amount of Fe-Ti oxides also increases markedly in the hybrids, compared with the granites. Alteration to titanite occurs frequently but is less strong, compared with the granites. Accessories are apatite needles and zircon.

The Tiveden hybrids are distinguished by the greenish black colour of their feldspars. This makes it sometimes difficult to recognize these rocks as granitoids, despite the abundance of large K-feldspars. The reason for this colouring is not known, but the feldspars do contain minute inclusions of darkish crystals or fluids, which are not seen in the normal granites. Probably, these small grains contain relatively more reduced iron in the form of magnetite. Where this iron component is oxidised to the "normal" state (hematite?), the K-feldspars gradually become red, while the plagioclase retains its dark colour longer. Large grains of plagioclase and occasionally K-feldspar are euhedral to subhedral and

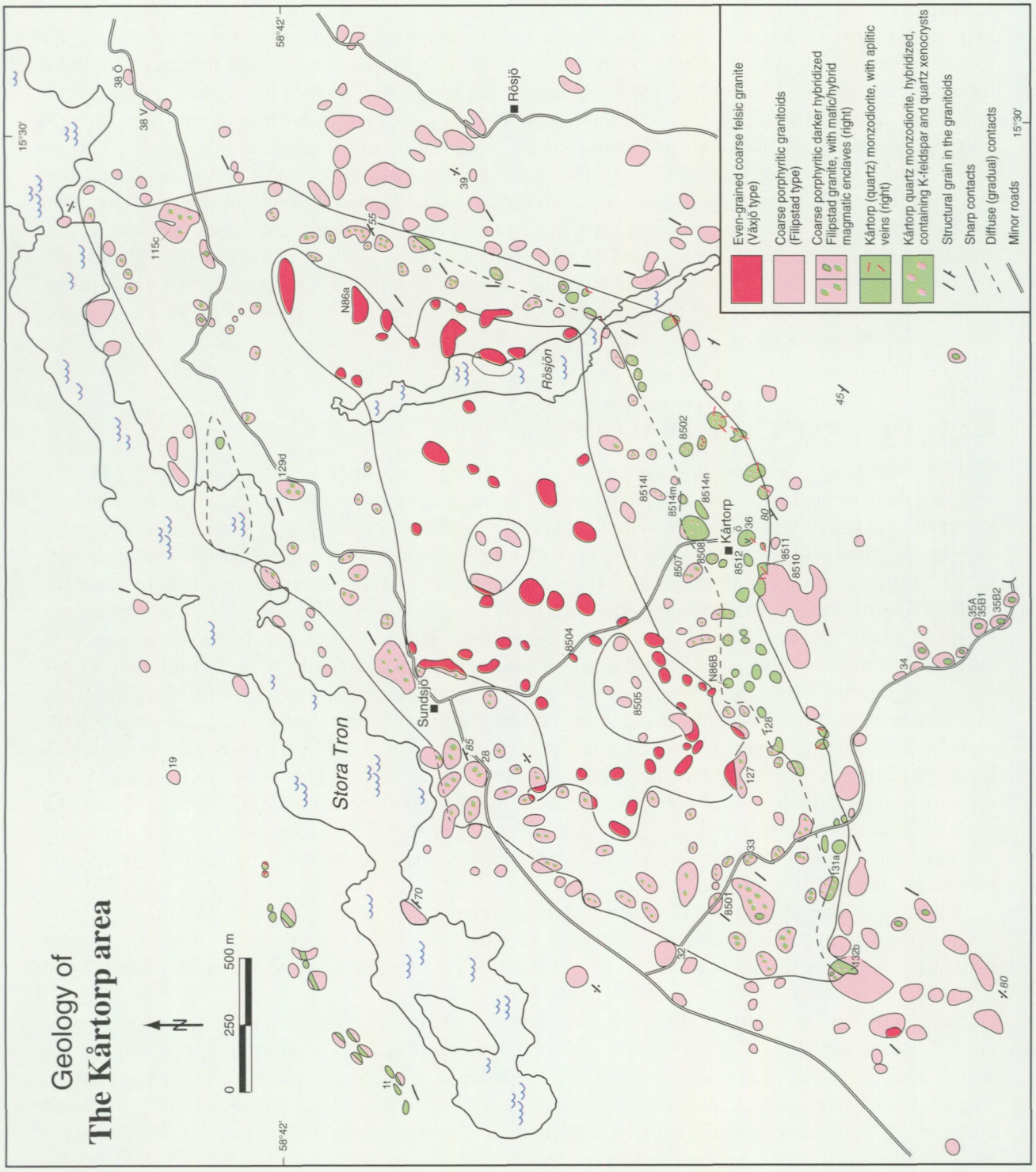

Fig. 6. Detailed geology of the Kårtorp area (for location, see Fig. 3). Coloured areas signify most outcrops in the area. The most basic type of hybrids are found in a zone along the southern contact (Kårtorp monzodiorites), and in a small area in the north. This area corresponds to the strongest aeromagnetic intensity (Fig. 23a; Wikström & Karis 1991). These most basic rocks show transitional contacts towards more silicic hybrids within the association. The contacts towards the surrounding Filipstad granitoids are, however, relatively sharp. A relatively primitive basic dyke (loc. 1t) is located northwest of the Kårtorp area (Fig. 6; cf. geochemistry section). The central part of the area is occupied by a silicic coarse even-grained granite (Växjö type), which shows sharp contacts to the Filipstad granitoids and hybrids. The aeromagnetic data indicate that it constitutes a relatively thin cap with a slightly thicker root zone in the northwest (cf. Fig. 23a; Wikström & Karis 1991). Further discussion in the text.



7a



7b

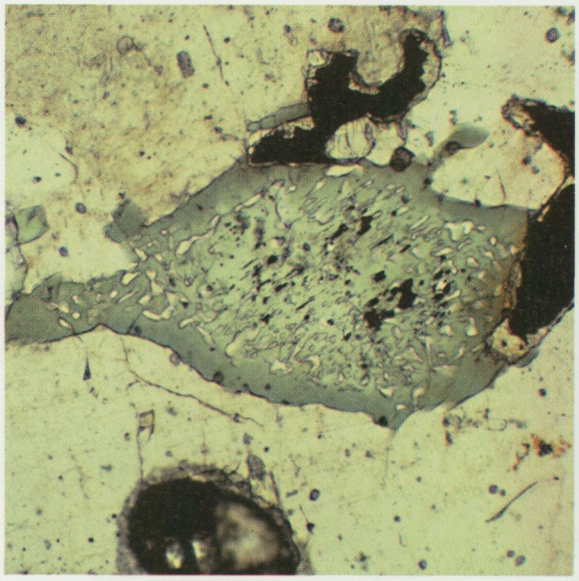

7c

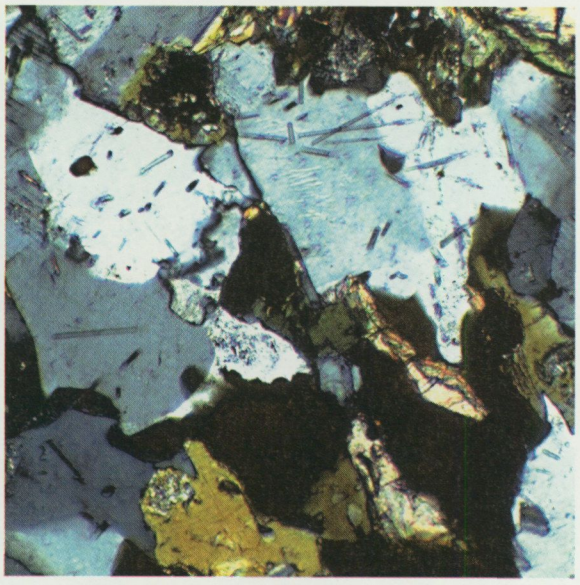

7d

Fig. 7. a) Black monzodiorite from the Tiveden hybrids (loc. 119/89; Fig. 4). Black colour due to dark colouring of plagioclase and K-feldspar. b) Example of silicic SVB granite in the TVZ (loc. 8820; Fig. 3). c) Typical amphibole-quartz-oxide pseudomorph after clinopyroxene. // nicols. The amphibole in the lighter areas in the centre is actinolitic and the greenish margin hornblende (cf. Table 1) (Kårtorp hybrids, loc. 36ö; Fig. 6). d) Apatite needles in MME. + nicols. Needles occur in groundmass feldspar and quartz, which were presumably the latest phases to crystallize and enclose the apatites formed in the melt due to rapid cooling. The rapid cooling was accomplished when the basic magma drop (the MME) was mingled into the considerably cooler granitoid crystal mush (cf. Didier & Barbarin 1991, and ref. therein).

Table 1. Representative analyses of minerals from the Småland–Värmland rocks.

	Kårtorp									
	Clinopyroxenes, hybrids					Biotites, hybrids and granites				
	3233 P1 (8511)	3237 P2 (8510)	3427 P1 (8512)	3238 P2 (8508)	3240 P3 (8507)	36VA P2	38Ö P3	26 P2	20 P3	17 P3
SiO_2	50.67	51.48	52.23	50.98	51.95	35.71	35.65	35.79	34.44	34.37
TiO_2	-	-	-	-	-	4.32	2.72	2.42	2.46	2.99
Al_2O_3	0.68	0.62	0.64	0.58	0.64	14.34	14.3	14.62	15.32	14.78
FeO	13.73	14.04	10.87	14.24	13.65	19.41	23.42	24.68	25.52	29.1
MnO	0.49	0.81	0.61	0.83	0.83	0.15	0.31	0.37	0.43	0.44
MgO	10.68	9	11.9	9.98	9.63	11.09	8.95	7.67	6.9	4.74
CaO	21.54	22.07	21.79	21.68	22.34	-	-	-	-	-
Na_2O	-	-	-	-	-	-	0.18	0.13	0.16	0.02
K_2O	-	-	-	-	-	9.77	9.61	9.31	9.93	9.43
	97.79	98.02	98.04	98.29	99.04	94.79	95.14	94.99	95.16	95.87
	Salite	Salite	Salite	Salite	Salite	Biotite	Biotite	Biotite	Biotite	Biotite

	Amphiboles, hybrids and granites														
	38Ö P3	26 P2	17 P2	36VAP3 (Av Px)	3271 P1 (35AA)	3269 P3 (29)	3268 P3 (8505)	3264 P3 (8514n)	3245 P3 (8510)	3244 P3 (8511)	3262 P3 (8507)	3259 P1 (8508)	3383 P2 (33)	3385 P1 (27)	3385 P2 (27)
SiO_2	42.42	41.06	41.77	43.25	43.46	43.44	42.95	41.98	42.7	43.79	42.27	43.07	48.01	52.45	42.36
TiO_2	1.48	0.54	1.15	1.01	0.61	1.53	1.69	0.78	1.6	1.5	1.3	1.91	0.45	0.12	1.64
Al_2O_3	10.22	11.76	12.09	11.03	9.76	9.53	9.31	11.88	9.36	9.52	10.74	9.65	5.09	2.76	9.6
FeO	20.75	23.94	23.62	17.96	22.02	21.05	21.5	19.6	20.99	19	20.39	19.42	17.88	16.81	21.71
MnO	0.63	0.46	0.63	0.37	0.1	0.1	0.1	0.1	0.1	0.1	0.1	0.1	-	-	-
MgO	7.38	5.28	4.66	9.5	7.87	8.43	7.19	8.86	8.11	9.44	8	8.76	11.32	12.28	7.32
CaO	11.38	11.45	11.19	11.43	11.56	11.19	11.47	11.76	11.68	11.74	11.7	11.43	11.9	11.92	11.53
Na_2O	1.54	1.21	0.97	1.19	0.56	1.53	1.65	1.05	1.3	1.17	1.39	1.42	1.19	0.19	1.25
K_2O	1.17	1.58	1.13	1.21	0.93	1.11	1.19	1.26	1.18	1.08	1.22	1.21	0.79	96.64	96.95
	96.97	97.28	97.21	96.95	96.87	97.91	97.05	97.27	97.02	97.34	97.11	96.97	96.63	Actinolite	Potassian ferro-
	Ferroedenitic hornblende	Potassian ferroan pargasitic hbl	Ferro-tscher-makitic hbl	Tschermakitic hornblende	Ferrian ferro hbl	Ferro hornblende	Ferro-edenitic hornblende	Tschermakitic hornblende	Ferro-edenitic hornblende	Magnesio hornblende	Ferroan pargasitic hbl	Ferro-edenitic hornblende	Magnesio hornblende		edenitic hbl

	Tiveden															
	Orthopyroxene	Clinopyroxenes, hybrids		gabbro	Amphiboles, hybrids					gabbro	Biotites, hybrids					Plagioclase, hybrid
	119:2 P2 Opx (2)	XE P5 Cpx (1)	8859C2 P3 Cpx	8859D1 P2	Cpx119:2 P9 Amf (3)	119:2 P5 Amf (1)	XE P3 Amf (1)	XE P8 Amf? (2)	8859C2 P12 Amf (2)	8859D1 P13 Amf (2)	8859D1 P7 Amf	119:2 Tr1 Bio (2)	XE P14 Bio Z92Z0	8859C2 P17 Bio (2)		119:2 Plag Tr1 (6)
SiO_2	49.54	51.13	50.74	50.75	43.1	40.14	43.47	51.39	41.94	41.51	42.33	35.14	34.84	34.77	SiO_2	57.48
TiO_2	0.05	-	0.01	0.04	1.08	0.26	0.17	0.07	1.37	0.7	0.63	4.96	4.12	4.56	Al_2O_3	26.1
Al_2O_3	0.41	0.5	0.72	1.01	10.2	12.09	8.68	2.09	9.85	10.54	10.68	13.88	13.9	14.35	FeO	0.11
FeO	35.45	13.27	15.2	8.83	20.83	22.74	20.89	16.46	21.92	19.64	16.75	23.16	23.71	23.6	MgO	-
MnO	1.4	1.4	1.02	0.39	0.27	0.23	0.74	0.7	0.59	0.25	0.24	0.12	0.38	0.29	CaO	8.64
MgO	12.08	10.02	9.14	12.69	8.09	6.46	8.31	12.94	7.25	8.26	10.41	8.39	7.89	7.93	Na_2O	6.69
CaO	0.66	22.7	22.04	24.07	11.52	11.56	11.76	11.85	11.22	12.15	12.22	-	-	-	K_2O	0.24
Na_2O	-	0.38	0.23	0.31	0.69	0.78	0.97	0.21	1.13	1.03	1.1	-	0.07	0.06	BaO	-
K_2O	-	-	-	-	1.17	1.52	0.95	0.14	1.17	1.4	1.19	9.6	9.74	9.32	SrO	-
	99.59	99.4	99.1	98.09	96.95	95.78	95.94	95.85	96.44	95.48	95.55	95.25	94.65	94.88		99.26
	Ferrohypersthene	Salite	Salite	Salite	Ferro hornblende	Ferrian pot. ferro-tschermakitic hbl	Ferro hornblende	Actinolite	Ferro-tschermakitic hornblende	Potassian Ferroan pargasitic hbl	Magnesian hastingsitic hbl	Biotite	Biotite	Biotite		An42 Andesine

occasionally brought together in a way suggesting a cumulus texture. Interstitial to these grains are quartz and biotite. Clinopyroxene and minor orthopyroxene (Table 1) have been identified in these hybrids. Amphibole+quartz pseudomorphs after pyroxenes are frequent also here. Otherwise, the same mineralogy is observed as in the Kårtorp hybrids.

The basic rocks are typically amphibolitic, containing dominantly plagioclase and amphibole. Biotite and Fe-Ti oxides are always present, but in varying amounts. Sometimes clinopyroxenes are well-preserved, but quite often only amphibole + quartz pseudomorphic aggregates remain. Orthopyroxene has been encountered only in sample 8839, where it is fresh and occurs abundantly. This sample is little hydrated compared with most other rocks. No olivine has been found. Epidote and titanite are sometimes common secondary minerals, as well as interstitial quartz. Elongated apatite is common as an accessory mineral.

The ultrabasic rocks are lherzolites or olivine-rich olivine websterites. They contain abundant, often strongly serpentinized olivine. The olivine occurs as chadacrysts in large (up to at least 5 cm) oikocrysts of clinopyroxene, orthopyroxene, or phlogopite. The pyroxenes are relatively fresh. Plagioclase occurs interstitially and is separated from the olivine by a reaction corona of dominantly clinopyroxene. The plagioclase is often strongly altered. Minor amounts of spinel are found, as well as accessory opaque phases.

The mineralogy of the mafic magmatic enclaves is identical to that of the amphibolitic basic rocks (e.g. the most basic Kårtorp rocks), except for the ubiquitous occurrence of small apatite needles. These are found in the groundmass quartz and feldspars (Fig. 7d). Clinopyroxenes have been found preserved only in a few instances. Xenocrysts of K-feldspar megacrysts, quartz, and plagioclase from the surrounding Filipstad granitoids are frequent in the enclaves.

The two supracrustal rocks, which have been analysed chemically and isotopically (the enclave 8857E and sample 124/89; cf. Table 3, Appendix 2a), are mineralogically similar. They are fine-grained with dominantly plagioclase and biotite. In addition, minor amounts of K-feldspar, and perhaps a little quartz, is found. 124/89 also carries opaque phases. A sedimentary origin of these samples seems most likely.

4.3. GEOCHEMISTRY

4.3.1. Major element characteristics

The new geochemical analyses of Småland-Värmland rocks of this study are compiled in Appendix 2a, and presented in major element discrimination diagrams in Fig. 8, together with analyses of SVB-rocks from the literature. The rocks from Kårtorp, TVZ, and Tiveden display a relatively distinct monzodioritic trend, between gabbro and granite, markedly similar to the trend of the Revsund granitoid suite (cf, Fig. 56, Chapter 7.3.1.). The trend of the SVB-data collected from the literature shows a more alkaline tendency, with quartz monzonites, monzonites, and even some syenites. Contrary to the Revsund suite, the SVB contain abundant associated basic and even ultrabasic rocks. A few of the mafic magmatic enclaves have more alkaline compositions, and plot in the syenodiorite field of Fig. 8a. In the A-B diagram of Debon & Le Fort (1982) (Fig. 8d), the rocks of this study are basically restricted to fields III (peraluminous; biotite essentially without muscovite and hornblende) and IV (metaluminous; hornblende ± biotite±pyroxene etc). The literature data, on the other hand, spread out also to more peraluminous compositions in field II (biotite>muscovite).

The alumina saturation diagrams in Fig. 9 contain, in addition to the samples of this study, a compilation of 471 SVB-samples from the literature. All SVB-rocks are metaluminous to peraluminous, except one peralkaline granite sample from the Linköping SW mapsheet (Persson et al. 1981). The centre of gravity in the data is close to molecular $Al_2O_3/CaO+Na_2O+K_2O$ (A/CNK) =1 (1.015). There is a tendency of an increase in A/CNK with increasing SiO_2, while the most peraluminous rocks occur at intermediate SiO_2 contents (64–69 %). This is consistent with the CIPW-norms, where the granites are slightly diopside to corundum normative, and the Tiveden intermediate rocks have the highest normative corundum (up to 2.36 %). The Kårtorp hybrids, on the other hand, are all diopside (and quartz) normative. The general character is similar to that of the Revsund granitoid suite (cf. Fig. 57), although much fewer data are available for the latter. The rocks of this study follow the general trend of the SVB,

but the Kårtorp rocks tend to be less aluminous at lower SiO_2 contents than average, whereas the Tiveden rocks in this range have higher A/CNK ratios. The basic rocks vary in normative composition from strongly olivine to strongly quartz normative, and the ultrabasic rocks have normative olivine up to 48 % (sample 203).

4.3.2. Trace element discrimination, granitoids

The rocks are plotted in the trace element discrimination diagrams of Whalen et al. (1987) and Pearce et al. (1984) in Fig. 10. The few trace element data that exist in the literature of the SVB-rocks have been included in the diagrams. They plot dominantly in the A-type fields of Whalen et al. (1987), but less distinctly than the rapakivi suites (cf. Figs. 36, 58), and trend partly into the orogenic fields. The FeO*/MgO ratios of the SVB-granitoids is generally substantially lower (3-6), compared with the rapakivis (mostly above 6). One group of SVB-granites have much higher Ga/Al ratios (6-7 x 10^4) than the others (Fig. 10a, b). Most of these occur on the map sheet Säfsnäs SW in eastern Värmland (M. Ripa, unpubl data), and two in the Äspö area of eastern Småland (Wikman & Kornfält 1995). The analyses of the rocks in this study follow the literature data relatively closely, but seem to be a little higher in the abundance of the high field strength (HFS) elements. Also here, there are marked similarities with the Revsund suite (Fig. 58). In the diagram after Pearce et al. (1984), the SVB-granites plot transitionally between the fields for volcanic-arc granites (VAG) and within-plate granites (WPG) (Fig. 10d), but dominantly in the VAG-field. The Revsund granites plot in the same general area of the diagram (cf. Fig. 58d). Some similarity with the Swedish rapakivi suites is also apparent in this diagram, especially the Jämtland–-Ångermanland rocks, which plot at lower Rb contents compared with the Rödö and Strömsbro rocks (cf. Fig. 36).

4.3.3. Spider diagrams, granitoids

Bulk earth normalized spider diagrams of silicic-intermediate SVB-rocks are shown in Fig. 11 together with averages of some other rock groups, in order to make comparisons simultaneously for a large number of elements. Average upper and lower crust (Taylor & McLennan 1985) have also been included for reference. It is clear from the uppermost diagram that the most silicic Filipstad, the "normal" Filipstad type granites, and the Tiveden hybrids in general have closely similar elemental charac-

Fig. 8. Classification diagrams using major element geochemical data of SVB rocks. Symbols are, crosses: 339 SVB rock analyses compiled from the literature (Kornfält 1975, Gorbatschev 1975, Gorbatschev et al. 1976, Wikman et al. 1980, 1982, Persson et al. 1981, 1985, Persson 1985, 1989, Björk 1985, Lundegårdh 1980, 1987, Gavelin 1984, Wikström et al. 1980, Wikström & Aaro 1986, Kresten 1986), inclined crosses: TVZ rocks, open diamonds: Kårtorp rocks, half-filled circles: Tiveden rocks, and filled diamonds: mafic-hybrid magmatic enclaves. a) R1-R2 diagram after De La Roche et al. (1980) based on the molecular parameters stated along the axes. Fields of different rocks types have been delineated empirically using a large data base. Numbered fields superimposed on the diagram are defined by Batchelor & Bowden (1985) as follows: 1=Mantle fractionates, 2=Pre-plate collision, 3=Post-collision uplift, 4=Late-orogenic, 5=Anorogenic, 6=Syn-collision, 7=Post-orogenic rocks. Rocks to the upper left of the diagonal line are silica undersaturated. The silicic to hybrid SVB rocks of this study display a typical monzotrend from the monzogranite to the monzodiorite field. A few of the most evolved MMEs fall in the syenodiorite field, while most of the basic rocks fall in the olivine gabbro field on both the under- and oversaturated parts. A few SVB rocks from the literature plot in the syenite field. b) SiO_2-total alkalies diagram after Middlemost (1985) showing an essentially consistent trend with the R1-R2 diagram. In comparison with the rapakivi granites (Figs. 34 and 56), the SVB granites are generally somewhat more Ca -rich, with very few data points falling in the syeno- and alkali-granitic fields. c) The Q-P diagram of Debon & Lefort (1983) relates the molecular parameters for quartz and feldspars with each other, and gives a trend entirely consistent with the two previous diagrams. d) The A-B diagram of Debon & Lefort (1983) is somewhat different as it relates a parameter of alumina saturation (A) with a parameter of the amount of mafic constituents (B). The fields are, I: muscovite alone or muscovite>biotite, II: biotite>muscovite, III: biotite alone, IV: biotite+hornblende±ortho- and clinopyroxene, ±primary epidote±sphene, V: clinopyroxene±hornblende±primary epidote±sphene, VI: exceptional compositions. LG=leucogranites. Fields I–III are peraluminous, and fields IV–VI are metaluminous. The SVB rocks spread out over the fields II–IV. The literature data are partly more strongly peraluminous, compared with the rocks of this study. The amount of leucocratic rocks in the SVB is fairly low (cf. rapakivi granites, Figs. 34 and 56). The granitoids and hybrids of this study spread out essentially in the biotite alone and biotite+hornblende fields, as do the majority of SVB rocks. This is consistent with petrographic observation.

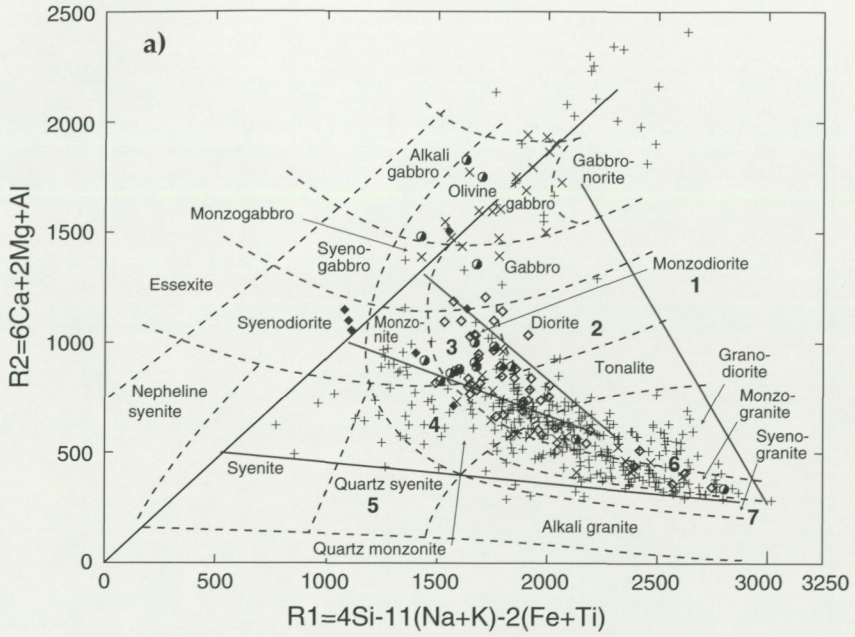
a)
R2=6Ca+2Mg+Al
R1=4Si-11(Na+K)-2(Fe+Ti)
Alkali gabbro
Olivine gabbro
Gabbro-norite
Monzogabbro
Syeno-gabbro
Gabbro
Monzodiorite
Essexite
Syenodiorite
Monzo-nite
Diorite
Tonalite
Grano-diorite
Monzo-granite
Syeno-granite
Nepheline syenite
Syenite
Quartz syenite
Alkali granite
Quartz monzonite
1
2
3
4
5
6
7

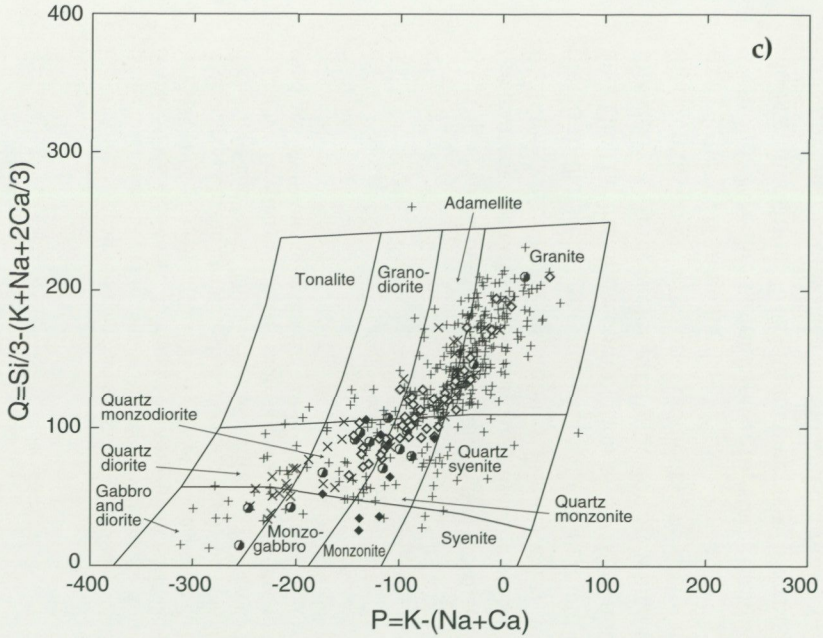
c)
Q=Si/3-(K+Na+2Ca/3)
P=K-(Na+Ca)
Adamellite
Granite
Tonalite
Grano-diorite
Quartz monzodiorite
Quartz diorite
Quartz syenite
Gabbro and diorite
Quartz monzonite
Monzo-gabbro
Monzonite
Syenite

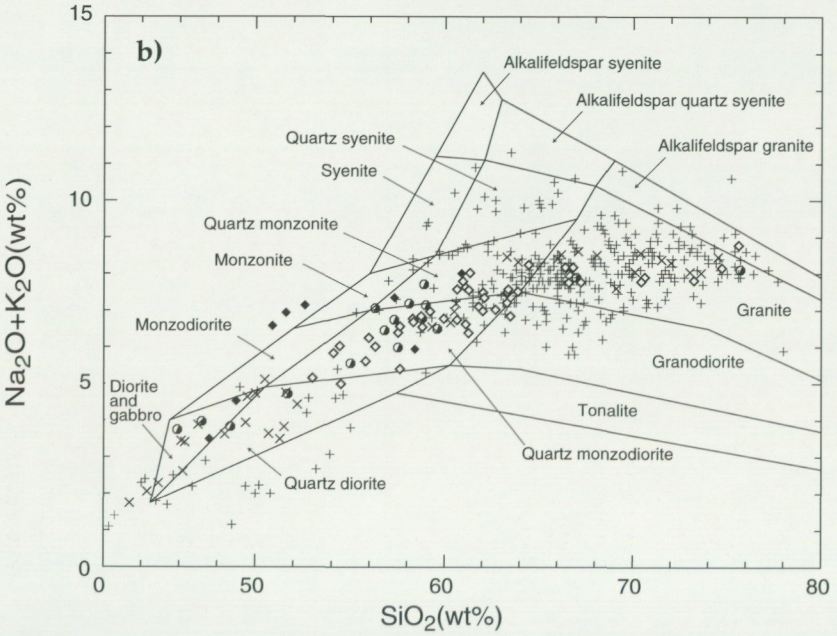
b)
Na2O+K2O(wt%)
SiO2(wt%)
Alkalifeldspar syenite
Alkalifeldspar quartz syenite
Quartz syenite
Alkalifeldspar granite
Syenite
Quartz monzonite
Monzonite
Granite
Monzodiorite
Granodiorite
Diorite and gabbro
Tonalite
Quartz monzodiorite
Quartz diorite

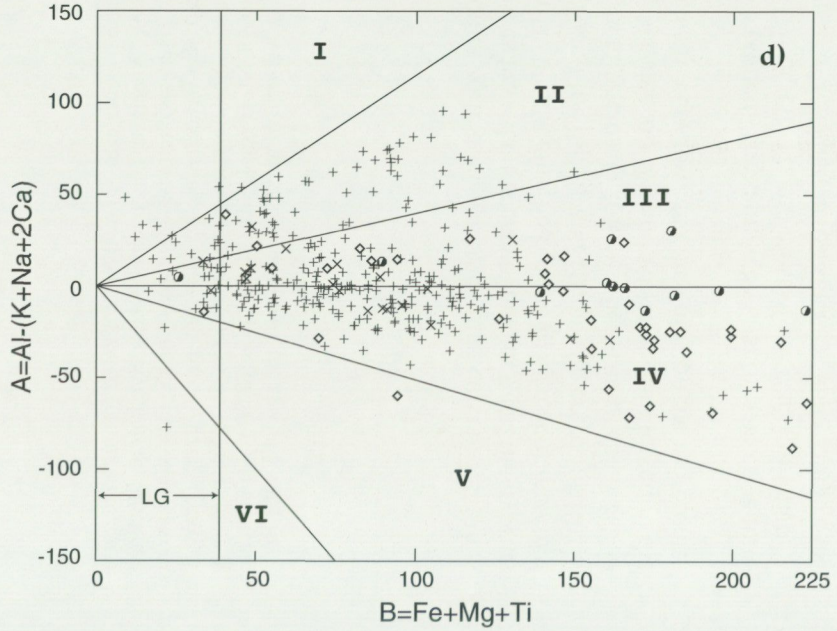
d)
A=Al-(K+Na+2Ca)
B=Fe+Mg+Ti
I
II
III
IV
V
VI
LG

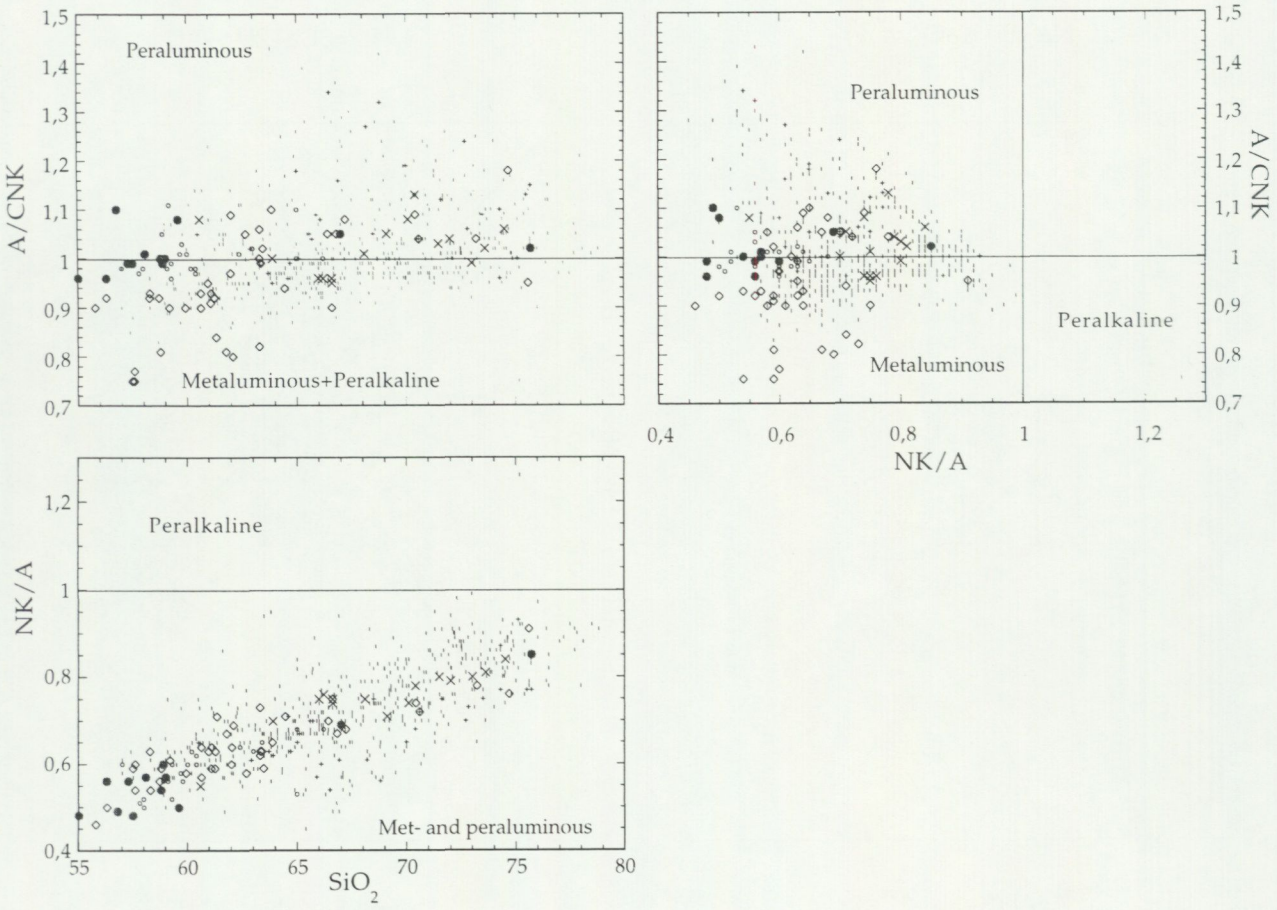

Fig. 9. Alumina saturation diagrams of SVB granitoids. Small vertical bars indicate 471 analyses compiled from the literature (same references as in Fig. 8 plus Ahl 1989, Wikman & Kornfält 1995, Annertz & Lindh unpubl. data). Symbols are, inclined crosses: TVZ granitoids, diamonds: Kårtorp granitoids, black dots: Tiveden granitoids, small crosses: SVB data of Wikström & Karis (1991), small circles: SVB data of the mapsheet Askersund SE (Tiveden area; A. Wikström unpubl. data). There is a large spread in the literature data, partly to highly peraluminous rocks. The most peraluminous rocks occur at SiO_2 contents between 65 and 70 %. The average of the data is, however, close to A/CNK=1 (molecular $Al_2O_3/CaO+Na_2O+K_2O$). Notable is that the Tiveden hybrids are more aluminous compared to those at Kårtorp. Marked similarity with the spread for the Revsund granitoid suite is observed (cf. Fig. 57).

ter (Fig. 11a). For the "mafic" elements the distribution is correlated with the silica content (and thus the content of mafic minerals) such that the silicic granites have the lowest abundances and the hybrids the highest. A similar situation is found for Eu, which is slightly enriched in the hybrids but most depleted in the silicic granites. An analogous relation is found for Ba, Zr and Hf, but reversed for Rb, U and Th. The literature compilation of SVB-granites generally closely follows the trend of the rocks in this study. Discrepancies are found for Sr, which is higher, and Be, Zr, and Hf, which are lower, in the literature average. For some elements, the literature data are very few, and thus may not be representative of the SVB in general.

In Fig. 11b, three anomalous Filipstad granitoids are plotted. The sample 8841 shows a very anomalous composition. It has high contents of Ba, Eu, Li, Be, Zr, Hf, Ti, and most of the transition metals. This chemistry suggests a substantial cumulus component of feldspar, mafic silicates, and oxides in the rock. Samples 8823 and 8827 have partly similar characteristics, e.g. high HREEs and Y. 8823 is also high in U and Rb, while 8827 is low in Th. In the lowermost spider diagram, a comparison with some other granitic suites in the Svecofennian is made. A marked resemblance between the average Filipstad granite and the average Revsund granitoid can be noted. Discrepancies can be noted for Cs and HREE

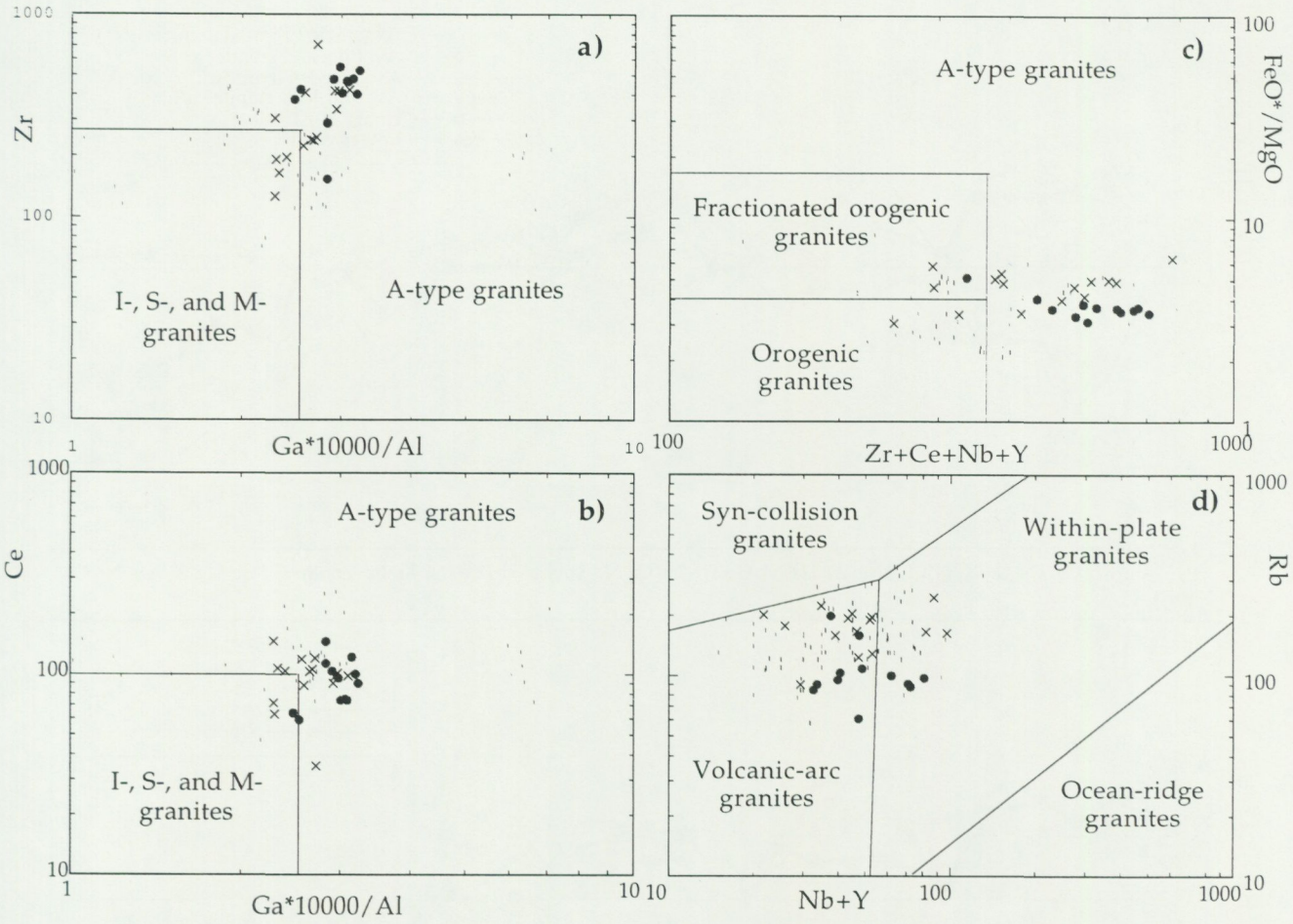

Fig. 10. Trace elements plots constructed to discern granites from different tectonic settings. a to c after Whalen et al. (1987), d after Pearce et al. (1984). Sources of literature data: Wilson et al. (1986), Ahl (1989), Wikman & Kornfält (1995), M. Ripa (unpubl. data). Symbols as in Fig. 9. The SVB granites essentially plot in the A-type (anorogenic) field of Whalen et al. (1987), however, they are partly transitional into the fields of orogenic granites (I-, S- and M-granites). In the Pearce et al. (1984) diagram, the SVB granites are transitional between the volcanic-arc (VAG) and within-plate granite fields, but with the majority of analyses in the VAG-field. The SVB granites tend not to plot in the syn-collision field. Closely similar charcteristics are recorded for the Revsund suite (cf. Fig. 58).

(higher in Revsund), and Be (higher in Filipstad granite). The Revsund granitoids are also slightly higher in the "mafic" elements, which may be due to comparatively more intermediate (lower SiO_2) rocks included in the average. The Härnö rocks stand out by having high Cu and LIL elements, but low Zr, Hf, Ti, and Fe. The large variation in the elemental abundances among the Fennoscandian rapakivi granites (see chapters below) generally encompass the composition of the c. 1.8 Ga granitoids (Härnö, Revsund, and SVB), except for the "mafic" elements where the rapakivis in general are lower.

4.3.4. Trace element discrimination, basic rocks

Some attempts to classify the basic SVB-rocks have also been made. Fig. 12 suggests that they are dominantly tholeiitic in character, with some alkalic tendencies, although the scatter is considerable. In the trace element discrimination diagrams of Fig. 13, there is also a considerable spread in the data set. In the diagram of Pearce & Cann (1973) there seem to be at least two clusters (13a). One in the field of calc-alkali basalts containing most of the TVZ and Tiveden rocks, as well as two of the enclaves,

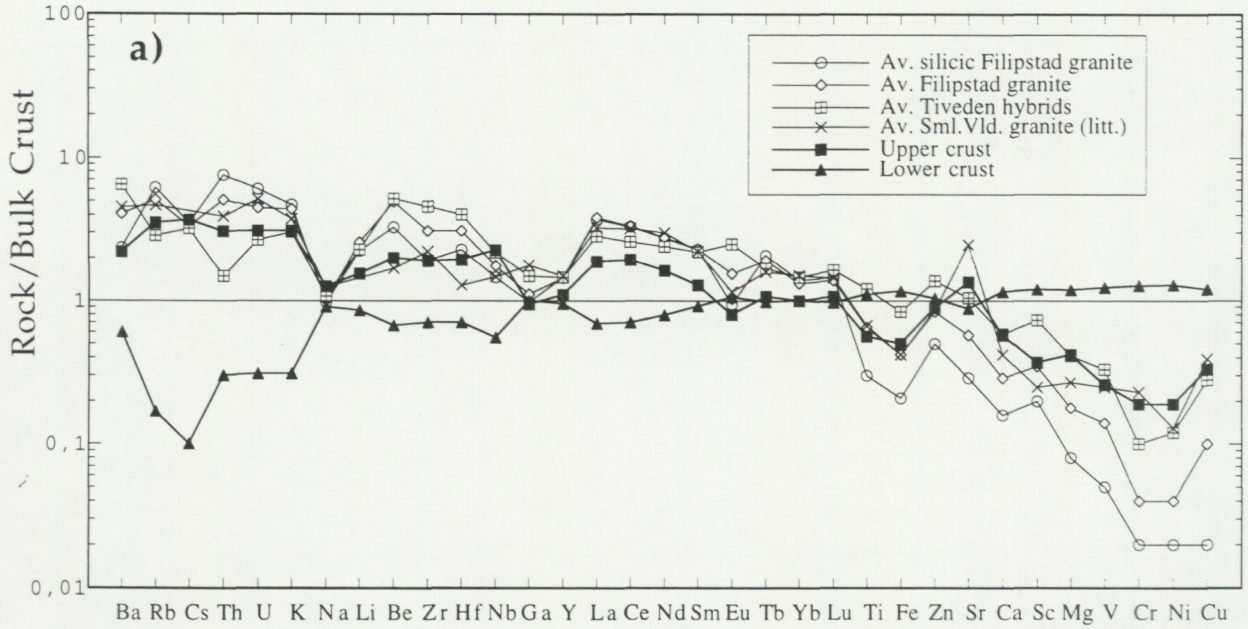
a)
Av. silicic Filipstad granite
Av. Filipstad granite
Av. Tiveden hybrids
Av. Sml.Vld. granite (litt.)
Upper crust
Lower crust
Rock/Bulk Crust
100
10
1
0,1
0,01
Ba Rb Cs Th U K Na Li Be Zr Hf Nb Ga Y La Ce Nd Sm Eu Tb Yb Lu Ti Fe Zn Sr Ca Sc Mg V Cr Ni Cu

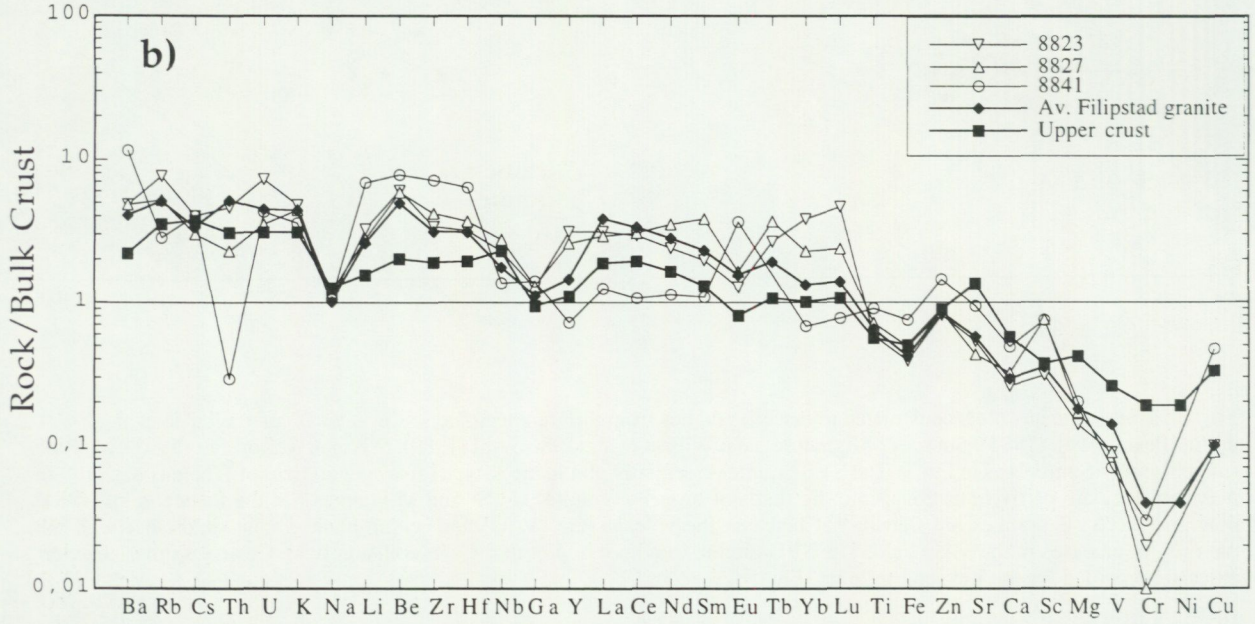
b)
8823
8827
8841
Av. Filipstad granite
Upper crust
Rock/Bulk Crust
100
10
1
0,1
0,01
Ba Rb Cs Th U K Na Li Be Zr Hf Nb Ga Y La Ce Nd Sm Eu Tb Yb Lu Ti Fe Zn Sr Ca Sc Mg V Cr Ni Cu

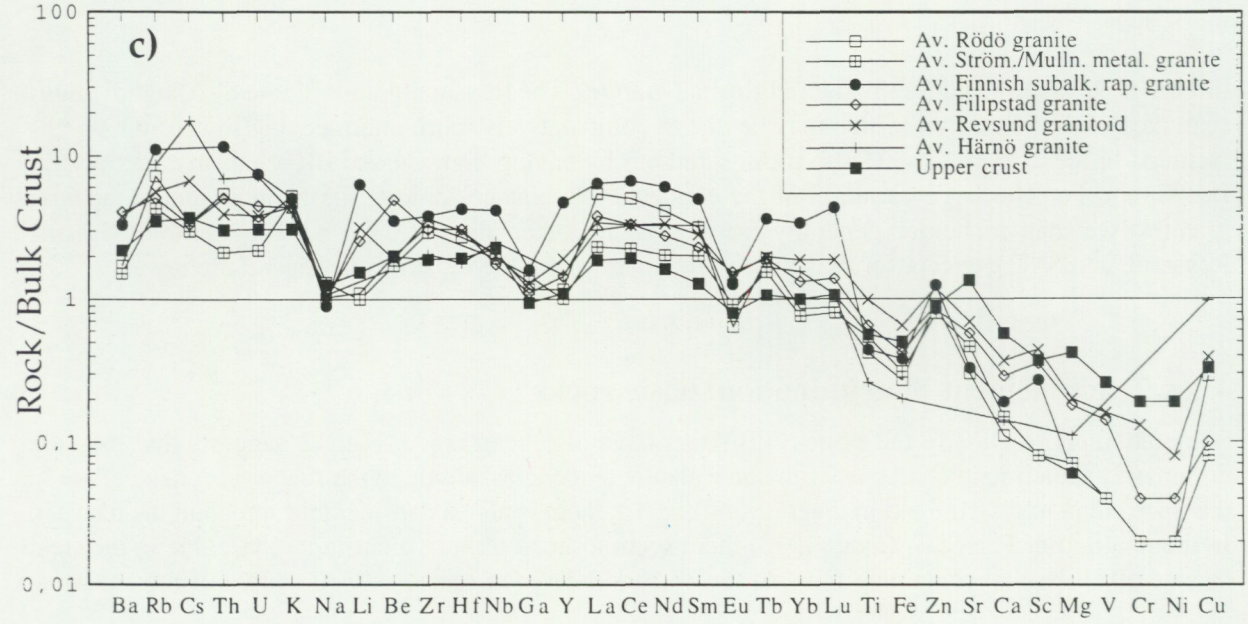
c)
Av. Rödö granite
Av. Ström./Mulln. metal. granite
Av. Finnish subalk. rap. granite
Av. Filipstad granite
Av. Revsund granitoid
Av. Härnö granite
Upper crust
Rock/Bulk Crust
100
10
1
0,1
0,01
Ba Rb Cs Th U K Na Li Be Zr Hf Nb Ga Y La Ce Nd Sm Eu Tb Yb Lu Ti Fe Zn Sr Ca Sc Mg V Cr Ni Cu

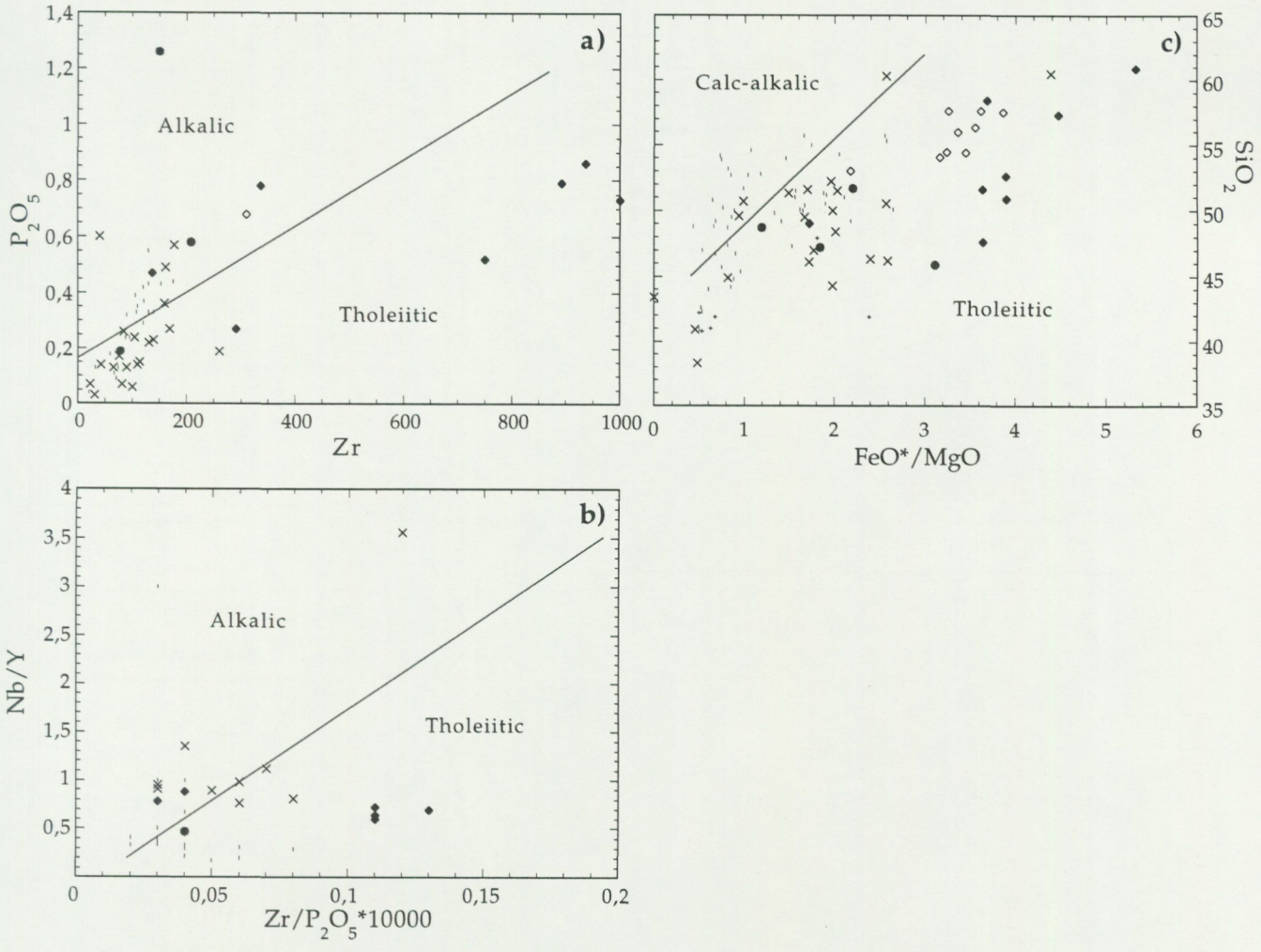

Fig. 12. Diagrams to separate tholeiitic from alkalic or calc-alkalic rocks. a) and b) after Floyd & Winchester (1975), and c) after Miyashiro (1974). The SVB basites are transitional between tholeiitic and alkalic-calc-alkalic. The rocks of this study tend to have a slight overweight for tholeiitic character. Vertical bars refer to literature data, inclined crosses to TVZ basites, dots to Tiveden basites, open diamonds to Kårtorp monzodiorites, and filled diamonds to mafic magmatic enclaves. Data sources in a) and b) are Ahl (1989), Wikman & Kornfält (1995), and M. Ripa (unpubl.). In c) in addition, Lundegårdh (1980, 1987), Wikman et al. (1982), Persson et al. (1981), Björk (1985), Persson (1985).

and one at very Zr-rich compositions outside the classification grid containing the two Kårtorp samples, most of the enclaves and two TVZ-rocks. In the classification by Meschede (1986) most of the TVZ-rocks and half of the enclaves plot in the AII-field, which is a combined field of within-plate alkali basalts and within plate tholeiites (13b). Three of the enclaves fall on the Zr-rich edge of the AI-field (within-plate alkali basalts only), while the SVB-rocks from the literature scatter between the C (within-plate tholeiites and volcanic-arc basalts) and B (E-type MORB) fields. In Fig. 13c (Cabanis & Lecolle 1989) most of the basic rocks of this study are found in the field of continental basalts (2A), while a few plot in the field of alkali basalts from intercontinental rifts (3A). The SVB-basites collected from the literature fall dominantly in the calc-alkali basalt field. There is, thus, a considerable vari-

Fig. 11. Bulk crust (Taylor & McLennan 1985) normalized spiderplots of average composition of different SVB granitoids, and other granitoids for comparison. Average upper and lower crust (Taylor & McLennan 1985) have been included for comparison. Considerable similarities are noted for different SVB granitoids in a). Some anomalous samples are plotted in b). In c) the average Filipstad granite is compared with different rapakivi, Revsund, and Härnö granitoids. The closest similarity is observed with the average Revsund granitoid. Discussion in text.

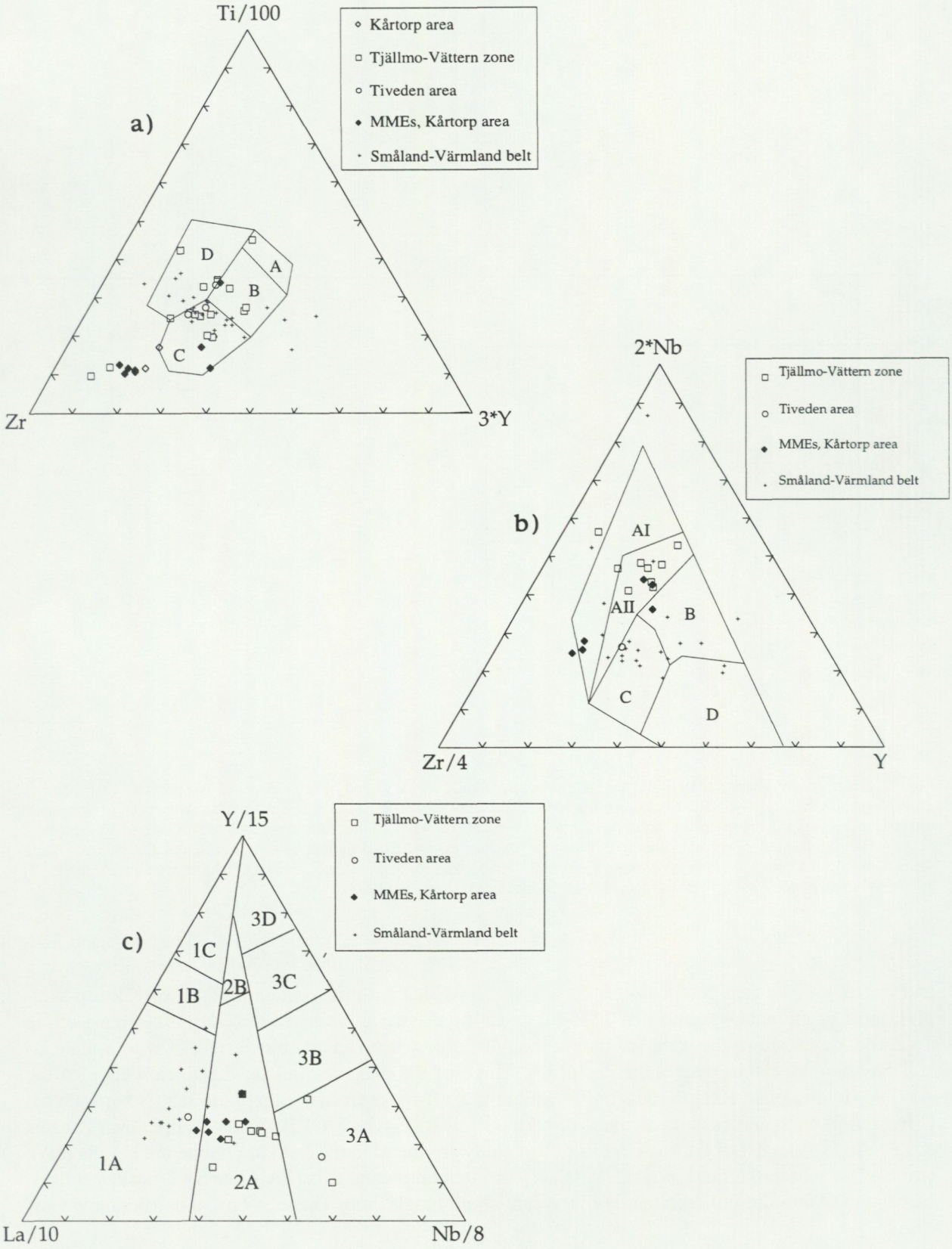
a)
Ti/100
Zr
3*Y
Kårtorp area
Tjällmo-Vättern zone
Tiveden area
MMEs, Kårtorp area
Småland-Värmland belt
A
B
C
D
b)
2*Nb
Zr/4
Y
Tjällmo-Vättern zone
Tiveden area
MMEs, Kårtorp area
Småland-Värmland belt
AI
AII
B
C
D
c)
Y/15
La/10
Nb/8
Tjällmo-Vättern zone
Tiveden area
MMEs, Kårtorp area
Småland-Värmland belt
1A
1B
1C
2A
2B
3A
3B
3C
3D

ation in geochemical character of the basic SVB rocks and these three diagrams do not give a consistent picture of the nature of this variation

4.3.5. Spider diagrams, basic rocks

Fig. 14 shows MORB-normalized spider diagrams for the analysed basic SVB-rocks, and other rocks for comparison. In the uppermost diagram, a group of the most "primitive" TVZ basites are plotted, i.e. those with the lowest concentration of LILE and HFSE. Primordial mantle (McDonough et al. 1992) is also included for reference. The average ultrabasic rock of the TVZ is also included, which in general has very low HFSE (except Nb and P), but similar LILE as the basites. The ultrabasites have naturally high contents of Ni and Cr (but not Sc), as also does sample 8850. Both average ocean island tholeiite (Thompson et al. 1984) and continental flood basalt (Thompson et al. 1983) have distinctly higher HFSE but similar LILE. In Fig. 14b the more "evolved" TVZ-basites have been collected and compared with the average Kårtorp basic hybrid (monzodiorites). There is a considerable overlap compared with the "primitive" group but a general tendency for higher contents for most elements, perhaps most pronounced for the LILE. This group in general has significantly lower Ni and Cr, which further attests to their more evolved character. The average most basic Kårtorp rock has considerably higher values for all HFSE, but similar in LILE, compared with the TVZ-basites.

In Fig. 14c, the mafic/hybrid magmatic enclaves have been plotted and compared with the average lamprophyre (Bergman 1987), the average of the most basic Kårtorp hybrids, and the ultrabasics of TVZ. Two enclaves that are anomalous compared with the rest, have been plotted separately, as well as two anomalous dyke rocks. There is an almost perfect match between the Kårtorp basic hybrids and the average enclave. There is also a strong resemblance between these rocks and the average lamprophyre. Lamprophyres are somewhat higher in Th and U, and lower in Hf, Zr, Y, and Yb, but these differences are small compared with the similarities, apart from the Ni spike for the lamprophyres. The enclave 8853C is essentially similar to the other enclaves, but slightly lower in most HFSE and higher (and even more similar to lamprophyres) in Th and U. The other enclave is similar to the more primitive parts of the TVZ basites. This is also true for the dyke 1t, while 118 is considerably more evolved and even intermediate in composition (SiO_2 60.5 %). In the lowermost spidergram (14d) the Tiveden basic rocks have been plotted, as well as the averages of the more evolved and more primitive TVZ basites, and average lamprophyre again. The Tiveden rocks display a wide variation in composition, especially so for the HFSE. The two most evolved ones (101/89 and 105/89), which belong to the same gabbro intrusion (Fig. 4), have in general higher HFSE than all TVZ-rocks, especially so for LREE and P, but are still lower than the average lamprophyre. The sample 8859D1, on the other hand, is very primitive in character, similar in HFSE composition to the ultrabasics, but with lower Cr and Ni. 139b/89 is similar to the most primitive of the TVZ-basites.

Fig. 63b illustrates a comparison between the SVB basic rocks and some basic rapakivi-related rocks. The Kårtorp most basic hybrids with lamprophyric character are considerably higher in the HFSE, while the less evolved TVZ basites are essentially similar to the rapakivi-related rocks, except being higher in HREEs and the transition metals.

Fig. 13. Trace element discrimination diagrams, designed to separate between different types of basalt. a) After Pearce & Cann (1973). The fields are A: island-arc tholeiites, C: calc-alkali basalts, D: within-plate basalts, and B: combination of MORB, island-arc tholeiites, and calc-alkali basalts. b) After Meschede (1986). The fields are AI: within-plate alkali basalts, AII: within-plate alkali basalts + within-plate tholeiites, B: E-type MORB, C: within-plate tholeiites + volcanic-arc basalts, and D: N-type MORB + volcanic-arc basalts. c) After Cabanis & Lecolle (1989). The fields are 1A: calc-alkali basalts, 1C: volcanic-arc tholeiites, 1B: area of overlap between 1A and 1C, 2A: continental basalts, 2B: back-arc basin basalts, 3A: alkali basalts from intercontinental rifts, 3D: N-type MORB, 3B: E-type MORB, 3C: E-type MORB, weakly enriched. MMEs are mafic magmatic enclaves and Småland–Värmland belt refers to literature data (same sources as in Fig. 12a, b). Discussion in text.

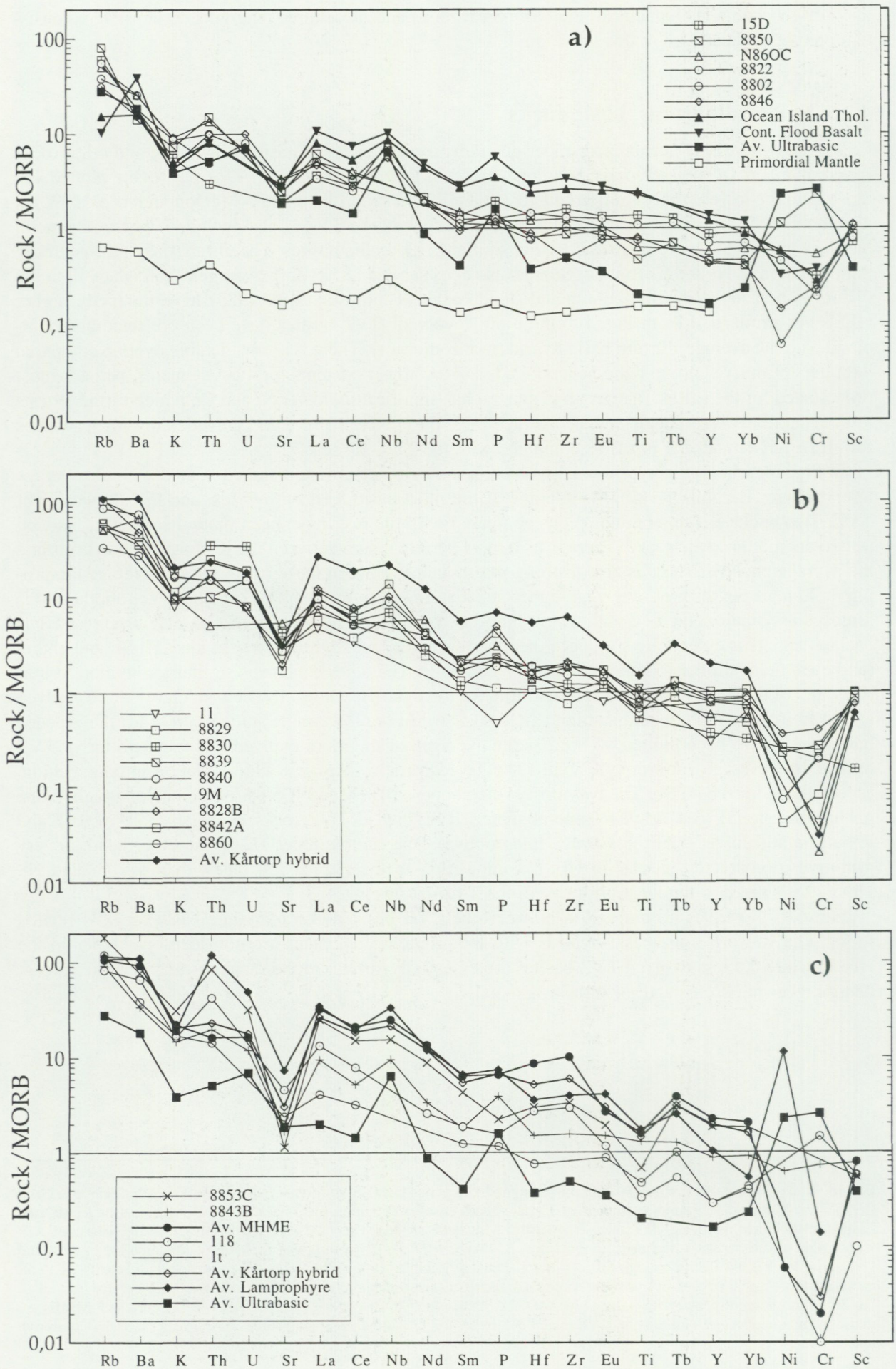
a)
15D
8850
N86OC
8822
8802
8846
Ocean Island Thol.
Cont. Flood Basalt
Av. Ultrabasic
Primordial Mantle
Rock/MORB
100
10
1
0,1
0,01
Rb Ba K Th U Sr La Ce Nb Nd Sm P Hf Zr Eu Ti Tb Y Yb Ni Cr Sc
b)
11
8829
8830
8839
8840
9M
8828B
8842A
8860
Av. Kårtorp hybrid
Rock/MORB
100
10
1
0,1
0,01
Rb Ba K Th U Sr La Ce Nb Nd Sm P Hf Zr Eu Ti Tb Y Yb Ni Cr Sc
c)
8853C
8843B
Av. MHME
118
1t
Av. Kårtorp hybrid
Av. Lamprophyre
Av. Ultrabasic
Rock/MORB
100
10
1
0,1
0,01
Rb Ba K Th U Sr La Ce Nb Nd Sm P Hf Zr Eu Ti Tb Y Yb Ni Cr Sc

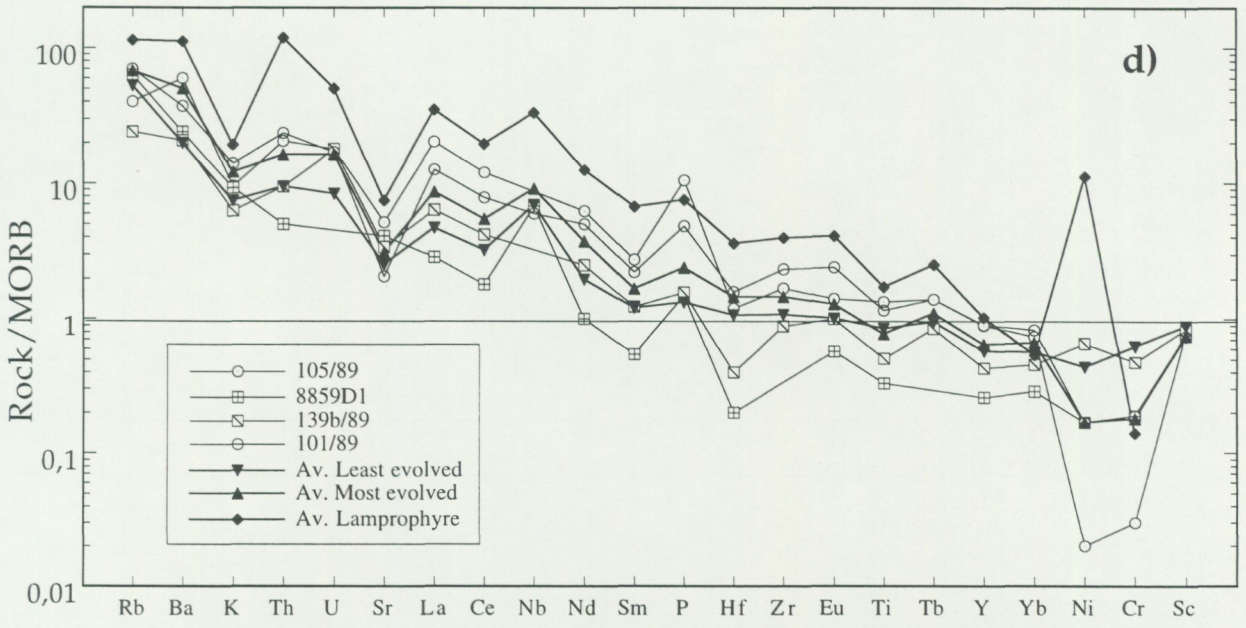

Fig. 14. MORB (mid-ocean ridge basalt) normalized (from MORB compilation in Rollinson 1993) trace element spiderplots basic SVB rocks of this study. Averages of lamprophyre (Bergman 1987), continental flood basalt (Thompson et al. 1983), ocean island tholeiite (Thompson et al. 1984), primordial mantle (McDonough et al. 1992) have been included for comparison. Numbers refer to sample numbers also found in Figs. 3 and 4, and Appendix 2a. Av. ultrabasic is the average of the ultrabasic rocks in this study. Av. Kårtorp hybrid is the average of the 6 most basic (SiO_2 <58 %) monzodiorites. Av. MHME refers to the average mafic-hybrid magmatic enclave, and includes all enclaves except 8853C and 8843B. Av. least evolved includes the least evolved basic rocks of TVZ (those in a), and av. most evolved refers to the more evolved basites of TVZ (those in b). Discussion in text.

4.3.6. Harker variation diagrams

The SVB-rocks of this study are plotted in Harker diagrams in Fig. 15. In these diagrams analyses of rocks from Wikström & Karis (1991) and Wikström (in prep.) have also been included, as these are from the same general areas. In many of the variation diagrams two distinct trends are clearly separable, one for the rocks in the Kårtorp area including most of the enclaves, and one for the TVZ and Tiveden rocks. The two trends diverge at the basic end of the spectrum and converge at the silicic end. The two trends are not clearly distinguished for all elements, but most distinct for TiO_2, P_2O_5, Sr, Zr, Hf, Nb, Zn, and the REEs (except Eu). The trends essentially follow straight lines in these element-element plots. The basic end of the Kårtorp trends (mafic enclaves) always contain larger amounts of the more incompatible elements (all elements mentioned above), and smaller amounts of compatible elements such as Cr, Ni, Cu, and V. Some of these enclaves are very high in elements such as e.g. P_2O_5 1.12 %, Zr 1430, Hf 33, Ga 32, Nb 77, Sc 50.4, Zn 261, Y 112, Ce 240, and Yb 8.8 ppm. All these elements are much higher compared with those of the associated granites (Fig. 15), which in general, e.g. have Zr contents lower than 500, Hf lower than 15, Ga lower than 25, Nb lower than 40, Zn lower than 120, Ce lower than 175, and Yb lower than 5.0 ppm.

Some inconsistency is also observed in the data. One of the enclaves, 8843B, follows the TVZ-trend rather than the Kårtorp trend, whereas some of the others show mixed behaviour, sometimes following the Tiveden-TVZ-trend. One sample (8811A) is consistently highest in the incompatible elements, while also 8812M, 8812L (dark margin and lighter core of the same enclave, respectively), 35B1, and 35B2 in most cases follow the trend defined by the suite of Kårtorp hybrids. Also within the rocks grouped together from the Kårtorp area, some variation exists. Thus, for example, a few of the granitoids from the surroundings of the Kårtorp hybrid association tend to plot with the TVZ-rocks, most markedly the somewhat anomalous sample 1gg (see REE-patterns below).

The two trends tend to converge close to 70 % SiO_2, which thus appear to represent the approximate high silica endpoint for both suites. In the basic end of the spectrum, there is an abrupt break in

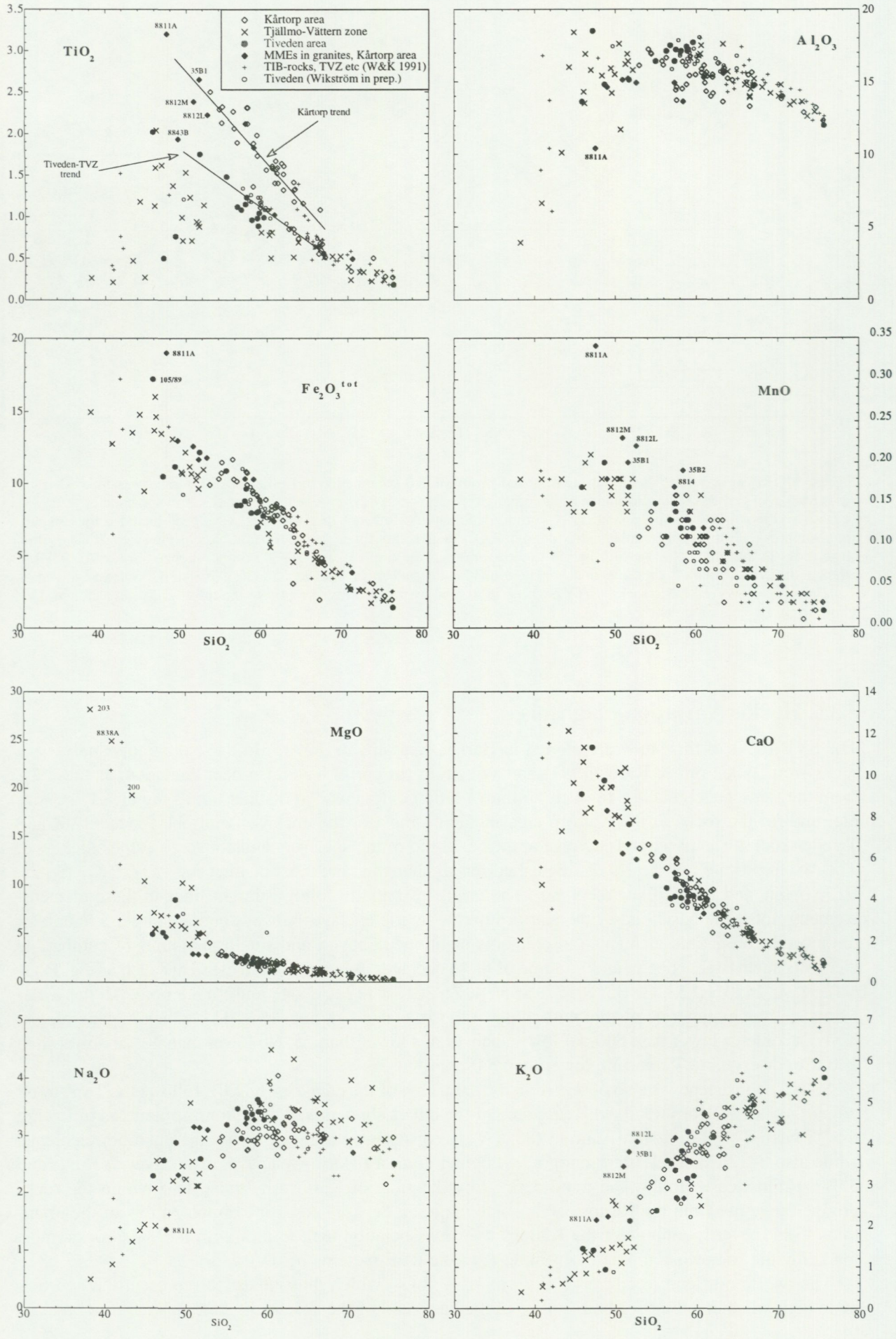
Kårtorp area
Tjällmo-Vättern zone
Tiveden area
MMEs in granites, Kårtorp area
TIB-rocks, TVZ etc (W&K 1991)
Tiveden (Wikström in prep.)
TiO2
Kårtorp trend
Tiveden-TVZ trend
8811A
35B1
8812M
8812L
8843B
Al2O3
Fe2O3 tot
105/89
MnO
35B2
8814
MgO
203
8838A
200
CaO
Na2O
K2O
SiO2

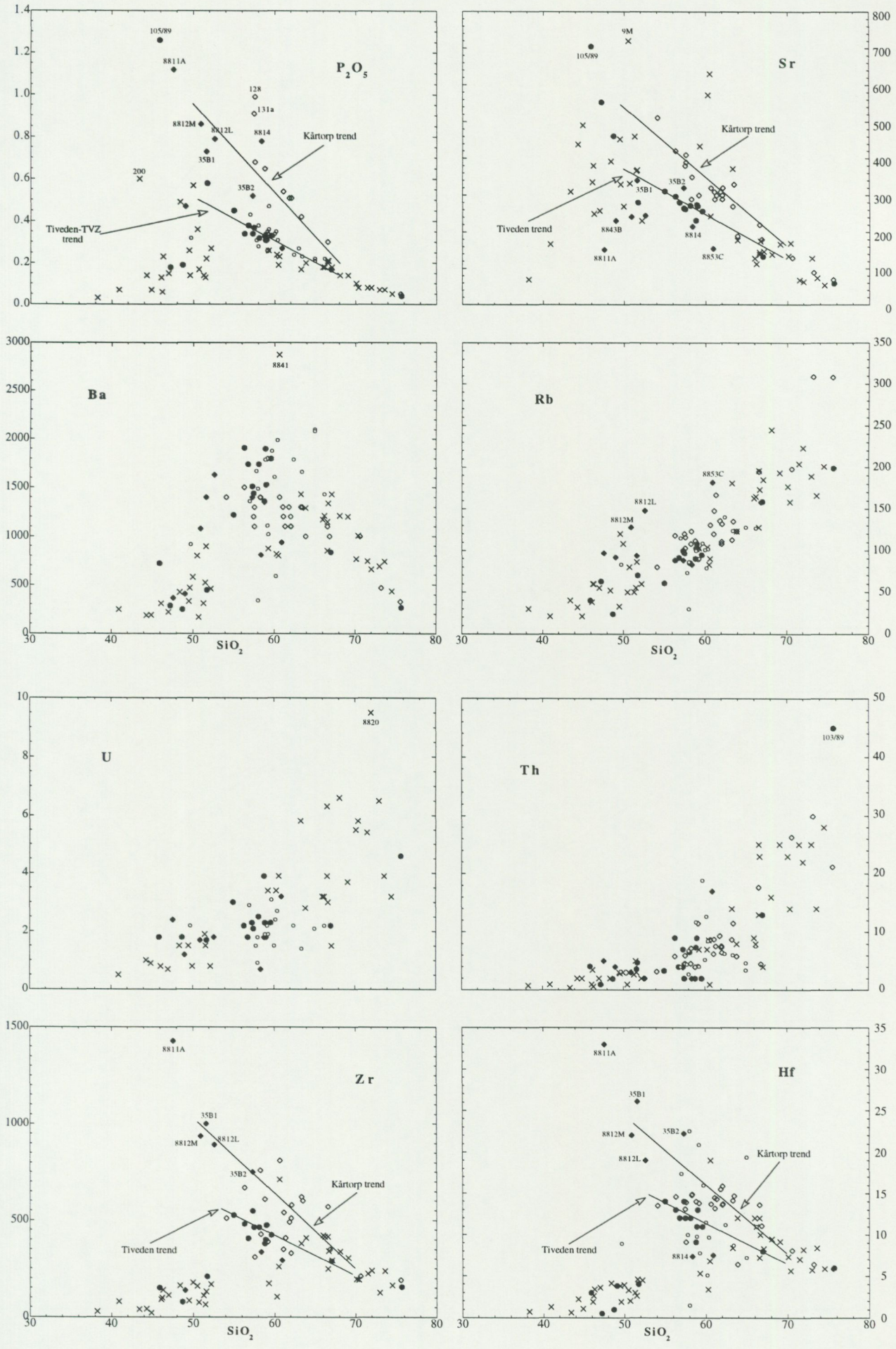
P2O5
105/89
8811A
128
131a
8812M
8812L
8814
35B1
200
35B2
Kårtorp trend
Tiveden-TVZ trend
Sr
9M
105/89
Kårtorp trend
35B2
35B1
Tiveden trend
8843B
8814
8811A
8853C
Ba
8841
SiO2
Rb
8853C
8812L
8812M
SiO2
U
8820
Th
103/89
Zr
8811A
35B1
8812M
8812L
35B2
Kårtorp trend
Tiveden trend
SiO2
Hf
8811A
35B1
8812M
35B2
8812L
Kårtorp trend
Tiveden trend
8814
SiO2

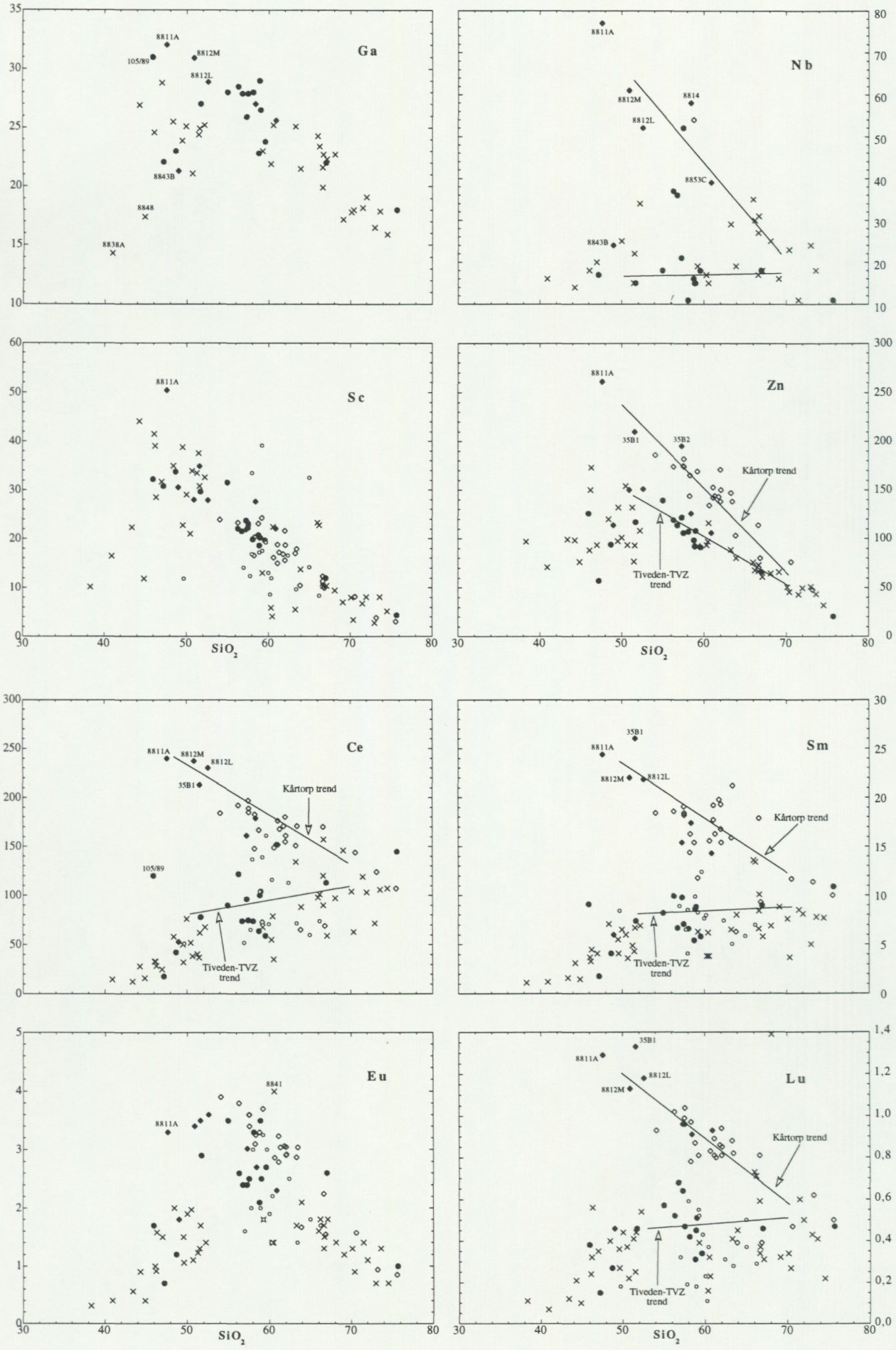
Ga
8811A
8812M
105/89
8812L
8843B
8848
8838A
Nb
8811A
8812M
8814
8812L
8853C
8843B
Sc
8811A
Zn
8811A
35B1
35B2
Kårtorp trend
Tiveden-TVZ trend
SiO2
Ce
8811A
8812M
8812L
35B1
Kårtorp trend
105/89
Tiveden-TVZ trend
Sm
35B1
8811A
8812M
8812L
Kårtorp trend
Tiveden-TVZ trend
Eu
8841
8811A
Lu
35B1
8811A
8812L
8812M
Kårtorp trend
Tiveden-TVZ trend
SiO2

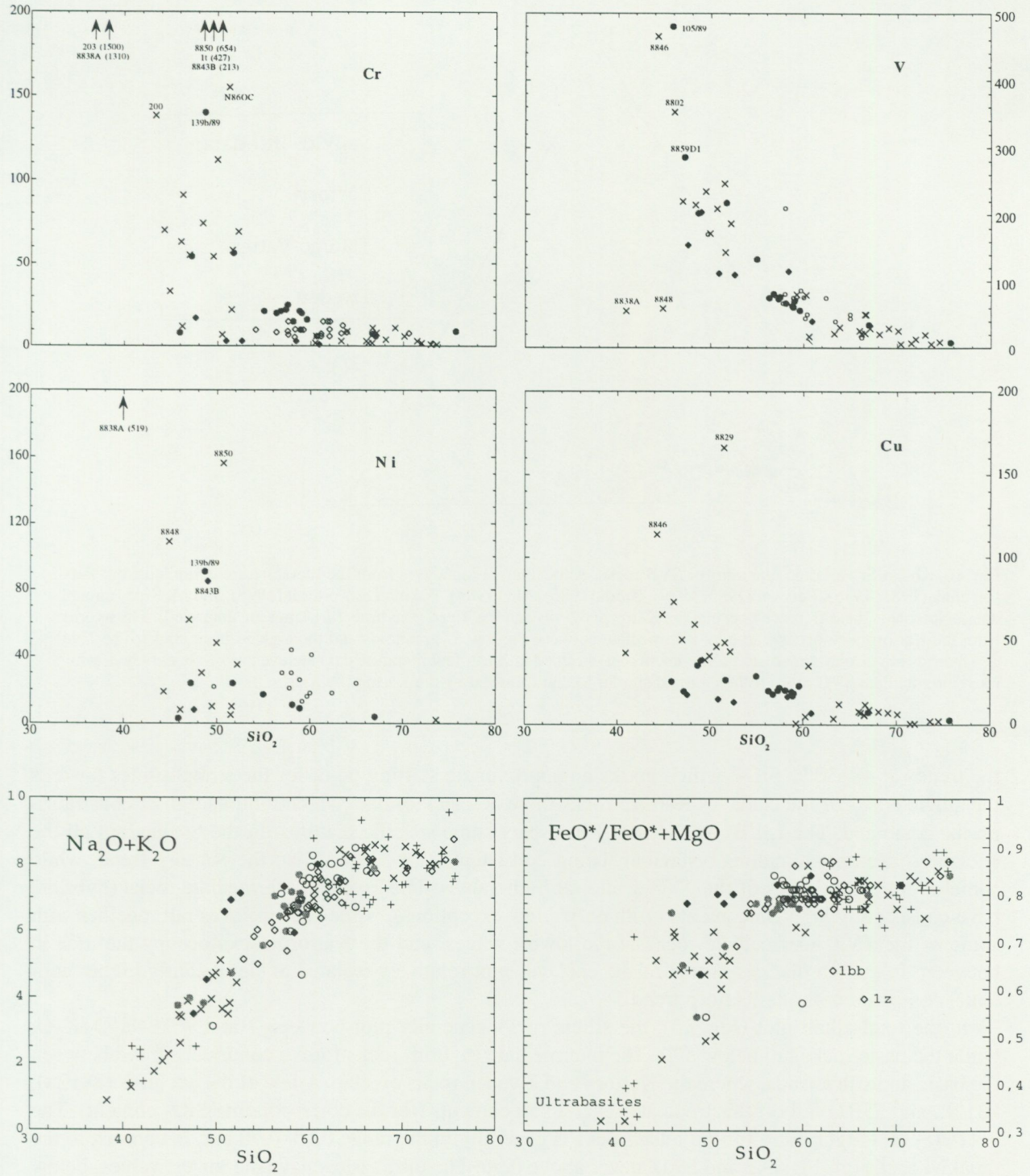

Fig. 15. Harker element variation diagrams of the rocks of this study. Additionally, SVB rocks from the Finspång mapsheets (Wikström & Karis 1991), and from the mapsheet Askersund SE (Tiveden area) (Wikström in prep.) have been included, as these cover the same general areas. Two separate linear trends are evident for many elements at intermediate compositions, one for the Kårtorp area and one generally for TVZ and Tiveden. For the other elements these trends overlap and are not clearly discernable. These differ mainly in the composition at the basic end of the trends. The mafic magmatic enclaves (MMEs) generally have a composition close to the basic endmember of the Kårtorp trend. At the silicic end of the spectrum these two trends converge at c. 70 % SiO_2. Some sample numbers have been included and refer to Figs. 3, 4, and 6. For Cr and Ni contents of some samples outside the range of the diagram have been stated in parenthesis. All analytical data is found in Appendix 2a. Detailed discussion in text.

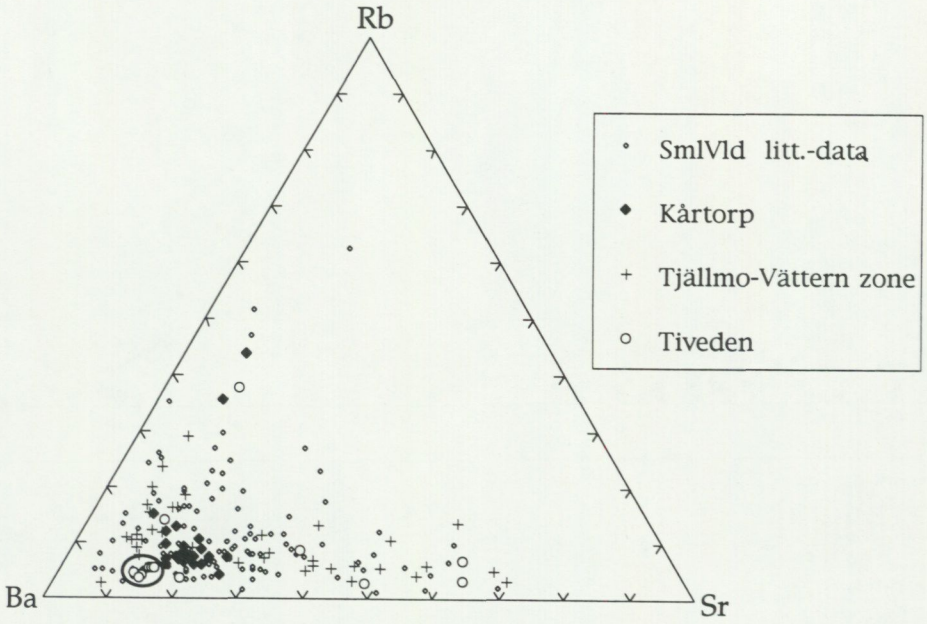

Fig. 16. Rb-Ba-Sr variation diagram for SVB rocks. Altogether 117 analyses from the literature are compiled from Persson et al. (1981, 1985), Persson (1985, 1989), Björk (1985), Ahl (1989), Wikman & Kornfält (1995), and M. Ripa (unpubl. data). Notable is the difference between the Kårtorp hybrids and the Tiveden hybrids (the latter are encircled). The hybrids from the Kårtorp area occupy an area intermediate between the low Sr granitoids and the high Sr basic rocks. The Tiveden hybrids are also intermediate in Sr content, but enriched in Ba. A few literature data are even more Ba enriched, while most intermediate SVB rocks follow a trend similar to that followed by the Kårtorp hybrids.

the trends at 48–50 % SiO_2, which marks an approximate starting point for the straight lines towards the silicic end. For the enclaves/Kårtorp rocks there is a lack of data which inhibits tighter constraints on the basic end. The LILEs Sr, Ba, and Rb display some specific features. In the Sr diagram all the enclaves have an anomalous behaviour, being consistently low, lower than the Kårtorp trend, while some intermediate rocks of the TVZ scatter at high values. The Tiveden intermediate rocks (hybrids) have consistently high Ba contents (with only a few exceptions), while two enclaves fall together with some of the TVZ intermediate rocks at the lowest values, and the Kårtorp rocks occupy the area in between. In the Rb diagram, some of the enclaves plot relatively isolated at significantly higher contents, compared with the Kårtorp trend.

In the total alkali plot (Fig. 15), the silicic rocks generally plot between 7 and 9 % Na_2O+K_2O, while the basic rocks fall below 5 %. The intermediate (hybrid) rocks form a continuous trend between the basic and silicic ends, where the Kårtorp and Tiveden rocks overlap. A few of the enclaves (8812M, 8812L, and 35B1) fall off this trend at higher alkali contents (for the corresponding SiO_2 content). The FeO*/(FeO*+MgO) ratio for the felsic rocks is generally in the range 0.75–0.90 but, in contrast to the rapakivi rocks (cf. Figs. 42 and 59d), never above 0.90. The ultrabasites have the lowest values, below 0.4, while the basic rocks are between 0.45 up to 0.80. The hybrid rocks tend to be slightly lower, compared with the granites, with the bulk of the data between 0.75 and 0.82. The Kårtorp area enclaves also have high values, around 0.8.

In Fig. 16, a Rb-Ba-Sr triangular diagram has been plotted, including also data from the literature. Compared with the rapakivi rocks (cf. Figs. 43 and 62), the SVB-rocks are relatively more Ba-rich. The Kårtorp hybrids fall essentially intermediate between the more granitic and the basic (more Sr-rich) parts, while the Tiveden hybrids (encircled) are comparatively enriched in Ba. Among the literature data even more Ba-rich rocks occur.

4.3.7. REE-patterns

REE-patterns of the rocks are displayed in Fig. 17. The most silicic SVB granites and "normal" Filipstad type granitoids, arbitrarily subdivided at 70 % SiO_2, have very similar patterns. The most silicic group have slightly deeper negative Eu-anomalies ($Sm_N/Eu_N = 2.3–4.6$, compared with 1.3–3.2 for the "normal" Filipstad granites). The Kårtorp hybrids have also been subdivided into two groups according to silica content, but are all extremely coherent with a restricted range in REE-compositions. In general, these patterns are similar to those of the granites, but the absolute amounts of the REEs are higher, the Eu-anomaly slightly less pronounced ($Sm_N/Eu_N = 1.4–2.6$), and the slope of the patterns somewhat less (lower $La_N/Yb_N = 8.9–10.7$, compared with the granites 6.3–23.9). Two samples of low silica granitoids (21 and 1gg), occurring slightly further away from Kårtorp, are anomalous. The Tiveden hybrids have another character. One group of hybrids show slight positive Eu-anomalies ($Sm_N/Eu_N = 0.8–1.1$), while the other group lack anomalies ($Sm_N/Eu_N = 1.1–1.5$). The slopes and amount of REEs for both groups are similar to that of the granites ($La_N/Yb_N = 6.2–13.0$). The absolute abundances are much lower compared with the Kårtorp hybrids (cf. Fig. 15).

As was mentioned previously the basic rocks are generally more or less "evolved". In general they have LREE-enriched patterns, but the amount of enrichment varies considerably (Fig. 17). The more evolved types approach the La_N/Yb_N ratios of the granites and have a small tendency for a negative Eu-anomaly, while the more primitive types are much less enriched ($La_N/Yb_N = 2.8–7.2$), without any indication of Eu-anomalies ($Sm_N/Eu_N = 1.0–1.5$). The ultrabasic rocks have very low abundances of REEs, but show some LREE-enrichment ($La_N/Yb_N = 2.5–10.3$). The dyke rocks display the same general variation as the basic plutonics. Sample 1t has a slight positive Eu-anomaly. The mafic magmatic enclaves are very alike the Kårtorp hybrids, perhaps with slightly deeper Eu-anomalies. One sample (8843B) differs, but compares instead well with the more evolved basic plutonics. Among the miscellaneous TIB rocks (Fig 17) only 8841 deserves special attention. This granitoid (SiO_2 60.6 %) has a pronounced positive Eu-anomaly ($Sm_N/Eu_N = 0.4$), and very high Ba content (2870 ppm). In general, the older early Svecofennian rocks in the area (tonalites to granites) have somewhat lower abundances with minor Eu-anomalies, but some of the most silicic ones have strong negative anomalies. Two samples of a fine-grained grey rock (124/89 and 8857E) dominated by plagioclase and biotite, of which one occurs as an enclave in the Filipstad type granite (8857E), have similar patterns. These patterns are very similar to those of metasediments in the Bothnian basin (cf. Fig. 44c and Claesson & Lundqvist 1995), which makes it probable that also the present rocks are metasediments.

4.4. ISOTOPE GEOLOGY

4.4.1. U-Pb zircon geochronology

A sample from the most basic rock at Kårtorp (sample 8511, Fig. 6), a monzodiorite, was selected for zircon geochronology. The rock was relatively rich in zircons. The crystals were generally very elongated with length:breadth ratios of 5:1 or more. They were brown, yellow to colourless with relatively abundant inclusions, with a small number of good quality clear crystals. Seven groups of clear crystals were handpicked from the size fractions 74 μm and larger, and two of these were air-abraded to less than half their original sizes. U and Pb were extracted using conventional chemical separation techniques (see Appendix 1), and analysed for their isotopic composition (Table 2). The analysed Pb and U blanks were 40 pg and 2.3 ng, respectively. Calculation of the errors and discordia line has been done with the programs PBDAT and ISOPLOT of Ludwig (1993, 1995).

Two fractions (K2 and K3) were not successfully analysed, and thus 5 fractions remained and are plotted on the concordia diagram of Fig. 45a. Three of these are highly discordant with large analytical errors. This includes the two abraded fractions. Fortunately, two fractions are good quality analyses, one of which is almost concordant. This is the size fraction with the 5 largest crystals (>210 μm). A discordia can be fitted through the three highly discordant and the two near concordant analyses, giving an age of 1802±10 Ma (MSWD = 2.6). The lower intercept is close to zero (23±73 Ma). A discordia fitted only through the two best analyses arrives at 1812±14 (MSWD = 0), with a lower intercept at 205±204 Ma. The $^{207}Pb/^{206}Pb$-ages of fractions K1 and K4 are 1810±12 and 1799±3 Ma, respectively. See discussion in chapter 4.5.1.1.

4.4.2. Nd isotopes

Thirty-five samples have been analysed for their Sm and Nd isotopic composition, 30 of these from the SVB plutonic suite and 5 from early Svecofennian rocks (Table 3). Of the SVB samples 7 are from the Kårtorp association (Kt), 8 from the Tiveden area (Tiv), and the rest (15) from the Tjällmo–Vättern zone (TVZ). The samples have been divided into several different groups on geological and geochemical grounds (Table 3), which will also be a basis for the isotopic discussion. Analytical techniques are detailed in Appendix 1. Sample numbers in Table 3 refer to Figs. 3, 4, and 6. SiO_2 and MgO contents have been included in Table 3 to allow comparisons with the geochemical character of the samples.

There is a significant overlap in the measured $^{143}Nd/^{144}Nd$ ratios for the granites and the different hybrid groups. Thus, for example, the granites range between 0.511462 and 0.511754, which includes the ranges of the Kårtorp hybrids (0.511695–0.511738) and the Tiveden hybrids (0.511633–0.511744). Among the three analysed microgranular enclaves one is higher (0.511799), whereas the basic and ultrabasic rocks have higher $^{143}Nd/^{144}Nd$ ratios (0.511868–0.512421), except sample 100/89 (0.511564). Higher $^{143}Nd/^{144}Nd$ in mantle-derived rocks is expected due to the usually depleted or less enriched nature of mantle compared with crustal sources.

The measured $^{147}Sm/^{144}Nd$ ratios are generally below 0.12 for the granites (0.0987–0.1192). The hybrids at Kårtorp fall in the range 0.1158–0.1189, and those in Tiveden 0.1147–0.1232. The microgranular enclaves (MMEs) are similar to the hybrids (0.1186–0.1264), whereas the basics and ultrabasics are generally higher (0.1248–0.1635), except for one sample (100/89) which is low (0.1017). The ultrabasics do not carry a depleted Sm/Nd signature, not even a near chondritic ($^{147}Sm/^{144}Nd_{CHUR}(0) = 0.1967$; Jacobsen & Wasserburg 1980, Faure 1986, DePaolo 1988), nor do the other basic rocks.

The initial ε_{Nd} values have been calculated at 1.80, which is a rough average age of the TIB I intrusive suite, adopted here for the purpose of comparison. An age of 1.84–1.85 Ga might be more appropriate for the Tiveden-TVZ region according to recent U-Pb zircon age determinations (Persson & Wikström 1993, Wikström 1996, see chapter 3). However, the U-Pb age for the Kårtorp monzodiorite

Fig. 17. Chondrite normalized (Taylor & McLennan 1985 after Evensen et al. 1978) REE plots of the SVB (TIB) rocks (and a few early Svecofennian rocks from the same areas) of this study. Sample numbers can be found in Figs. 3, 4, and 6. Discussion in text.

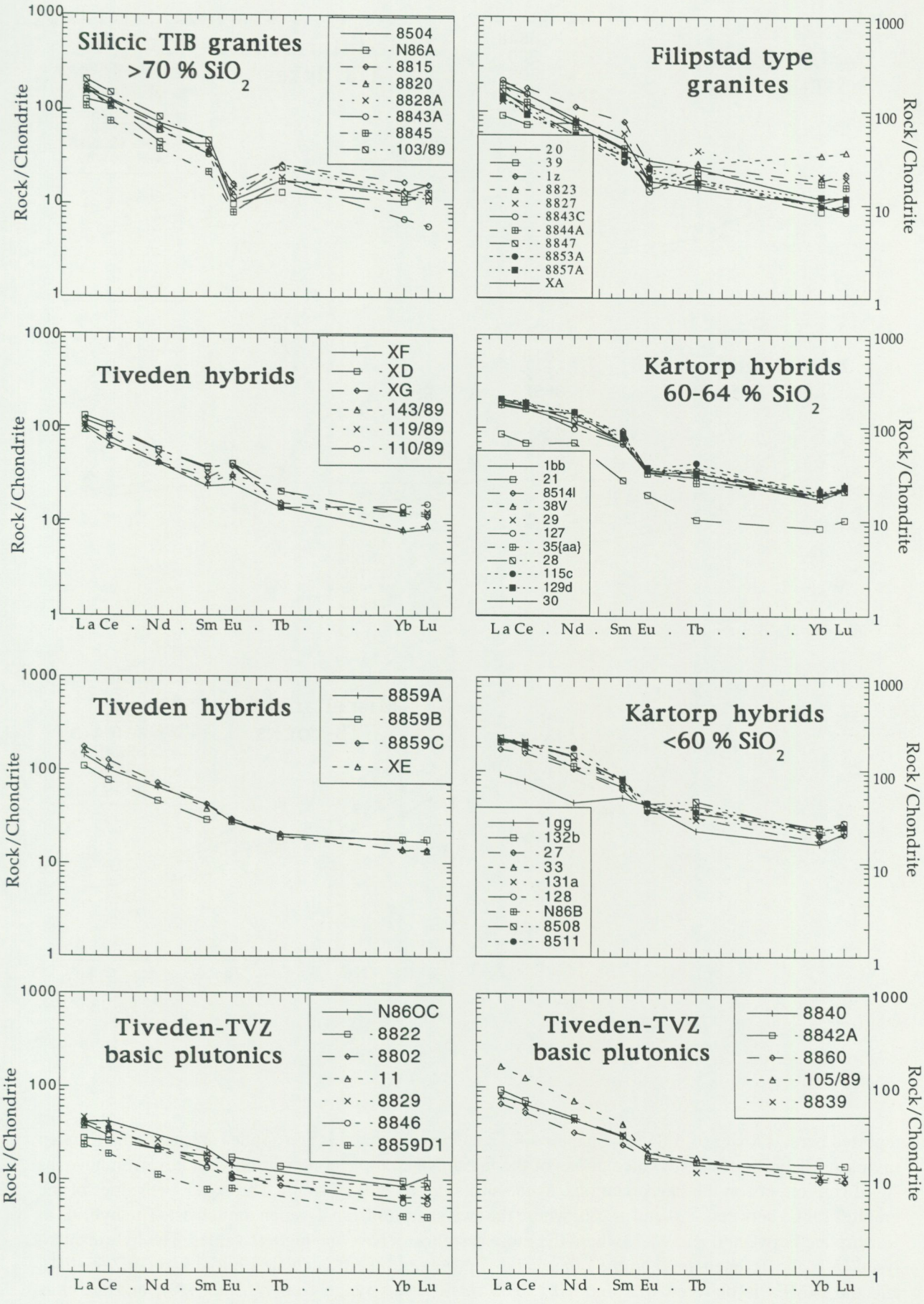
Silicic TIB granites
>70 % SiO2
8504
N86A
8815
8820
8828A
8843A
8845
103/89
Filipstad type
granites
20
39
1z
8823
8827
8843C
8844A
8847
8853A
8857A
XA
Tiveden hybrids
XF
XD
XG
143/89
119/89
110/89
Kårtorp hybrids
60-64 % SiO2
1bb
21
8514l
38V
29
127
35(aa)
28
115c
129d
30
Tiveden hybrids
8859A
8859B
8859C
XE
Kårtorp hybrids
<60 % SiO2
1gg
132b
27
33
131a
128
N86B
8508
8511
Tiveden-TVZ
basic plutonics
N86OC
8822
8802
11
8829
8846
8859D1
Tiveden-TVZ
basic plutonics
8840
8842A
8860
105/89
8839
Rock/Chondrite
1000
100
10
1
La Ce . Nd . Sm Eu . Tb . . . . Yb Lu

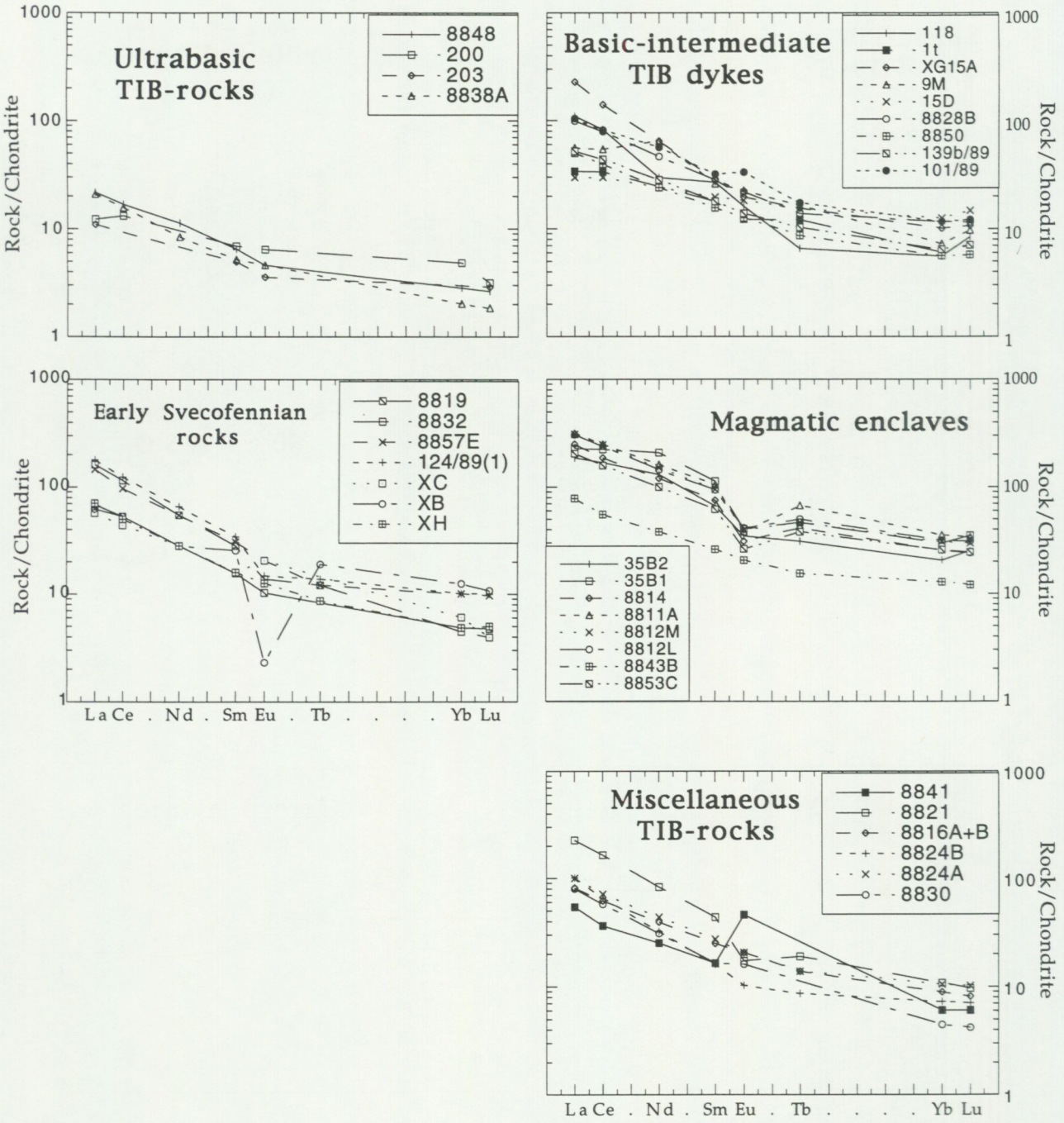

Fig 17, cont.

reported here, is lower (c. 1.81 Ga; chapter 4.4.1.) suggesting that this age applies at least to the Kårtorp samples. The age chosen for calculations of the initial Nd isotopic composition will, however, have insignificant effects on the interpretations, as the shifts in ε_{Nd} will be small. The $\varepsilon_{Nd}(1.80)$ values of the granites range between -1.0 and +0.66, where the two samples from Tiveden are lowest. The hybrids at Kårtorp are between 0 and +1.1, where the most basic rocks have the highest values. The hybrids analysed from the Tiveden area, on the other hand, are lower in their calculated initial ε_{Nd} (-0.7 to -0.4), and the MMEs is between -0.2 and +0.7. The mafic rocks range from -0.3 to +3.4, and are thus chondritic to depleted in character, where gabbro sample 8822 (TVZ) is the most strongly depleted. Notably, the ultrabasics are not generally more depleted than the other mafic rocks.

Table 2
U-Pb zircon results, Kårtorp monzodiorite

Fraction	Weight (µg)	number of crystals	U (ppm)	Pb_{tot} (ppm)	Pb_{com} (ppm)	$^{206}Pb/^{204}Pb$ (1)	rad. Pb atomic % 206-207-208Pb	$^{206}Pb/^{238}U$ (2)	$^{207}Pb/^{235}U$ (2)	$^{207}Pb/^{206}Pb$ (2)	$^{207}Pb/^{206}Pb$ (age)
K1 150-210 µm LP clear	30.0	5	190	68.5	0.98	1386	77.4-8.6-14.0	0.3204±22	4.889±47	0.11066±72	1810±12
K4 100-150 µm LP clear	118.8	20	194	62.8	0.44	3833	78.0-8.6-13.4	0.2907±36	4.408±56	0.10996±20	1799±3
K5 74-100 µm LP clear	94.4	26	216	50.5	1.35	1383	77.5-8.5-14.0	0.2054±41	3.111±67	0.10985±86	1797±14
K6 100-150 µm abraded	19.0	8	194	41.6	1.12	910	78.2-8.6-13.2	0.1895±103	2.884±159	0.11040±90	1806±15
K7 100-150 µm abraded	18.2	10	271	39.3	3.38	338	80.0-8.6-11.4	0.1231±39	1.827±68	0.10763±192	1760±31

LP = long prismatic, SP = short prismatic. Pb_{tot} is total lead, and Pb_{com} common lead. (1) $^{206}Pb/^{204}Pb$ only corrected for mass discrimination.

(2) Ratios corrected for mass discrimination, blank (0.01 ng U and 0.04 ng Pb), and common Pb ($^{206}Pb/^{204}Pb$=15.6, $^{207}Pb/^{204}Pb$=15.3, $^{208}Pb/^{204}Pb$=35.2). Errors are 2 σ.

Table 3. Nd and Sr isotopic data of SVB-rocks (and some Svecofennian).

Sample	Rocktype	SiO_2	MgO	Sm (ppm) (MS)	Nd (ppm) (MS)	$^{147}Sm/^{144}Nd$ (measured)	$^{143}Nd/^{144}Nd$ (measured)	ε_{Nd} (1.80 Ga)	ε_{Nd} (1.89 Ga)	T_{DM} (Ga)	Rb (ppm)	Sr (ppm)	Rb/Sr (XRF)	$^{87}Rb/^{87}Sr$ (XRF+MS)	$^{87}Sr/^{86}Sr$ (measured)	$^{87}Sr/^{86}Sr$ initial (1.80Ga)	ε_{Sr} (1.80)	ε_{Sr} (1.89)
	Granites																	
39	Coarse porphyritic granite (Kt)	66.83	1.03	7.045	35,72	0.1192	0.511754 (20)	0.66	-	2.08	140	180	0.79	2.31	0.762241 (12)	0.7024	1	-
8843C	Coarse porphyritic granite (TVZ)	69.1	0.86	8.843	54,13	0.0987	0.511462 (28)	-0.30	-	2.10	193	205	1.137	3.31	0.791084 (8)	0.7054	43	-
8844A	Coarse porphyritic granite (TVZ)	66.6	1.20	9.156	51,05	0.1084	0.511615 (21)	0.44	-	2.07	196	178	1.4	4.1	0.802076 (11)	0.6959	-92	-
8853A	Coarse porphyritic granite (TVZ)	66.6	0.82	7.333	40,24	0.1101	0.511609 (24)	-0.07	-	2.11	128	163	0.818	2.380	0.767609 (8)	0.7060	52	-
8823	Coarse porphyritic granite (TVZ)	68.1	0.76	7.831	40,59	0.1166	0.511659 (18)	-0.60	-	2.17	245	175	1.625	4.758	0.829671 (13)	0.7065	59	-
8815	Coarse porph. fels. granite (TVZ)	71.5	0.43	9.420	51,13	0.1113	0.511595 (4)	-0.62	-	2.16	204	78	2.97	8.8	0.926800 (16)	0.6990	-48	-
8845	Coarse porph. fels. granite (TVZ)	73.0	0.50	4.882	25,80	0.1144	0.511646 (9)	-0.34	-	2.15	189	167	1.525	4.459	0.813057 (16)	0.6976	-68	-
8504	Even-grained felsic granite (Kt)	73.21	0.43	8.165	45,43	0.1086	0.511627 (30)	0.63	-	2.05	270	90	3.21	9.51	0.940077 (17)	0.6939	-121	-
257/93	Coarse porphyritic granite (Tiv)	62.4	0.97	7.022	38.42	0.1105	0.511565 (3)	-1.02	-	2.19	140		0.445	1.292	0.737806 (18)	0.7044	28	-
AW9325	Coarse porphyritic granite (Tiv)	63.4	1.14	6.499	35.29	0.1113	0.511586 (4)	-0.80	-	2.17	124		0.4695	1.363	0.742955 (12)	0.7077	76	-
	Hybrids and mafics at Kårtorp																	
8508	Very dark hybrid (Kt)	56.3	2.58	18.28	94.85	0.1165	0.511736 (30)	0.93	-	2.05	120	420	0.2325	0.673	0.720439 (8)	0.7030	9	-
1bb	Light hybrid (Kt)	63.3	1.55	14.31	72.74	0.1189	0.511715 (12)	-0.03	-	2.14	120	270	0.421	1.22	0.734824 (9)	0.7032	13	-
129d	Medium-dark hybrid (Kt)	61.1	2.01	15.86	82.38	0.1164	0.511695 (28)	0.15	-	2.11	120	310	0.3421	0.992	0.727855 (13)	0.7022	-3	-
132b	Dark hybrid (Kt)	58.8	2.29	17.30	89.90	0.1163	0.511729 (11)	0.84	-	2.06	112	393	0.2951	0.8554	0.725691 (8)	0.7035	17	-
8511	Quartz monzodiorite (Kt)	54.08	2.90	17.52	91.46	0.1158	0.511738 (20)	1.14	-	2.03	100	510	0.1525	0.4416	0.714027 (8)	0.7026	3	-
	Mafics																	
11	Coarse hbl-gabbro (TVZ)	46.2	5.55	3.719	16.86	0.1333	0.511926 (13)	0.76	-	2.12	60	380	0.0991	0.287	0.710596 (17)	0.7032	11	-
9M	Quartz diorite dyke (TVZ)	50.5	3.93	5.883	27.61	0.1248	0.511885 (9)	1.93	-	1.98	50	720	0.0474	0.1371	0.706491 (14)	0.7029	8	-
8822	Fine-grained basite (TVZ)	47.0	6.88	4.596	16.99	0.1635	0.512421 (10)	3.45	-	1.88	55	260	0.185	0.536	0.713547 (22)	0.6997	-38	-
8840	Basite, slightly hybr. (TVZ)	51.6	5.11	7.137	32.49	0.1328	0.511868 (19)	-0.26	-	2.22	86	391	0.180	0.523	0.716681 (12)	0.7031	11	-
8859 D1	Basite (Tiv)	47.2	5.13	1.991	9.142	0.1317	0.511934 (8)	1.29	-	2.06	63	590	0.0709	0.205	0.708083 (18)	0.7028	6	-
100/89	Gabbro (Tiv)	49.7	7.08	3.798	22.61	0.1014	0.511564 (5)	1.07	-	2.01	83	210	0.0384	0.1111	0.705757 (9)	0.7029	7	-
	Ultramafics																	
203	Lherzolite (TVZ)	38.3	28.2	1.154	5.323	0.1310	0.511973 (17)	2.21	-	1.97	30	70	0.171	0.50	0.714356 (15)	0.7014	-13	-
200	Lherzolite (TVZ)	43.4	19.3	1.823	7.996	0.1378	0.511999 (16)	1.15	-	2.1	40	310	0.0393	0.1138	0.705837 (10)	0.7029	8	-
	Hybrids																	
119	Very dark hybrid (Tiv)	57.5	2.39	8.302	41.04	0.1223	0.511739 (8)	-0.35	-	2.18	97	307	0.3146	0.9118	0.727386 (11)	0.7038	20	-
8859B	Dark hybrid (Tiv)	56.8	2.44	7.157	35.11	0.1232	0.511744 (16)	-0.46	-	2.19	91	319	0.355	1.028	0.726011 (22)	0.6994	-42	-
XE	Light hybrid (Tiv)	59	2.08	9.592	50.53	0.1147	0.511633 (18)	-0.67	-	2.17	108	326	0.3706	1.075	0.732239 (15)	0.7044	29	-
143	Medium-dark hybrid (Tiv)	59.6	2.10	6.460	32.36	0.1207	0.511709 (23)	-0.57	-	2.19	95	314	0.3542	1.027	0.729902 (7)	0.7033	14	-
	Microgranular enclaves																	
8811A	Dark, xenocrystic enclave (TVZ)	47.6	4.70	33.64	160.8	0.1264	0.511799 (12)	-0.13	-	2.17	97	136	0.62	1.79	0.747503 (10)	0.7012	-17	-
8814	Hybrid enclave (TVZ)	58.4	2.52	20.6	105	0.1186	0.511750 (18)	0.72	-	2.07	83	235	0.368	1.068	0.731593 (10)	0.7039	23	-
8853C	Coarse hybrid enclave (TVZ)	60.9	1.25	15.54	76.89	0.1222	0.511745 (23)	-0.21	-	2.16	182	159	1.120	3.265	0.789167 (19)	0.7046	32	-
	Svecofennian rocks																	
8857E	Fine-grained encl., Svecof. (TVZ)	56.4	2.07	7.142	39.01	0.1107	0.511394 (17)	-4.42	-3.42	2.45	204	200	1.102	3.45	0.794625 (9)	0.7053	42	-21
8819	Tonalite (Svecof.) (TVZ)	67.9	1.37	3.590	18.43	0.1177	0.511687 (14)	-0.30	0.62	2.15	93	381	0.318	0.922	0.727635 (27)	0.7038	20	4
8832	Adamellite (Svecof.) (TVZ)	69.3	7.24	7.237	43.93	0.0996	0.511415 (39)	-1.43	-0.3	2.18	150	218	0.800	2.33	0.764410 (15)	0.7041	25	-17
124/89	Paragneiss (Svecof.) (Tiv)	60.8	8.97	8.971	51.44	0.1054	0.511394 (11)	-3.19	-2.13	2.33	15	204	0.0350	0.101	0.711024 (24)	0.7084	86	86
142:1/89	Tonalite (Tiv)	67.5	1.29	3.295	17.95	0.1110	0.511612 (5)	-0.22	0.78	2.13	75	140	0.222	0.643	0.720638 (32)	0.7040	23	13

TVZ=The Tjällmo–Vättern zone; Kt=Kårtorp; Tiv=Tiveden. SiO_2, MgO, Rb, and Sr extracted from Appendix 2a, except for samples 257/93, AW9325, 100/89, 142:1/89 (A. Wikström unpubl. data).
$^{143}Nd/^{144}Nd$ is corrected according to average La Jolla standard measurements at the time of analysis (see Appendix 1). Measured $^{87}Sr/^{86}Sr$ ratios corrected according to average standard (SRM987) measurements at the time of analysis (see Appendix 1).
Mass spectrometry data, errors: Sm. 2 std error of mean on av. 0.021 %; Nd. 2 std error of mean on av. 0.045 %; $^{143}Nd/^{144}Nd$. 2 std error of mean on av. 0.000018 (0.0036%). Number in parenthesis refer to within-run 2 std. error of the mean.
$^{147}Sm/^{144}Nd$: relative std dev. estimated to be better than 0.5%. Errors in Nd due to errors in $^{143}Nd/^{144}Nd$ measurements (2 std errors of mean) are on average ±0.4 and max. ±0.6. T_{DM}-values according to DePaolo (1988).
Rb/Sr measured by XRF. Normally 4 measurements on 2 briquettes. Average relative "spread" 0.012 %. Significant number of digits in relation to "spread" of data (see Appendix 1).
Mass spectrometry data, errors: $^{87}Sr/^{86}Sr$. 2 std error of mean on av. 0.000013 (=0.0018%); ratios normalized to $^{86}Sr/^{88}Sr$=0.1194. Errors in ε_{Sr} due to errors in $^{87}Sr/^{86}Sr$ measurements (2 std errors of mean) are on average ±0.2 and max. ±0.4.

The Nd and Sm contents of the granites range between 25.8 and 54.1 ppm and 6.5 and 9.4 ppm, respectively, which is generally significantly lower than the rapakivi granites (cf. Tables 13 and 22). The Kårtorp hybrids have high contents of the REEs, markedly higher than in the granites, (see geochemistry, chapter 4.3.7.); Nd is between 72.7 and 94.8 ppm and Sm between 14.3 and 18.3 ppm. The hybrids from Tiveden are lower, in the range of the granites (Nd: 32.4–50.5 and Sm: 6.5–9.6 ppm). The MMEs are extremely high in these elements, up to 160.8 ppm Nd and 33.6 ppm Sm. The mafic rocks range between 9.1 and 32.5 ppm Nd, and between 2.0 and 7.1 ppm Sm, which is normal compared with mafic rocks in general (cf. e.g. Faure 1986, p. 201). The ultrabasics have, as expected, the lowest REE contents: Nd 5.3–8.0 and Sm 1.2–1.8 ppm.

No WR-Sm-Nd isochrons could be calculated from the analytical data. Errorchrons calculated for the silicic and basic suites give "ages" of 2017±369 Ma (MSWD = 1.3) and 2245±364 Ma (MSWD = 24), respectively. Similarly, errorchrons calculated for the hybrids and all analysed rocks give 1113±310 Ma (MSWD = 1.2) and 2275±122 Ma (MSWD = 6.6). WR isochron calculations were performed with the program ISOCHRON (Provost 1990). Discussion in section 4.5.1.1.

4.4.3. Sr isotopes

The 35 samples investigated for Nd isotopic composition have also been analysed for Sr isotopes (Table 3). The measured $^{87}Rb/^{86}Sr$ values for the granites range between 2.3 and 9.5. The range is more restricted for the hybrid rocks (Tiveden and Kårtorp): 0.67–1.22. The MMEs range from 1.1 to 3.3, whereas the basic and ultrabasic rocks have very low values from 0.11 to 0.54. The intermediate rocks thus have intermediate $^{87}Rb/^{86}Sr$ values, and the Rb/Sr ratio is, as expected, low in the mantle-derived basic rocks.

Correspondingly, the granites have the highest measured $^{87}Sr/^{86}Sr$ ratios, since this is dependent on the Rb/Sr ratio and the time elapsed since crystallization, if the samples evolved in an undistrubed, closed system. Thus, samples with the highest $^{87}Rb/^{86}Sr$ ratios also show the highest $^{87}Sr/^{86}Sr$ values, ranging from 0.7378 to 0.9401. Also here the hybrids are intermediate, with values ranging from 0.7140 to 0.7348. Some of the MMEs have relatively high values, up to 0.7892, whereas the mafics and ultrabasics generally have low values: 0.7058 to 0.7167.

When calculating the $^{87}Sr/^{86}Sr$ ratios back to their initials (assumed at 1.80 Ga), the values for some rocks are appreciably lower than the bulk earth ("uniform reservoir" = UR) value (0.7024 at 1.80 Ga; cf. Faure 1986). These also give negative values of the initial ε_{Sr} parameter (Table 3). This is most common among the granites, but occurs also in the other groups. An approximate value of the depleted mantle at 1.80 Ga is 0.7012 (ε_{Sr} = -17). This value is obtained by assuming a straight line evolution between the BABI (basaltic achondrite best initial; Papanastassiou & Wasserburg 1969, Faure 1986) and an average of the most depleted modern MORBs (0.7025; cf. Faure 1986, DePaolo 1988), and represents a minimum value of DM at this time. Values lower than this are not considered realistic, but are the result of disturbance of the Rb-Sr system at some time significantly after crystallization, whereby the Rb/Sr ratio has increased or the rock has lost radiogenic Sr (cf. Romer et al. 1992). Hence, it is generally those samples with the highest $^{87}Rb/^{86}Sr$ in each group that have the lowest apparent initial ratios.

Low initial Sr values are found for the basic and ultrabasic rocks ($\varepsilon_{Sr}(1.80)$= -13 to 11, omitting 8822). The Kårtorp hybrids also have low $\varepsilon_{Sr}(1.80)$ from -3 to 17, whereas the Tiveden hybrids are slightly higher, 14 to 29 (excl. 8859B), similar to to the MMEs (23-32), except for 8811A at -17. The granites are somewhat more evolved (higher Rb/Sr and initial Sr ratio) with $\varepsilon_{Sr}(1.80)$ ranging from 1 to 76, excluding the negative ones. Although the overlaps between the rock groups are substantial, some general differences are evident. Discussion in section 4.5.1.3.

A test of the possible use of the WR-Sr data for age determination is seen in Fig. 18. An errorchron calculated from the silicic rocks gives an "age" as low as 1641±47 Ma (MSWD=281), whereas the basic rocks give 1674±127 Ma (MSWD = 36). Including all samples in the errorchron calculation results in the "age" 1781±25 Ma (MSWD = 232), whereas only the hybrids give 1876±52 Ma (MSWD=96). Discussion in section 4.5.1.1.

4.5. DISCUSSION

4.5.1. Isotopes

4.5.1.1. Geochronology

Two different U-Pb discordias have been calculated and plotted in Fig. 45a, giving ages that differ by 10 Ma. Since the discordia through the three highly discordant points extrapolates towards the origin and includes the abraded fractions, laboratory problems are suspected. U spike was added to the sample before aliquoting and Pb spiking. If Pb was lost during, e.g. aliquoting of the dissolved fractions due to inhomogeneity of the dissolutions so that the spiked fraction contained less Pb than indicated by the weights of the liquids, this would move the analyses of these fractions towards the origin of the diagram, and thus away from an original discordia, presumably with a higher lower intercept. The 1812±14 Ma age calculated from the two best analytical points is therefore the preferred age, although the difference is within errors. The $^{207}Pb/^{206}Pb$ age (1810±12 Ma) of the almost concordant fraction is also a good indication of the age of the rock.

No reliable data on the intrusion ages of the rocks could be obtained from the WR-Sr system (Fig. 18). Due to the very high MSWD-values the scatter cannot be ascribed to analytical uncertainty only, thus some geological "error" is inherent in the sample suite. There is no actual reason why these samples, which are scattered over a very large area (c. 150 km^2), should have identical initial $^{87}Sr/^{86}Sr$ values. On the contrary, heterogeneities in the source rocks would be transferred to the magmas and are not likely to be homogenized over wide areas, unless large-scale stirring can be inferred (Miller et al. 1988). As discussed by Romer (1994) such "isochrons" instead represent mixing lines of samples with variable initial ratios, and the obtained "age" may lack geochronological significance. The "ages" obtained from the errorchrons of the silicic and basic TIB-suites, 1.64 and 1.67 Ga respectively, suggest that the rocks (in each group) with the highest Rb/Sr ratios initially had somewhat lower $^{87}Sr/^{86}Sr$ ratios, since these ages are ca 150–200 Ma lower than the determined U-Pb zircon ages of correspond-

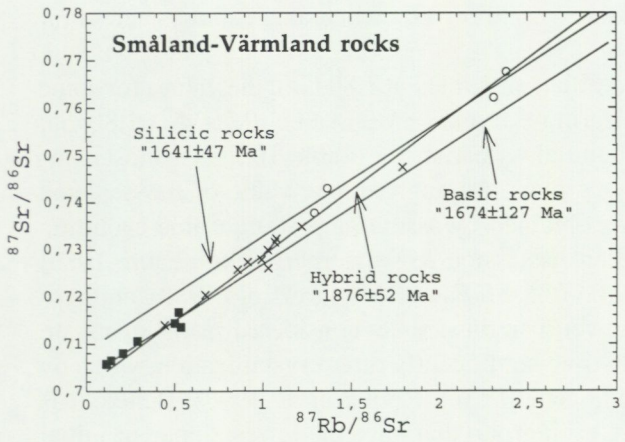

Fig. 18

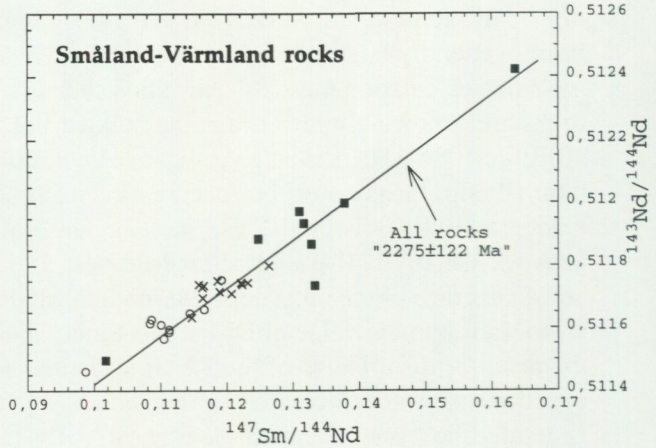

Fig. 19

Fig. 18. $^{87}Rb/^{86}Sr$-$^{87}Sr/^{86}Sr$ diagram for the SVB whole rock samples of this study. No isochrons could be calculated from the material, due to the large scatter. Errorchrons have been calculated for the granitoid (silicic) rocks (samples 39-AW9325; Table 3), the basic-ultrabasic (samples 11-203) rocks, and the hybrid (Kårtorp, Tiveden and enclaves) rocks. All of these are probably poorly constrained rotated mixing lines, and lack geological age significance. It is interesting to note, however, that the line fitted to the lumped together hybrids cross the other two lines at a relatively low Rb/Sr ratio for the granitoids and a relatively high ratio for the basic rocks. Discussion in the text.

Fig. 19. $^{147}Sm/^{144}Nd$-$^{143}Nd/^{144}Nd$ diagram for the SVB whole rock samples of this study. Also in this case (cf. Fig. 18) the data do not give any information pertaining to the age of the rocks. An errorchron calculated for the whole data set gives an "age" of 2275±122 Ma (MSWD=6.6). Similarly, reference lines calculated for the granitic and basic rocks indicate "ages" over 2 Ga, i.e. c. 200 Ma more than the true crystallization age. These results indicate that the data was initially correlated heterogeneously (Romer 1994), whereby rocks with higher Sm/Nd ratios had higher $^{143}Nd/^{144}Nd$ initials. Further discussion in the text.

ing rocks in the area (this study, Persson & Wikström 1993, Wikström 1996). Thus, the sample suite may be termed 'correlated heterogeneous' in the terminology of Romer (1994), i.e there is a negative correlation between $^{87}Rb/^{86}Sr$ and initial $^{87}Sr/^{86}Sr$. Alternatively, later disturbance of the Rb-Sr system in the area, e.g. by hydrothermal or late magmatic fluids may have been operative. In such a case, the redistribution affected the rocks inhomogeneously, such that the rocks gained Rb or lost radiogenic ^{87}Sr. Thus, rocks with higher Rb/Sr ratios (and thus higher amounts of radiogenic ^{87}Sr) should have been affected consistently more, to lower the apparent crystallization age. This process requires pervasive large-scale redistribution of probably mainly Rb, which may be possible in a postmagmatic fluid regime (e.g. Shirey 1991). Even if this is the cause the homogenization was only partial, as seen from the large scatter in the material, and may be superimposed on a heterogeneous primary magmatic isotopic distribution, and most probably does not represent any meaningful geologic age. These results are in accordance with earlier studies where WR-Rb-Sr-ages generally were 150–200 Ma younger than U-Pb zircon ages from the Svecofennian (e.g. Romer et al. 1992, Romer 1994, and ref. therein).

An errorchron calculated from the hybrid rocks gives an "age estimate" of 1876 Ma, i.e. about 200 Ma older than the endmember rock suites, and this is a mixing line without doubt as shown in the geochemistry section below (chapter 4.5.2.4). Thus, it seems that rocks in this study can be divided into at least three subsuites of rocks forming mixing lines: Two that have formed by differing magmatic evolution in different parts of the TIB endmembers, and one that has formed by mixing of these endmembers. The mixing line for the hybrids runs between a silicic endmember at $^{87}Rb/^{86}Sr$ c. 2.0 and a basic endmember at $^{87}Rb/^{86}Sr$ c. 0.4. In the light of this discussion, the seemingly relatively good (1781±25 Ma) errorchron calculated for the whole data set is no more than a superposition of at least three other mixing lines, which happens to fall comparatively close to the actual age of the rocks. Note that the MSWD-value is very high (232). But even if the MSWD is low this does not necessarily support the idea that the calculated line is an isochron, since solely the increasing of the age of the system has the effect of lowering the calculated MSWD, and thus tends to mask the initial heterogeneities (Romer 1994).

Neither could any reliable intrusion ages be extracted from the Sm-Nd WR-system. Instead the "ages" calculated from errorchrons fitted to the data are several 100 Ma older than intrusion ages (Fig. 19) obtained from U-Pb zircon data (Persson & Wikström 1993, Wikström 1996, this study). The reason for this is the varying initial $^{143}Nd/^{144}Nd$ ratios where rocks with higher Sm/Nd ratios also generally show higher $^{143}Nd/^{144}Nd$ in both the silicic and basic suites. The reason for this is not clear and may be typical for this specific sample suite only, and not generally applicable, especially since the errors are large. Later disturbance of the Sm-Nd system is less likely, compared with the Rb-Sr system. The "age" calculation for the basic suite strongly depends on one sample (8822) with a much higher Sm/Nd ratio than the others, and thus influences the calculation proportionally more. Thus, no isotopic homogenization in the plutonic magmas over large areas is observed for the Sm-Nd system. Furthermore the basic rocks both have higher Sm/Nd and initial $^{143}Nd/^{144}Nd$ ratios compared with the silicic rocks, resulting in the high apparent "age" calculated for all samples. The gentle slope in the distribution of the hybrid rocks in Fig. 19 gives a much lower "age". The reason for this may be sought in the specific geochemistries in the endmembers for specific hybrids (chapter 4.5.2.4 below).

The above discussion regarding the Rb-Sr and Sm-Nd WR isotopic systems clearly shows that regionally sampled igneous suites only result in a number of crude mixing lines of possibly various origin, where it is only by chance that the calculated ages are close to the actual intrusion ages (e.g. relatively homogeneous initial ratios in the suite, and no appreciable later disturbance). Even in more restricted areas with strictly defined sampling, variations in the initial ratios cannot be ruled out (cf. the Rödö example, chapter 6.5.3.1.). This topic has been elaborated in greater detail by, e.g. Wendt (1993) and Romer (1994).

4.5.1.2. Nd isotopic interpretation

The time-integrated Nd isotopic evolution of early Svecofennian metaigneous rocks in Bergslagen totally encompasses the $\varepsilon_{Nd}(1.80)$ values for the TIB granites measured in this and previous studies (Fig. 20). This fact, and the dominantly I-type geochemical characteristics of the TIB rocks, is compatible with a derivation from such early Svecofennian metaigneous crustal sources in Bergslagen.

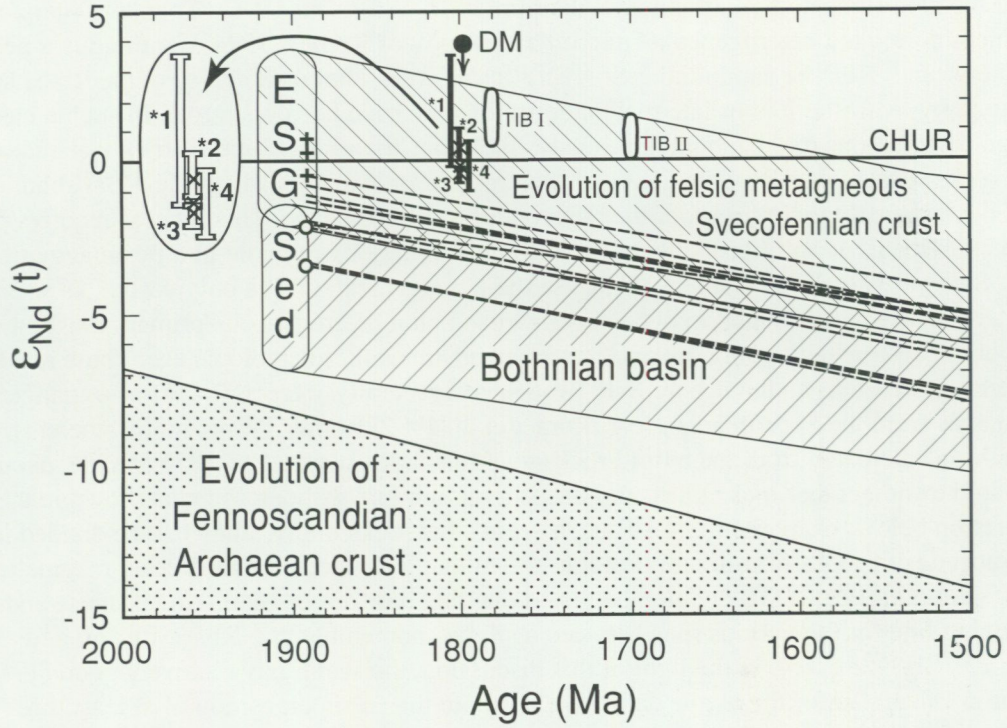

Fig. 20. ε_{Nd} vs. time diagram. The rocks of this study have been plotted together with other relevant data. DM is the depleted mantle (+3.9 at 1.80 Ga; DePaolo 1981). ESG is early Svecofennian metaigneous rocks (Wilson et al. 1985, 1987, Patchett & Kouvo 1986, Patchett et al. 1987, Huhma 1986, Valbracht 1991, Welin et al. 1993, Claesson & Lundqvist 1995). Sed is metasediments of the Bothnian basin (Miller et al. 1986, Claesson 1987, Patchett et al. 1987, Welin et al. 1993, Claesson & Lundqvist 1995, this study). TIB I and II denote previous data from the Transscandinavian igneous belt (Wilson et al. 1985, Patchett et al. 1987). Evolutionary lines (broken) are for metasedimentary rocks from the Bergslagen province (Miller et al. 1986, Patchett et al. 1987, Valbracht 1991, and this study (with circles at 1.89 Ga)). SVB rocks of this study have been plotted as lines showing the range in ε_{Nd} at c. 1.80 Ga. *1) is basic-ultrabasic rocks, *2) is the Kårtorp hybrids, *3) is the Tiveden hybrids, *4) is the granitoids, and inclined crosses the mafic-hybrid magmatic enclaves. Early Svecofennian granitoids measured in this study are marked with crosses at 1.89 Ga. Discussion in the text.

Early Svecofennian metasedimentary rocks from the Bergslagen area have partly somewhat less radiogenic compositions (Miller et al. 1986, Patchett et al. 1987, Valbracht 1991, Kumpulainen et al. 1996, this study), with lower initial ε_{Nd} values, compared with the metaigneous rocks (Fig. 20). There is, however, also a considerable overlap. Two samples of this study are most probably of early Svecofennian metasedimentary origin, 124/89 and 8857E. The latter is a xenolithic enclave occurring in the Filipstad granite (cf. Fig. 2), while 124/89 is a supracrustal plagioclase-biotite rock from central Tiveden (Fig. 4). The $\varepsilon_{Nd}(1.80)$ of 8857E is much lower compared with the surrounding SVB-granites (-4.2 vs. -1.0 to +0.7). It is also among the lowest of the Svecofennian metasediments measured in Bergslagen so far (Fig. 20). This suggests a significant Archaean input to the sediments represented by this small enclave. Archaean contributions to the early Svecofennian sediments in this southern Svecofennian province, have previously been documented by Claesson et al. (1993) and Kumpulainen et al. (1996). The former authors found several different generations of detrital zircons, at about 2.0–1.9, 2.95–2.6, and 3.3–3.1 Ga, and speculated about the possible provenance areas for this material. The samples measured here, together with previous Nd data (Patchett et al. 1987, Miller et al. 1986, Valbracht 1991, Kumpulainen et al. 1996), suggest that the Archaean influence in the early Svecofennian metasedimentary sequence in Bergslagen is relatively widespread. Compared with the Bothnian basin, however, the Archaean contribution to early Svecofennian sedimentation appears to be lower in Bergslagen (cf. Fig. 20). The TIB-granites do not show any sign of an Archaean component in the magmas, and the Nd isotopic data are consistent with a generation solely from early Svecofennian metaigneous sources in the lower crust. The lower crustal regions tapped by the SVB granitoids in this area thus seem to lack Archaean components (cf. Patchett et al. 1987). This contrasts with the case in central Sweden, where the rapakivi rocks contain a substantial Archaean component (cf. chapters 6.5.3.2. and 7.5.1.2.). The early Svecofennian metagranitoid samples measured in this study lie in the range of pre-

viously obtained data for this group (Fig. 20; Patchett et al. 1987, Valbracht 1991, Huhma 1986, Patchett & Kouvo 1986, Wilson et al. 1985, 1987, Welin et al. 1993, Claesson & Lundqvist 1995, Billström & Weihed 1996).

The sampled basic and ultrabasic SVB rocks have very variable Nd isotopic signatures, from depleted ($\varepsilon_{Nd}(1.80)$= +3.4) to near chondritic (-0.3). A concentration on mildly depleted compositions (0 to +1.5) can, however, be detected. This compositional range can be accomplished by a derivation from a depleted (+3.9) mantle source (DePaolo 1981) supplemented by addition of varying proportions of crustal material. The sample with the lowest ε_{Nd}, (8840), also shows field and petrographic evidence of mixing with the TIB granite magmas.

The lherzolites, which are probably pieces of the uppermost mantle from which the basic suite was generated, are not strongly depleted ($\varepsilon_{Nd}(1.80)$= +1.1 and +2.2). If these represent the mantle source of the basic magmas (see chapter 4.5.2.3.), only very little assimilation is needed to achieve the observed variations in initial Nd composition. One sample (8822) is, however, more depleted than the lherzolites and must consequently have its origin in a somewhat more depleted part of the mantle. Thus, the mantle source seems in general to be mildly depleted. However, the lherzolites contain abundant phlogopite and have slightly LREE enriched REE-patterns (cf. Fig. 17) with very low $^{147}Sm/^{144}Nd$ ratios (0.13–0.14) compared with CHUR (0.1936). They are, thus, geochemically enriched, but mildly depleted with respect to the Nd isotopes. This may be due to an enrichment episode shortly prior to or in conjunction with the generation of the basic SVB magmatism of a mantle slightly depleted in a previous melting event (early Svecofennian?) (cf. e.g. Matielli et al. 1996, Wiechert et al. 1997) , whereby the initial premetasomatic Nd isotopic composition is at least partly preserved (cf. Menzies & Hawkesworth 1987).

Three groups of hybrid rocks have been separated: i) hybrids in the Kårtorp association, ii) hybrids in Tiveden, and iii) mafic/hybrid microgranular enclaves. These are geochemically different with respect to Sm and Nd contents (Fig. 15; Nd is not shown but behaves almost identically to Ce and Sm). The hybrids at Kårtorp and those in Tiveden follow distinctly different trends. At Kårtorp the Sm and Nd contents increase substantially with decreasing SiO_2, i.e. the mafic rocks have higher abundances of these elements, whereas in Tiveden a slight decrease is noted towards the basic rocks. This means that the mafic endmember is radically different with respect to these elements in these cases. The Kårtorp basic endmember should thus be much more enriched in character compared with that in Tiveden (see geochemistry section, chapter 4.5.2.4.). The most mafic rock exposed at Kårtorp (e.g. sample 8511) is a monzodiorite which is already somewhat hybridized, so the actual endmember is not at hand. The two trends converge at increasing silica somewhere around 70 % SiO_2. The three sampled enclaves follow the Kårtorp trend, but the most mafic one is extremely enriched in Sm and Nd (33.6 and 160.8 ppm). This sample which occupies a position in the extension of the Kårtorp mixing trend (Fig. 15), can be inferred to approximately represent a mafic endmember for the Kårtorp suite.

With regard to the initial Nd isotopes, the rocks of this study are all relatively close in composition with substantial overlaps (Table 3, Fig. 20), which render the interpretations more difficult, partly because of the average estimated error in the calculated ε_{Nd} values (±0.5 ε-units). Some general trends may, however, be detected. The initial ε_{Nd} values for granites from the different areas vary in such a way that the lowest are found in Tiveden (c. -1.0), and the highest in the Kårtorp area (+0.6), whereas granites of the TVZ spread in between. There, thus, seems to be a slight but still detectable geographical variation of initial values of the silicic endmember for the hybrids. No geographical control on the variation in initial ε_{Nd} can be detected for the basic rocks. Since the endmembers are not isotopically distinctly defined, no unique mixing trend can be advocated for the whole area. In the $^{143}Nd/^{144}Nd$–$^{147}Sm/^{144}Nd$ diagram (Fig. 19) the intermediate compositional nature of the hybrids is confirmed also with respect to the Nd isotopes.

In Fig. 21a, $\varepsilon_{Nd}(1.80)$ have been plotted against SiO_2 as an example of the relations between chemical and isotopic parameters in the sampled SVB-suite. The distribution of the data is roughly consistent with mixing between the mantle-derived magmas and the crustal granitic melts with the hybrids intermediate along two different mixing trajectories: One at generally higher ε_{Nd} values corresponding to the Kårtorp rocks, and one at lower ε_{Nd} corresponding to the Tiveden rocks. The nature of the silicic endmembers thus appears to be slightly different: higher $\varepsilon_{Nd}(1.80)$ in Kårtorp compared with Tiveden, while SVB granitoids from TVZ scatter in between. The basic endmember is isotopically less well-defined, but appears to lie between ε_{Nd} (1.80) +2 and +4 (DM). Perhaps more or less depleted

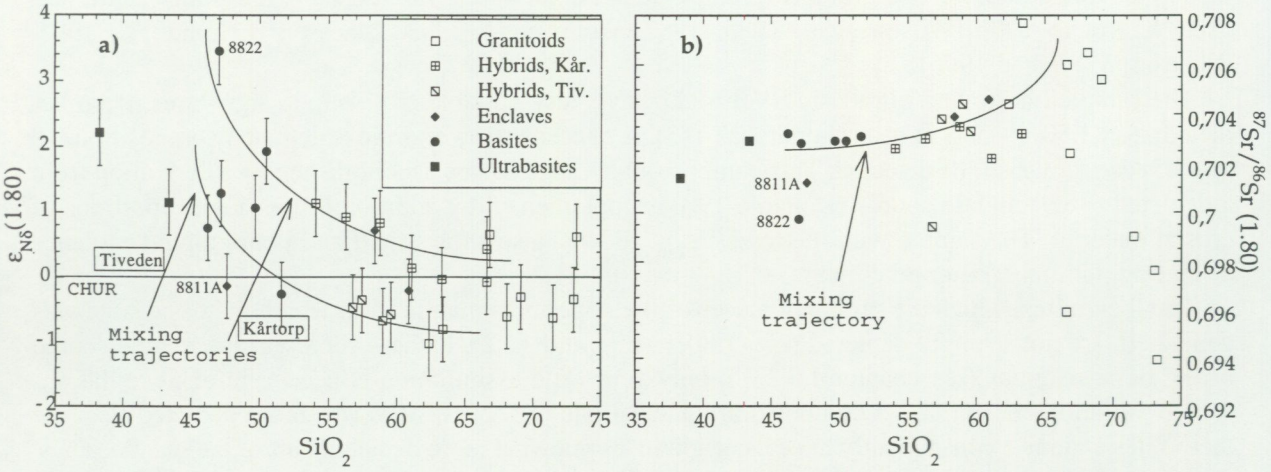

Fig. 21. a) Initial ε_{Nd} vs. silica for the SVB rocks of this study. Two separate mixing curves are discerned for the Kårtorp and Tiveden hybridization, respectively. b) Initial $^{87}Sr/^{86}Sr$ vs. silica diagram for the same rocks as in a). In many rocks the Rb-Sr system has been altered at some time after crystallization, which has shifted the initial compositions to lower (non-primary) values. Nevertheless, the majority of samples roughly follow a mixing trajectory also for the Sr isotopes, where the hybrids plot intermediate. Essentially all rocks below this mixing curve have suffered alteration of the primary igneous Rb-Sr system. Further discussion in the text.

mantle may be involved in the different basic magmas, as is indicated by relatively low ε_{Nd} values in the lherzolites (+1 to +2), while one gabbro is close to the depleted mantle (+3.45).

4.5.1.3. Sr isotopic interpretation

Although the Rb-Sr system has been disturbed after crystallization in many of the analysed rocks, some differences between the groups are still evident. Most of the rocks with negative initial ε_{Sr} values can be assumed to have an altered Sr-isotopic composition compared with that of primary crystallization (increased Rb/Sr ratio or loss of radiogenic ^{87}Sr), as well as a few others (Figs. 21b, 22). Fig. 21b displays initial Sr against SiO_2. Here the two separate trends for Kårtorp and Tiveden are not evident. An approximate mixing trajectory has been sketched between the endmembers, with the hybrid rocks occupying an intermediate position. Essentially all rocks below this mixing curve have suffered some postcrystallization change in the Rb-Sr system. The very low initial values for some rocks cannot be explained by heterogeneous regional compositions, as they are too low to be tenable for undisturbed igneous rocks. The range in heterogeneity in initial Sr compositions is represented by the rocks that follow the mixing trajectory, and can be assumed to show undisturbed values (cf. e.g. Romer et al. 1992, Romer 1994). Strongly disturbed Sr isotope systematics has also been reported from early Svecofennian rocks (Billström & Weihed 1996).

Fig. 22 shows the relation between initial ε_{Nd} and ε_{Sr} for the rocks analysed in this study. The strong disturbance of the Rb-Sr system in certain samples have shifted the data points to unrealistic values to the far left. If these data points are moved horizontally back to the right they would end up at realistic primary positions. This suggests that the Sm-Nd system remained essentially intact during the disturbance of the Rb-Sr system, although minor effects on the Nd system cannot be excluded. Even a few of the hybrids have suffered Rb/Sr alteration, notably two of the Kårtorp samples who have been shifted to values close to UR (uniform reservoir; Faure 1986) and the Tiveden curve. The fact that these samples actually are disturbed is indicated in Fig. 21b, where they plot below the mixing trajectory defined by the undisturbed rocks.

The enclave 8811A is the only sample that can be inferred to have been affected by disturbance also in the Sm-Nd system. This sample has geochemical characteristics which suggest that it may represent the basic endmember composition in the Kårtorp mixing event (see chapter 4.5.2.4.). However, its initial ε_{Nd} value should be at least three units higher to fulfill this requirement (Figs. 21a, 22), while the Rb-Sr system appears to be disturbed to a lesser degree (cf. Fig. 21b). The Nd isotopic composition

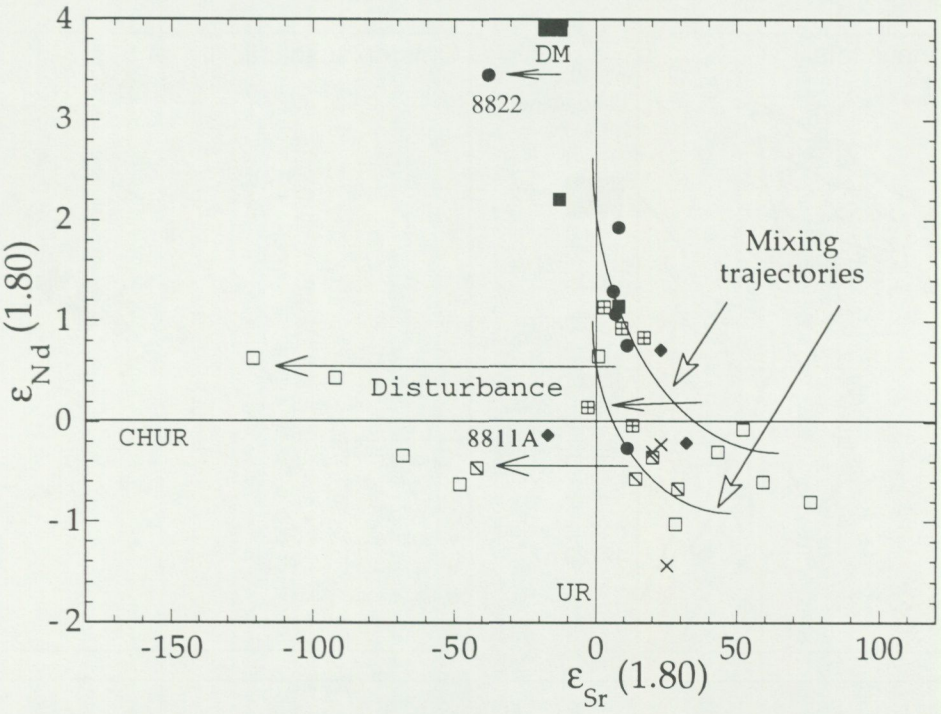

Fig. 22. Initial ε_{Nd}-ε_{Sr} diagram for the rocks of this study. Arrows indicate the presumed offset of the disturbed samples. Also the most depleted sample (8822) with regard to ε_{Nd} have suffered Rb-Sr alteration (cf. Fig. 21b), while the enclave 8811A probably have an altered Nd isotopic composition. Two separate mixing trajectories can be inferred for the Kårtorp and Tiveden cases also in this diagram, although less well-defined. Discussion in the text. Symbols as in Fig. 21, except inclined crosses: early Svecofennian granitoids.

of this enclave is thus similar to that of the granite host, suggesting isotopic readjustment with late magmatic granitic fluids. Such fluid readjustment may also have been operative in the two other enclaves, although this is not possible to separate from the effects of magmatic hybridization. Readjustment of the isotopic composition by host granitic fluids or melts is commonly described in the literature, although the effectivness of this process apparently has varied from case to case (e.g. Holden et al. 1987, 1991, Davidson et al. 1990, Pin et al. 1990, Allen 1991, Fourcade & Javoy 1991, Metcalf et al. 1995, Elburg 1996a, b, Poli et al. 1996). Even though isotopic equilibration proceeds much faster than chemical (e.g. Baker 1989, Lesher 1990, 1994), primary isotopic differences between enclave and host pairs have thus in many cases been preserved.

The undisturbed rocks can be inferred to roughly follow two separate mixing trends also in Fig. 22, although less well separated. The Kårtorp hybrids are considerably more primitive in nature than those from Tiveden. There is a strong overlap between the Kårtorp hybrids and the basic rocks of Tiveden and TVZ, which is not the case in Fig. 21a. It is suggested that the basic endmember of the Kårtorp hybridization is more depleted in nature, perhaps similar to sample 8822, compared with that of the Tiveden hybrids. The reason for the overlap may then be that the other basic rocks originate from a mildly depleted source, such as the lherzolites, and have assimilated small quantities of crustal material. The more strongly depleted basic magma, mixed with larger amounts of crustal material (SVB-granitoids), may thus end up with the same isotopic composition as the basites also for the Kårtorp hybrids. The more silicic chemical nature of the Kårtorp hybrids, compared with the basic rocks, is in accordance with this model. The early Svecofennian granitoids generally plot in the same area in Fig. 22 as the SVB granitoids. This supports the proposed model that the SVB granites are derived by melting of such source rocks (cf. geochemistry section). Frequent examples of mixing trends in ε_{Nd}-initial Sr space occur in the literature, suggesting a mixed origin for the rocks, although usually in younger rocks with better numerical separation of the endmember ratios (e.g. Gray 1984, Faure 1986, Davidson et al. 1990, Fleck 1990, Voshage et al. 1990, Sandiford et al. 1992, Arakawa & Shinmura 1995, Moreno-Ventas et al. 1995, Siebel et al. 1995). Based essentially on Sr-isotopes, Nielsen et al. (1996) suggested an origin by c. 50 % mixing of leuconorite and granitic roof melts for the mangerites and quartz mangerites in the Bjerkreim-Sokndal intrusion, SW Norway.

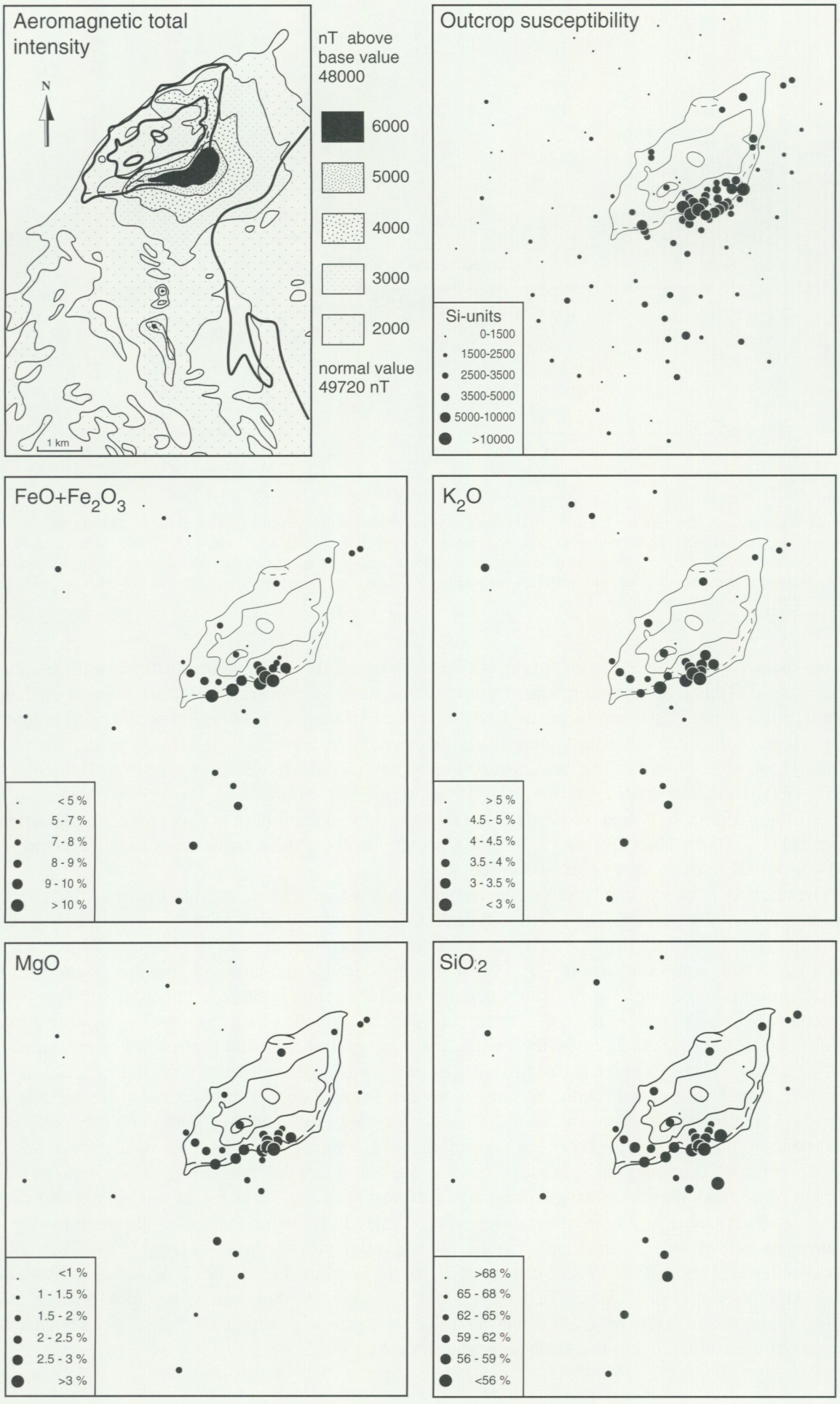
Aeromagnetic total intensity
N
1 km
nT above base value 48000
6000
5000
4000
3000
2000
normal value 49720 nT
Outcrop susceptibility
Si-units
0-1500
1500-2500
2500-3500
3500-5000
5000-10000
>10000
FeO+Fe2O3
< 5 %
5 - 7 %
7 - 8 %
8 - 9 %
9 - 10 %
> 10 %
K2O
> 5 %
4.5 - 5 %
4 - 4.5 %
3.5 - 4 %
3 - 3.5 %
< 3 %
MgO
<1 %
1 - 1.5 %
1.5 - 2 %
2 - 2.5 %
2.5 - 3 %
>3 %
SiO2
>68 %
65 - 68 %
62 - 65 %
59 - 62 %
56 - 59 %
<56 %

4.5.2. Geochemistry

4.5.2.1. Kårtorp area: correlation with magnetic characteristics

In the Kårtorp area outcrop susceptibility measurements have been performed (Appendix 2a), partly to qualitatively see if the rocks present at the surface could be responsible for the strong aeromagnetic anomaly, but mainly to correlate with the geochemistry. A more adequate aeromagnetic map, in the scale of 1:50 000, is found in Wikström & Karis (1991). In Fig. 23 the magnetic characteristics are compared with some whole rock geochemical parameters in two-dimensional space. A preliminary discussion on this correlation was given in Andersson (1989). There is a strong correlation between increasing outcrop susceptibility and increasingly basic whole rock chemistry, as exemplified by MgO in Fig. 24a. This means that the amount of magnetite increases with increasing hybridization from granite to the most basic monzodiorites or gabbros, as magnetite is the totally dominating magnetic mineral in igneous rocks (e.g. Haggerty 1979, Frost 1991). The aeromagnetic anomalies correlate well with the outcrop susceptibilities (Figs. 23a and b), suggesting that the rocks at the surface are at least partly responsible for the magnetic anomalies. It is clear that the low-magnetic leucocratic granite in the centre forms a sheet that gives rise to a low in the overall high positive anomaly. The aeromagnetic anomaly further indicates that high-magnetic rocks prevail in the southeastern part of the association and continues at depth. This also corresponds with the area of the most basic rocks exposed, with the highest outcrop susceptibility. Whether rocks at depths become more basic than the Kårtorp monzodiorites or not, cannot be determined since the amount of magnetite is not only related to the whole rock chemistry but even more to the oxygen fugacity and equilibria among Fe-Ti oxides and silicate phases during crystallization and cooling (e.g. Frost & Lindsley 1991, Frost 1991, and ref. therein). Nevertheless, the huge anomaly indicates that the monzodiorites (or more basic/magnetic) rocks become increasingly widespread at depth. There is also a relation between the Fe/Mg ratio of biotite and susceptibility, where iron in biotite decreases as susceptibility increases (Fig. 24b). Thus, as the magnetite content in the rock increases, the biotite becomes increasingly Mg-rich, suggesting an increase in f_{O_2} relative to f_{H_2O} according to the simplified equilibria: $2\ KFe_3AlSi_3O_{10}(OH)_2 + O_2 = 2\ KAlSi_3O_8 + 2\ Fe_3O_4 + H_2O$ (cf. e.g. Frost & Lindsley 1991). No quantitative investigations of the oxygen fugacity and mineral equilibria relations have been performed in the present study.

4.5.2.2. Granites

4.5.2.2.1. General

The Filipstad-type granites and their more silicic equivalents can be derived by partial melting of preexisting early Svecofennian source rocks in the deep crust. Such a model is supported by the isotopic data (chapter 4.5.1.2. above). This melting was caused by large volumes of basic mantle derived magma that underplated the lower early Svecofennian crust. No other means of generating the enormous volumes of SVB-granitoids appears realistic, as was also suggested by Johansson (1988). Remnants (mega enclaves) of this basic underplate, brought up by the granitoid batholith, are represented by the basic rocks associated with the SVB-granitoids in many areas, e.g. those in this study.

The early Svecofennian rocks can be represented by a composite of such rocks analysed in this study (Appendix 2a), dominated by tonalitic material such as samples XH and 8819 and excluding strongly fractionated rocks such as XB, which probably are very subordinate in the lower crust. This type of source has a LREE-enriched rare earth pattern with little or no Eu-anomaly and considerably

Fig. 23. Comparison between magnetic and geochemical characteristics in the Kårtorp area. The outline of the relation among the rock types (Fig. 6) has been superimposed on the diagrams. a) Shows a simplified version of the aeromagnetic intensity map (Wikström & Karis 1991). b) Shows outcrop susceptibility measurements separated into classes of increasing intensity (SI-units). A strong correlation with rock type is evident, as well as with the aeromagnetics. The most basic rocks occurring along the southern margin have the highest susceptibility, while the silicic central granite is very low. South of the Kårtorp association minor aeromagnetic anomalies occur, which are also evident in outcrop. c–f) show the spatial distribution of some geochemical parameters. There is a clear correlation between the whole rock chemistry and degree of magnetism, suggesting that at least part of the strong aeromagnetic anomaly can be explained by rocks seen at the surface.

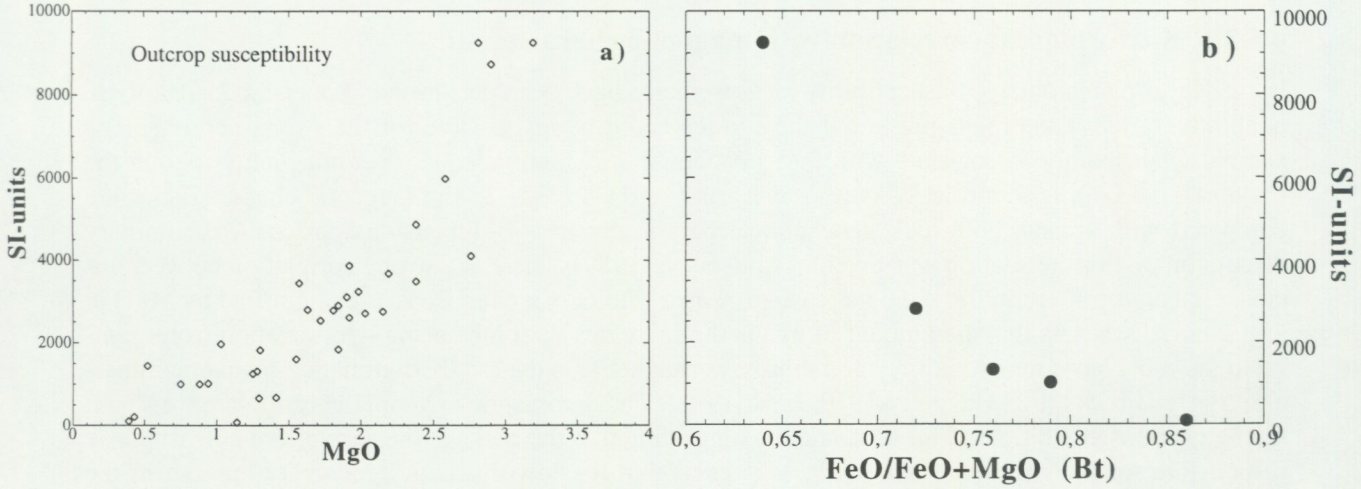

Fig. 24. Kårtorp area. a) Relation between outcrop susceptibility and whole rock MgO, showing the strong correlation between increasing susceptibility and basicity of the rocks. b) The Fe content of biotites shows a negative correlation with increasing susceptibility. This suggests an increasing f_{O_2} and concomitant increase in magnetite stability, with increasingly more basic magmas.

lower absolute abundances (Fig. 17), which are appropriate source characteristics.

Skjerlie & Johnston (1993) have performed dehydration-melting experiments of a tonalite which, in composition, closely resembles sample 8819 of this study (Table 4). At 10 kbar above 1075°C the percentage of melt produced in their experiment increases to 50 % or more, and this melt has a composition fairly similar to the Filipstad granites (Table 4). Notable differences are observed for FeO_{tot}, Na_2O and K_2O and may be related to differences in starting composition. If the sources for the SVB-granites in general are slightly more felsic than sample 8819, this will magnify the difference. The residue after this melting is composed dominantly of plagioclase (oligoclase), orthopyroxene (En_{61}), and quartz, with minor ilmenite, apatite and zircon. At 1000°C only 25 % melt is produced. This melt is very similar in composition to the average of the most silicic (>71 % SiO_2) SVB-granites (Table 4), and leaves a residue of the same phases with additional biotite and a little magnetite. This experimental evidence is thus in accordance with the generation of SVB-type granites by lower crustal partial melting of tonalitic to granodioritic sources.

Table 4. Comparison of SVB-chemistry with experimental melts.

	8819	S&J93T1	Filip 1	Filip 2	S&J93T7:10/1075	SVB >71	S&J93T7:10/1000
SiO_2	67.9	67.05	66.86	70.38	69.1	73.76	70.25
TiO_2	0.36	0.48	0.65	0.41	0.76	0.3	0.28
Al_2O_3	15.9	15.19	14.57	13.94	13.52	12.94	14.42
FeO^{tot}	3.05	3.84	3.85	2.81	4.45	2	2.15
MnO	0.06	0.04	0.06	0.05	0.06	0.03	0.03
MgO	1.37	1.88	0.98	0.68	0.69	0.39	0.36
CaO	3.17	2.56	2.24	1.55	1.82	1.09	1.05
Na_2O	4.26	4.83	3.2	2.96	4.37	2.9	2.41
K_2O	2.38	1.85	4.82	4.95	3.48	5.32	4.94
P_2O_5	0.1	0.13	0.2	0.1	0.29	0.06	0.15
	98.55	97.85	97.43	97.83	98.54	98.79	96.04

8819 = early Svecofennian tonalite, TVZ; S&J93T1 = tonalitic starting compostion in the experiments. Experiments after Skjerlie & Johnston (1993)
Filip 1 = Average Filipstad granite (n=10) 66–70 % SiO_2; Filip 2 = Average Filipstad granite (n=3) 70–71 % SiO_2

S&J93T7:10/1075 = Glass composition in experiment at 10 kbar/1075°C. 50 % melt generated; SVB >71 = Average SVB-granite (n=9) >71 % SiO_2
S&J93T7:10/1000 = Glass composition in experiment at 10 kbar/1000°C. 25 % melt generated

4.5.2.2.2. Major element modelling, partial melting

To test this genetic hypothesis and to see if different degrees of partial melting could generate the range in composition of the SVB-granites, major and trace element modelling was attempted. Table 5 summarizes the most consistent major element models. Models were calculated with the XLFRAC software of Stormer & Nicholls (1978) and Stormer (pers. comm. 1995), which solves linear least-squares mass-balance equations. According to the experiments (Skjerlie & Johnston 1993), a Filipstad granite with a composition of 66–70 % SiO_2 should be the result of 50 % melting or slightly more. If 8819 is used as the source and an average of Filipstad granites in this silica range (Filip 1) as the resulting melt, 54 % residue comprising 68 % oligoclase, 23 % quartz and 9 % orthopyroxene (En_{61}) is obtained (Table 5). Mineral compositions used are those reported by Skjerlie & Johnston (1993). If a more calcic plagioclase (labradorite) is used for the residue, this translates to an increased percentage of melting (c. 65 %). Since equilibrium (batch) melting should leave an increasingly calcic plagioclase as more of the plagioclase component enters the melt, this may be a realistic model. Skjerlie & Johnson (1993), however, did not observe any significant increase in An-content in the plagioclase upon increasing temperature (and melting) and suggested that Ca in the plagioclase was consumed in a garnet-forming reaction. This garnet broke down at 975°C and the Ca entered the melt, where it was incorporated into plagioclase again, which grew as euhedral grains (Skjerlie & Johnston 1993). These reactions thus buffered the Ca content of plagioclase, while at 1075°C, melt was produced by the reaction plagioclase + quartz = melt and a small increase in An-content was observed. Thus, at the advanced stages of melting when no other Ca-containing phase is present the restitic plagioclase becomes progressively more An-rich.

The major element models calculated for the more silica-rich SVB-granites (Table 5), suggest c. 40 % melting of 8819, leaving a residue of 70–73 % plagioclase, 14–18.5 % quartz, 11–13 % orthopyroxene, and very little biotite. Oligoclase composition was used in this case as this should be more in agreement with a lower melt percentage, and using a more calcic residual plagioclase gave unreasonable results. The pyroxene composition used in this case was that reported by Skjerlie & Johnson (1993) from their 1000°C, 10 kbar experiment, which was slightly more Fe-rich (En_{52}). More Mg-rich pyroxene does not give reasonable results. Furthermore, biotite was included in the calculations as it was a minor residual phase in their experiment. The calculated proportions of the residual phases closely resemble that of the experiments, leaving only very little biotite. This supports the validity of the models. However, the major element models calculated here give 10–15 % more melt, compared with the experiments. The conclusion from these calculations and comparison with the experiments is that SVB-granites with >70 % SiO_2 can be derived by 25–40 % melting of an early Svecofennian dominantly tonalitic lower crustal source, while the slightly more basic granites (66–70 % SiO_2) may be derived by 45–65 % melting of this same source.

Table 5. Summary of the major element modelling, Småland–Värmland granites. Partial melting.

Source rock	Partial melt	Calculated modal composition of residue
8819	Filip 1	54% Residue composed of 68% Oligoclase + 23% Quartz + 9% Orthopyroxene (En61)
	Filip 1	34% Residue composed of 58% Labradorite + 35% Quartz + 7% Orthopyroxene (En61)
	Filip 2	58% Residue composed of 70% Oligoclase + 18.5% Quartz + 11% Orthopyroxene (En52) + 0.5% Bt
	SVB >71	60% Residue composed of 73% Oligoclase + 14% Quartz + 13% Orthopyroxene (En52) + <1% Bt

4.5.2.2.3. Trace element modelling, partial melting

The conclusion from the major element considerations was tested by batch melting calculations for a number of trace elements (Table 6). Also here the composition of sample 8819 was used as starting composition. The residual assemblages and melt degrees derived above were utilized. The mineral/melt partition coefficients (K_D-values) for the phases were extracted from the compilation of Rollinson (1993), essentially using those reported by Arth (1976), Pearce & Norry (1979), and Nash & Crecraft (1985). In Fig. 25 the results are displayed in graphical form.

For the 25–40 % melting and comparison with the more silicic SVB-granites the agreement is fairly good. The composition of Filip 2 and SVB >71 averages are mostly within the range between the 25 and 40 % melting calculations. Notable exceptions are Eu, Ba, Sr, Sc, Zr and U. Reasons for these discrepancies may include: Eu in 8819 is amongst the lowest of the early Svecofennian rocks (0.9 ppm), some of which have contents up to 2.1 ppm (cf. Appendix 2a). A composite source may thus contain more Eu than 8819. This, together with possibly a too high $K_D^{plag/melt}$(Eu) in the calculations (5.417) may explain this discrepancy. The low calculated contents of Sc are controlled by opx, and may be due either to a too high proportion in the residue or to a too high K_D. Since the proportion of opx in the residue is relatively small, the K_D is possibly too high (20). Too high Zr and U are also calculated, which may be due to a very small amount of zircon left in the residue. Calculated Ba is generally too high and partly also Sr. This may be due to a too low proportion of biotite in the model residue (<1 %). A few percent of biotite with high K_D(Ba) are sufficient to explain this. Some feldspar fractionation may have contributed to this effect.

Regarding the more basic SVB-granites (Filip 1), the fit is much poorer. In Table 6 and Fig. 25 sample 8811A has been included, as representing the basic endmember in mixing trends (see below). Mixing, e.g. Filip 2 with a minor proportion of basic magma of this composition can explain the composition of Filip 1, which is generally intermediate between the calculated composition and 8811A. A part-

Table 6. Trace element modelling, Småland–Värmland granites. Batch partial melting.

	8819	F=50 F3	F=65 G3	Filip 1	8811A	F=40 H3	F=25 H3	Filip2	F 40 I3	F 25 I3	SVB >71
La	25.1	39.55	34.38	57.36	116	44.18	54.54	63.95	43.65	53.54	57.93
Ce	51	85.35	72.06	113.38	240	97.6	126.49	124	96.55	124.3	110.38
Nd	20	34.55	28.72	54.63	115	39.98	53.28	50	39.53	52.3	43.5
Sm	3.6	6.33	5.22	10.88	24.4	7.38	10.01	9.65	7.3	9.82	8.68
Eu	0.9	0.38	0.51	1.75	3.3	0.33	0.29	1.44	0.32	0.28	1
Tb	0.5	0.9	0.73	1.45	3.9	1.05	1.45	0.98	1.04	1.41	1.16
Yb	1.2	2.11	1.74	3.59	8.8	2.42	3.25	2.55	2.36	3.12	3.03
Lu	0.18	0.31	0.26	0.54	1.29	0.36	0.48	0.41	0.35	0.46	0.47
Rb	93	180.91	141.25	169.63	97	220.09	334.3	187.5	222.09	340.12	224.88
Ba	631	1043.29	885.21	1064.63	366	1168.78	1485.23	883	1178.1	1504.14	541.5
Sr	257	128.77	166.15	153.25	152	113.99	100.07	132.5	110.95	97.15	76.08
Sc	8.4	5.9	7.55	13.75	50.4	4.78	4.32	8.1	4.16	3.69	5.3
Y	10.3	17.78	14.86	36.59	112	20.16	26.51	22.9	19.67	25.46	30.46
Nb	7	12.58	10.29	23.83	77	14.33	19.4	-	14.25	19.22	16
Zr	100	184.15	148.17	377.13	1430	218.65	310.87	203	217.51	307.99	190.71
U	3.1	5.76	4.61	3.75	2.4	6.89	9.92	5.5	6.86	9.83	5.52
Th	7	13.4	10.56	14.4	5	16.26	24.3	24.65	16.22	24.19	26.26

8819 = Early Svecofennian tonalite, starting composition
F=50 F3 = 50% melting with 68% Plag +23% Qz + 9% Opx in the residue
F=65 G3 = 65% melting with 58% Plag + 35% Qz + 7% Opx in the residue
Filip 1 = Average of Filipstad granites, 66-70% SiO_2 8811A = Basic endmember magma (enclave)
F=40 H3 = 40% melting with 70% Plag + 18.5% Qz + 11% Opx + 0.5% Bt in the residue
F=25 H3 = 25% melting with 70% Plag + 18.5% Qz + 11% Opx + 0.5% Bt in the residue
Filip 2 = Average of Filipstad granites, 70-71% SiO_2
F 40 I3 = 40 % melting with 73% Plag + 14% Qz + 13% Opx + <1% Bt in the residue
F 25 I3 = 25 % melting with 73% Plag + 14% Qz + 13% Opx + <1% Bt in the residue
SVB >71 Average silicic SVB-granites, >71% SiO_2

ly mixing origin for the granites in the range 66–70 % SiO_2 is supported by the trends in Fig. 15, where these granites generally follow trends towards the basic endmember (e.g. 8811A), while the trends converge at a silicic endmember at c. 70 % silica. The trace element modelling thus rejects the major element model of 50–65 % melting of the early Svecofennian tonalite to give the more basic (66–70 % SiO_2) granites, and rather suggests an additional component of mixing in the chemistry for the granites below c. 70 % SiO_2.

In summary: the trace elements indicate that the SVB-granites around or slightly above 70 % SiO_2 can be derived by 25–40 % melting of a tonalitic source, probably with minor more granitic components, leaving a residue of dominantly oligoclase, orthopyroxene (c. En_{50}–En_{60}), quartz, and minor biotite. Similarly, Rämö (1991) derived the primary silicic magma in the Suomenniemi rapakivi batholith by modelling c. 20 % melting of an early Svecofennian granodioritic source. Very small amounts of zircon and apatite (<0.5 %) may also be left in the residue, as indicated also by the experiments of Skjerlie & Johnston (1993). Granitoids more basic than this contain a component of mixing with a basic endmember (see below). An origin for the suite (66 to 76 % SiO_2) by fractional crystallization is not likely, in view of the small variation in trace elements over this evolutionary range. Limited removal of e.g. feldspar may have occurred in places to account for the decrease in Ba.

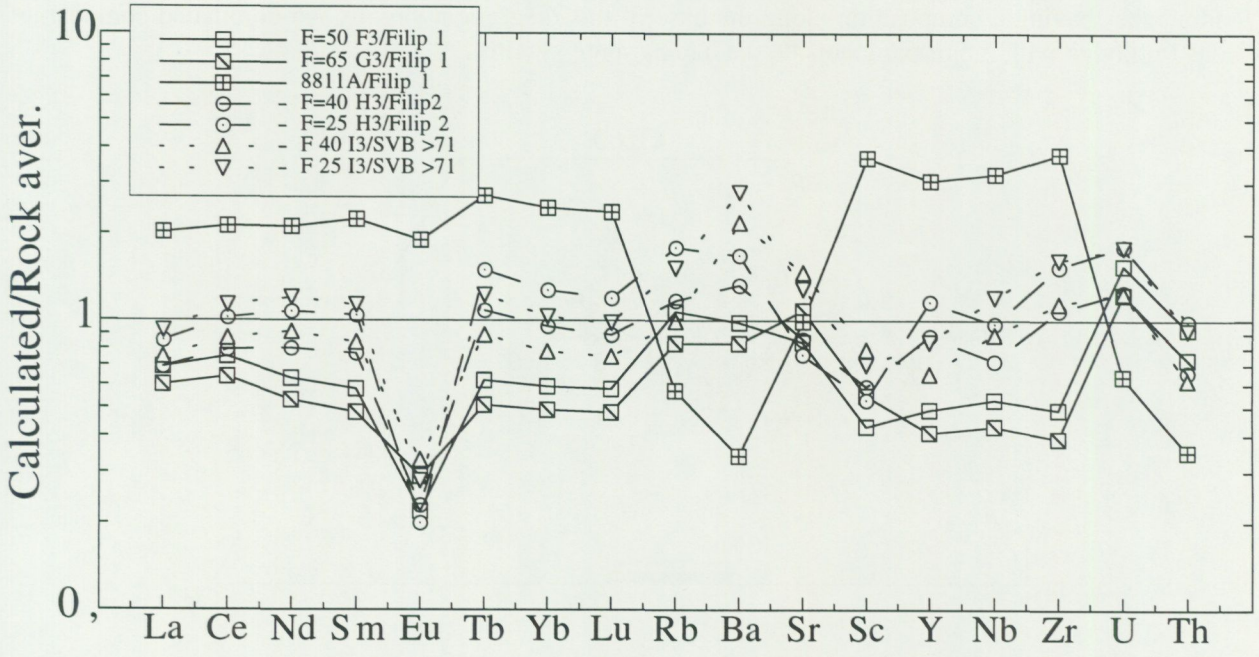

Fig. 25. Trace element distribution from batch partial melting modelling of an assumed lower crustal protolith, having the composition of tonalite sample 8819. Models are calculated using the residual assemblages derived in the major element modelling (Table 5), and are summarized in Table 6. The batch melting equation is $C_L/C_0=1/[D_{rs}+F(1-D_{rs})]$ (e.g. Hanson 1978), where C_L is the concentration of an element in the liquid, C_0 is the initial concentration in the unmelted residue, D_{rs} is the bulk distribution coefficient for the residual assemblage, and F is the degree of melting. Distribution coefficients used were extracted from the compilation in Rollinson (1993). The calculated compositions were compared and normalized to the averages Filip 1, Filip 2, and SVB >71, which represent increasingly higher SiO_2 contents (Table 6). Sample 8811A has been included for comparison and has a pattern completely opposite to those calculated. Discussion in text.

4.5.2.2.4. Haplogranite system relations

SVB-granitoids with more than 63 % SiO_2 have been plotted on the haplogranite system in Fig. 26. They all plot off to more Or-rich compositions compared with the minimum melt compositions at water saturated melting, indicating water undersaturated conditions (e.g. Whitney 1975, Holtz et al. 1992). Water undersaturated minima experimentally determined (Holtz et al. 1992; Johannes & Holtz 1996) have been plotted as small crosses. The more Or-rich melt compositions at lower a_{H_2O} have also been verified in experiments on natural rocks (e.g. Conrad et al. 1988). Granites with more than 70 % SiO_2 have more than 28 % quartz in the norm and comprise approx. the group in Fig. 26 above 30 % relative Qz. These have also Qz+Ab+Or>83 %, while the more basic ones are between 67 and 83 %. As the less silicic samples contain a significant component of mixing with a basic endmember they are only included for reference. An An-component of the system also shifts the beginning of melting compositions towards the Qz-Or side if projected onto the haplogranite system (e.g. James & Hamilton 1969, Johannes & Holtz 1996, and ref. therein). This effect may contribute to the higher Or contents compared with minimum melts in Fig 26 (cf. Anderson & Cullers 1978, Rämö 1991), but it is not possible to separate this from the effect of low water activity since the shifts in the diagram are similar.

The normative compositions of two melts produced by melting of tonalite by Skjerlie & Johnston (1993) (discussed above) have been included in Fig. 26: **a)** c. 50 % melting at 1075°C and 10 kbar, and **b)** c. 25 % melting at 1000°C at 10 kbar, suggested to be appropriate for lower crustal generation of the SVB-granites. Both lie to the right of the water-saturated minimum melts. The 25 % melt is far away from the 10 kbar haplogranitic minima, even the water undersaturated ones, while the 50 % melt is actually closer. These are clearly no minimum melts, but rather show the change in composition as melting proceeds. At lower degrees of melting the composition of the melt is dominated by the breakdown of biotite and melting of quartz, while at increasing temperatures progressively more plagioclase enters the melt (Skjerlie & Johnston 1993), which drives it towards the Ab-corner in the Qz-Ab-Or-triangle. However, most of the more silicic (>70 % SiO_2) granites are bracketed by the composition of these experimental melts, supporting the derivation of these granites by the 25–40 % melting proposed above. The more basic granitoids plot at lower Qz-contents, consistent with a mixing trend towards a basic endmember having a composition along the base of this diagram at slightly Ab-dominated compositions (although with major parts outside the haplogranite system).

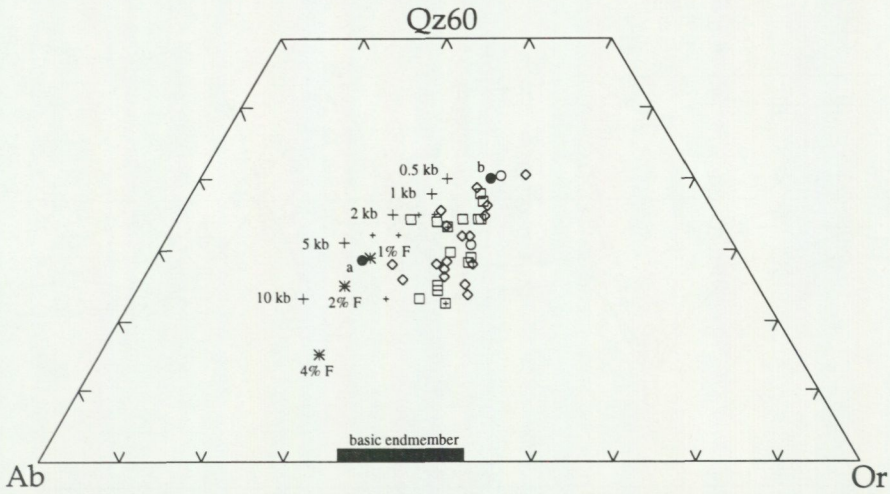

Fig. 26. SVB granitoids of this study (SiO_2 >63 %) plotted on the haplogranite system. Crosses labelled 0.5 through 10 kb represent minimum melt compositions in the haplogranite system at water-saturated conditions (Tuttle & Bowen 1958, Luth et al. 1964, Holtz et al. 1992). Small crosses to the right of 2 kb represent melting at a_{H_2O}=0.5 and 0.25, respectively (Holtz et al. 1992), to the right of 5 kb a_{H_2O}=0.6 and 0.4 (Holtz et al. 1992), and to the right of 10 kb a_{H_2O}=0.5 and 0.3 (Johannes & Holtz 1996). Stars represent melting with 1, 2, and 4 % F at 1 kb water saturated conditions (Manning 1981). Dots labelled a and b are the normative compositions of the average experimental melts derived by Skjerlie & Johnston (1993) for c. 50 % melting at 10 kb/1075 °C and 25 % melting at 10 kb/1000°C, respectively. Basic endmember refers to the approximate normative compositions of the basic rocks as represented in this diagram. Rocks with SiO_2 >70 % generally have Qz higher than 30 %. Rocks below 30 % Qz trend towards the composition of the basic endmember as would be expected if they were hybridized. Symbols: diamonds are Kårtorp granitoids, squares TVZ granitoids, and circles are Tiveden granites. Further discussion in the text.

4.5.2.3. The basic suite

4.5.2.3.1. General

The basic suite contains samples collected from differently sized plutonic bodies, enclaves and dykes over a wide area, which are thus heterogeneous in nature. The likelihood that all samples were derived by differentiation in the same magma "chamber" is very little. On the other hand, every sample in this suite should represent some stage in the evolution of one or several lower crustal basic magma systems associated with the generation of SVB-granites. This suggests that the physical conditions in the system may have been broadly similar (same approximate P and T) in separate parts of the basic underplate. The basic system most probably experienced several episodes of replenishment, with concomitant mixing of evolved and primitive magmas. Since these magmas were generated more or less continuously during the same tectonic event and probably from similar source areas in the mantle, their chemistry should also be essentially similar.

The ultrabasic rocks found at three locations within the TVZ are fragments of the upper mantle, which have survived the transport to middle crustal levels fairly well. Since all samples contain plagioclase and spinel they derive from the uppermost mantle (e.g. Wyllie 1979). The large amounts of unaltered phlogopite show that this is a piece of hydrated mantle. The olivine and plagioclase are usually strongly altered to serpentine and white mica+calcite, respectively. This alteration most probably occurred during or after transport of the ultrabasite into the crust, and may have enriched and changed its original mantle composition. The analysed ultrabasic rocks show LREE-enriched patterns (Fig. 17), which thus partly may be due to crustal influence, but in general they are closely similar to the spinel lherzolite average of McDonough (1990). The major elements and, e.g. Cr and Ni, in these ultrabasic rocks are less refractory in nature than spinel lherzolites in general, while the incompatible elements are consistently higher (cf. McDonough 1990). The abundance of phlogopite suggests that these rocks were modally metasomatized by hydrous fluids in the upper mantle (cf. e.g. Harte 1987). These fluids most likely caused an enrichment in LILE and HFSE before the lherzolites entered the crust. It is possible that most of the enrichment is of mantle origin, since the REE-patterns fall in the uppermost part of the variation for spinel lherzolites (Basaltic volcanism study project 1981). The petrology of the lherzolites has not been investigated further in this study.

The lherzolites, or slightly less enriched equivalents, may represent the source lithology for the basic SVB-suite. The most primitive parts of this suite have REE-patterns only slightly more enriched than the ultrabasites. The chemical variation among the rocks in the basic suite is interpreted as a result of a combination of partial melting and crystal fractionation processes (see below). Individual samples from different parts of the area may have been incorporated in the SVB-granitoids at widely different times, thus representing different stages of evolution and/or replenishment.

In general, the least evolved rocks are of two types: i) plutonic rocks of the TVZ and Tiveden, and ii) dyke rocks in the whole area. Some of the dykes (139b/89, 8850, and 1t) are among the most primitive rocks in the area. These presumably represent injections of new mantle melts at the vaning stages of granitoid magmatism in the SVB. Although they represent the latest stages of basic magmatism, magmas of similar composition can be assumed to approximate the parental magmas of the whole suite, followed by an evolution by fractional crystallization. There is a decrease in CaO, MgO, Cr, and Ni, but an increase in TiO_2, Na_2O, K_2O, P_2O_5, and all incompatible elements, with evolution. This evolution is subvertical in the Harker diagrams, and thus not so well represented (Fig. 15). The trends are almost vertical at around 50 % SiO_2, which is natural if they are controlled by cpx, opx, and labradorite, minerals with SiO_2 contents near 50 %. To better illustrate the evolution in the basic suite selected elements have been plotted against MgO (Fig. 27).

It is not possible to derive the very large variation observed in the compatible elements Ni and especially Cr, by variable partial melting of the same mantle source. Additional crystal fractionation of a phase with high partition coefficient (K_D) for Cr is necessary, undoubtedly cpx. Fe-Ti oxides, on the other hand, cannot be part of a fractionating assemblage, since TiO_2, and partly $Fe_2O_3^{tot}$ and MnO are increasing with decreasing MgO. Furthermore, V should be much more strongly depleted in the evolved rocks if an oxide phase had participated ($K_D^{magnetite/melt}(V)=26$; cf. Rollinson 1993). In fact, V is at its highest level in the evolved sample 105/89. Neither is apatite a fractionating phase, since P_2O_5 shows a strong increase in the more evolved rocks. The Ni content varies from 156 ppm in the most primitive dyke (8850) to less than 1 ppm in the most evolved enclaves. If the lherzolite source contains

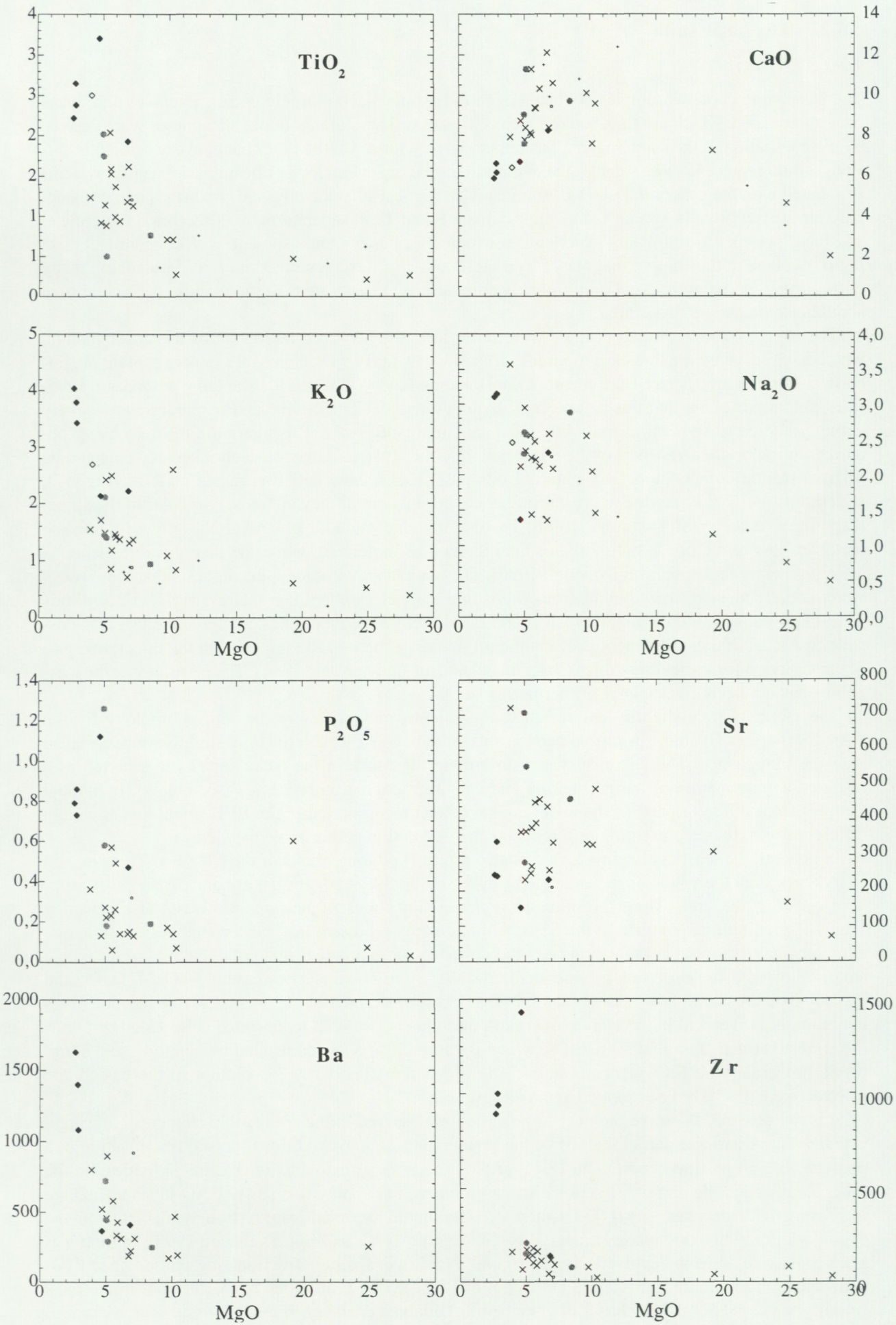
TiO2
CaO
K2O
Na2O
P2O5
Sr
Ba
Zr
MgO
MgO
MgO
MgO

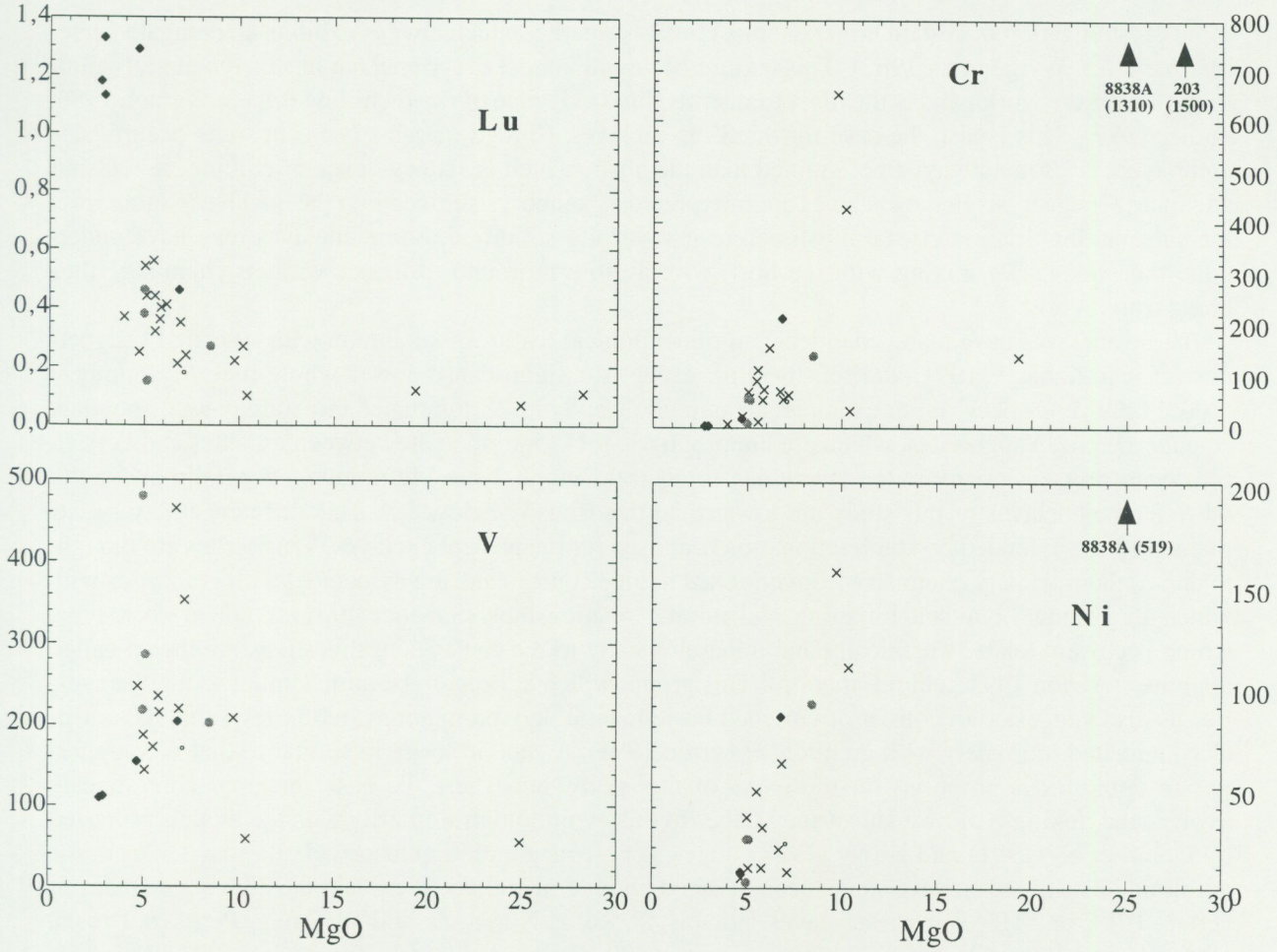

Fig. 27. Selected MgO variation diagrams for the basic SVB rocks in this study. The evolution is more clearly seen compared with the Harker diagrams (SiO_2-abscissa, Fig. 15). Symbols as in Fig. 15. The enclaves are clearly the most strongly evolved basic rocks. CaO, Cr, and Ni decrease strongly with MgO, while most others increase. Plagioclase fractionation deriving the enclaves is indicated by decrease in Sr (cf. Fig. 15). Further discussion in the text.

519 ppm (sample 8838A) or more, the whole range of compositions in the basic suite down to contents below 10 ppm cannot be the result of partial melting of a single source alone. Some other process, such as crystal fractionation (of e.g. olivine and pyroxenes), have to be invoked.

4.5.2.3.2. Enclaves

Regarding the group of most evolved basic rocks, i.e. the mafic enclaves, fractionation of plagioclase seems to be required by the data: lower Al_2O_3, Sr, Ca (8811A is also lower in Na_2O). Eu increases relatively strongly with evolution, but not as strongly as the other REEs. This is accounted for by the low (lower than unity) $K_D^{plag/melt}$(Eu), but even lower (one order of magnitude) K_Ds for the other REEs in plagioclase in basic melts (cf. compilation in Rollinson 1993). Large degrees of fractionation (depending on how primitive the parental magma is assumed to be) are necessary to achieve the elevated contents of the incompatible elements in these rocks (see section 4.5.2.3.6. below).

Nowadays a large majority of workers seem to agree that mafic microgranular enclaves have a magma mingling origin (e.g. Didier & Barbarin 1991, and ref. therein). They represent globules of basic or hybrid magma mingled into the host granitoid during some event of dynamic interaction, where they form pillows that are more or less rapidly chilled depending on the initial temperature differences between the magmas (e.g. Sparks & Marshall 1986, Frost & Mahood 1987). The chilling often causes

rapid crystallization of certain minerals, most notably apatite, which always exhibits an elongated acicular habit (cf. Wyllie et al. 1962). This texture occurs in almost every enclave of this type in all granitoids around the world, and is the most frequently cited evidence of rapid chilling (cf. e.g. Vernon 1983, Didier 1987). This is also the case for the SVB-enclaves. Chilled margins occur in some occurrences and the enclaves are always finer grained than the hosts, which is also evidence of chilling. K-feldspar and quartz megacrysts in the enclaves are interpreted as xenocrysts mixed into the enclave magma from the surrounding granitic crystal mush before it was fully solidified. Some enclaves may have undergone more extensive mixing with the host, with a more profound influence of their chemistry, thus being truly hybrid.

These enclaves have many chemical and mineralogical features in common with so-called vaugnerites (cf. e.g. Sabatier 1991, and ref. therein), except for significantly lower whole-rock Mg-numbers (100*MgO/MgO+FeO^{tot}). For example, an amphibole and biotite dominated mineralogy with abundant acicular apatite. Vaugnerites, which are lamprophyric rocks intermediate between minettes and kersantites occurring essentially in the Hercynian of central Europe, have Mg-numbers generally above 40, whereas the enclaves of this study are lower than this (mostly below 20). This difference may be explained by the extended crystal fractionation proposed for the present enclaves. Vaugnerites are thought to derive their primary chemistry from enriched mantle sources and are associated with granitoids with which they show abundant mingling and mixing relationships (Sabatier 1991). Another rock type, which is closely related chemically and mineralogically to the enclaves of this study, are the so-called appinites (Ayrton 1991, and ref. therein). This group, which appears to be quite similar to the vaugnerites, is also suggested to consist of enriched basic mantle derived magmas rich in H_2O that have usually interacted intimately with granitoids (Ayrton 1991). A genetic scenario similar to that of vaugnerites or appinites is proposed for the rocks of this study, but where the basic magmas continuously evolve, and mixing is allowed at various stages of this evolution, in similarity with the models proposed by Orsini et al. (1991) and Bussy (1987). Late- to post-magmatic liquid or volatile transfer from the granitoid hosts to the enclaves have been invoked by several authors to explain the high abundances of certain LILE and HFSE in the enclaves, notably K, Rb, P, Nb, Y, Zr, and REE (e.g. Petrik & Broska 1989, Bédard 1990, Christiansen & Venchiarutti 1990, Orsini et al. 1991, Zorpi et al. 1991, Blundy & Sparks 1992, Elburg & Nicholls 1995, Stimac et al. 1995, Sisson et al. 1996). The mechanism for this transfer remains unclear, however, since these elements usually are more strongly enriched in the enclaves than in the host (cf. Figs. 15 and 27). In the SVB the enrichment may be explained largely by crystal fractionation (see below), although indications of late enclave-host interactions are recorded, e.g. by the resetting the Nd isotope composition in enclave sample 8811A (see chapter 4.5.1.2.). A fractional crystallization origin for strongly incompatible element-enriched mafic-hybrid enclaves has been advocated by, e.g. Wiebe (1996) and Wiebe et al. (1997).

4.5.2.3.3. Partial melting modelling. Major elements

To put some quantitative constraints on the magmatic evolution of the basic SVB-suite in the present area, major and trace element modelling was attempted. At first it was tested if the lherzolites could represent fragments of the mantle source rock. Results of major element tests of partial melting are summarized in Table 7. The program XLFRAC (Stormer & Nicholls 1978) was used in the calculations. Table 8 lists the composition of the rocks utilized that are representative of the compositional variation in the suite, and Table 9 gives the composition of the crystalline phases used in the calculations. Since no analyses of the minerals in the lherzolites are available, these mineral compositions have been compiled from the literature. Moreover, the lherzolite minerals do not represent the residual mineralogy and may not have an appropriate composition. This is, of course, a major source of uncertainty in these models, but the results are nevertheless consistent. The mineral compositions used here are slightly more Fe-rich compared with mantle xenoliths in general (cf. e.g. Wilson 1989, p. 46). An attempt to use more Mg-rich mineral compositions proved unsuccessful and gave unreasonable results. Residual minerals in the uppermost mantle may, however, be more Fe-rich than in deeper sections of the mantle.

The presumably most primitive basic rock sampled in the TVZ, 8850 (Cr 654 and Ni 156 ppm), can be derived by 25–30 % melting of a lherzolite similar in composition to sample 203 (Table 7). This

Table 7. Partial melting models, Småland–Värmland basites.
Major element models. Compositions in Tables 8 and 9 were used.

Source	Melt degree (F)	Rock (melt)	Composition of residue	Sum of sq. res.
203	25	8850	86 % Olivine + 16 % Opx	5.1
8838A	48	8850	97 % Olivine + 2 % Opx	12.5
203	25	1t	85 % Olivine + 16 % Opx	3.3
8838A	39	1t	80 % Olivine + 14 % Cpx + 6 % Opx	9
203	22	139b/89	80 % Olivine + 20 % Opx	4
8838A	37	139b/89	75 % Olivine + 16 % Opx + 9 % Cpx	10.5
203	18	8859D1	76 % Olivine + 24 % Opx	3.4
8838A	30	8859D1	68 % Olivine + 23 % Opx + 9 % Cpx	9
203	20	8842A	84 % Olivine + 14 % Opx + 2 % Cpx	5
8838A	31	8842A	79 % Olivine + 18 % Cpx + 3 % Opx	13.5
203	20	8860	82 % Olivine + 18 % Opx	4.3
8838A	33	8860	76 % Olivine + 12 % Opx + 12 % Cpx	11.7
203	20	8839	78 % Olivine + 22 % Opx	6
8838A	30	8839	69 % Olivine + 16 % Opx + 15 % Cpx	15.9
203	16	8812M	78 % Olivine + 15 % Opx + 7 % Cpx	7.1
8838A	25	8812M	71 % Olivine + 23 % Cpx + 6 % Opx	19.3
203	12	8811A	69 % Olivine + 21 % Opx + 10 % Cpx	13.3
8838A	19	8811A	56 % Olivine + 28 % Cpx + 16 % Opx	34.9

would leave a residue with c. 85 % olivine and 15 % orthopyroxene, but no clinopyroxene. Also dyke 1t, with a primitive composition, can be derived by c. 25 % melting, leaving a residue of the same composition. In the case of sample 139b/89, slightly smaller melt degrees are indicated, with residues containing a little more opx relative to olivine, but still no cpx.

In the case of the more evolved gabbros, they could also be directly derived by partial melting from 203, according to the major element models (Table 7). The melt degrees are, however, somewhat smaller, around 20 %. In this case the models mostly indicate that some additional cpx may be left in the residue. This result is also valid for the high-Al gabbro 8859D1. With respect to the major element models it appears possible to derive also the very evolved enclaves 8812M and 8811A by partial melting of 203 (Table 7). The melt degrees are 12–16 %, but the fit is poor (sum of squared residuals is high) indicating that the models may not be valid.

If the more enriched lherzolite 8838A is considered as the source rock, the degree of melting required increases substantially, but the fit of the models decreases (Table 7), suggesting that this composition is less appropriate as a source.

Table 8. Summary of composition of basic SVB-rocks. Recalculated to 100 %.

		SiO_2	TiO_2	Al_2O_3	FeO^{tot}	MgO	CaO	Na_2O	K_2O	Cr	Ni
203	Ultrabasite	44.01	0.30	4.50	15.48	32.40	2.29	0.57	0.45	1500	n.d.
8838A	Ultrabasite	45.40	0.23	7.35	12.79	27.64	5.16	0.84	0.58	1310	519
8850	Primitive dyke	52.70	0.74	12.16	10.01	10.11	10.50	2.65	1.13	654	156
1t	Primitive dyke	51.36	0.74	14.70	9.97	10.56	7.87	2.11	2.69	427	n.d.
139b/89	Primitive dyke	50.53	0.79	15.36	10.46	8.81	10.08	2.99	0.98	140	90
8859D1	High-Al gabbro	49.14	0.52	19.26	9.84	5.34	11.76	2.68	1.46	54	24
8842A	Evolved gabbro	54.21	1.18	16.41	10.28	5.24	8.08	3.06	1.54	69	35
8860	Evolved gabbro	51.97	1.04	16.69	10.21	6.11	9.85	2.59	1.53	54	10
8839	Evolved gabbro	50.52	1.43	16.08	12.31	6.13	9.76	2.31	1.47	74	30
105/89	Evolved gabbro	47.99	2.15	14.48	16.48	5.29	9.63	2.45	1.53	8	3
8812M	Evolved enclave	53.36	2.50	15.83	11.89	3.05	6.47	3.30	3.60	3	<1
8811A	Evolved enclave	51.08	3.43	11.16	18.35	5.04	7.19	1.46	2.29	17	8

n.d.=not determined

Table 9. Mineral compositions used in major element modelling. Småland–Värmland, basic rocks. Recalculated to 100 %.

	Ol R72b	Opx DHZ63 T3:2	Cpx DHZ63 T17:6	Pl DHZ92 T38:5
SiO_2	39.24	55.53	52.17	52.62
TiO_2	0.04	0.32	0.49	0.09
Al_2O_3	0.06	1.26	3.09	29.82
FeO^{tot}	20.26	13.18	8.51	0.45
MgO	40.11	29.31	16.11	0.08
CaO	0.29	0.4	19.34	12.7
Na_2O	0	0	0.27	4.03
K_2O	0	0	0.02	0.21
	100	100	100	100

Ol R72b. Olivine (Chrysolite) from Postjotnian dolerite, Rödö area (Table 11 below).
Opx DHZ63 T3:2. Bronzite (Deer, Howie & Zussman 1963, Table 3 analysis 2)
Cpx DHZ63 T17:6. Augite (Deer, Howie & Zussman 1963, Table 17 analysis 6)
Pl DHZ92 T38:5. Labradorite (Deer, Howie & Zussman 1992, Table 38 analysis 5)

4.5.2.3.4. Partial melting modelling. Trace elements

In order to test if the result of the major element modelling above is consistent also with the trace element compositions, batch partial melting models were calculated for a number of elements. The results are compiled in graphical form in Fig. 28. The models assume the same mineralogical composition of the residues as was calculated for the major elements (Table 7). In equilibrium (batch) partial melting,

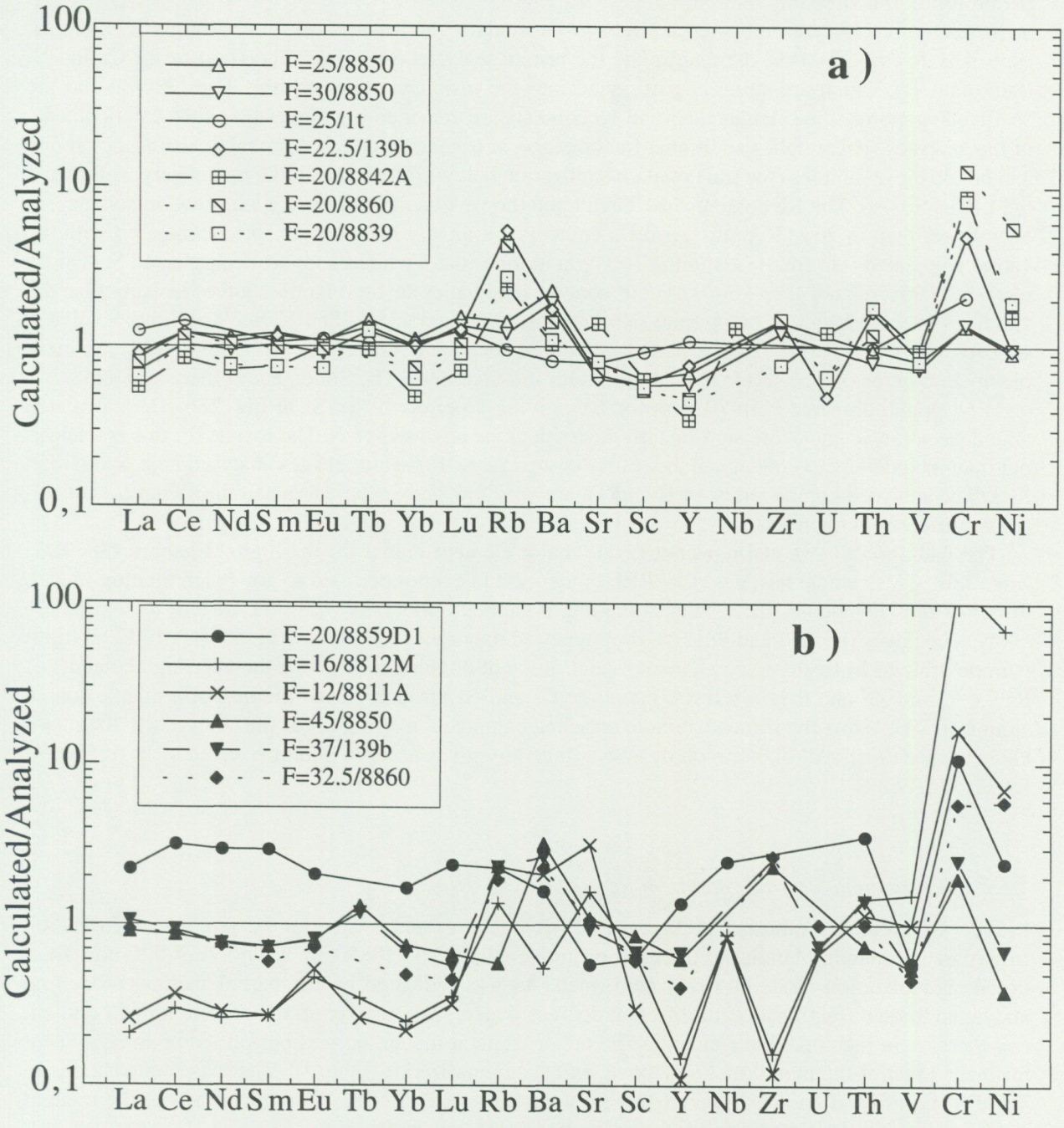

Fig. 28. Trace element batch partial melting models for the basic SVB rocks of this study. Distribution coefficients used were extracted from the compilation in Rollinson (1993). Models are calculated using the most appropriate residual assemblages derived in the major element modelling (Table 7). Lherzolite sample 203 was used as source rock. Calculated contents are normalized to the the rock in question. Perfect correspondence between calculated and analytical data would thus yield a value of 1 for all elements. **a)** Models F=25/8850 to F=22.5/139b represent 22.5 to 30 % melting to yield the primitive dykes. The fit of the models is very good except for Rb. F=20/8842A to F=20/8839 represent 20 % melting models for the more evolved gabbros. Also these fit reasonably well, except for Cr and Ni, which are higher in the calculated composition. This suggests that these rocks have experienced additional fractionation of particularly cpx. **b)** The fit of the strongly evolved enclaves (8812M and 8811A) to batch partial melting models of 203 is very poor. This is also true of the high-Al gabbro (8859D1). For example, the REE contents of the enclaves are much higher than those obtained by calculation from the major element models, while 8859D1 has much lower REE contents than calculated. F=45/8850 to F=32.5/8860 are models using the ultrabasite 8838A as source rock instead of 203. These models give poorer fits than when using 203 as the source (a). Further discussion in text.

only the bulk distribution coefficient of the residual phases and the degree of melting determines the composition of the melt in relation to the original source (cf. e.g. Hanson 1978). Distribution coefficients were extracted from the compilation of Rollinson (1993). Lherzolite sample 203 was generally used as the model source. Due to lack of analytical data, some of the elements had to be estimated based on the composition of the other ultrabasites and chemically similar elements. This necessarily introduced extra uncertainty in the calculations, but relative to the overall uncertainty of the composition of the protolith, it is probably minor.

A relatively close resemblance between the calculated and analytical compositions is obtained, especially for the 22–30 % melting giving the primitive dykes (Fig. 28a). The good fit for Cr and Ni (8850 and 1t), which are strongly partitioned into the residues, is noteworthy. For 139b/89 and the "evolved" gabbros, the calculated Cr and Ni contents are considerably higher than the actual contents of the analyses. This implies additional fractionation of especially cpx, but probably also some olivine and opx in these samples (see fractional crystallization below). The REEs fit the model very well, while the LILEs less so. The Rb contents in 139b/89 and the "evolved" gabbros are very low, in some cases even lower than in 203 (30 ppm). Also Ba contents are mostly lower in the rocks compared with the values calculated (not for 1t) assuming 100 ppm in the source, while the opposite applies to Sr. This is most probably related to a very variable content of alkalies in the mantle source, in particular the variation in the content of phlogopite (Rb and Ba) and plagioclase (Sr). 139b/89 and the "evolved" gabbros may thus derive from a particular source rock with much less phlogopite, whereas more plagioclase in the source seems to be required for most samples. The Sr content of lherzolite 8838A, is e.g. 167 ppm, compared with 70 ppm for 203, giving a perfect fit for Sr in Fig. 28b. The calculated abundances for Sc and Y are significantly lower than the analysed ones. The reason for this is unclear, but may include higher contents in the source compared with the ultrabasites analysed here or too high K_Ds. The analysed compositions of U and Th are very low and analytical uncertainties have a considerable influence in the variations.

The batch melting model does not fit the major element model for the high-Al gabbro (8859D1) (Fig. 28b). This sample has, e.g., low REE contents, and cannot be fitted to any batch melting model. This fact thus invalidates the results of the major element model above. In the case of the extremely evolved enclaves (8812M and 8811A), the suggested major element melting model (12–16 % melting) is impossible to fit to any trace element model. It is not possible to generate the very high contents of REEs, Y, and Zr, and the very low contents of Cr and Ni through partial melting of a mantle source similar to 203. Using the somewhat more enriched composition of 8838A as the source with the major element models above (higher melt degrees), generally gives an even poorer trace element fit (except for Sr; Fig. 28b).

4.5.2.3.5. Fractional crystallization. Major elements

In order to test the hypothesis that the more evolved gabbros and enclaves are derived by fractionation from parental magmas similar to the most primitive basic rocks (8850, 1t, 139b/89) of the suite, fractional crystallization modelling was performed. As was indicated by the partial melting modelling above, additional fractionation of different degrees is necessary to explain the depletion in Cr and Ni, and increase in incompatible elements. The major element modelling was performed in an equivalent manner to that of the partial melting above, and is summarized in Table 10. The rock compositions in Table 8 and mineral compositions in Table 9 were utilized also here. Minor variations in the mineral compositions had little effect on the general outcome of the results.

The slightly more evolved character of sample 139b/89, compared with 8850, can be accommodated by c. 20 % fractionation of cpx and opx. In general, in the models deriving the more evolved gabbros from the primitive dykes, cpx is the dominating fractionating phase accompanied by minor amounts of opx, olivine, and plagioclase. If the most primitive dyke (8850) is used as the parental magma, the degree of crystallization to form the gabbros 8860, 8839, and 8842A is c. 30–45 %. If, instead, 139b/89 is used as the parental magma the crystallization degrees are 10-20 %, consistent with the previous 20 % fractionation to derive 139b/89 from 8850. If the high-alumina gabbro 8859D1 is considered parental to the other gabbros, major plagioclase crystallization has to be invoked, and the fits of the models are worse. The high-Al gabbro itself seems to be possible to generate by fractionation of a

Table 10. Fractional crystallization models, Småland–Värmland basites.
Summary of the more consistent major element models. Compositions in Tables 8 and 9 were used.

Evolved rock	Parental rock	% cryst.	Calculated proportion of phases in the fractionating assemblage	Sum of sq.res.
139b/89	8850	20	72 % Cpx + 28 % Opx	4.4
8860	8850	29	64 % Cpx + 36 % Opx	1
8860	139b/89	11	56 % Olivine + 44 % Cpx	1.4
8860	8859D1	23	77 % Plag + 23 % Cpx	11.7
8839	8850	30	68 % Cpx + 32 % Opx	5.8
8839	8850	46	45 % Cpx + 30 % Opx + 25 % Plag	2.8
8839	139b/89	12	63 % Cpx + 32 % Opx + 5 % Olivine	5.5
8839	8859D1	30	84 % Plag + 9 % Cpx + 7 % Olivine	5.2
8842A	8850	31	81 % Cpx + 19 % Olivine	0.5
8842A	8850	33	79 % Cpx + 21 % Opx	1.7
8842A	8850	35	75 % Cpx + 18 % Ol + 7 % Plag	0.3
8842A	1t	17	73 % Olivine + 27 % Cpx	6.4
8842A	139b/89	18	62 % Cpx + 38 % Olivine	10.4
8859D1	8850	37	50 % Cpx + 50 % Opx	7.8
8859D1	139b/89	19	80 % Opx + 20 % Cpx	1.6
105/89	8859D1	46	78 % Plag + 22 % Cpx	2.9
105/89	139b/89	73	49 % Plag + 25 % Opx + 22 % Cpx + 4 % Olivine	1.4
105/89	8860	45	64 % Plag + 36 % Cpx	10
8812M	8842A	39	53 % Plag + 27 % Opx + 20 % Cpx	2.7
8812M	8842A	28	55 % Plag + 35 % Cpx + 10 % Opx	4.2
8812M	8860	43	54 % Plag + 33 % Cpx + 13 % Olivine	2
8812M	8860	57	51 % Plag + 25 % Cpx + 24 % Opx	1.1
8812M	8839	53	45 % Plag + 33 % Opx + 22 % Cpx	9
8811A	8850	70	38 % Plag + 36 % Cpx + 26 % Opx	1.7
8811A	1t	67	55 % Plag + 27 % Opx + 10 % Olivine + 8 % Cpx	4.3
8811A	139b/89	64	58 % Plag + 23 % Cpx + 17 % Olivine + 2 % Opx	1.3
8811A	8839	45	72 % Plag + 15 % Cpx + 13 % Olivine	0.8
8811A	8839	43	70 % Plag + 20 % Cpx + 10 % Opx	2.9
8811A	8860	56	70 % Plag + 17 % Cpx + 13 % Opx	0.7
8811A	8842A	52	75 % Plag + 25 % Olivine	6.7
8811A	8859D1	63	77 % Plag + 13 % Cpx + 10 %Olivine	8

combination of pyroxenes from the primitive dyke magmas.

The strongly evolved gabbro 105/89 may be derived by c. 45 % crystallization from the high-Al gabbro of 3/4 plagioclase and 1/4 cpx (Table 10). It is also possible to produce 105/89 by c. 73 % crystal removal from the dyke 139b/89, which includes 8859D1 as an intermediate step in the evolution. For the two strongly evolved enclaves (8812M and 8811A), high degrees of crystallization are calculated. These models are always dominated by plagioclase, with lesser amounts of pyroxene, mostly cpx, and occasionally olivine. For 8811A the highest degrees of fractionation are calculated if the primitive dykes are used as parental magmas (64–70 %). The proportion of plagioclase is lower and that of the mafic minerals higher, compared with models where the "evolved" gabbros are used as parental magmas. The latter give crystallization degrees of 43–56 %. Adding this crystallization to the previous one, where the gabbros were derived from the parental primitive dyke magma (8850), gives total amounts of crystallization for 8811A (from 8850) in the range 61–70 %, which is the same as calculated directly from the primitive dykes (Table 10). 8812M gives crystallizations essentially in the range 40-55 % from the evolved gabbros, similar to 8811A, but with a lower proportion of plagioclase.

4.5.2.3.6. Fractional crystallization. Trace elements

To test the major element calculations, Rayleigh crystal fractionation models based on the results of the major element modelling were calculated, using the NewMelt module of the Newpet program (Clarke et al. 1994). Results are depicted graphically in Fig. 29. Fig. 29a shows the models deriving the more evolved gabbros by fractionation from the primitive ones (8850 and 139b/89). The composition of sample 139b/89 is consistent with c. 20 % crystallization of two pyroxenes as indicated by the major elements above, except for Rb. The Rb content of 8850 is higher than in 139b/89 (80 and 24 ppm, respectively), which is inconsistent with an incompatible behaviour. Similarly, for the gabbros, much higher Rb contents are calculated compared with that actually present in these rocks. If 139b/89 is considered as parental to the gabbros, the results are consistent also for Rb. On the contrary, calculated Ba contents appear to be somewhat too low, whereas Sr are more consistent. These variations in LILEs are probably related to variable degrees of enrichment in the original mantle source that was tapped, as was suggested by the partial melting modelling above. 8850 is enriched in Rb compared with the other rocks, and should thus come from a source slightly richer in this element. Calculated contents of Sc, Y and Zr (except for 8860) are usually lower than the actual rock analyses, and may be ascribed to slightly too high K_Ds and/or minor crustal contamination. Variations in U and Th are probably enhanced by the low concentrations, close to the detection limits. Cr, which is largely controlled by cpx, is reproduced well, whereas calculated Ni contents are too high. This seems to indicate that olivine has been more important as a fractionating phase than estimated by the major element models, since olivine has the highest K_D for Ni. Another possibility is that the K_Ds used for Ni in olivine, and especially cpx (15 and 5, respectively), are too low, since the latter is the dominating phase. They were chosen as intermediate in the wide K_D-variation reported by Rollinson (1993). By inserting higher $K_D^{cpx/melt}$(Ni) (10–14), the analytical data are approached closely.

Fig. 29b shows fractional crystallization trends calculated on the basis of the major element models for the most evolved basic rocks in the area. The large discrepancies clearly show that the major element models in these cases are not valid. The high-Al gabbro (8859D1) cannot be derived by simple fractionation from a parental magma similar to the primitive dykes. The contents of, e.g. REEs, are much too low. One possible explanation may be that this rock has assimilated substantial amounts of restitic crustal material strongly dominated by plagioclase, and thus diluted the original composition. This process should, however, lead to enhanced Eu and Sr contents which is not observed. The strongly evolved gabbro 105/89 cannot be derived from the high-Al gabbro, as was suggested above. 75 % crystallization from 139b/89 gives better results. Somewhat too high HREEs and Cr indicate that a slightly higher proportion of cpx in the fractionating assemblage is required. Ni should also be removed more thoroughly, by more olivine or higher $K_D^{cpx/melt}$(Ni). Thus, the high-Al gabbro (8859D1) cannot be obtained as an intermediate step in this evolution.

The strongly evolved enclave magmas are much too high in REEs, Zr and Y to be derived either from the primitive dyke magmas or the more evolved gabbros, by the fractionation degrees suggested in the major element modelling above (Table 10). Extended fractionation of the same assemblages to 80–90 % from the "evolved" gabbro magmas reproduces the composition of the enclaves fairly well (Fig. 29b), except for U, Th, V, Cr, and especially Ni. This means that the enclave magmas represent c. 10–15 % residual melt from an original primitive magma, such as sample 8850. The discrepancies for V, Cr, and Ni can be accounted for by somewhat more cpx in the fractionating assemblage, and perhaps somewhat higher $K_D^{cpx/melt}$(Ni) as indicated for the gabbros above. Furthermore, if e.g. gabbro 8860 (instead of 8842A) is used as the parental magma, Cr and Ni are reproduced much more closely, because of the lower initial contents. Thus, slight variations in the parental compositions and/or the fractionating assemblage can explain the variations in the transition elements. U and Th, however, cannot be accounted for in this way and seem to indicate lower degrees of fractionation (c. 50 %), more in concert with the major element models. Due to the low contents close to their detection limits, the analytical uncertainty of U and Th is high, and possibly too high in the parental magmas. Although admittedly speculative, most of the above evidence indicates that the enclaves represent samples of very highly differentiated magmas of the basic suite. Late to post magmatic modification of the enclave chemistry by exchange with the host granitoids (e.g. Petrik & Broska 1989, Bédard 1990, Christiansen & Venchiarutti 1990, Orsini et al. 1991, Zorpi et al. 1991, van der Laan & Wyllie 1993, Elburg & Nicholls 1995, Stimac et al. 1995) may, however, also have contributed to some degree.

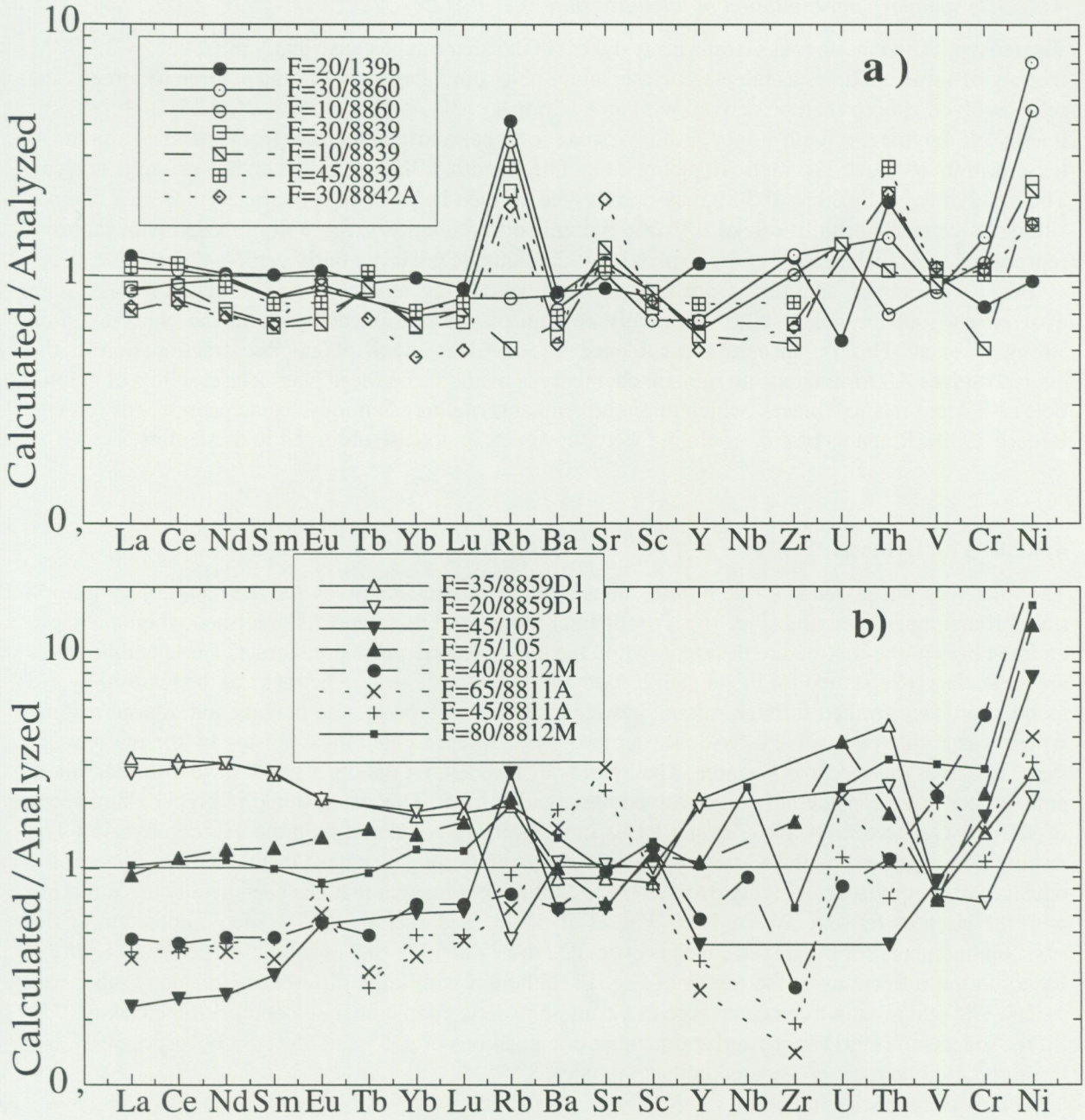

Fig. 29. Closed system (Rayleigh) fractional crystallization models for the basic SVB rocks of this study. Rayleigh fraction ation is described by $C_L/C_0=F^{(D-1)}$ (e.g. Rollinson 1993), where C_L is the concentration of an element in the liquid, C_0 is the concentration of an element in the parental liquid, F is the fraction of melt remaining, and D is the bulk distribution coefficient of the fractionating assemblage. The most appropriate models from the major element modelling (Table 10) was used in the calculations. K_Ds were taken from the compilation by Rollinson (1993). Generally, the primitive dykes (8850 and 139b/89) were used as parental magmas. a) The trace elements are consistent with the slightly less primitive 139b/89 being derived from the most primitive 8850 by c. 20 % crystallization of pyroxenes. There is a relatively good fit for the "evolved" gabbros calculated as daughter magmas of 8850 (30-45 % crystallization, e.g. F=30/8839) and 139b/89 (10 % crystallization), except for Rb and Ni, as suggested by the major element models. b) It is not possible to derive the high-Al gabbro (8859D1) from a parental magma similar to the primitive dykes. F=45/105 and F=75/105 refer to derivation of 105/89 from 8859D1 and 139b/89, respectively. F=40/8812M represents 40 % crystallization to 8812M with the "evolved" gabbro 8842A as parent. F=65/8811A represents 65 % crystallization from 139b/89 to 8811A, while F=45/8811A is 45 % crystallization from the "evolved" gabbro 8839. F=80/8812M denotes 80 % crystallization of 8842A to 8812M. The models calculated from the fractionation degree derived in the major element models (Table 10) do not fit the evolved enclaves. Extended fractionation to >80 % gives a somewhat better correspondence. Further discussion in the text.

4.5.2.3.7. Summary interpretation of the basic suite

The most primitive basic rocks (some basic dykes) in the area can be consistently modelled by 25–30 % melting of similar sources as the plagioclase-spinel-phlogopite lherzolites found at three localities. The more evolved gabbros can be derived with an additional c. 30–45 % fractional crystallization of dominantly clinopyroxene, with minor orthopyroxene, olivine, and plagioclase, from magmas similar to these primitive dykes. The high-Al gabbro cannot be fitted into this evolution and its origin is unclear. The highly evolved gabbro 105/89 may possibly be derived by c. 75 % crystallization from a composition similar to the primitive dyke 139b/89. Extreme differentiation (>80 % from the evolved gabbros) reproduces the geochemistry of the evolved mafic magmatic enclaves fairly well.

Fe-Ti oxides, and apatite are not part of the fractionating assemblage. The enclaves and more evolved parts of the basic suites commonly contain plagioclase phenocrysts, in the enclaves often strongly zoned. This is petrographic evidence in accordance with plagioclase fractionation at the evolved stages. Unfortunately, no mineral chemistry is available on these plagioclases. Clots of amphibole also occur in some places, which might be remnants of altered clinopyroxene phenocrysts (cf. e.g. Bédard 1990). Remants of cpx or olivine were, however, in no case observed in these clots.

4.5.2.4. The hybrids

The relatively linear trends in the hybrid suites strongly suggest that they are the result of hybridization through magma mixing (Fig. 15). Two distinct mixing trends can be distinguished where the basic endmembers in the mixing are different, while the silicic endmembers are similar. These endmembers are most clearly separated for incompatible elements in the basic suite. The rocks of the Kårtorp hybrid association have formed through mixing between a Filipstad type granite magma and a basic magma which was highly evolved and residual ('lamprophyric'), represented most closely by the mafic magmatic enclaves that occur in the area. The hybrids in Tiveden, on the other hand, have a similar silicic endmember but a considerably less evolved basic endmember. This has resulted in higher abundances of TiO_2, P_2O_5, Sr, Zr, Hf, Nb, Zn, and REEs in the Kårtorp compared with the Tiveden hybrids. The mixing trends defined by the Kårtorp hybrid plutonics thus strongly suggest that the composition of the enclaves truly represents a highly evolved basic endmember magma that has been available for mixing with the granites (cf. e.g. Wiebe 1996, Poli et al. 1996, Wiebe et al. 1997). The composition of the basic endmembers for the mixed suites is estimated to be 48–50 % SiO_2 for both Tiveden and Kårtorp, based on the inflections in the trends of Fig. 15, although with large differences for many other elements. The two mixing trends converge to a common silicic endmember at a compsition close to 70 % SiO_2. Andersson (1991) suggested endmember compositions of c. 55 and 65 % SiO_2, respectively, but those reported here are considered better estimates.

Some discrepancies include:

a) much lower Sr contents in the enclaves compared with that required by an endmember in the Kårtorp trend (Fig. 15). Most of the Rayleigh fractional crystallization models yield, however, Sr contents in the range 350–500 ppm. This is highly dependent on starting composition since the bulk distribution coefficient generally is close to one, but indicates that the model calculations could reproduce also the Sr composition of the Kårtorp basic endmember (c. 550 ppm) fairly good. The low Sr contents measured in the enclaves are therefore attributed to late stage fluid exchange with the surrounding granitoid, related to the hydrothermal alteration of plagioclase.

b) K_2O and Rb show anomalously high contents in some of the enclaves (Fig. 15). This is probably also the result of late to post magmatic fluid exchange with the host granitoid (cf. e.g. Petrik & Broska 1989, Bédard 1990, Christiansen & Venchiarutti 1990, Orsini et al. 1991, Zorpi et al. 1991, Elburg & Nicholls 1995, Stimac et al. 1995), associated with the widespread formation of biotite and amphibole in the enclaves.

c) The Tiveden hybrids have higher contents of especially Ba and Eu than required by the mixing relation. Since some of them even display positive Eu-anomalies (Fig. 17), this is attributed to accumulation of feldspar components. This is also reflected in higher contents of Al_2O_3 and Na_2O. There is unequivocal petrographic evidence of cumulus textures in these rocks. Subhedral to euhedral plagioclase tables, as well as even subhedral large K-feldspars lie closely packed with an interstitial mass of

quartz and biotite. The reason for this feldspar accumulation is presently not known, but it may even involve restitic feldspar. Apart from this departure, the Tiveden hybrids follow the mixing trends.

d) In the case of Zr and Hf, however, a basic endmember more enriched in these elements than available in the TVZ-Tiveden basic rocks is required to match the Tiveden hybrids (Fig. 15). The composition of the enclaves indicates that such an intermediate endmember should be produced during fractionation, although not sampled by the rocks in the present data set. Alternatively, also zircon accumulation in the hybrid rocks has to be invoked.

The bulk of the geochemical data are in strong support for a mixing origin for the intermediate rocks in this study. A plutonic mixing which took place in the lower-middle crust and formed large volumes of magma. Analogous rocks occur in southern Östergötland, Småland, and probably elsewhere but unrecognized as hybrids, as was discussed in a previous preliminary paper (Andersson 1991). Plutonic magmatic hybridization (mixing) is a major rock-forming process which has been neglected to a large degree in the past. Although occasionally proposed earlier (e.g. Wager et al. 1965) this process has only recently begun to receive proper attention (e.g. Goldie 1978, Hibbard 1981, 1991, Whalen & Currie 1984, Reid et al. 1983, Reid & Hamilton 1987, Hyndman and Foster 1988, Lindberg & Eklund 1988, Zorpi et al. 1989, Barbarin 1989, 1990, Larsen & Smith 1990, Sabatier 1991, Barbarin & Didier 1992, Castro et al. 1995, Collins 1996, Poli et al. 1996), and has even entered the scene as a specific type of granitoid (H-type) in classifications (Barbarin 1990, Castro et al. 1991).

4.5.3. Concluding discussion on the origin of the Småland–Värmland belt rocks

The regionally extensive high magnetic anomalies in the SVB, e.g. Tiveden, and large areas in northeastern Småland and southern Östergötland (e.g. Persson 1985, 1989, Eriksson & Henkel 1994), which can be broadly correlated with intrusive rocks of intermediate compositions (quartz monzonites to monzodiorites), may represent relatively deeper sections through the batholith, compared with areas of lower regional magnetic anomalies. They should thus often have been tectonically uplifted in relation to areas with lower degree of magnetism. This type of relationship is quite obvious for the eastern Tiveden area, where the eastern block most probably has moved down in relation to the western, along the Aspa fault zone (A. Wikström pers. comm. 1996). The intermediate rocks are here suggested to result from extensive plutonic mixing in the deep crust between the voluminous mantle-derived basic magmas underplating likewise voluminous crustal melts (SVB granites). The crustal melts were generated from lower crustal protoliths of mainly early Svecofennian age and dominantly tonalitic-granodioritic composition, in response to the heat advected from the underplated mantle magmas. Whether the mixing occurred already partly in the lower crustal regions or mainly during rise and emplacement, is presently not clear.

Cruden et al. (1995) showed that under the appropriate rheological conditions thorough mixing can occur between silicic and entrained basic magmas during flow in channels on the way to their final emplacement. This is mainly dependent on the viscosity and density contrasts in the system at the time of buoyant rise of the granitoid magma. Progressively increasing entrainment of basic rocks within the rising crustal magma facilitates more extensive mixing (Cruden et al. 1995). In rising convecting two-magma diapirs, coupled circulation (i.e. the magmas convect together, rather than separate) and mixing is enhanced by low contrasts in viscosity and density between the magmas, as well as a low average density relative to the surrounding crust (Weinberg 1992). Magma mixing and coupled circulation are mutually reinforcing processes that may lead to complete chemical homogenized hybrid magmas (Weinberg 1992).

Initially, entrainment of basic magma in the SVB-granites was limited, as evidenced by the limited mixing in e.g. TVZ, where the basic rocks are set in relatively silicic granites, perhaps because smaller volumes of the basic magmas were able to interact with the uppermost parts of the overlying crustal melt layer. Similarly, scattered enclaves are also evidence of little entrainment and thus chilling of the basic magma in "droplets" distributed in the granitoid. With time and continued supply of more mantle magma to the underplate, more crustal material melts. Higher temperatures in the crustal melts lower the viscosity contrasts, which is followed by increasing entrainment and mixing, giving rise to the homogenized hybrid areas in the SVB.

The lithological structure of the SVB as proposed here with more silicic rocks in the upper parts and increasing amounts of hybrid (mixed) rocks with depth, suggests that the first melts to escape from the stratified lower crustal magma system were the uppermost most silicic and unmixed parts. These entered the "conduits" first and were evacuated to higher levels before the lower more basic parts. The most silicic parts of the SVB only contain few scattered mafic enclaves, testifying to little mafic-felsic magma interaction. In areas of Filipstad type granites with compositions generally below 70 % SiO_2, such as, e.g., in the area south of Kårtorp, enclaves occur more abundantly. Many of these enclaves seem to have formed by intermingling and mixing of strongly evolved basic rocks, and the coarse porphyritic Filipstad granites. As successively more basic magma was entrained into the channelways, more mixing during transport was possible and homogenized hybrids were produced. Since the processes were continuous, the hybrid magmas were generally emplaced below the more silicic magmas, which might have acted as viscous caps in the middle crustal magma reservoirs. Mafic enclaves are uncommon in areas of hybrid rocks in accordance with the predominance of mixing over mingling processes. The hybrid rocks have formed through mixing between crystal mushes of silicic SVB (Filipstad type) magmas and basic magmas in different stages of evolution (see geochemistry section above; cf. Poli et al. 1996). The Kårtorp hybrids result from mixing with a strongly evolved basic endmember, similar in composition to that recorded by the scattered mafic enclaves in the same general area, while the Tiveden hybrids have a less evolved character of the basic endmember. This indicates that the basic rocks involved in the Kårtorp/enclave mixing system represent a highly differentiated portion of the underplated magma system, probably in its uppermost part (cf. Wiebe 1996).

If the low-magnetic, more silicic areas of SVB generally represent higher levels of intrusion, the basic rocks occurring in such areas should have been emplaced as entrained fragments of the underlying basic underplate in the granitic source region. TVZ represents such an area, as was also suggested by Wikström (1987), where also ultrabasic fragments have been entrained and brought to their present position by the SVB-granitoids. These mantle fragments must have been carried from their source regions in the upper mantle by the underplated basic magmas and become accidentally entrained in the silicic intrusives, presumably at relatively early stage. The non-refractory character of the fragments indicates that they represent xenoliths of the uppermost mantle that was unmodified by the melting event that produced the basic rocks which brought them into the crust. In the TVZ, mixing of the basic and silicic magmas is limited and local in nature, and interaction is dominated by mingling processes, which supports the concept of minor amounts of basic magma entrained in a much cooler and larger volume of silicic magma (cf. Sparks & Marshall 1986, Frost & Mahood 1987, Fernandez & Barbarin 1991). An area similar to TVZ, containing associated basic rocks and Filipstad type granites with relatively low-magnetic characteristics, occurs on the Linköping SW mapsheet (Persson et al. 1981, Wilson et al. 1986).

The Kårtorp area (and areas further south into the mapsheet Linköping NE; Gorbatschev et al. 1976) may represent an intermediate level between, e.g., TVZ and Tiveden, where only the uppermost part of the highly magnetic hybrid rocks appear at the present erosion level. The concentration of highly magnetic, intermediate to basic rocks at Kårtorp may indicate a site of upward flow in the batholith. What we see here is probably the top of the first entrained most evolved basic magmas, mixed with the granitic layer during rise. Going downwards in the Kårtorp area one would thus expect to encounter hybrid rocks formed from less evolved basic magmas and perhaps partly refractory crustal material (cf. chapter 4.5.2.4.), similar to those we see in Tiveden. The highly silicic SVB-granite (Växjö type) occupying a central position in the Kårtorp association, may be remnants of the slightly earlier intruded unmixed granites, which have acted as a cap and forced the hybrid magmas sideways.

Preliminary hornblende barometry (Hammarstrom & Zen 1986, Hollister et al. 1987, Johnson & Rutherford 1989, Schmidt 1992) on the SVB rocks of Tiveden and Kårtorp, which contain the appropriate mineral assemblages, suggests middle crustal intrusion depths of 16-25 km. Barometric studies on the SVB-granitoids must, however, be correlated with tectonic kinematics, contact metamorphic assemblages of the country rocks, distribution of high-magnetic intermediate rocks on a regional scale etc., to obtain reliable differences in intrusion depths in different areas. Recently, Andersson (1997b) has calculated temperatures and pressures from the upper amphibolite to granulite facies metamorphic assemblages close to TIB intrusions in this region, and obtained essentially the same general range in depths, consistent with their interpretation as contact-related. No hornblende data are at present available from the TVZ which, in this model, is suggested to represent a slightly higher crustal intrusion lev-

el compared with Tiveden and Kårtorp.

The overall plate-tectonic environment during the formation of the SVB (and TIB) is not clear-cut. Some authors have previously favoured a model where the rocks were formed in an andino-type magmatic arc during subduction (e.g. Nyström 1982, Wilson 1982), whereas extensional ensialic tectonism has been proposed by e.g. Wilson et al. (1985), Johansson (1988), and Öhlander & Zuber (1988). Recent geophysical data indicate that Postsvecofennian extension along deep crustal detachment zones was active in response to the overthickened Svecofennian crust, formed during the early Svecofennian collisional event (Korja et al. 1993, Korja & Heikkinen 1995). Such extensional collapse may have been instrumental in the generation of the mantle-derived magmas that underplated the crust and caused the lower crustal melting and formation of the Transscandinavian Igneous Belt granitoids and volcanics (Korja et al. 1993). This model adds the interesting aspect of extensional delamination along deep listric shear zones as an important factor in magma generation and intrusion. In the southern part of SVB, in central Småland, the essentially E–W striking Åsene shear zone can be correlated with a major jump in Moho depth, indicating c. 10 km relative uplift of the southern block (Guggisberg & Berthelsen 1987, Guggisberg et al. 1991). This may be one expression of this extensional delamination tectonics, inducing astenospheric upwelling and mantle and crustal melting (Beunk et al. 1996). One drawback of this model is perhaps the very scarce occurrence of basic dykes associated with the TIB, while numerous such dykes are associated with the later anorogenic extension-related rapakivi complexes. However, such dykes are not entirely absent and occur, e.g., in the Tjällmo–Vättern zone discussed in this study. The low frequency of basic TIB-dykes can be explained by the close temporal association of the TIB with the infracrustal magmatism ("late-orogenic" granites) formed in response to the crustal thickening. The implication is that the crust that was underplated by the mantle-derived magmas was still relatively hot and ductile, which prevented major dyke swarms from reaching upper crustal levels. The accumulating basic underplated magmas were therefore essentially confined to the lower crust, where they induced voluminous melting and granitoid production. The dykes that occur were intruded late, shortly after the consolidation of the granitoid SVB mass, and represent the waning stages of intermittent basic injections in the crust during this magmatic episode. In conclusion, most evidence - both chemical and structural - appears to favour an extensional environment for the TIB, in a crust that was not thermally relaxed after the previous collision event.

5. The Fennoscandian rapakivi granite complexes

The classical Fennoscandian rapakivi complexes of the Subjotnian period comprise a number of batholiths and smaller plutons extending from Russian Karelia in the east to central Sweden in the west (Fig. 30). There seems to be a systematic geographical distribution of crystallization ages of the complexes. Excluding the Salmi batholith, the complexes become progressively younger westwards (Fig. 30). The major batholiths are, from east to west: Salmi (and Uljalegi; 1.56–1.53 Ga), Wiborg (1.65–1.61 Ga), Laitila (1.57–1.54 Ga), Vehmaa (1.57 Ga), Åland (1.58–1.57 Ga), Nordingrå (1.58 Ga), and Ragunda (1.51 Ga) (Vaasjoki 1977, Vaasjoki et al. 1991, Suominen 1991, Neymark et al. 1994, Welin & Lundqvist 1984, Persson 1995, Amelin et al. 1997). Minor intrusive rapakivi complexes in southern and western Finland include the Ahvenisto (1.64–1.63 Ga) and Suomenniemi (1.64 Ga) satellites on the northern margin of the Wiborg batholith, and the Onas (1.63 Ga), Bodom, Obbnäs, Kökarsfjärden (1.57 Ga), Fjälskär (1.58 Ga), Reposaari (1.58 Ga), and Siippy (1.56 Ga) plutons (Vaasjoki 1977, Vaasjoki et al. 1988, 1991, 1993, Suominen 1991, Idman 1989). The present study deals with 5 of the 7 minor Subjotnian plutonic complexes in Sweden, namely from southeast to northwest: the Rödö, the Mårdsjö, the Nordsjö, the Mullnäset, and the Strömsund complexes, and their associated dyke rocks (cf. Figs. 30, 31). The petrogenesis of the Subjotnian Strömsbro complex, further south (Fig. 30), is discussed in Andersson (1997a). The pluton which is only outcropping at some small skerries off the coast of Västerbotten county (Bonden; Nilsson & Kero 1989) is not included in the study. The intrusion ages of five of the complexes have been determined according to the U-Pb zircon method of dating, and the determined ages range from 1526 to 1497 Ma (see chapters 6.4.1., and 7.4.1 below, and Andersson 1997a). Recently, also the small 1.47 Ga Noran granite intrusion in central southern Swe-

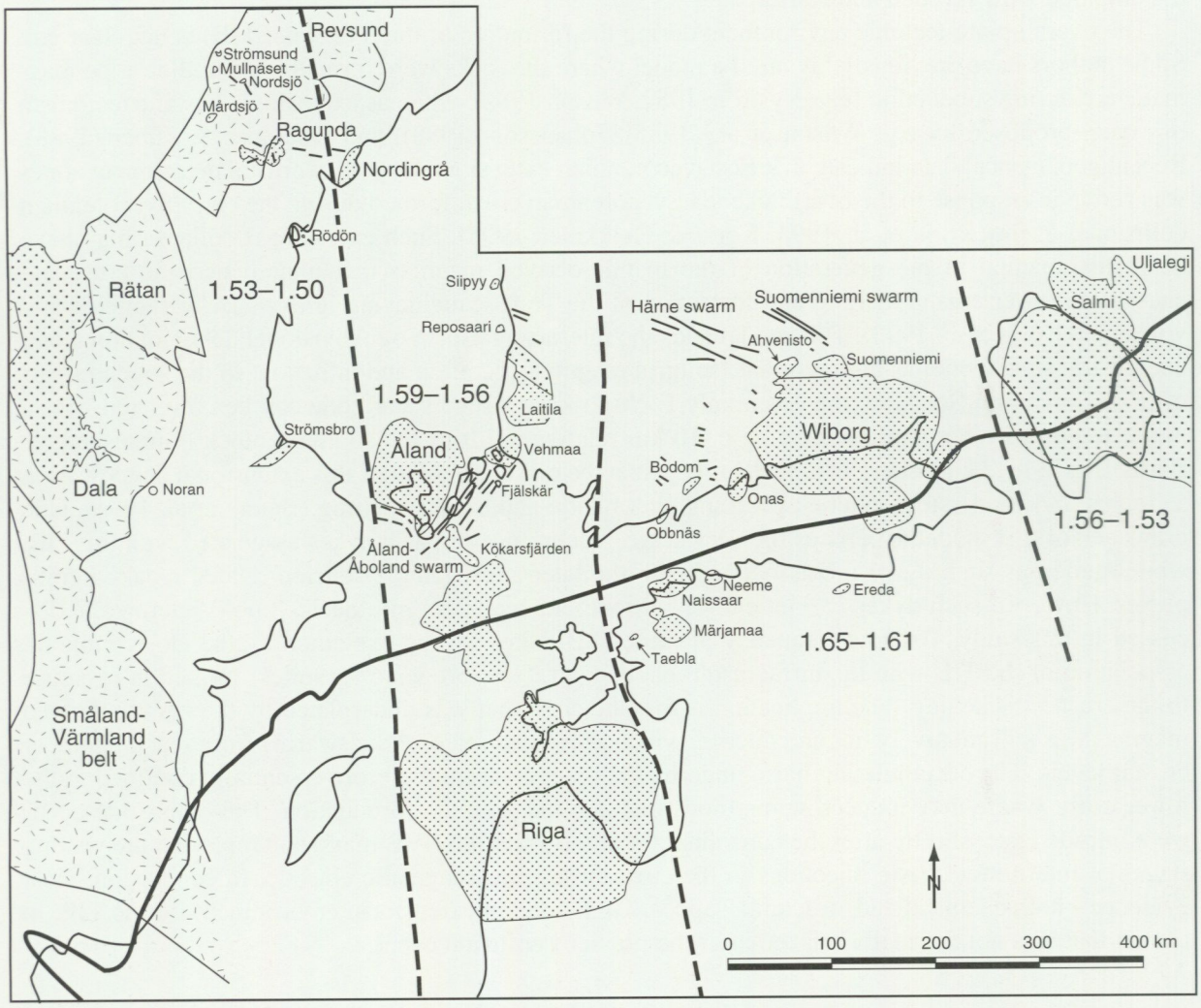

Fig. 30. Distribution in space and time of the Fennoscandian rapakivi complexes. Densely stippled: Rapakivi complexes, lightly stippled: Jotnian sedimentary rocks (>1.26, <1.50 Ga). Thick solid line marks the northern limit of the Palaeozoic platform cover rocks. The Transscandinavian Igneous Belt (TIB) is outlined in the west. The TIB have been subdivided into the Småland–Värmland belt, the Dala province, the Rätan batholith, and the Revsund intrusive suite. Apart from at Salmi in the east, a systematic younging of the rapakivi complexes to the west, is apparent. The map is prepared from various sources including Lundegårdh et al. (1984), Lundqvist et al. (1990), Gaál & Gorbatschev (1987), Rämö (1991), and Koistinen et al. (1994). Sources of age data are found in the text.

den has been related to the Fennoscandian rapakivi magmatism (Claesson & Kresten 1997).

Beneath the Phanerozoic cover of the east-European platform in the Baltic states, several Subjotnian complexes have been identified in drillcores (Kirs et al. 1991), among them the huge Riga batholith (1.58 Ga), and some small plutons in northern Estonia (Ereda, Taebla, Märjamaa 1.63 Ga, Naissaare 1.62 Ga; Rämö et al. 1996) (Fig. 30). Other, somewhat younger, anorogenic granitoids (generally not classified as Subjotnian or rapakivis) are present within and at the margin of the Svecofennian domain in SE Sweden; the Götemar (1.40–1.35 Ga), the Blekinge (1.45–1.40 Ga), and the Vaggeryd (1.23–1.20 Ga) suites (e.g. Åberg 1988, Johansson 1990). The rocks of these suites generally lack the textural characteristics of rapakivi granitoids, but are geochemically similar. The granitoids and silicic volcanics belonging to TIB II (cf. chapter 3) in Dalarna county, partly have both textural and geochemical similarities with the typical rapakivis (e.g. Hjelmqvist 1966, Ahl 1994, Ahl et al. in prep.). They are classified as Subjotnian as they form basement for extensive Jotnian sediments but are slightly older compared with the classical rapakivi complexes, c. 1.70–1.68 Ga (Lee et al. 1988, Lundqvist & Persson 1996, Ahl et al. in prep.). The Dala igneous province seems to be an area where the character of the magmatism changes with time from an earlier (TIB I) generally I-type to a later (TIB II) A-type (Ahl et al. in prep).

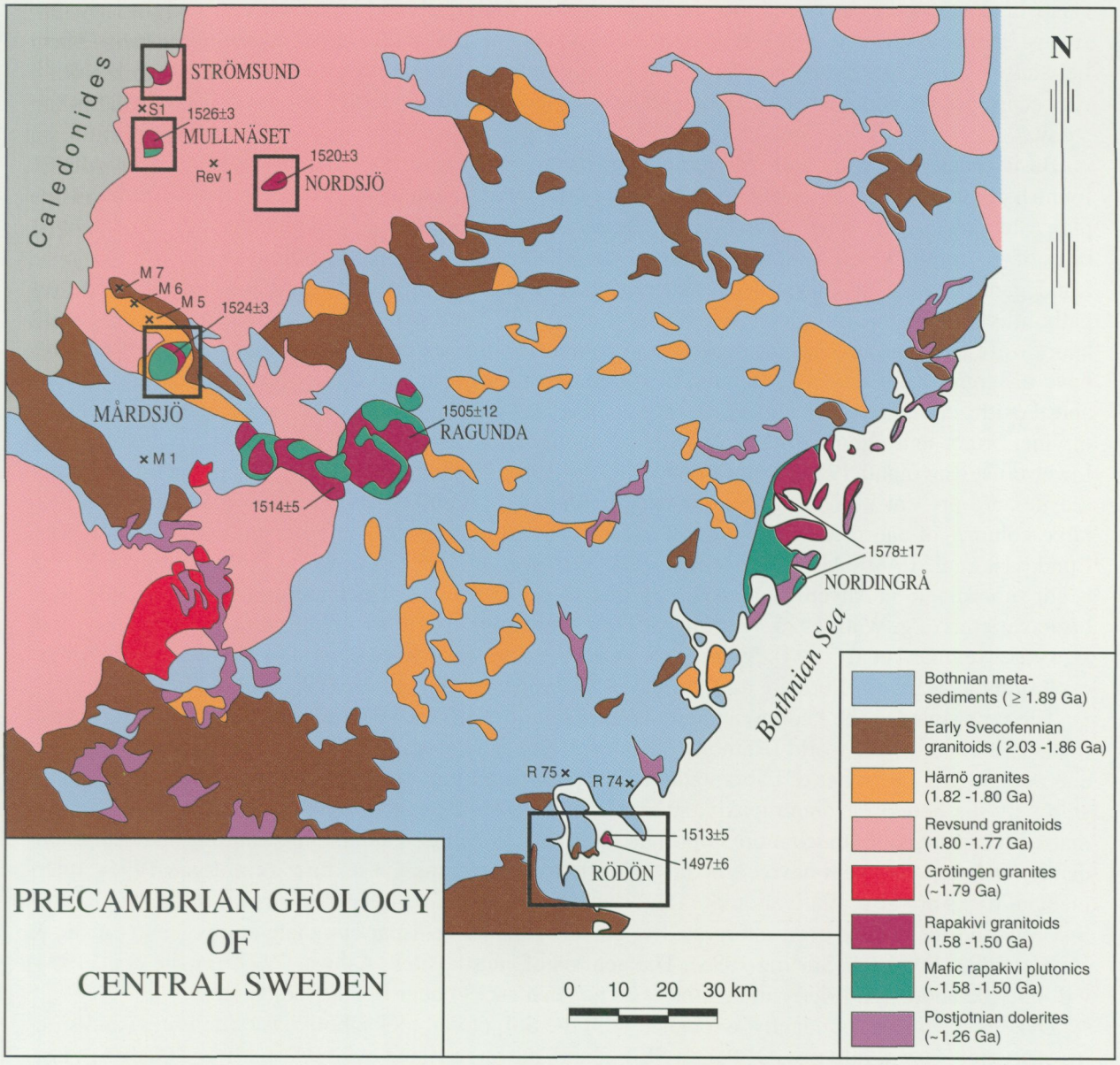

Fig. 31. Precambrian geology of central Sweden. Modified after Lundegårdh et al. (1984) and Lundqvist et al. (1990). Ages after Welin & Lundqvist (1984), Welin (1994), A. Persson (pers. comm. 1997), and this work. Frames outlines Figs. 32 and 55. The position of Fig. 31 is shown in Fig. 1.

Geochemically (e.g. Vorma 1976, Rämö & Haapala 1995) the rapakivi granitoids in the Fennoscandian suite belong to the anorogenic type of silicic magmatism, with generally higher contents of Si, K, F, Rb, Zr, Hf, Ga, U, Th, Zn, and the REEs (except Eu), as well as high K/Na, Fe/Mg, and Ga/Al ratios than average granite. Low contents of Ca, Mg, Al, P, and Sr are typical (Sahama 1945, Kornfält 1976, Vorma 1976, Haapala 1977, Nurmi & Haapala 1986, Rämö 1991). The youngest, and most evolved silicic phases, often show lowered K/Na ratios and strong enrichments in e.g. F, Ga, Rb, Th, U, Nb, and Sn, and depletions in Ba and Sr (Vorma 1976, Haapala 1977, Rämö 1991, and this thesis).

The characteristics of the rapakivi texture have been summarized by Vorma (1976): i. the ovoidal shape of alkali feldspar insets, 3–4 cm and more in diameter. ii. mantling of the ovoids by oligoclase-andesine shells, 1–3 mm in thickness; some ovoids, however, remain unmantled. iii. the ubiquitous occurrence of two generations of alkali feldspar and quartz; the idiomorphic older generation of quartz having been crystallized as high quartz. These characteristics apply to the typical wiborgitic and pyterlitic varieties that dominate the Finnish massifs, whereas the large ovoids are missing in the Swedish occurrences, except in the Rödö and to some extent Strömsbro granites. Since these strict textural characteristics are only fulfilled by a few granites worldwide, Haapala & Rämö (1992) and Rämö &

Haapala (1995) have suggested that the term rapakivi granite should be defined as any granites with A-type chemical characteristics irrespective of age that, at least in the larger batholiths, contain varieties showing the rapakivi texture. Since this definition is not strictly followed by the majority of Swedish occurrences (Lundqvist et al. 1990, and below), the relative age term Subjotnian is preferred in this study.

Basic rocks associated with silicic rapakivi magmatism occur both as plutonics and dykes. In the Finnish complexes, the basic plutonics have only minor areal extension, except in the Ahvenisto complex (Savolahti 1956), whereas in Sweden the associated basic plutonics often constitute large proportions of the complexes, e.g. Nordingrå, Ragunda, Mårdsjö, and Mullnäset (Sobral 1913, Kornfält 1976, Lundegårdh et al. 1984, Lundqvist et al. 1990, and below). The latter is also true for the Salmi and Riga batholiths (e.g. Neymark et al. 1994, Rämö et al. 1996). The basic rocks comprise gabbros (norites), anorthosites, and monzodiorites, and belong to anorthositic suites (NAM series), which presumably have differentiated from high-alumina basalt compositions to monzodiorites or monzonites, forming anorthositic cumulates (Eklund et al. 1994). The geochemical trends also suggest the removal of olivine, ortho- and clinopyroxene, of which cumulates are not observed but most likely reside in the lower crust (Savolahti 1956, Kornfält 1976, Rämö 1991, Eklund et al. 1994). Small amounts of anorthosites are present in Wiborg, Suomenniemi, Ahvenisto, Laitila (Kolinummi), and Åland, whereas large volumes of anorthosites are present in Salmi, Riga, but exposed only in Nordingrå (Sobral 1913, Lundqvist et al. 1990). Also intermediate rocks are of little areal extent in the Finnish complexes, but occur subordinate in Ahvenisto and Wiborg (the so-called tirilites, which are green even-grained more basic varieties, e.g. Wahl 1925, Hackman 1934). Monzonites occur as a major unit in Salmi (Sviridenko 1968, Neymark et al. 1994). Syenitic rocks occur as major units in several of the Swedish complexes, Ragunda, Mårdsjö, Nordsjö, and Mullnäset (Kornfält 1976, Persson 1996, and below).

The rock suites of the Fennoscandian rapakivi (Subjotnian) complexes show many similarities with rocks elsewhere in the world (Rämö & Haapala 1995). The so-called AMCG (anorthosite-mangerite-charnockite-granite) suites of Labrador and the Grenville province both have textural and chemical kinship with the Fennoscandian rapakivi suites (Emslie 1978, 1991, Ryan 1991). Anorthosites and other mafic rocks are areally much more important there than in Fennoscandia, but granitoids do occur abundantly, and some of them have exceedingly well-developed rapakivi textures (e.g. Ryan 1991). Intermediate rocks are also relatively more important in Grenville and Labrador, similar to the situation in Sweden, and these have been interpreted to contain a major feldspar cumulate component (Emslie & Hegner 1993, Emslie & Stirling 1993). The genesis of anorthosites (Ashwal 1993, Emslie et al. 1994) will only be addressed briefly in this thesis as no such rocks occur in the studied areas.

Dyke rocks occur abundantly associated with the Subjotnian rocks, both basic (dolerites) and silicic (quartz feldspar porphyries, QFPs). In SE Finland, the large Häme dyke swarm (over 200 dykes; Laitakari 1991) extends from the northernmost parts of the Wiborg area northwestwards about 250 km (Laitakari 1991). It contains, together with the spatially associated Suomenniemi dyke swarm, dominantly dolerites and minor QFPs (Rämö 1991). In SW Finland, the large (about 500 dykes) Åland-Åboland dyke swarm trends NE from SE of the Åland batholith up to the Vehmaa batholith (Lindberg et al. 1991). Also this swarm contains both basic and silicic dykes, but the overwhelming majority are dolerites. In both swarms, composite QFP-dolerite dykes occur, formed by intermingling of the basic and silicic magmas in the same conduits (Eklund & Lindberg 1992, Rämö 1991), and giving rise to numerous delicate (disequilibrium) textures (e.g. Andersson & Eklund 1994). In Sweden, only a few doleritic dykes are associated with the Strömsbro (Asklund 1939; Andersson 1997a) and Mårdsjö (K.-A. Kornfält pers. comm. 1995) complexes. Relatively more, both dolerites and silicic to intermediate dykes, are associated with the Ragunda (Kornfält 1976) and Nordsjö (Lundqvist et al. 1990; chapter 7) complexes, and exceptionally many, and diversified, with the Rödö granite (Holmquist 1899, and chapter 6). No dykes have been found in association with the Nordingrå and Strömsund complexes. Some dykes have been found geographically intermediate between the complexes (Lundqvist et al. 1990, Lundegårdh et al. 1984). Recently, numerous dykes and small intrusions of varying composition have been found both during mapping in the field and from aeromagnetic anomalies in the areas west and south of the Mårdsjö complex (Lundqvist & Korja 1997). These have macroscopic and geochemical features suggestive of a close relation with the Subjotnian rocks.

Geophysical modelling by Laurén (1970) suggests that the rapakivi granite massifs constitute relatively thin sheets (<10 km) of low density material with a deeper root in the margin. Elo & Korja (1993)

modified this interpretation based on gravity and magnetic studies of the Wiborg batholith. They conclude that the upper 30 km consists dominantly of several separate rapakivi granite intrusions with an intercalated thin (at 8–14 km depth) layer with relatively high seismic velocities, interpreted to represent gabbro-anorthositic rock types. Mafic underplated rocks and mantle upwelling is indicated in the lower crust beneath the low density upper crust (Elo & Korja 1993). The crust is thinner (42–46 km) in an E–W direction along the Gulf of Finland where the rapakivi complexes have intruded (Korja et al. 1993), but also in the area of the major Subjotnian complexes in central Sweden (< 50 km). The crust in southern Finland experienced Postsvecofennian extension along deep crustal detachment zones that caused this thinning (Korja et al. 1993, Korja & Heikkinen 1995), which was associated with mafic underplating, crustal fusion, and generation of the bimodal rapakivi complexes (Haapala & Rämö 1992, Korja & Heikkinen 1995).

The geophysical modeling indicates a sheetlike form of the rapakivi granite intrusions with feeder channels in the margin (Laurén 1970, Elo & Korja 1993). This shape suggests that the rapakivi magmas may have intruded by relatively rapid flow to the emplacement levels through localized channels (feeder dykes), and then spread out laterally (e.g. Elo & Korja 1993, Rämö & Haapala 1995). The silicic rapakivi magmas should then have had a relatively low viscosity to be able to follow fracture zones in the crust up to their final high emplacement levels. This is in accordance with the experimental data which show that high F contents drastically lower the viscosity of highly silicic magmas, due to depolymerization of the melt (e.g. Dingwell et al. 1985, 1993). A sheetlike form is also inferred for the Nordingrå granite, directly overlying the gabbro-anorthosites (Lundqvist et al. 1990). Aeromagnetic data from the Ragunda complex strongly suggest that the magmas have intruded in several pulses, successively younging eastwards (Lundqvist et al. 1990, Persson 1996). The large amounts of exposed basic rocks in several of the Swedish complexes compared with their Finnish counterparts are most likely the result of deeper levels of exposure, similar to many of the Labradorian examples (e.g. Emslie et al. 1994). It is also noteworthy that the granitoids in the Swedish occurrences associated with large basic components generally lack the typical coarse porphyritic ovoidal rapakivi texture, and hence are even-grained or small porphyritic (cf. Kornfält 1976, Lundqvist et al. 1990). This may be related to their relative spatial closeness to the hot associated basic rocks, where different thermal conditions prevented the ovoid growth. Furthermore, the sparse development of the rapakivi textures in the Swedish granites (except Rödön), closely associated to basic plutonics, is plausibly connected with deeper levels of exposure compared with their Finnish equivalents, since the typical rapakivi textures are thought to develop during decompression while the magma intrudes to subvolcanic levels, < 3 km (Nekvasil 1991, Eklund et al. 1996).

6. The Subjotnian Rödö rapakivi complex

6.1. FIELD RELATIONS

The small Rödö rapakivi complex is situated in eastern central Sweden, as indicated on Fig. 31. The area around the Rödö rapakivi granite massif has been mapped in some detail (Foldout map). The mapping was concentrated on the granite massif itself and its nearest surroundings, and on and around the large number of reported dyke occurrences believed to be associated with the massif (Holmquist 1899, Lundqvist et al. 1990, Th. Lundqvist unpubl. field notes). The map in Fig. 32 shows the extension of the area where the assumed rapakivi related dykes occur. It covers an area of approx. 12 km E–W, and 7 km N–S. Since a large part of the area is water-covered, numerous dykes can be assumed to be hidden below sea level. On this map (Fig. 32), and on the close-up map of the central Rödö area (Foldout map), dykes have been indicated that may be assumed to be part of the same dyke system on structural, geochemical and petrographic grounds.

The *Rödö granite* itself is a coarse porphyritic, red granite (SiO_2 = 68.2–74.7 %). The megacrysts are large (≤ 3 cm) ovoidal K-feldspars, and rounded (≤1 cm), drop-like quartz grains. The K-feldspars are both mantled and unmantled by plagioclase, but mantled grains usually predominate. The mantles may be difficult to see, since they commonly also are brick red in colour. The thickness of these mantles varies, but is usually a couple of mm. The predominance of this mantled ovoid (rapakivi) texture

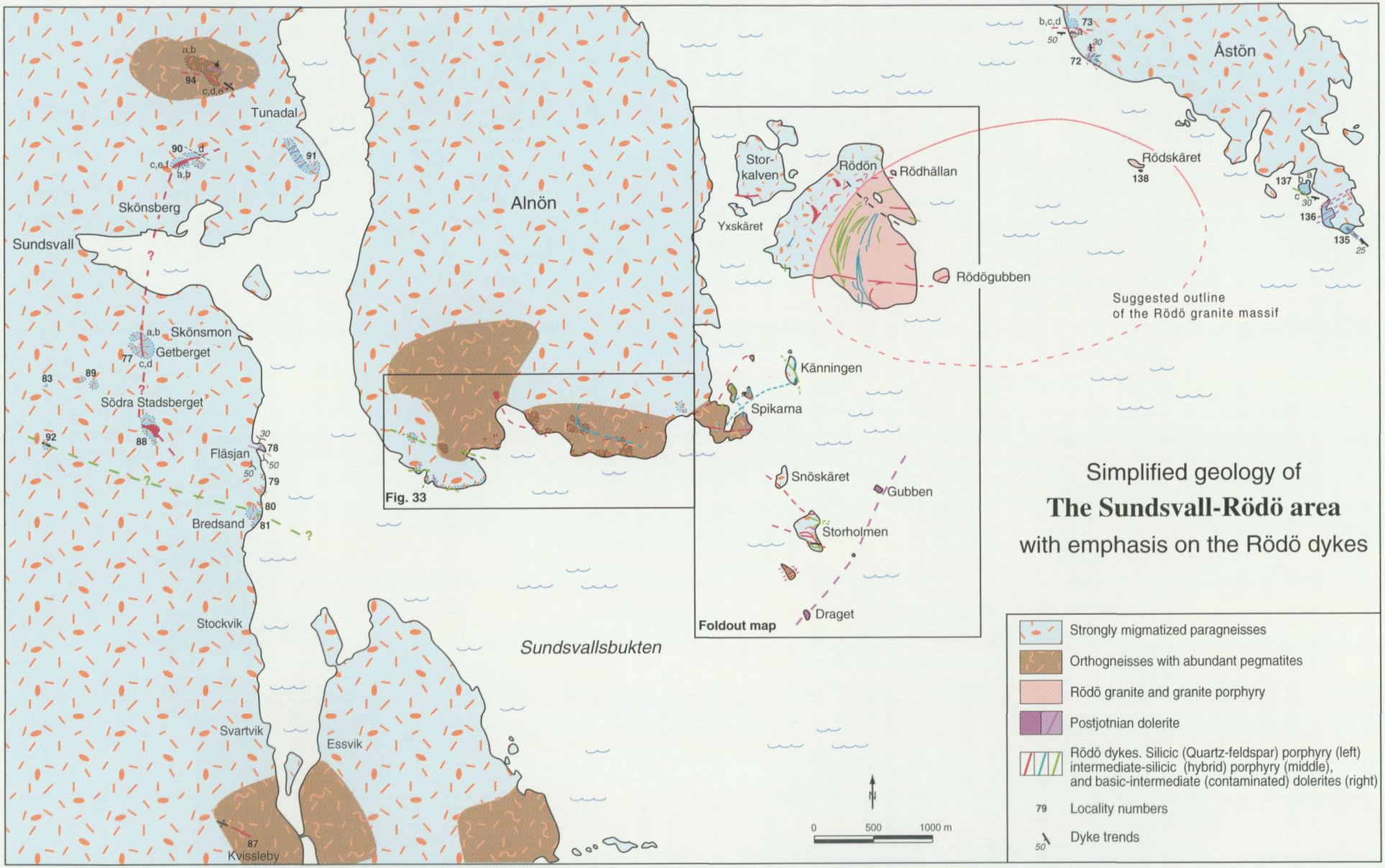
Sundsvall
Skönsberg
Tunadal
Alnön
Skönsmon
Getberget
Södra Stadsberget
Fläsjan
Bredsand
Stockvik
Svartvik
Essvik
Kvissleby
Sundsvallsbukten
Fig. 33
Foldout map
Stor-
kalven
Yxskäret
Rödön
Rödhällan
Rödögubben
Rödskäret
Åstön
Suggested outline
of the Rödö granite massif
Känningen
Spikarna
Snöskäret
Gubben
Storholmen
Draget
0
500
1000 m
Simplified geology of
The Sundsvall-Rödö area
with emphasis on the Rödö dykes
Strongly migmatized paragneisses
Orthogneisses with abundant pegmatites
Rödö granite and granite porphyry
Postjotnian dolerite
Rödö dykes. Silicic (Quartz-feldspar) porphyry (left)
intermediate-silicic (hybrid) porphyry (middle),
and basic-intermediate (contaminated) dolerites (right)
Locality numbers
Dyke trends

makes the Rödö granite a wiborgite according to Finnish rapakivi terminology, the only one in Sweden (Plate 1a) . K-feldspar and quartz also dominate the groundmass, and thus appear in two generations, which is typical for rapakivi granites (cf. Vorma 1976). The granite is strongly miarolitic, and the vugs contain crystals of quartz, calcite, feldspar, and sometimes fluorite. The size of the vugs is up to about 15 cm.

The areal extension of the granite intrusion is poorly known, since large parts of the area are water-covered and no geophysical data are available. A possible outline has been sketched in Fig. 32, suggesting an area of c. 20 km^2. The extension to the NE is indicated by the islet Rödskäret (loc. 138), which is composed of Rödö granite.

Aplitic dykes, a few cm to about two dm in width, crosscut the granite (Plate 1f). They are grey or red and very fine-grained. They often thin out and disappear into the granite, suggesting a formation as late liquids squeezed out of the granite crystal mush. *Dark schlieren* structures are common in the Rödö granite on the southern coast of Rödön (Plate 1d and e). They are stretched out, arc-like structures and consist of dominantly Fe-Mg silicates, with lesser amounts of quartz and feldspar. They are often associated with vugs and aplitic dykes.

Pillows of *granite porphyry*, from one dm to about one m in size, are distributed throughout the granite (Plate 1b). They have a finely medium-grained groundmass (coarser than the quartz-feldspar porphyries), but otherwise contain the same type of megacrysts as the granite (cf. Holmquist 1899). This type of granite porphyry also occurs as larger irregular enclaves in the granite, from a few meters to several hundreds of meters. Larger areas with coherent granite porphyry have been marked by a deeper red colour on the Foldout map. This is especially common in the higher areas of central Rödön. The granite porphyry has essentially the same mineralogy and geochemistry as the granite, and it is interpreted as a chilled marginal facies which has been disrupted and distributed into the granite magma as semisolid enclaves of variable size.

Apophyses of granite porphyry can be observed to emanate from the Rödö granite into the country rocks at one locality on central Rödön (loc. 32; Foldout map). A set of similar dykes subparallel to the granite-country rock contact also occur in the sedimentary gneiss at the southwestern shore of Rödön at loc. 25. These, however, cannot be followed into the granite due to lack of exposure. These dykes are 1 dm to 1 m wide, and also suggested to be apophyses from the granite.

Country rock xenoliths are very scarce in the Rödö granite. At loc. 12, close to the contact on SW Rödön, a few occur. They are dark angular pieces of micaceous metasedimentary rocks. No contact metamorphic hornfels assemblage is preserved in them, but they are retrograded and very chloritic. This applies to the whole contact area. No contact aureole has been found. The country rocks at the contact have been thoroughly retrogressed (or little affected by the intrusion?). This has prevented calculations of metamorphic P-T conditions during the intrusion.

The dykes can be divided into three main categories: i) quartz-feldspar porphyries (QFPs), which contain phenocrysts of quartz, K-feldspar, and more seldom plagioclase in varying amounts and sizes (red dykes in Figs. 32, 33 and Foldout map), ii) dolerites, which are more or less evolved, and/or contaminated by felsic material, usually quartz and feldspar xenocrysts (light green), and iii) hybrid porphyries, which are magmatic mixtures of the two previous types in different proportions (bluish green in Fig. 32, and with additional red dots in Fig. 33 and the Foldout map). Some occurrences of these are quite spectacular (Plate 2f).

A few localities with *composite dykes* occur. The composite dyke at loc. 12 (Foldout map) on the SW shore of Rödön is about 5 m wide. The margins consist of ca 1 m of a black dolerite, which relatively sharply turns into a 30 cm wide hybrid zone (Plate 2h). The latter transforms over 10 cm into the central almost 2 m wide QFP. Both the QFP and the hybrid zone contain enclaves of fine-grained maf-

Fig. 32. Geological sketch map of the Rödö area (based on Lundqvist et al. 1990). Rödö granite intrusion is indicated as an oval delineated in red. Blue and brown illustrate early Svecofennian country rocks. Rödö dykes are indicated as quartz-feldspar porphyries (QFPs; red), dolerites (greenish), and hybrid porphyries (HPFs; greenish blue). The proposed outline of the Rödö granite is tentative, due to the lack of exposure and geophysical data. However, the Rödö granite on the islet of Rödskäret indicates that at least the northern extent is fairly well-constrained. Dykes suggested to be part of common systems have been indicated. Three localities of the Sundsvall porphyry are proposed to form a continuous dyke system (loc. 88, 77, and 90). Frames outline areas of Fig. 33 and the Foldout map. Localities not included on these maps are included here. Only studied outcrops are indicated (outside the frames).

ic material similar to the margins, but they are smaller in the QFP. K-feldspar phenocrysts of the QFP also occur in the hybrid where they have more clearly developed plagioclase mantles. Also skeletal plagioclases can be found in the hybrid zone.

At loc. 135, on the tip of Åstholm promontory east of Rödön (Fig. 32), another composite dyke occurs. This one is at least 3 m wide, but only one contact is exposed. It consists of a slightly hybridized 0.5 m wide black marginal zone (SiO_2=67.9 %), and a several meters wide central QFP-zone (SiO_2=74.4 %). Both contain megacrysts of K-feldspar, plagioclase and quartz up to a size of two cms. The K-feldspars are sometimes resorbed and mantled by a skeletal plagioclase. The QFP contains numerous dark rounded enclaves, some tens of cms and smaller. Also these contain the megacrysts described above.

The QFPs come in several modifications. Mainly three types can be distinguished: i) one which is coarse porphyritic, with big crystals of K-feldspar, skeletal plagioclase and quartz, similar to the Rödö granite itself, but with finer grained matrix (only at loc. 55 and 112). This type also contains numerous rounded mafic-hybrid enclaves (SiO_2=59.1 %) and is closely associated with the coarse porphyritic hybrids described below (Plate 2a).

ii) The second type carries phenocrysts of slightly smaller size, generally crystals of quartz and K-feldspar less than 2 cm in diameter. This type occurs at loc. 46, 47 and 52 on western Spikarö and Lergrundet, probably forming an interconnected system (Foldout map). Hybrid, quartz and K-feldspar xenocryst-rich enclaves, c. 3 cm to 3 dm in size, occur at loc. 46 and 47 (SiO_2=63.6 %). This is the most common type of QFP, with occurrences at, e.g. loc. 96 on southern Alnön (Fig. 33), 122, 171, and 175 on Storholmen, 107 on Snöskäret, the Sundsvall porphyries, 73 on Åstön, 156 and 160 on western Rödön, and those on eastern Rödön (127b, 128, 126c, 130, 132, 133c, and 140a) (SiO_2=69.5–76.6 %). Quartz phenocrysts are small and subordinate in some occurrences (e.g. loc. 46, 47, 52, 96, and 140a). This type of QFP often contains abundant small (usually less than 5 mm) miarolitic cavities filled with mainly chlorite, calcite and quartz. Due to the abundance of chlorite in these, the rocks have a mottled appearance. The enclaves generally contain more and slightly bigger cavities with dominantly calcite, chlorite and quartz, more similar to those in the dolerites.

The localities of the silicic (SiO_2=74.7–75.7 %) so-called *Sundsvall porphyries* in the west (loc. 88, 77, and 90, Fig. 32, north and south of the city of Sundsvall) probably represent one large dyke (or perhaps a few subparallel ones), because of their strong similarities. They are yellowish red quartz-feldspar porphyries with a fine-grained matrix and phenocrysts of euhedral K-feldspar (≤1 cm) and rounded quartz (≤0.5 cm). At loc. 88 and 90 (Fig 32) the dykes are very large with widths of 150 m or more. The QFP at loc. 94 may be connected to this system.

iii) The last type has the smallest phenocrysts, generally less than 0.5 cm, usually only a couple of millimeters. These are also the most fractionated rocks of the silicic Rödö magmatism (see the geochemistry below). Examples are the presumably connected QFPs at loc. 18 and 45 on Skorven and Spikarö (Foldout map). Other examples include loc. 117f and g and 118b on Storholmsfläsjan and Norrgrundet, 144 on Rödön, 166 and 167 on Storkalven (SiO_2=71.1–77.2 %). In this group, mafic/hybrid magmatic enclaves occur only at loc. 18 and 45 (Plate 1h). They are numerous small (< 1 dm) and green to black. These QFPs usually do not contain any miarolitic cavities.

Mafic/hybrid enclaves occur only in those QFP localities described above. The enclaves are evidence of coeval, co-mingled and partly mixed silicic and basic magmas (cf. e.g. Didier & Barbarin 1991, and ref. therein)

The dolerites are usually black and very fine-grained. They are commonly very homogeneous in width, 1-3 m. Almost ubiquitously they contain some felsic xenocrysts, such as quartz or K-feldspar (Plate 2d), more or less resorbed and coated with mafic minerals or plagioclase. Sometimes a more general "monzonitization" of the dolerite into a violet-red rock of hybrid character is observed (loc. 62 on Långfläsjan and 50 on central Rödön). The dolerites contain abundant vugs, up to almost 1 dm in size, generally coated with chlorite and filled with calcite and quartz. At loc. 62 (Foldout map) small (usually < 1 dm) country rock xenoliths are found, and a few quartz lumps similar to those described by Eklund & Lindberg (1992) as xenoliths, where the feldspar component has been dissolved into the basic magma.

South of Sundsvall, two occurrences of Rödö dolerites have been indicated to belong to the same system (loc. 81 and 92), based on the strikes of the dykes. This is strengthened by petrographic and geochemical similarities. On the southern parts of Alnön (Fig. 33) a number of dyke occurrences have

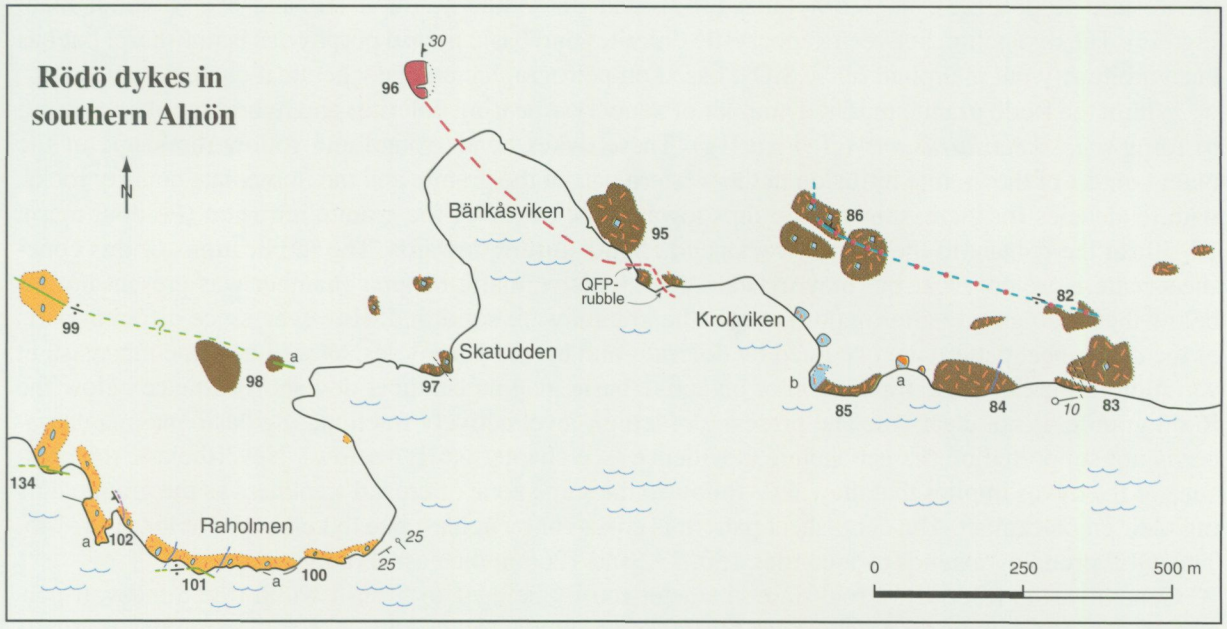

Fig. 33. Rödö dykes on southernmost Alnön. Brown is orthogneisses, blue: metasedimentary gneisses, orange: palingenic (c. 1.82 Ga) granites, green: Rödö dolerites, red: Rödö quartz-feldspar porphyries, greenish blue with red dots: intermediate hybrid porphyries, violet: Postjotnian dolerites, and dark blue: carbonatites (same legend as on the Foldout map). Only studied outcrops are included.

been indicated to be part of the same system, mainly based on their structural trends. The evidence is strongest in the case of the hybrid porphyries at loc. 82 and 86, and QFPs at 95 and 96, since the petrographic similarities are very strong in these cases (at loc. 95 only local rubble indicates the presence of a QFP).

Composite dolerite/hybrid dolerite dykes occur in some instances, characterized by a lateral zoning pattern. At loc. 115a (southern Rödön) a ca 5 m wide dyke with a 1–2 m brown marginal zone (Foldout map) is found. The margin is slightly more silicic (SiO_2 = 59.1 %) compared with the grey-green central zone (SiO_2 = 56.6 %). The transition is gradual, and both facies contain scattered xenocrysts of quartz (≤1 cm), K-feldspar (≤3 cm), and large megacrysts of skeletal plagioclase. 115b is thinner (ca 2 m). In this case the central part is browner (SiO_2 = 66.4 %; silicic hybrid porphyry) and the c. 0.5 wide margins darker (SiO_2 = 55.8 %). Numerous small dark rounded enclaves of the margin can be found in the brown central zone (Plate 2b). Megacrysts similar to those found in 115a are met with. Yet another slightly zoned dolerite-hybrid porphyry dyke occurs on Storholmen (loc. 123). It is 1.5–2 m wide and consists of a ca 1 m wide brown central zone (SiO_2 = 59.3 %) and a black (30–40 cm wide) marginal zone (SiO_2 = 61.1 %). Megacrysts of plagioclase and some K-feldspar occur mainly in the central zone.

The *hybrid porphyries* occur in two major types: i) a dark coarse porphyritic type, with large crystals of K-feldspar (around 3 cm), more or less intergrown or overgrown by plagioclase, quartz (≤1 cm), and large skeletal plagioclases. They are geochemically rather silicic (SiO_2 = 66.5–69.3 %), and very different from the other main group of hybrids. This type occurs in some spectacular occurrences on Långfläsjan, Gråfläsjan, Skorven, Spikarö and Känningen (loc. 3, 43, 44, 53, 57, 58, 68, and 112; Foldout map, Plate 2e). These occurrences form an interconnected system of flatlying dykes. The coarse QFP of locality 55 shares the same system, since it can be seen to mingle with the hybrid porphyries at loc. 55 and 57. These hybrid porphyries also contain hybrid enclaves, with more sparsely distributed megacrysts of the same type as in the surrounding hybrid porphyries (Plate 2f). These enclaves are, however, much more basic in nature (SiO_2 = 56.6–59.1 %). The enclaves often contain abundant small (< c. 1 cm) vugs, open or filled with calcite, chlorite and quartz. These vugs are characteristically concentrated in the centre of the enclaves, while the margins are devoid of them (Plate 2g).

ii) The second group of hybrid porphyries are more basic in character (SiO_2 = 61.5–64.3 %), and usually contain smaller resorbed K-feldspar and quartz xenocrysts (Plate 2c). They occur more widely, e.g. in some dykes of the cone-sheet intrusion (see below) in the Rödö granite (loc. 116c, 146c, 151h),

on western Rödön (33), on Storholmen (169), and on southern Alnön (82 and 86) (Foldout map; Fig. 33). The distinction between xenocrystic dolerites and basic hybrid porphyries is not sharp, but has been arbitrarily put at around 60 % SiO_2, based on petrographic and geochemical characteristics.

Within the Rödö granite massif a number of xenocryst-bearing dolerites and hybrid porphyries seem to form *cone-sheet intrusions* (cf. Plate 1g). These dykes bend around and follow the shape of the outer contact of the granite intrusion in the western part of the granite and the immediate country rocks, with tendencies for increasingly steep dips towards the centre of the granite intrusion (Foldout map); 10–30° at the contact to the country rocks and 55–80° further inwards. The implications of this cone-sheet pattern are not clear but may indicate that an active mafic magma chamber was present not far below the Rödö granite after major parts of the granite were solidified. However, since different parts of the cone-sheet pattern are occupied by dolerites and hybrid porphyries, as well as some inconsistent variation in the dips, the implication of an active basic magma chamber at a short distance below the Rödö granite, is not clear-cut. The presence of a high-level actively fractionating basic magma chamber is not supported by the geochemical evidence (see chapter 6.5.1.7 below). Nevertheless, the presence of the dykes implies that they have followed the same zone of crustal weakness as the granite during their emplacement. The cone-sheet pattern is cross-cut by at least one dyke of QFP at loc. 144–145. This QFP probably extends to localities 130, 132 and 126c in the east (Foldout map).

Generally, the Rödö dyke rocks are characterized by being 1 to 5 m in width (the Sundsvall porphyries are exceptional in reaching up to 150 m in width), often with a slightly irregular intrusive pattern; bended, bulging, or zigzagging, especially the silicic ones. This contrasts with, e.g. the Post-jotnian dykes in the area, which are thinner than 1 m and cut straight through the country rock.

The *country rocks* in the Rödö area consist of highly migmatitic early Svecofennian gneisses. These are dominated by *metasedimentary supracrustals of metagreywacke type* (Lundqvist et al. 1990). These metasediments are often so strongly melted that they have turned into schollen migmatites, actually dominated by the palingenic material. On the Foldout map, areas dominated (>50 %) by the *palingenic grey granites* (orange) have been separated from areas where the metasediments still are the volumetrically most important (blue). They are intimately interfingering almost everywhere, which is why this division is subjective in nature, but nevertheless regarded as relatively correct in the scale of the map. It shows the spatial distribution and very high degree of anatexis which the supracrustals in the area have suffered. The areas dominated by palingenic granite contain numerous restitic enclaves of the metasediments, from single crystals up to blocks of several meters or sometimes tens of meters, often rounded and more quartzofeldspatic than the metasediment in general. The granite contains irregularly distributed large crystals (up to 15 cm) or glomerocrysts of K-feldspar, which give it a conspicuous appearance. Locally on central-northern Rödön a grey-red finely medium-grained palingenic granite occurs (red on the Foldout map).

Orthogneisses are present in the southern parts of the area, on southern Alnön, Spikarö, Skorven, Långfläsjan, Gråfläsjan, and Storholmsfläsjan (Foldout map). These orthogneisses are very similar to the palingenic granites described above, and contain, e.g. also large K-feldspar mega/glomerocrysts, but much fewer metasedimentary enclaves. The border between orthogneisses and the palingenic granites is very difficult to establish, and perhaps artificial. The similarities in texture and structure may indicate a genetic relationship, but this is outside the scope of this paper. However, in the field the difference is sufficiently clear to enable the division to be made at the scale of the maps.

Both the metasediments (and the palingenic granites) and the orthogneisses are crosscut by a network of usually straight *pegmatitic dykes*. These are generally white and of a size ranging from a few cm to a few dm wide. The network of dykes is interconnected in three dimensions, often at right angles. Black tourmaline is ubiquitous in the pegmatites, and occasionally blue-green apatite is observed. The thin pegmatites can often be seen to thin out and disappear in the surrounding gneisses, indicating that they are of local derivation.

The *structures in the country rocks* west of the Rödö intrusion is dominated by very flat lineations (Foldout map). As the rapakivi intrusion is approached from the west the deformation increases and a pronounced, steep, foliation is developed. This foliation follows the outer contours of the Rödö granite and is interpreted as resulting from the intrusion. Discrete brittle deformational zones crosscut both the rapakivi rocks and the country rocks. These have dominantly northwesterly or northeasterly strikes and are subvertical. They have been marked with broken lines on the Foldout map, and are in general related to the tectonic action of the c. 550 Ma alkaline Alnö intrusion (Kresten 1990) 7 km NW of

Rödön. An intense alteration and dark brick-red colouring of the rock in the zones is typical, as well as carbonate veins.

Carbonatitic dykes related to the Alnö intrusion are common and the youngest intrusives in the area. They are usually some dm to a couple of m in width and greyish green or beige in colour. They strike NW- to NNW and are subvertical. Usually they are deeply weathered and form minor canyons in the shorelines, concealed by rubble. But a few are exposed and the most prominent are marked by a dark blue colour on the Foldout map and Fig. 33. At loc. 18 (on Skorven) a carbonatitic dyke is observed to crosscut the Rödö-related QFP. Similarly, at loc. 25 on southern Rödön, a carbonatite dyke is observed to crosscut the granite porphyry dykes and the metasedimentary gneisses.

Postjotnian dolerite dykes are common in the area (violet on the maps). This dolerite generation (c. 1260 Ma; Suominen 1991) is expressed as a number of one to a few dm wide subvertical dykes, some with northeasterly strikes (e.g. on Storholmsfläsjan, loc. 117e, and neighbouring islets, and Åstön, 136), and some with northwesterly strikes (e.g. on Skorven (18, 19) and Gråfläsjan (56). They are generally fine-grained ophitic olivine dolerites with variable but usually not strong alteration. In the southeastern part of the area a zone of medium-grained Postjotnian dolerites occurs, striking NE on the islets of Draget (120), Österåsen (121), and Gubben (103) (Foldout map and Fig. 32). These are probably part of a flatlying sheet, dipping gently to the east, similar to those described further north (e.g. Lundqvist & Samuelsson 1973, Larson 1980, Lundqvist et al. 1990). It may even be connected to the large (diameter of 100 km) lopolith in Ångermanland, continuing southwards to the dolerites south of Sundsvall Bay (Lundqvist et al. 1990). The nearby thin subvertical dykes may be feeder dykes (or apophyses) to the sheet. Such flatlying sheets are typical of the Postjotnian magmatism (central Scandinavian dolerite group; Gorbatschev et al. 1979) in central Sweden (Lundqvist et al. 1990). Within the medium-grained dolerites, irregular pods of coarse pegmatitic dolerite are commonly found, ranging from a few dm to several meters in size. On Gubben, some albite aplites, a few cm wide, cut the dolerites. These, which have a very specific Si-Al-Na-dominated chemistry (Sample R103d; Appendix 2b), may represent the final differentiation product of the magmatism.

6.2. PETROGRAPHY / MINERALOGY

The Rödö granites are characterized by a coarse porphyritic texture, with large (≤ 3 cm) ovoidal crystals of Kfsp. These are heavily brown-pigmented, presumably by submicroscopic grains of Fe-oxides. No twinning is found in the Kfsp, which thus are less ordered in their structure, probably of orthoclase type. Mantles of plagioclase around the Kfsp ovoids are frequent, but not ubiquitous. The mantled ovoids which usually predominate, vary in thickness from very thin to several mm. The plagioclase also occurs sparsely as discrete grains and is usually strongly affected by sericite and saussurite alteration. A few analyses of plagioclases (albite) and Kfsp in the granite have been performed (Table 11). The quartz (as well as the Kfsp) occurs in two generations, namely as large 0.5–1 cm rounded crystals with embayments, and in the granophyric groundmass, where it often shows featherlike intergrowths with Kfsp. The Fe-Mg-minerals are almost totally altered to chlorite. Fine-grained opaque phases are also present. Zircon and apatite are prominent accessory phases. Allanite or monazite have not been identified.

The dark schlieren structures within the granite are enriched in Fe-rich chlorite (Table 11), zircon, apatite, and opaque phases. Kfsp, quartz and plagioclase are present in reduced amounts. Kfsp sometimes forms a mantle around quartz. The aplites cutting the granite contain quartz, Kfsp, and more plagioclase than the granite. Furthermore, some greyish yellow-brown biotite (Li-rich?) often associated with fluorite occurs, possibly also topaz.

The granite porphyries are mineralogically very similar to the granites with, e.g. two generations of Kfsp and quartz, brown biotite (often altered to chlorite), and some fluorite. Additionally, relatively big zircons and apatite rods are found.

The QFPs vary a great deal in grain size, both in matrix and phenocrysts. The basic characteristics are, however, similar: euhedral to rounded and embayed phenocrysts of quartz and Kfsp, and sometimes plagioclase. The feldspars are usually strongly altered. Occasionally the phenocrysts are aggregated to glomerocrysts. Spherulites are typical (e.g. in the dykes at loc. 18, 45, 122, 128, 77, 88, and

Table 11. Representative analyses of minerals from the Rödö complex and Postjotnian dolerites.

	Silicic rocks			
	Rödö granite	Rödö granite	Most evolved QFP	Dark schlieren
	R139b Kfs P1	R139b P1 Pl	R117f2 TR1 6	R115s2 P5
SiO_2	65.06	68.93	68.91	24.29
TiO_2	-	-	-	-
Al_2O_3	17.92	19.89	19.74	17.72
FeO	0.04	-	0.61	40.89
MnO	-	-	-	0.23
MgO	-	-	-	5.03
CaO	-	0.1	0.03	-
Na_2O	0.56	11.07	10.02	-
K_2O	15.56	0.06	0.12	-
BaO	-	-	-	-
SrO	-	-	-	-
	99.14	100.05	99.43	88.16
	K-feldspar	Albite	Albite	Chlorite-Fe

Rödö dolerites, feldspars

	R99 TR1 Pl 14	R99 TR4 Pl 8	R99 P9 Pl	R99 P10 Pl	R111 TR1 Pl 74	R111 P1 Pl	R150 P22	R81b P15 Pl	R81b P14 Ksp	R134 Pl P2	R134 Pl TR 3
SiO_2	53.72	55.85	56.76	65.66	51.67	55.8	64.9	68.72	63.63	67.65	67.69
Al_2O_3	28.61	27.25	26.93	18.99	31.1	26.24	21.99	19.52	18.29	20.32	20.36
FeO	0.46	0.45	0.48	0.24	0.2	0.54	0.52	0.02	0.08	0.08	-
MgO	0.06	0.06	0.03	-	0.06	0.09	0.08	0.03	-	-	-
CaO	11.32	10.18	9.03	0.37	12.18	10.16	1.21	0.12	-	0.81	0.64
Na_2O	4.72	5.46	5.56	5.16	4.24	4.98	9.56	10.77	0.2	11.05	10.6
K_2O	0.43	0.67	0.91	8.74	0.31	0.59	1.16	0.09	16.16	0.16	0.16
BaO	0.04	-	0.13	-	-	-	-	-	0.44	-	0.06
SrO	0.13	0.15	0.26	-	0.03	-	-	-	-	-	0.2
	99.49	100.07	100.09	99.16	99.79	98.4	99.42	99.27	98.8	100.07	99.71
	Labr An_{57} Plag pheno	Labr An_{51} Plag pheno	Andes An_{47} Plag matrix	$Or_{52}Ab_{46}An_2$ Alkfsp matrix	Labr An_{61} Plag pheno	Labr An_{53} Plag matrix	Albite An_7 Plag matrix	Albite An_1 Plag matrix	K-fsp matrix	Albite An_4 Plag xeno?	Albite An_3 Plag xeno?

Rödö dolerites, mafic minerals

	R99 TR3 14	R99 TR3 11	R99 P5 Px	R111 TR2 Px 15	R111 P6 Px	R150 TR2 Cpx 27	R150 TR1 Cpx 1	R150 P18	R81b P10 Px	R81b P12 Px	R81b P9 Px	R134 P2
SiO_2	51.57	49.82	47.75	51.13	50.4	51.58	51.36	52.88	48.7	48.96	48.44	28.8
TiO_2	0.52	0.8	1.7	0.7	1.02	0.67	0.7	0.69	1.21	0.63	1.4	-
Al_2O_3	4.09	4.01	4.48	2.6	3.02	2.53	1.38	2.03	2.16	0.85	1.12	16.07
FeO	7.35	11.52	14.03	9.69	10.98	9.75	15.23	10.36	16.72	21	33.12	29.08
MnO	0.11	0.22	0.26	0.19	0.23	0.17	0.26	0.17	0.37	0.46	0.4	0.23
MgO	16.98	13.73	10.17	17.63	15.9	15.53	13.15	16.4	8.92	6.14	2.56	12.6
CaO	18.42	18.35	20.16	16.88	16.53	18.93	16.47	17.35	20.18	19.97	6.15	0.31
Na_2O	0.48	0.49	0.54	0.2	0.32	0.25	0.28	0.22	0.31	0.35	4.08	-
K_2O	-	0.04	-	-	-	-	0.03	-	-	0.18	1.1	-
	99.52	98.98	99.09	99.02	98.4	99.41	98.86	100.1	98.57	98.54	98.37	87.11
	Cpx core micropheno	Cpx rim micropheno	Cpx matrix	Cpx micropheno	Cpx matrix	Cpx core micropheno	Cpx rim micropheno	Cpx matrix	Cpx core matrix	Cpx rim matrix	Cpx matrix	Chlorite pseudom.

Postjotnian dolerites

	R120a TR 26	R120a TR 49	R72b TR1 Pl 16	R72b TR1 Pl 11	R120a TR3 Opx 5	R120a TR 10	R72b TR2 Ol 4	R72b TR3 Px 18
SiO_2	48.94	56.37	49.37	53.15	34.35	51.49	39.07	46.2
	TiO_2	-	-	-	-	-	1.08	0.04
3.57		Al_2O_3	32.19	27.47	31	27.83	0.03	1.91
0.06	4.35		FeO	0.28	0.4	0.34	0.41	42.45
11.23	20.18	15.21		MnO	-	-	-	-
0.69	0.23	0.19	0.22		MgO	-	-	0.11
0.06	22.4	13.29	39.95	8.85		CaO	15.44	9.19
14.58	11.37	0.14	20.48	0.29	20.52		Na_2O	2.74
5.7	2.86	4.39	-	0.35	-	0.56		K_2O
0.14	0.41	0.07	0.37	-	-	-	-	
BaO	-	0.03	-	-	-	-	-	-
	SrO	0.07	0.12	-	-	-	-	-
-			99.8	99.69	98.33	97.58	100.06	100.06
99.78	99.48							
	Bytow An_{76} core	Andes An_{47} rim	Bytow An_{74} core	Labr An_{59} rim	Olivine (Hortonolite)	Cpx	Olivine (Chrysolite)	Cpx

140a) but not generally occurring (e.g. not in the dykes at loc. 117f and g, 118b, 144, 160, 73). The spherulites are commonly developed as rosettes around corners of the phenocrysts (Plate 3c)). The geochemically evolved QFPs contain albite (Table 11) and Kfsp phenocrysts, often forming an anti-rapakivi texture (Plate 3d) Fluorite is varyingly abundant. Clots of chlorite occur sometimes together with opaque phases, rutile and zircon. Such mafic clots are also usually associated with small (≤1 cm) miarolitic cavities in some dykes (e.g. 46, 47, 57, 96). The cavities are filled with calcite and/or quartz. Abundant small grains of CaLREE-fluorocarbonates of the bastnäsite group have been encountered in some QFPs and the schlieren (Plates 3a and b). These are discussed thoroughly in section 6.5.1.4. Isolated grains of, e.g. columbite and xenotime, have been encountered in the most evolved QFPs, while allanite and monazite appear to be absent. Sphalerite has also been found in some more primitive QFPs.

The dolerites are characterized by a usually very fine-grained matrix, with more or less well-preserved plagioclase tables, and unidentified probably hydrous Fe-Mg-silicates. Microphenocrysts of augite of varying Fe/Mg composition occur in some dykes (Table 11). Often they are zoned towards more Fe-rich margins. In addition, relatively abundant opaque oxides occur and sometimes sulphides.



1a

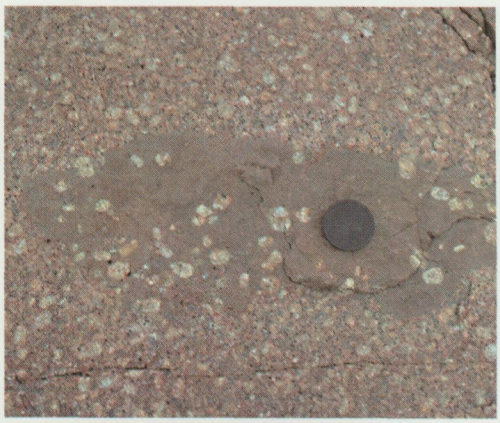

1b



1c



1d

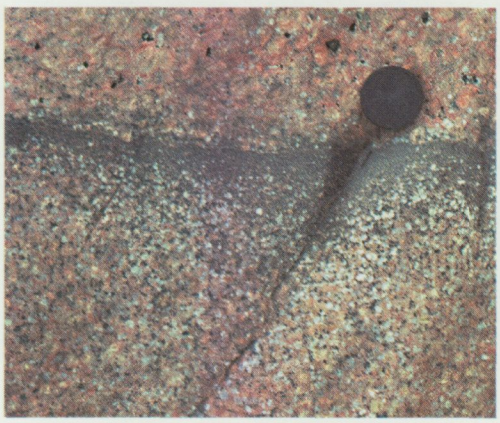

1e



1f



1g



1h

Plate 1a) Rödö granite with well-developed plagioclase-mantled K-feldspar ovoids (wiborgite). Rödskäret, loc. 138, Fig. 32 (cf. also the cover). b) Granite porphyry enclave with bulging margin towards the enclosing granite. Some megacrysts transgress the margin. Eastern Rödön, loc. 127, Foldout map. c) Calcite-filled vugs in the Rödö granite. Diameter of lens cap is c. 5 cm. Southern Rödön, loc. 114, Foldout map. d) Dark schlieren in Rödö granite. Southern Rödön, loc. 114, Foldout map. e) Close-up of schlieren zone in Rödö granite. The schlierens are often associated with vugs and aplites. Southern Rödön, loc. 114, Foldout map. f) Grey aplite veins in the Rödö granite, thinning out in a typical manner. Southern Rödön, loc. 114, Foldout map. g) Composite dyke (dolerite margin and hybrid porphyry centre, cf. Plate 2b) cutting the Rödö granite as a part of the cone-sheet intrusions. Southern Rödön, loc. 115b, Foldout map. h) Strongly evolved quartz-feldspar porphyry (type B, cf. chapter 6.3.1., Fig. 37) with small mafic magmatic enclaves. Small porphyritic (<5 mm). Eastern Skorven, loc. 18, Foldout map.



2a



2b



2c



2d

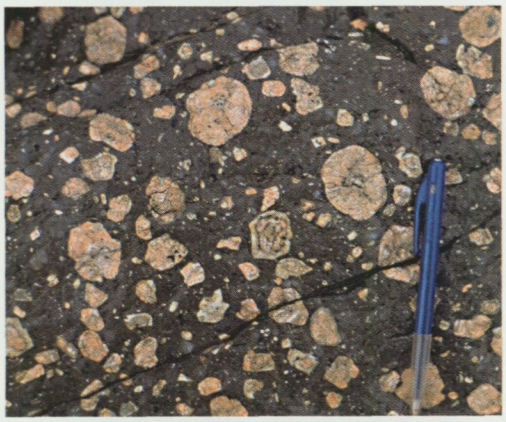

2e

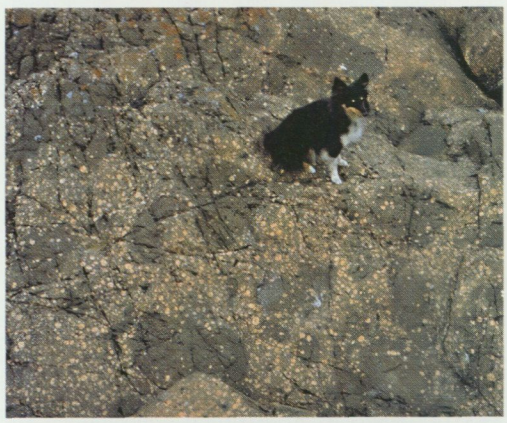

2f



2g



2h

Plate 2a) Rounded hybrid magmatic enclave in coarse silicic hybrid porphyry. A megacryst is seen to transgress the margin. Gråfläsjan, loc. 55, Foldout map. b) Hybrid porphyry (silicic group, SiO_2 66.4 %, cf. chapters 6.1. and 6.5.1.8.) in centre of composite dyke. The same dyke as in Plate 1g. Small rounded mafic magmatic enclaves, similar to the marginal dolerite. c) Sample of intermediate hybrid porphyry, with K-feldspar megacrysts generally smaller than 1 cm. Central Rödön, loc. 151h, Foldout map. d) Xenocryst-rich "contaminated dolerite". Eastern Rödön, loc. 133b, Foldout map. e) Coarse silicic hybrid porphyry. K-feldspar megacrysts are up to 3 cm in diameter, euhedral to rounded, occasionally mantled by plagioclase. Quartz megacrysts are also euhedral to rounded, up to 1 cm. Large skeletal plagioclases also occur, often with a small K-feldspar core. Northern Skorven, loc. 3, Foldout map. f) Mafic-hybrid magmatic enclaves in coarse silicic hybrid porphyry. Numerous megacrysts of the porphyry were engulfed in the mafic enclaves during the magma mingling event. Långfläsjan, loc. 58, Foldout map. g) Close-up of a mafic enclave from the locality in the previous figure (f). The central portions of the enclave contain abundant small vugs (such vugs usually contain calcite etc.). h) Hybrid zone between marginal dolerite and central quartz-feldspar porphyry in composite dyke. Enclaves of the marginal dolerite occur in the hybrid zone. Southeastern Rödön, loc. 12, Foldout map.

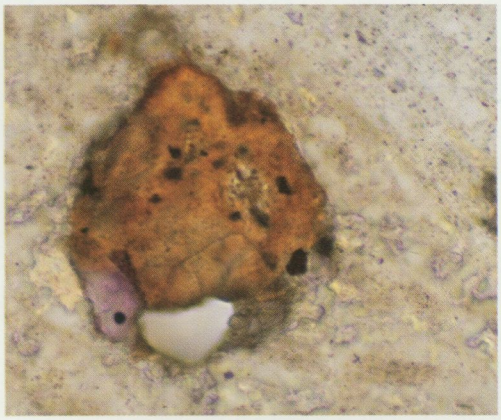

3a

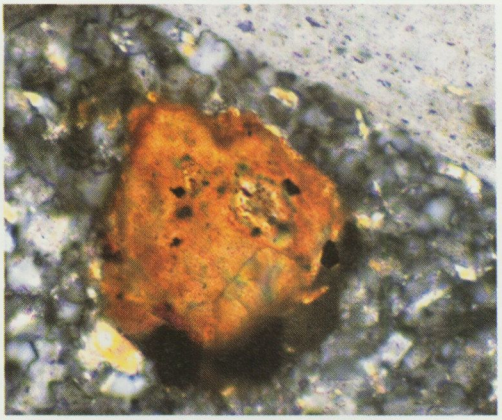

3b

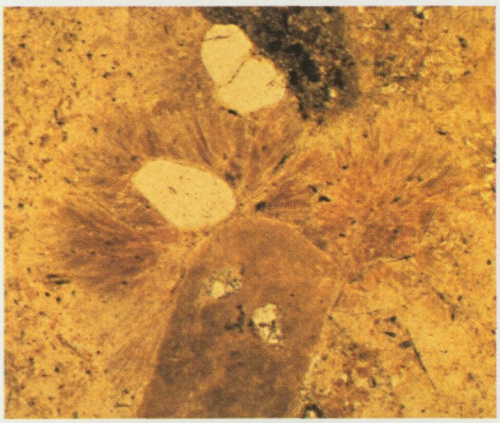

3c



3d



3e



3f

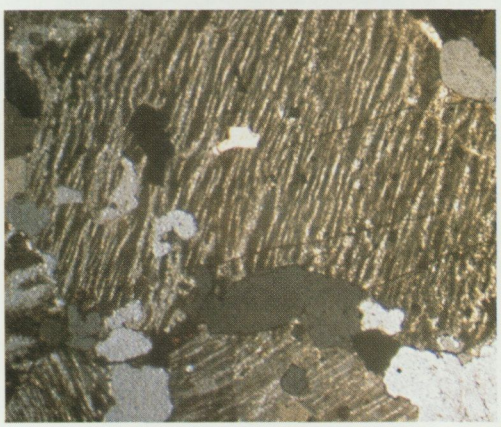

3g

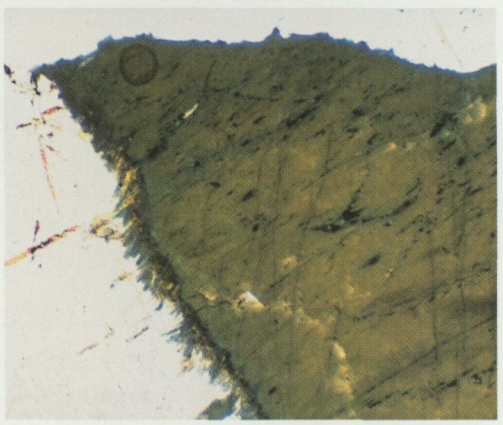

3h

Plate 3a) Ca-LREE-fluorocarbonate grain (brown), and fluorite (violet) in quartz-feldspar porphyry. The fluorocarbonate contains two small inclusions of xenotime in its upper right. Micrograph, // nicols, diameter of the grain is c. 0.12 mm. Loc. 167, Storkalven, Foldout map. b) Same grain as in a., + nicols. c) Spherulitic feldspar growth, nucleated on phenocrysts of quartz and K-feldspar. Micrograph, // nicols, altered K-feldspar phenocryst is c. 0.7 mm across. d) Anti-rapakivi texture in strongly evolved quartz-feldspar porphyry (type A, cf. chapter 6.3.1., Fig. 37). Albite microphenocryst rimmed by K-feldspar. (green colour is from marker pen). Micrograph, + nicols, length of feldspar grain c. 0.24 mm. Loc. 117f, Storholmsfläsjan, Foldout map. e) Typical contact relationship between Mårdsjö gabbro and granite, indicating magma mingling. Loc. M15, Fig. 55a. f) Intricate feldspar texture of Nordsjö syenite, Very irregular, serrated grain boundaries between plagioclase and K-feldspar. Micrograph, + nicols, width of the field is c. 5.8 mm. Loc. N11, Fig. 55b. g) Mesoperthite in peralkaline granite. The mesoperthite grains are the sole feldspar in the rock, and the plagioclase in this perthite is pure albite (cf. Table 19). Micrograph, + nicols, perthite grain is c. 5 mm long. Loc. Mu6, Fig 55c. h) Alkali amphiboles in peralkaline granite. Deep blue marginal phase is riebeckite, while the bluish brown-green is ferrorichterite (cf. chapter 7.2. and Table 19). Micrograph, // nicols, base of figure c. 1.4 mm across. Loc. S3, Fig. 55d.

Megacrysts of plagioclase are present in places (e.g. at loc. 99, 111, 151, 140b, and 134), and are relatively well-preserved. Compositions are labradorite-andesine or albite (Table 11). The latter are probably xenocrysts incorporated from a silicic source (e.g. the associated QFP magmas). Sometimes the plagoclase megacrysts exhibit skeletal or cellular textures (e.g. at loc. 134 and 137). The dolerites also often contain xenocrysts of Kfsp and quartz. These are always more or less dissolved around the margins, and the quartz grains usually have a reaction rim of pyroxene or amphibole (ocelli formation; cf. e.g. Bussy & Ayrton 1990, Vernon 1990). The Kfsp is often overgrown by skeletal plagioclase mantles. Finely cellular rimzones occasionally occur on plagioclase megacrysts (cf. Andersson and Eklund 1994). Sometimes abundant vugs contain dominantly calcite, chlorite and quartz.

The more basic hybrid porphyries (SiO_2 c. 60–65 %) have mineralogical features similar to that described for the dolerites above, with the difference that the amount of xenocrysts and the degree of alteration are higher. Several of these dykes are syenitic, and have alkaline tendencies containing greenish blue amphibole and blue-greenish pyroxene. Furthermore, occasionally quartz and Kfsp are met with also in the matrix. The most silicic hybrid porphyries (SiO_2 c. 65–70 %; e.g. loc. 3, 43, 44, 53, 57, 58, 68, 112) have an almost granitic mineralogy, with a slightly larger amount of chloritzed Fe-Mg-silicates. The megacrysts are euhedral to rounded Kfsp and quartz. The Kfsp megacrysts are sometimes mantled by plagioclase of varying thickness (up to 0.5 cm), but often completely unmantled (Plate 2e)). Inside the mantle, the Kfsp is heavily dissolved and rounded, sometimes with only a small core left. The mantle is usually cellular in texture, with optical continuity across the cellular network.

Some mineral analyses from the Postjotnian dolerites have been included in Table 11. The plagioclase is usually strongly zoned from bytownite cores to andesine rims. The olivine and clinopyroxene appear unzoned. Orthopyroxene has not been found. Fe-Ti oxides are abundant, while biotite and apatite are present in minor amounts.

6.3. GEOCHEMISTRY

Altogether 143 samples from the Rödö area were analysed for their major and trace element composition; 116 rocks belonging to the Subjotnian Rödö suite, 15 Postjotnian rocks, and 12 older country rocks (Appendix 2b).

In the major element geochemical plots in Fig. 34 the Rödö rocks plot in a relatively consistent manner in the diagrams. For comparative purposes, rocks from the Suomenniemi (Rämö 1991), Laitila (Vorma 1976) and Åland (Eklund & Lindberg 1992, Lindberg & Eklund 1992, Eklund et al. 1994, Eklund et al. 1996d, and Lindberg & Eklund unpubl. data) rapakivi complexes have been included. The Postjotnian dolerites from the Rödö area are also included. The silicic Rödö rocks plot very coherently in the granite fields, generally dominantly in the syenogranite or alkali feldspar granite of De la Roche et al. (1980) and Middlemost (1985). The aplites and a few QFPs are distinguished in the P-Q diagram of Debon & LeFort (1982) by plotting in the adamellite field (Fig. 34c), due to higher Na/K ratios. The basic Rödö rocks are characterized by a quartz-rich monzotrend, similar to that of the Åland area. In the Åland rapakivi area, however, some more calc-alkaline rocks (plotting in the granodiorite-tonalite fields) are also present, which have no counterparts in the Rödö area. The rocks of the Suomenniemi area also display marked similarities with the Rödö complex. The silicic rocks of the Suomenniemi, however, have a slight tendency towards more Ca-rich monzogranitic compositions, as well as containing some silica-undersaturated basic rocks (syenogabbros, Fig. 34a). Silica-undersaturated basic rocks also constitute a significant part of the Åland–Åboland dyke swarm. A majority of the Post-

Fig. 34. Major element geochemical classification diagrams of rock types in the Rödö complex. Rocks from the Suomenniemi (Rämö 1991), Laitila (Vorma 1976), and Åland (Eklund & Lindberg 1992, Lindberg & Eklund 1992, Eklund et al. 1994, Eklund et al. 1996d, and Lindberg & Eklund unpubl. data) rapakivi complexes have been included for comparison. Diagrams are after De la Roche et al. (1980) (a), Middlemost (1985) (b), and Debon & Lefort (1983) (c-d). A more detailed explanation is found in Fig. 8. Symbols are: open squares: Rödö granite, open triangles, apex up: Rödö aplites, open diamonds: Rödö granite porphyries, open circles: Rödö quartz-feldspar porphyries, stars: Rödö dark schlieren, half-filled squares: Rödö hybrid porphyries, filled squares: Rödö dolerites, filled circles: Rödö "contaminated" dolerites. Filled diamonds: Postjotnian dolerites. Open diamonds, apex down: Laitila batholith. Inclined crosses: Suomenniemi complex. Crosses: Åland batholith. Discussion in the text.

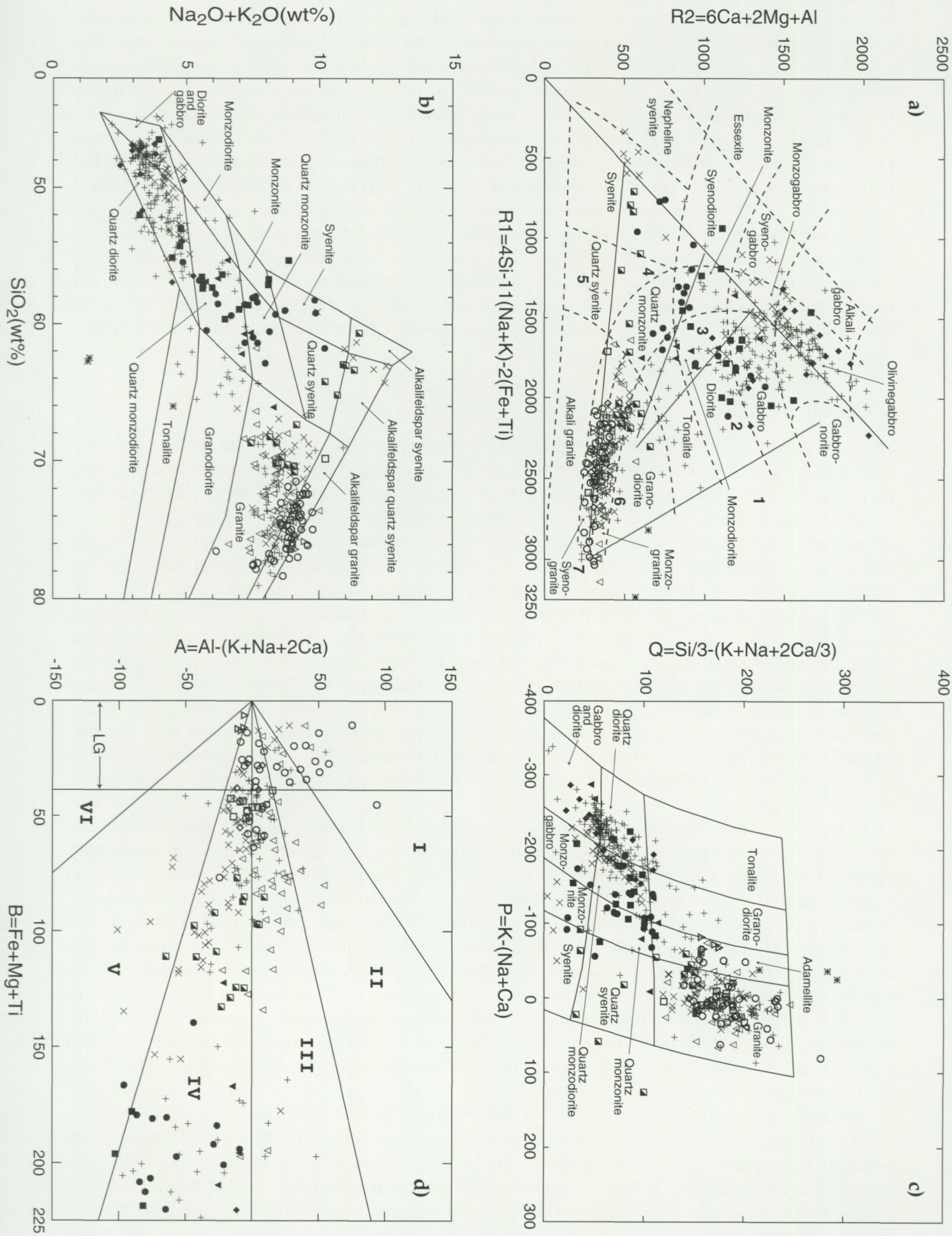
a)
R2=6Ca+2Mg+Al
R1=4Si-11(Na+K)-2(Fe+Ti)
Olivinegabbro
Alkali gabbro
Monzogabbro
Monzonite
Essexite
Syenodiorite
Nepheline syenite
Syenite
Quartz syenite
Alkali granite
Syeno-granite
Monzo-granite
Granodiorite
Tonalite
Diorite
Gabbro
Gabbro-norite
Monzodiorite
Quartz monzonite
Syeno-gabbro
1
2
3
4
5
6
7
b)
Na2O+K2O(wt%)
SiO2(wt%)
Diorite and gabbro
Monzodiorite
Quartz monzonite
Monzonite
Syenite
Quartz syenite
Alkalifeldspar syenite
Alkalifeldspar quartz syenite
Alkalifeldspar granite
Quartz diorite
Tonalite
Granodiorite
Granite
Quartz monzodiorite
c)
Q=Si/3-(K+Na+2Ca/3)
P=K-(Na+Ca)
Quartz diorite
Gabbro and diorite
Tonalite
Granodiorite
Adamellite
Granite
Monzogabbro
Monzonite
Syenite
Quartz syenite
Quartz monzonite
Quartz monzodiorite
d)
A=Al-(K+Na+2Ca)
B=Fe+Mg+Ti
LG
I
II
III
IV
V
VI

jotnian dolerites are also undersaturated with respect to silica, plotting in the field of olivine gabbro in Fig. 34a. The Laitila rocks (only silicic) are generally all granitic, with a tendency to somewhat lower total alkalies (Fig. 34b). In the Suomenniemi complex, a few distinctly syenitic rocks also occur (alkali feldspar syenitic dykes; Rämö 1991). In the Rödö complex only a few specific rocks have syenitic affinities. In this work, these are referred to as "evolved hybrids" and are suggested to have formed from magma mixing between highly evolved basic and silicic endmembers (see chapter 6.5.1.8. below). The most highly evolved Rödö dolerites are also syenitic in composition. In the A-B diagram of Debon & LeFort (1982) (Fig. 34d) the different rock groups display some interesting features. The Laitila granites are all in the peraluminous fields at relatively high content of mafic minerals (high B, biotite alone field), compared with the silicic Rödö rocks. The Rödö granites plot close to the leucogranite field, and most of the QFPs are within this field, trending towards strongly peraluminous compositions (muscovite>biotite field). The aplites are very leucocratic and slightly metaluminous. The granitic rocks in the Suomenniemi complex display a distinctly metaluminous trend (in the biotite+hornblende±pyroxene etc field, IV), with some late, evolved, leucocratic and peraluminous rocks. The Åland rocks show a wider compositional variation, but are otherwise similar to the Rödö rocks.

6.3.1. Silicic rocks

In Fig. 35 the Rödö rocks of granitic composition have been plotted in conventional alumina saturation diagrams. Also here, rocks from the Laitila and Suomenniemi batholiths are included for comparative purposes. The Strömsbro granitoids (Andersson 1997a) are also included. No peralkaline rocks have been identified in the Rödö suite, in contrast to the complexes to the NW in Jämtland–Ångermanland (see chapter 7.3.1.). The granites and the granite porphyries straddle the boundary between the metaluminous and peraluminous fields (subaluminous), whereas the aplites are slightly metaluminous. The QFPs ranges from slightly metaluminous to strongly peraluminous (up to A/CNK = 1.33; R117f2, except for the anomalous sample R87a; A/CNK=1.56). As a consequence, the silicic Rödö rocks are also slightly to strongly corundum normative, with a few exceptions that are slightly diopside normative. The most peraluminous ones are also those that show the highest contents of incompatible elements (cf. below). Some rocks of the Suomenniemi suite, however, show peralkaline geochemistry (alkali feldspar syenites; Rämö 1991). The trend of the Suomenniemi rocks is overall distinctly more metaluminous in character compared with Rödön, even if some peraluminous rocks occur also there. The Laitila rocks, on the other hand, exhibit a strongly peraluminous trend, that is less alkaline than the corresponding Rödö rocks. Hence, distinct differences in Al-saturation between the rapakivi complexes of the shield are apparent.

In Fig. 36 some discrimination diagrams which attempts to separate granitoids from different tectonic settings, based on trace element geochemistry, are shown. The granitic Rödö rocks are plotted, again together with the Suomenniemi rocks for comparison. No data from Laitila is available here. In Figs. 36a–c after Whalen et al. (1987) the Rödö rocks clearly plot in the field of A-type (anorogenic) granites, chiefly due to high Ga/Al ratios. Some of the QFPs have low contents of HFSE, for reasons discussed below, and thus plot in the field of I-, S-, and M-granites in Fig. 36c. Marked similarities with the Suomenniemi rocks are evident, even if the latter generally have slightly higher abundances of Ga and HFSE. In Fig. 36d, after Pearce et al. (1984), a large majority of the analyses of the Rödö rocks fall within the WPG-field (within-plate granites). Due to the generally relatively low HFSE-contents in the Rödö granites, granite porphyries, and certain QFPs, these fall across the border into the VAG-field (volcanic-arc granites). Furthermore, some of the most peraluminous QFPs fall in the the syn-COLG-field (syn-collision granites).

To facilitate simultaneous comparison of different rock groups and complexes with respect to major and trace elements, bulk crust-normalized (Taylor & McLennan 1985) spider diagrams of the silicic rocks are presented in Fig. 37. Upper and lower crust averages (Taylor & McLennan 1985) have been included for reference. In Fig. 37a it can be seen that the Rödö granites are lower in all elements except K, Na, Ti, Zn, Sr, and Mg, compared with the average Finnish subalkaline rapakivi granites (Rämö & Haapala 1995). The granite porphyries (usually occurring as rounded enclaves or larger masses within the granite) have a chemistry almost identical to that of the granites. The aplite dykes cutting the granite, on the other hand, are strongly enriched in relation to the granites in LILE (except Ba and

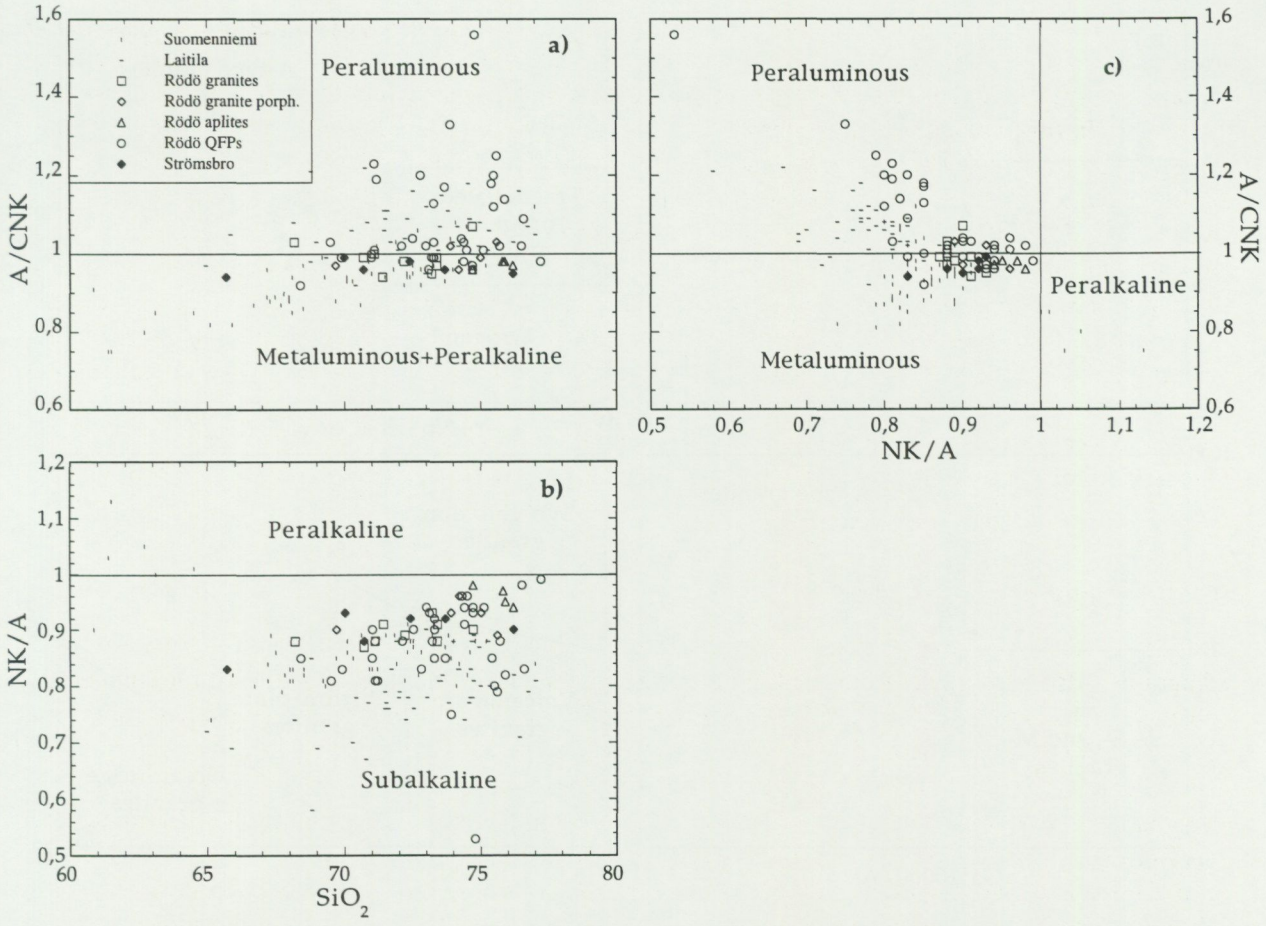

Fig. 35. Alumina saturation diagrams for the silicic Rödö and Strömsbro rocks. Rocks from the Strömsbro (Andersson 1997a), Suomenniemi (Rämö 1991) and Laitila (Vorma 1976) complexes have been included for comparison. A strongly peraluminous character is shown by some of the QFPs. No peralkaline rocks have been encountered in the Rödö suite, but a few occur in Suomenniemi. The Laitila granites are distinctly more aluminous compared with the Rödö granites, and even more so compared with the dominantly metaluminous Suomenniemi granites. The Strömsbro granites are all slightly metaluminous.

K), Nb, Y, and the HREE, but depleted in Zr, LREE, Eu, Sr, Ca, and the transition metals. The dark schlieren structures in the granites are strongly enriched in HFSE but depleted in LILE. The transition metals are also higher in the schlieren due to higher percentage of mafic minerals. In Fig. 37b the close geochemical resemblance between the Rödö granites and the least evolved (primitive) QFPs is obvious. Among the most evolved QFPs two distinct groups can be distinguished on geochemical grounds. One group (A in Fig. 37b) is exceptionally enriched in certain trace elements: Rb, Cs, Th, U, Zr, Hf, Nb, Ga, and the HREE, but depleted in Ba, Ti, Fe, and especially LREE and Eu. The other group (B in Fig. 37b) shows similar depletions in LREE and Eu, Ti, and Fe, but are enriched only in Rb, Cs, Nb, and Ga. Contrary to group A, group B is strongly depleted in Zr and Hf, and has relatively low contents of U, Th, Y, and HREE. In Fig 37c, some geochemically anomalous silicic dykes are plotted, most of which are low in LREE and high in HREE. Generally they are intermediate in composition between the least evolved and most evolved QFPs. Most anomalous is R87a, which is extremely low in Na (Na_2O=0.64 %), but rich in LREE and Zn. The values from this dyke differ considerably from the trends of the rest of the suite. This, together with its occurrence relatively far away from Rödön (Fig. 32), indicates that it may not be related to the Rödö suite at all.

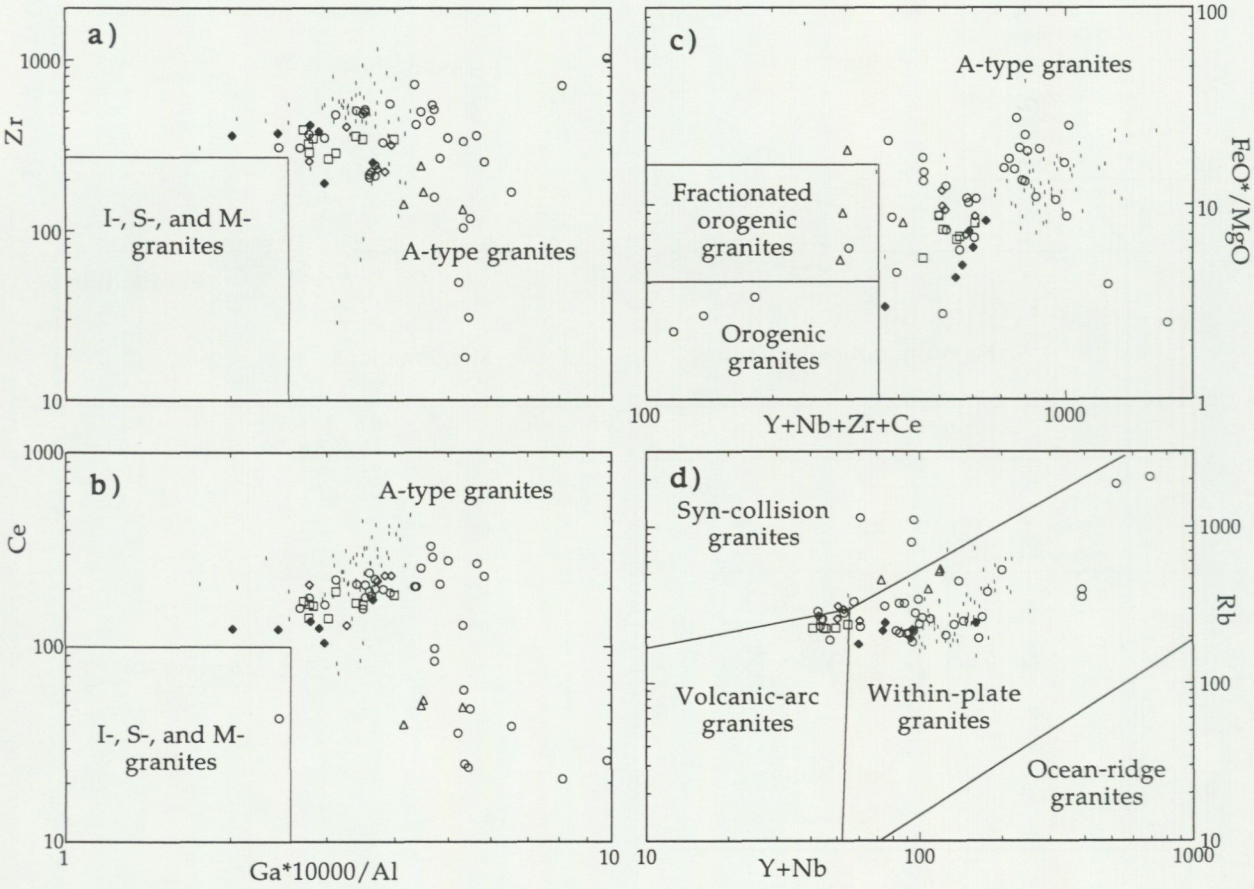

Fig. 36. Trace element diagrams designed to reveal the tectonic setting of granitoids. a-c) after Whalen et al. (1987), d) after Pearce et al. (1984). Same rock types and symbols as in Fig. 35 (no data for the Laitila rocks). The Rödö and Strömsbro rocks clearly fall in the anorogenic (A-type) field. The aplites and some of the QFPs have lower HFSE (e.g. Ce and Zr) which make them fall in the orogenic fields in Fig. 36c. This is due to effects of fractionation as discussed in the text. In d) the Rödö rocks are transitional between the volcanic-arc (VAG) and within-plate (WPG) fields. The granites and granite porphyries fall in the corner of the VAG field, while most of the QFPs are in the WPG field and some even in the syn-collision field. The Suomenniemi and Strömsbro granites are all in the WPG field.

Fig. 37. Bulk crust (Taylor & McLennan 1985) normalized spiderplots for the silicic Rödö rocks and some other rocks. Upper and lower crustal averages (Taylor & McLennan 1985) have been included for comparison. Average Finnish subalkaline (rapakivi) granite is from Rämö & Haapala (1995). The different rock types are displayed as averages since each group has relatively coherent geochemical characteristics, to allow general comparisons. In a) it can be seen, e.g., that the schlieren are rich in HFSE but poor in LILE, while the aplites are rich in LILE but poor in transition metals. The average Finnish rapakivi granite is generally more enriched in both LILE and HFSE compared with the Rödö granites. In b) the extremely evolved character of some of the QFPs is shown. Two main groups of evolved QFPs are present, one which is very rich in Rb, Th, U, Zr, Hf, Nb, and HREEs, and one which is depleted in Zr, Hf and low in the REEs. c) shows some of the other highly evolved QFPs that were not fitted into the averages in b). R87a is anomalous, being very high in the LREEs and very low in Na. Numbers refer to sample numbers also found on Figs. 32 and 33, and the Foldout map. Further discussion in the text.

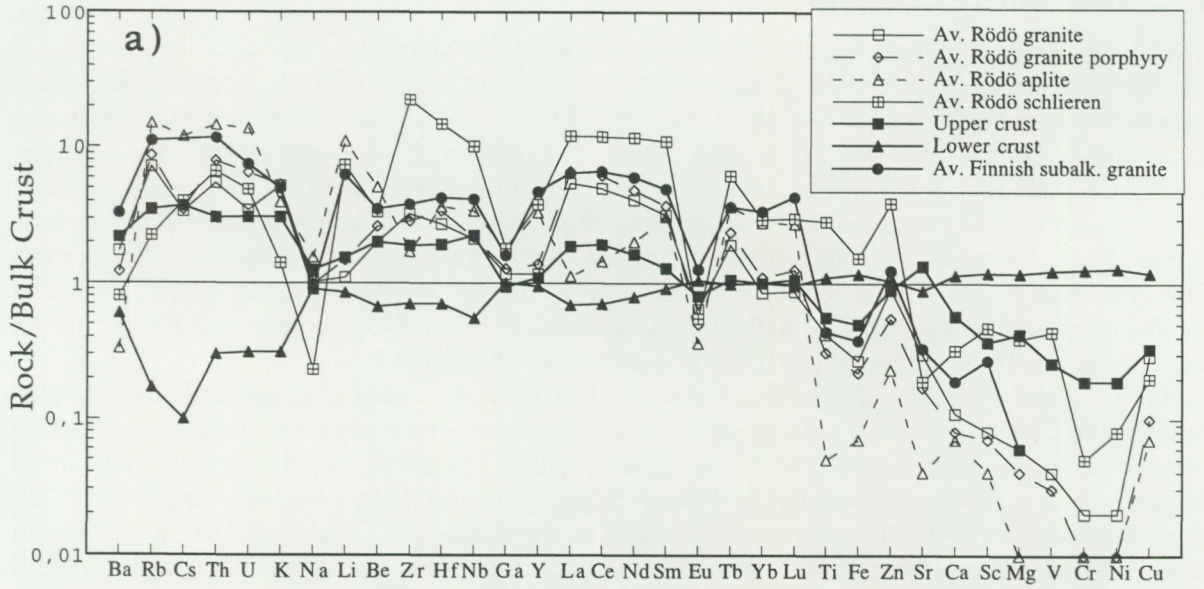
a)
Rock/Bulk Crust
100
10
1
0,1
0,01
Av. Rödö granite
Av. Rödö granite porphyry
Av. Rödö aplite
Av. Rödö schlieren
Upper crust
Lower crust
Av. Finnish subalk. granite
Ba Rb Cs Th U K Na Li Be Zr Hf Nb Ga Y La Ce Nd Sm Eu Tb Yb Lu Ti Fe Zn Sr Ca Sc Mg V Cr Ni Cu

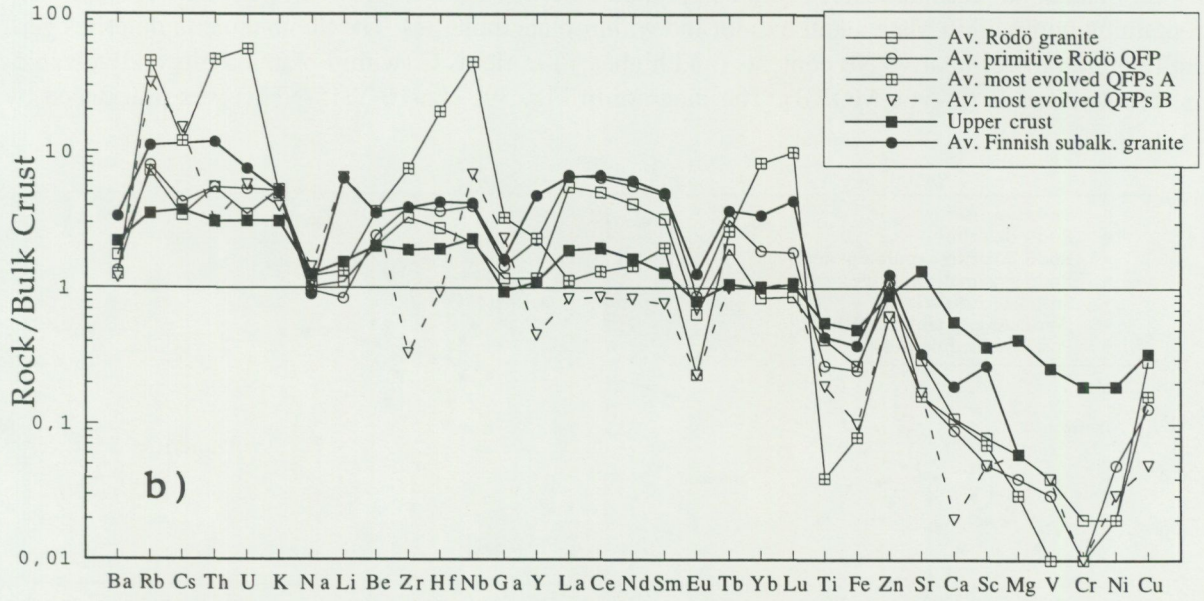
b)
Rock/Bulk Crust
100
10
1
0,1
0,01
Av. Rödö granite
Av. primitive Rödö QFP
Av. most evolved QFPs A
Av. most evolved QFPs B
Upper crust
Av. Finnish subalk. granite
Ba Rb Cs Th U K Na Li Be Zr Hf Nb Ga Y La Ce Nd Sm Eu Tb Yb Lu Ti Fe Zn Sr Ca Sc Mg V Cr Ni Cu

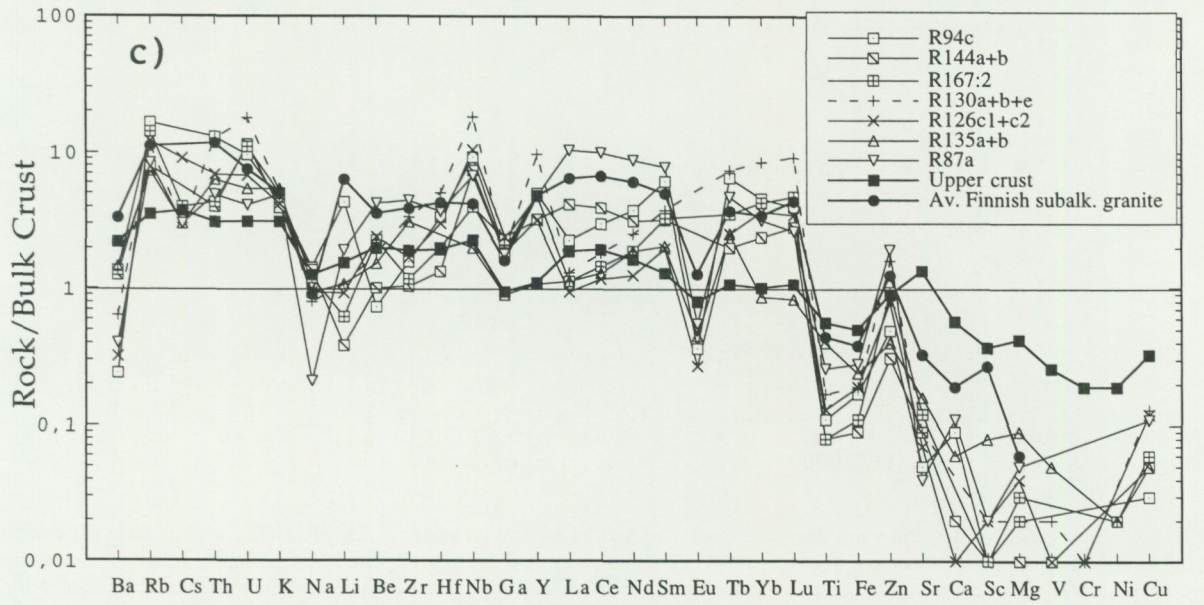
c)
Rock/Bulk Crust
100
10
1
0,1
0,01
R94c
R144a+b
R167:2
R130a+b+e
R126c1+c2
R135a+b
R87a
Upper crust
Av. Finnish subalk. granite
Ba Rb Cs Th U K Na Li Be Zr Hf Nb Ga Y La Ce Nd Sm Eu Tb Yb Lu Ti Fe Zn Sr Ca Sc Mg V Cr Ni Cu

6.3.2. Basic-intermediate rocks

The basic-intermediate rocks are plotted in some classification diagrams in Fig. 38. In the Zr vs. P_2O_5-plot of Floyd & Winchester (1975) (Fig. 38a) the Rödö rocks exhibit tholeiitic to weakly alkalic chemistry, whereas in Fig. 38b (Zr/P_2O_5*10000 vs. Nb/Y; Floyd & Winchester 1975) they plot dominantly in the alkalic field (with a few exceptions). The same holds for the Postjotnian dolerites, which are clearly tholeiitic in Fig 38a (lower Zr concentrations than the Rödö dolerites), but mostly alkalic in Fig. 38b. For the basic rocks in the Suomenniemi area (the Häme and Suomenniemi dolerite swarms, Rämö 1991), the opposite situation applies: they are alkalic in 38a and have a tendency to more tholeiitic character in 38b. In Fig. 38c (FeO*/MgO vs. SiO_2; Miyashiro 1974) both the Postjotnian and the Suomenniemi rocks show clearly tholeiitic character, with lower SiO_2 contents compared with the Rödö dolerites. The latter group partly grade into the calc-alkalic field.

In Fig. 39a (Zr-Ti/100-3*Y; Pearce & Cann 1973) the Rödö dolerites plot in the field of within-plate basalts (the D-field), trending towards increasing Zr contents. The Postjotnian dolerites also mainly plot in the within-plate basalt-field, but at higher relative Ti contents. Partly they also plot in the B-field, which is a combined field of mid-ocean ridge basalts (MORB), island-arc basalts (IAB), and calc-alkali basalts (CAB). The Suomenniemi rocks plot in the B- and C-fields (CAB). In the diagram devised by Meschede (1986)(Zr/4-2*Nb-Y; Fig. 39b) all Rödö rocks fall in field AI, corresponding to within-plate alkali basalts, whereas the Postjotnian dolerites trend from AI to AII, where AII is a field containing both within-plate alkali basalts and within-plate tholeiites. The Suomenniemi dolerites generally plot at lower relative Nb contents (and higher Y) in fields C (within-plate basalts and volcanic-arc basalts) and B (E-type MORB). The diagram in Fig. 39c (La/10-Y/15-Nb/8) was introduced by

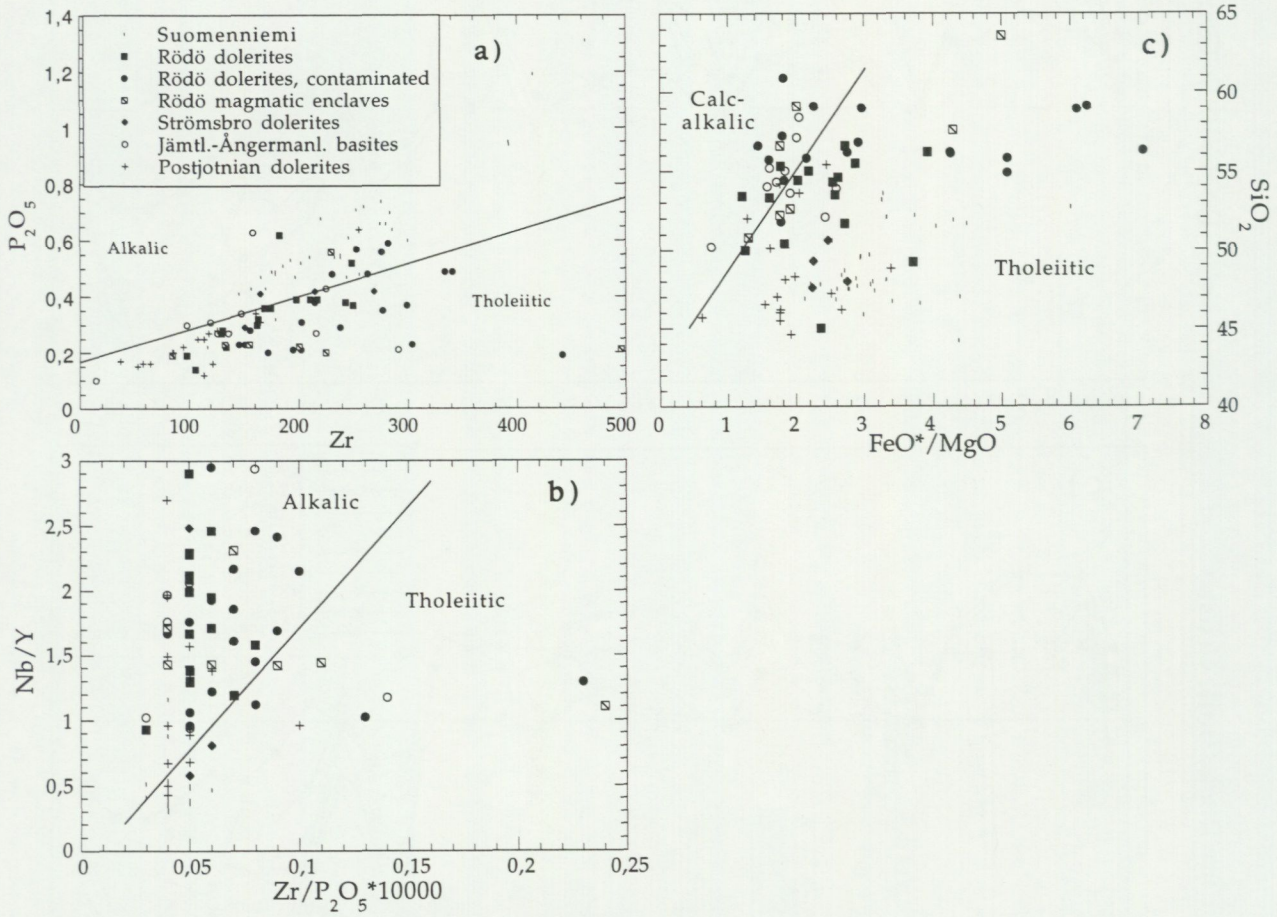

Fig. 38. Some classification diagrams for basic rocks. a) and b) after Winchester & Floyd (1975), and c) after Miyashiro (1974). All basic rapakivi-related rocks of this study are included as well as those reported for the Suomenniemi dyke swarm by Rämö (1991). The classification in relation to tholeiitic and alkalic/calc-alkalic characters is ambiguous. Evidently the Suomenniemi rocks are richer in P_2O_5, while the Postjotnian dykes are lower in Zr. The SiO_2 contents of the Rödö dolerites are generally higher than in the Suomenniemi and Postjotnian dykes (cf. Fig. 41). Discussion in the text.

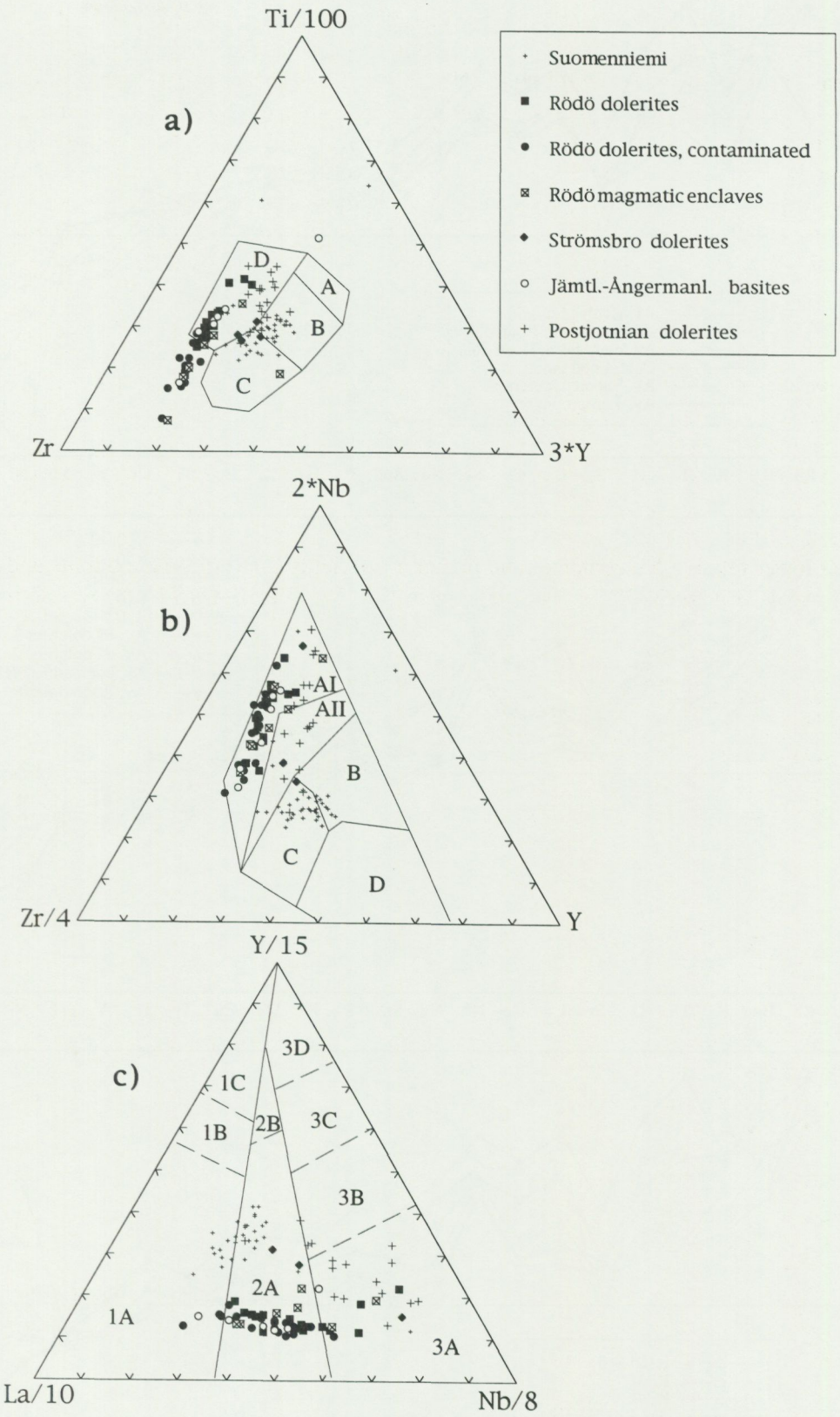

Fig. 39. Trace element geochemical-tectonic classification of the basic rapakivi-related rocks of this study, the Suomenniemi dykes (Rämö 1991), and some Postjotnian dykes. The Swedish rocks tend to indicate continental, within-plate, alkalic to tholeiitic affinities. The Suomenniemi differ in having higher relative Y contents, in some diagrams suggesting a more orogenic-type chemistry. The Postjotnian differ by having higher relative Nb and Ti contents, indicating a slightly more alkalic character. Diagrams after Pearce & Cann (1973) (a), Meschede (1986) (b), and Cabanis & Lecolle (1989) (c). Explanation of the fields is found in Fig. 13. Discussion in the text.

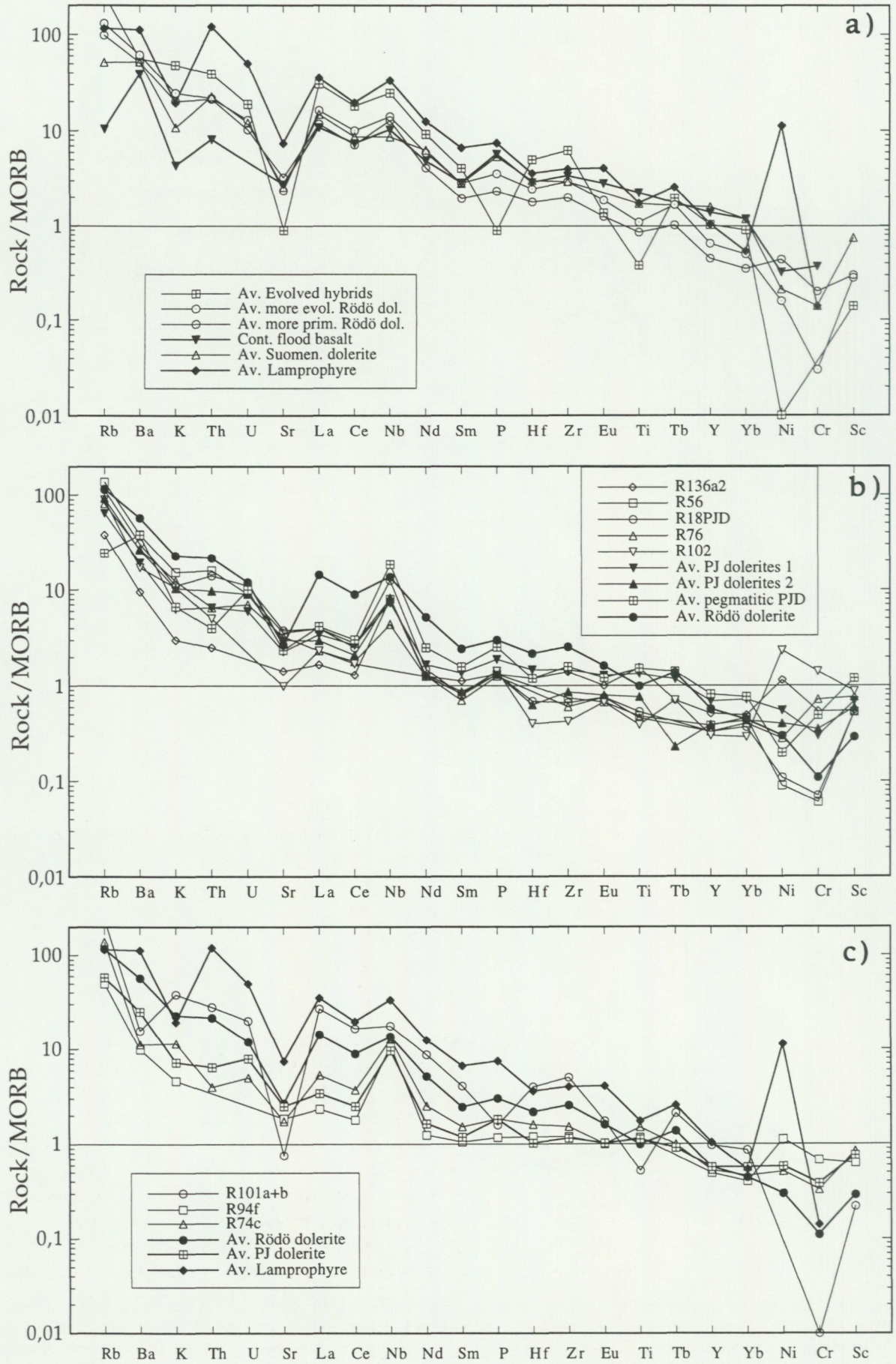
a)
Rock/MORB
100
10
1
0,1
0,01
Av. Evolved hybrids
Av. more evol. Rödö dol.
Av. more prim. Rödö dol.
Cont. flood basalt
Av. Suomen. dolerite
Av. Lamprophyre
Rb Ba K Th U Sr La Ce Nb Nd Sm P Hf Zr Eu Ti Tb Y Yb Ni Cr Sc
b)
Rock/MORB
R136a2
R56
R18PJD
R76
R102
Av. PJ dolerites 1
Av. PJ dolerites 2
Av. pegmatitic PJD
Av. Rödö dolerite
Rb Ba K Th U Sr La Ce Nb Nd Sm P Hf Zr Eu Ti Tb Y Yb Ni Cr Sc
c)
Rock/MORB
R101a+b
R94f
R74c
Av. Rödö dolerite
Av. PJ dolerite
Av. Lamprophyre
Rb Ba K Th U Sr La Ce Nb Nd Sm P Hf Zr Eu Ti Tb Y Yb Ni Cr Sc

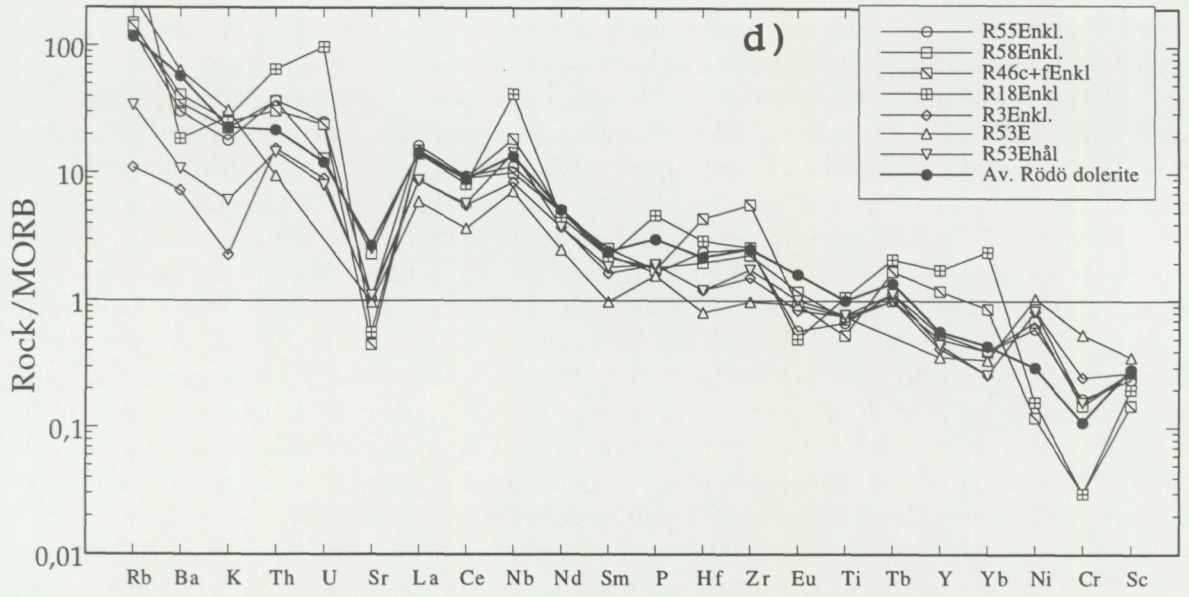

Fig. 40 cont.

Cabanis & Lecolle (1989). The Rödö, Suomenniemi and Postjotnian dolerites are here clearly separated. The Rödö rocks have lower relative Y and plots in field 2A (continental basalts), whereas the Suomenniemi rocks trend from field 2A into 1A (calc-alkali basalts) at higher relative Y contents. The Postjotnian dolerites are found in field 3A (alkali basalts from intercontinental rifts) and a few in 3B (E-type MORB; enriched) at lower relative La but higher Nb. All basic Rödö rocks are distinctly quartz normative (except R134a which has 3.22 % olivine in the norm), while the Postjotnian dolerites are typically olivine normative. The Rödö dolerites are thus quartz tholeiites and the Postjotnian dolerites olivine tholeiites according to the CIPW norms.

The analyses of the basic-intermediate Rödö rocks are also plotted in MORB-normalized spider diagrams (Fig. 40). To facilitate the inspection, average values of rock groups with similar patterns are plotted instead of individual analyses. Individual analyses are included for specific (anomalous) samples. In Fig. 40a a general comparison between the major basic-intermediate Rödö rocks and other relevant rocks is shown. The Rödö dolerites are separated into two groups, one more primitive (higher in Ni and Cr, as well as e.g. MgO, CaO) and one more evolved. They show very similar patterns, but the latter (which also includes the "contaminated"/more evolved dolerites) have higher contents of all LILE and HFSE. The Suomenniemi dolerites show relatively marked similarities with the Rödö dolerites, although with some exceptions: the Suomenniemi rocks are higher in Y, Yb, Ti, P, but lower in Rb, K, Nb, which was partly evident already in Fig. 39. The continental flood basalt average of Thompson et al. (1983) shows marked similarity to the Rödö dolerites, but even more so to the Suomenniemi rocks, except for the LILE. Average lamprophyre (Bergman 1987) shows little resemblance to the rapakivi-related dolerites, having higher abundances of most elements. The trace element

Fig. 40. MORB (mid-ocean ridge basalt) normalized (from MORB compilation in Rollinson 1993) trace element spider diagrams of basic rapakivi-related rocks of this study. Averages of lamprophyre (Bergman 1987), continental flood basalt (Thompson et al. 1983), and average Suomenniemi dolerite (Rämö 1991) have been included for comparison. Numbers refer to sample numbers also found on Figs. 32 and 33, and Foldout map. a) Average lamprophyre is higher in most LILE and HFSE, compared with the Rödö dolerites, while average continental flood basalt is much closer in composition. Especially the Suomenniemi average is very close to the continental flood basalt average. b) The Rödö dolerites are dissimilar to the Postjotnian dolerites in having distinctly higher LREEs and somewhat higher LILE and most HFSE. The Postjotnian dykes in the Rödö area are enriched in Nb compared with other elements. Some anomalous rocks are plotted in c). Samples R94f and R74c appear to have been erroneously included in the Rödö dolerite group, as geochemically they are most similar to the Postjotnian dykes (cf. Fig. 41). R101a+b is close to the "evolved hybrids" (cf. a) in composition. d) Mafic-hybrid magmatic enclaves. The majority are relatively similar to the average Rödö dolerite. R18Enkl and R46c+fEnkl are considerably enriched in certain HFSE compared with the other enclaves. Discussion in the text.

characteristics of the hybrid porphyries derived from the mixing of the evolved basic and silicic endmembers reflect the strong influence of the silicic components, compared with the dolerites (i.e. increased contents of granitophile elements and decreased (=diluted) contents of others).

The Postjotnian dolerites (Fig. 40b) generally have lower contents of LILE and most HFSE (except Nb, Y, and HREE) compared with the Rödö dolerites, although a large variation in composition is evident. The compositional spread may probably be attributed to different stages of evolution represented by the sampled dykes. This is indicated by the large spread in the Ni and Cr contents, where the samples with highest Ni and Cr are lower in LILE and HFSE (generally incompatible in basic systems). This is corroborated by the relatively high contents of incompatible elements in the late Postjotnian pegmatitic pods. The Postjotnian dolerites from the Rödö area are characterized by a strong positive anomaly for Nb, compared with other HFSE. This contrasts with other Postjotnian dolerites further south in the Dala province (Patchett et al. 1994). In Fig. 40c some anomalous dolerites are compared with, for example, average Rödö dolerite and average Postjotnian dolerite. R101a+b has been classified as "contami-nated" dolerite but is geochemically very close to the evolved hybrids. R74c and R94f have been assigned to the Rödö dolerites based on field appearance, but this may be incorrect as their geochemistry is more akin to that of the Postjotnian dolerites.

The different mafic/hybrid magmatic enclaves are plotted in Fig. 40d. Apart from R18Enkl and R46c+fEnkl, there is a more or less pronounced similarity between the enclaves and the Rödö dolerites. The enclaves are generally somewhat more primitive in composition compared with the average Rödö dolerite, being especially clear for the LILE in some enclaves. R18Enkl is completely different with high contents of Th, U, Nb, P, Tb, Y, and Yb as well as low Ba, Sr, and Eu, which is consistent with hybridization with an evolved silicic magma (QFP). Similarly, but less pronouncedly, R46c+fEnkl show evidence of mixing with a less evolved silicic (QFP) magma by the increased contents of, e.g. Nb, Hf, Zr, Tb, Y, and Yb.

6.3.3. Variation diagrams

Figs. 41a–d show Harker variation diagrams for all the Rödö rocks, divided into specific types as stated in the legend. The analyses of the Postjotnian rocks of the Rödö area, as well as rocks from the Suomenniemi batholith and associated dykes in SE Finland (Rämö 1991), are also included for comparative purposes. These diagrams give a lucid overview of the total geochemical variation for all elements analysed for all rocks.

The analyses of the dark schlieren segregations within the granite clearly deviate from the trend of the rest of the samples of the rapakivi complex, showing high abundances of, e.g. TiO_2, Fe_2O_3*, Zr, Y, Zn, Li, Th, REE except Eu, and low abundances of, e.g. Al_2O_3, Na_2O, and K_2O.

The silicic parts of the Rödö suite are characterized by a large variation in certain elements. The granites, granite porphyries, and the majority of the QFPs, however, show the typical rapakivi chemistry with low contents of, e.g. MgO, CaO, P_2O_5, Al_2O_3 and Sr, but high contents of K_2O (generally between 5 and 6 %), Rb, F, Ga, Zr, Hf, Th, U and the REEs (cf. e.g. Rämö 1991, Vorma 1976, Rämö & Haapala 1995). The geochemical variation in the Rödö suite also compares well with that of Cenozoic topaz rhyolites in western North America (cf. e.g. Christiansen et al. 1983, 1984, 1986, Christiansen 1996). The strong variation in the silicic suite is manifested, e.g. by increased contents of Al_2O_3

Fig. 41a–d. Harker variation diagrams for the rocks of the Rödö complex. Postjotnian dolerites of the Rödö area have been included for comparison, as well as rocks from the Suomenniemi complex (Rämö 1991). Rocks have been subdivided according to the legend). The dark schlieren in the granite are geochemically clearly offset in relation to the other rocks. The hybrid porphyries define two separate mixing trends (roughly straight lines) for many elements (indicated in the diagrams), one with more primitive endmembers for the silicic hybrids and one with more evolved endmembers for the intermediate hybrids. For many elements, this division is not resolved, due to small differences in the endmembers. The basic dykes of the Suomenniemi swarm are generally lower in SiO_2 and K_2O, but higher in, e.g., TiO_2, Fe_2O_3, CaO, Y, Sc, and REEs, compared to the Rödö dolerites. The Postjotnian dolerites are generally more primitive in character being higher in, e.g., MgO, CaO, Sc, and V, but lower in, e.g., SiO_2, K_2O, Ba, and LREEs. Suggested trends of fractionation in the basic Rödö suite are indicated with arrows. The Suomenniemi granitoids are distinctly higher in Ba, Y, Sc, and HREEs, compared with the silicic Rödö rocks. Cf. Figs. 37 and 40. Sample numbers have been included occasionally and refer to Figs. 32, 33, and the Foldout map. Discussion in the text.

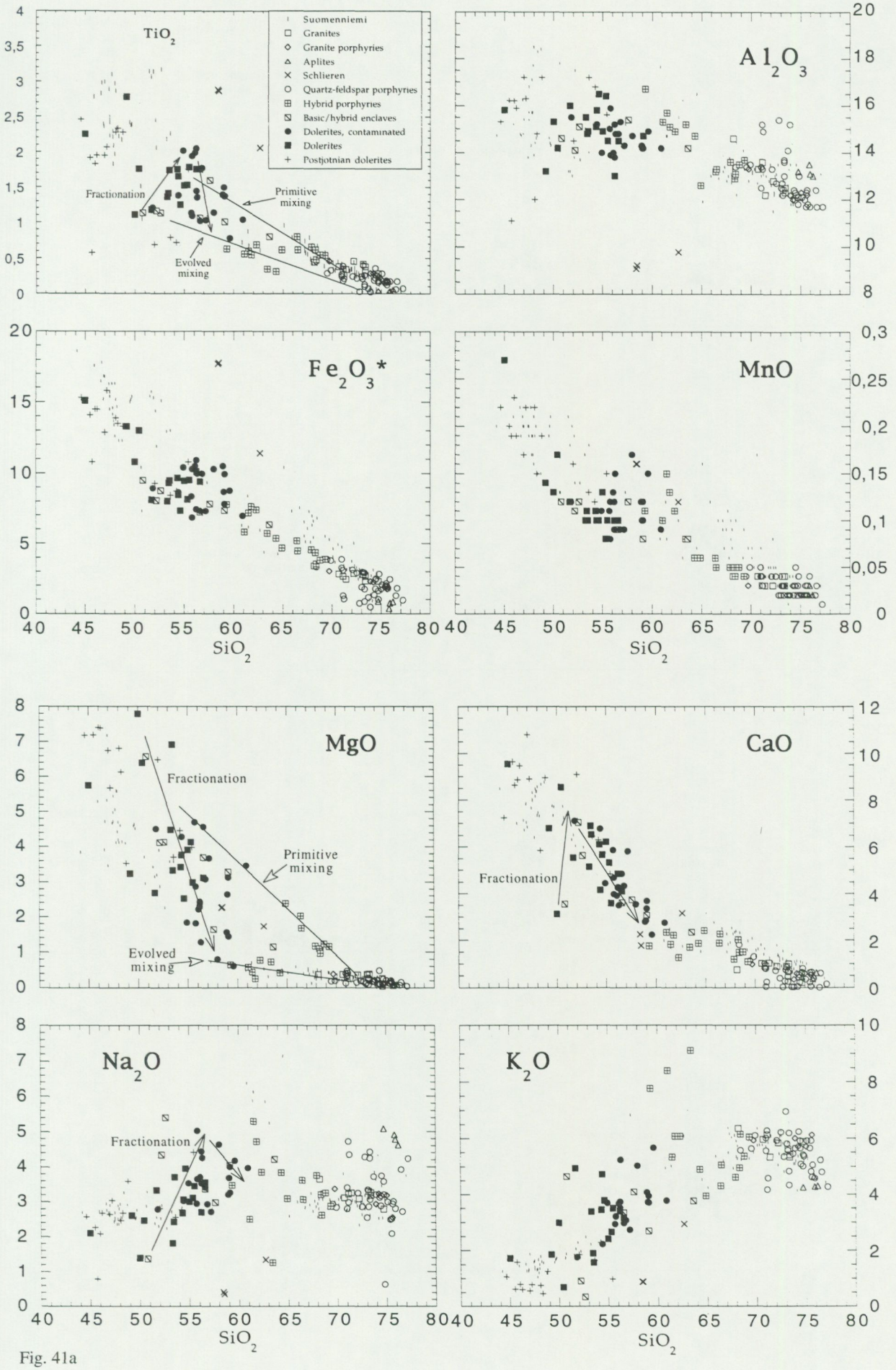
TiO2
Suomenniemi
Granites
Granite porphyries
Aplites
Schlieren
Quartz-feldspar porphyries
Hybrid porphyries
Basic/hybrid enclaves
Dolerites, contaminated
Dolerites
Postjotnian dolerites
Fractionation
Primitive mixing
Evolved mixing
Al2O3
Fe2O3*
MnO
MgO
CaO
Na2O
K2O
SiO2

Fig. 41a

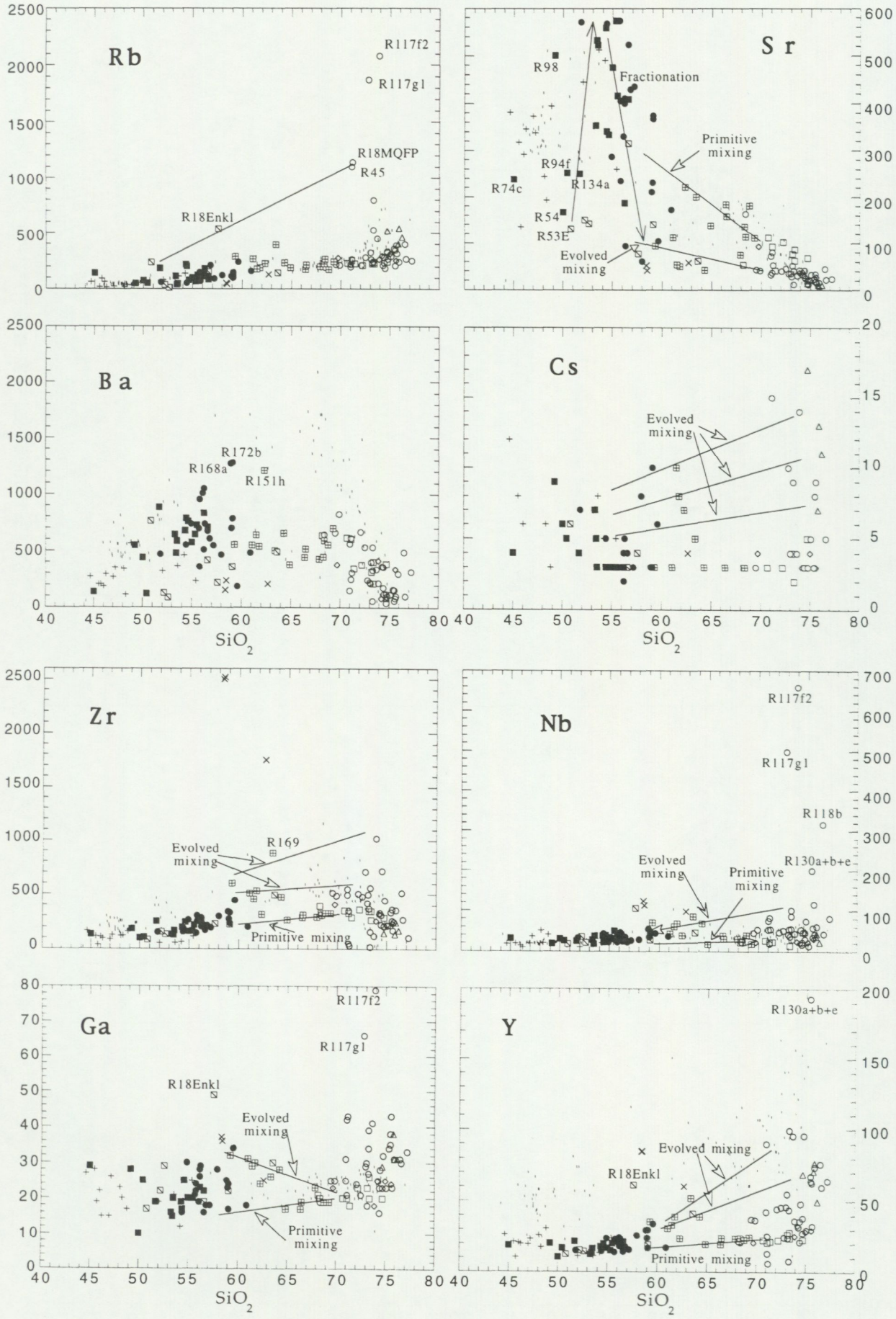
Rb
R117f2
R117g1
R18MQFP
R45
R18Enkl
Sr
R98
Fractionation
Primitive mixing
R94f
R74c
R134a
R54
R53E
Evolved mixing
Ba
R172b
R168a
R151h
Cs
Evolved mixing
Zr
Evolved mixing
R169
Primitive mixing
Nb
R117f2
R117g1
R118b
R130a+b+e
Evolved mixing
Primitive mixing
Ga
R117f2
R117g1
R18Enkl
Evolved mixing
Primitive mixing
Y
R130a+b+e
Evolved mixing
R18Enkl
Primitive mixing
SiO2
SiO2

Fig. 41b

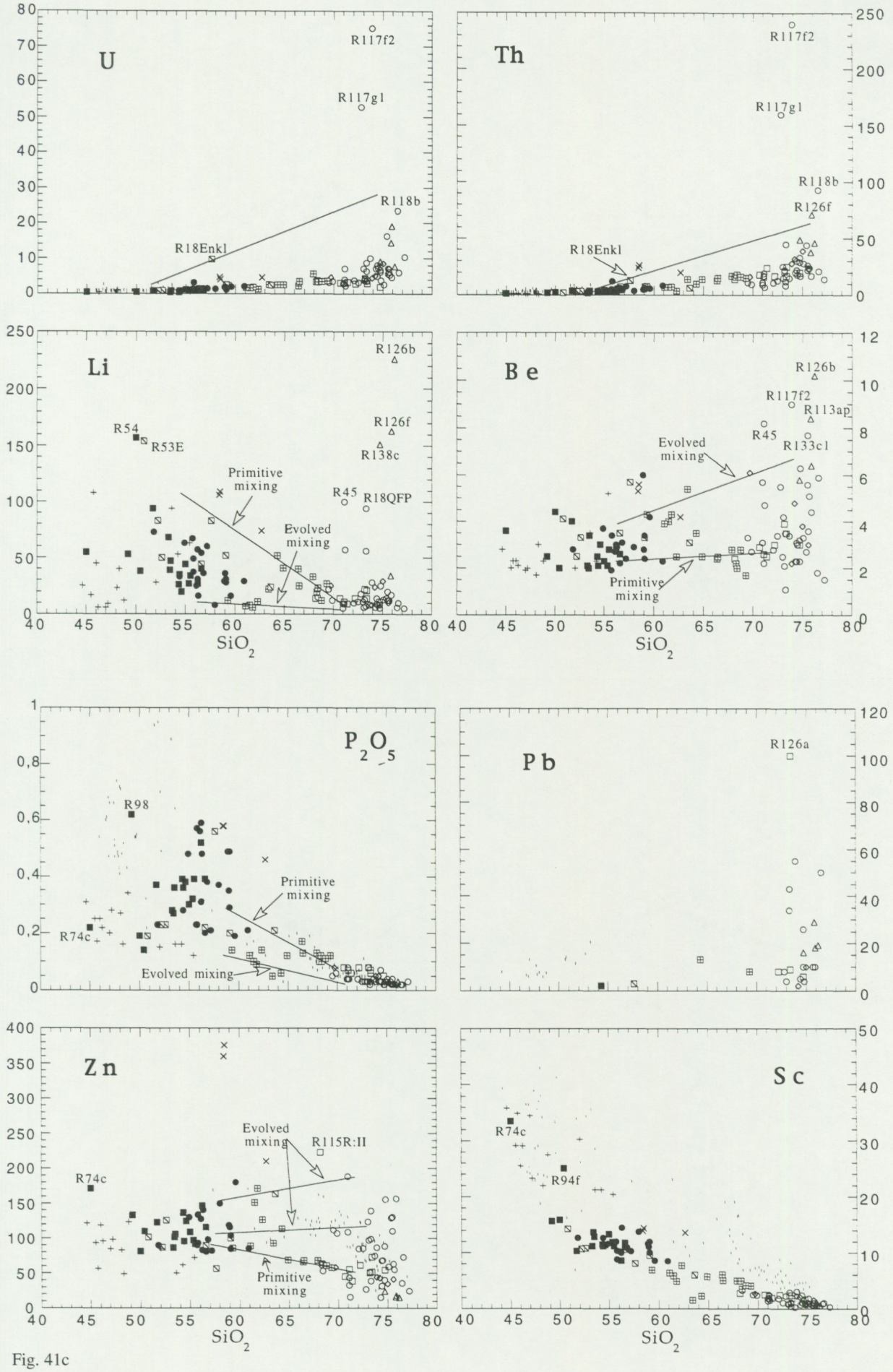
U
R117f2
R117g1
R118b
R18Enkl
Th
R117f2
R117g1
R118b
R126f
R18Enkl
Li
R126b
R54
R53E
R126f
R138c
Primitive mixing
R45
R18QFP
Evolved mixing
SiO2
Be
R126b
R117f2
R113ap
R45
R133c1
Evolved mixing
Primitive mixing
SiO2
P2O5
R98
Primitive mixing
R74c
Evolved mixing
Pb
R126a
Zn
Evolved mixing
R115R:II
R74c
Primitive mixing
SiO2
Sc
R74c
R94f
SiO2

Fig. 41c

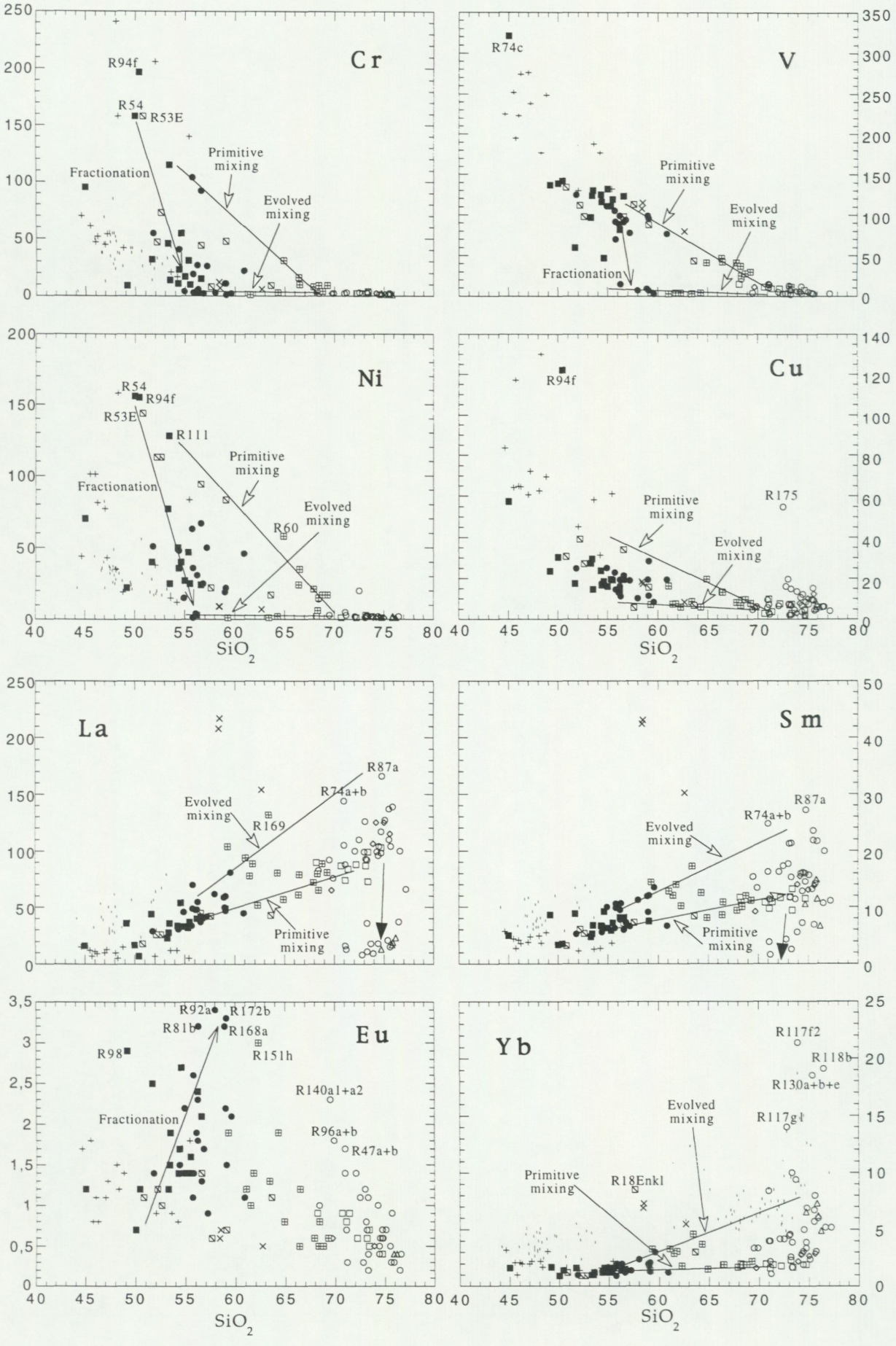
Cr
R94f
R54
R53E
Primitive mixing
Fractionation
Evolved mixing
V
R74c
Primitive mixing
Evolved mixing
Fractionation
Ni
R54
R94f
R53E
R111
Primitive mixing
Fractionation
Evolved mixing
R60
Cu
R94f
R175
Primitive mixing
Evolved mixing
La
R87a
R74a+b
Evolved mixing
R169
Primitive mixing
Sm
R87a
R74a+b
Evolved mixing
Primitive mixing
Eu
R92a
R172b
R81b
R168a
R98
R151h
R140a1+a2
Fractionation
R96a+b
R47a+b
Yb
R117f2
R118b
R130a+b+e
Evolved mixing
R117g1
Primitive mixing
R18Enkl
SiO2
SiO2

Fig. 41d

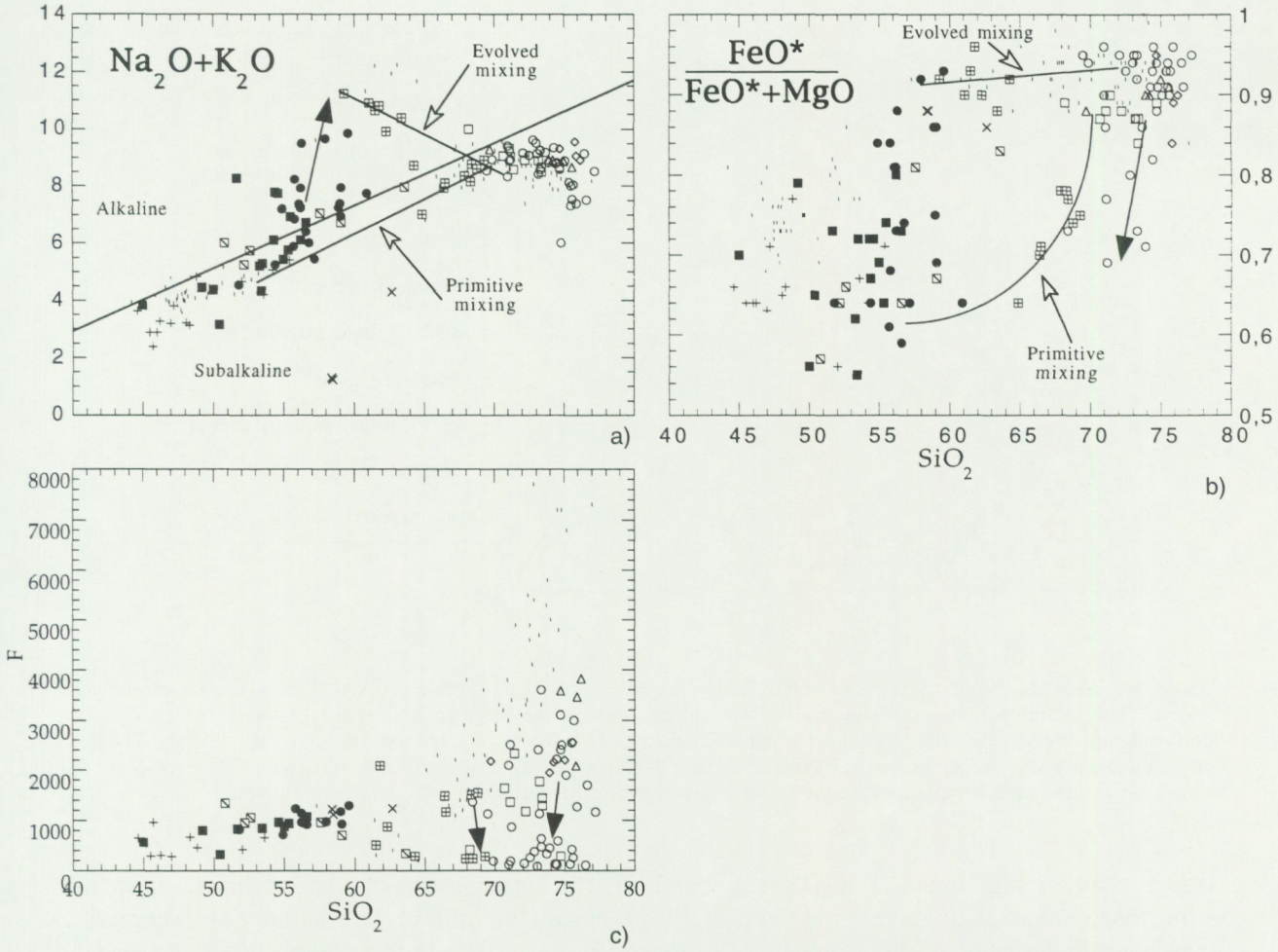

Fig. 42. Variation diagrams for total alkalies, iron-magnesium ratio, and fluorine. The two mixing trends are distinctly separated in the total alkalies diagram. The most evolved basic dykes are strongly enriched in alkalies. The silicic rocks are generally very high in the FeO*/FeO*+MgO ratio, generally above 0.85, typical for rapakivi granitoids (e.g. Rämö & Haapala 1995). This contrasts with, e.g. the Småland–Värmland granitoids (cf. Fig. 15). The most evolved rocks in the basic suite are also very high in iron/magnesium, and thus also the intermediate hybrids. In contrast, the silicic hybrids follow a trend towards a decreasing iron-magnesium ratio, suggesting mixing with the more primitive parts of the basic suite. The Suomenniemi granitoids are richer in F, compared with their Rödö counterparts. A number of silicic Rödö rocks are distinctly depleted in F.

(up to 15.4 %) in some QFPs, Na_2O (especially in the aplites, up to 5.08 %), Rb (up to 2080 ppm), Cs (17 ppm), Nb (659 ppm), Ga (79), Y (193 ppm), Pb (55 ppm), U (75.2 ppm), Th (240 ppm), Li (226 ppm, especially the aplites), Be (10.2 ppm), the HREEs (Yb 21.4 ppm), and F (3820 ppm, Fig. 41d).

Elements that show depleted values in certain parts of the suite comprise: K_2O (down to 4.24 %), Ba (39 ppm), Zr (18 ppm), Y (6.1 ppm), Be (1.1 ppm), the LREEs (La 8 ppm), the MREEs (Sm 1.6 ppm), Eu (0.2 ppm or less), and F (85 ppm). The total alkali content is generally high (c. 8–9 %, Fig. 42a), but decreases partly in the most silicic samples. The Fe-number is generally high (FeO*/FeO*+MgO > 0.85, Fig. 42b), which is typical for rapakivi rocks. In some of the QFPs, however, it decreases to 0.69.

The Rödö dolerites (including the "contaminated" dolerites and the mafic/hybrid enclaves), show a relatively large spread in composition, not least for SiO_2 (45.0 to around 60 %). The distinction between the most silicic dolerites (evolved and/or "contaminated") and the hybrid porphyries is not clear and the limit has been set somewhat arbitrarily to around 60 % SiO_2. A more or less arbitrary limit between dolerites and the "contaminated"/more evolved dolerites has been set at about 55 % SiO_2, based mainly on the occurrence of quartz and feldspar xenocrysts in the rock. Most elements show a considerable variation, e.g. K_2O (0.69–5.66 %), MgO (0.58–7.79 %), Ba (88–1280 ppm), Cr (<1–197 ppm), and Eu (0.7–3.4 ppm). Generally, the Rödö dolerites are low in TiO_2, Cr, V, Ni and Sc,

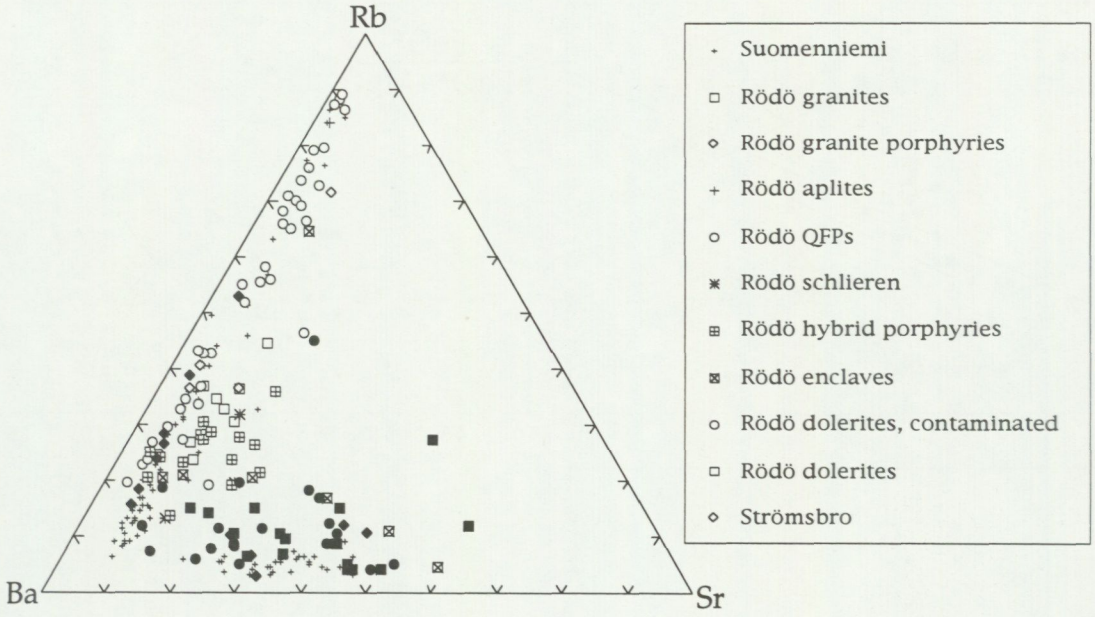

Fig. 43. Rb-Ba-Sr diagram for the rocks of the Rödö complex. Parts of the highly evolved Rödö QFPs are strongly Rb enriched. The hybrid porphyries are generally intermediate between the basic rocks and the granites. The rocks of the Suomenniemi complex generally lack the intermediate character of the Rödö suite, but trend to higher Ba contents. The Rödö complex generally lack rocks enriched in Ba (cf. the Jämtland–Ångermanland complexes, Fig. 62). Intermediate rocks are also lacking in the Strömsbro complex, where the granites have variable Rb enrichment. Discussion in the text.

whereas they are high in Na_2O, K_2O, Ba, Cs, and Eu. The high contents of alkali elements, especially in the "contaminated" dolerites (up to almost 10 %), make them plot in the alkaline field in Fig. 42a. Regarding the Fe-number, this is generally substantially lower than in the silicic Rödö rocks, around 0.6–0.7, but some samples extend to higher values (0.93).

The hybrid porphyries generally have an intermediate composition between the dolerites and the silicic rocks. The petrological delimitation towards the "contaminated" and/or most evolved dolerites is, as mentioned above, somewhat arbitrary. This also partly applies to the limit towards the QFPs. Within the suite of hybrid porphyries, two distinct groups can be separated with characteristic geochemistries: i) one group with a marked silicic composition (SiO_2 65.0–69.3 %), somewhat overlapping with granites and QFPs, and ii) one group with more intermediate composition (SiO_2 c. 60–65 %). These groups differ by showing divergent trends for many elements. The more silicic group, for example, exhibits a separate MgO-trend at higher contents (Fig. 41a), whereas the intermediate group partly shows extremely high K_2O contents (up to 9.12 %). Also with regard to Al_2O_3, MnO, Cs, Zr, Nb, Ga, Y, Zn, Be, and REE, the intermediate group has trends at higher abundances, whereas the silicic group is higher in Sr, V, Ni, and Li (Figs. 41a-d). Furthermore, the intermediate group is strongly alkaline in character (Fig. 42a), whereas the silicic group connects to the suite of silicic Rödö rocks (granites, QFPs, etc) on the subalkaline side of the diagram. The intermediate group of hybrid porphyries is also strongly enriched in Fe compared with Mg, while the opposite is true for the silicic hybrid porphyries (Fig. 42b).

The Postjotnian dolerites show elemental similarities to the Rödö dolerites, but differ by, e.g. having generally lower contents of SiO_2, K_2O, Ba, P_2O_5, and LREE, but higher contents of, e.g. V and Cu (cf. Fig. 40). They are clearly subalkaline in Fig. 42a, and have a tendency for lower FeO*/FeO*+MgO (Fig. 42b).

The rocks of the Suomenniemi suite differ from the Rödö suite by having higher abundances of Fe_2O_3*, MnO, CaO, Ba, Y, Sc, Yb, and F in the silicic part of the suite. In the basic rocks a tendency for higher contents of Fe_2O_3*, Zr, Y, P_2O_5, Sc, and REE is observed for the Suomenniemi rocks. The latter are also clearly subalkaline in Fig. 42a, and a tendency for higher FeO*/FeO*+MgO can be traced in Fig. 42b.

In the triangular plot in Fig. 43, the relative distribution of the LIL-elements Ba-Rb-Sr in the rocks of the Rödö suite is visualized. The rocks of the Strömsbro (Appendix 2b and Andersson 1997a) and Suomenniemi complexes are included for comparison. The QFPs plot generally at lower relative Sr contents, compared with the granites, extending towards high Rb contents. The hybrid porphyries overlap with the granites, but also show a trend to intermediate compositions between the granites and dolerites at higher relative Sr content. The Rödö dolerites tend to have significantly higher relative Rb contents compared with the Suomenniemi dolerites. The spread for most of the different rock types is large in the diagram.

6.3.4. REE-patterns

Chondrite-normalized plots of the rock types in the Rödö suite are shown in the diagrams of Fig. 44a–c. The Rödö granites are enriched in the LREEs ($La_N/Yb_N = 25.6–39.4$), with a distinct negative Eu-anomaly ($Sm_N/Eu_N = 4.6–9.9$). The patterns of the granite porphyries are identical to that of the granites. The rocks of the dark schlieren structures are strongly enriched in the REEs (e.g. La up to 217 ppm and Yb up to 7.3 ppm), except Eu (see also Fig. 41d), and thus have deeper negative Eu-anomalies ($Sm_N/Eu_N = 22.7–26.6$) than the granites in which they occur. Otherwise their patterns are parallel to that of the granites. The majority of the QFPs have patterns very similar to that of the granites (Fig. 44a), however, they are generally slightly less enriched in the LREEs ($La_N/Yb_N = 11.6–20.9$). The Eu-anomalies are partly deeper for the QFPs ($Sm_N/Eu_N = 2.8–27.2$), compared with the granites. A minor group of QFPs have patterns indistinguishable from the granites. Another small group of QFPs have very different patterns, with strong negative Eu-anomalies ($Sm_N/Eu_N = 5.4–20.1$), enrichment of the HREEs, and depletion of the LREEs ($La_N/Yb_N = 0.39–6.4$). The absolute abundances of the LREEs are sometimes very low (e.g. La down to 8 ppm), and very high for the HREEs (Yb up to 21.4 ppm). The aplites exhibit flat REE-patterns ($La_N/Yb_N = 2.1–3.2$), with significant Eu-anomalies ($Sm_N/Eu_N = 6.3–11.5$). The granites of the studied Jämtland–Ångermanland complexes (chapter 7.3.4., below) generally have flatter REE-patterns, and less deep negative Eu-anomalies (cf. Fig. 60).

A majority of the Rödö dolerites have LREE-enriched patterns without any Eu-anomaly (Fig. 44b). The patterns are slightly flatter than those of the granites ($La_N/Yb_N = 14.3–22.8$). A number of "contaminated"/evolved dolerites have patterns with similar LREE-enrichments ($La_N/Yb_N = 18.0–25.7$), but with a weak negative Eu-anomaly ($Sm_N/Eu_N = 1.6–4.0$).

The silicic group of hybrid porphyries have REE-patterns identical to the granites, whereas the intermediate ones have slightly weaker Eu-anomalies ($Sm_N/Eu_N = 2.5–5.0$), and higher contents of HREEs ($La_N/Yb_N = 14.8–19.4$; Fig. 44b). The basic/hybrid enclaves exhibit considerable similarity in REE-pattern to the xenocrystic ("contaminated") dolerites, except for R18Enkl, which is strongly enriched in the HREEs ($La_N/Yb_N = 3.4$).

The REE-patterns of 5 composite dykes have been plotted in Fig. 44b. R74 consists of a QFP part and a dolerite part. The QFP part is rich in the REEs, and shows a deep Eu-anomaly, similar to the other QFPs. The pattern of the dolerite is flatter ($La_N/Yb_N = 6.8$) than the average Rödö dolerite; in fact, showing more of a similarity to the patterns of the Postjotnian dolerites (Fig. 44c). R12 is comprised of three parts, where the QFP and hybrid porphyry parts are similar and in accordance with the other QFPs. The dolerite part corresponds to the Rödö dolerites without Eu-anomaly. R135a+b is the QFP part, which is markedly depleted in the LREEs ($La_N/Yb_N = 6.4$), whereas the dark, hybrid porphyry part (R135h), which occurs along the contact, is very similar in REE-pattern to the silicic hybrid porphyries (Fig. 44b). The dykes at 115a and 115b do not contain any QFP part. Samples R115a1 and R115a4 from the eastern dyke are actually quite close in their REE-patterns, which fall in the lower range of the Rödö dolerites and lack Eu-anomaly. R115b1+b2 represents the centre of the western dyke and belongs to the silicic hybrid porphyry group (SiO_2 66.4 %). It has a well-developed negative Eu-anomaly ($Sm_N/Eu_N = 6.5$). The mafic margin (R115b5+b6; $SiO_2 = 55.8$ %) has a less pronounced anomaly ($Sm_N/Eu_N = 2.9$). Otherwise the REE-patterns of the centre and marginal portions are almost identical, and closely similar to the silicic hybrid porphyries.

The Postjotnian dolerites have flat REE-patterns ($La_N/Yb_N = 1.5–6.2$), compared with the Rödö dolerites, with in particular low abundances of the LREEs (Fig. 44c). Only weak tendencies for Eu-anomalies exist, negative ($Sm_N/Eu_N = 1.2–1.7$) in some of the medium-grained and pegmatitic

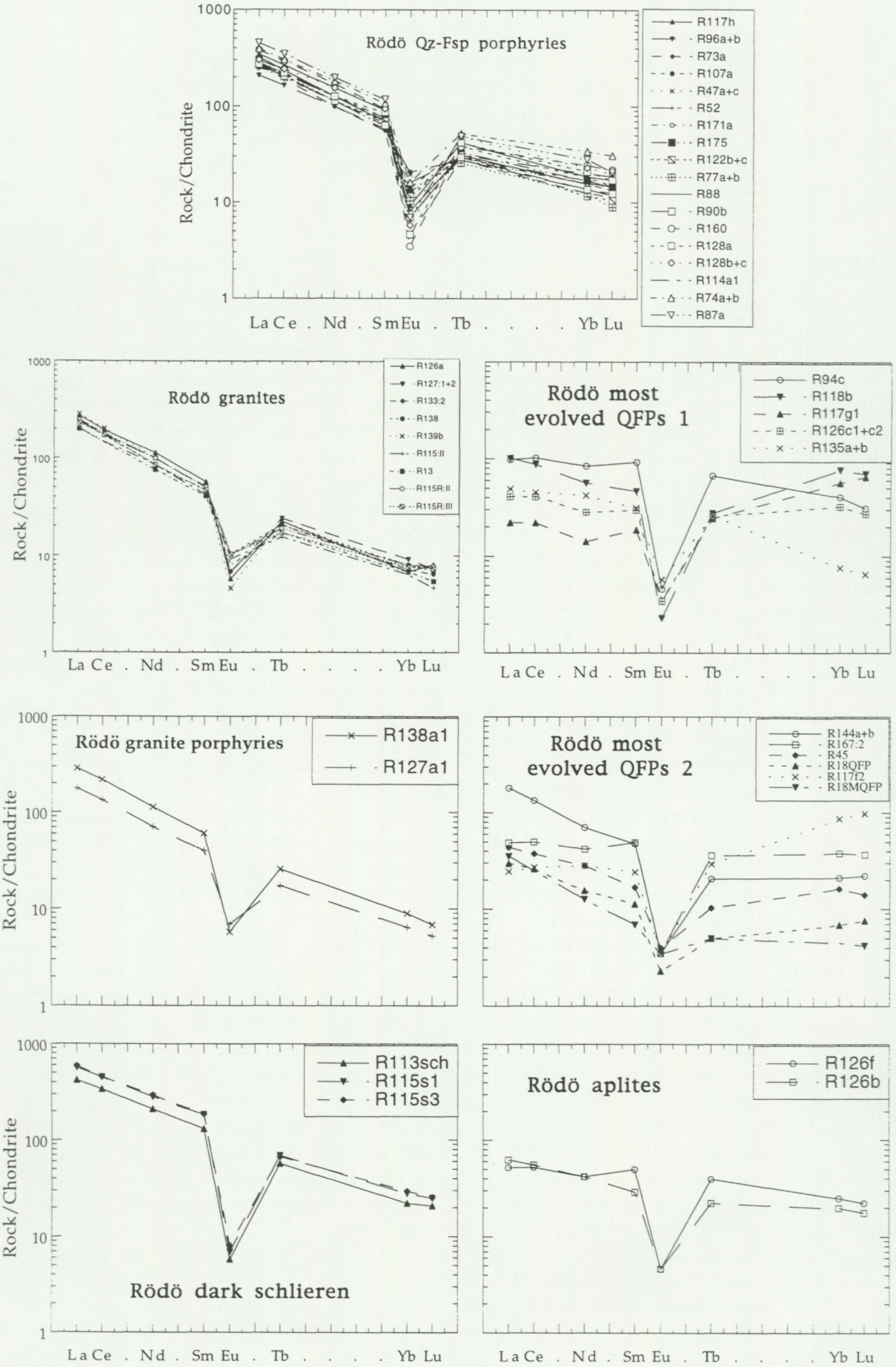
Rödö Qz-Fsp porphyries
Rock/Chondrite
1000
100
10
1
La Ce . Nd . Sm Eu . Tb . . . . Yb Lu
R117h
R96a+b
R73a
R107a
R47a+c
R52
R171a
R175
R122b+c
R77a+b
R88
R90b
R160
R128a
R128b+c
R114a1
R74a+b
R87a
Rödö granites
R126a
R127:1+2
R133:2
R138
R139b
R115:II
R13
R115R:II
R115R:III
Rödö most evolved QFPs 1
R94c
R118b
R117g1
R126c1+c2
R135a+b
Rödö granite porphyries
R138a1
R127a1
Rödö most evolved QFPs 2
R144a+b
R167:2
R45
R18QFP
R117f2
R18MQFP
Rödö dark schlieren
R113sch
R115s1
R115s3
Rödö aplites
R126f
R126b

Fig. 44a

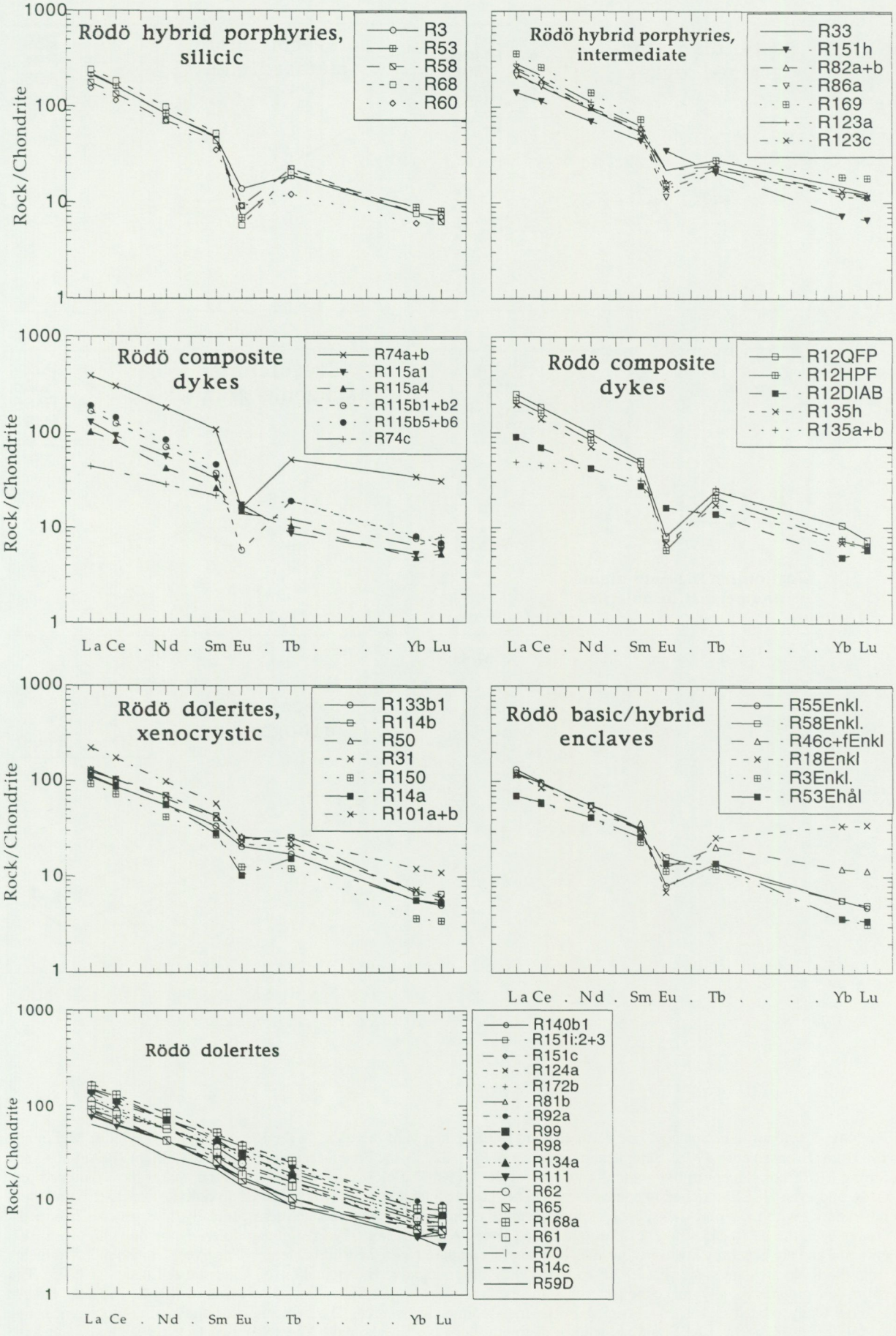
Rödö hybrid porphyries, silicic
R3
R53
R58
R68
R60
Rödö hybrid porphyries, intermediate
R33
R151h
R82a+b
R86a
R169
R123a
R123c
Rödö composite dykes
R74a+b
R115a1
R115a4
R115b1+b2
R115b5+b6
R74c
Rödö composite dykes
R12QFP
R12HPF
R12DIAB
R135h
R135a+b
Rödö dolerites, xenocrystic
R133b1
R114b
R50
R31
R150
R14a
R101a+b
Rödö basic/hybrid enclaves
R55Enkl.
R58Enkl.
R46c+fEnkl
R18Enkl
R3Enkl.
R53Ehål
Rödö dolerites
R140b1
R151i:2+3
R151c
R124a
R172b
R81b
R92a
R99
R98
R134a
R111
R62
R65
R168a
R61
R70
R14c
R59D
Rock/Chondrite
1000
100
10
1
La Ce . Nd . Sm Eu . Tb . . . . Yb Lu

Fig. 44b

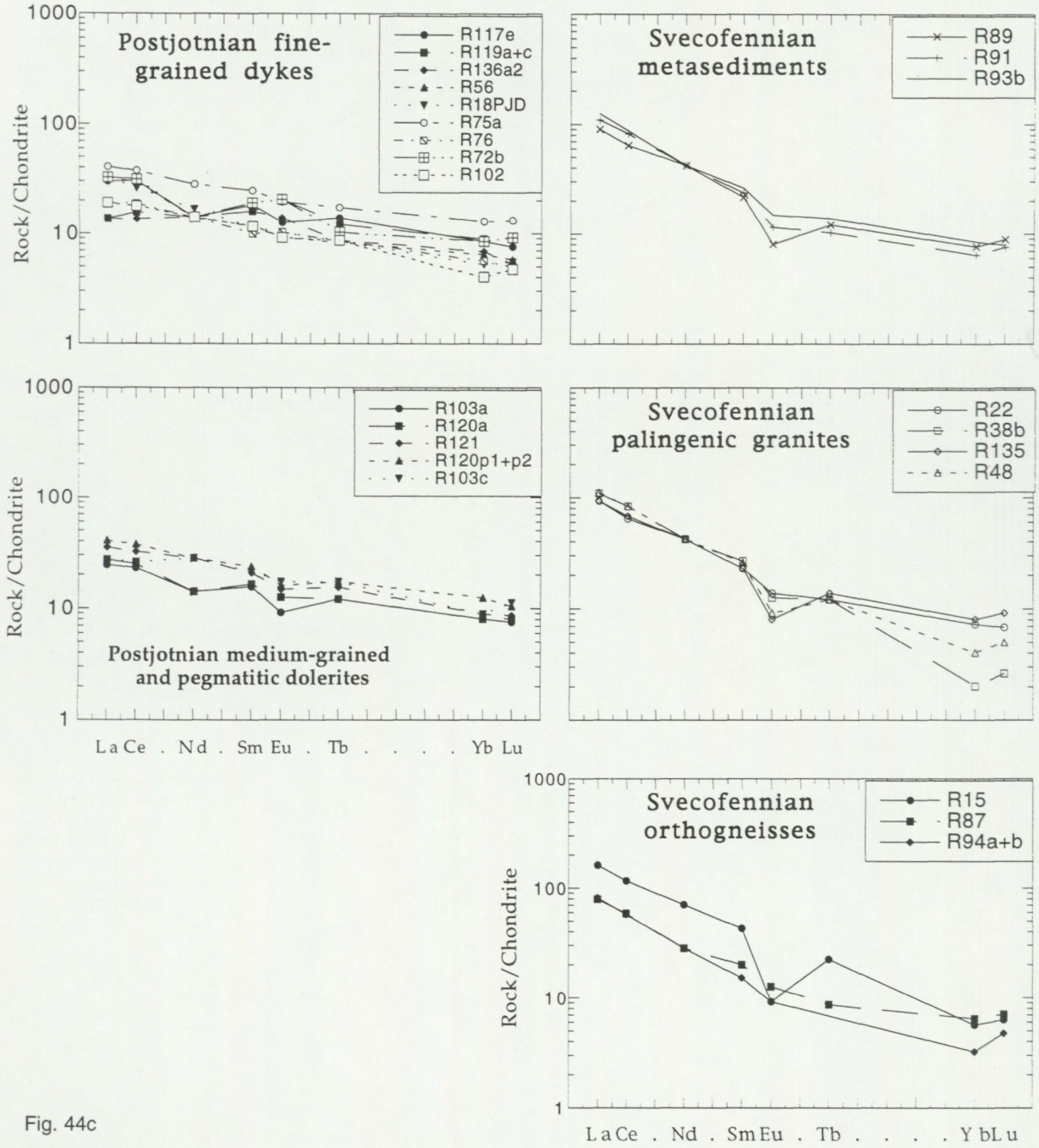

Fig. 44c

Fig. 44a–c. Chondrite normalized rare earth element (REE) patterns of the rocks in the Rödö complex (Taylor & McLennan 1985 after Evensen et al. 1978). Sample numbers refer to Figs. 32, 33, the Foldout map, and Appendix 2b). a) The silicic rocks. Strong LREE enrichment in the granites and most of the QFPs. The most evolved QFPs and the aplites have flattened patterns, and even HREE enriched in some cases. b) The intermediate and basic rocks. The Rödö dolerites are LREE enriched, in similarity with the silicic rocks, but lack in general Eu anomaly. The intermediate rocks generally have patterns intermediate between the basic and silicic. c) Postjotnian and Svecofennian rocks. The Postjotnian dolerites are only slightly LREE enriched and are generally lower in absolute abundances, compared with the Rödö dolerites. The Svecofennian metasediments from the Rödö area are somewhat LREE enriched with minor negative Eu anomalies (cf. Claesson & Lundqvist 1995). The palingenic granites closely image the patterns of the metasediments, apart from some being lower in HREE. The latter feature is most likely related to garnet remaining in the metasedimentary source. The orthogneisses show some divergence, one sample being higher in LREE and showing a distinctly negative Eu anomaly. The other two lack Eu anomaly and have patterns similar to other early Svecofennian granitoids in Bergslagen (cf. Fig. 17). Discussion in the text.

varieties, and positive ($Sm_N/Eu_N = 0.77–0.96$) in some of the thin dykes.

The REE-patterns for the metasediments and the related palingenic granites of the country rocks show large similarities (the metasediments: $La_N/Yb_N = 11.7–16.9$; $Sm_N/Eu_N = 1.8–2.7$; Fig. 44c), except that some of the granites have lower HREE contents. Two of the orthogneisses do not show any Eu-anomalies and differ in this way from the third which also has higher contents of the L- and MREEs.

6.4. ISOTOPE GEOLOGY

6.4.1. U-Pb zircon geochronology

Zircon geochronology was performed on rocks from the Rödö granite. Several small samples from the Rödö granite were utilized and mixed together, as one single big sample was not collected for practical reasons. These small samples were R126a, R127:1+2, R13, R133. Their location is displayed on the Foldout map. Nine fractions of zircons of different types and sizes were handpicked. Two of these were air-abraded. The zircons were of two different types, one long prismatic with a length:breadth ratio around 4:1, and one short prismatic with a length:breadth ratio around 1:1. The former were generally brown and turbid, but with well-developed crystal forms. The latter were clear, slightly yellow, also with sharp crystal forms. The analysed U and Pb blanks were 0.01 and 0.05 ng, respectively. The analytical results are shown in Table 12. All 9 fractions give a poor discordia with an upper intercept age of 1500±26 Ma (MSWD = 22) (Fig. 45b). The data for the most discordant fraction (R2) is of lower analytical quality and a bit off the discordia line to the right. If this fraction is omitted from the discordia calculation, the upper intercept age becomes 1504±19 Ma (MSWD=10). The relatively large MSWD value indicates a relatively large scatter among the fractions, more than can be accounted for by analytical errors. If all fractions with positions slightly to the right of the discordia above (R1, R2, R6, and R10) are omitted from the age calculation, the age obtained is, within errors, the same as before (1493±12 Ma, MSWD = 1.8). The two abraded fractions (R9 and R10) are the most concordant (3 and 0.3 % discordancy, respectively). They yield $^{207}Pb/^{206}Pb$ ages of 1490 and 1503 Ma, respectively. An age calculation using only these two abraded fractions gives 1507±47 Ma. One fraction is above the concordia curve (R4). If this fraction together with those that are slightly displaced to the right (R1, R2, R6) are omitted the statistically most well constrained age is calculated (1497±6 Ma, MSWD=1.3; lower intercept is 229±21 Ma).

Table 12
U-Pb zircon results, Rödö granite

Fraction	Weight (µg)	number of crystals	U (ppm)	Pb_{tot} (ppm)	Pb_{com} (ppm)	$^{206}Pb/^{204}Pb$ (1)	rad. Pb atomic % 206-207-208Pb	$^{206}Pb/^{238}U$ (2)	$^{207}Pb/^{235}U$ (2)	$^{207}Pb/^{206}Pb$ (2)	$^{207}Pb/^{206}Pb$ (age)
R1 >210 µm LP brown	138.6	2	746	183.8	-	2107	90.2-8.4-1.4	0.2236±9	2.879±14	0.09336±28	1495±4
R2 150-210 µm SP clear	104.0	8	97	17.0	0.526	801	76.7-7.1-16.2	0.1507±31	1.922±42	0.09252±77	1478±12
R3 150-210 µm LP brown	215.5	9	455	94.6	5.48	835	78.4-7.1-14.5	0.1786±2	2.227±10	0.09044±35	1435±6
R4 100-150 µm SP clear	132.9	16	79	25.0	0.381	1578	76.7-7.2-16.1	0.2789±8	3.590±23	0.09335±52	1495±8
R5 100-150 µm LP brown	241.1	23	601	118.7	5.40	1058	77.1-6.9-16.0	0.1687±2	2.083±7	0.08951±28	1415±4
R6 74-100 µm SP claer	180.1	50	200	45.0	2.89	710	78.8-7.2-14.0	0.1927±3	2.436±13	0.09168±42	1461±7
R7 74-100 µm LP brown	444.3	94	486	99.0	3.37	1456	78.3-7.1-14.6	0.1789±2	2.230±11	0.09043±42	1435±7
R9 >100 µm abraded	60.1	17	237	65.3	1.20	1540	80.0-7.4-12.6	0.2515±5	3.228±10	0.09310±21	1490±3
R10 >100 µm abraded	48.6	11	64	19.8	1.22	413	77.4-7.3-15.3	0.2605±16	3.367±36	0.09375±81	1503±13

LP = long prismatic, SP = short prismatic. Pb_{tot} is total lead, and Pb_{com} common lead. (1) $^{206}Pb/^{204}Pb$ only corrected for mass discrimination.

(2) Ratios corrected for mass discrimination, blank (0.01 ng U and 0.05 ng Pb), and common Pb ($^{206}Pb/^{204}Pb$=15.8, $^{207}Pb/^{204}Pb$=15.2, $^{208}Pb/^{204}Pb$=35.3). Errors are 2 σ.

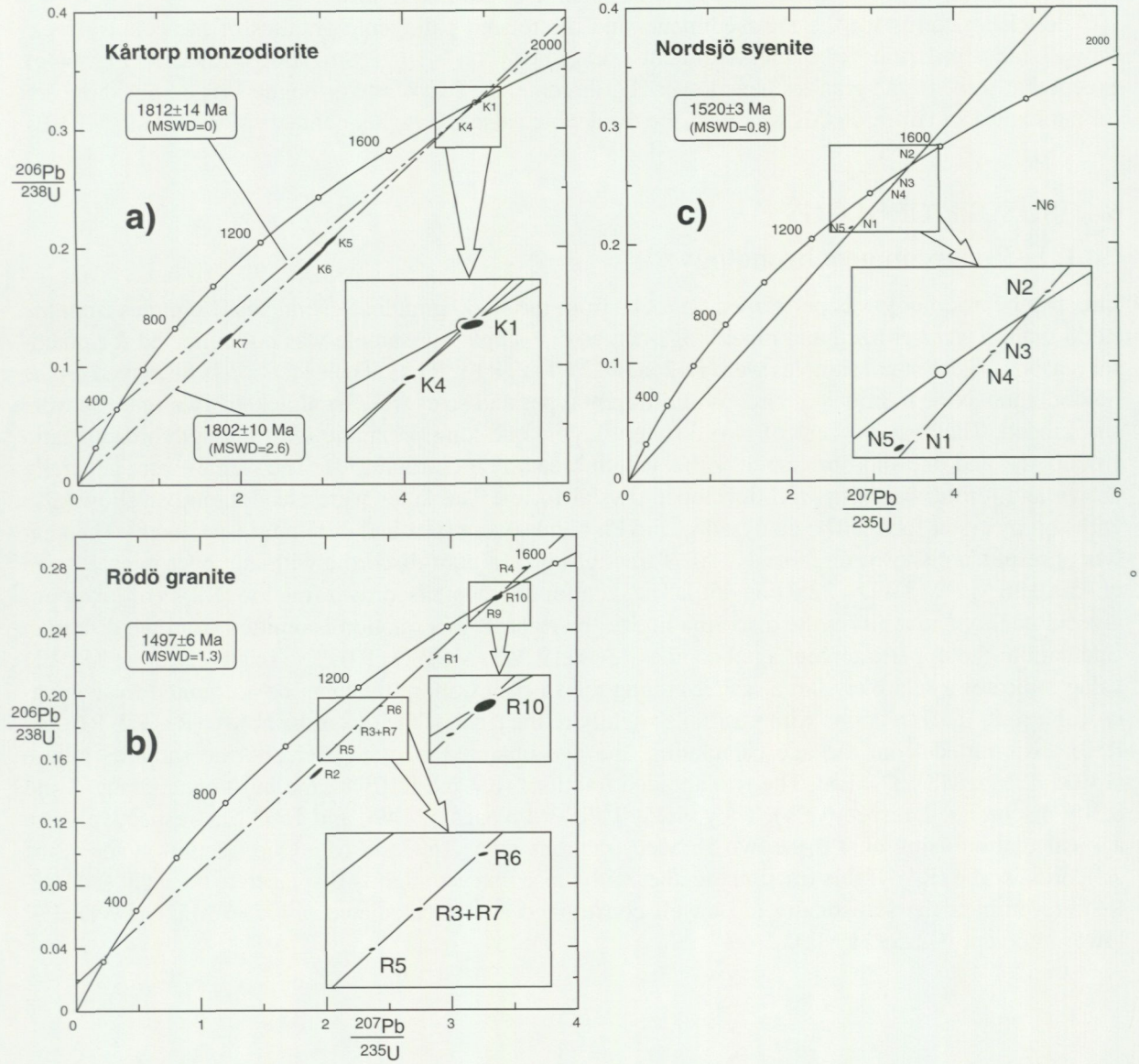

Fig. 45. Concordia U-Pb zircon diagrams for three of the five dated rocks in this study. The preferred ages are indicated in the diagrams. a) The Kårtorp monzodiorite. Seven fractions were analyzed, two air-abraded (K6 and K7). The analyses of fractions K2 and K3 were unsuccessful. Fractions K5-K7 are very discordant and extrapolate towards the origin. This indicates problems in preparation and if these fractions are omitted a two fraction discordia gives the preferred age 1812±14 Ma (MSWD=0 since only two fractions). $^{207}Pb/^{206}Pb$ ages of fractions K1 and K4 are 1810 and 1799 Ma, respectively. b) The Rödö granite. Nine fractions were analyzed; two air-abraded (R9 and R10). The analyses show some scatter around the discordia. The preferred age is obtained by omitting fractions R1, R2, R4, and R6. c) The Nordsjö syenite. Six fractions were analyzed. The discordia was calculated omitting fractions N5 and N6. Fraction N6 is strongly offset to the right of the rest of the analyzed fractions, with a $^{207}Pb/^{206}Pb$ age of 2390 Ma. Discussions in the text.

6.4.2. Nd isotopes

Twenty-nine WR-samples from the Rödö area have been analysed for their Nd isotopic composition (Table 13). Twenty-one belong to rocks of the Rödö suite, 2 are Postjotnian dolerites, 2 orthogneisses, 2 metasediments, and 2 palingenic granites. Among the analysed Rödö rocks, most of the different types are represented: granites, QFPs, hybrid porphyries, dolerites, one aplite, and one enclave. The analysed $^{143}Nd/^{144}Nd$ ratios are low for the granites (0.511254–0.511296), while the values for the

Table 13. Nd and Sr isotopic results, Rödö area.

	SiO_2 (XRF)	MgO (XRF)	Sm (MS)	Nd (MS)	$^{147}Sm/^{144}Nd$	$^{143}Nd/^{144}Nd$	$\varepsilon_{Nd}(1.50)$	$\varepsilon_{Nd}(t)$	T(DM)	$f_{(Sm/Nd)}$	Rb (XRF)	Sr (XRF)	$^{87}Rb/^{86}Sr$	$^{87}Sr/^{86}Sr$	$^{87}Sr/^{86}Sr(1.50)$	$^{87}Sr/^{86}Sr(i)$
Rödö granites																
R126a	73.4	0.36	13.54	88.18	0.0928	0.511274 (6)	-6.65	->	2.23	-0.53	223	58	10.74	0.913555 (15)	0.6823	->
R127:1+2	73.2	0.38	12.86	80.98	0.0960	0.511295 (12)	-6.86	->	2.27	-0.51	226	96	8.59	0.881124 (13)	0.6962	->
R133:2	72.2	0.36	12.06	77.73	0.0937	0.511296 (6)	-6.40	->	2.22	-0.52	208	151	5.80	0.820179 (21)	0.6953	->
R138	70.7	0.37	11.61	74.13	0.0947	0.511254 (13)	-7.41	->	2.30	-0.52	227	131	5.429	0.811473 (27)	0.6946	->
Quartz-feldspar porphyries																
R73a	74.4	0.12	12.82	77.46	0.1001	0.511336 (8)	-6.85	->	2.30	-0.49	281	41	30.0	1.235583 (20)	0.5897	->
R96a+b	69.9	0.20	13.96	77.77	0.1076	0.511384 (8)	-7.36	->	2.37	-0.45	208	56	14.5	0.978438 (16)	0.6663	->
R117g1	72.8	0.17	4.10	11.24	0.2204	0.512606 (15)	-5.20	->	-	0.12	1 870	35	218	4.728422 (156)	0.0352	->
R160	75.9	0.08	24.47	134.45	0.1100	0.511405 (4)	-7.41	->	2.42	-0.44	237	<10	41.0	1.447649 (211)	0.5650	->
R167:2	73.7	0.17	11.95	33.24	0.2174	0.512598 (8)	-4.78	->	-	0.11	451	41	43.8635	1.563732 (89)	0.6194	->
R144a+b	77.2	0.01	11.55	48.05	0.1454	0.511800 (8)	-6.51	->	2.81	-0.26	251	23	30.5723	1.092798 (148)	0.4346	->
Aplite																
R126f	75.9	0.08	10.65	34.18	0.1883	0.512214 (11)	-6.68	->	-	-0.04	540	<10	239	5.198968 (15521)	0.0537	->
Rödö dolerites																
R101a+b	59.6	0.61	14.38	82.42	0.1055	0.511346 (6)	-7.69	->	2.40	-0.46	237	89	6.4582	0.845026 (22)	0.7060	->
R111	53.4	6.91	5.56	30.29	0.1110	0.511424 (12)	-7.23	->	2.41	-0.44	41	564	0.2421	0.708770 (9)	0.7036	->
R134a	51.7	2.69	9.31	50.89	0.1106	0.511353 (3)	-8.54	->	2.51	-0.44	185	265	2.218	0.758789 (28)	0.7110	->
R14c	53.5	3.32	7.61	41.41	0.1110	0.511340 (18)	-8.87	->	2.54	-0.44	48	522	0.1398	0.708316 (14)	0.7053	->
Hybrid porphyries																
R86a	61.5	0.45	13.49	78.38	0.1040	0.511367 (10)	-6.99	->	2.33	-0.47	178	63	8.60	0.869521 (38)	0.6844	->
R133b1	56.2	2.43	7.70	42.89	0.1085	0.511414 (19)	-6.94	->	2.37	-0.45	129	455	0.9920	0.727760 (20)	0.7064	->
R68(1)	68.8	1.23	12.07	75.13	0.0971	0.511262 (5)	-7.72	->	2.33	-0.51	172	270	2.4541	0.760926 (14)	0.7081	->
R68(2)			12.12	75.31	0.0972	0.511305 (8)	-6.89	->	2.28	-0.51			2.4542	0.761140 (13)	0.7083	->
R115a1	59.1	3.12	8.24	47.50	0.1054	0.511358 (8)	-7.44	->	2.38	-0.46	147	446	2.408	0.770593 (15)	0.7188	->
R151h	62.3	0.78	10.39	56.69	0.1108	0.511370 (5)	-8.25	->	2.49	-0.44	225	243	1.012	0.733373 (15)	0.7116	->
Hybrid enclave																
R18Enkl	57.6	1.64	8.88	37.88	0.1416	0.511709 (23)	-7.55	->	2.85	-0.28	538	65	20.74	1.10547 (31)	0.6590	->
Postjotnian dolerites																
R72b	45.5	7.19	4.40	17.49	0.1521	0.512436 (13)	->	3.27	1.49	-0.23	17	301	0.194	0.706567 (14)		0.7031
R120a	47.0	6.75	3.88	15.07	0.1557	0.512453 (8)	->	3.02	1.54	-0.21	22	372	0.064	0.704610 (12)		0.7035
Sedimentary gneisses																
R91	68.7	2.15	5.29	28.88	0.1106	0.511418 (6)	-7.27	-2.92	2.41	-0.44	142	254	1.7041	0.752605 (29)	0.7159	0.7063
R89	68.0	2.29	5.24	28.51	0.1110	0.511397 (5)	-7.76	-3.43	2.45	-0.44	105	253	1.505	0.745135 (26)	0.7127	0.7042
Palingenic granites																
R22	67.3	1.95	5.34	29.53	0.1092	0.511435 (13)	-6.67	-3.04	2.35	-0.44	130	259	1.708	0.751064 (18)	0.7143	0.7063
R38b	69.4	1.86	6.07	31.73	0.1156	0.511501 (13)	-6.61	-3.25	2.4	-0.41	146	215	2.206	0.766978 (35)	0.7195	0.7092
Orthogneisses																
R94a+b	69.1	1.14	4.07	23.79	0.1035	0.511560 (13)	-3.12	1.59	2.05	-0.47	101	287	1.026	0.729691 (19)	0.7076	0.7018
R15	70.0	1.23	10.06	53.09	0.1145	0.511558 (12)	-5.28	-1.13	2.29	-0.42	164	198	2.947	0.782908 (13)	0.7195	0.7027

SiO_2, MgO, Rb, and Sr extracted from Appendix 2b. Initial values calculated at 1.89 Ga for the sedimentary gneisses and orthogneisses; at 1.82 Ga for the palingenic granites and at 1.26 Ga for the Postjotnian dolerites.

$^{143}Nd/^{144}Nd$ is corrected according to average La Jolla standard measurements at the time of analysis (see Appendix 1). Measured $^{87}Sr/^{86}Sr$ ratios corrected according to average standard (SRM987) measurements at the time of analysis (see Appendix 1).

$^{147}Sm/^{144}Nd$: relative std dev. estimated to be better than 0.5%. Rb/Sr measured by XRF. Normally 4 measurements on 2 briquettes. Average relative "spread" 0.012 %. Significant number of digits in relation to "spread" of data (see Appendix 1).

QFPs range up to very high values (0.511336–0.512606). Also the aplite shows a very high measured $^{143}Nd/^{144}Nd$ value (0.512214). The dolerites and hybrid porphyries have intermediate values (0.511262–0.511424), whereas the analysed enclave lies somewhat higher (0.511709).

The $^{147}Sm/^{144}Nd$ values are also low for the granites (0.0928–0.0960), whereas some of the QFPs and the aplite exhibit values strongly depleted in Nd (0.1001–0.2204). The dolerites and hybrid porphyries have distinctly low values for basic rocks (0.0971–0.1110), while the enclave is higher (0.1416).

The measured isotope ratios are generally higher for the gneisses and palingenic granites than for the Rödö granites (Table 13), and are typical for similar Svecofennian rocks elsewhere (cf. e.g. Patchett et al. 1987, Claesson & Lundqvist 1995). Also the Postjotnian samples have measured ratios in accordance with previous measurements of rocks of the same suite (Claesson 1987, Rämö 1990, Patchett et al. 1994, Andersson 1997a), and thus initial ε values that are relatively depleted, though not as depleted as the DM represented by the DM curve of DePaolo (1981).

The initial ε_{Nd} values for the Rödö rocks have been calculated at the 1.50 Ga U-Pb crystallization age of the granite (Table 13). The range of initial ε_{Nd} values are visualized in Fig. 46, together with data from other Fennoscandian rapakivi complexes and other relevant rocks. The rocks of the

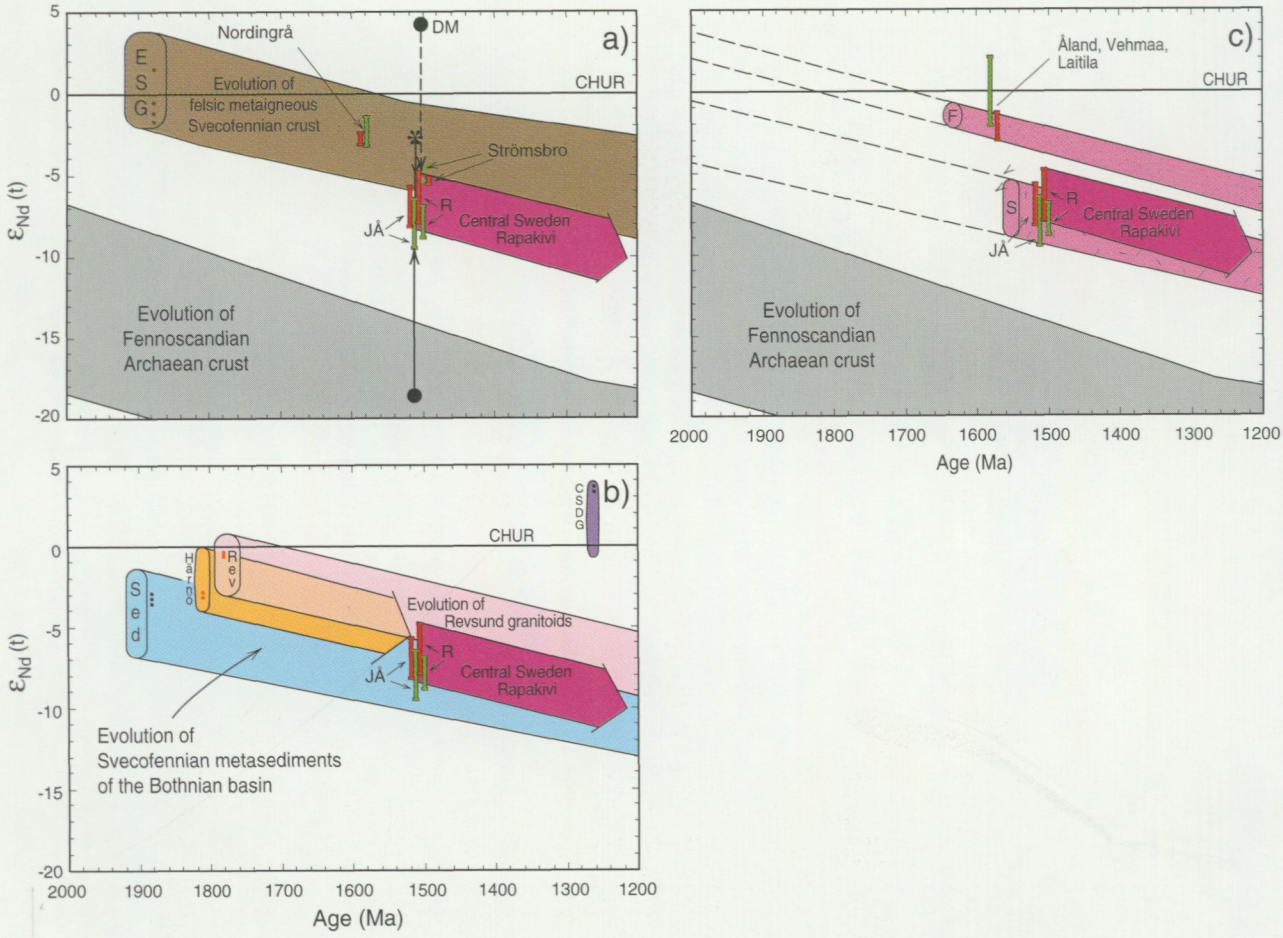

Fig. 46. ε_{Nd} evolution vs. time for rocks from Fennoscandian rapakivi complexes. ESG is early Svecofennian metaigneous rocks. Sed is sedimentary rocks in the Bothnian basin. Härnö is Härnö suite (c. 1.82 Ga) granites. Rev is the Revsund granitoid suite. F is silicic rocks of the Suomenniemi complex (excluding topaz-bearing types). S is rocks of the Salmi batholith. Central Sweden rapakivi denotes the evolution of silicic-intermediate rocks of this study. DM is the approximate composition of the depleted mantle at 1.51 Ga (DePaolo 1981). Black dot in the Archaean field denotes the average composition of Fennoscandian Archaean rocks, and the star similarly denotes the early Svecofennian metaigneous rocks. Sources of data: this study, Martin et al. 1983, Jahn et al. 1984, Wilson et al. 1985, 1987, Miller et al. 1986, Patchett & Kouvo 1986, Öhlander et al. 1987, Patchett et al. 1987, 1994, Claesson 1987, Huhma 1986, 1987, Valbracht 1991, Welin et al. 1993, Claesson & Lundqvist 1995, Rämö 1991, Andersson 1994, Neymark et al. 1994, Fröjdö et al. 1996, Lindh & Johansson 1996, Andersson 1997a, Fröjdö, Andersson & Eklund unpubl. data). Discussion in the text.

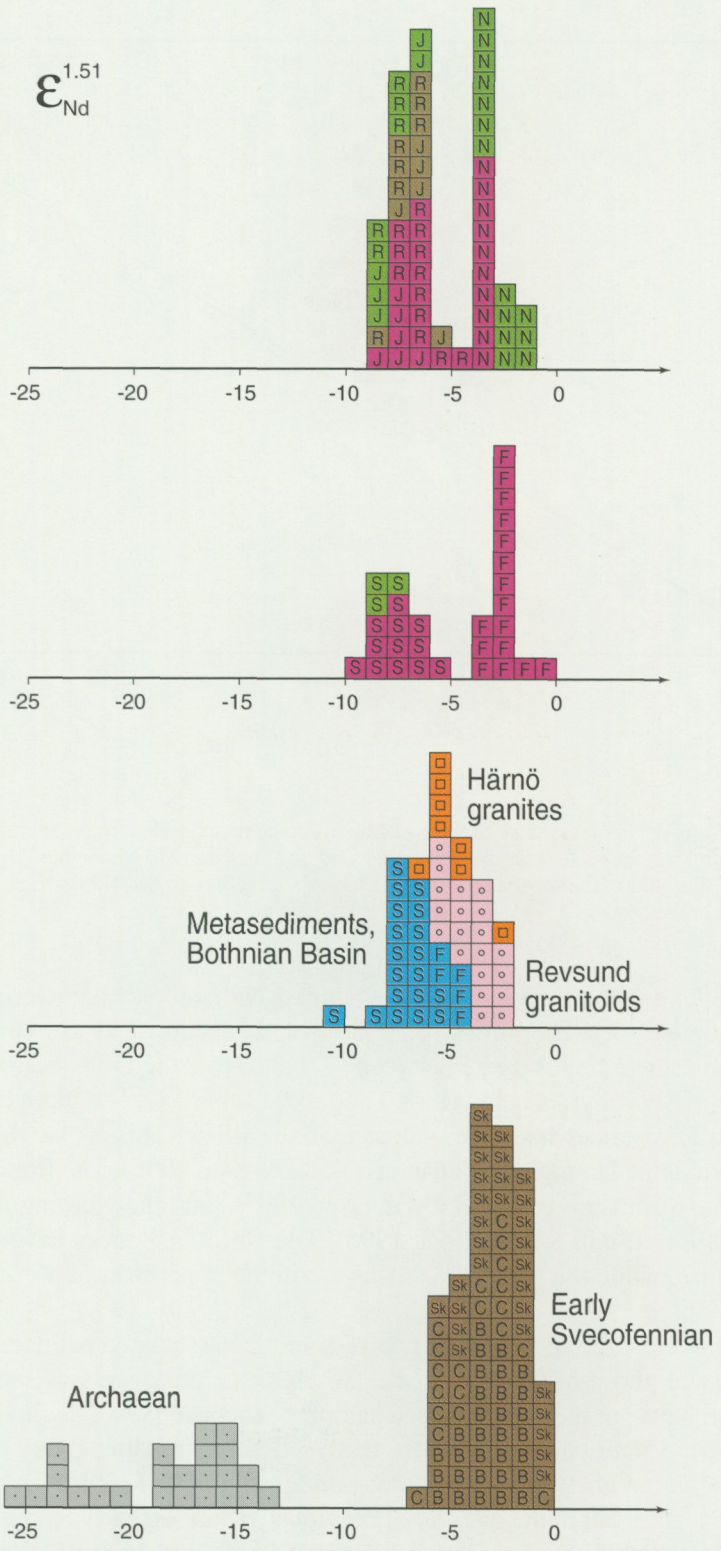

Fig. 47. Histogram showing the ε_{Nd} spread at 1.51 of analyses for different Fennoscandian rapakivi complexes and pertinent rocks. The lettering refers to the following. Early Svecofennian (metaigneous): B is Bergslagen region, C is central Sweden (Bothnian basin), and Sk is the Skellefte district. Metasediments: S is in the Swedish part and F in the Finnish part. Two upper levels refer to rapakivi complexes: S is Salmi, F is Suomenniemi (excluding topaz-bearing rocks), N is Nordingrå, R is Rödön, and J is Jämtland–Ångermanland. Green is basic rocks, red is silicic rocks, and brownish green is intermediate rocks. There is a "bimodal" distribution of Nd isotopic characteristics, where the Salmi and the central Swedish (excluding Nordingrå) complexes have lower initial ε_{Nd} compared to Nordingrå and the Finnish equivalents. The SW Finnish complexes are similar in Nd characteristics to the other Finnish complexes (not shown; Rämö 1991, Fröjdö, Andersson & Eklund unpubl. data). At 1.51 Ga (age of rapakivi magmatism in central Sweden) the central Swedish complexes have lower ε_{Nd} than the early Svecofennian metaigneous rocks of the region, but are similar to the metasediments of the Bothnian basin, while the Finnish complexes and Nordingrå compare well with the metaigneous Svecofennian rocks. Sources of data are the same as in Fig. 46 (excluding Fröjdö, Andersson & Eklund unpubl. data). Discussion in the text.

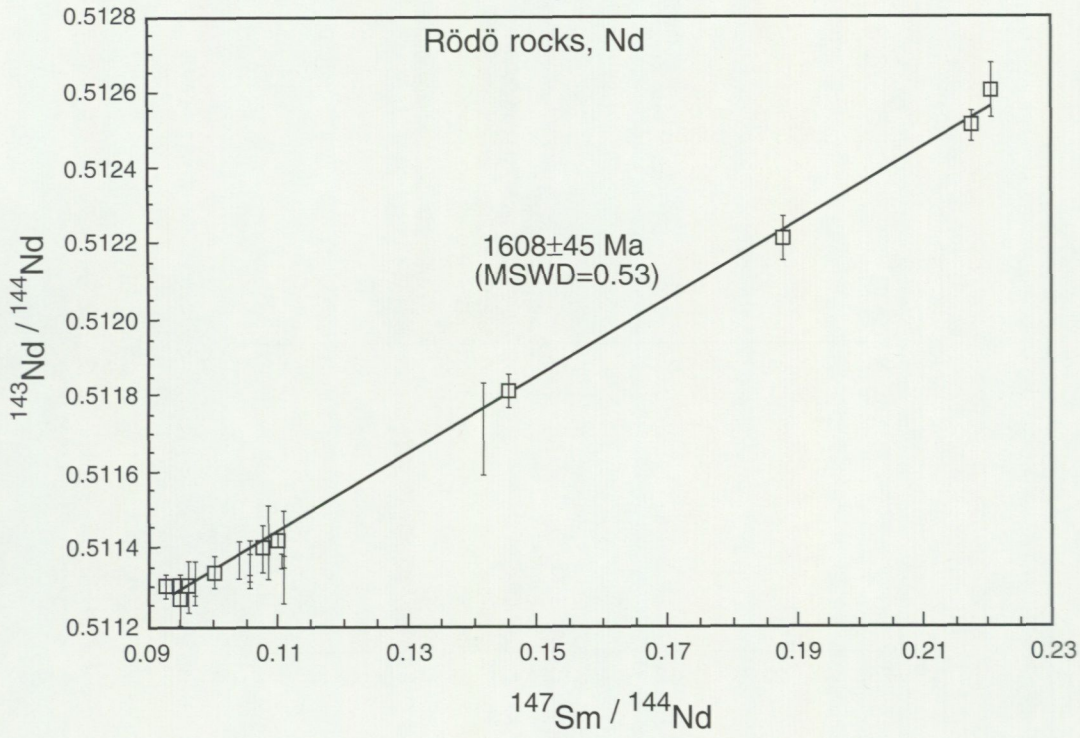

Fig. 48. $^{147}Sm/^{144}Nd$-$^{143}Nd/^{144}Nd$ diagram for the rocks of the Rödö complex. Silicic rocks are marked with squares. An isochron of acceptable quality was calculated for the silicic rocks, giving an age c. 110 Ma higher (1608±45 Ma) compared with the U-Pb zircon age (cf. Fig. 45b). The most evolved rocks have extremely high Sm/Nd ratios and control the isochron to a large extent. Discussion in the text.

Jämtland–Ångermanland complexes have closely similar Nd isotopic characteristics and only slightly higher ages (see chapter 7.4.). The initial ε_{Nd} values of the Rödö rocks are very low, irrespective of chemical composition: the granites range between -7.4 and -6.4, the QFPs between -7.4 and -4.8, and the dolerites and hybrid porphyries between -8.9 and -6.9 (Table 13). The more basic rocks of the suite thus actually tend to have somewhat lower values than the silicic. This is also the case for the rocks in the Jämtland–Ångermanland complexes (chapter 7.4.2., Persson 1996). The Rödö rocks differ in initial ε_{Nd} from those of the Strömsbro complex (Andersson 1997a) and the Nordingrå complex (Andersson 1994, Fröjdö et al. 1996, Lindh & Johansson 1996). The Nordingrå rocks have distinctly more radiogenic (higher) ε values, while the Strömsbro rocks are in the uppermost part of the range for the silicic Rödö rocks (Fig. 46a).

The ε_{Nd} (1.50) values of the sedimentary gneisses and the associated palingenic granites show considerable similarity with those of the Rödö rocks, whereas the orthogneisses show higher values even if the spread is large between the two analysed samples. The samples of sedimentary gneiss analysed in this study fall in the interval of previously analysed corresponding rocks of the Bothnian basin (Claesson 1987, Patchett et al. 1987, Claesson & Lundqvist 1995). This is also true for the palingenic granites. The orthogneisses fall in the interval of previously analysed early Svecofennian granitoids (cf. Patchett et al. 1987, Huhma 1986, Patchett & Kouvo 1986, Valbracht 1991, Welin et al. 1993, Claesson & Lundqvist 1995), even if sample R15 is on the lower edge. In the Bothnian basin area of central Sweden there is a slight tendency towards lower ε_{Nd} values in the early Svecofennian granitoids (Welin et al. 1993, Claesson & Lundqvist 1995, this study), compared with other parts of the Svecofennian domain (cf. Fig. 47). The initial ε_{Nd} value (at 1.26 Ga) of the analysed Postjotnian dolerites lies in the depleted area (+3.0 to +3.3), but is not as depleted as the DM curve (+4.5) of DePaolo (1981). This is similar to values obtained previously of rocks in this suite (Claesson 1987, Rämö 1990, Patchett et al. 1994, Andersson 1997a). Patchett et al (1994) and Andersson (1997a) also in parts received lower $\varepsilon_{Nd}(1.26)$ (-0.7 to +1.8) for this group of dolerites in the Dala region and Strömsbro area further south.

An attempt to extract geochronological information from the Sm-Nd WR data of the Rödö rocks is

shown in Fig. 48. All Rödö rocks have been plotted, but only the silicic (unfilled squares) have been utilized in the isochron calculation. This gives an age of 1608±45 Ma (MSWD = 0.53), which is an isochron of acceptable quality. All but one sample are within analytical error on the isochron line. This age is significantly higher and outside the calculated error limits compared with the 1497±6 Ma age derived from the U-Pb zircon data above and the 1513±5 Ma U-Pb zircon age of Welin (1994). The data from the basic and intermediate rocks do not give any meaningful age results.

6.4.3. Sr isotopes

The same 29 samples that were analysed for Nd isotopes were also analysed for Sr isotopes (Table 13). The granites have measured $^{87}Sr/^{86}Sr$ between 0.8118 and 0.9135, whereas the Sr in the QFPs and the aplite is partly strongly radiogenic with values between 0.9784 and 5.1989. The dolerites and hybrid porphyries have very varying $^{87}Sr/^{86}Sr$, but generally somewhat lower (0.7082–1.1054). The two Postjotnian dolerites have low values (0.7045–0.7065), whereas the older Svecofennian rocks have measured $^{87}Sr/^{86}Sr$ in the interval 0.7296–0.7829.

Also the $^{87}Rb/^{86}Sr$ ratios vary considerably. The silicic rapakivi rocks often have high (5.43–43.84) ratios, sometimes very high (218–239). Among the basic to intermediate rocks this ratio varies between 0.1398 and 20.74. (The numerical values of the ratios have been rounded off according to the calculated errors in Table 13.)

The analytical errors in the $^{87}Sr/^{86}Sr$ ratios are very high in some analyses, which may have propagated in the calculation of the initial $^{87}Sr/^{86}Sr$ ratios (at 1.50 Ga). All apparent initial Sr values are very to extremely low and unrealistic for the silicic rocks. They are, e.g. considerably lower than the value for an assumed bulk earth (UR = uniform reservoir) at this time (0.7027). The initial ratios for the basic and intermediate rocks are, with some exceptions, realistic. Some of these are relatively primitive (0.7036–0.7053), others somewhat higher (0.7060–0.7064) and a third group distinctly higher (0.7110–0.7188). The Postjotnian dolerites exhibit primitive values (0.7031–0.7035; at 1.26 Ga). The Svecofennian metasediments and the palingenic granites have intermediate initial Sr values (at 1.89 and 1.82 Ga, respectively). At the time of 1.50 Ga these rocks have values between 0.7127 and 0.7195. The orthogneisses on the other hand, are initially (at 1.89 Ga) rather primitive (0.7018–0.7027). At the time of rapakivi magmatism the two samples have developed quite differently, to 0.7072 and 0.7186 respectively, where the latter is within the interval of the metasediments. This is also in agreement with the low $\varepsilon_{Nd}(1.50)$ value for this sample.

To see if these WR-Sr measurements could be used geochronologically the results were plotted in Fig. 49a. All analyses are included but only the silicic rocks were used in the isochron calculation. The calculated "age" is 1340±39 Ma (MSWD = 154), which is c. 270 Ma lower than the age calculated from the WR-Nd isochron and 160 Ma less than the U-Pb zircon age. The very high MSWD value, however, indicates that there is considerable scatter around the line, and it cannot be regarded as an isochron. This is more clearly shown in a diagram of the type seen in Fig. 49b (Provost 1990). Here the basic to intermediate rocks have been encircled and not used for the age calculation. This type of diagram is a transformation of the axes on the conventional one, where the fit of individual analyses to the regression line is more clearly seen and the quality thus more lucidly displayed (cf. Fig. 49a). Furthermore, it is constructed in such a manner that the intersection with the right-hand axis shows the age, and the intersection with the left-hand axis shows the initial $^{87}Sr/^{86}Sr$ ratio (Provost 1990). As can be seen from this diagram, almost none of the analyses are within error on the line. Calculations omitting certain samples do not improve the results. If, e.g., the two samples with the most elevated Rb/Sr ratios (R126f, aplite, and R117g1, QFP) are omitted, this gives an almost identical age result (1346±28 Ma, MSWD = 48).

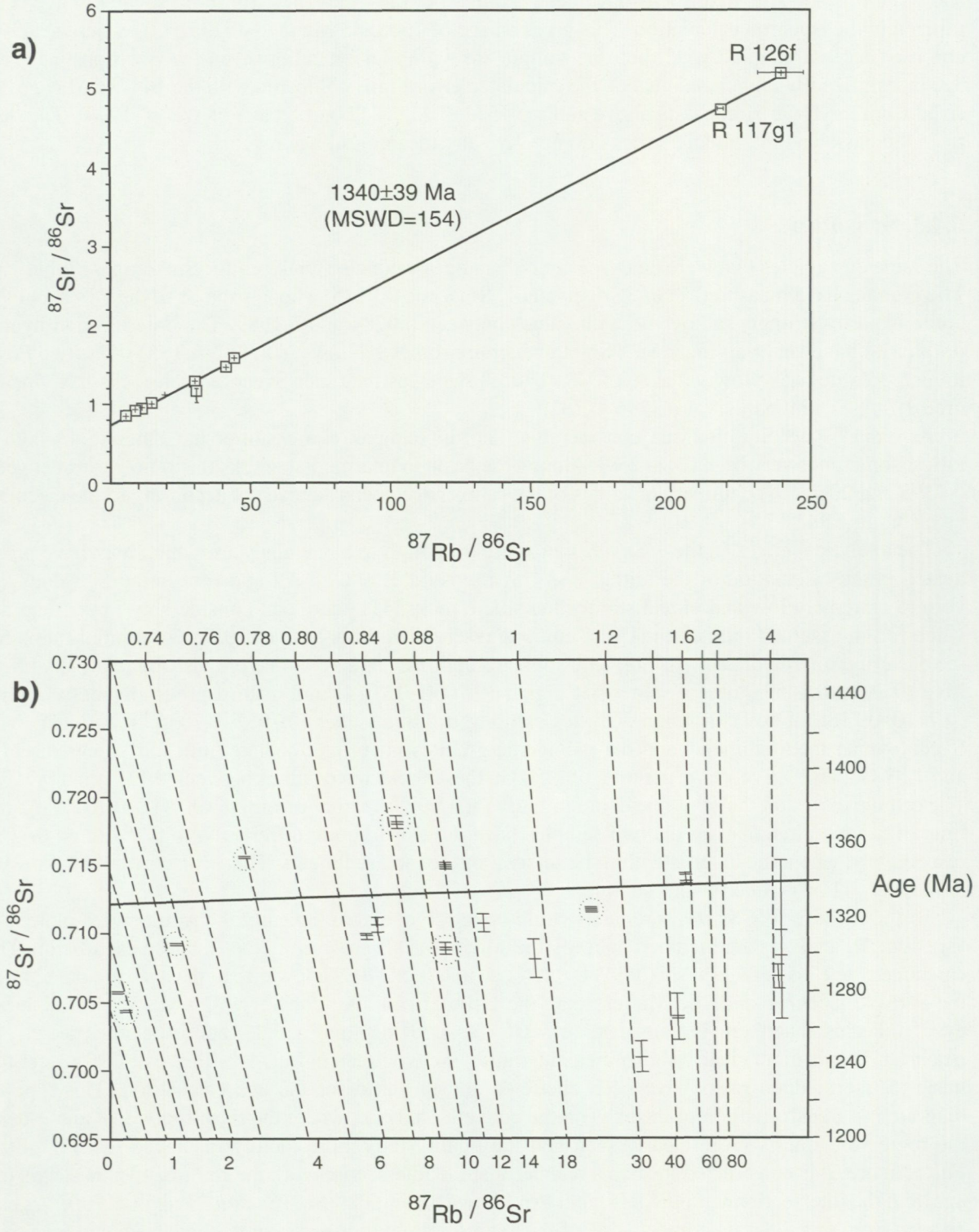

Fig. 49. a) $^{87}Rb/^{86}Sr$–$^{87}Sr/^{86}Sr$ diagram for the rocks of the Rödö complex. The calculated errorchron give an "age" c. 160 Ma younger than the U-Pb zircon age (cf. Fig. 45b). The large MSWD value indicates very low adherence to the line and the "age" may have no geological meaning. Two samples, one aplite (R126f) and one QFP (R117g1), have very high Rb/Sr ratios and totally control the slope of the reference line. b) "Improved isochron" diagram of Provost (1990) for the Rödö rocks. In this diagram the axises has been transposed in such a way that the adherence to the calculated line of individual analyses is more clearly displayed irrespective of their Rb/Sr ratio. The left vertical axis gives the initial Sr ratio and the right vertical axis the age. Only one of the silicic Rödö rocks overlaps within error the errorchron, explaining the high MSWD value. Discussion in the text.

6.4.4. Pb whole rock isotopes

Eight samples of rocks from the Rödö complex have been analysed for WR-Pb (Table 14), 4 granites, 3 QFPs and 1 aplite. These are plotted in a $^{207}Pb/^{204}Pb$–$^{206}Pb/^{204}Pb$ diagram in Fig. 50, in relation to Fennoscandian Pb isotopic data from galena and feldspar (cf. Fig. 65). Since these are WR samples, where U has been present in the samples up to the present, the Pb isotopic signatures are strongly radiogenic. Especially two samples have very high $^{207}Pb/^{204}Pb$ and $^{206}Pb/^{204}Pb$ ratios (R126f and R117g1), i.e. the same samples that are also the most evolved in the Nd and Sr systems. The samples cannot be fitted together in a single secondary isochron. An errorchron fitted through the six least radiogenic samples, which appear to form a linear array, gives an "age" of 1762±1100 Ma (Fig. 50).

In comparison with corresponding analyses from granitoids in Finnish rapakivi complexes (Rämö 1991), these samples generally have lower $^{207}Pb/^{204}Pb$ ratios. Lines with slopes corresponding to the crystallization age of the Rödö granite (c. 1.50 Ga, chapter 6.4.1.), extrapolate back from the WR-compositions to the composition measured for the more radiogenic of the feldspars of the Jämtland–Ångermanland complexes (cf. Fig. 65, chapter 7.4.4.), except for R117g1.

Table 14. Rödö whole-rock Pb-results.

Sample	*Rocktype*	*$^{206}Pb/^{204}Pb$*	*$^{207}Pb/^{204}Pb$*	*$^{208}Pb/^{204}Pb$*
R138	Rödö granite	19.47	15.49	40.58
R126a	Rödö granite	20.617	15.673	42.610
R127:1+2	Rödö granite	20.169	15.649	41.468
R133:2	Rödö granite	18.856	15.558	40.345
R73a	Qz-fsp porphyry	21.540	15.786	42.912
R96a+b	Qz-fsp porphyry	18.88	15.45	38.38
R117g1	Qz-fsp porphyry	34.554	16.520	55.166
R126f	Rödö aplite	29.753	16.587	45.993

Samples with two decimals have somewhat lower precision. Sample numbers can be found in Figs. 32, 33, the Foldout map, and Appendix 2b.

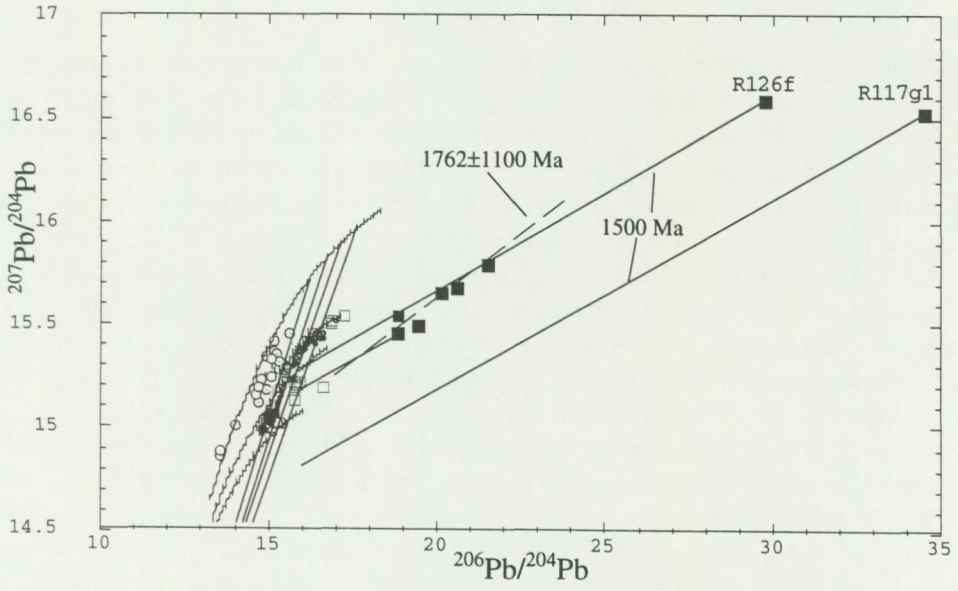

Fig. 50. $^{206}Pb/^{204}Pb$–$^{207}Pb/^{204}Pb$ diagram for the silicic WR-samples (filled squares) from Rödön (Table 14). The diagram also includes the galena and feldspar data compiled in Fig. 65, including the feldspar data from the Jämtland–Ångermanland complexes (unfilled squares; cf. Table 23). Included are also the second stage growth curves and isochrons plotted in Fig. 65. A secondary errorchron fitted through the six least radiogenic WR-samples gives an "age" of 1.76 Ga, which has no geological meaning and probably is a function of the variation in initial compositions. Lines with slopes representing the crystallization age of the Rödö complex (1.50 Ga), have been indicated. All except one of the Rödö WR-samples extrapolate approximately back (at 1.50 Ga) to the isotopic composition (initial) of the Jämtland–Ångermanland feldspars. Discussion in the text.

6.5. DISCUSSION

6.5.1 Geochemistry

6.5.1.1. General

The geochemical characteristics presented above show that the silicic Rödö rocks belong to a metaluminous to peraluminous rapakivi suite, with A-type affinity (Figs. 35, 36). The documented chemical spread in the silicic Rödö suite shows that strong fractionation has operated in the silicic part of the magma system. This fractionation partly follows typical rapakivi trends with, e.g. increasing Na_2O, and Na/K (especially in the aplites). The trace elements with most incompatible behaviour and high abundances in certain samples are Cs, Rb, Nb, Ga, Y, Pb, U, Th, Li, Be, F, and the HREE. Apart from the "mafic" elements, also P_2O_5, Ba, Zr, LREE, MREE, and Eu are compatible, and to some degree also F, Y, Be, and Li (cf. e.g. Christiansen et al. 1986, Haapala 1988). Some of the QFPs and the aplites exhibit extreme differentiation with very high contents of the incompatible elements, indicating that no minerals with high mineral-melt partition coefficients (K_Ds) for these elements have crystallized. This means, e.g. that biotite (Rb, Cs), columbite (Nb, Ta), or xenotime (HREE) are not part of the fractionating assemblage. The two latter minerals have, however, been encountered as minute grains in the most evolved QFPs. On the other hand, quartz, K-feldspar (K_2O, Ba) and plagioclase (Sr, Eu) are the major fractionating phases, as evidenced by their ubiquitous occurrence as phenocrysts. Although zircon (Zr, Hf, Y, HREE [less LREE]) has very low solubility in peraluminous melts (Watson & Harrison 1983) it has only precipitated in certain parts of the system affecting some of the most evolved dykes, and not others. The partly high F content in the magma system should have increased the solubility of zircon and HFSE-oxides (e.g. columbite, $(Fe,Mn)(Nb,Ta)_2O_3$) (e.g. Keppler 1993, London 1995 and ref. therein), postponing the precipitation of these phases. This might explain the strong enrichment in, e.g. Zr, Hf, HREE, Nb, Ta, Y, U, and Th in the most evolved silicic rocks. Furthermore, the solubility of e.g., xenotime ($(Y, HREE)PO_4$) is high in silicic melts and not related to the F content of the magma (Keppler 1993). Amphibole (Y, M-HREE), or perhaps clinopyroxene, has probably precipitated in minor amounts in the early stages, but should not have been a major fractionating phase in the advanced stages because of the strong increase in Y and HREE in the most evolved magmas.

6.5.1.2. Major element modeling of the silicic suite

Major element modelling was attempted to try to put some constraints on the proportion of phases responsible for the geochemical evolution in the silicic Rödö suite. The least-square mass balance program XLFRAC developed by Stormer & Nicholls (1978) was utilized for the calculations. The Rödö granite was used as parental magma (samples R126a or R138, representing the possible variations in starting composition), and three types of strongly evolved rocks were selected for testing. These were the aplites (sample R126f), the most highly evolved QFPs, type A (sample R117f2), and B (samples R18QFP and R45). Mineral phases used in the calculations comprise quartz, plagioclase, Kfsp, amphibole, and Fe-Ti-oxide and their compositions (recasted as 100 % of 8 major oxides) are listed in Table 15. Due to the limited amount of analyses acquired from minerals of the Rödö rocks, compositions of plagioclase, amphibole, and clinopyroxene from Rämö (1991), and of Fe-Ti-oxide from the Jämtland–Ångermanland complexes (see chapter 7.2. below) were utilized. This will not, however, affect the major outcome of the calculations, as the actual compositions of the fractionating phases probably are close to those used. The most reasonable results from the calculations are summarized in Table 16.

The aplite (R126f) can be modelled by c. 93 % crystallization of a fractionating assemblage consisting of 27 % quartz (Qz), 31 % plagioclase (Pl), 34 % Kfsp, 4 % amphibole (Amf), and 1 % oxide (Ox). This is the only reasonable model that was obtained for the aplite, and it is in general agreement with the mineral composition of the granite. Other models were tested, e.g. with a more An-rich plagioclase (from the Hammarudda complex, Åland; Andersson & Eklund 1994) and clinopyroxene (Cpx) instead of amphibole (from Rämö 1991), but resulted in either unrealistically low degrees of crystallization or more than 100 % crystallization.

Modelling of the evolution to obtain the composition of the most evolved of all QFPs (R117f2) also resulted in very high degrees of crystallization, 83–96% depending on model. Using exactly the same fractionating phases as for the aplite, but the granite R126a (slightly more silicic) instead of R138 as

Table 15. Phase compositions used for major element modelling in the silicic Rödö suite.

	Qz	Pl R139b	Pl TR91	Pl A&E94	Kfsp R139b	Hbl TR91	Cpx TR91	Oxid N3b
SiO_2	100	68.94	64.78	59.99	65.3	40.4	47.8	0
TiO_2	0	0	0	0	0	2.12	0.31	26.36
Al_2O_3	0	19.88	20.74	24.8	18.32	9.82	0.85	0.08
FeO^{tot}	0	0	0.82	0.26	0	32.27	29.42	73.48
MgO	0	0	0.33	0	0	1.51	1.46	0.08
CaO	0	0.33	2.6	6.86	0	10.39	19.89	0
Na_2O	0	10.85	9.33	7.24	0.54	1.64	0.27	0
K_2O	0	0	1.4	0.85	15.84	1.85	0	0
Sum	100	100	100	100	100	100	100	100

Pl R139b: Albite analyzed from Rödö granite. Pl TR91: Oligoclase from Deer et al. (1963), used by Rämö (1991).
Pl A&E94: Andesine from the Hammarudda complex, Åland (Andersson & Eklund 1994).
Kfsp R139b: K-feldspar analyzed from the Rödö granite.
Hbl TR91: Amphibole average, used by Rämö (1991). Cpx TR91: Clinopyroxene average, used by Rämö (1991).
Oxid N3b: Magnetite+ilmenite average from a trachyte dyke of the Nordsjö complex (cf. Table 19).

Table 16. Summary of the major element modelling of the silicic Rödö suite.

Evolved rock	Starting rock	% cryst.	Calculated proportion of phases in fractionating assemblage
R126f	R138	93	27 % Qz + 31 % Pl (Pl TR91) + 34 % Kfsp + 4 % Amf + 1 % Ox.
R117f2	R126a	96	30 % Qz + 28 % Pl (Pl R139b) + 35 % Kfsp + 6 % Amf + 1 % Ox.
	R126a	93	34 % Qz + 31 % Pl (Pl TR91) + 31 % Kfsp + 2 % Amf + 2 % Ox.
	R126a	94	33 % Qz + 32 % Pl (Pl TR91) + 32 % Kfsp + 1 % Cpx + 2 % Ox.
	R126a	85	30 % Qz + 29 % Pl (Pl R139b) + 35 % Kfsp + 4 % Amf + 2 % Ox.
	R138	85	27 % Qz + 31 % Pl (Pl TR91) + 36 % Kfsp + 5 % Amf + 1 % Ox.
	R138	82	27 % Qz + 30 % Pl (Pl R139b) + 36 % Kfsp + 6 % Amf + 1 % Ox.
R18QFP	R126a	68	32 % Qz + 22 % Pl (Pl R139b) + 37 % Kfsp + 8 % Amf + 1 % Ox.
	R138	63	25 % Qz + 23 % Pl (Pl TR91) + 43 % Kfsp + 8 % Amf + 1 % Ox.
	R126a	54	35 % Qz + 20 % Pl (Pl TR91) + 37 % Kfsp + 6 % Amf + 2 % Ox.
	R126a	48	32 % Qz + 16 % Pl (Pl R139b) + 42 % Kfsp + 7 % Cpx + 3 % Ox.
R45	R126a	90	31 % Qz + 26 % Pl (Pl R139b) + 35 % Kfsp + 7 % Amf + 1 % Ox.
	R138	79	28 % Qz + 27 % Pl (Pl TR91) + 38 % Kfsp + 6 % Amf + 1 % Ox.
	R126a	78	35 % Qz + 26 % Pl (Pl TR91) + 33 % Kfsp + 4 % Amf + 2 % Ox.
	R126a	71	33 % Qz + 22 % Pl (Pl R139b) + 38 % Kfsp + 5 % Cpx + 2 % Ox.
	R126a	63	37 % Qz + 20 % Pl (Pl TR91) + 37 % Kfsp + 4 % Cpx + 2 % Ox.
	R138	52	27 % Qz + 15 % Pl (Pl TR91) + 47 % Kfsp + 8 % Cpx + 2 % Ox.

Table 17. Closed system fractional crystallization, Rödön silicic system.

	La	Ce	Nd	Sm	Eu	Tb	Yb	Lu	Rb	Ba	Sr	Y	Nb	Zr	U	Th	Sc
Average Rödö granite (Starting composition)	87	166	66	11.2	0.7	1.16	1.88	0.26	230	434	77	24	24	327	3.1	19	2.3
R126f (analysis), aplite	19	50	30	11.5	0.40	2.3	6.2	0.85	540	(70)	9	77	43	240	19.1	71	1.1
Calculated*)	381	779	189	26.8	0.20	2.1	3.7	0.52	966	104	12	40	61	240	17.9	177	1.3
R117f2 (analysis), evolved QFP A	9	26	20	5.6	(0.1)	1.7	21.4	3.74	2080	216	42	37	659	1020	75.2	240	3.1
Calculated**)	352	783	282	46.0	0.24	4.7	8.0	1.16	1114	229	32	92	103	1407	22.2	151	3
R18QFP (analysis), evolved QFP B	11	25	11	2.6	0.20	0.5	1.7	0.29	797	331	40	8	86	18	6.3	8	1.0
Calculated***)	184	357	118	18.3	0.27	1.55	1.5	0.18	511	209	37	18	41	24	2.1	30	1.3
R45 (analysis), evolved QFP B	16	36	20	393.9	-0.1	0.6	4.0	0.53	1100	251	37	13	82	50	7.0	17	1.8
Calculated****)	265	540	183	28.9	0.27	2.7	3.4	0.44	770	229	36	40	63	91	6.1	66	2.0

*) 95 % crystallization of 27 % Qz, 30 % Pl, 33.97 % Kfsp, 8 % Amf, 1 % Ox, and 0.03 % Zirc.
**) 90 % crystallization of 34 % Qz, 31 % Pl, 31 % Kfsp, 2 % Amf, and 2 % Ox.
***) 65 % crystallization of 25 % Qz, 23.5 % Pl, 42 % Kfsp, 8 % Amf, 1 % Ox, and 0.5 % Zirc.
****) 80 % crystallization of 34.90 % Qz, 26 % Pl, 33 % Kfsp, 4 % Amf, 2 % Ox, and 0.1 % Zirc.
Values in parenthesis are estimated due to contents lower than detection limits of the method.

K_Ds used for		Kfsp	Plag	and for		Kfsp	Plag
R117f2, R45,	Rb	0.34	0.041	R126f:	Rb	0.487	0.105
R18QFP:	Sr	3.87	4.4		Sr	5.4	15.633
	Ba	6.12	0.36		Ba	11.45	1.515

parental magma, results in 93 % crystallization of 34 % Qz, 31 % Pl, 31 % Kfsp, 2 % Amf, and 2 % Ox. Using Cpx instead of Amf does not alter the result. Inserting an albitic plagioclase (Pl R139b), as is observed in the phenocrysts of the dyke, changes the total amount of crystallization only marginally to 96 %, but the relative amounts of Kfsp and Amf increase somewhat (Table 16). Using R138 as starting magma lowers the total crystallization required to around 85 %, and suggests higher proportions of Kfsp in the fractionating assemblage (27 % Qz, 30 % Pl, 36 % Kfsp, 6 % Amf, and 1 % Ox). Plagioclase composition has very little effect on the result in this case, while replacing Amf with Cpx results in probably unrealistically low degrees of crystallization (66–74 %). Based on these calculations it is suggested that the residual magma of the dyke R117f2 has developed by 85–95 % crystallization of the major phases Qz (27–31 %), Pl (29–31 %), Kfsp (29–36 %), Amf (or other Fe-Mg-silicate; 2–6 %), and Ox (1–2 %). The composition of plagioclase has probably become progressively albitic during fractionation.

The models calculated for the other group of most evolved QFPs (group B) arrive at lower degrees of crystallization, compared with R117f2. The realistic models calculated for the QFP sample R18QFP indicate amounts of crystallization varying between 48–68 %, depending on parental magma composition, plagioclase composition, and use of Amf or Cpx in the fractionating assemblage (Table 16). The lowest degree of crystallization is obtained with Cpx in the assemblage. This is probably the least likely of the calculated models, due to the relatively highly refractory nature of the magma (high contents of incompatible elements; Figs. 37, 41, Appendix 2b) and the lower probability of having anhydrous Cpx fractionating (all mafic silicates in the silicic rocks are hydrous). The composition of the parental magma has a relatively strong influence on the result, as well as the Pl composition. Nevertheless, these compositional variations mark the uncertainty in the model. Thus, the actual amount of crystals removed from the parental magma to arrive at R18QFP should be between c. 55 and 65 %, probably closer to the higher value, and comprise 25–35 % Qz, 20–23 % Pl, 37–43 % Kfsp, 6–8 % Amf, and 1–2 % Ox.

In the case of R45, the major element modelling suggests that crystallization has proceeded further, compared with R18QFP. Reasonable models fall in the wide range of 52–90 % crystallization, where the Cpx-containing calculations are in the lowermost part of this range (Table 16). The models with albitic plagioclase show very diverging results depending on which parental magma is assumed (R138 or R126a), while the calculations with oligoclase (Pl R91) give similar results (although varying proportions of Qz and Kfsp), irrespective of starting composition. It is suggested that R45 has developed through c. 80 % crystallization of an assemblage of major phases consisting of 28–35 % Qz, 26–27 % Pl, 33–38 % Kfsp, 4–7 % Amf, and 1–2 % Ox.

Even if these models are approximate they give a rough relative estimate of the variation in amount of crystallization and proportions of the crystallizing phases between the evolved rocks. The statistical fit of these least-squares calculations is very good, with the sum of squared residuals always below 0.3. The calculations indicate that Kfsp is the dominating fractionating phase, which is supported by its dominance as phenocryst in the porphyries and granites. In the most highly evolved systems (90 % crystallization, or more) the increase in importance of Pl is noted. This is also supported by petrographic evidence, as albite is a prominent phenocrystic phase in these residual magmas, probably due to massive removal of early Kfsp and more anorthitic plagioclase. Abundant antirapakivi mantling in R117f2 and related dykes, suggest an even later return to Kfsp precipitation (Plate 3d).

6.5.1.3. Trace element modelling of the silicic Rödö suite

Trace element modelling using closed system fractional crystallization has been attempted using the NewMelt module in the Newpet program (Clarke et al. 1994), in order to test the suggested major element models (selected results are shown in Table 17). However, due to the large variation in suggested mineral/melt K_Ds for the various elements (cf. e.g. Rollinson 1993), these calculations are only crude tests of the models. The effect of the fluorocarbonates (see below) on the LREE could not be assessed in the calculations, leading to calculated contents that were much too large. The proportions in the fractionating assemblages obtained in the major element modelling were used in these calculations, supplemented with trace amounts of zircon, and the calculated amount of the trace elements at the approximate degree of crystallization was checked against the actual analysis. The same rock

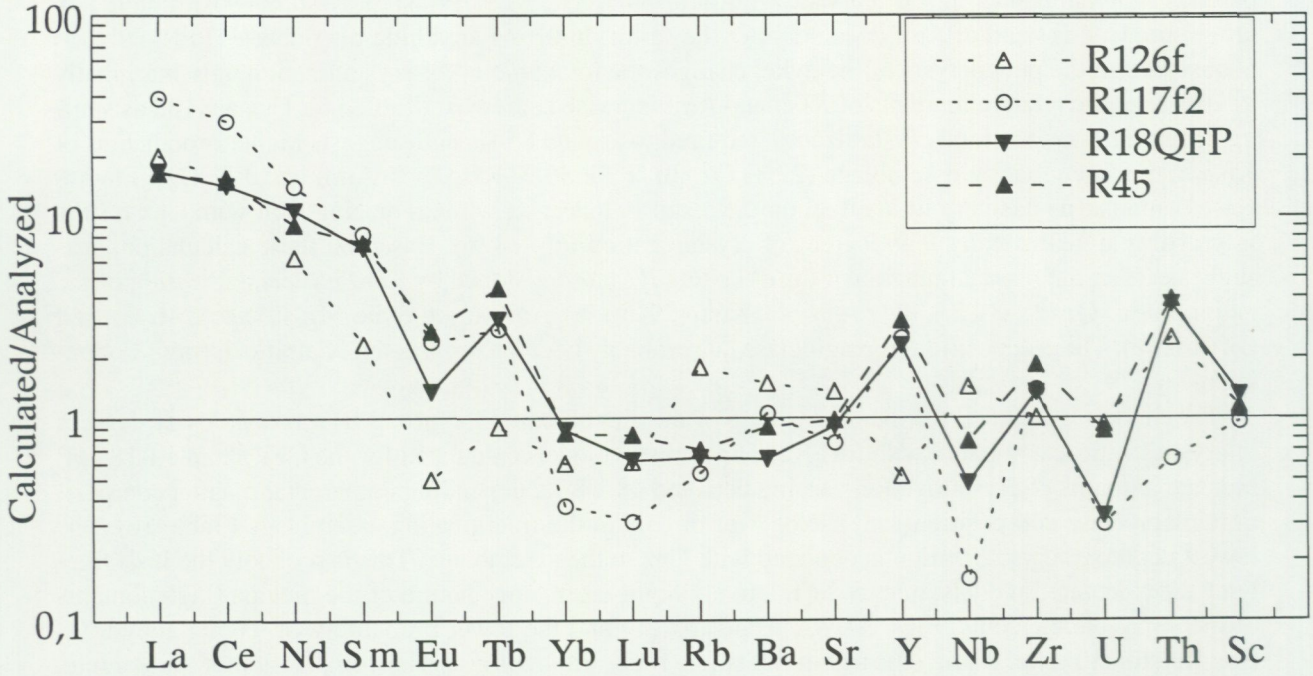

Fig. 51. Graphical display of the trace element modelling of fractionation in the silicic Rödö suite (Table 17). Calculated contents are normalized to those analyzed. The starting composition (parental magma) used was the average Rödö granite (Table 17). The degree of fractionation used was estimated from the major element models (Table 16). For the LREEs the fit is very poor, and for the other elements fairly good but variable. Discussion in the text.

samples were used also in these calculations (cf. Appendix 2b). Mineral/melt K_Ds from the compilation of Rollinson (1993, and ref. therein) were utilized. K_Ds for Zr, Y, and Tb in zircon was estimated at 4000, 200, and 20, respectively, based on comparison with other element K_Ds. Results are summarized in Fig. 51.

The match for the aplite (R126f) is rather poor (Table 17). An assumed content of 0.03 % zircon in the fractionating assemblage give relatively good agreement with the analyses for Zr, U, and Tb, but too low values of HREE, and too high Th and Y. The reported K_D-values of Mahood & Hildreth (1983) perhaps overestimate the difference in K_D between U (340.50) and Th (76.80). Reported K_D-values for Rb, Ba, Sr in the feldspars vary widely (e.g. Arth 1976, Mahood & Hildreth 1983, Nash & Crecraft 1985). For Ba and Sr the highest K_Ds give almost the observed depletion in these elements for the aplites, whereas intermediate K_D-values seem appropriate for Rb. Too much Y is removed by amphibole and zircon. No zircon and less amphibole in the crystallizing assemblage gives a better fit. Nb has high K_Ds for amphibole and magnetite (4 and 2.5, respectively; Pearce & Norry 1979). No K_D is reported for Nb in zircon. The calculated removal of amphibole and Fe-Ti-oxides can almost account for the observed Nb content.

In the case of the most evolved dyke (R117f2), the very high contents of Rb, HREE, Nb and U cannot be modelled adequately. However, excluding amphibole from the fractionating assemblage gives an almost perfect match with the measured contents of HREE. Using the lowest reported K_Ds for Rb in feldspars (Arth 1976) gives values approaching the actual value. No zircon in the fractionating assemblage gives a close match for Zr and Th. The highest K_Ds for Ba and Sr give too low contents in the calculations (contrary to the case with aplite), while intermediate K_Ds (used in Table 17, Fig. 51) give a close match. Too high Y values compared with the content in the dyke are also calculated. If a fractionation without amphibole and Fe-Ti-oxides is calculated (which may be appropriate for the late stages), this may account for the high HREE and partly Nb, but gives too high Sc, Y, Zr and Tb.

For the dykes R18QFP and R45, a slightly better match between calculated and analytical contents is obtained. 0.5 % zircon for R18QFP and 0.1 % for R45 imitates the analysed contents of Zr and HREE relatively closely, but less so for U and Th. The discrepancy between K_Ds for U and Th in zircon is obvious also here. Calculated Y contents are also high which may be due to values of estimated $K_D^{zircon/melt}(Y)$ (200) that are too low. Low K_Ds for Rb and intermediate for Ba and Sr (Table 17) give reasonable results.

The relatively poor agreement between calculated and analysed trace element contents in the evolved rocks may be caused by several factors: 1) incomplete and inconsistent database of mineral/melt K_Ds, giving widely varying results, 2) incorrectly assumed proportion of fractionating phases or degree of crystallization, 3) influence of geological factors other than closed system fractional crystallization.

Among these factors 2) is probably of least importance, since the major element modelling put some constraints on the phase proportions. Christiansen et al. (1983, 1984, 1986) invoked a very similar fractionating assemblage to account for the geochemical variation among Cenozoic topaz rhyolites in western North America, except that they propose biotite instead of amphibole. In the case of Rödön, biotite is less probable due to the strong increase in Rb with evolution, since $K_D^{Bt/melt}(Rb)$ is high in silicic magmas (cf. Rollinson 1993). The effect of uncertainty in the K_Ds has been evaluated to some extent above, and may have contributed significantly in some cases. However, unrecognized geological factors seem to play an important role. For the LREEs, this problem is solved by the discovery of Ca-LREE-fluorocarbonates in the Rödö rocks (see below), since allanite and monazite appear to be lacking. Other geological factors that may cause discrepancies include: a) an incorrect assumption that the Rödö granite represents the parental magma, and maybe most important, b) the influence of fluids which may have altered the original magma composition either by extracting elements during exsolution of a fluid phase from the magma, enrichment by not removing the enriched fluid phase from the magma, or later subsolidus redistribution. The very strong enrichment in HREE, Nb, U, Th, etc in, e.g. the most evolved sample (R117f2), may be connected with a fluid-related process, or an even more residual nature of the magma (>90 % crystallization) (see below). Congdon & Nash (1991), e.g., suggest more than 75 % fractional crystallization for very enriched topaz rhyolites in western USA.

6.5.1.4. Fluids and fluorocarbonates

During the search for possible phases that could explain the strong depletion in LREE (and concomitant enrichment in HREE) in the most evolved rocks, relatively abundant grains of a reddish brown phase, often associated with fluorite, were encountered. Qualitative compositional data obtained on this material showed that it contained Ca-LREE (La, Ce, Pr, Nd, Sm, Gd, Dy, and Ho in varying proportions)-F as major elements, but no trace of HREE. The relative proportion of Ca to LREE was variable, and the grains were easily burnt under the electron beam of the microprobe. These qualitative results indicate that these grains are composed of minerals of the bastnäsite ($LREECO_3F$) group (parisite $CaLREE_2(CO_3)_3F_2$, röntgenite $Ca_2LREE_3(CO_3)_5F_3$, and synchysite $CaLREE(CO_3)_2F$; Burt 1989). The small anhedral grains were found in the dark schlieren, some little evolved QFPs, and in some of the more evolved QFPs (Plate 3a and b). Their chemistry varies with rock type. In the little evolved QFP (sample R107b) they are typically richest in Ca, La, and Ce, whereas in the more evolved QFP (R167:2) they are dominated by Nd with lower Ca contents, including also small amounts of Y and Th. In the schlieren (R115s2), the fluorocarbonate has the lowest Ca combined with dominating La and Ce. Bastnäsite has previously been reported from the small Fjälskär rapakivi intrusion in SW Finland (Lahti & Suominen 1988). No monazite or allanite have been encountered and thus removal of these fluorocarbonates from the magma system is suggested to explain the depletion in LREE, but incompatible behaviour of the HREE (Figs. 37, 41, 44a). The abundance of fluorite, calcite, and fluorocarbonates indicates that the silicic Rödö magmas were originally rich in F and CO_2 (relative to H_2O). The c. 0.2–0.3 % F obtained in the whole rock analyses of the least evolved silicic rocks may significantly underestimate initial contents due to losses from degassing of these high-level intrusions. However, lack of petrographic evidence of primary magmatic fluorite indicates that the magma was never saturated in this phase, i.e. not exceptionally rich in fluorine.

F is strongly partitioned into the melt phase over the fluid phase (e.g. Webster 1990, Carroll & Webster 1994, Johannes & Holtz 1996) in peraluminous magmas. Up to at least 7 % F can readily be accommodated in the melt. In silicic melts having more than 7 % F coexisting with an aqueous fluid phase, however, F preferentially partitions into the fluid phase (Webster 1990). F appears to be even slightly more soluble in CO_2-containing magmas (Webster 1990). CO_2, on the other hand, is much less soluble (e.g. Fogel & Rutherford 1990, Blank et al. 1993, Blank & Brooker 1994). CO_2 solubility is also highly dependent on P and T. At constant P, more CO_2 can be dissolved in the melt at lower Ts.

The effect of P is, however, much stronger, so that at 7 kbar (1050°C) c. 0.5 % can be contained in the melt, compared with only 0.05 % at 1 kbar (Fogel & Rutherford 1990).

The numerous small cavities occurring in the least evolved Rödö QFPs do not usually contain any fluorocarbonates, but rather calcite, chlorite, quartz and sometimes rutile and zircon. This suggests, together with the experimental data, that a CO_2-rich aqueous fluid was exsolved early, primarily as a result of pressure drop during emplacement of these dykes. This fluid phase contained apparently abundant Si, some Ti and Zr (and presumably Mg, Al and Fe to precipitate chlorite). According to the experiments of Webster (1990) the solubility of silicate melt in the exsolving fluid increases with increasing F in the system. F has the effect of depolymerizing the melt, forming mainly AlF_6^{3-}-complexes (Manning et al. 1980; Schaller et al. 1992). This produces an increased amount of non-bridging oxygen atoms in the melt (i.e. O atoms not wholly bonded within the polymerized Al-Si-O network of the melt), which are free to react and form complexes with, e.g. TiO_2 and ZrO_2 in the melt (Keppler 1993). Further complexing with H_2O and CO_2 species may bring these elements into the fluid phase upon exsolution, where they eventually precipitate as hydrothermal phases (rutile, zircon, chlorite and quartz). Since small quantities of sphalerite have been found interstitially in some of the least evolved QFPs, this indicates the presence of minor amounts of sulphur in the fluids. At this stage, however, very little F is removed into the fluid phase due to its high solubility in the melt.

The REE^{3+}-ions may form strong complexes with a variety of ligands including F^-, Cl^-, OH^-, SO_4^{2-}, and CO_3^{2-} (Wood 1990, Haas et al. 1995, Gieré 1996). Wood (1990) suggested that fluoride and carbonate complexes were the most likely candidates for transport of REEs in hydrothermal systems. Haas et al. (1995) pointed out that the type of ligand is strongly dependent on pH of the fluid and predicted, on the basis of theoretical modelling, that REE-chlorides should be dominant under acidic, REE-fluorides under neutral, and REE-hydroxides under basic conditions. REE-carbonate complexes would be important at neutral pH, lower Ts, and high CO_3^{2-} concentrations. High carbonate concentrations are clearly at hand in the Rödö fluids, while no analytical control on chlorine has yet been established. Thus the major form of REE transport in the Rödö fluids may nevertheless be carbonate and fluoride complexes (cf. Kosterin 1959, Wood 1990). Mixed fluoride-carbonate complexes may also be important (Wood 1990, Ngwenya 1994). Fluid inclusions in granitic systems enriched in REEs and especially LREEs have been documented (e.g. Banks et al. 1994), as well as crystallized bastnäsite and parisite in fluid inclusions (Salvi & Williams-Jones 1990, Taylor & Pollard 1996). A mechanism to fractionate between the LREE and HREEs, where the LREEs are extracted to the fluid phase while the HREEs remain within the melt, is needed. As demonstrated by Haas et al. (1995), the light and heavy REEs are complexed more or less strongly by different ligands at acidic to neutral conditions, which may promote fractionation in hydrothermal solutions. Wendlandt & Harrison (1979) determined that the LREEs partition into a vapour phase in equilibrium with a silicic melt much more efficiently than the HREEs. The reason for this is not known, but may be of considerable relevance to the fractionation seen in the Rödö rocks, where the LREEs obviously have been preferentially transferred to the late fluid phase and crystallized as fluorocarbonates.

At the latest stage of crystallization in the primitive QFPs, the F contents have increased to such a degree that more F is partitioned into the fluid phase where it crystallizes as fluorocarbonates, mainly together with calcite and muscovite. This fluorocarbonate is the first to crystallize and is enriched in La and Ce (and Ca), since the lightest REEs are structurally most preferred (Gieré 1996 and ref. therein).

The more evolved QFPs contain lower amounts of CO_2 (and thus higher relative F/CO_2), since this was previously removed by the fluids which crystallized the early calcite and fluorocarbonates in the primitive QFPs. These residual melts exsolve later stage fluids, richer in F. This fluid brings Ca and LREEs in complexed form, precipitating CaLREE-fluorocarbonates and fluorite interstitially. In these most evolved melts, the Ca content is lower (due primarily to previous plagioclase fractionation), and so is the Ca content of the fluorocarbonates, suggesting that the fluoride ion successfully competes for Ca^{2+}, in comparison with the REE^{3+}. Since this late stage melt is depleted in La and Ce, due to the earlier fluorocarbonate crystallization, the fluorocarbonates crystallizing here are dominated by Nd (with minor Gd, Dy, and Ho), and some refractory Y and Th. The presence of xenotime as inclusion in fluorocarbonate (Plate 3a and b) in one of the more evolved QFPs shows that this phase also has precipitated very late from the fluid phase. As the solubility of xenotime is high in haplogranitic melts (not a function of F content; Keppler 1993), Y and HREE may be enriched in residual fluid-rich melts. These elements may be extracted into the fluid phase, together with parts of the small amounts of P in the

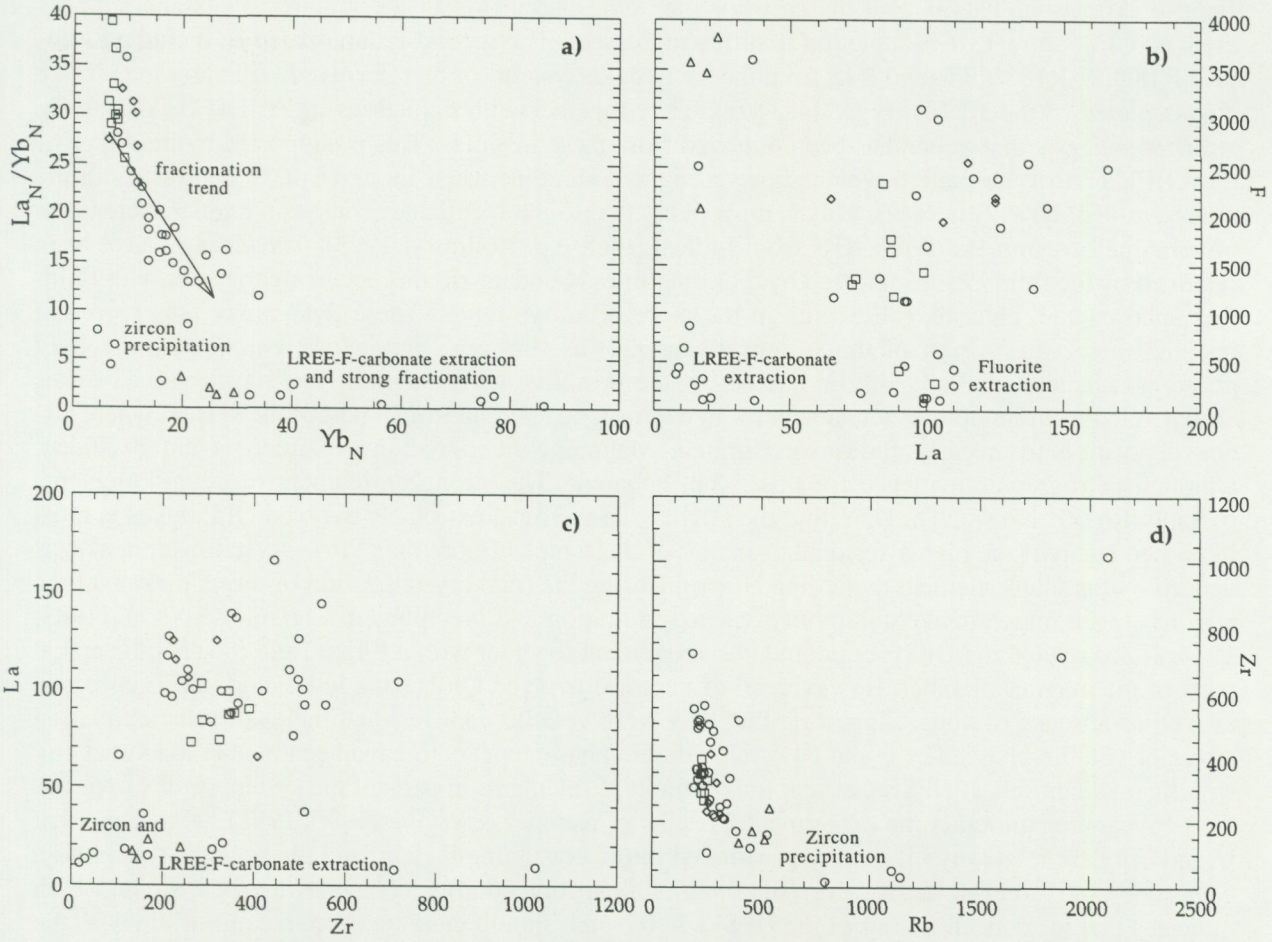

Fig. 52. Diagrams to highlight the influence of accessory phases in the evolution of the silicic Rödö system. The general fractionation trend involves increasing HREE and decreasing La/Yb ratios (a). Parts of the system is depleted in fluorine (b, and Fig. 42). Some of these rocks have also suffered depletion in LREEs (a and b), due to the extraction of Ca-LREE-flurocarbonates. A specific group of QFPs (group B in Fig. 37b) have very low Zr contents (R18QFP, R18MQFP, and R45 in Fig. 44a), controlled by zircon extraction (a, c and d). The other group of highly evolved QFPs (group A in Fig. 37b) have instead increasing Zr and HREE, not compatible with zircon removal (cf. R117f2, R117g1, R118b in Fig. 44a). Symbols the same as in Fig. 41. Further discussion in the text.

system, by these very late expelled fluids where the phosphate and Y+HREE combined into hydrothermal xenotime [(Y, Yb, Er, Dy, Gd, Ho)PO_4].

The crystallization of the associated calcite from the early and fluorite from the late fluids lowers the activities of CO_3^{2-} and F^- in these fluids, respectively (e.g. Gieré 1996). This should facilitate the precipitation of the fluorocarbonates in each system. According to Williams-Jones and Wood (1992) the coexistence of parisite and fluorite indicates relatively higher temperatures (close to magmatic?), and absence of fluocerite ($REEF_3$) suggests high activity of CO_3^{2-} relative to F^-. Since the fluorites contain no detectable REEs and no fluocerite has been found, this suggests that the activity of CO_3^{2-} is still relatively high in these late stage fluids. The textures even allow the interpretation that some of these phases may have crystallized directly from the melt. It has been shown experimentally (Hsu 1992) that F-bastnäsites may form at magmatic conditions up to 860°C and from environments relatively low in F.

Fig. 52 illustrates the effects of the accessory phases on the trace element geochemistry in the silicic Rödö rocks. The extraction of fluorite together with the fluorocarbonates can account also for the sharp drop in the F content of the evolved rocks, down to 104 ppm (Fig. 42). Some rocks which are not affected by LREE-depletion show also a sharp decrease in F (Fig. 52b). This group includes many of the least evolved QFPs and a few granites, and suggests that there has been an early loss of volatiles from parts of the magma system.

The most highly evolved dykes do not contain any fluorocarbonates at all and have thus crystallized from residual melts that were highly depleted in the LREE due to the previous fluorocarbonate and

fluorite extraction. This is also the case for the aplites occurring in the granite. All of the strongly evolved QFPs show LREE-depletion to different degrees. The second group (group B, including samples R18QFP, R18MQFP, and R45 from the same dyke system) of most evolved QFPs in Fig. 37b are also depleted in the HREE (Figs. 44a, 52a). This, together with depletions in Zr, Hf, U, Y, and Th, strongly suggests that zircon has been removed from these magmas. This is supported by the shape of the LREE part of the pattern which shows a marked slope between La and Sm, in contrast with the other evolved dykes (Fig. 44a). This is most likely due to the fact that zircon has a regular increase in mineral/melt (or mineral/fluid) K_Ds from La to Lu (cf. e.g. Rollinson 1993). The Zr may have been removed by the fluids, as is indicated by the sometimes abundant zircons occurring together with fluid-deposited calcite, chlorite, rutile, etc., in the more primitive QFPs. These dykes may thus represent residual melts after a part of the system where Zr was strongly complexed, removed by the fluid phase, and deposited abundantly in cavities of the primitive QFP-magmas. The most evolved dykes enriched in the zirconophile elements, may, in contrast, be residual from a part of the system where zircon deposition from early fluids was limited. Magmatic fractionation of zircon is not excluded, although petrographic evidence for this is not apparent. The strong enrichment of certain elements (notably Rb, Zr, Nb, Ta, Th, U, Y, and the HREEs) in the most extremely evolved QFP dykes is most likely the result of the highly residual character of these melts (more than 90 % crystallization, as evidenced by the major element modelling above). During the final crystallization of these, most evolved magmas, even minerals like columbite, reached saturation and precipitated. Christiansen et al. (1983, 1984, 1986) related the HFSE-enrichment to movement together with a F-rich fluid towards the apical parts of the magma chamber. However, all of the most evolved QFPs have low F and LREE contents, as well as absence of vugs, suggesting that they were volatile-poor residual melts after the extraction of major volatile phase. The F and CO_2 rich volatile phase appears to have been unable to extract any significant quantities of HFSEs, except for zirconophile elements in parts of the system (QFPs, type B). This appears to contradict the experimental results of Keppler & Wyllie (1990, 1991), who found that U and Th were relatively efficiently partitioned into a coexisting F-rich fluid phase and U also into a CO_2-rich (but F-free) fluid. However, the fluid/melt partition coefficients are always below one, which indicates that the concentrations of the HFSEs in the melt should increase even in equilibrium with the F-rich fluid. The REE-pattern of the dyke R135a+b in addition indicates that this magma may have been affected by the removal of some unidentified HREE-containing phase (Fig. 44a).

The aplites have similar geochemical characteristics as the most evolved QFPs, with relatively low contents of both LREE and HREE (Figs. 52a and 44a). Their chemistry suggests that they represent residual liquids squeezed out of the granite in which they occur, i.e. low in elements that are preferentially incorporated into the phases present in the granite, e.g. Eu and Sr retained in the plagioclase of the granite, transition metals retained in the Fe-Ti-oxides of the granite, Ba retained in the Kfsp, and LREE retained in some fluorocarbonates (in the absence of allanite and monazite). They are, however, markedly enriched in F (and fluorite) expelled from the crystallizing granite. The contents of HREE are higher than in the granite but not conspicuously so, and Zr is lower (Figs. 41, 52). This indicates that some of these elements are retained in early crystallized zircon but this is counteracted by the extreme amount of crystallization (close to 100 % as suggested also by the major element modelling above). Such a highly residual liquid should show some enrichment in these elements unless early zircon precipitation was very extensive. These data support an origin by filter pressing for the aplite veins in the granite.

The dark schlieren structures and the Rödö granite are rich in $Fe_2O_3^*$, TiO_2, Zr, Nb, Y, P_2O_5, Zn, and Li, but also all REE (except Eu), and Th (Figs. 41, 44a). They are often associated with the largest vugs (up to 10 cm) and aplite veins. This field evidence supports an interpretation where the schlieren form very late in the evolution. The schlieren represent areas of strong fluid flow and late autometasomatic alteration of the granite. The fluids have a strong dissolving effect on the feldspars, which are partly leached and carried away by the fluid. Reprecipitating feldspar can be observed, e.g. around some quartz grains and in the vugs. The fluids contain appreciable amounts of the elements mentioned above, precipitating, e.g. as hydrothermal zircon and apatite (abundant), fluorocarbonates (present), but also Fe, Ti, Zn, and to a lesser extent transition metals crystallizing as Fe-Ti-oxides and mafic silicates, mostly chlorite. The abundant hydrothermal apatite in the schlieren, which is not found in the QFPs, is presumably related to the higher primary magmatic contents of Ca and P in the granite compared with the QFPs. The leaching effect on the feldspars has lowered the concentrations of elements like K, Na, Ba, Eu, and Sr.

6.5.1.5. Origin of the silicic parental magma

The Rödö granites are interpreted to represent the most primitive part of the silicic Rödö suite, close to a silicic parental magma. If so, the negative Eu anomaly of the REE patterns of the granites indicates that plagioclase remains in the source. The LREE enrichment character of the patterns indicates the presence of one or more HREE retaining phases in the unmelted source residue. Clinopyroxene, amphibole, garnet or zircon may contribute to this (cf. Christiansen et al. 1983, 1984, 1986), but not monazite. A protolith giving these REE characteristics to a partial melt could very well be an orthogneiss similar to those in the country rocks, with the relatively flat REE pattern displayed in Fig. 44d. Experimental and other data support that A-type granitic magmas can be generated from undepleted granodioritic-tonalitic sources in the lower crust, during H_2O-undersaturated melting due to heat influx brought by basic magmas underplating the lower crust (e.g. Anderson 1983, Creaser et al. 1991, Emslie 1991, Skjerlie & Johnston 1993). Typical early Svecofennian and Archaean successions are composed of such lithologies. 20 % melting of early Svecofennian dominantly granodioritic or slightly more felsic sources has been modelled as the most probable source lithology for the rapakivi granites of the Suomenniemi batholith in SE Finland (Rämö 1991). Plagioclase and pyroxene are likely to dominate a residue after such a melting event (e.g. Conrad et al. 1988, Rutter & Wyllie 1988, Skjerlie & Johnston 1993, Emslie et al. 1994), but not garnet (Rämö 1991), explaining the REE-patterns of the granites. Some metasomatic enrichment with, e.g. alkalies and LREEs in the source region prior to melt generation cannot, however, be ruled out. Moreover, Landenberger & Collins (1996) suggested that the source lithologies of A-type granite melts were previously enriched in K-feldspar by a previous melting event according to the principal reaction Bt+Qz+Pl=Opx±Cpx+Kfsp+melt. No attempt to model the melting processes leading to a primary silicic Rödö magma has been made in this work, but similar modelling was presented for the Småland-Värmland granites in chapter 4.5.2.2. above. In analogy with this modelling and Rämö (1991), a slightly lower degree of melting (compared with the SVB granites; <25 %) of a similar tonalitic-granodioritic lower crustal source is qualitatively consistent with the more incompatible element-enriched nature of the Rödö granite. Such crustal A-type (rapakivi) magmas are thus considered to represent the parental magmas in the magmatic evolution of the rapakivi complexes, in this case approximated by the Rödö granite and the least evolved QFPs.

6.5.1.6. Relation to the haplogranitic system

In Fig. 53 the silicic Rödö rocks are plotted in the normative haplogranitic system Qz-Or-Ab. The Rödö rocks approximate this simplified system as the sum of normative Qz+Or+Ab is always above 85 %, and mostly above 91 %. Normative An is usually low (<3.5 %), but is up to 5-6 % in a few of the QFPs. In the aplites and the more evolved dykes, An is 0. The effects of additional An in the system should thus be very small. Normative corundum is usually very low (<2 %), but may reach 4 % in the most evolved dykes. The anomalous sample R87a has 5.92 % normative corundum. All the granites and granite porphyries, as well as most of the QFPs, plot to the right of the water-saturated minimum melt or eutectics at more Or-rich compositions (Fig. 53). Such Or-rich compositions indicate conditions of low water activity, according to experimental data (e.g. Holtz et al. 1992a, Johannes & Holtz 1996). If these WR data can be considered to represent rocks that were fairly close to melt composition at some stage, their position in the diagram suggests that the a_{H_2O} should have been generally below c. 0.3 for the pressure range 10–2 kbar. There is a tendency for a subvertical trend in the diagram for the bulk of the rocks which may indicate an effect of magma ascent at constant or slightly increasing a_{H_2O} (cf. Holtz et al. 1992a). If, however, the bulk rock chemistry partly represents some accumulation of feldspar and quartz, a part of the shift away from Ab is an artifact of this (e.g. Holtz et al. 1992a, Shebanov et al. 1996).

A number of samples lie at compositions more Qz-rich than the experimental 0.5 kbar minimum melt composition. These have more than average corundum in the norm (c. 2 %), but the observed relative Qz values appear too high to be due to the additional effect of alumina only (cf. e.g. Joyce & Voigt 1994, Holtz et al. 1992b, Johannes & Holtz 1996). These rocks are heavily altered and may have suffered some autometasomatic dissolution of feldspars that has raised the relative Qz content. The low Ab content of sample R87a clearly separates it from the evolutionary trend of the rest of the Rödö

rocks. The aplites and some of the more evolved QFPs trend towards more Ab-rich compositions. This may be a combined effect of elevated F contents and increasing activity of H_2O in the latest residual magmas. F contents of 1 % or less are indicated, even if this is not completely comparable as the experiments were performed under H_2O-saturated conditions (Manning 1981). Nevertheless, F should be responsible for this trend because otherwise an increase in pressure is required, which is unlikely. An increase of a_{H_2O} to approx. 0.5 is also suggested for these residual rocks. The consideration of the normative compositions in the haplogranitic system is thus consistent with the mineralogical and geochemical data that the magmas were generally rich in CO_2 and F.

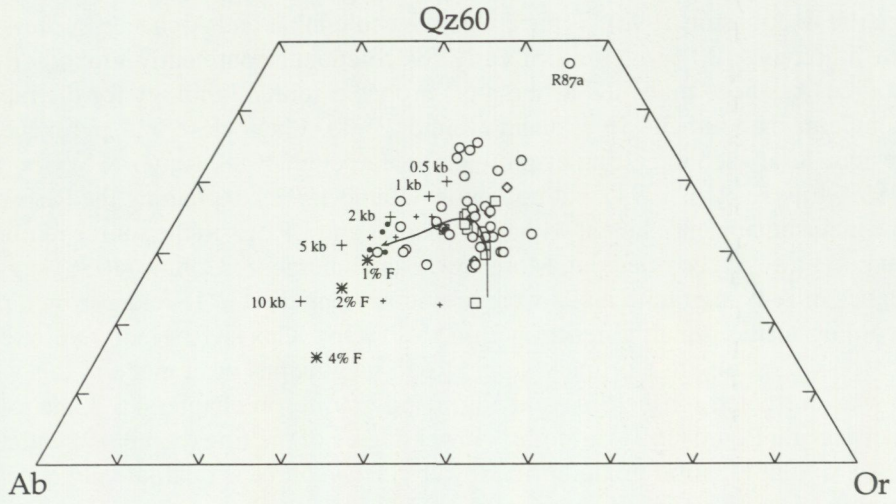

Fig. 53. The silicic Rödö rocks plotted in the haplogranite system (normative Qz-Ab-Or). All samples have Qz+Ab+Or > 85 %, and most > 91 %. Symbols the same as in Fig. 41, except for aplites (small black dots). Crosses and stars refer to experimental minima in the system and are detailed in Fig. 26. The majority of the rocks plot distinctly to the right of the water-saturated minima (labelled in kilobars; kb), suggesting water undersaturated conditions (Or-rich). Some of the most evolved QFPs and aplites plot closer to water saturated conditions (and F-rich minima), suggesting increasing activity of H_2O and/or F in the residual magmas. A possible evolutionary trend is indicated by the arrow in the diagram. Sample R87a is anomalous (very low in the Ab component), and is probably not related to the rest of the suite by magmatic fractionation. Further discussion in the text.

6.5.1.7. Rödö (and Postjotnian) dolerites

The Rödö dolerites are characterized by large variability in geochemistry (Fig. 41). They are generally relatively high-K continental within-plate quartz normative tholeiites, although some trace element diagrams suggest an alkali basaltic character (Fig. 39). The alkali-rich character of the more evolved/contaminated dykes is clearly displayed in the Na_2O+K_2O diagram (Fig. 42). In the R1-R2 diagram (Fig. 34a) a small number of basic dykes have a syenitic trend falling in the syenodiorite and syenite fields at approximately saturated compositions. This trend is separated from the general monzonitic trend of the majority of the samples. The latter trend is towards the compositions of the associated silicic Rödö rocks in the diagram, and thus a significant part of the chemical spread of this monzonitic trend could be ascribed to the contamination by the associated silicic magmas. This is manifested petrographically by a reddish colour (Kfsp and quartz in the matrix) and/or xenocrysts of Kfsp and quartz. The "contamination" is also seen in the Rb-Ba-Sr diagram (Fig. 43), where the basic suite trends towards the composition of the granites at lower Sr and higher Rb. A minor trend towards high Ba is also discernable. Although it may be difficult in detail to separate the effects of fractional crystallization and contamination in the chemical evolution of the basic Rödö suite, the operation of the former process is apparent since a large part of the chemical variability cannot be ascribed to contamination.

The REE-patterns of the majority of Rödö dolerites are relatively LREE-enriched with no noticeable Eu-anomaly (Fig. 44b). The Eu contents of the most evolved dykes are actually the highest of all rocks of the Rödö complex, but even so not giving rise to any anomaly. These rocks are thus markedly rich in the REEs, especially the LREEs, suggesting that they are highly differentiated. A minor group of dolerites have a small negative Eu-anomaly (Fig. 44b), suggesting that plagioclase has been removed or that they have been more contaminated by interaction with the rapakivi magmas.

The concomitant decrease of CaO and MgO, as well as a strong depletion in Cr, in the element variation (Harker) diagrams (Fig. 41), suggests fractionation of clinopyroxene (cpx) as a major cause for the geochemical variation (cf. Kolker et al. 1990). The composition of this cpx may have varied from an early more Mg-rich to a later more Fe-rich type, which is indicated by the change in composition of cpx microphenocrysts along with dyke chemistry as well as zoning to more Fe-rich compositions in the margins (cf. Table 11). Olivine phenocrysts have not been found, but may have contributed in the early stages when, e.g. the Ni content decreases rapidly. In contrast to Cr, the depletion in Ni is not so strong for the evolved stages in differentiation, suggesting that olivine was not coprecipitating with cpx. This is supported by the lack of olivine phenocrysts in the rocks. The sharp drop in MgO and Ni at the earliest stage, between the most primitive rocks and the rest of the suite, indicates early olivine involvement. Additionally, CaO is seen to increase from the most primitive rocks to the rest of the suite (Fig. 41a), which is not consistent with early cpx removal. Since these are generally quartz normative rocks, early crystallization should have involved opx together with olivine.

The most primitive composition encountered among the analysed basic rocks is represented by sample R54 and the mafic enclave R53E (Fig. 41). These may be regarded as parental to the rest of the suite. R111 and R98 are also among the least evolved. This is most evident in the MgO, Cr and Ni diagrams, where these rocks have the highest contents. R111 is from the dyke on the islet of Känningen (Foldout map) proposed by von Eckermann (1938) to be a natural example of an anorthositic melt (kenningite). It is obvious, however, from the geochemistry and petrography that this dyke is not particularly different from the other Rödö dolerites (e.g. high in alumina, Al_2O_3 is only 14.8 %). This was realized by Lundqvist (1975), who carefully examined several samples of this dyke, including those collected by von Eckermann. He therefore concluded that no evidence of anorthositic melts could be found at this locality and proposed that the term kenningite should be abolished (Lundqvist 1975). The geochemistry of samples R74c and R94f (Figs. 40c and 41) suggests that they most probably are part of the Postjotnian magmatism, and have thus been mislabelled in the diagrams.

During the earliest stage (from R54 to the rest) the Sr content increases strongly (Fig. 41b), which is inconsistent with plagioclase removal. Al_2O_3 also seems to increase slightly, whereas Na_2O increases markedly. In the rest of the suite, Sr decreases strongly, while Al_2O_3 turns from a roughly positive to a negative trend. Eu increases over the whole range of compositions. This is true also for Na_2O, although perhaps less markedly at the evolved stage. This is consistent with considerable plagioclase fractionation from the beginning of the evolved stage (at c. 53 % SiO_2) and on. Labradorite phenocrysts are relatively widespread in the dykes (cf. Table 11), which shows that the melt was saturated in plagioclase. The evolved trend thus suggests a cotectic fractionation of cpx and plagioclase. This means that the conditions changed in the magma, whereby cpx and plagioclase replaced early olivine and opx in the fractionation assemblage. Fractionation of Fe-Ti oxides is also indicated to start at about 57 % SiO_2, as there is an inflexion point for the TiO_2 and possibly also for $Fe_2O_3^*$, combined with a sharp drop in V. Similarly, P_2O_5 first increases strongly, followed by a sharp drop at c. 57 % SiO_2 (Fig. 41c), indicating saturation in apatite. Sporadic observation of oxide and apatite microphenocrysts corroborates these geochemical conclusions.

The proposed parental magmas (R54 and R53E) are not likely to represent the primary unfractionated mother magma for this magmatism. Substantial high pressure removal of olivine and orthopyroxene from an initial olivine tholeiite primary magma in a lower crustal magma (or uppermost mantle) chamber should have preceded the evolution as seen here (e.g. Green et al. 1967, Presnall et al. 1978, 1979, Emslie 1980, 1985, Ashwal 1993 and ref. therein). The low CaO contents in the most primitive rocks (R54 and R53E) are consistent with opx rather than cpx stability (cf. Fram & Longhi 1992). The existence of high-Al opx megacrysts in many anorthosite complexes supports early high pressure opx fractionation (Emslie 1975, Fram & Longhi 1992, Longhi et al. 1993, Emslie et al. 1994). This is indicated by the relatively low contents of MgO, Cr, Ni, etc. even in the most primitive rocks sampled. This is probably also the major cause of the strong REE, and especially LREE enrichment of the Rödö

dolerites (cf. e.g. Emslie 1985, Kolker et al. 1990, Mitchell et al. 1995). Fractionation of olivine and opx should not lead to any Eu anomaly (cf. compilation of partition coefficients in Rollinson 1993), which is consistent with the data (Fig. 44b). The plagioclase fractionation at the evolved stage is, however, expected to cause relative Eu depletion, but this can be counteracted by the strong coprecipitation of cpx until the very last stages (cf. Emslie 1985, Kolker et al. 1990, Emslie et al. 1994, Mitchell et al. 1995).

The stability fields of cpx and opx increase with pressure (e.g. Green et al. 1967, Presnall et al. 1978, 1979, Emslie 1985, Fram & Longhi 1992), while that of plagioclase decreases. This suggests that the basic Rödö magmas first resided in a lower crustal chamber, within the stability field of olivine + opx. The trends discussed above suggest that the residual magma was withdrawn from this chamber and emplaced at upper crustal levels, shifting it into the stability field of cpx + plagioclase, probably in connection with the emplacement of the associated Rödö granite. Thus, high-P fractionation proceeded during the heating and melting, producing the granitic magma, induced by the basic magma. The buoyant rise of the granitic magma to the upper crust also facilitated the rise of the basic magma. The rise to high levels in the crust occurred before the magma was saturated in plagioclase and cpx. This is probably the reason why no high-Al rocks, commonly thought to be parental to anorthosites (e.g. Emslie 1980, 1985, Olson & Morse 1990, Ashwal 1993, Emslie et al. 1994), are present in the Rödö area. Moreover, the Rödö dolerite suite lacks the compositional characteristics of ferrodioritic to monzodioritic rocks (e.g. high TiO_2, FeO_{tot}, P_2O_5, etc.), usually regarded as residual after anorthosite formation (cf. e.g. Mitchell et al. 1996). Due to the early pressure-drop there was not enough time and the magma jumped into the plagioclase stability field before significant Al-enrichment developed. This means that no anorthositic rocks were produced in the high-P chamber, which readily explains the general lack of anorthositic rafts or fragments in the dykes. In the high-level chamber the low-P fractionation was supplemented also by Fe-Ti oxides and apatite, before any strong enrichment of Fe developed.

The marked LREE enrichment of the Rödö dolerites, usually without any Eu anomaly, is a typical feature that separates them from the Postjotnian dolerites which are only very slightly LREE enriched (Fig. 44b). Qualitatively a relatively low degree of melting of a plagioclase-free mantle source may give a REE pattern like that of the Rödö dolerites. The Postjotnian dolerites, on the other hand, should in such a case have been generated by a larger degree of melting, giving a lower LREE enrichment, if a similar source is assumed. Different mantle sources are also possible (perhaps at different levels), having different degrees of enrichment or depletion. Tendencies for both positive and negative Eu anomalies can be detected for the Postjotnian dolerites, and can be interpreted as resulting from incipient plagioclase precipitation.

Another possible (and more probable) reason for the LREE-enrichment in the Rödö dolerites is the substantial early removal of opx and olivine in the lowermost crust since these minerals have low mineral/melt K_Ds for the REEs and especially the LREEs. The Postjotnian dolerites are, on average, slightly more primitive in character for the major elements (Fig. 41), and most of the trace elements (LILE and HFSE), except Nb, Y and the HREE (Figs. 40, 41). This may be interpreted in the following way. The extent of high-pressure fractionation (of opx, cpx and olivine in a subcrustal or lowermost crustal chamber) is less advanced, compared with that of the Rödö basites. In fact, most of the fractionation in the Postjotnian basic rocks has probably occurred at high levels in the crust. The olivine tholeiitic nature and depletion in Ni of the Postjotnian dolerites suggests a major role for olivine fractionation. The less pronounced depletion in Cr also suggests removal of some cpx, and the variable Sr contents indicate some additional plagioclase contribution to the trends. These are also the main minerals observed in the rocks (cf. Table 11). The high mineral/melt K_Ds for Ni and Cr results in strong depletion even at relatively minor fractionation. The assemblage olivine+cpx+plagioclase indicates low-pressure fractionation commonly observed for continental flood basalts (e.g. Cox 1980, Basaltic Volcanism Study Project 1981), which has also been suggested for Subjotnian dolerites in Finland (Boyd 1972, Rämö 1990, 1991). The low-pressure fractionation of these minerals (and additional Fe-Ti oxides) is verified from the Postjotnian dolerites intruded as large sills which differentiated in situ and developed extensive mineral layering (Lundqvist & Samuelsson 1973, Larson 1973, 1980, Lundqvist et al. 1990). The trace element variation within the suite of Postjotnian dolerites, compared with average Rödö dolerite is displayed in Fig. 40b.

The reason for this difference between the Subjotnian and Postjotnian basic magmatism may be that the rheological and thermal state of the crust 240 Ma later (at 1.26 Ga) was quite different. By this time

the cooling and thermal relaxation (cratonizing) of the crust should have progressed considerably, compared with the conditions at 1.50 Ga. This means that the brittle regime of the crust extended deeper, allowing deeper fracturing associated with the Postjotnian extensional event. Thus, the different tectonic environment facilitated the deep chambers to be more easily tapped to higher levels.

Within the suite of Rödö dolerites the trace element variation is relatively limited (Fig. 40a). The average composition of the Suomenniemi dykes (Rämö 1991) is closely similar to the Rödö rocks, suggesting similar conditions of formation. The majority of the Suomenniemi rocks are, however, more primitive in character, as is evident in the Harker variation diagrams (Fig. 41). The more evolved Suomenniemi rocks are similar to the Rödö dolerites, except for a few elements, e.g., Y, and the REEs; especially Y are higher in the Suomenniemi case. This difference is also borne out in the trace element classification diagrams in Fig. 39. This high Y relative to other HFSEs distinguishes the Suomenniemi dykes clearly from the Rödö dolerites, whereby the Suomenniemi rocks trend towards more "orogenic" fields in the diagrams. In fact, the Suomenniemi dykes are in many respects more similar to the Postjotnian dolerites. The reason for this discrepancy is at present unclear. The relatively strong resemblance between continental flood basalts and the rapakivi-related dolerites, especially the Suomenniemi dykes (Fig. 40a), is in accordance with their tectonic setting and suggests a similar petrogenesis.

6.5.1.8. Hybrid porphyries and enclaves

Two groups of intermediate rocks of differing character can be distinguished between the dolerites and the granites/QFPs. Due to their difference in SiO_2 content they have been designated the silicic and intermediate hybrid porphyries. The diverging trends between the two types of hybrid porphyries are most clearly seen in the Harker diagrams for MgO, Al_2O_3, Sr, Zr, Ga, Y, V, Ni, and the REEs (Fig. 41). The silicic (SiO_2 65–70 %) hybrid porphyries are thus the result of mixing between a silicic endmember corresponding to the Rödö granite and a basic endmember corresponding to some of the less evolved (more primitive, with e.g. higher MgO, Ni, Cr content, etc) parts of the dolerite suite. The other hybrid porphyries (intermediate: c. 60–65 % SiO_2) have more evolved endmembers: a fractionated (but not strongly fractionated) QFP magma as the silicic endmember mixed with the more evolved parts of the basic suite.

Some of the intermediate hybrid porphyries show anomalously high K_2O contents and concomitantly low Na_2O, not consistent with mixing. These porphyries may, however, rather represent the most evolved (syenitic) stage in the evolution of the basic magmas, combined with some mixing with the silicic endmember, explaining the apparent inconsistency. The "contaminated" dolerite R101a+b, should probably be grouped with the intermediate hybrid porphyries as indicated most clearly in the R1-R2 diagram (Fig. 34a) and the REE-pattern (Fig. 44b). A summary of the geochemical character of the intermediate (evolved) hybrids is shown in Fig. 40a, in comparison with the Rödö dolerites. The combination of strong fractionation and mixing with the QFPs results in high contents in all incompatible elements.

It is clear from several of the Harker diagrams that the intermediate hybrid porphyries represent mixtures between differently evolved endmembers (e.g. K_2O, Ba, Cs, Zr, Zn, and the REEs; Fig. 41). This shows that mixing processes operated contemporaneously with fractionation in both the basic and silicic magma systems, up to the most evolved stage of the basic system. The most highly fractionated QFPs and the aplites do not have any matching hybrid porphyries, intermediate to the dolerites. This can be most clearly seen for Rb, Ba, Nb, Ga, Y, U, Th, Li and the REEs, and suggests that the fractionation in the silicic magma continued after the mixing processes ceased. These highly evolved QFPs thus probably represent the last magmatism in the Rödö complex.

The most silicic hybrid porphyries have REE patterns very similar to the granites (Fig. 44b). This is not surprising since their chemistry as a whole is close to the granites. They are, however, still clearly distinct from the granites, perhaps most convincingly demonstrated by the FeO*/FeO*+MgO ratio (Fig. 42b). The division between the intermediate hybrid porphyries and contaminated highly evolved dolerites (syenites) is, as noted above, somewhat arbitrary and the similarity in REE patterns is also considerable (Fig. 44b). The content of HREE of the intermediate hybrid porphyries tends to be higher than the silicic hybrid porphyries, and thus more resembles the QFPs. The silicic hybrid porphyries show more coherent mixing trends, compared with the evolved group, consistently plotting between

the least evolved parts of the endmember suites. There is also a distinct textural difference between the two suites of hybrid porphyries. The silicic hybrid porphyries have large megacrysts of feldspar (≤3 cm) and quartz (≤1 cm), which closely resemble those of the Rödö granite. The megacrysts of the intermediate hybrid porphyries are generally smaller (≤1 cm) and more akin to those encountered in many QFPs.

The mixing between the granite and the primitive dolerites should have occurred before that between the QFPs and the evolved dolerites, if they belong to the same evolutionary system. Hence, there should also be a corresponding succession in age between the different types of dykes. This has only been possible to verify in very few instances in the field, since crosscutting relationships between Rödö dykes are rarely exposed. At loc. 144 on Rödön (Foldout map), however, an evolved QFP can be seen to cut a relatively primitive dolerite. Another, not completely exposed locality, seems to indicate that an evolved QFP-dyke cuts silicic (early) hybrid porphyry (loc. 44 on Spikarö; Foldout map). The geochemical trends can thus be used to infer the relative geologic age of the dykes, even if no contacts are exposed.

The basic/hybridized enclaves generally follow the trend of the basic suite, at relatively primitive compositions as seen, e.g. from the comparatively high Ni and Cr contents (e.g. Fig. 41). Most of the analysed enclaves occur in the silicic hybrid porphyries of the early mixing episode, and should thus be rather primitive. Two of the analysed enclaves, however, differ markedly (Fig 40d). One occurs in one of the most evolved QFPs (R18Enkl), and has anomalously high contents of Rb, Nb, Ga, Y, U, and Yb, with respect to the mixing trends. This is most likely due to postmagmatic fluid circulation and transfer from the QFP host (cf. e.g. Petrik & Broska 1989, Bédard 1990, Christiansen & Venchiarutti 1990, Orsini et al. 1991, Zorpi et al. 1991, Elburg & Nicholls 1995, Stimac et al. 1995). The other enclave (R46c + fEnkl) occurs in a relatively primitive QFP. It clearly represents a hybrid rock (SiO_2 63.6 %), but does not follow either of the trends for the hybrid porphyry groups (Figs 41a–d). The most likely explanation consistent with the geochemistry is that it was formed by mixing between the QFP in which it resides and a doleritic magma of intermediate fractionation level.

6.5.2. Notes on the composite dykes

Composite dykes are usually interpreted to be formed from two magmas intruding along the same fissure simultaneously (e.g. Blake & Campbell 1986, Freundt & Tait 1986, Carrigan & Eichelberger 1990). The usual case to find the more basic material along the margins of composite dykes (e.g. Walker & Skelhorn 1966, Carrigan & Eichelberger 1990) is related to fluid mechanical differences between the two magmas. Basic magmas are normally considerably less viscous compared with silicic ones (e.g. Murase & McBirney 1973), i.e. before crystallization has progressed to the critical crystal fraction where crystals start to interact and behave more rigidly (e.g. Arzi 1978, Van der Molen & Paterson 1979, Spera et al. 1988, Lejeune & Richet 1995, Johannes & Holtz 1996). This means that the energetically most favourable way of transport is by basic magma acting as a low-viscous lubricant along the margins of the composite dyke, transporting the more silicic component relatively passively along during intrusion (Carrigan & Eichelberger 1990, Carrigan 1994). This is most probably the reason why the interaction between the magmas has usually been fairly limited. The intrusion has been by laminar flow along the basic margins which have taken up all the magmatic deformation preventing turbulent mixing with the more viscous centre. In the more unusual cases where the silicic magmas are found along the margins (e.g. Rämö 1991), the silicic magma has most likely entered the fissure first from a stratified magma chamber with a silicic upper part. Shortly after, basic magma is entrained into the conduit centre, where it travels at higher velocities than the silicic margin due to its much lower viscosity (e.g. Freundt & Tait 1986, Blake & Campbell 1986). This situation is unstable and promotes strong turbulent interaction and mixing between centre and margin (Freundt & Tait 1986), which may lead to a reverse (and more stable) situation with basic margin and silicic centre higher up along a conduit (Blake & Campbell 1986). Complete mixing between the magmas can result if the silicic magma initially occupies the margin of the dyke. Formation of net-veined dykes may also be possible in this initial situation as the silicic magma becomes superheated and low-viscous and may act as marginal lubricant, while the basic magma is chilled and becomes semi-rigid at the critical melt fraction. This package is transported upwards and concurrently the amount of silicic magma diminishes.

In the case of the Rödö composite dykes, overturn of dykes with initially more silicic margins may be indicated by the frequent occurrence of small mafic enclaves in the more silicic centres, and abundant silicic xenocrysts in the marginal dolerite (hybrid porphyry, loc. 135). In the case of loc. 115b, for example, the centre of the dyke is a hybrid porphyry with numerous enclaves of marginal material. Such strong effects of mixing and mingling is not expected if the more viscous centre (the "silicic" magma) were transported all the way from the source region relatively passively in the middle with lubricating margins (the dolerite magma), but rather suggest a preceding more violent stage where an initially silicic magma (QFP magma) entered the fissure first. Some of the mixing as seen may, however, have developed prior to dyke injection. At loc. 12, a 3 m wide QFP is flanked by 1m dolerite margins and a narrow hybrid, enclave-containing zone in between. This appears to be a case of relatively stable flow, where the marginal doleritic magma has transported the more viscous central QFP magma passively, resulting in only limited mixing.

6.5.3. Isotopes

6.5.3.1. Age

Welin (1994) has previously determined an U-Pb zircon age from 4 zircon fractions to 1513±5 Ma. The analytical quality of the data points is, however, not stated. The scatter obtained in the U-Pb data of this study significantly exceeds the analytical errors (MSWD values >>1), suggesting involvement of geological factors, such as e.g. remnants of older material or differences in intrusion ages among the four samples combined in the analyses (see chapter 6.4.1.). The latter is considered highly unlikely, due to the small size of the Rödö granite intrusion, as well as very homogeneous petrographic nature of the samples. The analysed fractions plotting slightly to the right of the discordia may contain an older component (Fig. 45b). This component is either minor in volume and much older, or larger in volume but only slightly older, since the points are still close to the discordia. The former alternative is more likely in the light of the low ε_{Nd} values for the Rödö granites and associated rocks (chapter 6.5.3.2. below), suggesting a major Archaean input to the magmas. Thus, a small amount of zircon material of possibly Archaean age is suggested by the data, even though no specific inherited type of zircons have been identified, such as in the case of the Nordsjö syenite (chapter 7.4.1.). Even the most concordant fraction (R10) seems to be slightly displaced to the right of the discordia and may contain small amounts of an older component. However, the analytical error of this fraction is relatively large and may account for some of the displacement.

The fraction plotting above the concordia (R4) has most likely experienced U loss due to incomplete digestion of the crystals, where some of the bound U (but not the more loosely bound Pb) was lost. If this is the case, the U has been lost today, which means that this point has moved directly away from the origin in the diagram. Since the calculated discordia line does not run through the origin, but has a lower intercept of 229±21 Ma, a more recent U loss in fraction R4 should have moved this point somewhat off the discordia to the left. If this fraction, together with those that are slightly displaced to the right (R1, R2, R6), are omitted the statistically most well-constrained age is calculated (1497±6 Ma, MSWD=1.3). This age is the preferred age estimate, as it probably reflects only a minimum influence of older components (Fig. 45b).

Within errors, all these calculations give the same age around 1500 Ma, which is slightly but probably significantly lower than the 1513±5 Ma age obtained by Welin (1994). Based on these results, and the low initial ε_{Nd}, one may argue that the result of Welin (1994), calculated from only 4 fractions may also contain unidentified older components, giving a slightly too old intrusion age. Thus, the age preferred from the present data may more accurately define the intrusion age.

The isochron 1608±45 Ma (MSWD=0.53) age calculated from the Sm-Nd WR system of the silicic rocks in the Rödö suite, is thus about 110 Ma too old compared with the U-Pb age suggested above (Fig. 48). There is a large spread in the $^{147}Sm/^{144}Nd$ ratios, but only a few samples have very high ratios. These samples therefore have the largest impact on the isochron calculation, and small biases in their determined values will have relatively large effects on the determined age. Since the analytical data have been collected over a relatively long period (930329–940514), and the measured values of the Nd standard have varied considerably in time, the raw analyses have been corrected by different

factors accordingly (cf. Appendix 1). This may have influenced the isochron. On the other hand, all but one analytical point fall within error on the isochron (Fig. 48), which makes it a relatively well-determined WR isochron. Any difference in the initial $^{143}Nd/^{144}Nd$ ratios in the system would of course also make the isochron unreliable. If the 1497 Ma U-Pb age is accepted as the true intrusion age the calculated initial ε_{Nd} values show a significant spread, where the samples with the highest Sm/Nd ratios have the highest ε_{Nd} values (Table 13). This means that those samples that have the largest impact on the isochron calculation probably had higher initial $^{143}Nd/^{144}Nd$ than the others, giving a too high age estimate. The reason for this may be sought in the strong fluid control exerted on the magmatic evolution, and especially on the LREEs (cf. chapter 6.5.1.4. above). The fluid extraction of the LREEs could have caused a fractionation between Sm and Nd and a decoupling of $^{143}Nd/^{144}Nd$ and the Sm/Nd ratio, leading to inadequate initial ratios calculated for some samples. Fluid exchange with the country rocks is also a possibility for some change in the isotopic parameters. The suite of basic Rödö rocks did not give any meaningful Sm-Nd WR geochronological data at all.

6.5.3.2. Nd isotopic relations

The very low calculated initial ε_{Nd} values (Table 13) for the Rödö rocks (at 1.50 Ga) suggest the involvement of an older low radiogenic component in the magmas. This is true irrespective of the chemistry of the rocks, in fact the basic-intermediate rocks tend to have even slightly lower initials, -8.9 to -6.9 (av. -7.6) compared with -7.4 to -4.8 (av. -6.6) for the silicic rocks. The investigated rocks from the rapakivi complexes of Jämtland and Ångermanland (chapter 7.4.2. below) have completely overlapping Nd isotopic characteristics with the Rödö rocks, and the following discussion is thus equally applicable to them.

In order to try to put some quantitative constraints on possible sources for the Rödö rocks, a compilation of Nd isotopic data obtained from rocks in the Svecofennian and Archaean provinces of the Fennoscandian shield was made from the literature. This compilation is summarized in Fig. 47, as histograms of the $\varepsilon_{Nd}(1.51)$ of all rocks for comparative purposes. The age 1.51 Ga was chosen as it represents an average age of the Swedish rapakivi complexes (excl. Nordingrå). In comparison with rocks from SE and SW Finnish rapakivi complexes (Rämö 1991, Fröjdö, Andersson & Eklund unpubl. data), the Rödö rocks (and the Jämtland/Ångermanland rocks) have markedly lower ε_{Nd} values (Figs. 46, 47). The rocks of the Salmi complex in Russian Karelia (Neymark et al. 1994), on the other hand, show complete overlap with the Swedish ones. The Strömsbro rocks in Fig. 46 are discussed in Andersson (1997a). The Salmi complex is emplaced on the border between the exposed Archaean craton and the Svecofennian domain (see Fig. 1), and its low initial ε_{Nd} values were explained by a mixture of these components (Rämö 1991, Neymark et al. 1994).

Fig. 46 shows the Nd evolution with time of different Fennoscandian crustal lithologies. The Finnish rapakivi granites and related silicic rocks and the Nordingrå granite are clearly included within the evolution of the early Svecofennian metaigneous rocks, and can thus, with regard to the Nd isotopes, be interpreted as derived by crustal melting solely of such sources (Rämö 1991, Andersson 1994, Lindh & Johansson 1996). This solution is not available for the Rödö rocks. The presently investigated rocks (incl. also those in Jämtland/Ångermanland) occur more than 300 km away from the nearest exposed Archaean crust in the Luleå area (Lundqvist et al. 1996, Wikström et al. 1996), with a juvenile arc-like terrain (the Skellefte district) in between, but still show similarly low values as the Salmi complex.

The calculated depleted mantle ages, T_{DM} (DePaolo 1981), and chondritic ages, T_{CHUR}, listed in Table 13 are in the range 2.5–2.0 Ga for the rapakivi granitoids. These mantle model ages imply that possible juvenile mantle derived protoliths of the rapakivi granitoid magmas should have been extracted from the mantle in this time span. Possible material with ages between 2.5 and 2.0 Ga suitable as protoliths for the rapakivi magmatism have not been recorded in this region. In the shield as a whole, rocks formed in this time span are dominated by metasediments and mafic to ultramafic volcanics and intrusions, belonging to the Lapponian and Karelian supergroups, covering the eroded Archaean basement in the northeast (e.g. Gaál & Gorbatschev 1987), with only minor intercalations of felsic igneous rocks. One single U-Pb zircon dating of early Svecofennian rocks in the region gives an age of more than 2 Ga (2.03 Ga) (Welin et al. 1993), otherwise the early Svecofennian ages are constrained to the period 1.95–1.86 Ga. Recent ion-probe U-Pb work on early Svecofennian metasediments has identified

Table 18
Concentration of Nd and ε_{Nd} at the time of rapakivi magmatism for potential source rocks.

	C_{Nd}	$\varepsilon_{Nd}(1.51)$
Depleted mantle[1)]	5-15	+4.5
Non-depleted mantle[2)]	30-47	±0
Archean[3)]	21	-18.5
Metasediments, Bothnian basin[4)]	30	-7.0
Svecofennian, metaigneous[5)]	35	-3.0
Revsund granitoids[6)]	40	-4.1
Rapakivi granitoids[7)]	61	-6.7
Rapakivi-associated basic rocks[8)]	35	-7.8

1) Expected range in C_{Nd} estimated from data of Huhma (1986), Patchett & Kouvo (1986), DePaolo (1988), Björklund & Claesson (1992), and Kumpulainen et al. (1996). $\varepsilon_{Nd}(1.51)$ after DePaolo (1981); $\varepsilon=0.25T^2-3T+8.5$.

2) C_{Nd} based on the Suomenniemi and Häme swarms (Rämö 1991), being a possible non-depleted source. C_{Nd}=30, assumed initial diabase magma of Rämö (1991). C_{Nd}=47, average of the Häme and Suomenniemi diabase analyses.

3) Averages of analyses from Martin et al. (1983); Jahn et al. (1984); Huhma (1986), and Öhlander et al. (1987). C_{Nd}, n=14. ε_{Nd}, n=24.

4) Averages of 19 analyses from this work, Miller et al. (1986), Claesson (1987), Patchett et al. (1987), and Welin et al. (1993), and Claesson & Lundqvist (1995).

5) Averages of 81 analyses from this work, Wilson et al. (1985, 1987), Huhma (1986), Patchett & Kouvo (1986), Patchett et al. (1987), Valbracht (1991), Welin et al. (1993), Claesson & Lundqvist (1995), and Kumpulainen et al. (1996).

6) Averages of 19 analyses from this work, Wilson et al. (1985), Patchett et al. (1987), and Claesson & Lundqvist (1995).

7) This work. n=25 (Tables 13 and 22).

8) This work. n=11 (Tables 13 and 22).

essentially no zircons in the age range 2.5–2.1 Ga (Claesson et al. 1993). Most of the zircons are in the range 2.1–1.9 Ga and a limited number (30 %) are Archaean (>2.6 Ga). These data do not support the existence of a major crustal segment of the age 2.5–2.1 Ga in the Svecofennian part of the Fennoscandian shield, although the existence of such rocks at depths cannot be ruled out.

The alternative is mixing of two or more components, crustal or crustal plus mantle. As can be seen in Figs. 46 and 47, only an Archaean crustal component has distinctly lower ε_{Nd} isotopic composition than the measured rapakivi granitoids. This is, thus, the only known potential source capable of lowering the ε_{Nd} of the rapakivi magmas significantly. Rämö (1991) concluded that the Finnish rapakivi granitoids could be satisfactorily explained as derived by remelting of the early Svecofennian metaigneous rocks (cf. Fig. 46, 47). Such an explanation is obviously not applicable here. A Svecofennian metaigneous derivation needs to be complemented by an input of Archaean material. Table 18 lists the average concentration of Nd (C_{Nd}) and $\varepsilon_{Nd}(1.51)$ for different potential source rocks, compiled from literature data supplemented by the data of this study, and will be used below to calculate proportions in different mixtures of possible source rock components.

The Svecofennian metasediments of the Bothnian basin show a Nd evolution completely overlapping that of the silicic Rödö rocks, with a spread in ε_{Nd} (1.51) between -10.2 and -5.7, and an almost identical average (-7.0; Table 18) (this study, Claesson & Lundqvist 1995, Welin et al. 1993, Patchett et al. 1987, Claesson 1987, Miller et al. 1986). The data of Huhma (1987) for the Tampere schist belt in southern Finland is slightly less negative (-5.3 to -4.4) and has not been included. Metaigneous rocks of the early Svecofennian episode are generally more radiogenic, with only little overlap with the rapakivis (Fig. 46). The spread in ε_{Nd}(1.51) is wide (-5.9 to +0.7), but the average is almost four units higher than for the rapakivi granitoids (-3.0). The Svecofennian rocks represent samples collected over a geographically large area, from the Skellefte district in the north (Wilson et al. 1985, 1987) to the relatively juvenile Bergslagen district in the south (this work, Patchett et al. 1987, Valbracht 1991, Kumpulainen et al. 1996), with recent data from central Sweden (this study, Claesson & Lundqvist 1995, Welin et al. 1993) as well as data from southern Finland (Huhma 1986, Patchett & Kouvo 1986). The average ε_{Nd}(1.51) value of the Revsund suite granitoids is somewhat lower compared with the early Svecofennian metaigneous rocks (-4.1), and the range is more restricted (-5.8 to -2.3) (this study, Wilson et al. 1985, Claesson & Lundqvist 1995, Patchett et al. 1987). However, also the Revsund rocks generally display a more radiogenic Nd evolution compared with the investigated rapakivis (Fig. 46). The Revsund suite rocks are restricted geographically to central Sweden and northwards to the Skellefte district. The Archaean rocks of the Fennoscandian shield analysed for Nd isotopes (Öhlander et al. 1987, Huhma 1986, Martin et al. 1983, Jahn et al. 1984) have an average ε_{Nd}(1.51) of -18.5 and a spread between -25.1 and -13.7.

A likely range in Nd concentration (C_{Nd}) for a possible depleted mantle component in the Svecofennian is 5–15 ppm (cf. e.g. Huhma 1986, Patchett & Kouvo 1986, Björklund & Claesson 1992, DePaolo 1988, Kumpulainen et al. 1996), and the ε_{Nd}1.51 is +4.5 (DePaolo 1981). A possible non-depleted mantle source of this particular age could be similar to the source of the Suomenniemi and Häme dolerite swarms, which are related to the SE Finnish rapakivi complexes and have initial ε_{Nd} values close to 0 (Rämö 1991). The average Nd concentration of these dolerites is 47 ppm. Rämö (1991), however, in his calculations assumed an initial mafic magma in these dykes with a C_{Nd} of 30 ppm, based on the most depleted dykes (highest initial ε_{Nd}). Thus, a reasonable range in Nd concentration for a non-depleted mantle source associated with the rapakivi magmatism may be 30–47 ppm. The Nd concentration in Archaean rocks from the NE parts of the Fennoscandian shield is quite variable, 7–69 ppm (Jahn et al. 1984, Huhma 1986, Öhlander et al. 1987), with an average of 21 ppm. C_{Nd} for Svecofennian metasediments of the Bothnian basin varies between 12 and 44 ppm with an average of 30 ppm (this study, Miller et al. 1986, Patchett et al. 1987, Claesson 1987, Welin et al. 1993, Claesson & Lundqvist 1995). Early Svecofennian metaigneous rocks are also quite variable in C_{Nd} (10–102 ppm), but a majority are in the range 20-40 ppm with an av. of 35 ppm (this study, Wilson et al. 1985, 1987, Patchett et al. 1987, Welin et al. 1993, Patchett & Kouvo 1986, Huhma 1986, Valbracht 1991, Claesson & Lundqvist 1995). Revsund granitoids range in C_{Nd} between 13 and 68 ppm, but 64 % are between 30 and 50 ppm with an av. of 40 ppm (this study, Wilson et al. 1985, Claesson & Lundqvist 1995, Patchett et al. 1987).

As far as the Nd isotopic composition is concerned, the Rödö rapakivis could be entirely derived by melting of metasedimentary rocks (Fig. 46b). This is, however, a very unlikely source for A-type granitoids. The sediments are in part muscovite-bearing, Al-rich rocks (with Al_2O_3 up to 21 %; Lundqvist et al. 1990), and melts from such a source would be peraluminous, two-mica S-type granites (e.g. Chappell & White 1974), like the Härnö granites, occurring exclusively within the sedimentary basin in question (Fig. 31) (Lundqvist et al. 1990, Claesson & Lundqvist 1995). Another possibility would be an early Svecofennian metasedimentary source depleted by a previous extraction of granitic melts, e.g. the Härnö granitic suite. Such a depleted crustal source is, however, not likely to contain an appropriate mineralogical composition. A previous melt extraction event from semipelitic (greywacke) sources would proceed by the dehydration melting of micas, depleting the protolith in, e.g. K, and LIL elements, leaving a residue dominated by quartz, plagioclase, garnet and sillimanite (e.g. Vielzeuf & Holloway 1988, Clemens 1992). Such a depleted source composition will not be capable of producing A-type granitic magmas rich in K, LIL and other characteristic elements (e.g. Creaser et al. 1991, Emslie 1991). Furthermore, recent Pb-feldspar and Sr-whole rock data preclude metasedimentary sources (chapter 7.4. below).

All other models require mixing of at least two components. Mantle sources are possible, but re-

quire substantial crustal additions, unless the Subsvecofennian mantle at the time was highly enriched in LREE. There are data supporting mantle sources for silicic rocks, both for Tertiary to Recent rhyolites (DePaolo et al. 1992, Perry et al. 1993), and Proterozoic A-type granitoids (Kerr & Fryer 1993, Emslie & Hegner 1993). In these cases, however, the rocks exhibit positive $\varepsilon_{Nd}{}^{t}$ values, suggesting depleted mantle sources or sources with short crustal residence times. The latter are, as shown above, not applicable in this case. Furthermore, the $\varepsilon_{Nd}{}^{t}$ in the rapakivis is lower than in any known mantle source from the shield.

Substituting relevant data into the general two-component mixing equation (cf. Faure 1986), the mixing of Archaean material with a mantle or crustal component can be described as:

$$x = \frac{C_{Nd}(S)[\varepsilon_{Nd}{}^{1.51}(S)-\varepsilon_{Nd}{}^{1.51}(Rap)]}{C_{Nd}(S)[\varepsilon_{Nd}{}^{1.51}(S)-\varepsilon_{Nd}{}^{1.51}(Rap)] + C_{Nd}(Arch)[\varepsilon_{Nd}{}^{1.51}(Arch)-\varepsilon_{Nd}{}^{1.51}(Rap)]},$$

where (Rap) denotes the rapakivi magma, (Arch) the Archaean component, (S) source material other than the Archaean component, and x is the fraction of Archaean material in the mixture.

In order to obtain some approximate quantitative constraint on the mixing of possible source components, the averages in Table 18 were used in the calculations. A derivation of the rapakivi granitoids from a depleted mantle source requires the input of 18–40 % Archaean material, depending on the mantle C_{Nd} (5–15 ppm). A non-depleted mantle source requires even more, 45–56 % Archaean material. To obtain the rapakivi magmas from such mantle sources requires extreme fractionation (>90 %; cf. e.g. Hess 1989, p. 231), in addition to the large degrees of assimilation implied from the calculations. If assimilation in the lower crust is the major process, this lower crust has to be made up almost exclusively of Archaean material, otherwise an even larger degree of assimilation is necessary. Such large degrees of assimilation cause substantial energy loss and crystallization of the magma (e.g. McBirney 1979, Hess 1989). The magma would tend to crystallize before reaching upper crustal levels. No field evidence for massive assimilation has been observed, e.g. restite enclaves. On the other hand, an already enriched mantle source will need very little crustal assimilation, and may thus be more realistic. Archaean material might have been added to the subcontinental mantle at some previous orogenic stage (e.g. during the Svecofennian), by e.g. percolating slab-derived fluids and/or melts (cf. e.g. Zindler & Hart 1986).

Crustal sources are, however, more petrologically tenable. Most workers suggest non-depleted metaigneous lower crustal protoliths for A-type granitoids (Anderson 1983, Creaser et al. 1991, Emslie 1991, Skjerlie & Johnston 1993). In this case, a magma derived from an early Svecofennian metaigneous source (Table 18), requires an Archaean contribution of about 34% to arrive at $\varepsilon_{Nd}1.51 = -6.7$. For a Revsund source, 30 % Archaean contribution is necessary. These calculations are strongly dependent on the Nd concentration in the averages. The reported Nd content in the Archaean rocks is very variable (Jahn et al. 1984, Huhma 1986, Öhlander et al. 1987), with only a few with more than 50 ppm and most below 20 ppm. Using an average calculated without the few with high contents (14 ppm) gives an Archaean contribution to the rapakivi magmas of 44 %, and thus 56 % early Svecofennian material. The distribution of Revsund suite rocks (Fig. 31) suggests that this potential source is available primarily for the western intrusions and not for the Rödö granite. In the western area a combination of early Svecofennian and Revsund protoliths is permissible, although the former probably dominate in the lower parts of the crust.

A combination of three sources is also possible. The association of the rapakivi granites with intermediate and mafic rocks points to this option. In such a case it is impossible to separate the relative importance of mantle and Svecofennian sources. It is evident, however, that a major Archaean component is present in the Rödö rapakivi magmas.

In *summary*, it is suggested that the source of the central Swedish rapakivi granitoid magmatism is derived from a mixture of early Svecofennian metaigneous and Archaean material, where the Archaean proportion is c. 35–40 %. This Archaean source is presumably of tonalitic, trondhjemitic or granodioritic (TTG) composition, similar to the majority of both the early Svecofennian granitoids, and the Archaean gneisses in the NE parts of the shield (cf. e.g. Gaál & Gorbatschev 1987). The existence of Archaean material in the lower crust of central Sweden has been verified by Claesson et al. (1997), who found 2.7 Ga zircons in the Nordsjö syenite (see chapter 7).

The similarly low values of the associated basic rocks cannot, however, be explained in a model of

only crustal sources. The basic magmas must have their ultimate origin in the mantle. Most likely the heat supplied by these basic magmas as they were emplaced in the lower crust started the melting and generation of the rapakivi magmas (Huppert & Sparks 1988, Andersson 1991, Haapala & Rämö 1992, Korja et al. 1993). This is supported by the bimodal nature of almost all Fennoscandian rapakivi complexes. However, the Nd isotopic nature of such mantle-derived basic magmas would be expected to be quite different from a crustal magma, especially when the crustal magma has such low initial ε_{Nd}. Two possible explanations of the low initial ε_{Nd} of the basic to intermediate rocks are: i) these magmas derive from a strongly enriched mantle source, or ii) they were originally chondritic or depleted in character but assimilated sufficient lower crustal material to completely change their Nd isotope characteristics. No basic enriched rocks have previously been reported for the part of the Svecofennian domain that lies outside areas known to be underlain by Archaean basement, e.g. in the early Svecofennian 1.95–1.86 Ga (e.g. Huhma 1986, Patchett et al. 1987, Valbracht 1991, Björklund & Claesson 1992, Kumpulainen et al. 1996), the Transscandinavian igneous belt (TIB) and related rocks 1.85–1.65 Ga (chapter 4.4.2. above), or the Postjotnian, 1.26 Ga (Claesson 1987, Rämö 1990, Patchett et al. 1994, Andersson 1997a, this work). Thus, the reason why the mantle should be enriched at 1.52–1.50 Ga and not before or after, remains obscure. Moreover, the Svecofennian province in central Sweden was stabilized at c. 1.77 Ga after the regional metamorphism and magmatism culminating with the Revsund granitoid suite. Further orogenic activities that could enrich the mantle with crustal components should have been minimal after this time. If the mantle was enriched at the TIB stage this should also be evident in the mafic rocks of this suite, which is not the case in the south Svecofennian province. The basic TIB rocks show in general a mildly depleted character (chapter 4.5.1.2. above). No basic rocks associated with the Revsund granitoids have been analysed to date.

Nevertheless, LREE-enriched mantle sources cannot be ruled out. These sources then appear to be restricted to the subcontinental mantle in a region localized only beneath central Sweden (leaving the sources for the Nordingrå basites less enriched, cf. Fig. 46), and not in the rest of the shield (except Salmi; Neymark et al. 1994), as basic magmas associated with the rapakivi complexes in Finland and Estonia are near chondritic (Rämö 1991, Rämö et al. 1996). Furthermore, the Postjotnian dolerites occurring in the same general areas in central Sweden as the rapakivi complexes derive from relatively depleted sources (Claesson 1987, Patchett et al. 1994, Andersson 1997a, this work). This must mean that the Postjotnian magmas were extracted from completely different mantle sections compared with the basic rapakivi-related rocks. Similar depleted mantle sources supplemented by different degrees of crustal assimilation, where the rapakivi-related basites are relatively more contaminated by crustal material, could also be envisaged (Rämö 1990, see below).

It seems more probable that the low ε_{Nd}-initials of the basic rocks are derived predominantly by crustal assimilation. This requires a very high proportion of Archaean, compared with early Svecofennian, component in the assimilated material. Otherwise the original basic character of the magmas would be changed too much to be consistent with the observed compositions. A basic magma with a depleted mantle source ($\varepsilon_{Nd}(1.51) = +4.5$) and an assumed Nd content of 5–15 ppm, requires an Archaean addition of between 20 and 50 %, depending also on the Nd content of the Archaean source. If Svecofennian material occurs in the assimilant, these figures would be even higher. Another possible source may be a non-depleted mantle with $\varepsilon_{Nd}(1.51) \approx 0$, giving a primary LREE enriched mantle-derived magma with an Nd content of 30–50 ppm. Such a basic component has been suggested by Rämö (1991) on the basis of the most primitive dolerites in the Häme and Suomenniemi swarms in SE Finland, which are associated with SE Finnish rapakivi complexes. This sort of mantle source requires an even larger amount of Archaean input to the mantle magma (> 50 %) to reach the low initials of the basic Rödö rocks. This is due to the much higher Nd content in this magma. Bulk assimilation of 20 to 50 % or more of crustal rocks of tonalite-granodiorite composition is probably not reasonable, as it would change the original basic composition too much (cf. Rämö 1990).

A typical feature of the central Swedish complexes is the strongly overlapping initial ε_{Nd} values of the associated basic rocks with the rapakivi granitoids. This is also the case for complexes with less negative initial ε_{Nd} values, Nordingrå (Andersson 1994, Fröjdö et al. 1996, Lindh & Johansson 1996) and Strömsbro (Andersson 1997a). In fact, in the complexes with the lowest initials, the basic rocks trend to even lower values than the granitoids. This is not the case, e.g. in the Nordingrå and Åland areas, where the basic rocks instead tend to include slightly less enriched compositions (cf. Fig. 46). In

the Ragunda complex a gabbro with $\varepsilon_{Nd}(1.51)$ as low as -10.1 has been recorded (Persson 1996). The overlapping initial ε_{Nd} values of the basic and silicic rocks in the central Swedish complexes could be taken as an indication of a common origin for all magmas in an enriched upper mantle. However, the discrepancies noted above suggest that the granitoid and basic rocks originate from different sources.

As regards rhyolitic volcanics and granitoids associated with basic rocks elsewhere, common sources in the mantle have been invoked (e.g. Perry et al. 1993, Kerr & Fryer 1993). In these cases, however, all the rocks have depleted signatures, i.e. also the silicic ones. These authors suggest that all rocks belong to a common line of differentiation from an original basic mantle-derived magma. A differentiation origin from a common primary magma is unlikely in this case because the relative amount of silicic magma is large in most complexes, much larger than can be derived by fractional crystallization of a basic parental magma (<10 %; cf. e.g. Hess 1989). This could partly be overcome if assimilation is also large, but probably not fully since generally basic and silicic rocks broadly occupy similar volumes in rapakivi complexes. The latter is a crude estimate because the different levels of exposure make it hard to judge reliably in each case. In addition, a dominantly intermediate rather than bimodal compositional character of the complexes would be expected. Another major problem with this model is that an extended fractional crystallization would yield huge amounts of mafic cumulates to account for this amount of silicic rocks, of which there is no sign. Anorthositic cumulates of considerable volume exist in some complexes, but there is no field evidence relating these to fractionation yielding a rapakivi type residual magma. Magma-mingling structures are common between basic and silicic magmas in the complexes. This suggests that the basic and silicic magmas were actually active contemporaneously, rather than the silicic being a late fractionate from the basic. Thus separate sources of the associated granitoid and basic magmas in the rapakivi complexes is most likely.

Recently, a new model to explain crustal Nd compositions in anorthosite massifs, associated with rapakivi granites has been proposed by Emslie & Hegner (1993), and Emslie et al. (1994). They suggest that as the mantle-derived basic magmas come into the lower crust and induce partial melting, forming the rapakivi magmas, while the restite material left behind after the crustal melting is largely dissolved in the mantle magmas below. This restite would supply the basic magmas with material contributing a crustal Nd isotopic signature (Archaean-dominated in this case). The restite would be dominated by refractory phases after the melting event such as pyroxene, plagioclase, and probably some accessory phases such as apatite and zircon (cf. the experiments of Skjerlie & Johnston 1993, Singh & Johannes 1996). If this restitic assemblage is dominated by these minerals with only insignificant zircon and/or garnet, it would be somewhat LREE enriched, which would be appropriate (cf. compilation in Grauch 1989).

However, also this model encounters some major difficulties, e.g. the contents of REEs in lower crustal granulites are low, similar to that of the most primitive basic rocks in the rapakivi complexes (cf. compilation in Table 6 of Emslie et al. 1994, mineral REE compilation in Grauch 1989, and sample R54 in Appendix 2b), while all more evolved basic rocks, e.g. in the Rödö complex, have substantially higher LREEs. A depleted lower crustal contaminant would thus not be able to increase the LREE content to the observed level. The addition of some undepleted material to the magmas is therefore likely. Accompanying fractionation of olivine and pyroxenes could also contribute significantly to the increase in REE, and especially the LREE contents of the basic magmas (cf. Emslie 1985, Mitchell et al. 1995, chapter 6.5.1.7.)

The following scenario is proposed to account for the enriched character of the Subjotnian basic rocks in central Sweden: 1) mantle-derived magmas associated with the rapakivi magmatism underplate the crust. These magmas are mildly depleted to slightly enriched (similar to those in Finland), however, with initially relatively low REE contents (perhaps similar to the least enriched Postjotnian dolerites, Nd≈5–10 ppm, Appendix 2b and Th. Lundqvist unpubl. data). 2) Melting of the undepleted lower crust is induced. This crust is dominantly tonalitic to granodioritic in composition, and is composed of both Archaean and early Svecofennian components. The Archaean components are suggested to be dominant in the lowermost parts closest to the lithospheric mantle, being remnants of an old basement in this part of the shield. This Archaean basement was intruded and overlain by calcalkaline rocks in the early Svecofennian. The melting of this composite material results in the strongly LREE-enriched rapakivi granite melts and a pyroxene and plagioclase dominated residue. The granites are derived from a mixture of c. 35–40 % Archaean material in this mixed source (see above).

In the lowermost levels the percentage of Archaean material available for assimilation in the basic

magmas is higher. Both the crustal residue and the newly generated rapakivi magmas, as well as undepleted crustal material, should be potentially available as contaminants in this environment. The residue contains plagioclase with a substantial positive Eu peak, which is counteracted by a negative one in the pyroxenes (and also apatite, if present; cf. Grauch 1989). The net effect is suggested to be a minor positive anomaly (cf. Taylor & McLennan 1985, p. 81). Undepleted Archaean-Svecofennian material is generally expected to lack or show a minor positive Eu anomaly and be strongly LREE-enriched (cf. Jahn et al. 1984, Öhlander et a. 1987, Fig. 44c). The rapakivi magmas are more LREE-enriched, but with a substantial negative Eu anomaly (cf. e.g. Fig. 44a). Due to the much higher REE concentration in the rapakivi magma only a minor assimilation of this component would erase a positive anomaly induced by the other two.

It is thus suggested that the main part of the assimilated material, causing the low initial ε_{Nd} values in the Subjotnian basic rocks, is composed of the depleted residue after extraction of the rapakivi magma. This is supplemented by a relatively minor component of undepleted Archaean-dominated lowermost crust and considerable high-P fractionation of mainly pyroxenes and olivine to arrive at the LREE-enriched composition of the basic rocks. If the mantle magma is mildly depleted and the assimilant is Archaean-dominated (depleted or undepleted), 15 up to 40 % assimilation is calculated, which is realistic since most of the Subjotnian basic rocks are quartz tholeiites showing abundant chemical and petrographic signs of crustal interaction (Figs. 34, Plates 1 and 2). If the lowermost crust also contains substantial amounts of more basic rocks, which appears likely in light of the numerous basic granulitic xenoliths recovered from volcanic pipes and kimberlites worldwide (e.g. Taylor & McLennan 1985), more assimilation can be accommodated without changing the composition of the basic magma too much. A model of this kind has been entertained by Neymark et al. (1994) for the Salmi batholith. Small additions of the newly extracted rapakivi magma may also be incorporated in parts of the suite, which is corroborated by an abundance of felsic xenocrysts and negative Eu anomalies (Figs. 44b, Plate 2d). This might have occurred during transport in conduits to the upper crustal emplacement levels. The less enriched character of the Postjotnian dolerites is consistent with much more limited interaction with the crust (cf. Rämö 1990).

6.5.3.3. Sr isotopic relations

Unfortunately, the Rb-Sr system in the silicic rocks of the Rödö suite has been severely disturbed, obscuring the primary igneous Sr isotopic compositions. All samples have unrealistically low initial $^{86}Sr/^{87}Sr$ (Sr_i) ratios (Table 13), lower than, e.g. the estimated bulk earth (UR, Sr(1.51) = 0.7027), which is due to a postcrystallization increase in the Rb/Sr ratio or loss in radiogenic Sr (cf. e.g. Romer et al. 1992). The reason and timing for this remains unclear, although it may be related to fluid circulation connected to the c. 550 Ma (Kresten 1990) Alnö intrusion, nearby. Some of the basic to intermediate rocks also have a disturbed Rb-Sr system, with high Rb/Sr ratios and low apparent initials. A few, however, have realistic Sr_i values, and can be divided into two groups: one with relatively primitive initial Sr ratios (0.7036–0.7064) and one with more evolved (0.7081–0.7188).

The $^{87}Sr/^{86}Sr(1.51)$-ratio is plotted against $\varepsilon_{Nd}(1.51)$ in Fig. 54 for the Rödö and Jämtland-Ångermanland rocks, together with other rocks in the Bothnian basin area (Tables 13, 22, and Claesson & Lundqvist 1995) and a few Archaean rocks from the NE part of the shield (Martin et al. 1983). The strongly disturbed rocks plot far off the diagram to the left. Very little information on the primary initial Sr composition of the silicic rocks can be extracted, due to the strong disturbance. Only one granite (M14a) from Jämtland shows an undisturbed (?) composition, which is identical to the uniform reservoir (UR; Fig. 53; Table 22). This meagre evidence suggests that the silicic rapakivi magmas may be characterized by a primary low-radiogenic Sr composition, close to that of the basic rocks, which precludes Revsund and metasedimentary source components in the magmas. A depleted mantle origin combined with assimilation of mainly Archaean material is indicated (curve in Fig. 54). More probably, and in accordance with the proposed model based on the Nd isotopes (chapter 6.5.3.2. above), this is a mixture of source rocks of Archaean and early Svecofennian origin (other curve in Fig. 54). This relies on the early Svecofennian metaigneous source having high ε_{Nd} and low $^{87}Sr/^{86}Sr$, similar to the most primitive sample shown in Fig. 54 (sample 82021; Claesson & Lundqvist 1995).

The crustal assimilant that has lowered the initial ε_{Nd} in the basic rocks should have been relative-

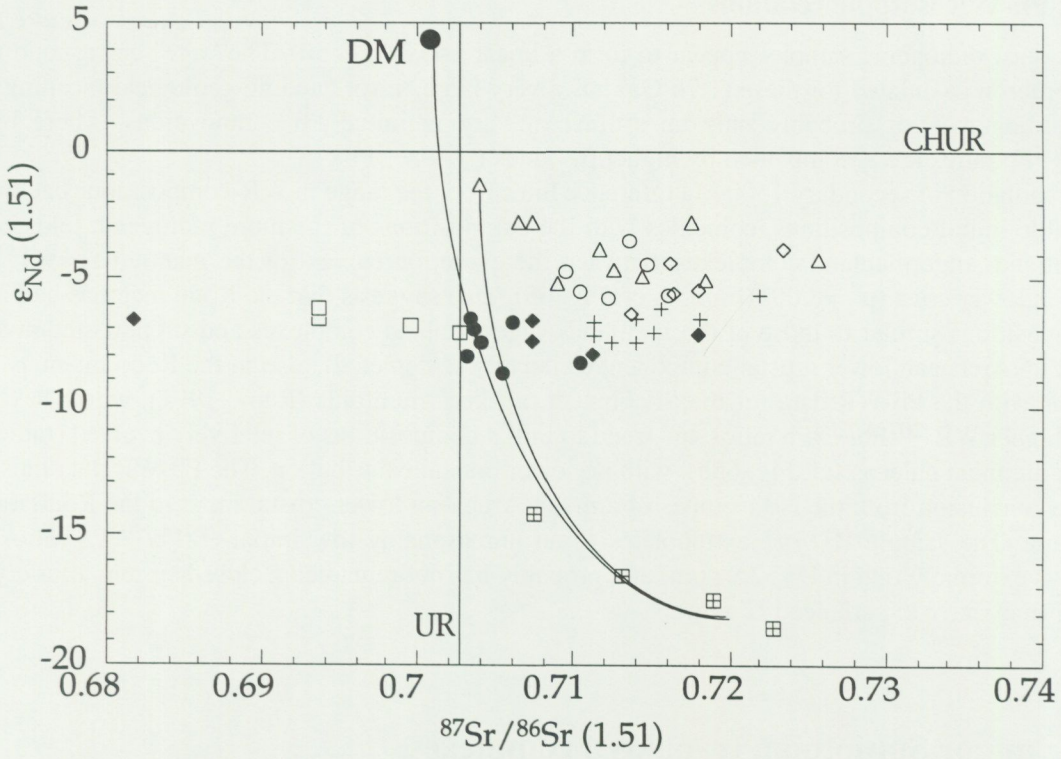

Fig. 54. ε_{Nd} vs. $^{87}Sr/^{86}Sr$ diagram at 1.51 Ga for the rapakivi rocks of this study (Tables 13 and 22) and relevant country rocks in the Bothnian basin (Claesson & Lundqvist 1995, this study). A few Archaean rocks from the NE part of the shield are included (Martin et al. 1983), as representative of a possible Archaean component. Symbols are, unfilled squares: rapakivi granites, filled circles: basic rapakivi-related rocks, filled diamonds: hybrid porphyries, Rödön, crosses: metasediments in the Bothnian basin, triangles: early Svecofennian granitoids, unfilled circles: Revsund granitoids, unfilled diamonds: Härnö granites. Two possible mixing curves are shown: one between the DM and and an Archaean component, and one between a primitive early Svecofennian granitoid and an Archaean component. CHUR is the chondritic uniform reservoir (Nd), and UR is the hypothetical uniform reservoir (Sr). Many samples plot off the diagram to the far left. These have disturbed (not preserved magmatic) Rb-Sr systematics. Discussion in the text.

ly depleted in Rb (low Rb/Sr ratio) for those rocks which plot close to UR (Fig. 54). The group of basic-hybrid rocks having higher initial Sr, on the other hand, should have assimilated material with high Rb/Sr ratios and thus more radiogenic $^{87}Sr/^{86}Sr$ ratios. The trend towards the metasediments in Fig. 54 suggests that these could be a substantial assimilant in some of these magmas. However, since $^{87}Sr/^{86}Sr(1.51)$ ratios for the early Svecofennian granitoids also range up to high values, mixtures between such granitoids and Archaean sources may account for the spread in initial Sr ratios in the basic-hybrid rocks. In any case, undepleted components have been assimilated in these rocks, presumably in the upper crust. For the hybrid porphyries there is abundant evidence of magma mixing with crystal-bearing rapakivi magmas (see chapter 6.5.1.8.), but in some cases there is petrographic evidence also for upper crustal assimilation. For example, sample R134a contains large scattered pink Kfsp megacrysts dissimilar to those in the rapakivi rocks as well as cellular megacrysts of albite (Table 11), of unknown, presumably xenocrystic, origin.

Even though all basic-intermediate rocks have low initial ε_{Nd} values, their Sr initials thus vary from primitive to evolved. This is consistent with primitive (but not Rb depleted) mantle sources for the basic magmatism combined with different types and degrees of crustal assimilation. The Sr isotopic composition of a combination of early Svecofennian and Archaean metaigneous more or less depleted lower crustal material, residual after extraction of the rapakivi granite magmas, will be close to that of the basic rapakivi-related rocks (curve). The residue will be dominated by pyroxene and plagioclase and be rich in Sr and poor in Rb (cf. Emslie et al. 1994), but since the $^{87}Sr/^{86}Sr(1.51)$ ratio of the residue probably will be close to that of the basic magmas, assimilation will have only a negligible effect on the Sr isotopic ratio of the basic magmas. A model of assimilation of dominantly residual lower crustal components in the basic rocks with lowest initial Sr values, is therefore supported by the Sr data.

6.5.3.4. Pb-WR isotopic relations

The six least radiogenic samples appear to form a linear array (Fig. 50). The "age" corresponding to the errorchron calculated for these (1.76 Ga) has a very large "error" and no geological meaning. The linear arrangement is probably only an artifact of varying initial Pb compositions, where higher $^{207}Pb/^{204}Pb$ ratios are accompanied by higher μ-values ($^{238}U/^{204}Pb$).

Extrapolation of secondary 1500 Ma reference lines from the range in WR-compositions backwards to possible initial compositions, coincides with the compositions of the more radiogenic feldspars of the Jämtland-Ångermanland complexes, between the evolution curves for the mantle ($\mu_2 = 9.17$) and Archaean lower crust ($\mu_2 = 8.00$) (Fig. 50, cf. Fig. 65). This suggests that the Rödö magmas had initial Pb compositions similar to those of the Jämtland-Ångermanland complexes and supports the involvement of an Archaean lower crustal component (relatively U-depleted), also in the Rödö magmas. This contrasts with the Pb-WR data for the SE Finnish rapakivi granitoids (Rämö 1991), which have distinctly higher WR-$^{207}Pb/^{204}Pb$ ratios and trend to initial compositions of relatively evolved (radiogenic) Svecofennian galenas (cf. Fig. 65b), with no lower crustal contribution. The Pb-WR data thus support the conclusion from the Nd isotopes of a major Archaean lower crustal input to the Rödö rapakivi magma. The sample R117g1 extrapolates to an unreasonably low initial $^{207}Pb/^{204}Pb$ ratio. This sample is extremely rich in U (52.8 ppm) and probably has not remained a closed system after crystallization (may have experienced U gain).

7. The minor Subjotnian (rapakivi) complexes in Jämtland–Ångermanland

Four minor intrusive complexes situated in the western part of the Bothnian basin have been investigated. They have traditionally been included in the suite of Fennoscandian rapakivi granite complexes on structural and petrographic grounds (e.g. Lundqvist 1979). None of them have, however, been subjected to modern petrogenetic studies, and their petrology has thus been poorly known.

7.1. FIELD RELATIONS

7.1.1. The Mårdsjö complex

The Mårdsjö complex in central Jämtland is about 60 km^2, the largest of these four. It intrudes early Svecofennian granitoids in the east and sedimentary gneisses with palingenic granites in the west (Fig. 55a). Gabbro is the dominating rock type (Lundegårdh et al. 1984). Here and there the gabbro contains spots or crystals of K-feldspar and quartz. It is, furthermore, often penetrated by granitic veins, commonly forming net-vein structures (Plate 3e). This relationship between the granitic veins and the

Fig. 55. Geological maps of the four small Subjotnian complexes in Jämtland and Ångermanland counties investigated in this study. Their regional position is shown in Fig. 31. Numbers indicate sampling localities. Only studied outcrops are included. These sample numbers refer to all tables and figures. **a)** The Mårdsjö complex is the largest of these around 60 km^2 (after Lundegårdh et al. 1984, and K.-A. Kornfält unpubl. data). It is dominated by gabbro, often containing veins of granite in a mingling relationship (cf. Plate 3e). An arc-like structure with brownish to greenish syenite occur in the eastern parts, and only minor areas of granite (metaluminous) are present. The syenites of the different massifs are macroscopically very similar. **b)** The Nordsjö massif consists entirely of syenite (after Lundqvist et al. 1990). Numerous dyke rocks are associated with this massif, cutting both the syenite and the country rocks (see Lundqvist et al. 1990). Only those sampled in this study are indicated on the map (N3 are trachytic, N4 peralkaline aplitic (ap), N10 quartz syenitic (trachytic), and N7 doleritic (D). PJD refers to a Postjotnian dolerite occurring close to the contact. **c)** The Mullnäset complex is dominated by syenites (after Lundegårdh et al. 1984). The southern parts of the complex consist of gabbro and an area in northeast of granite (metaluminous). One locality of peralkaline granite (Mu6) was found in the northern part of the syenite. More peralkaline rocks may occur in this area, which is poor in exposures. **d)** The Strömsund massif is the most poorly exposed of the four (modified from Lundegårdh et al. 1984). The localities marked are the only ones known to the present author. The massif is partly covered by Caledonian rocks and may extend considerably beneath this cover. One locality in the south indicates slightly less quartz-rich compositions. Two localities contain metaluminous granite (S7 and S8), while three contain peralkaline granite (S3, S4, and S6; orange on the map). The peralkaline rocks appear to occupy the northeasternmost parts, but otherwise the relations between the granite types are not known. An area of a grey fine-grained granite of unknown, but presumably early Svecofennian, position occurs in the southeast.

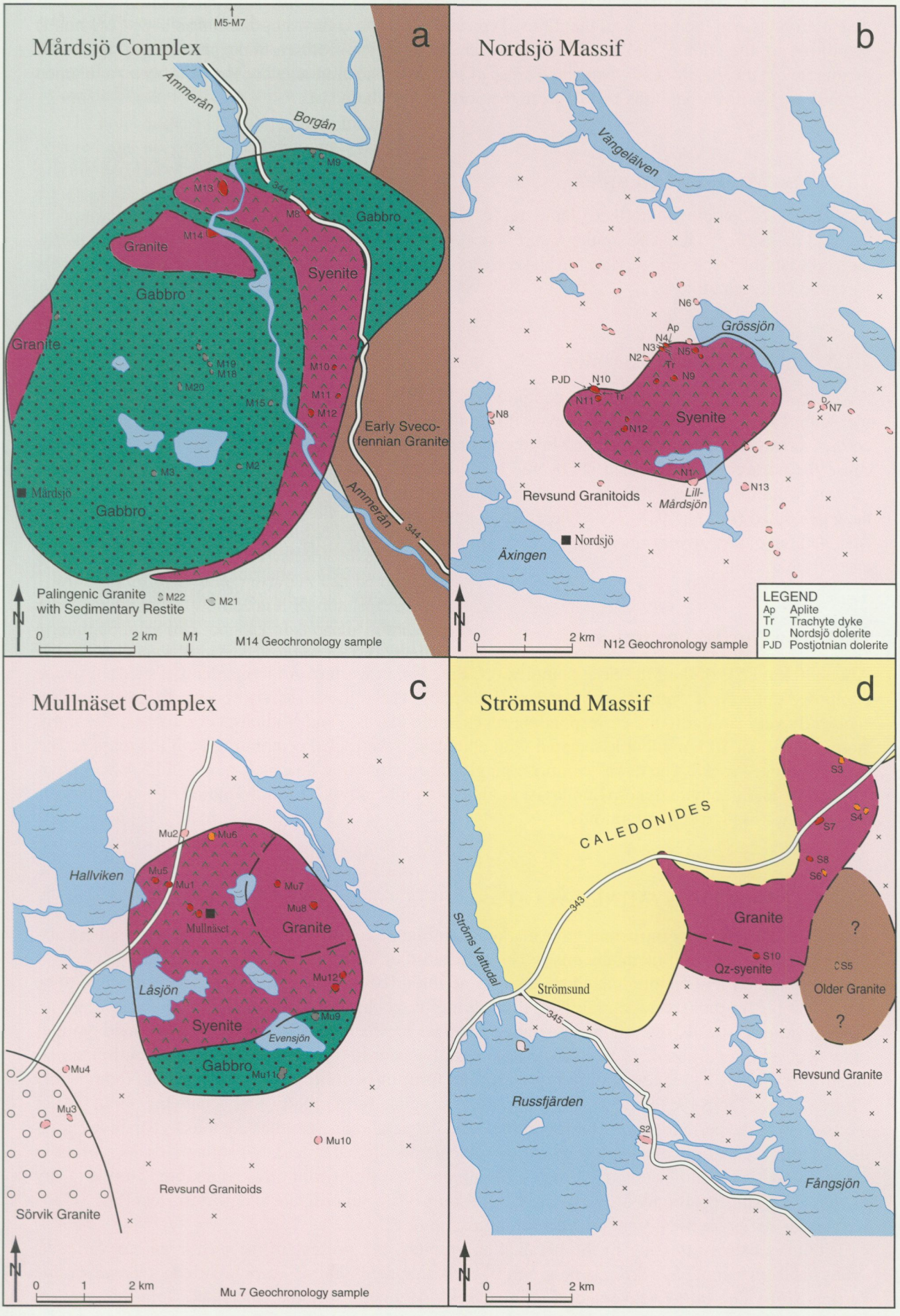
a
Mårdsjö Complex
M5-M7
Ammerån
Borgån
M9
M13
344
M8
Gabbro
M14
Granite
Syenite
Gabbro
Granite
M19
M18
M20
M10
M11
M15
M12
Early Sveco-fennian Granite
M3
M2
Mårdsjö
Gabbro
Ammerån
344
Palingenic Granite with Sedimentary Restite
M22
M21
N
0 1 2 km
M1
M14 Geochronology sample
b
Nordsjö Massif
Vängelälven
N6
Ap
Grössjön
N4
N3
N5
N2
Tr
N9
PJD
N10
N11
Tr
D
N7
N8
Syenite
N12
N1
Revsund Granitoids
Lill-Mårdsjön
N13
Nordsjö
Äxingen
N
0 1 2 km
N12 Geochronology sample
LEGEND
Ap Aplite
Tr Trachyte dyke
D Nordsjö dolerite
PJD Postjotnian dolerite
c
Mullnäset Complex
Mu2
Mu6
Hallviken
Mu5
Mu1
Mu7
Mu8
Mullnäset
Granite
Mu12
Låsjön
Syenite
Mu9
Evensjön
Gabbro
Mu11
Mu4
Mu3
Mu10
Revsund Granitoids
Sörvik Granite
N
0 1 2 km
Mu 7 Geochronology sample
d
Strömsund Massif
CALEDONIDES
S3
S4
S7
S8
S6
343
Granite
?
S10
Qz-syenite
S5
Older Granite
?
Ströms Vattudal
Strömsund
345
Revsund Granite
Russfjärden
S2
Fångsjön
N
0 1 2 km

gabbro suggests that the magmas were coeval, and that magma mingling occurred where the magmas essentially retained their physical identities. Typically, the gabbro forms convex outer contacts against, or pillows in, the granite, and sometimes show chilled margins. Locally, minor amounts of aplite and pegmatite cut the gabbro. Only two small areas of pure Mårdsjö granite occur. An arc of brown to green syenitic rocks runs around the massif from the north to the southeast.

7.1.2. The Mullnäset complex

The Mullnäset complex in northern Jämtland (c. 20 km^2) is dominated by brown to green intermediate syenitic rocks (Fig. 55c). The southern part is occupied by gabbros, whereas a small area in the northeast consists of brick-red granite. No dyke rocks are known, and the complex intrudes exclusively Revsund suite granitoids.

7.1.3. The Strömsund complex

About ten km north of the Mullnäset complex (cf. Fig. 31), an intrusion with similar characteristics is met with (Fig. 55d). In this case, however, it is comprised entirely of granites to quartz syenites. Their colour varies from brick-red over red-brown to green. The size of the massif is difficult to assess because the northwestern part of it is covered by Caledonian rocks. Assuming a roughly circular form, the size would be around 30 km^2. No dyke rocks are known, but boulders of quartz porphyries have been described (Frödin 1918). Also here, the country rock is almost exclusively Revsund suite rocks. A small area of a relatively fine-grained, grey granitoid, possibly early Svecofennian, is situated southeast of the massif.

7.1.4. The Nordsjö complex

About 30 km ESE of the Mullnäset complex (cf. Fig. 31), in western Ångermanland, a small intrusion composed entirely of syenitic rocks occurs (Fig. 55b). These rocks are also brown to green, macroscopically very similar to the corresponding rocks in the Mårdsjö and Mullnäset complexes. The intrusion is small (ca 10 km^2), but associated with abundant dyke rocks, penetrating both the massif itself and the country rocks. The dykes comprise plagioclase porphyritic dolerites, quartz-feldspar porphyries, aplitic, and trachytic dykes (Lundqvist et al. 1990, and below). The surrounding country rocks are exclusively Revsund suite granitoids

7.2. PETROGRAPHY / MINERALOGY

The rocks in these minor intrusions have markedly similar petrographic characteristics and are here discussed as a group. The mineral chemistry is summarized in Table 19.

The *granitic rocks* are dominated by strongly perthitic K-feldspar. The K-feldspars often tend to be somewhat bigger than average grainsize, thus giving the rocks a small-porphyritic appearance. Even-grained varieties are also common, and gradual changes between porphyritic and even-grained granites often occur. Minor amounts of free plagioclase usually occur in the metaluminous granites. In the peralkaline granites, plagioclase is only present in the form of perthitic exsolution lamellae (completely Ca-free albite; Table 19, Plate 3g). Typically, these lamellae form broad veins occupying about half of the volume of the perthite grains (mesoperthite), and the peralkaline granites are thus hypersolvus granites. Quartz is generally abundant (especially in the peralkaline granites), but sometimes decreasing in amount to quartz syenitic compositions (metaluminous). No significant rapakivi texture is found in any of these massifs; no rounded quartz grains and only very subordinate plagioclase mantling of the K-feldspars (if present, only in the metaluminous granites).

Biotite is usually missing in the peralkaline granites, but present in the *metaluminous* varieties. Analyses from sample S7 (Strömsund granite), show that the biotite is Fe-rich with an average atomic Fe/(Fe+Mg)-value of 0.73 (average of 23 analyses). A mineral formula calculated from this average

Table 19. Representative analyses of minerals from the Jämtland–Ångermanland rapakivi complexes.

Feldspars

	Mesoperthites, peralkaline granites				Mesoperthites, syenites				Plagioclases, syenites			
	S6 Per P2	S6 Per P5	Mu6 Per P3	Mu6 Per P5	N5 Per P2	N5 Per P5	Mu1 Per P2	Mu1 Per P1	M13 Per P1	M13 Per P2	Mu1 Plag P5	Mu1 Plag P3
SiO_2	64.37	68.94	65.59	68.45	64.68	66.04	65.07	67.16	65.2	66.68	64.21	65.89
Al_2O_3	17.9	19.12	18.16	19.27	18.32	21.28	18.34	20.57	18.49	21.02	22.02	21.06
FeO	0.06	0.54	0.08	0.23	0.05	0.11	0.04	0.09	-	0.06	0.11	0.12
MgO	-	-	-	-	-	-	-	-	-	-	-	-
CaO	-	-	-	-	-	2.37	0.04	1.8	-	1.61	3.36	1.88
Na_2O	0.11	11.49	0.13	12.12	0.42	10.18	0.34	10.29	1.14	10.9	9.38	10.72
K_2O	15.76	0.09	15.9	0.1	15.64	0.4	16.15	0.22	15.02	0.14	0.39	0.2
BaO	-	-	0.09	0.04	0.18	-	0.29	-	0.15	0.02	-	0.02
SrO	-	0.18	-	-	-	-	-	-	-	-	0.18	0.12
	98.2	100.36	99.95	100.21	99.29	100.38	100.27	100.13	100	100.43	99.65	100.01
	K-feldspar	An_0 Albite	K-feldspar	An_0 Albite	K-feldspar	An_{11} Oligoclase	K-feldspar	An_9 Albite	K-feldspar	An_8 Albite	An_{17} Oligoclase core	An_9 Albite rim

	Feldspars, trachyte dyke					
	M13 Plag P3	N3b Fsp P2	N3b Fsp P5	N3b Fsp P1	N3b Fsp Mx P1	N3b Fsp Mx P2
SiO_2	65.04	63.33	63.13	63.43	65.18	68.95
Al_2O_3	21.52	21.81	18.9	22.98	18.27	19.99
FeO	0.1	0.17	0.16	0.03	0.07	0.07
MgO	-	0.02	-	-	-	-
CaO	2.79	3.51	0.08	3.97	-	0.78
Na_2O	10.12	6.98	0.54	9.56	0.38	11.01
K_2O	0.29	3.57	14.08	0.14	15.82	0.14
BaO	-	0.49	0.7	0.07	0.44	-
SrO	-	0.1	-	0.08	-	0.12
	99.86	99.98	97.59	100.26	100.16	101.06
	An_{13} Oligoclase	$Or_{21}Ab_{62}An_{17}$ Anorthoclase	K-feldspar after anorth	An_{19} Oligocl after anorth	K-feldspar matrix	An_4 Albite matrix

Mafic silicates

	Peralkaline granites					Metaluminous granites			Syenites			
	S3 Amph2 P2	S3 Amph2 P1	S6 ? P1	S6 ? P6 Lam	S6 ? P5	Mu6 ? P2	S7 Bio1 P1	Mu7 Amp2 P4	Mu5 Ol P6	Mu5 Cpx P11	Mu5 TR 33	N5 Ol P6
SiO_2	47.07	52.07	51.22	34.71	44.21	45.44	35.78	41.13	29.65	48.31	39.64	30.18
TiO_2	1.5	0.35	0.07	2.76	0.14	0.91	3.48	1.91	0.04	0.2	2.45	-
Al_2O_3	1.97	0.33	0.06	7.17	3.24	3.35	11.59	7.05	-	0.55	7.65	-
FeO	34.36	37.03	37.59	41.68	41.49	33.67	29.12	30.2	67.54	28.35	30.6	64.78
MnO	0.82	0.19	1.1	0.2	2.24	0.38	0.33	0.5	1.46	0.68	0.36	1.95
MgO	*0.1*	*0.13*	0.29	*0.8*	0.23	*1.54*	*6.01*	2.61	1.34	2.13	*1.83*	2.99
CaO	5.23	-	0.2	-	-	9.43	-	10.32	0.07	19.69	10.66	0.18
Na_2O	4.73	6.7	6.16	-	0.06	1.6	0.03	2.16	-	0.36	2.11	-
K_2O	1.4	0.1	-	8.14	3.37	0.64	9.15	1.09	-	-	1.46	-
ZnO	0.19	0.06					-	-	0.02	-	-	-
	97.37	96.96	96.69	95.46	94.98	96.96	95.49	96.97	100.12	100.27	96.76	100.08
	Ferro-richterite	Riebeckite margin to Fe-richterite	Riebeckite in oxide	Fe-mica? Intergr w P5 in oxide	Mn-K grunerite? in oxide	Ferroactin hornblende in oxide	Biotite (lepidomelane)	Ferroedenitic hornblende	Fayalite	Augite (Ferrohedenb)	Ti-K ferroeden hornblende	Fayalite

	Trachyte dyke				Gabbro		
	N5 Cpx1 (8)	N5 Amph P9	N3b ? P6	N3b Ox P2	N3b Rim P1	Mu9 Opx P2	Mu9 Cpx P3	Mu9 Bio P5
SiO_2	49.71	40.42	51.55	36.04	28.74	50.84	52.26	37.26
TiO_2	0.33	3.07	0.63	0.05	0.4	0.16	0.21	4.85
Al_2O_3	0.85	8.8	1.58	0.03	13.56	0.51	1.18	13.05
FeO	21.23	26.24	13.26	46.46	37.24	30.1	11.45	20.42
MnO	0.49	0.39	0.43	0.85	0.31	0.42	0.23	0.04
MgO	5.73	4.14	11.17	8.35	6.65	16.28	12.58	10.75
CaO	21.06	10.54	20.63	3.38	0.33	1.36	21.78	-
Na_2O	0.34	2.52	0.5	1.35	0.06	-	0.35	0.15
K_2O	-	1.42	-	0.68	1.36	-	-	9.16
ZnO	0.1	0.08				0.07	-	BaO 0.40
	99.84	97.62	99.75	97.19	88.65	99.74	100.04	96.08
	Hedenbergite	Ti-K ferroparg hornblende	Augite phenocryst	Ca-Na cummingtonite? oxide margin	Fe-chlorite oxide margin	Ferro-hypersthene	Diopside (Salite)	Biotite

Fe-Ti oxides and apatite

	Peralkaline granites		Syenites				Trachyte dyke			
	S6 Ilm P2	S6 Mag P1	N5 Ilm P1	N5 Mag P4	Mu1 Ilm P3	Mu Mag P8	Mu 1 Ap P11	N3b Ilm P1	N3b Mag P1	N3b Ap P1
SiO_2	-	0.41	-	0.06	-	0.11	0.24	-	-	0.16
TiO_2	50.2	0.3	50.61	0.84	51.56	1.56	-	49.35	1.67	-
Al_2O_3	-	-	-	0.45	0.03	0.39	-	-	0.31	-
FeO	47.09	93.54	46.94	92.32	45.11	91.62	0.07	45.39	92.26	0.4
MnO	2.5	0.07	2.31	-	2.45	0.04	0.03	4.65	0.1	0.05
MgO	-	0.1	-	0.03	0.12	0.18	-	-	0.13	-
CaO	-	-	-	0.05	-	0.19	55.88	0.1	0.04	55.13
Na_2O	0.04	-	-	0.09	-	-	0.02	0.12	-	0.06
K_2O		-	-	-	-	-	-	-	-	0.02
P_2O_5							42.3	-	-	43.8
	99.83	94.42	99.86	93.84	99.27	94.09	98.54	99.61	94.51	99.62
	Ilmenite	Magnetite	Ilmenite lam in magnetite	Magnetite host	Ilmenite	Magnetite	Apatite	Ilm intergr with magnetite	Magn intergr with ilmenite	Apatite

gives: $K_{0.98}(Fe^{II}_{1.95}Mg_{0.71}Mn_{0.01}Ti_{0.22}Al_{0.11})(Si_{2.94}Al_{1.06})0_{10}(OH)_2$, based on 7 cations in octahedral and tetrahedral coordination. A formula based on the average of 15 analyses of amphibole from the metaluminous Mullnäset granite (Mu7) has been calculated based on 13 cations in the C and T positions and gives:
$(K_{0.23}Na_{0.46})(Ca_{1.78}Na_{0.22})(Fe^{II}_{3.73}Fe^{III}_{0.38}Mg_{0.56}Mn_{0.07}Ti_{0.22}Al_{0.04})(Si_{6.67}Al_{1.33})O_{22}(OH)_2$, corresponding to ferroedenitic hornblende (cf. e.g. Leake 1978, Hawthorne 1981; Table 19). It is also Fe-rich, with an average Fe/(Fe+Mg)-ratio of 0.87. Accessory minerals are abundant, relatively big, zircons and minor apatite.

In the *peralkaline* granites, blue to bluegreen amphiboles were observed. They are usually zoned with wide bluegreen cores and thin blue rims (Plate 3h). Along cleavage planes and associated with inclusions in the crystals, deep blue areas also occur. These amphiboles have been analysed from samples S3 and S6 (Strömsund granite) and are alkali and calcalkali amphiboles (Table 19). A formula based on average of 7 analyses of the blue type gives:
$(K_{0.10}Na_{0.12})(Ca_{0.06}Na_{1.94})(Fe^{II}_{3.08}Fe^{III}_{1.65}Mg_{0.06}Zn_{0.01}Mn_{0.04}Al_{0.14})(Si_{7.97}Al_{0.03})O_{22}(OH)_2$, corresponding to riebeckite, with very high sodium and iron but low Al, Ca and Mg. The bluegreen type is higher in Ca, but still very high in Na and Fe and low in the other cations (except Si; Table 19), and classifies as the calc-alkali amphibole ferrorichterite. A formula from the average of 14 analyses gives:
$(K_{0.27}Na_{0.36})(Ca_{0.93}Na_{1.07})(Fe^{II}_{4.41}Fe^{III}_{0.26}Mg_{0.05}Mn_{0.10}Zn_{0.02}Ti_{0.21})(Si_{7.66}Al_{0.34})O_{22}(OH)_2$. This mineralogical data thus clearly corroborates with the peralkaline whole rock chemistry of these granites. Fe-Ti oxides occur relatively abundantly, as well as some minor apatite and a few zircons.

The *syenites* contain dominantly mesoperthite. Grain boundaries between different perthite grains are generally serrated and intergrown (Plate 3f). The perthite feldspar is the principal mineral, but small amounts of free plagioclase (albite-oligoclase; Table 19) and sometimes quartz, are occasionally met with. The composition of the plagioclase in the perthites is more calcic, compared with that in the peralkaline granites (c. An_{10}; Table 19). Mafic minerals are more abundant compared with the granites, and comprise olivine, clinopyroxene and amphibole. The olivine is fayalite (Table 19), with an average Fe/(Fe+Mg)-ratio of 0.04 in the Mullnäset monzonite (Mu5), and 0.08 in the Nordsjö monzonite (N5). Also the clinopyroxenes are Fe-rich (Table 19), with an average Fe/(Fe+Mg) of 0.87 for those from the Mullnäset monzonite (Mu5), and 0.67 for those from the Nordsjö monzonite (N5). According to the classification in Deer, Howie & Zussman (1963), they are ferrosalites in Mu5 and ferrohedenbergites in N5. The amphibole in the syenite generally seems to be of late origin. It often occurs as coronas around clinopyroxene, sometimes with only tiny remnants of cpx in the middle or completely pseudomorphic. These are also iron-rich calc-amphiboles comparable with those in the metaluminous granites above (Table 19), with Fe/(Fe+Mg)-ratios of 0.90 (aver. of 19 analyses) and 0.78 (aver. of 11 analyses) in Mu5 and N5, respectively. They are classified as Ti- and K-rich ferroedenitic and ferropargasitic hornblendes, respectively (e.g. Leake 1978, Hawthorne 1981). Ilmenite and magnetite occur in substantial amounts, often intergrown (Table 19). Accessories comprise relatively abundant apatite and some zircon.

The trachytic dykes (N3a and N3b) in Nordsjö contain phenocrysts of anorthoclase, augite, Fe-Ti oxides, and minor apatite (Table 19). The anorthoclase is often decomposed to Kfsp and oligoclase, and exsolution-intergrowth of magnetite and ilmenite is common in the phenocrysts. The augites are fresh and essentially unzoned, and considerably more Mg-rich compared with those in the associated syenite (N5) (Table 19). Very iron-rich secondary minerals occur together with the Fe-Ti oxide phenocrysts (Table 19). The matrix is composed dominantly of feldspars (albite+Kfsp) and hydrous Fe-Mg silicates, mainly biotite and amphibole.

The mineralogy of the *gabbros* is dominated by plagioclase and mafic minerals. They are generally even-grained, fine- to medium-grained rocks, sometimes slightly plagioclase porphyritic. The mafic minerals comprise biotite, orthopyroxene, and clinopyroxene, but typically no olivine. They are all more Mg-rich compared with those in the silicic and intermediate rocks. The biotite has a Fe/Fe+Mg-ratio of 0.52 (aver. of 10 analyses), and a formula calculated from the average gives:
$(K_{0.92}Ba_{0.01}Na_{0.02})(Fe^{II}_{1.35}Mg_{1.26}Ti_{0.28}Al_{0.11})(Si_{2.90}Al_{0.09})O_{10}(OH)_2$. The orthopyroxenes are hypersthenes, with Fe/(Fe+Mg)-ratios of 0.52 (Table 19; aver. of 10 analyses). The clinopyroxenes are even more Mg-rich (Fe/(Fe+Mg)=0.35; average of 6 analyses), corresponding to salite (Deer, Howie & Zussman 1963). Apatite is the only significant accessory mineral.

7.3. GEOCHEMISTRY

7.3.1. Major element characteristics

Altogether 59 samples from Jämtland and Ångermanland were analysed in this study, with respect to major and trace elements (Appendix 2b). Of these, 39 analyses are from the rapakivi complexes, 18 from the older country rocks, and 2 from younger Postjotnian dolerites.

The rocks of the Jämtland-–Ångermanland complexes are plotted in major element discrimination diagrams in Fig. 56. For comparison, rocks from the c. 1.82 Ga Härnö granite and the c. 1.79 Ga Revsund granitoid suites are included (Lundqvist et al. 1990, Claesson & Lundqvist 1995, L. Lundqvist unpubl. data, Lundegårdh et al. unpubl. data), as well as rocks from the c. 1.51 Ga Ragunda rapakivi complex (Kornfält 1976). A few analyses are also from the Strömsbro rapakivi complex (Andersson 1997a). The Jämtland–Ångermanland rocks display a distinct syenitic trend with abundant syenites and quartz syenites. Some of these are also slightly undersaturated and one even plots in the nepheline syenite field in the R1–R2 diagram (Fig. 56a). However, only one sample (N3a) is nepheline normative (CIPW-norm), while the other syenites are quartz normative and in a few cases slightly olivine normative. Also the silicic rocks have a clearly alkali-rich character, falling in the syeno to alkali granite fields (Fig. 56a).

The basic rocks are generally saturated, quartz normative gabbros, with one exception (N7), which is slightly olivine normative, falling in the syenogabbro field of the R1–R2 diagram (Fig. 56a). One of the basic Mårdsjö rocks (M3) is an olivine normative leucogabbro. Only two rocks tend to follow a more monzonitic trend towards the silicic end of the spectrum, M20 and Mu11a. M20 is a monzodiorite of the Mårdsjö complex, while Mu11a is a relatively quartz-rich (normative Qz=11.06 %) gabbro in the Mullnäset complex. The Ragunda rocks have very similar distribution of major elements as the smaller complexes, but appear to have slightly more abundant undersaturated (olivine normative) gabbros similar to N7 of the Nordsjö complex (Fig. 56a). The Härnö suite is restricted to silicic compositions generally in the monzogranite field, while the Revsund suite displays a distinct monzo-trend from monzogranite to monzodiorite, similar to the Småland–Värmland suite (chapter 4.3.1. above). A part of this suite also trends to more Ca-rich compositions in the fields of granodiorite and tonalite (Fig. 56).

The felsic and intermediate rocks are plotted in alumina and alkali saturation diagrams (Fig. 57). For comparative purposes, granitoids from the Härnö, Revsund, Åland, and Ragunda suites are included. The pronounced peraluminous nature of the Härnö suite granites is evident here (average A/CNK=1.18), while the Revsund suite displays a wide variation in alumina saturation but centres almost exactly on the met- to peraluminous border (average A/CNK=0.99). Both the Åland and Ragunda rocks show a wide variation from distinctly metaluminous to strongly peraluminous, whereas the granitoids of the small Jämtland–Ångermanland complexes all have low degrees of alumina saturation, particularly the intermediate rocks. A number of silicic rocks have a peralkaline chemistry, three of the analysed Strömsund granites (S3, S4, and S6), one Mullnäset granite (Mu6), and two of the Nordsjö dykes (N10b, peralkaline quartz syenite, and N4a, peralkaline aplite).

7.3.2. Trace element discrimination

Some trace element diagrams designed to recognize the tectonic environment of the magmatism are displayed in Fig. 58. In the Rb vs. Y+Nb diagram (Pearce et al. 1984) the Jämtland–Ångermanland complexes are transitional between the fields of volcanic arc granites (VAG) and within-plate granites (WPG) (Fig. 58d). The Rb contents are lower than in the Härnö granites and mostly lower also than in the Revsund granitoids. Some overlap, however, is noted at higher Nb+Y contents. The few analysed Åland porphyries overlap substantially with the Jämtland–Ångermanland rocks. The Härnö granites plot unambiguously in the syncollision granite (syn-COLG) field, whereas the Revsund suite plots dominantly within the VAG-field, but somewhat stretching out into the WPG-field. In the diagrams after Whalen et al. (1987), the Jämtland–Ångermanland rapakivi granitoids generally plot in the field of A-type granites. Among the Mårdsjö rocks, which generally have comparably low Ga/Al ratios, some fall in the field of orogenic granites (Fig. 58a–c).

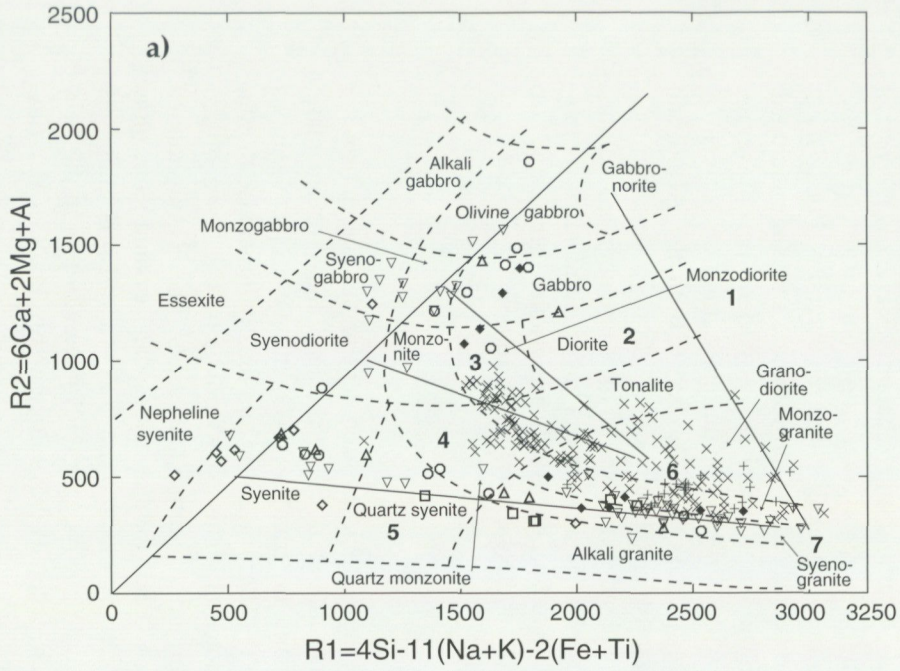
a)
R2=6Ca+2Mg+Al
R1=4Si-11(Na+K)-2(Fe+Ti)
Alkali gabbro
Gabbro-norite
Olivine gabbro
Monzogabbro
Syeno-gabbro
Gabbro
Monzodiorite
Essexite
Syenodiorite
Monzo-nite
Diorite
Tonalite
Grano-diorite
Monzo-granite
Nepheline syenite
Syenite
Quartz syenite
Alkali granite
Syeno-granite
Quartz monzonite
1
2
3
4
5
6
7

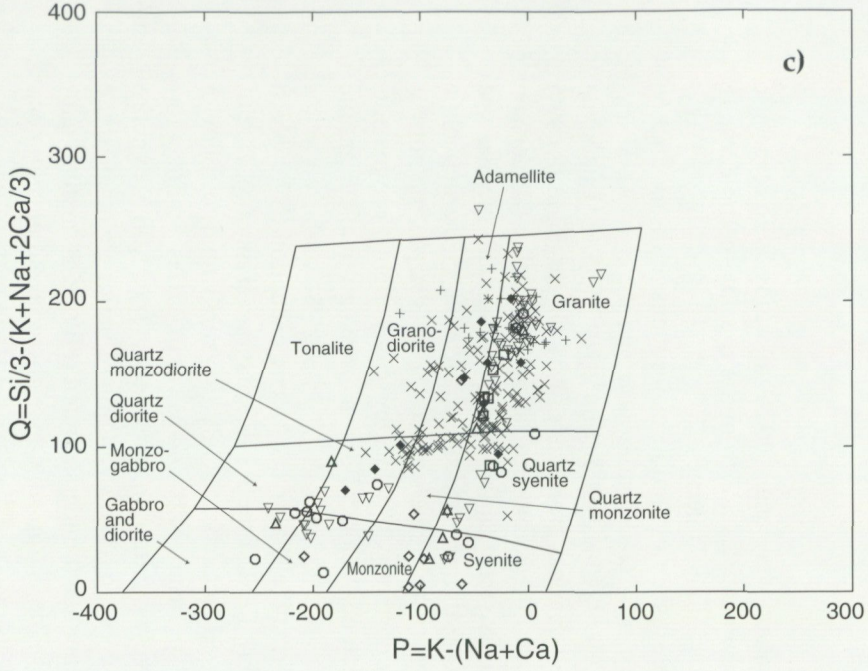
c)
Q=Si/3-(K+Na+2Ca/3)
P=K-(Na+Ca)
Adamellite
Granite
Tonalite
Grano-diorite
Quartz monzodiorite
Quartz diorite
Monzo-gabbro
Gabbro and diorite
Quartz syenite
Quartz monzonite
Monzonite
Syenite

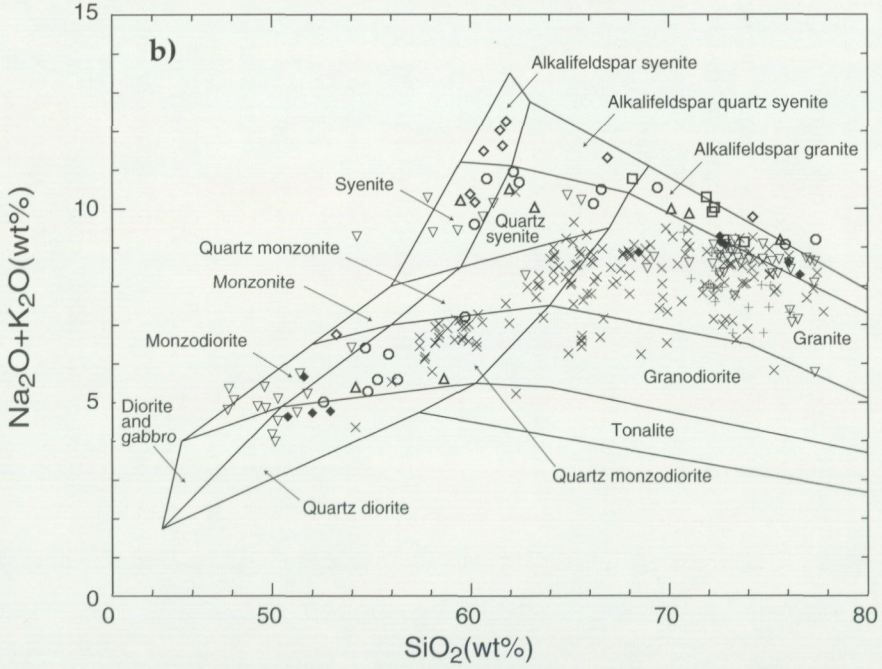
b)
Na2O+K2O(wt%)
SiO2(wt%)
Alkalifeldspar syenite
Alkalifeldspar quartz syenite
Alkalifeldspar granite
Syenite
Quartz syenite
Quartz monzonite
Monzonite
Monzodiorite
Granite
Granodiorite
Diorite and gabbro
Tonalite
Quartz monzodiorite
Quartz diorite

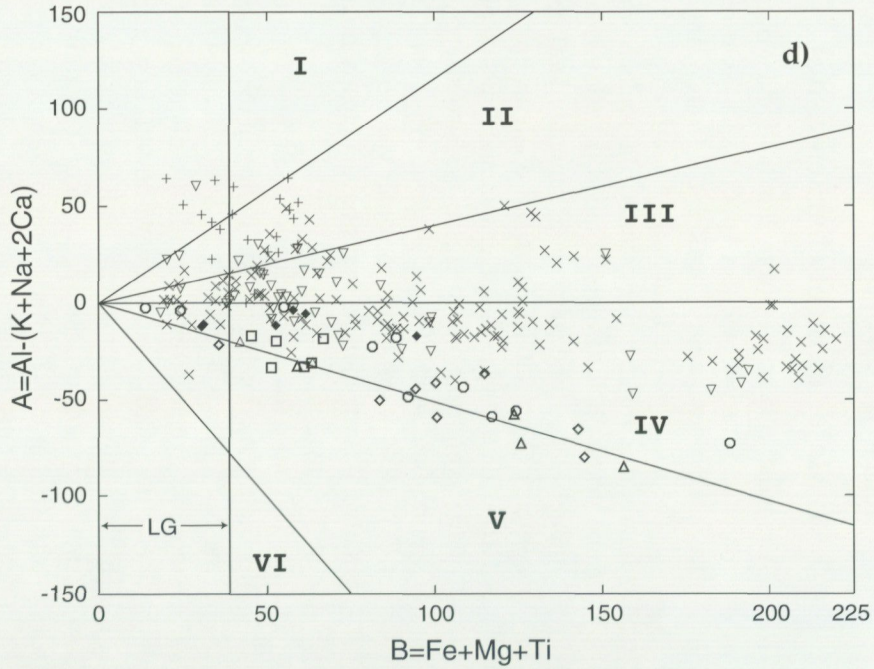
d)
A=Al-(K+Na+2Ca)
B=Fe+Mg+Ti
I
II
III
IV
V
VI
LG

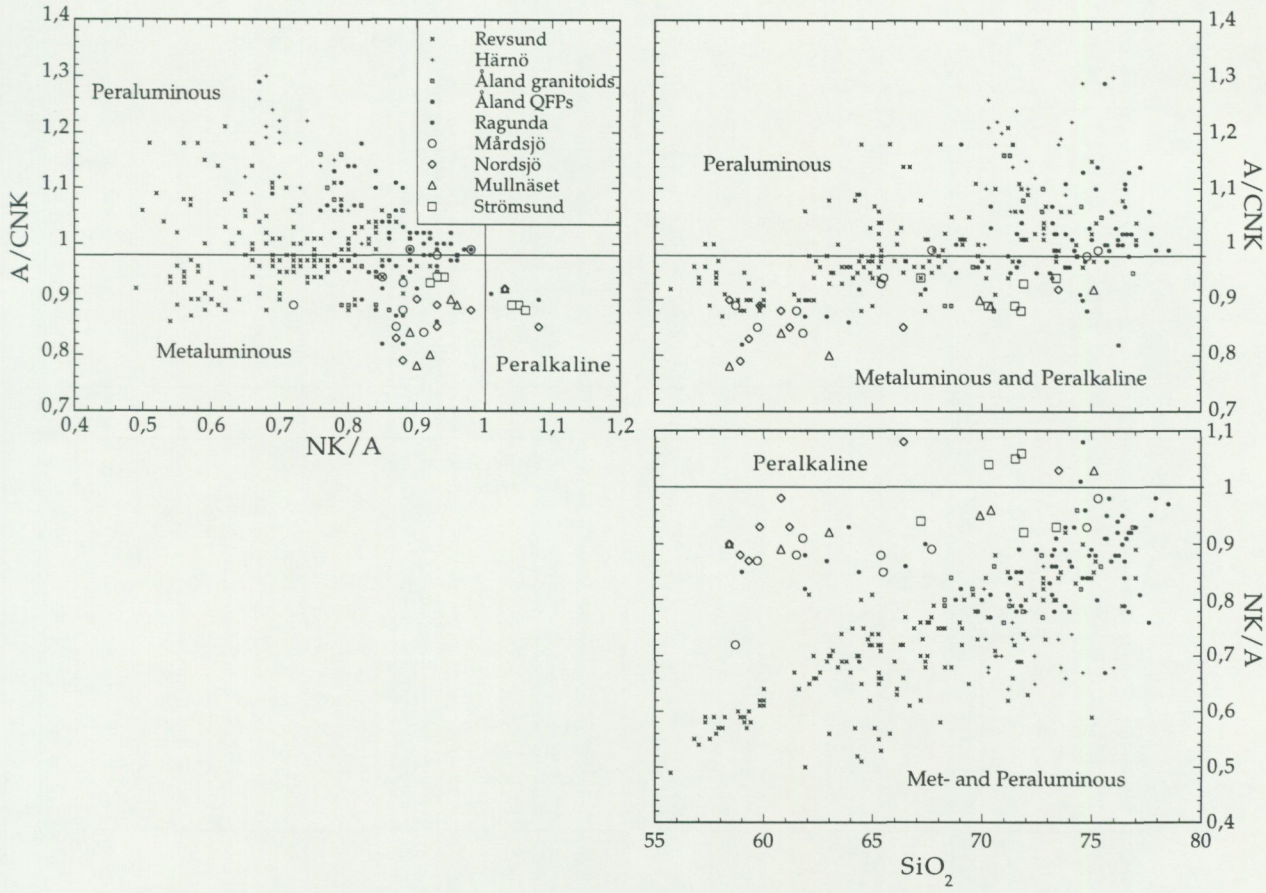

Fig. 57. Alumina saturation diagrams for the silicic-intermediate rocks of the Jämtland–Ångermanland complexes. Also here Ragunda, Revsund, and Härnö rocks have been included (same data sources as in Fig. 56). Data from granitoids and quartz-feldspar porphyries in the Åland rapakivi batholith (Eklund 1993, unpubl. data, Eklund et al. 1996d, B. Lindberg unpubl. data) are also included. The rocks in this study are metaluminous to peralkaline, whereas in the Ragunda complex strongly peraluminous rocks occur as well. The alkaline nature of the rocks in these complexes, compared with other rock suites (except Ragunda), is clearly shown in c). The Härnö granites are strongly peraluminous (Av. A/CNK=1.18), while the Revsund suite centres on the met- to peraluminous border (Av. A/CNK=0.99). Discussion in the text.

Fig. 56. Major element discrimination diagrams of the Jämtland–Ångermanland rocks, and some other rocks for comparison. Included are data from the Ragunda complex (Kornfält 1976), Härnö granites and Revsund granitoids (this study, Lundqvist et al. 1990, Th. Lundqvist unpubl. data, L. Lundqvist unpubl. data, Lundegårdh et al. unpubl. data), and the Strömsbro complex (Andersson 1997a). Symbols are, open circles: Mårdsjö complex, open triangles, apex up: Mullnäset complex, open squares: Strömsund granite, open diamonds: Nordsjö complex. Filled diamonds: Strömsbro complex. Open triangles, apex down: Ragunda complex. Inclined crosses: Revsund suite granitoids. Crosses: Härnö granites. Explanations of the diagrams are found in Fig. 8. The rocks of the Jämtland–Ångermanland complexes display typical syenitic trends (incl. Ragunda). The Revsund granitoid suite shows a typical monzotrend, from monzogranite to monzodiorite, similar to that of the SVB rocks in Fig. 8. Discussion in the text.

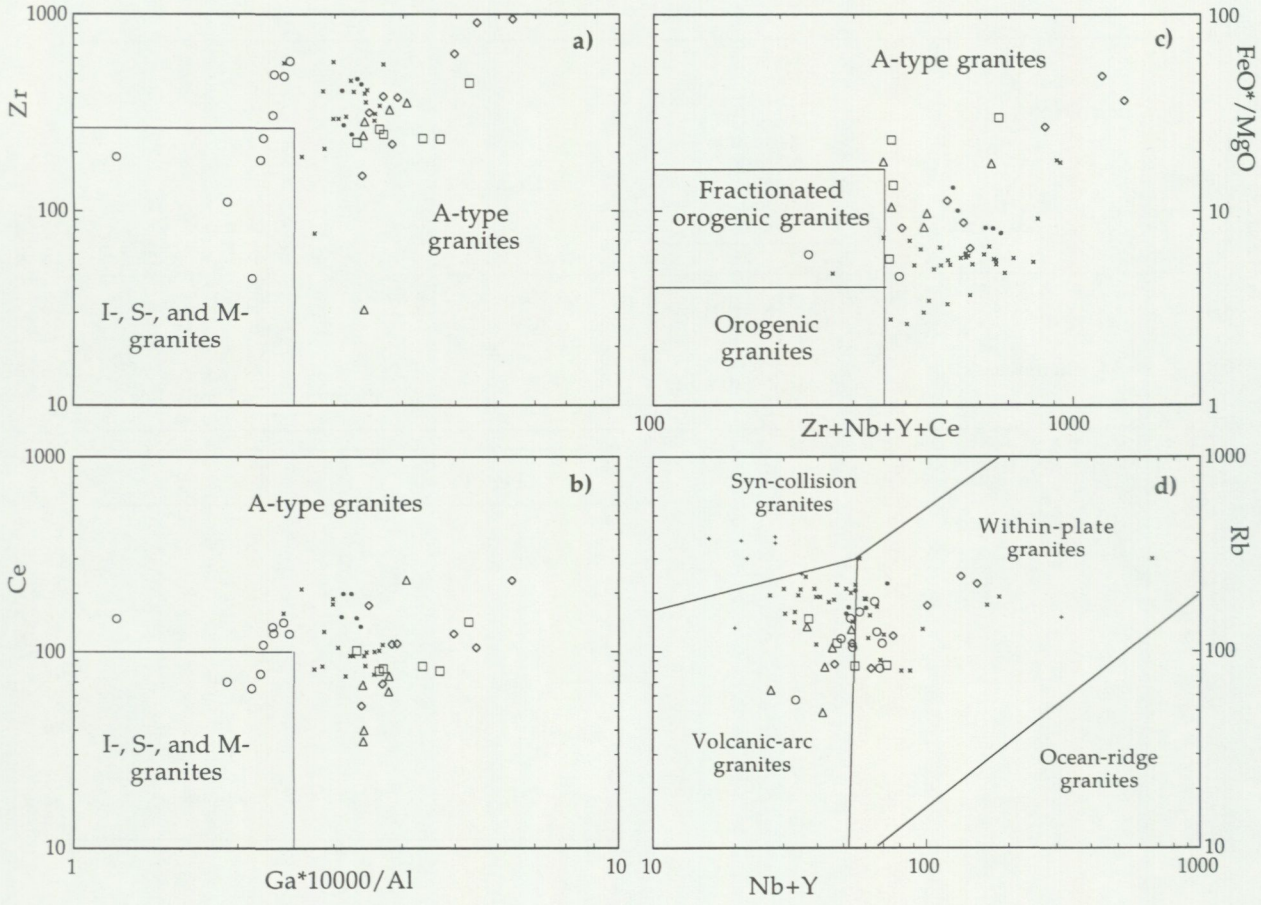

Fig. 58. Trace element diagrams designed to reveal the tectonic setting of granitoids. a–c) after Whalen et al. (1987), d) after Pearce et al. (1984). The same rock types and symbols as in Fig. 57 (no data for Ragunda rocks). The rocks generally plot in the fields of A-type granites of Whalen et al. (1987), except a few of the Mårdsjö aplite/pegmatites and syenites. Also the Revsund granitoids fall in the A-fields, but in c) at comparatively lower FeO*/MgO ratios (cf. the SVB granitoids in Fig. 10c). In the Pearce diagram (d), the Subjotnian rocks of the Jämtland-Ångermanland complexes are transitional between the volcanic-arc (VAG) and within-plate (WPG) fields, which was also the case for the Rödö rocks (cf. Fig. 36d). The Revsund granitoids tend to be dominantly in the VAG-field, while the Härnö granites plot clearly in the syn-collision field. Discussion in the text.

7.3.3. Harker variation diagrams

The geochemistry is displayed in a series of Harker variation diagrams, to show the chemical variation within and between the complexes, and to compare them with some other rapakivi complexes (Fig. 59). The latter is represented by the Ragunda complex just to the south (Kornfält 1976) and the Laitila massif in SW Finland (Vorma 1976). Especially noteworthy is the enrichment of certain elements in the intermediate rocks, compared both with the mafic and the felsic rocks, e.g. Al_2O_3, K_2O, Na_2O, MnO,

Fig. 59a–d. Harker variation diagrams for the Subjotnian Jämtland–Ångermanland complexes. Ragunda (Kornfält 1976) and Laitila (Vorma 1976) rocks have been included for comparison. Some data from Lundqvist et al. (1990; Nordsjö) and K.-A. Kornfält (unpubl. data; Mårdsjö) are included. Numbers refer to samples that can be found in Fig. 55 and in Appendix 2b, except LPxx:xx (Lundqvist et al. 1990), and KAKxxxx (K.-K. Kornfält unpubl. data). These data partly deviate from those in the present study which may, in the case of e.g. Cr, be due to low analytical quality. The intermediate rocks (syenites) are enriched in elements like Al_2O_3, alkalies, Ba, and Eu, and clearly do not follow any mixing trends between the silicic and basic rocks. The trachytic-peralkaline dykes in Nordsjö are typically enriched in HFSE such as Zr, Y, Nb, Ga, and U, compared with the other rocks. The Nordsjö rocks are rich in Na_2O. The Ragunda rocks in general have a variation very similar to the rocks of this study (except for higher Rb in the granites), while the Laitila rocks deviate substantially. The latter have lower contents of alkalies, but higher contents of, e.g. Rb, Ba, U, and the REEs. The intermediate rocks have very high iron/magnesium ratios (d), closer to the peralkaline silicic rocks than to the metaluminous. The latter have distinctly lower Fe-enrichment, compared with the peralkaline rocks. The intermediate rocks have elevated Eu contents and Ba/Sr ratios (d), compared with the other rocks. Discussion in the text.

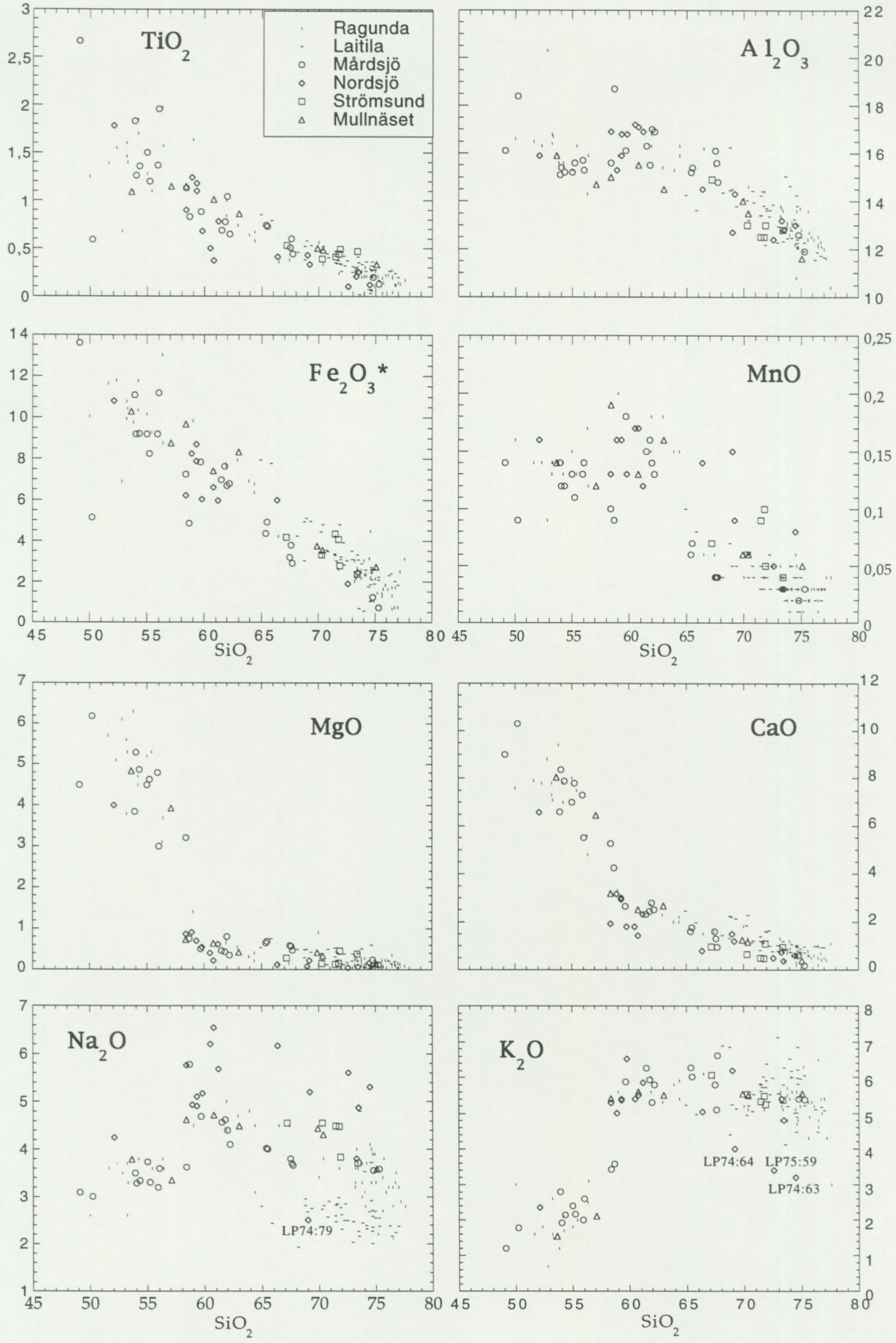
TiO2
Ragunda
Laitila
Mårdsjö
Nordsjö
Strömsund
Mullnäset
Al2O3
Fe2O3*
MnO
MgO
CaO
Na2O
K2O
LP74:79
LP74:64
LP75:59
LP74:63
SiO2
SiO2

Fig. 59a

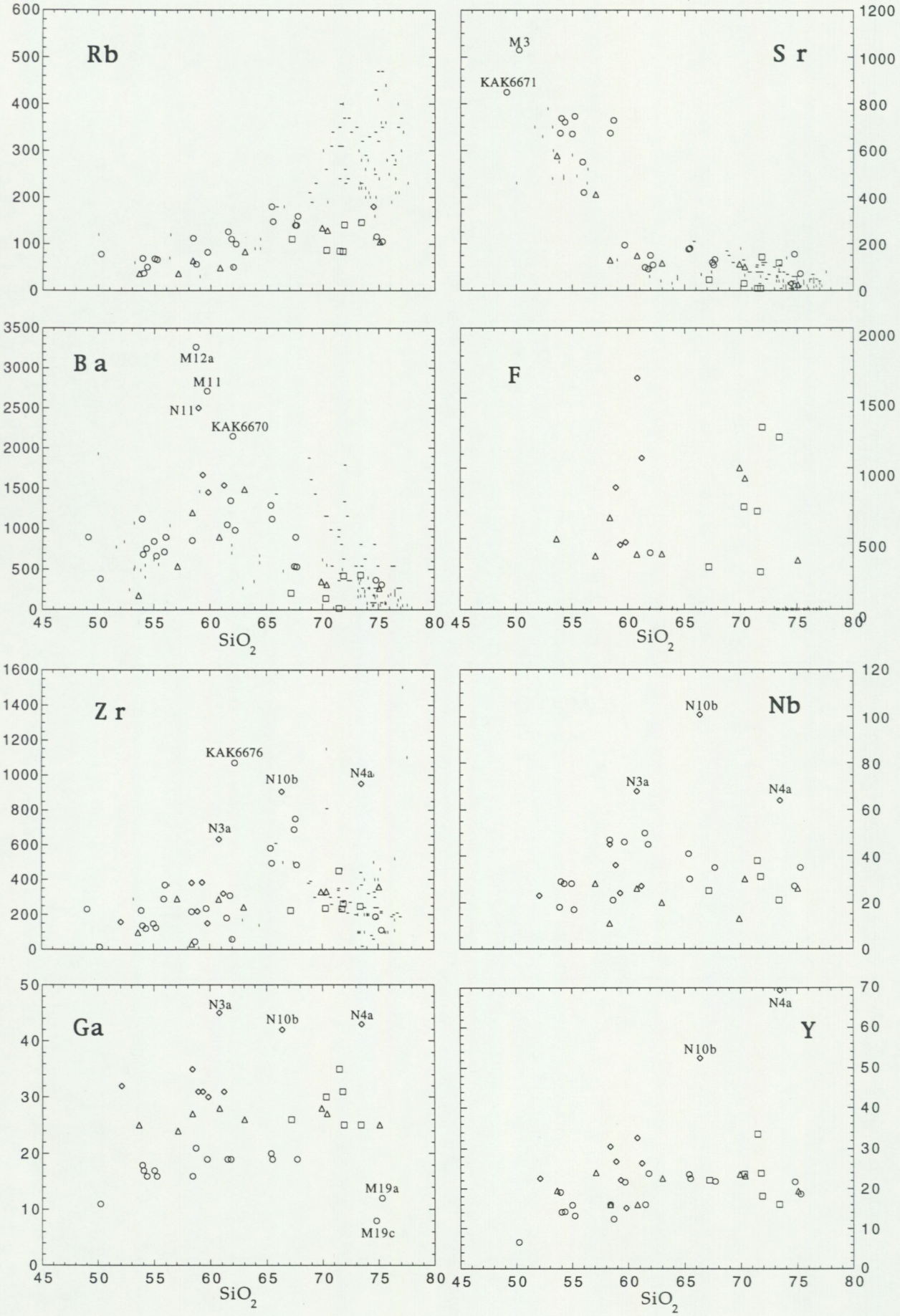
Rb
Sr
M3
KAK6671
Ba
M12a
M11
N11
KAK6670
F
Zr
KAK6676
N10b
N4a
N3a
Nb
N10b
N3a
N4a
Ga
N3a
N10b
N4a
M19a
M19c
Y
N4a
N10b
SiO2
SiO2
SiO2
SiO2

Fig. 59b

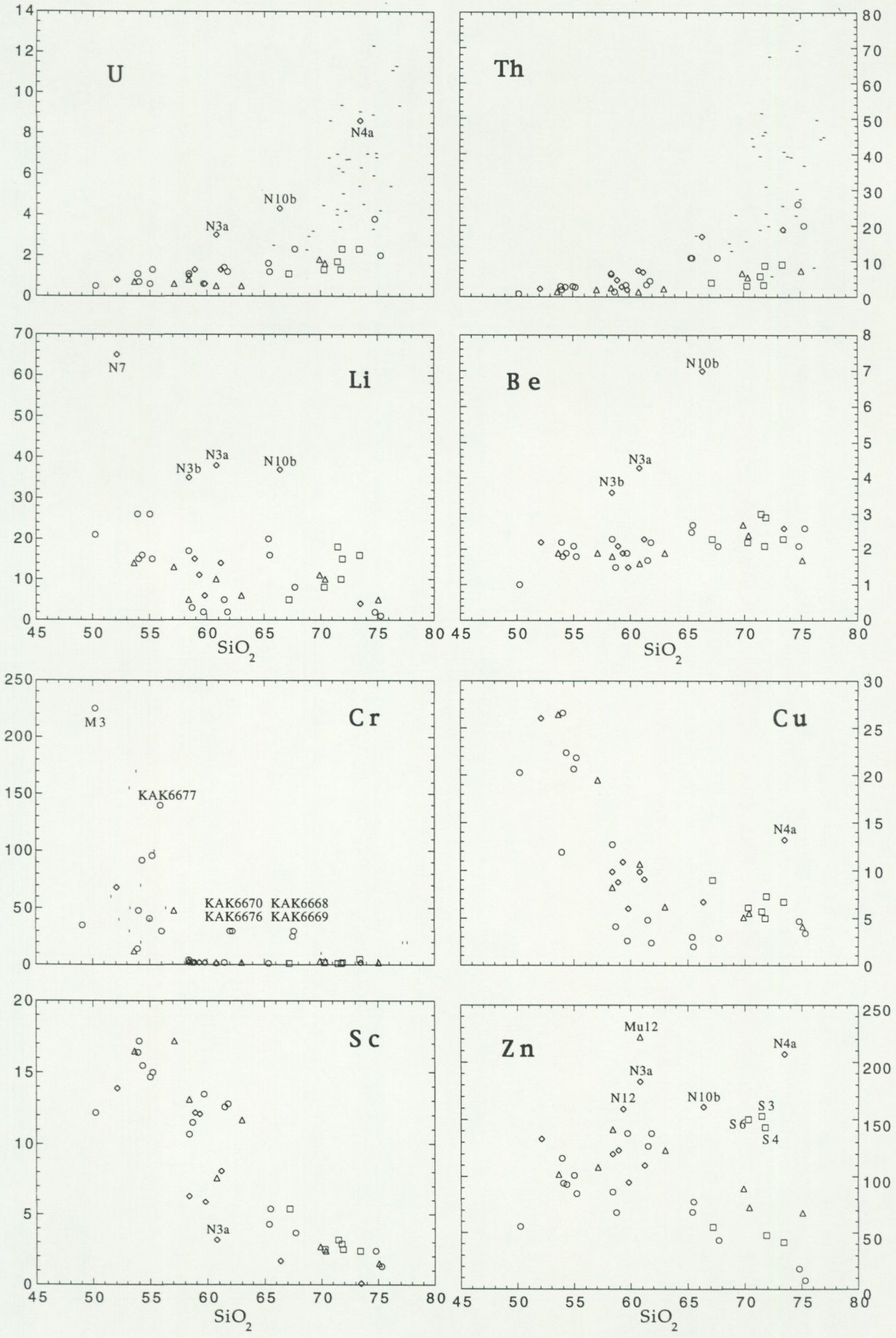
U
N4a
N10b
N3a
Th
Li
N7
N3a
N3b
N10b
Be
N10b
N3a
N3b
Cr
M3
KAK6677
KAK6670 KAK6668
KAK6676 KAK6669
Cu
N4a
Sc
N3a
Zn
Mu12
N4a
N3a
N12
N10b
S3
S6
S4
SiO2
SiO2
SiO2
SiO2

Fig. 59c

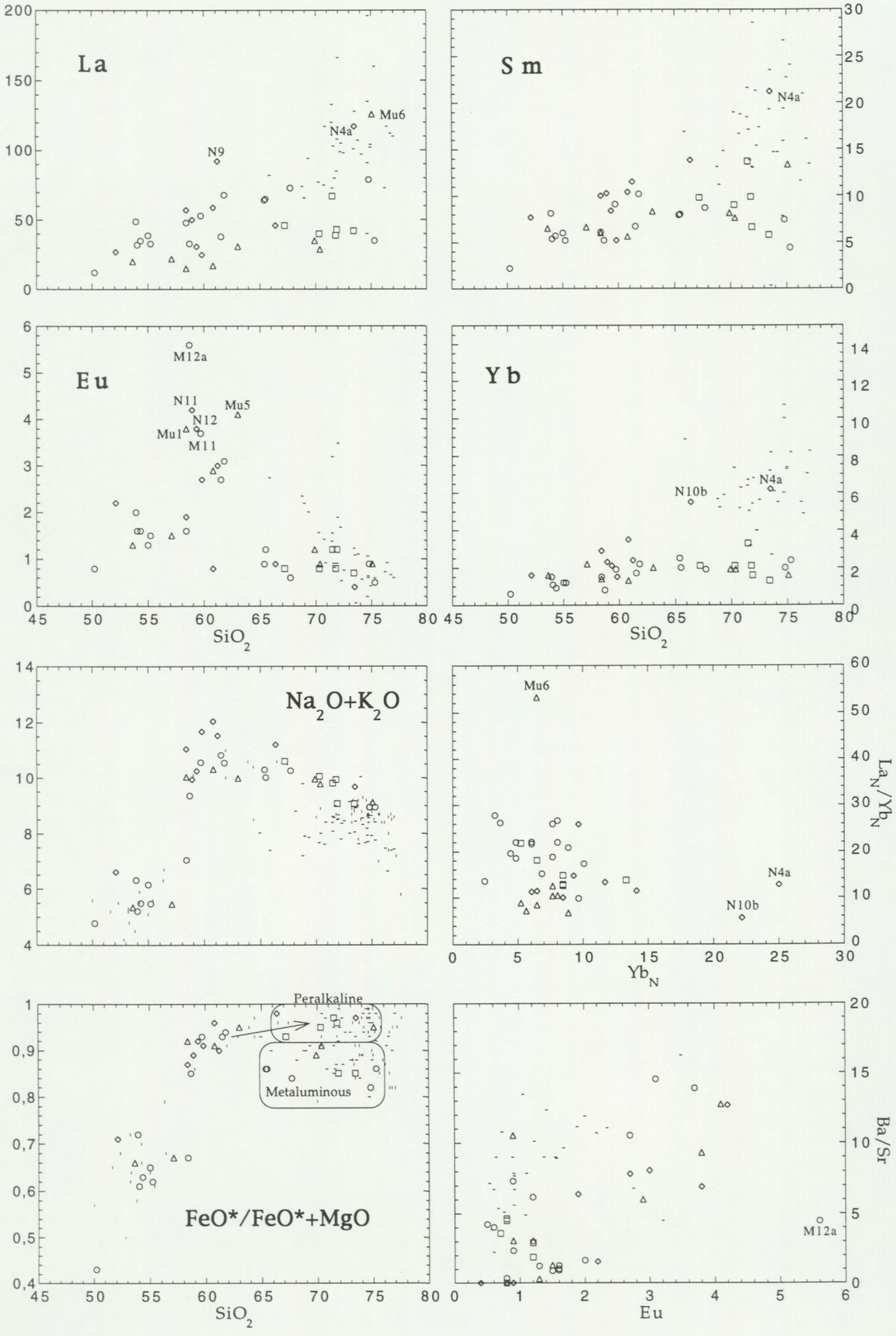
La
N9
N4a
Mu6
Sm
N4a
Eu
M12a
N11
Mu5
N12
Mu1
M11
Yb
N10b
N4a
SiO2
SiO2
Na2O+K2O
Mu6
N4a
N10b
LaN/YbN
YbN
Peralkaline
Metaluminous
FeO*/FeO*+MgO
M12a
Ba/Sr
Eu
SiO2

Fig. 59d

Zn, and most pronouncedly Ba and Eu. Correspondingly they are relatively depleted in elements like CaO, MgO, Sr, Cu and to some degree Li.

The geochemical similarity with the Ragunda complex is apparent (Fig. 59), except maybe for Rb where the most felsic Ragunda rocks have higher amounts, generally above 200 ppm, whereas those investigated here are all below 200 ppm. The similarity with the Laitila massif, which is dominated by silicic rocks, is also relatively marked. Certain exceptions are, however, noticeable. The Laitila rocks have higher contents of such elements as Rb, Ba, U, Th and REE except Eu, whereas Na_2O-content is significantly lower compared with that of the Jämtland–Ångermanland rocks. K_2O and Al_2O_3 are also slightly higher in the Laitila massif.

The geochemical similarity between the investigated complexes is striking with a few exceptions: i) the Nordsjö rocks are markedly enriched in Na_2O (up to 6.55 %), Ga (up to 45 ppm) and Y (up to 70 ppm), ii) some of the analysed Nordsjö dykes have a very specific chemistry with extra high contents of also MnO, Zn, Zr, Nb, Rb, Li, Be, U (but not Th) and the REE (except Eu; e.g. Sm up to 21.2 and Yb up to 6.2 ppm), together with low contents of above all K_2O, iii) a weak tendency of chemical separation of the Mårdsjö and Nordsjö rocks in one group and Mullnäset and Strömsund in another group can be seen, especially for Zr and Th. Regarding Ga, on the other hand, the Mårdsjö rocks show the lowest abundances, Nordsjö the highest, and Mullnäset and Strömsund are intermediate.

The alkali enrichment is clearly displayed in Fig. 59d (Na_2O+K_2O vs. SiO_2). The Ragunda rocks have an identical trend, whereas the Laitila rapakivi is much less alkali enriched. The Fe-enrichment in relation to Mg is the same, or even more marked in the intermediate rocks, compared with the felsic ones, whereas the mafic rocks have much lower FeO*/FeO*+MgO ratios (Fig. 59d). The peralkaline silicic rocks are distinctly more iron enriched, compared with the metaluminous ones. The specific character of the intermediate syenites is visualized in Fig. 59d where Ba/Sr is plotted against Eu. They are distinctive in their high Eu and Ba but low Sr, and thus form a separate group in this diagram.

7.3.4. REE-patterns and spider diagrams

Looking at the REEs, the granites of the different investigated complexes show similar patterns (Fig. 60), with an enrichment in the LREE (La_N/Yb_N varies between 12.2; Mu8, and 53.2; Mu6), and a marked negative Eu-anomaly ($Sm_N/Eu_N = 2.5–5.6$). The similarity with the Rödö granites is apparent. The latter, however, have a slightly higher LREE enrichment and deeper Eu-anomaly (cf. Fig. 44a). Among the Nordsjö dykes, the most silicic is also the one with the highest absolute REE abundances, but also the deepest Eu-anomaly ($Sm_N/Eu_N = 20.0$). The other intermediate to felsic Nordsjö dykes show patterns reminiscent of the granites from the other investigated complexes (Fig. 60c).

Fig. 61 shows bulk-crust normalized spider diagrams of the average compositions of the intermediate-silicic Jämtland–Ångermanland rapakivi rocks in comparison with other relevant rocks. There is a strong resemblance between the metaluminous Mårdsjö and Strömsund/Mullnäset granites, where the latter group, however, are somewhat lower in the LREE (Fig. 61a). The Mårdsjö pegmatite/aplites show normal enrichment (mainly Th and U) and depletion (Li, Zr, Ga, Eu, transition metals) in elements related to residual liquid generation from a granitic parent fractionating quartz, feldspars and some ferromagnesian silicates (cf. e.g. the trend in the silicic Rödö suite, above). Similarly to the Rödö granites (cf. Fig. 37) also these granites are less enriched in most LILE and HFSE compared with the average Finnish subalkaline rapakivi granites. Interestingly, the rapakivi granites are relatively similar also to the older Härnö and Revsund granitoids. The latter two groups, however, tend to be somewhat richer in the LILE and the HREEs.

The Jämtland–Ångermanland peralkaline granites (Fig. 61b) are generally much lower in both LILE and HFSE compared with the global average of such granites, compiled by Rämö & Haapala (1995). The average Jämtland–Ångermanland syenites are also completely different from the average alkali feldspar syenites of the Suomenniemi complex (Rämö & Haapala 1995). The latter are generally also much higher in most elements compared with the Swedish ones, and have a negative Eu-anomaly in contrast to the positive in the Swedish syenites. The Swedish syenites are actually closer to their associated peralkaline granites in geochemistry than to the Finnish syenites. Some of the more anomalous rocks are plotted in Fig. 61c. N3a and N3b are two syenitic (trachytic) dykes from the Nordsjö complex with strong geochemical similarity, although discrepancies can be noted for, e.g. Cs, U, and Eu.

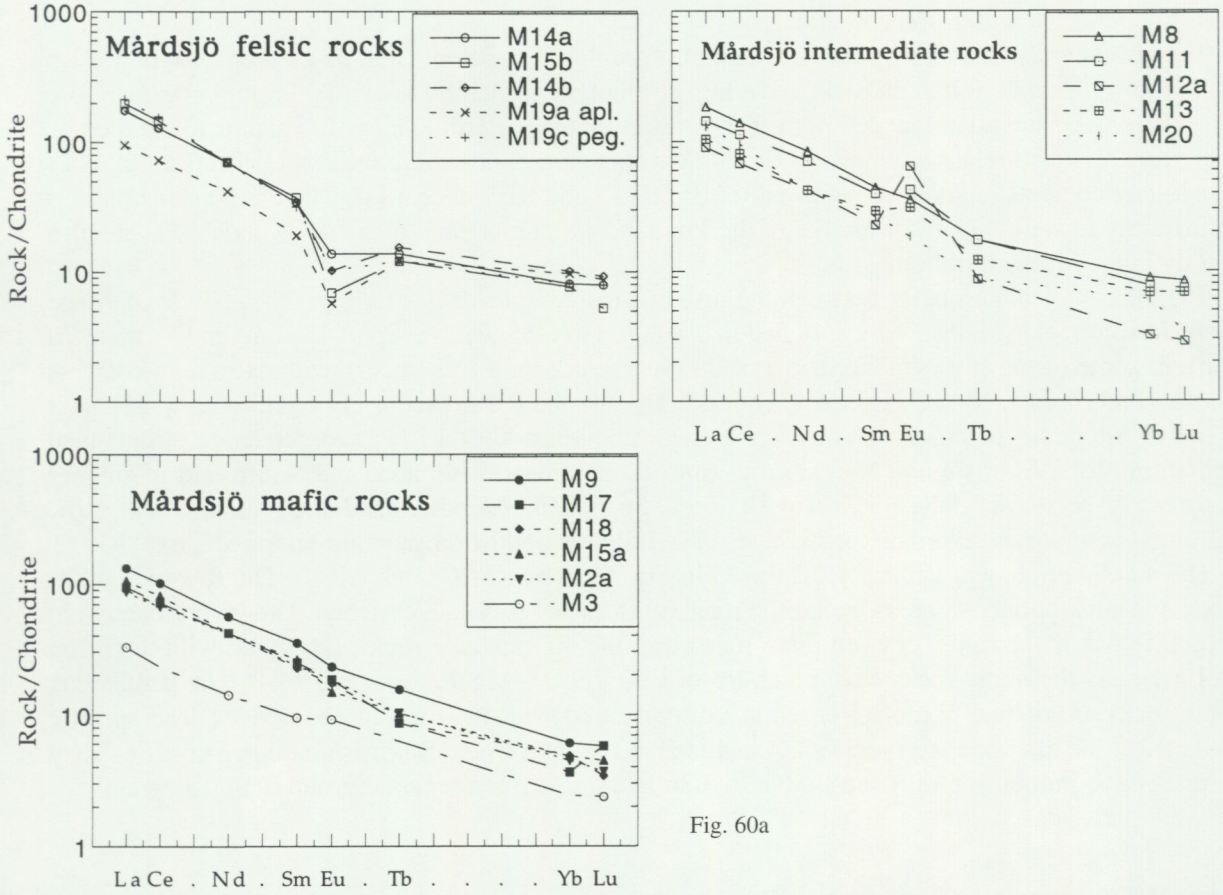

Fig. 60a

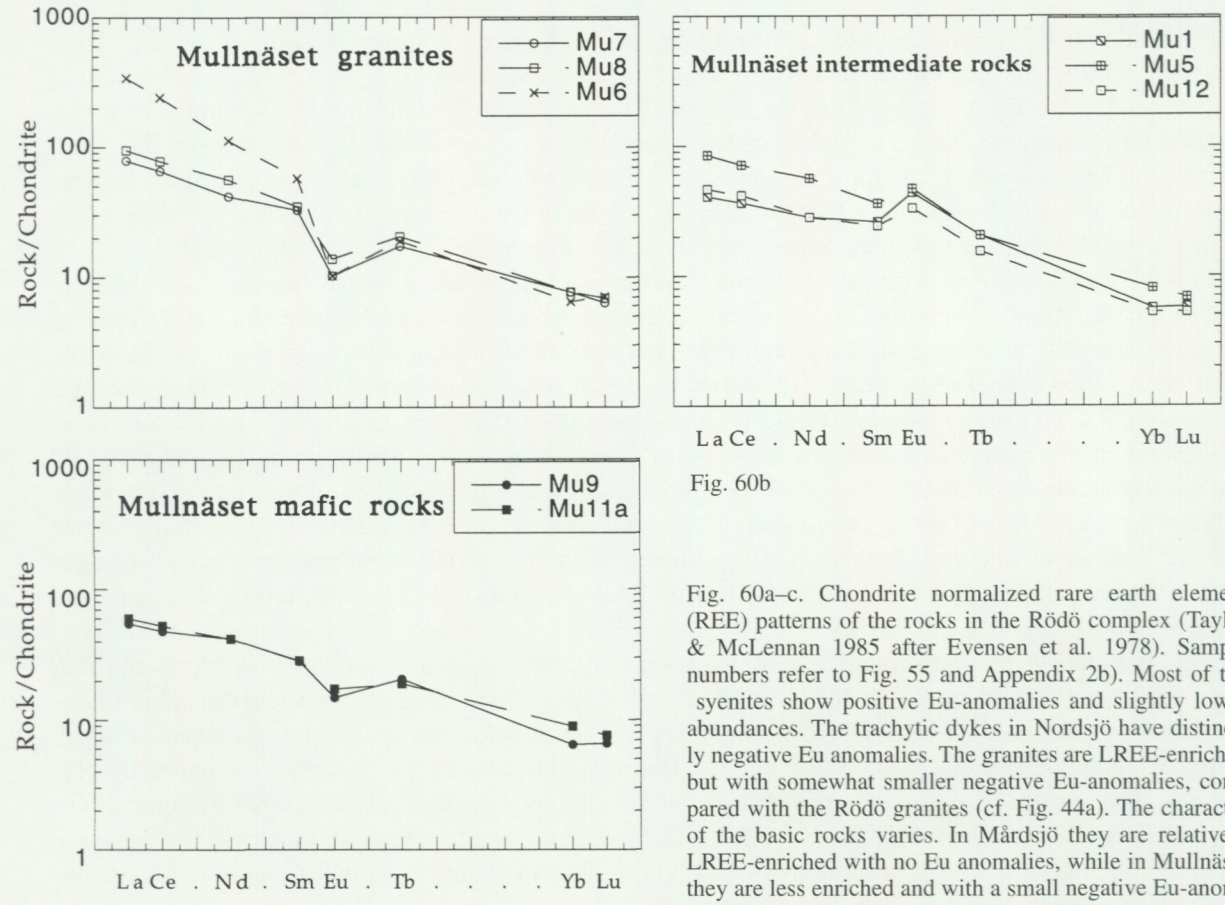

Fig. 60b

Fig. 60a–c. Chondrite normalized rare earth element (REE) patterns of the rocks in the Rödö complex (Taylor & McLennan 1985 after Evensen et al. 1978). Sample numbers refer to Fig. 55 and Appendix 2b). Most of the syenites show positive Eu-anomalies and slightly lower abundances. The trachytic dykes in Nordsjö have distinctly negative Eu anomalies. The granites are LREE-enriched but with somewhat smaller negative Eu-anomalies, compared with the Rödö granites (cf. Fig. 44a). The character of the basic rocks varies. In Mårdsjö they are relatively LREE-enriched with no Eu anomalies, while in Mullnäset they are less enriched and with a small negative Eu-anomaly. The leucogabbro (M3) has lower REE contents and a slight positive Eu-anomaly. Discussion in the text.

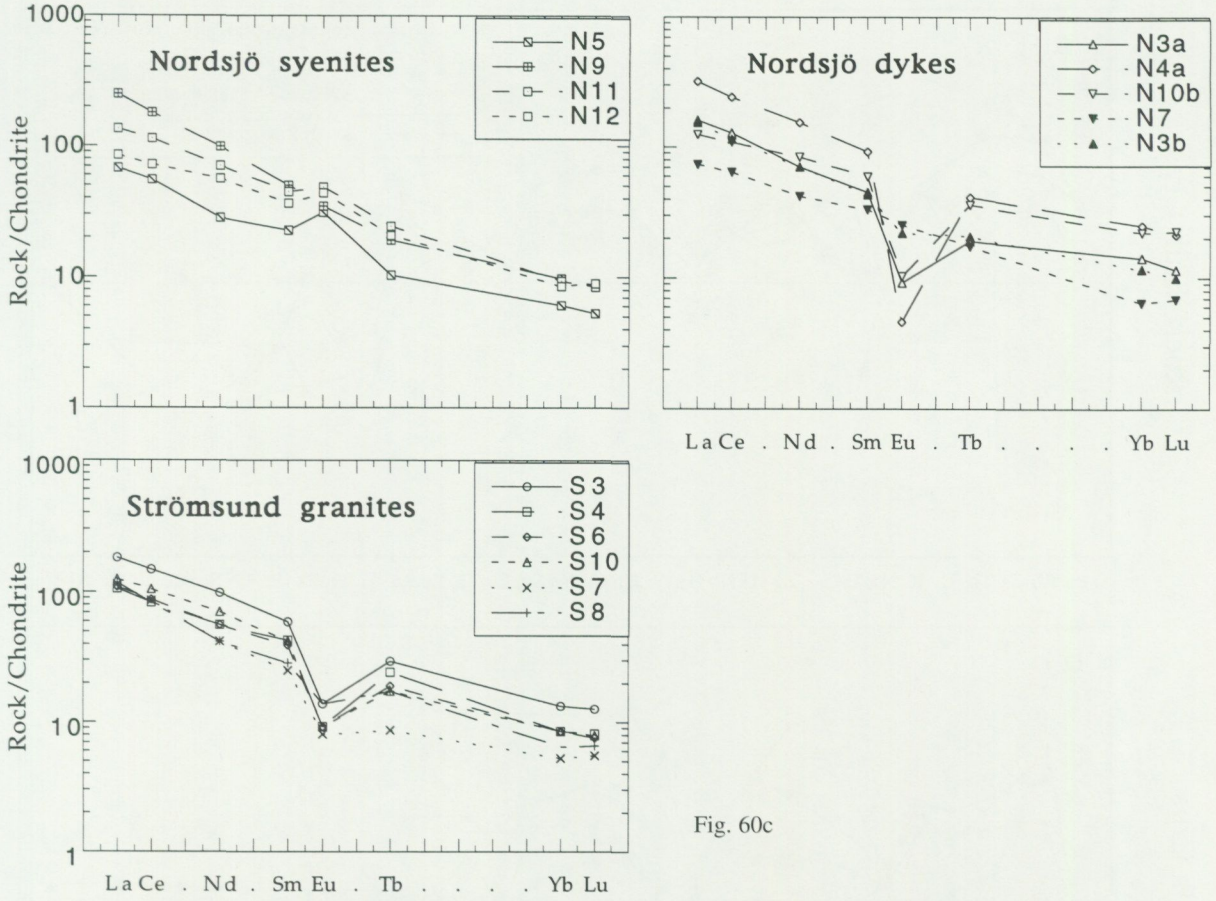

Fig. 60c

Compared with other (plutonic) syenites, they are richer in Th, U, Li, Eu, and HREE, and poorer in, e.g. Ba. N10b is a peralkaline quartz syenite, relatively rich in most elements except the LREE, compared with the syenites. N4a is a peralkaline aplitic dyke with strong enrichment in most elements except Li, Be, and Eu.

The associated mafic rocks also show a pronounced enrichment in LREE (Fig. 60). In the Mårdsjö gabbros, this enrichment is as strong as in the granites, but the absolute abundances are generally lower. The Mårdsjö gabbros do not show any Eu-anomaly. On the contrary, the gabbros of the Mullnäset complex are less LREE enriched ($La_N/Yb_N = 6.8–8.4$) and show a small negative Eu-anomaly ($Sm_N/Eu_N = 1.7–1.9$). The mafic dyke associated with the Nordsjö complex (N7) are LREE enriched ($La_N/Yb_N = 11.4$), without Eu-anomaly.

The intermediate (syenitic) rocks produce a small positive Eu-anomaly ($Sm_N/Eu_N = 0.35–0.95$), except M20 which is more mafic in character (monzodioritic), M8 and N9 (Fig. 60). Except for the positive Eu-anomaly, the REE patterns of the intermediate rocks are similar to those of the felsic rocks in the same complex. A tendency towards slightly lower absolute abundances of the elements can be detected, however. Some differences between the complexes also exist, e.g. the Mullnäset syenites have lower LREE contents compared with those in Mårdsjö, and the Nordsjö syenites have a wide variation in REE contents, where one sample N5 has significantly lower absolute abundances than the others. The positive Eu-anomalies distinguish the intermediate rocks here from the hybrid rocks of the Rödö complex, which all have negative anomalies (cf. chapter 6.3.4. above).

In a triangular plot of Ba-Rb-Sr (Fig. 62), the Ba-enriched intermediate rocks (syenites) form a group of their own in the Ba-corner, whereas the mafic rocks trend towards the Sr-corner. The granitic rocks plot at higher Rb concentrations, and one of the peralkaline Strömsund granites (S3) almost in the Rb-corner. This is not due to a high Rb content (85 ppm), but to extremely low Ba and Sr contents (188 and 9.6 ppm, respectively). The granitic rocks in these complexes generally seem to be relatively richer in Sr than both Laitila and Ragunda (Fig. 62).

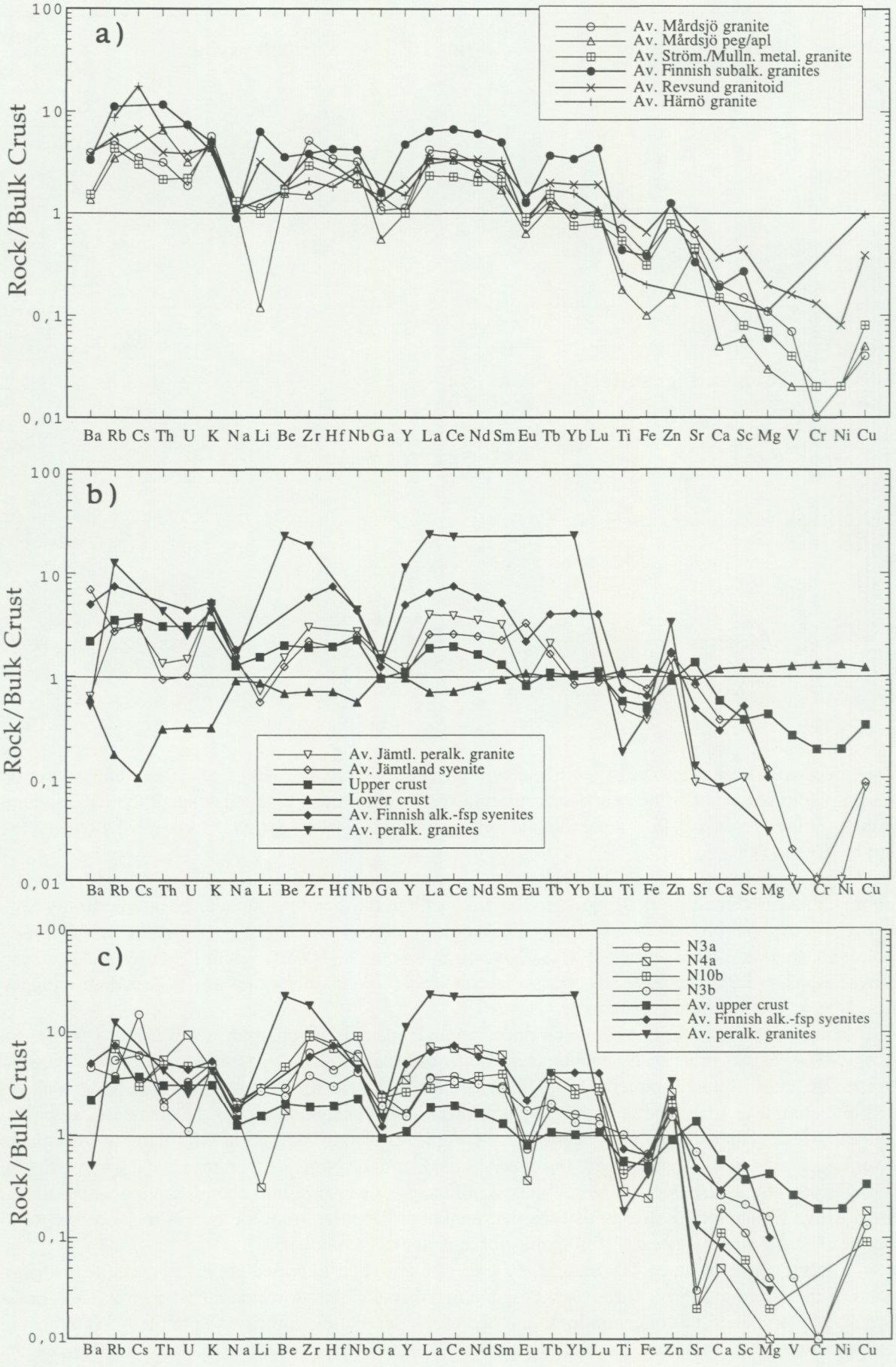
a)
Av. Mårdsjö granite
Av. Mårdsjö peg/apl
Av. Ström./Mulln. metal. granite
Av. Finnish subalk. granites
Av. Revsund granitoid
Av. Härnö granite
b)
Av. Jämtl. peralk. granite
Av. Jämtland syenite
Upper crust
Lower crust
Av. Finnish alk.-fsp syenites
Av. peralk. granites
c)
N3a
N4a
N10b
N3b
Av. upper crust
Av. Finnish alk.-fsp syenites
Av. peralk. granites
Rock/Bulk Crust
100
10
1
0,1
0,01
Ba Rb Cs Th U K Na Li Be Zr Hf Nb Ga Y La Ce Nd Sm Eu Tb Yb Lu Ti Fe Zn Sr Ca Sc Mg V Cr Ni Cu

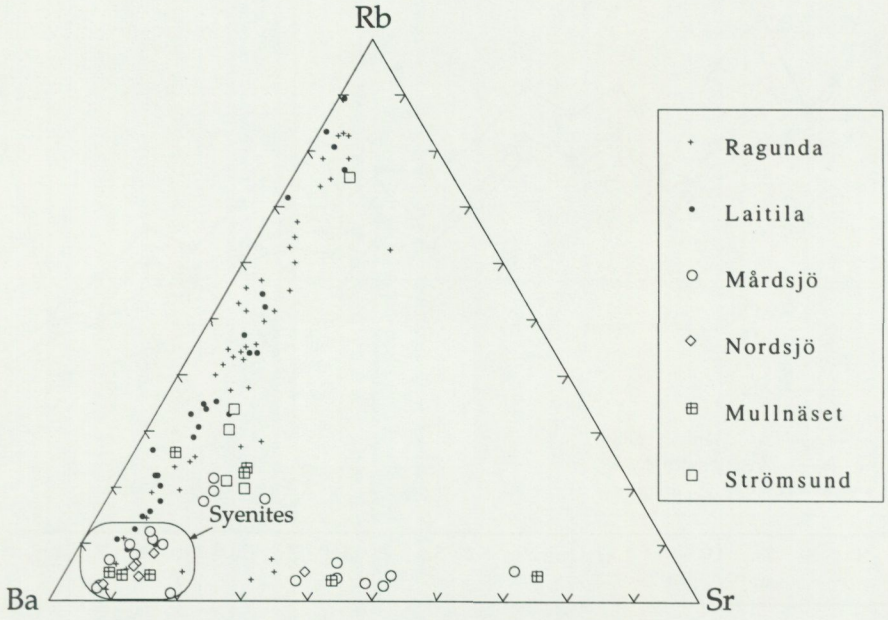

Fig. 62. Rb-Ba-Sr diagram for the Subjotnian Jämtland–Ångermanland rocks. Ragunda (Kornfält 1976) and Laitila (Vorma 1976) rocks have been included for comparison. The syenitic rocks occupy a position close to the Ba corner, distinctly offset in relation to the granites and basic rocks. The Ragunda and Laitila rocks trend at low Sr from Ba to Rb rich compositions, while the metaluminous granites of the JÅ complexes are more Sr rich. Discussion in the text.

The geochemical character of the basic Jämtland–Ångermanland rocks is identical to that of the Rödö dolerites (chapter 6.3.2. above), suggesting them to be continental within-plate quartz normative tholeiites, although some trace element diagrams suggest an alkali basaltic character (Figs. 38, 39). For comparison, the basic rocks of the Jämtland–Ångermanland complexes have been plotted in MORB-normalized spider diagrams (Fig. 63). A strong similarity is obvious for all trace elements with the rapakivi-related Rödö and Suomenniemi dolerites, as well as average continental flood basalts, but not average lamprophyre. Some of the rocks which are most anomalous are plotted in Fig. 63a. Only one is strongly anomalous, M3. This is the high alumina (18.4 %) leucogabbro of the Mårdsjö complex, which in general has lower contents of all HFSE, but higher contents of e.g. Sr, CaO, Al_2O_3, MgO, Ni and Cr. It also has the lowest FeO*/FeO*+MgO ratio (0.43) of all basic rocks (Fig. 59d). The REE pattern of M3 is slightly less LREE enriched with significantly lower absolute abundances of the REEs, but with with no or only a very small positive Eu-anomaly. A comparison of the rapakivi-related basic rocks and Småland-Värmland (SVB) basic rocks (cf. chapter 4.3.) is also made in Fig. 63b. The average most basic rock in the Kårtorp hybrid association is considerably more enriched than all rapakivi-related basic rocks in HFSE, but less so for the LILE. This is the most strongly fractionated part of the SVB-suite, which is similar geochemically to lamprophyres (cf. chapter 4.5.2.3.). The less fractionated part of the basic SVB-suite (average TVZ basite), however, is similar to the basic rapakivi-related rocks, except for higher contents of HREE and the transition metals.

Fig. 61. Bulk crust (Taylor & McLennan 1985) normalized spiderplots for the silicic-intermediate Jämtland–Ångermanland (JÅ) rocks and some other rocks. Upper and lower crustal averages (Taylor & McLennan 1985) have been included for comparison. Average Finnish subalkaline (rapakivi) granite, av. peralkaline granites, and av. Finnish alkali feldspar syenites, are from Rämö & Haapala (1995). Average Revsund and Härnö granitoids are extracted from the data of this study, Th. Lundqvist (unpubl. data), L. Lundqvist (unpubl. data). The different rock types are displayed as averages to allow general comparisons. a) Displays the metaluminous to peraluminous rocks. The average Finnish rapakivi granite is generally higher in most LILE and HFSE, compared with the JÅ rocks. b) the JÅ peralkaline granites are much lower in most elements compared with the global average compiled by Rämö & Haapala (1995). Similarly, the JÅ syenites have much lower contents of almost all LILE and HFSE, compared with the peralkaline alkali-feldspar syenites of Suomenniemi. In fact, the JÅ syenites and peralkaline silicic rocks have very similar patterns, where the peralkaline rocks are slightly higher in most elements, except Ba and Eu. c) The trachytic to peralkaline silicic dykes in Nordsjö. These are closer in composition to the Suomenniemi syenites, especially the peralkaline rocks. There is a strong increase in the negative Eu-anomaly from N3b to N4a. Discussion in the text.

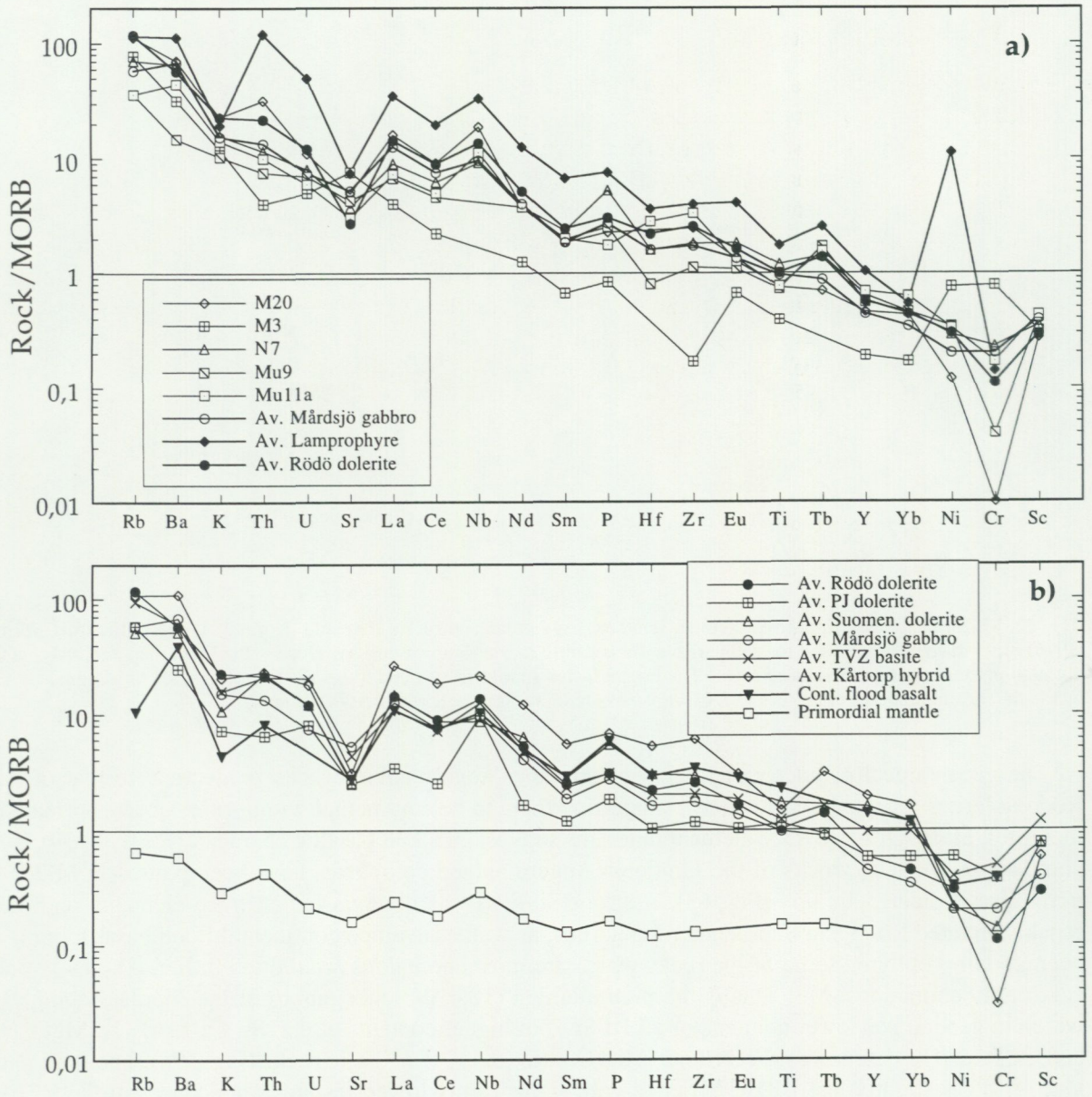

Fig. 63. MORB (mid-ocean ridge basalt) normalized (from MORB compilation in Rollinson 1993) trace element spiderplots basic rapakivi-related rocks of this study. Averages of lamprophyre (Bergman 1987), continental flood basalt (Thompson et al. 1983), primordial mantle (McDonough et al. 1992), and average Suomenniemi dolerite (Rämö 1991) have been included for comparison. In addition, average Rödö, Strömsbro and Postjotnian dolerite (Rödö area), as well as TVZ basite and Kårtorp hybrid (Fig. 14) have been included in b). Numbers refer to sample numbers also found on Fig. 55. The JÅ basic rocks are essentially very similar in composition to the Rödö dolerites, except being slightly lower in LILE. The leucogabbro sample (M3) from Mårdsjö is substantially lower in HFSE, but higher in Ni and Cr. Average lamprophyre is higher for almost all elements. Both the Suomenniemi dolerites, TVZ basites, and continental flood basalts are similar in composition to the JÅ rocks, but the Kårtorp hybrids are closer to av. lamprophyre, while the Postjotnian dolerites in general have lower HFSE abundances. Discussion in the text.

7.4. ISOTOPE GEOLOGY

7.4.1. U-Pb geochronology

Three of the complexes have been dated by the U-Pb zircon technique. Two samples, Mårdsjö granite (M14a) and Mullnäset granite (Mu7), were selected for single grain zircon analysis. Three zircon grains, in the >100 μm fraction, from each sample were carefully selected by handpicking. These were among the clearest and most inclusion-free that could be found. Each grain was dissolved separately using the chemical procedure described in Appendix 1. The risk of including inherited older crystals or crystals with inherited cores overgrown with younger rims is minimized with this technique. The data are shown in Table 20. The weight of each fraction (=grain) is very low, between 1.7 and 4.6 μg, and the content of U and Pb in the zircons is low, 59–160 and 27–116 ppm, respectively. The measured $^{206}Pb/^{204}Pb$-ratios are also low: 325 to 905, making the common lead correction relatively large. This, together with the low total amount of U and Pb measured, makes the errors in the calculated $^{206}Pb/^{238}U$- and $^{207}Pb/^{235}U$-ratios relatively large. Fortunately, all of the analysed grains are near concordant (Fig. 64).

Table 20
U-Th-Pb isotopic data for air-abraded single zircon grains from rapakivi rocks, central Sweden

Weight	U	Pb_{tot}	Th	$^{206}Pb/^{204}Pb$	Measured ratios		Ages (Ma)[1]			
(μg)	(ppm)	(ppm)	(ppm)		$^{206}Pb/^{207}Pb$	$^{206}Pb/^{208}Pb$	$^{206}Pb/^{238}U$	$^{207}Pb/^{235}U$	$^{208}Pb/^{232}Th$	$^{207}Pb/^{206}Pb$
Mårdsjö granite (sample M14a, cf. Fig. 55)										
3.4	89.8	22.4	61.5	325.3	7.491	3.226	1510	1516	1575	1525±8
3.9	95.9	28.6	72.4	512.6	8.496	3.511	1447	1472	1437	1509±6
1.7	160.1	47.9	116.5	905.1	9.462	3.975	1490	1504	1516	1524±4
Mullnäset granite (sample Mu7, cf. Fig. 55)										
4.5	58.8	18.2	26.9	385.1	7.919	4.399	1496	1507	1574	1524±6
4.5	67.9	20	32.7	816.8	9.255	5.702	1535	1532	1465	1527±4
4.6	66.6	20	29.6	431.2	8.121	4.731	1530	1529	1550	1526±7

1) Ages based on radiogenic Pb corrected for mass-fractionation, spike compostion, total blank, plus initial common Pb according to Stacey & Kramers (1975) model for an age of 1525 Ma.

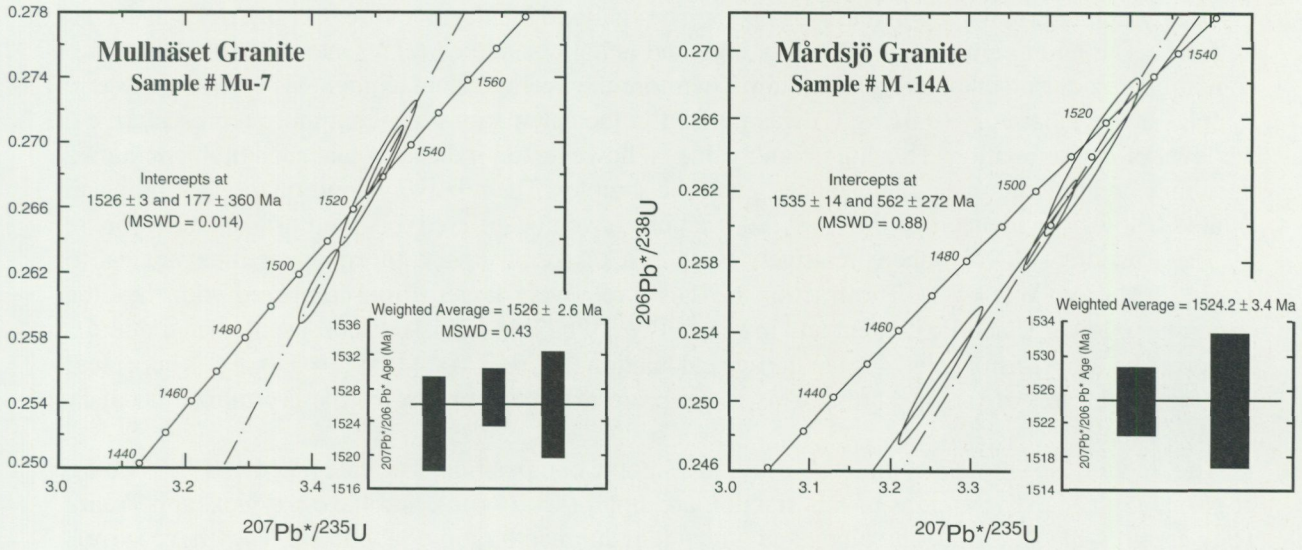

Fig. 64. Concordia diagrams for Mullnäset granite (a), and Mårdsjö granite (b). Analyses are performed on air-abraded single zircon grains, giving relatively high errors but concordant or near concordant results. For the Mullnäset granite, all three grains follow a discordia line with an upper intercept of 1526±3 Ma, interpreted to represent the crystallization age. For the Mårdsjö granite, two analyses are near concordant and one slightly less so. Regression through all three analyses gives an upper intercept of 1535±14 Ma. However, the weighted average of the $^{207}Pb/^{206}Pb$ age of the two most concordant gives an age of 1524±3 Ma, which is considered a more reliable estimate of the crystallization age. This age is, within errors, the same as the regressed age.

Table 21
U-Pb zircon results, Nordsjö syenite

Fraction	Weight (µg)	number of crystals	U (ppm)	Pb_{tot} (ppm)	Pb_{com} (ppm)	$^{206}Pb/^{204}Pb$ (1)	rad. Pb atomic % 206-207-208Pb	$^{206}Pb/^{238}U$ (2)	$^{207}Pb/^{235}U$ (2)	$^{207}Pb/^{206}Pb$ (2)	$^{207}Pb/^{206}Pb$ (age)
N1 >210 µm LP	741.7	5	286	68.2	0.002	19909	78.9-7.5-13.6	0.2189±4	2.853±6	0.09452±7	1519±1
N2 >210 µm SP clear	276.9	7	267	78.6	0.190	6611	80.1-7.6-12.3	0.2735±5	3.567±8	0.09460±13	1520±2
N3 150-210 µm LP	187.5	8	440	124.3	0.340	6245	76.5-7.2-16.3	0.2505±3	3.261±6	0.09442±13	1516±2
N4 150-210 µm SP clear	258.4	15	173	44.8	0.119	6325	81.7-7.7-10.6	0.2446±4	3.192±7	0.09464±14	1521±2
N5 45-74 µm SP clear	101.8	205	95	21.4	0.116	811	82.2-7.7-10.1	0.2137±10	2.745±32	0.09313±90	1491±14
N6 45-74 µm SP dark	52.5	84	612	171.3	14.0	508	76.6-11.8-11.6	0.2285±5	4.849±50	0.15393±132	2390±21

LP = long prismatic, SP = short prismatic. Pb_{tot} is total lead, and Pb_{com} common lead. (1) $^{206}Pb/^{204}Pb$ only corrected for mass discrimination.
(2) Ratios corrected for mass discrimination, blank (0.01 ng U and 0.066 ng Pb), and common Pb ($^{206}Pb/^{204}Pb$=15.8, $^{207}Pb/^{204}Pb$=15.2, $^{208}Pb/^{204}Pb$=35.3). Errors are 2 σ.

For the Mullnäset granite, all three analysed zircons follow the calculated discordia line closely, giving an upper intercept age of 1526±3 Ma (MSWD=0.014). This is regarded as the crystallization age of the intrusion (Fig. 64a). The lower intercept at 177 Ma has a large calculated error (±360 Ma), and can not be given any geological meaning. A discordia through all three of the analysed Mårdsjö zircons gives an upper intercept age of 1535±14 Ma (MSWD=0.88) (Fig. 64b). One grain is, however, more discordant than the other two, and a discordia running through only the latter two gives the intercept age of 1524±3 Ma (MSWD=0, only two points). This latter age, calculated from the two most concordant points, is regarded as the best estimate of the true crystallization age of the Mårdsjö granite. The calculated $^{207}Pb/^{206}Pb$-ages of the two most concordant points are also very close to the intercept age (Table 20). In spite of their relatively large analytical errors these analyses are considered to be very good estimations of the intrusion ages, due to their near concordant nature.

One sample of the Nordsjö syenite (N12) was also subjected to zircon age determination. This was done by conventional multigrain analysis. Six fractions were handpicked from different size fractions, dissolved and analysed separately (Table 21). The sample was very rich in zircons of good quality. The majority were clear and short-prismatic, with a length:breadth ratio of about 2:1. A minority were long-prismatic, but more abundant among the larger crystals. The length:breadth ratio of these was often around 5:1, and they were clear to somewhat brown. The weight of the dissolved fractions varied between 52 and 742 µg. The U and Pb contents of the zircons were also generally significantly higher than in the single zircon analyses, 95–613 and 21–171 ppm, respectively. The fraction N6 is especially rich in U and Pb, whereas N5 is poor. The analysed blank values are 0.11 ng for Pb and 1.116 ng for U. The latter value is exceptionally high and is not considered representative of the amount of contamination during chemical preparation. Therefore the average blank content for a large number of samples at the laboratory (0.01 ng U) was utilized in the calculations as being more representative of the level of contamination. This high blank value is, however, an indication that such high contaminations may, in unfavourable circumstances, enter the samples. The relatively good-quality discordia calculated below, is evidence that the analysed fractions have not suffered this kind of contamination.

The fractions N1–N5 adhere relatively well to a discordia line with an upper intercept age of 1522±22 Ma (MSWD=5.2). The fraction N5 has a relatively larger error, compared with the other ones, due to lower U and Pb content and lower $^{206}Pb/^{204}Pb$ (Table 21). A discordia calculated omitting N5, gives better precision (Fig. 45c) in the age calculation (1520±3 Ma, MSWD=0.8). N5 is here clearly offset to the left of this discordia. This is the preferred age estimate for the crystallization of the Nordsjö syenite.

The fraction N6 shows a completely different isotopic composition. The calculated $^{207}Pb/^{206}Pb$-age of N6 is 2390 Ma. The zircons of this fraction are small (45–74 µm), and have a typical appearance. They are grey-black, turbid, and elongated with a length:breadth ratio of about 3:1. They have surprisingly well-preserved crystal faces, although usually somewhat rounded. The highly discordant $^{207}Pb/^{206}Pb$-age of 2390 Ma is a minimum age, since among the 84 small analysed grains some younger ones may have been included, as well as younger overgrowths, although none has been optically noted. Furthermore, the lower intercept of a discordia line calculated for several fractions of this type of crystals may be higher than zero, which means that the $^{207}Pb/^{206}Pb$ ratio of the discordant N6-fraction will significantly underestimate the upper intercept age. These crystals thus contain inherited

material with much higher crystallization age than the other fractions, suggesting that the syenite contains material that is at least 900 Ma older than the rock itself. This is, thus, evidence in strong support of the conclusions drawn from the Sm-Nd isotope systematics, that an older, most probably Archaean, lower crust is involved in the genesis of these rocks (see chapters 6.5.3.2 and 7.5.1.2). Recent ion-probe analyses of this group of zircons have confirmed their Archaean age (2.70±0.04 Ga; Claesson et al. 1997).

7.4.2. Nd isotopes

Twenty-three whole rock Sm-Nd isotopic analyses of rocks from Jämtland and Ångermanland are reported in Table 22. Sixteen of these are from rocks of the four investigated rapakivi complexes, and the rest from the different country rocks. Duplicate analyses from separate dissolutions of the same samples show good correspondence (Table 22). Also the runs of the USGS basalt standard BCR-1 show good agreement with the literature value (average of many runs from different labs; Gladney et al. 1990). The duplicate sample, M15a, analysed both in St. Petersburg and Stockholm show excellent interlab reproducibility. Analytical details are given in Appendix 1.

Notably, there is a big overlap in measured values between the different rock types and complexes. The measured $^{143}Nd/^{144}Nd$ ratios vary between 0.511286 and 0.511688 for the mafic rocks, between 0.511180 and 0.511578 for the intermediate rocks, and between 0.511140 and 0.511460 for the granites. Likewise, the measured $^{147}Sm/^{144}Nd$ values overlap markedly. The highest value for the granites is 0.1135, and the lowest value for the mafic rocks is 0.1026. The intermediate rocks range between 0.0942 and 0.1254. There is, furthermore, a large overlap also in the Sm- and Nd-contents between the different rock types. The granites and syenites, however, tend to have somewhat higher contents, up to 79 ppm Nd and 12.0 ppm Sm, whereas the lowest contents in the associated mafic rocks are 30 ppm Nd and 5.8 ppm Sm. The contents of the latter are fairly high compared with mafic rocks in general (Faure 1986, cf. e.g. the Postjotnian and other dolerites, Appendix 2b, Rämö 1990, Johansson & Johnsson 1990, Patchett et al. 1994), which is typical for the Subjotnian rapakivi-associated basic rocks in general (Rämö 1990, 1991, Andersson 1994, Neymark et al. 1994, Appendix 2b), and agrees with the enrichment in LREE that is evident in the geochemistry (chapter 7.3.4. above).

The ε_{Nd} values at the time of magma crystallization (c. 1.52 Ga for all complexes), are consistently very low, between -8.5 and -5.7. Irrespective of composition, rocks from the same complex have similar initial ε-values (Table 22). In the Mårdsjö and Nordsjö samples the basic rocks have slightly lower values than the silicic-intermediate, whereas for the Mullnäset complex the opposite is observed. There are also some differences between the complexes. The most negative $\varepsilon_{Nd}(1.52)$-values are displayed by the Strömsund massif -8.2 to -7.5, whereas Nordsjö has the least negative values: -6.5 to -5.7. There is thus no overlap between these complexes. The Mårdsjö rocks are relatively more negative, -8.5 to -7.1, and overlap the Strömsund values completely. The Mullnäset rocks, on the other hand, are slightly less negative, -6.8 to -6.2, and thus overlap with Nordsjö. The differences thus seem to be more related to geography than to composition. Calculated depleted mantle ages (T_{DM}; DePaolo 1981) are, as well as CHUR-ages, high (Table 22) compared with the crystallization ages of these rocks (see above). T_{DM} varies between 2.64 and 2.16 Ga. No rocks of such ages are known in the region, and very few in the shield as a whole.

7.4.3. Sr isotopes

Rb and Sr isotopes were measured on 7 samples from the area, 4 from the rapakivi complexes and 3 from the older country rocks (Table 22). The analytical errors ($2\sigma_M$) are low (Appendix 1). Two of the samples from the rapakivi complexes are granites and two are gabbros. All samples have also been analysed for Nd isotopes. The measured $^{87}Sr/^{86}Sr$ ratios are low for the basic rocks and high for the silicic, and likewise for the $^{87}Rb/^{86}Sr$ ratios, which is normal. The contents of Rb and Sr are also within the limits expected for these rock types (cf. Appendix 2b). The $^{87}Sr/^{86}Sr$ at the time of crystallization of the rocks is low for all measured rocks from the rapakivi complexes (0.6994–0.7034). This is close to the value for the estimated bulk earth (uniform reservoir, UR), at this time (0.7027). One granite value (Mu8) is even lower, which is unrealistic and suggests that the primary magmatic Rb-Sr

Table 22
Nd-Sr isotopic results, Jämtland-Ångermanland

Sample no	*Description*	SiO_2	*Sm*	*Nd*	$^{147}Sm/^{144}Nd$	$^{143}Nd/^{144}Nd$	$\varepsilon_{Nd}(1.52)$	$\varepsilon_{Nd}(t)$	T_{DM}	T_{CHUR}	$f_{Sm/Nd}$	*Rb*	*Sr*	$^{87}Rb/^{86}Sr$	$^{87}Sr/^{86}Sr$	Sr_i (1.52)	Sr_i	$\varepsilon_{Sr}(1.52)$
		wt%	*ppm*	*ppm*														
M18	Mårdsjö gabbro	55.2	5.80	33.32	0.1052	0.511317 (4)	-7.96	<-	2.43	2.19	-0.47							
M15a(1)	Mårdsjö gabbro	55.0	6.87	40.61	0.1026	0.511286 (3)	-8.06	<-	2.42	2.18	-0.48	65.63	715.13	0.2656	0.70884 (07)	0.7030	->	5
M15a(2S)	Mårdsjö gabbro	55.0	6.90	40.40	0.1033	0.511295 (8)	-8.03	<-	2.42	2.18	-0.47			0.269	0.70894 (17)	0.7031	->	5
M20	Monzodiorite, Mårdsjö	58.4	6.68	43.02	0.0942	0.511180 (10)	-8.50	<-	2.38	2.16	-0.52							
M11(1)	Mårdsjö syenite	59.7	11.32	67.21	0.1022	0.511298 (6)	-7.75	<-	2.39	2.15	-0.48							
M11(2)	Mårdsjö syenite	59.7	9.87	58.48	0.1024	0.511306 (7)	-7.63	<-	2.39	2.14	-0.48							
M14a	Mårdsjö granite	65.5	11.90	76.34	0.0946	0.511257 (6)	-7.06	<-	2.29	2.05	-0.52	153.57	195.03	2.2882	0.75275 (08)	0.7027	->	1
M15b(1)	Mårdsjö vein granite	67.7	9.37	62.45	0.0910	0.511196 (7)	-7.55	<-	2.30	2.07	-0.54							
M15b(2)	Mårdsjö vein granite	67.7	9.15	65.15	0.0852	0.511140 (5)	-7.52	<-	2.26	2.04	-0.57							
N7	Nordsjö dolerite	52.1	7.87	39.39	0.1211	0.511551 (6)	-6.50	<-	2.47	2.18	-0.38							
N9(1)	Nordsjö syenite	61.2	10.19	70.09	0.0881	0.511264 (6)	-5.67	<-	2.16	1.92	-0.55							
N9(2)	Nordsjö syenite	61.2	12.02	79.24	0.0920	0.511287 (7)	-5.97	<-	2.20	1.96	-0.53							
N11	Nordsjö syenite	58.9	10.60	57.05	0.1127	0.511496 (6)	-5.93	<-	2.34	2.07	-0.43							
Mu11a(1)	Mullnäset gabbro	57.1	6.68	30.01	0.1350	0.511688 (6)	-6.53	<-	2.64	2.34	-0.31	43.77	456.39	0.2775	0.70943 (08)	0.7034	->	9
Mu11a(2)	Mullnäset gabbro	57.1	6.72	30.24	0.1347	0.511684 (5)	-6.55	<-	2.64	2.33	-0.32							
Mu5	Mullnäset syenite	63.0	8.32	42.69	0.1183	0.511536 (6)	-6.23	<-	2.42	2.13	-0.40							
Mu12	Mullnäset syenite	60.8	5.95	28.78	0.1254	0.511578 (4)	-6.80	<-	2.54	2.26	-0.36							
Mu8	Mullnäset granite	69.9	8.06	43.08	0.1135	0.511460 (5)	-6.79	<-	2.42	2.15	-0.42	133.04	115.39	3.3571	0.77290 (10)	0.6994	->	-44
S7	Strömsund granite	73.4	5.99	36.66	0.0991	0.511263 (5)	-7.83	<-	2.37	2.14	-0.50							
S6	Strömsund granite	70.3	8.71	47.46	0.1113	0.511367 (7)	-8.18	<-	2.51	2.26	-0.43							
S4	Strömsund granite	71.8	9.31	50.12	0.1127	0.511416 (14)	-7.49	<-	2.47	2.21	-0.43							
M1	Svecof. metasediment	66.3	3.84	21.72	0.1072	0.511363 (8)	-7.45	-3.16	2.41	2.16	-0.46	150.43	244.52	1.7878	0.75308 (08)	0.7139	0.7044	162
M7(S)	Early Svecof. granitoid	63.2	6.02	33.44	0.1088	0.511463 (7)	-5.81	-1.60	2.30	2.03	-0.45			2.180	0.76092 (22)	0.7134	0.7016	151
M5(1)	Early Svecof. granitoid	69.6	4.46	23.21	0.1166	0.511616 (9)	-4.34	-0.51	2.24	1.94	-0.41	290.50	101.27	8.4646	0.91111 (12)	0.7258	0.6809	337
M5(2)	Early Svecof. granitoid	69.6	4.57	24.00	0.1154	0.511596 (7)	-4.51	-0.61	2.25	1.95	-0.41							
Mu2	Revsund granitoid	64.9	9.13	46.69	0.1186	0.511682 (7)	-3.45	-0.72	2.18	1.86	-0.40	213.25	197.30	3.1500	0.78241 (10)	0.7135	0.7013	156
Mu4	Dark Revsund granitoid.	57.3	10.74	52.52	0.1240	0.511762 (6)	-2.93	-0.39	2.18	1.83	-0.47							
N2	Revsund granitoid	67.6	8.13	43.11	0.1143	0.511630 (6)	-3.62	-0.74	2.17	1.86	-0.41							
N8	Pink Revsund granitoid	64.6	7.02	35.36	0.1203	0.511707 (5)	-3.29	-0.62	2.18	1.85	-0.41							
BCR-1	USGS Basalt standard		6.40	27.96	0.1388	0.512646 (6)												
BCR-1	USGS Basalt standard		6.44	28.26	0.1383	0.512640 (8)												
BCR-1	USGS Basalt standard		6.67	28.56	0.1390	0.512643 (9)												
BCR-1(S)	USGS Basalt standard		6.63	28.88	0.1387	0.512628 (12)									0.705052 (10)			
BCR-1(S)	USGS Basalt standard														0.705083 (20)			
BCR-1(S)	USGS Basalt standard		6.62	28.88	0.1387	0.512620 (5)									0.705158 (14)			
BCR-1(S)	USGS Basalt standard		6.60	28.78	0.1387	0.512628 (20)									0.705004 (12)			
BCR-1(S)	USGS Basalt standard		6.60	28.68	0.1392	0.512703 (32)									0.705020 (10)			
BCR-1(S)	USGS Basalt standard														0.705082 (12)			
Literature values (Gladney et al. 1990)			*6.59*	*28.8*	*0.1371*	*0.512640*									*0.70501*			

(1) and (2) are duplicate analyses. (S) are analyzed at LIG-NRM in Stockholm. The rest at IPGGC St. Petersburg. SiO_2 is extracted from Appendix 2b. Rb and Sr were determined by IDMS. Numbers in parenthesis denote within run $2\sigma(m)$ in $^{143}Nd/^{144}Nd$ and $^{87}Sr/^{86}Sr$ ratios in the fifth and sixth decimals. T_{DM} after DePaolo (1981); $\varepsilon_{DM}(t)=0.25t^2-3t+8.5$. $f_{Sm/Nd}=[^{147}Sm/^{144}Nd(sample)/^{147}Sm/^{144}Nd(CHUR)]-1$. Measurements on the WR-standard BCR-1 in St. Petersburg and Stockholm are included. $\varepsilon_{Nd}(t)$ and Sr_i at 1.89 Ga for M1, M5, and M7, and at 1.79 Ga for Mu2, Mu4, N2, and N8.

system has suffered disturbance some time after the crystallization, in such a way that the original Rb/Sr ratio has increased or radiogenic Sr has been lost. The $^{87}Sr/^{86}Sr(1.52)$-values for the country rocks are all markedly higher than for the rapakivi rocks (cf. Table 22, Fig. 54), whereas their initial values (calculated at 1.89 and 1.79 Ga for the early Svecofennian and Revsund rocks, respectively) are primitive, and even unrealistically low in one case (M5).

7.4.4. Pb feldspar isotopes

Feldspars from 10 rocks have been separated for analysis of their lead isotopic compositions; 7 from the rapakivi complexes and 3 from the country rocks (Table 23). All of these WRs have been analysed for their Nd and some for their Sr isotopes (Table 22). The $^{206}Pb/^{204}Pb$ values for the leached (see Appendix 1) rapakivi feldspars vary between 15.308 and 16.610. The latter value is significantly higher than the others, which are lower than 15.941, and indicates that this feldspar fraction probably contained some primary U that decayed and added more radiogenic Pb. The other rapakivi feldspars are regarded as essentially unradiogenic, showing the isotopic composition at the time of crystallization.

The $^{207}Pb/^{204}Pb$ ratios vary between 15.018 and 15.217, which is between the evolution curves for the mantle ($\mu 2=9.17$) and the lower crust ($\mu_2=8.00$), in the two-stage evolutionary model of Stacey and Kramers (1975) (Fig. 65b). μ_2 is the $^{238}U/^{204}Pb$ ratio in stage two. A large number of analyses of feldspar and galena lead from the Fennoscandian shield have been added for reference in Fig. 65, and are referred to in the discussion. The Pb isotopic composition cannot be related to WR chemistry in any straightforward way. The range in Pb isotopic composition is as large within the complexes as between them.

The $^{208}Pb/^{204}Pb$ values are between 34.971 and 35.878, and spread out in a way similar to the $^{207}Pb/^{204}Pb$ values. The two samples showing the lowest Pb isotopic ratios (most primitive having the lowest U-Pb ratios in their source; Mu12 and M15a) are located slightly above the mantle curve, near the feldspars from the Salmi massif (Neymark et al. 1994). The other ones are distributed near the mantle and upper crustal curves (Fig. 65a). The Salmi feldspars and galenas, however, generally have higher relative $^{208}Pb/^{204}Pb$. The curves are from the Zartman and Doe (1981) plumbotectonics model.

The three feldspars from the older country rocks show pronouncedly higher Pb isotopic ratios, especially $^{206}Pb/^{204}Pb$. The latter suggests an addition of uranogenic lead. The $^{207}Pb/^{204}Pb$ values conform relatively well with the evolutionary curve for "Svecofennian juvenile crust" of Rämö (1991). Most of the analysed feldspars and galenas from Finnish rapakivi complexes (Vaasjoki 1981, Rämö 1991) fall along this trend (Fig. 65b). The feldspars from the Subjotnian complexes analysed here thus have substantially more primitive (i.e. less radiogenic) compositions.

Table 23. Pb-feldspar isotopic results.

Sample	*mineral*	$^{206}Pb/^{204}Pb$	$^{207}Pb/^{204}Pb$	$^{208}Pb/^{204}Pb$
M15a	plagioclase	15.308	15.019	35.037
M11	mesoperthite	15.758	15.130	35.057
M14a	perthite	15.941	15.215	35.662
Mu11a	plagioclase	15.809	15.217	35.231
Mu12	mesoperthite	15.286	15.018	34.971
Mu8	perthite	16.610	15.191	35.878
N12(1)	mesoperthite	15.856	15.201	35.359
N12(2)	mesoperthite	15.790	15.187	35.296
M1	plagioclase	16.462	15.452	36.295
M5	feldspar	16.879	15.500	35.932
Mu2(1)	feldspar	16.893	15.521	35.706
Mu2(2)	feldspar	17.220	15.542	35.835

(1) and (2) denote replicate analyses. Sample numbers can be found in Figs. 31, 55, and Appendix 2b.

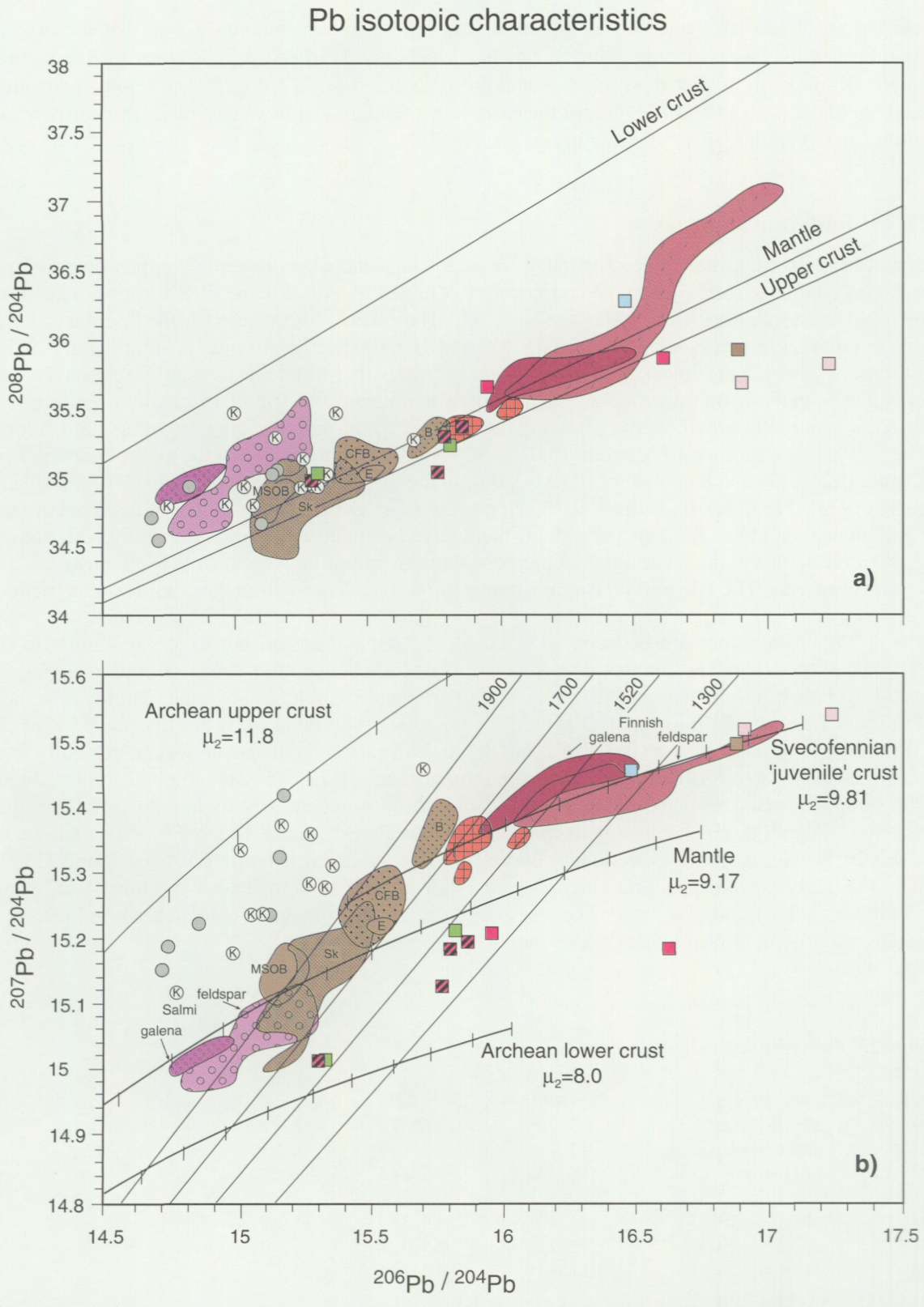

Fig. 65. Pb isotopic composition of the feldspar fractions of this study (Jämtland–Ångermanland area), in the frame of other Fennoscandian Pb data compiled from the literature. Brown fields are early Svecofennian galenas from different geographic/geological areas: B is Bergslagen, CFB is the central Finnish batholith area, E is the Enåsen deposit in the Bothnian basin, Sk is the Skellefte district, and MSOB is the main sulphide ore belt in Finland. Violet fields are Salmi galenas and feldspars and wine red fields galenas and feldspars from Finnish rapakivi complexes. Checkered bright red fields are galenas from Postsvecofennian granite-related galenas. Grey circles represent galenas from Archaean rocks and circles with a K are galenas from Karelian cover rocks on the Archaean craton. Samples of this study (feldspars, Table 23), are plotted as coloured squares: red are rapakivi granites, green are basic rocks from the rapakivi complexes, striped red-green are syenites from the rapakivi complexes, light blue is from an early Svecofennian metasediment, brown is from an early Svecofennian granitoid, and pink are from a Revsund granitoid. Evolutionary curves are stage two curves (Stacey & Kramers 1975) for different postulated reservoirs with different μ_2 ($^{238}U/^{204}Pb$) values: Archaean upper crust, μ_2=11.8, Archaean lower crust, μ_2=8.0, depleted mantle, μ_2=9.17, and Svecofennian "juvenile" crust, μ_2=9.81 (Rämö 1991). Stage two model isochrons (Stacey & Kramers 1975) for 1300, 1520, 1700, and 1900 Ma have also been included. Evolutionary curves in $^{208}Pb/^{204}Pb$-$^{206}Pb/^{204}Pb$ space are after Zartman & Doe (1981). Data sources for the compiled data are: Vaasjoki (1981), Rickard & Svensson (1984), Sundblad (1991), Sundblad et al. (1993), Hallberg (1989), Johansson & Rickard (1985), Rämö (1991), Neymark et al. (1994), Vaasjoki & Vivallo (1990), Vaasjoki & Sakko (1988), Åberg & Charalampides (1986), Billström (1985), and Sundblad et al. (1988). Discussion in the text.

7.5. DISCUSSION

7.5.1. Isotopes

7.5.1.1. Ages

The U-Pb zircon ages presented above for three of the investigated complexes are considered to represent the ages of crystallization with relatively good precision. Including the errors, they are in the narrow range 1529–1517 Ma. This is c. 60 Ma younger than the U-Pb zircon age determined for the Nordingrå complex (1578±19 Ma; Welin & Lundqvist 1984, T. Mårtensson pers. comm. 1996). Other recent age determinations from Subjotnian complexes in central Sweden give slightly lower ages in the range 1513–1497 Ma, including those of this study: Rödön 1497±6 Ma and Strömsbro (Andersson 1997a) 1500±19 Ma. Recent age data on the Ragunda complex have yielded 1513±9 and 1506±13 Ma (Persson 1996), and Welin (1994) reported an age of 1513±5 Ma for the Rödö granite.

The Swedish rapakivi complexes, which occupy the westernmost part of the Fennoscandian suite of rapakivi granite complexes, are thus the youngest (cf. Fig. 30). The Nordingrå complex is older and similar in age to the SW Finnish and the Riga complexes (1.59–1.56 Ga; Vaasjoki 1977, Vaasjoki et al. 1988, Idman 1989, Suominen 1991, Rämö et al. 1996). The otherwise youngest complex in the suite is the easternmost Salmi massif in Russian Karelia (1.56–1.53 Ga; Neymark et al. 1994, Suominen 1991, Amelin et al. 1997). The Wiborg complex and the smaller plutons in SE Finland are the oldest (1.65–1.61 Ga; Suominen 1991, Vaasjoki et al. 1991, 1993), including some small intrusions in northern Estonia (Rämö et al. 1996).

Excluding the Salmi batholith there is thus a westerly younging age trend among the Fennoscandian rapakivi complexes. This trend, however, does not seem to record a smooth geographical age distribution. Instead, rocks of similar ages appear to form roughly discrete north–south trending belts (cf. Fig. 30). The youngest belt (1.53–1.50 Ga) trends from Strömsbro in the south to Mullnäset and Strömsund (no age determined) in the north, followed to the east of an older belt (1.59–1.56 Ga) from Riga in the south over SW Finland to Nordingrå in the north. Next to the east is the oldest belt (1.65–1.61 Ga) trending from northern Estonia to SE Finland (and SW Russian Karelia) with the huge Wiborg batholith as its major expression, and in the eastern end the Salmi complex, ca 100 Ma younger than the Wiborg complex (c. 1.56–1.53 Ga.). The reason for this age distribution is unclear, but the belt-like geometry argues for a relation to large-scale tectonic processes. These "belts" are more or less perpendicular to the direction of thinner crust along southern Finland (Korja et al. 1993). A relation to plate tectonic activities along the western margin of the shield during the Gothian (1.75–1.55 Ga) crust-forming event (e.g. Connelly & Åhäll 1996, Connelly et al. 1996), perhaps in response to propagating continental back-arc extension, does not seem to be too farfetched.

7.5.1.2. Nd isotopic relations

The low initial ε_{Nd} values obtained (Table 22 and Fig. 46), indicate a major component of older crustal (low-radiogenic) material in the Jämtland–Ångermanland magmas, both the silicic, intermediate, and basic. These results correspond closely with the results from the Rödö complex. A more thorough discussion on the implications of this is therefore given in chapter 6.5.3.2. above. Some specific points will, however, also be made here. The differences in initial ε_{Nd} are generally larger between the four Jämtland–Ångermanland complexes than between rocks of different composition within each complex (Table 22). This suggests a derivation from geographically slightly heterogeneous sources in the lower crust (and perhaps upper mantle). If the model suggested for the Rödö rocks (chapter 6.5.3.2.), where the silicic rocks are derived from melting of a lower crust composed of a heterogeneous mixture of early Svecofennian and Archaean metaigneous sources (see also concluding discussion below, chapter 8), the proportions of these two components have varied in the sources for the different complexes in accordance with their respective initial ε_{Nd} values. The Strömsund and Mårdsjö complexes with their lower $\varepsilon_{Nd}(1.52)$, compared with Nordsjö and Mullnäset, should thus contain slightly more of an Archaean source component. A spatial chemical variation with respect to the concentration of Nd within each source component could, however, also give such a variation. This is perhaps less likely since such differences would probably be small-scale and tend to average out during magma generation in a

source region. Areally consistently varying average (Nd-) compositions of the source components in this geographically relatively small area are not likely.

If a generation of the complexes from an upper mantle source is favoured, this mantle should also have had a spatial variation in the degree of LREE enrichment. In the Mårdsjö complex, the basic rocks have systematically lower initial ε_{Nd} values than the granitoids. This seems to be the case also for the Nordsjö rocks, but not for those from Mullnäset where the values overlap (Table 22). This might be an indication that the basic and silicic/intermediate rocks derive from different sources, mantle and crustal, respectively. The mantle-derived magmas, have in this case, not necessarily a higher percentage of the Archaean component, since a small Archaean component may have a large effect on the ε_{Nd} if it is much richer in Nd. However, inspection of Table 22 reveals the relatively high contents of Nd in the basic rocks (30–40 ppm), which favour substantial additions of crustal material to the magmas if a depleted original nature is assumed. High-P fractionation of olivine and orthopyroxene can also contribute significantly to LREE enrichment in the residual magma (cf. discussion on Rödö dolerites, chapter 6.5.1.7.). If, on the other hand, the mantle-derived magmas initially had c. 30 ppm Nd (as proposed by Rämö 1991, for the Suomenniemi dykes), the low ε_{Nd} values must be reflecting an enriched mantle source.

The overlap in the $\varepsilon_{Nd}(1.51)$ values for the rapakivi complexes and the metasediments of the Bothnian basin (Figs. 46, 47) is merely coincidental (the age 1.51 Ga is chosen for comparative purposes). As discussed previously (chapter 6.5.3.2.), a generation of the A-type rapakivi granitoids from metasedimentary sources is petrologically untenable. The early Svecofennian granitoids from the Bothnian basin area analysed in this study have relatively low $\varepsilon_{Nd}(1.52–1.50)$ (Tables 13 and 22) compared with this group in the shield as a whole (average of -3.0, cf. Table 18). This is in accordance with data from previous studies (Welin et al. 1993, Claesson & Lundqvist 1995) giving a general average $\varepsilon_{Nd}(1.51)$ value of -3.8 for the early Svecofennian granitoids in the Bothnian basin (cf. Fig. 47). The values are, however, still clearly higher than the values for the rapakivi granitoids in Jämtland–Ångermanland, and thus an Archaean contribution is necessary (see chapter 6.5.3.2. for further discussion).

The Nd-data of the Jämtland–Ångermanland intrusions are very similar to those obtained from the Salmi rapakivi complex in Russian Karelia (Rämö 1991, Neymark et al. 1994). The Salmi batholith has intruded at the margin of the exposed Archaean craton, which is why a large Archaean component in its magmas is expected (Rämö 1991, Neymark et al. 1994). The Nd-evolution with time for this batholith strongly overlaps that of the Jämtland–Ångermanland and Rödö complexes (Fig. 46c). This circumstance supports the presence of an Archaean basement also beneath central Sweden.

7.5.1.3. Sr isotopic relations

The few analysed samples from Jämtland–Ångermanland show primitive initial Sr-ratios, both for the mafic and granitic rocks (Table 22). At least one value is clearly disturbed, not showing primary igneous composition (Mu8). The initial $^{87}Sr/^{86}Sr$ value for this sample is below that of the bulk earth (=UR=uniform reservoir) at this time ($Sr_{UR}(1.52)=0.7027$, which is also seen in the negative $\varepsilon_{Sr}(1.52)$-value. In Fig. 54 the Sr(1.51)-values are combined with the $\varepsilon_{Nd}(1.51)$-values for these rocks, and other rocks in the Bothnian basin area and Archaean rocks from the NE part of the shield. Since also analyses of rocks from the 1.50 Ga Rödö complex are included, 1.51 Ga is chosen as an average age for plotting reasons. The Sr isotopic relations are discussed in more detail in chapter 6.5.3.3.

7.5.1.4. Pb feldspar isotopic relations

The results of the Pb feldspar analyses from the Jämtland–Ångermanland rocks (Table 23) spread out in a relatively large interval between the model curves for the mantle and lower crust (Fig. 65b) (cf. Rämö 1991). Sample Mu8 has an enhanced $^{206}Pb/^{204}Pb$-ratio compared with the others, which can be ascribed to some remaining U, which has resulted in excess radiogenic Pb. This is the same sample that exhibits a clearly disturbed signature in the Sr system. The low Pb isotopic ratios indicate a marked but apparently more heterogeneous Archaean component in the magmas, compared with the Nd isotopes. This Archaean component is indicated to be U-depleted (low-radiogenic). No indications of U-rich

Archaean upper crustal components are present in these magmas.

Two of the samples (M15a, gabbro, and Mu12, syenite) from different complexes, plot at very primitive (low-radiogenic) compositions near the lower crustal curve in Fig. 65b, whereas the others spread towards higher $^{207}Pb/^{204}Pb$ values closer to the mantle curve. Most of the samples plot relatively close to the 1520 Ma second-stage model isochron after Stacey & Kramers (1975), which is an indication that the samples essentially have retained their values since the time of crystallization (c. 1520 Ma, chapter 7.4.1.). The Pb isotopic composition of these samples is significantly more primitive than those of the corresponding rapakivi feldspars in Finland (Fig. 65b, Rämö 1991). The latter can be correlated with a Pb evolution from relatively evolved early Svecofennian sources (CFB or B in Fig. 65b) in agreement with the Nd isotopes (Rämö 1991).

The Pb results of the central Swedish rapakivi feldspars can be interpreted similarly to the Nd isotopes above, i.e. as being formed by a mixture of Archaean and Svecofennian source components. In this case, however, the relative importance of these components appears to differ substantially from sample to sample even within the same complex, while the Nd isotope systematics suggested a more homogeneous mixture of components (cf. Table 22). One explanation of this might be the large spread in possible Pb isotopic compositions for the Svecofennian component.

Measured Pb isotopic compositions in galena from a large number of Svecofennian mineralizations have been plotted in Fig. 65 (explanations and references are given in the figure caption), and the compositional spread is substantial. There appears to be a geographic control on the Pb isotopic composition of the early Svecofennian galenas. The most primitive, U-poor sources are present in the Skellefte district in the north and the most evolved U-rich ones in the Bergslagen district in the south, with the Bothnian basin samples (E and CFB) in between. This trend also correlates with the distance from the exposed Archaean craton and the most primitive galenas in the Skellefte district may thus contain a significant component of U-depleted Archaean lower crust, while the Pb-ores in Bergslagen are derived entirely from early Svecofennian sources. The role of the mantle component is, however, difficult to constrain, and the implication of this distribution regarding mixed sources has been discussed by several authors (e.g. Vaasjoki 1981, Huhma 1986, Billström 1989, Sundblad 1991, Sundblad et al. 1993, Billström & Vivallo 1994). This means that it is hard to postulate the isotopic composition of an early Svecofennian source component.

The most probable composition is, however, represented by the areas labelled E or CFB in Fig. 65. E is the Enåsen mineralization (Hallberg 1989) located in the Swedish part of the Bothnian basin, and CFB is the central Finnish batholith area (Vaasjoki 1981), corresponding to galena Pb compositions from the eastern, Finnish, segment of the Bothnian basin. A Svecofennian component with this composition can be mixed in different proportions with an Archaean component represented by, e.g. the hypothetical evolution curve of Archaean lower crust (μ_2=8.00; Rämö 1991), to yield the range in the analysed silicic-intermediate rapakivi samples. However, since the compositions of the components in the mixture cannot be unequivocally determined, it is not possible to quantify their relative proportions. If the compositions of the components are the same for all the granitoid samples the proportions will not be the same as calculated from the Nd isotopes. It is, however, probable that the Pb isotopes are more sensitive tracers of small-scale variations in the U-Pb ratio in the lower crustal source regions, and that this has influenced the data. Also the U-Th-Pb character of the Archaean lower crust component might have varied, due to different degrees of depletion, giving compositions deviating from the μ_2=8.00-curve. Sample Mu12 appears to contain a higher depleted Archaean component, compared with the other syenites. This may, however, be due to a more primitive composition of the Svecofennian component, similar to galenas from the Skellefte district (Sk in Fig. 65). The gabbro of the same complex (Mu11a) is substantially more radiogenic, which possibly is related to a mantle source with μ_2=9.17 or slightly higher, which has assimilated relatively undepleted Archaean material. This is consistent with the quartz-rich, high-silica character of this rock. The other granite-syenites require more radiogenic Svecofennian components, similar to those of CFB or E, and the Archaean component may be less depleted. The low-radiogenic composition of the Mårdsjö gabbro (M15a) should be related to an assimilated strongly U-depleted Archaean component (cf. ε_{Nd} values Table 22), which is consistent with its more basic character, compared with Mu11a.

The analysed Svecofennian feldspars show markedly evolved (radiogenic) Pb compositions, which suggest that they contain U giving excess radiogenic Pb (Table 23). They conform relatively well to the

evolution curve for "juvenile Svecofennian crust" (μ_2=9.81) suggested by Rämö (1991), which has its starting point in the CFB-field (Fig. 65b). This suggests that if the excess radiogenic Pb is removed they would have an original composition (at the time of crystallization) in this field.

With regard to thorogenic lead (^{208}Pb), the samples spread between primitive compositions in the area of Archaean Pb and evolved compositions near those of the Finnish rapakivis. Sample Mu8 and the Svecofennian feldspars clearly show evidence of excess radiogenic Pb. Curves for the evolution of the mantle and upper and lower crust have been added in Fig. 65a (after Zartman & Doe 1981). The thorogenic isotopic compositions can also be interpreted in terms of different degrees of mixing of a Th-depleted Archaean component with a Svecofennian or mantle component, but it is impossible to determine the quantitative contribution of these components in each rock sample. It is, however, evident also here that samples M15a and Mu12 have more primitive compositions and appear to contain a higher degree of Th-depleted material than the others, which is not generally supported by the Nd isotopic systematics. In comparison with feldspars from the Salmi complex, the central Swedish ones are less primitive (more radiogenic). The Salmi feldspars have, e.g. high ^{208}Pb/^{204}Pb at lower ^{206}Pb/^{204}Pb values and thus higher Th/U ratios, suggesting lower crustal protoliths more strongly depleted in U than in Th (cf. Larin et al. 1990, Neymark et al. 1994). This is not the case for the Jämtland–Ångermanland feldspars, suggesting, in general, less strongly depleted character of the lower crustal component.

In conclusion: the Pb isotopes do not give any conclusive evidence about the relative importance of the different source components, but still clearly show that a major contribution of a much older U and Th depleted lower crust is involved in this magmatism. Ashwal et al. (1986) and Ashwal (1993) have also interpreted similar Pb isotopic variations in Mesoproterozoic anorthosite-granite complexes in Labrador as resulting from interactions with a depleted, low-radiogenic Archaean crust.

7.5.2. Geochemistry

7.5.2.1. The Härnö and Revsund suites

The generation of the Härnö granitic suite from sources similar to the Svecofennian metasediments of the Bothnian basin (supplemented by minor metaigneous sources) is supported by their restricted silicic composition (Fig. 56), marked peraluminous S-type character, trace element modelling, and Sr-Nd isotopes (Claesson & Lundqvist 1995). Their field occurrences, which are mainly restricted to the metasedimentary basin areas, where they generally form minor intrusions of heterogeneous character, often carrying abundant, more or less dissolved, fragments of the country rocks (Lundqvist et al. 1990), are in accordance with a relatively local anatectic origin.

The geochemistry of the Revsund suite is on the whole much less aluminous, although locally it may sometimes be relatively peraluminous (cf. Fig. 57), containing garnet in areas of assimilation of metasediments (Lundqvist et al. 1990). The relatively well-confined monzotrend suggests that the chemical evolution of the Revsund suite rocks may be controlled by plutonic mixing processes between monzogranitic silicic endmembers and monzogabbroic basic endmembers (Fig. 56a; cf. chapter 4 on the SVB rocks). The basic endmember of this mixing trend is poorly known due to the general scarcity of such rock types (cf. Lundegårdh et al. 1984, Lundqvist et al. 1990). Minor amounts of associated basic rocks in the Revsund suite do, however, occur locally (e.g. Björk 1988, 1995, and pers. comm. 1996, Th. Lundqvist pers. comm. 1996, P. Weihed unpubl. res.). Mafic magmatic enclaves within the Revsund granitoids indicating the co-mingling of basic and silicic magmas have been found (Lundqvist et al. 1990, P. Weihed pers. comm. 1996). The monzotrend of the Revsund granitoids is strikingly similar to that observed in the Filipstad-type (coarse porphyritic) Småland-Värmland granitoids (Fig. 8), which have also been interpreted in terms of plutonic mixing processes (Andersson 1989, 1991, chapter 4 above). There is also a more diffuse granodioritic-tonalitic trend in the Revsund suite which tentatively may be interpreted as resulting from a more primitive mixing between less evolved gabbros and the granites. In contrast, Persson (1978) interpreted the monzotrend in the Revsund suite as a result of magma differentiation, rather than mixing.

Since the Revsund granitoids occur in a series of interconnected vast batholiths the volume of magma is huge, in contrast to the Härnö granites. This suggests a substantially different mode of origin. The Revsund magmas were generated at depths substantially below the present level of erosion, coalesced into large magma volumes and rose to the emplacement levels. Their average subaluminous geochem-

istry suggests dominantly metaigneous source rocks. Such source rocks may have consisted dominantly of early Svecofennian (2.0–1.86 Ga) granitoids and volcanics. This is consistent with isotopic data which also suggests a minor admixture of Archaean and metasedimentary material (Patchett et al. 1987, Claesson & Lundqvist 1995, chapter 6.5.3.2. above). Low initial Sr ratios of some Revsund granites may indicate that the source is partly LILE-depleted. Such voluminous silicic magma generation in the lower parts of the crust strongly suggests that heat was supplied by underplating basic magmas.

Associated basic plutonism is much more abundant in the similar Småland–Värmland belt (e.g. Persson 1985, 1989, Wilson et al. 1986, Andersson 1989, 1991), where such a model thus finds support in the field (cf. chapter 4.5.3.). As noted above, basic rocks do occur in the Revsund suite and may be more common than previously recognized. The geochemical mixing trends and occurrence of enclaves supports this. Furthermore, relatively higher magnetic anomalies in certain areas of the Revsund suite (e.g. compilation of Eriksson & Henkel 1994; P. Weihed pers. comm. 1996) may indicate mafic or hybridized rocks at depths, even if magnetite contents have been observed to increase locally also in silicic Revsund types (L. Björk pers. comm. 1996). Although magma mixing is important in controlling the magnetic susceptibility in plutonic suites (cf. the Småland–Värmland belt, chapter 4.5.2.1. above), the variation of oxygen fugacity in this context plays a significant role for the modal variation of Fe-oxides and Fe-silicates in granitic rocks (e.g. Czamanske & Wones 1973, Czamanske et al. 1981, Ishihara 1984, Frost 1991).

Even if the Revsund suite rocks plot in the A-type field in essentially the same areas as the rapakivi rocks in the trace element discrimination diagrams (Fig. 58), they are clearly less alkali-rich and more calc-alkaline in character (Fig. 56), with no syenitic trend. This is unequivocal evidence of different modes of origin. The Revsund granitoid suite represents a huge amount of presumably dominantly crustal-derived magmatism, and if considered belonging to the TIB (e.g. Gorbatschev & Bogdanova 1993) which is strongly indicated by geochemical, petrographical and geochronological data, it becomes part of an elongated belt of enormous magma volumes. This clearly suggests formation due to some orogenic process (subduction or extensional collapse), rather than anorogenic intracratonic extension. An orogenic origin is also supported by the relatively more calcic chemistry and the general absence of coeval dyke swarms. If similar source rocks (granodioritic to tonalitic older crust) are envisioned for the subaluminous Revsund and rapakivi granites in central Sweden, the former should be generated by considerably higher melt percentages as, for instance, evidenced by their, on average, higher CaO and MgO and lower alkali contents, as well as the much larger volumes. Their large volumes should also mean that the Revsund granites were extracted from more extensive source regions, compared with the rapakivi granites, perhaps at variable depths. The Nd isotopes (see above) may be interpreted in agreement with such a scenario. The rapakivi granitoids were generated more locally in the lowermost crust (deeper than the Revsund granites), where the Archaean component is higher (giving lower ε_{Nd}) compared with the lower/middle crust in general (cf. chapters 6.5.3.2. and 8).

7.5.2.2. The Subjotnian complexes

The geochemistry of the minor Jämtland–Ångermanland complexes (Mårdsjö, Nordsjö, Mullnäset, and Strömsund) clearly suggests that these are A-type rocks with the same general characteristics, with high (although not as high as the average Finnish rapakivi granite) and low contents of the same elements as the other rapakivi rocks of the shield (e.g. Figs. 58, 61). A distinctive feature of the Jämtland-Ångermanland complexes is the metaluminous to peralkaline character, with only subordinate peraluminous rocks (Fig. 57). The strong resemblance with the Ragunda complex is conspicuous. The latter, however, also carry abundant peraluminous rocks. This geochemical signature thus seems to be characteristic of the rapakivi complexes in the western part of central Sweden, whereas syenitic and peralkaline rocks are very subordinate to absent in the eastern central Swedish complexes (Nordingrå, Sobral 1913, Lundqvist et al. 1990, Rödön, chapter 6.3.1. above, and Strömsbro, Andersson 1997a).

The geochemical trends in Fig. 59, clearly show that the syenites cannot have formed by hybridization, as a result of magma mixing between a silicic and basic endmember. In such a case they should have followed a straight line trend between the granites and gabbros for all elements in these element-to-element diagams. For some elements this is approximately the case, but for others it is clearly not.

The syenites are higher in K_2O, Na_2O, Al_2O_3, MnO, Ba, Eu, and especially Na_2O+K_2O compared with an expected gabbro-granite mixing trend, but lower in MgO, CaO, Sr, and Cu (partly also Li). The iron enrichment is high (generally over FeO*/FeO*+MgO=0.85), and similar to that of the granites (Fig. 59d), but much higher compared with the gabbro suite (0.6–0.7). The peralkaline silicic rocks have generally distinctly higher FeO*/FeO*+MgO ratios (>0.95) compared with the metaluminous silicic rocks (0.82–0.93). Such a relation has also been observed by Persson (1996) in the Ragunda complex. The syenites show an increase in the Fe-Mg ratio with SiO_2 in the direction of the peralkaline silicic rocks.

Regarding the REE-patterns, the LREE-enrichment is similar to slightly less enriched in the syenites compared with the granites. The Eu-anomaly is, however, generally negative in the latter and positive in the former. The Eu-enrichment is similar in size for syenites from all complexes, with a few exceptions (N9 and M8 lack anomaly, while M12a has a more pronounced). The monzodiorite M20 has a chemistry separate from the syenites, which is consistent with mixing between granitic and gabbroic endmembers. Otherwise, mixed rocks appear to be of very restricted importance in these complexes, contrary to the cases in, e.g. the Rödö complex (chapter 6.5.1.8.) and the Åland rapakivi batholith (Lindberg & Eklund 1992, Eklund et al. 1994).

The markedly uniform petrographic and geochemical character of the rock associations between the complexes indicates that similar processes have operated at all four sites. Strong similarity with the Ragunda complex is also apparent (cf. Kornfält 1976, Persson 1996). Also the latter contain abundant syenites and two suites of silicic rocks, one metaluminous to peraluminous and one metaluminous to peralkaline (Persson 1996). The former group is, however, much more abundant in Ragunda than in the small complexes studied here.

The iron-enrichment in the ferromagnesian minerals is also strong, Fo_{4-8} in the olivines and Di_{13-33} in the clinopyroxenes of the syenites (cf. Table 19). This is typical for the intermediate and felsic rocks of rapakivi complexes (cf. e.g. Simonen & Vorma 1969, Salonsaari 1995), but lacking in the associated mafic rocks (e.g. Di_{65} and En_{48}) (Table 19). This Fe-enrichment is also apparent in the biotites and amphiboles of the granitic rocks, especially in the peralkaline group the alkali amphiboles are nearly devoid of Mg (Table 19). The presence of alkali amphiboles has previously been noted also from Ragunda (Kornfält 1976) and in porphyry boulders in the vicinity of the Strömsund complex (Frödin 1918).

Both mineral chemistry and geochemistry are thus most consistent with a genetic connection between the syenites and the granites, rather than with the basic rocks. Moreover, the intimate spatial relation between syenites and peralkaline silicic rocks, together with the trend of Fe-enrichment (Fig. 59d), suggests that these rocks share some part of magmatic history. The magmatic relation between the syenites and the metaluminous granites is more doubtful. The distinct geochemical gaps between the gabbros and the syenites argue against a genetic relationship, as does the marked difference in the composition of the mafic silicates. Furthermore, the occurrence of dykes of metaluminous trachytic (syenitic) composition (N3a and N3b) associated with the Nordsjö complex (carrying phenocrysts of anorthoclase, augite, Fe-Ti oxides and some apatite), is strong evidence of the original presence of syenitic magmas, which may have been parental to the peralkaline silicic rocks. The fractionating assemblage in equilibrium with such a parental magma is indicated by these phenocryst phases.

The leucogabbro, M3, in the Mårdsjö complex has a more primitive chemistry compared with the rest of the gabbros, e.g. higher contents of MgO, CaO, and Cr, and lower SiO_2, LILE and HFSE (Fig. 62a). It is similar in composition to the high-Al gabbros (Al_2O_3 18.4 %; although lower in Fe and somewhat higher in K) which some workers have proposed as parental to basic suites in anorthositic complexes (e.g. Berg 1980, Emslie 1980, 1985, Emslie et al. 1994, Eklund et al. 1994, Mitchell et al. 1995). The trend from M3 to the other gabbros (low in alumina, <16 % Al_2O_3), may qualitatively be related by combined fractionation of cpx and plagioclase (cf. Rödö dolerites, chapter 6.5.1.7). The trends of Sr and Eu can be accounted for since Sr is removed by plagioclase, while Eu actually has a mineral/melt K_D below one in basic systems (cf. Rollinson 1993) and thus should increase with plagioclase removal from the melt, as is the case in the Mårdsjö suite.

The geochemistry of the syenites, at least those which contain the highest amounts of Al_2O_3, Ba, and Eu, suggests some feldspar accumulation. The consistently low Sr contents indicate that plagioclase is not part of this cumulus assemblage, but rather alkali feldspar. The discovery of anorthoclase (Table 19) as phenocryst phase in a trachytic (syenitic) dyke (N3b) from Nordsjö, strongly implies that

this is the original fractionating feldspar. This anorthoclase has, however, decomposed to an intricate mesoperthitic intergrowth of K-feldspar and albite/oligoclase (Table 19; Plate 3f), during the slow cooling of the plutonic syenites. In the trachyte dyke, it is also partly decomposed but is preserved in the central parts of the phenocrysts, due to more rapid cooling. This dyke additionally contains abundant augite and Fe-Ti oxide phenocrysts (Table 19), as well as some apatite, but no olivine was found. Thus there is petrographic evidence that cpx and oxides may be fractionating phases. The geochemistry is consistent with some accumulation of these phases, as e.g. MnO, Sc, and Zn are relatively enriched in the syenites. The high contents of, e.g. CaO, Fe_2O_3, and TiO_2 in the gabbros tend to mask an enrichment of these elements in the syenites in the Harker diagrams (Fig. 59). Thus fractionating an assemblage of anorthoclase, augite, Fe-Ti oxide, and possibly fayalite with minor apatite may account for a magmatic evolution from an originally not cumulus enriched syenite (or quartz syenite) magma to the peralkaline granites. The transition into the peralkaline field can be accomplished by fractional removal of plagioclase or, as in this case, anorthoclase relatively rich in Ca (cf. Bowen 1945, Gittins 1979). Similar fractionating assemblages has been reported by. e.g. Upton (1960, 1964) in the Gardar syentic intrusives of south Greenland.

Peralkaline granites are not previously reported from the Fennoscandian rapakivi complexes, but are documented in three of the four complexes studied here (not in Mårdsjö). The geochemical peralkalinity is supported by the existence of alkaline minerals (riebeckite and ferrorichterite; Table 19). It is worth noting that the Nordsjö rocks are especially rich in Na_2O, except one dyke reported by Lundqvist et al. (1990), while some dykes also are concurrently low in K_2O (Lundqvist et al. 1990). The strong enrichment in certain trace elements (e.g. Ba, Y, Nb, Zr, Li, Be, U) in some of the metaluminous to peralkaline dykes in Nordsjö (Fig. 59) is probably related to the fractionation processes described below.

7.5.2.3. Major element modelling

In order to test the possibility of generating the peralkaline silicic rocks by crystal fractionation from a syenitic or quartz syenitic parental magma, major element modelling was performed (Stormer & Nicholls 1978). Mineral compositions used in the calculations are all taken from analyses of the rocks involved (trachyte dyke and syenites, recalculated to 100 % and summarized in Table 24). The peralkaline rocks Mu6, S3, S6, N10b, and N4a are considered as residual melts in the modelling. Different starting magmas (syenites and trachytes) and fractionating phase assemblages were used to calculate possible proportions of phases removed from the parental magma to arrive at the residual melt. Table 25 is a summary of the results.

Table 24. Phase compositions used for major element modelling in the Jämtland–Ångermanland syenites-peralkaline silicic suites.

	Cpx N3b	Cpx Mu5	Cpx N5	Fay Mu5	Fay N5	Anort N3b	Plag M13	Oxid N3b	Oxid Mu1	Apatit N3b	Apatit Mu1
SiO_2	51.20	49.12	50.41	30.15	30.72	63.66	65.14	0	0	0	0.26
TiO_2	0.68	0.13	0.34	0	0	0	0	26.36	27.49	0	0
Al_2O_3	1.65	0.38	0.88	0	0	22.02	21.74	0.08	0.16	0	0
FeO^t	13.87	27.8	22.17	68.4	66.08	0.17	0	73.48	72.27	0.4	0.18
MgO	11.2	1.82	4.76	1.4	3.09	0	0	0.08	0.08	0	0
CaO	20.87	20.43	21.01	0.05	0	3.38	2.81	0	0	55.5	56.17
Na_2O	0.53	0.32	0.43	0	0	7.24	10.09	0	0	0	0
K_2O	0	0	1.4	0	0	3.53	0.22	0	0	0	0
P_2O_5	0	0	0	0	0	0	0	0	0	44.1	43.39
Sum	100	100	100	100	100	100	100	100	100	100	100

Cpx N3b: Average augite (n=11) from the Nordsjö trachyte dike
Cpx N5: Average ferrosalite (n=25) from the Nordsjö syenite
Fay N5: Average fayalite (n=10) from the Nordsjö syenite
Plag M13: Average plagioclase (n=4) from the Mårdsjö syenite.
Cpx Mu5: Average hedenbergite (n=13) from the Mullnäset syenite
Fay Mu5: Average fayalite (n=12) from the Mullnäset syenite
Anort N3b: Average anorthoclase (n=4) from the Nordsjö trachyte dike.
Oxid N3b: Average Fe-Ti oxide (50% ilm+50% magn; n=4) from the Nordsjö trachyte dyke.
Oxid Mu1: Average Fe-Ti oxide (50% ilm+50% magn; n=5) from the Mullnäset syenite. Apatit N3b: Apatite (n=1) from the Nordsjö trachyte dyke.
Apatit Mu1: Average apatite (n=3) from the Mullnäset syenite.

Table 25. Summary of the major element modelling of the intermediate-silicic Jämtland–Ångermanland suites.

Rocks	% cryst.	Calculated proportion of phases in fractionating assemblage	Sum Sq. res.
Trachytes, Nordsjö			
N3b -> N3a	17	81 % Anorthoclase + 10 % Augite + 7 % Fe-Ti Oxides + 2 % Apatite	1
N3a->N10b	49	91 % Anorthoclase + 8.9 % Fe-Ti Oxides + 0.1 % Apatite	3.7
Syenites -> peralkaline aplite, Nordsjö			
N3b->N4a	77	89 % Anorthoclase + 7 % Fe-Ti Oxides + 3 % Fayalite + 1 % Augite (N3b)	6
N9->N4a	71	88 % Anorthoclase + 7 % Fe-Ti Oxides + 3 % Augite (N3b) + 2 % Fayalite	6.8
N12->N4a	73	80 % Anorthoclase + 9 % Fe-Ti Oxides + 7 % Cpx (N5) + 4 % Fayalite	5.6
N12->N4a	68	81 % Anorthoclase + 8 % Fe-Ti Oxides + 7 % Fayalite + 3 % Apatite + 1 % Cpx (N5)	5.1
N12->N4a	66	80 % Anorthoclase + 13 % Fe-Ti Oxides + 6 % Cpx (N3b) + 1 % Apatite	5.8
Syenites -> peralkaline granite, Mullnäset			
Mu5->Mu6	54	78 % Anorthoclase + 9 % Fayalite + 7 % Fe-Ti Oxides + 3 % Cpx (N3b) + 3 % Apatite	2.8
Mu5->Mu6	58	78 % Anorthoclase + 9 % Cpx (Mu5) + 8 % Fe-Ti Oxide + 5 % Fayalite	3.3
Mu5->Mu6	51	77 % Anorthoclase + 15 % Fe-Ti Oxides + 6 % Cpx (N3b) + 2 % Apatite	3.9
Mu12->Mu6	64	85 % Anorthoclase + 8 % Fe-Ti Oxides + 5 % Fayalite + 2 % Apatite + 1 % Cpx (N3b)	4.3
Mu12->Mu6	62	83 % Anorthoclase + 12 % Fe-Ti Oxides + 3 % Cpx (N3b) + 2 % Apatite	4.8
Mu12->Mu6	67	83 % Anorthoclase + 8 % Fe-Ti Oxides + 6 % Cpx (Mu5) + 3 % Fayalite	5
Syenites -> peralkaline granites, Strömsund			
N12->S3	66	81 % Anorthoclase + 9 % Fe-Ti Oxides + 5 % Fayalite + 3 % Cpx (N3b) + 2 % Apatite	3.9
N12->S3	70	81 % Anorthoclase + 9 % Fe-Ti Oxides + 7 % Cpx (N5) + 3 % Fayalite	4.6
Mu12->S3	60	82 % Anorthoclase + 8 % Fe-Ti Oxides + 7 % Cpx (N3b) + 3 % Fayalite	4.2
Mu5->S3	49	76 % Anorthoclase + 10 % Cpx (N3b) + 8 % Fe-Ti Oxides + 6 % Fayalite	2.9
Mu12->S6	57	79 % Anorthoclase + 9 % Fe-Ti Oxides + 8 % Cpx (N3b) + 4 % Fayalite	3.6
M8->S6	54	81 % Anorthoclase + 8 % Fe-Ti Oxides + 6 % Cpx (Mu5) + 5 % Fayalite	4.8
M14a->S6	34	85 % Anorthoclase + 9 % Fe-Ti Oxides + 3 % Cpx (N3b) + 2 % Apatite + 1 % Fayalite	3.7
M14a->S6	36	85 % Anorthoclase + 8 % Fe-Ti Oxides + 6 % Cpx (N3b) + 1 % Fayalite	3.7

All fractionating assemblages are totally dominated by anorthoclase (76–91 %). This is consistent with the mineralogy of the syenites, where mesoperthite with complex intergrowths is the dominating mineral (Plate 3f), as well as with the dominance of anorthoclase as phenocryst phase in the associated trachyte dykes. The average composition of the anorthoclase from N3b was used in the calculations, which is close to the composition of the feldspar in the syenites if the mesoperthite is integrated. In general, Fe-Ti oxides are the next abundant mineral according to the calculations, around 10 %. The oxide used in the calculations is a mixture of magnetite/ilmenite in equal amounts, which appears realistic from petrographic observation. The relation between the other three phases considered in the calculations, varies according to the model. Generally, if apatite is included in the calculation, fayalite becomes the most abundant mafic silicate, while if apatite is omitted, cpx is dominating over fayalite. This is somewhat problematic. A small amount of apatite has obviously crystallized, since it is an abundant accessory phase in the syenite and occurs as microphenocrysts in the trachyte dykes. This is also indicated by the depleted P_2O_5 contents in the residual peralkaline melts. However, models including apatite usually give unrealistically low cpx percentages, sometimes lower than apatite. This is not consistent with the fact that cpx is much more abundant in the syenites. This is probably related to some imbalancing of the CaO, MgO, and FeO contents in the phases used in the calculations.

Regarding the Nordsjö trachytic dykes, no olivine was found as phenocryst phase, and calculations involving fayalite were not successful. Seventeen per cent crystallization of the assemblage anorthoclase+augite+Fe-Ti oxide+apatite, which all occur as phenocryst phases in N3b, reproduces the composition of N3a very well. Further crystallization to obtain the peralkaline quartz trachytic dyke N10b is most consistent with an additional c. 50 % crystallization without augite, but with over 90 % anorthoclase. The extensive anorthoclase crystallization can readily explain the transition from metaluminous to peralkaline character of the magma from N3a to N10b. Removal of the anorthite component of the feldspar causes a relative depletion in Ca and Al in the magma, since more Al is removed compared with what is required for alkali feldspar formation (cf. e.g. Bowen 1945, Gittins 1979).

The composition of the highly silicic aplite dyke, N4a, can be reproduced by fractionation from the trachytes, but models starting with syenitic (plutonic) parental magmas appear to fit slightly better, with higher and more realistic contents of cpx in the fractionating assemblage (Table 25). Around 70 % crystallization of c. 80 % anorthoclase, 8 % Fe-Ti oxides, 6 % cpx, 5 % fayalite and 1 % apatite is consistent with the mineralogy of the syenites. N4a is thus considered representing a residual melt after the crystallization of the syenites of the massif. The sum of squared residuals for these Nordsjö models are a bit high (Table 25), but the results are consistent with the petrographic and geochemical data.

In the case of Mullnäset, the amount of crystallization depends on which of the syenites is chosen as parental magma. Mu12 is slightly more basic than Mu5 and thus requires a little more crystallization before arriving at the composition of Mu6 (c. 83 compared with 78 %). This is essentially a difference in the amount of anorthoclase. Anorthoclase is considered as an appropriate fractionating phase also in the other complexes because of the marked similarities in petrographic and geochemical characteristics. Delicately intergrown mesoperthites are typical in the syenites from all complexes. Mu6 may thus be derived by c. 55–65 % crystallization of c. 78–85 % anorthoclase, 7–15 % Fe-Ti oxide, 3–6 % cpx, 2–7 % fayalite, and 1–2 % apatite. In some cases small amounts of free plagioclase have been found in the syenites (Table 19). The influence of a small amount of plagioclase on the calculations is probably negligible, and may be looked upon as included in the anorthoclase. In the Mårdsjö complex no peralkaline rocks have been encountered so far, which may be related to a deeper level of exposure.

In the Strömsund complex no syenites are met with, so the composition of parental magmas was assumed by analogy with the other complexes. Petrographic and geochemical similarities with the other complexes are clear, although no age has yet been obtained for the complex proving it to be part of the same generation. Peralkaline granites have the widest areal extent in the Strömsund complex (Fig. 55). This, together with the lack of associated basic rocks, suggests that the erosional level is higher up in the Strömsund pluton. Unfortunately, however, the complex is poorly exposed. Depending on which syenite is chosen as parental magma and which of the Strömsund granites is used as the derivative, the crystallization required varies between 50 and 70 % (Table 25). The crystallizing assemblage is similar to the other cases: 76–82 % anorthoclase, 8–10 % Fe-Ti oxide, 3–10 % Cpx, 3–6% fayalite, and 1–2 % apatite. It is also noteworthy that the peralkaline Strömsund granite theoretically can be derived by c. 35 % crystallization of the same assemblage (but even more anorthoclase dominated) from the metaluminous Mårdsjö granite (quartz syenite). This dry assemblage is not, however, consistent with that observed in the Mårdsjö granite. An assemblage of two feldspars, amphibole, oxides, and apatite can, in theory, give similar results, but in general such a relation is not favoured by the available field and petrographic evidence.

7.5.2.4. Trace element modelling

To make an independent test of the major element models above, trace element calculations using closed system fractional crystallization were performed using the NewMelt module in the NewPet program (Clarke et al. 1994) (Table 26). Mineral/melt K_Ds from the compilation of Rollinson (1993, and ref. therein) have been utilized. Due to the variation in suggested mineral/melt K_Ds for the various elements and minerals, the calculations can only crudely indicate if the model is possible at all. The partition coefficients for the dominating fractionating phase, anorthoclase, are estimated from interpolation of a combination of those of K-feldspar and plagioclase ($K_D^{anor/melt}$ Rb 0.5, Ba 10, Sr 10, Eu 4.5). This may be too high, compared with K_Ds determined from phenocrysts and glass in volcanics (e.g. Mahood & Stimac 1990, Macdonald et al. 1994). However, as the calculations in most cases are not able to reproduce the strong depletion in Ba and Sr elements in the peralkaline rocks (see below), these K_Ds do not seem unreasonable. Some variations in K_Ds with peralkalinity of the melt have been observed in volcanics (e.g. Mahood & Stimac 1990, Macdonald et al. 1994), but Ba and Sr have their highest values at lowest peralkalinity, i.e. in the trachytic systems which are most important here. For Rb it is the other way around; $K_D^{feldspar/melt}$ increases with peralkalinity, suggesting that it may be too high in these calculations. On the other hand, most of the calculations (see Table 26, and below) suggest that the K_D used for Rb (0.5) may be even too low. K_Ds for Zr, Y, and Tb in zircon was estimated at 4000, 200, and 20, respectively, based on comparison with other element K_Ds. The rest of the

mineral/melt K_Ds used in the calculations are close to those reported by Mahood & Stimac (1990) from Pantelleria.

The approximate average proportions in the fractionating assemblages obtained in the major element modelling (Table 25) was used in these calculations and the calculated amount of the trace elements at the approximate degree of crystallization was checked against the actual analysis. Different starting compositions (i.e. different parental syenites or trachyte N3b) were tested in the calculations, as well as amount and proportion of the accessory phases apatite and zircon. In general, larger proportions of apatite, compared with zircon, give more consistent results. This is in accord with the larger abundance of apatite in the syenites. Rocks assumed as parental magmas were chosen from samples which showed little or negligible indication of cumulate components, i.e. not those rocks having the highest Ba and Eu contents. The syenites M8, N9, and the trachyte dyke N3b seemed generally most appropriate. In most cases, the trachyte dyke (N3b) from Nordsjö gave results with the closest fit to analytical data, in contrast with the major element calculations above. The difference compared with M8 and N9 was generally, however, relatively small. A selection of the best fit results are summarized in Table 26 and Fig. 66.

In the case of the evolution from trachyte N3b to N3a by c. 15 % crystallization of the assemblage derived by the major element modelling, the trace elements fit very well (Table 26 and Fig. 66), except for Ba and Sr, which should be removed even more strongly. Some of the more incompatible elements (Rb, Nb, Zr, and U) seem to indicate that slightly more than 15 % should have crystallized. Going from N3a to the peralkaline quartz trachyte dyke N10b (50 % crystallization), the trace elements are consistent with the model derived from the major elements, except for the LREEs which should be removed slightly more. For example, small amounts of undetected allanite (cf. Kornfält 1976) could account for this. The incompatible elements match the analysis more closely here, compared with N3a. The lowering of the Sc content may indicate that minor amounts of cpx were fractionated also in this case.

There is, in general, a close similarity between calculated and analysed compositions for the REEs (Fig. 66), except some deviation for Eu. The latter may be related to some variation associated with cumulation or extraction of anorthoclase. N3b, for example, has probably already experienced some feldspar extraction, as indicated by its negative Eu-anomaly, compared with, e.g. M8 which lacks Eu-anomaly. In most cases, the very low contents of Ba and Sr in the peralkaline rocks are not quite obtained in the calculations, although nearly so. For M8 to Mu6 a close fit is obtained. Rb is usually decreasing slightly from syenites to peralkaline granite, except in N4a. This indicates that the $K_D^{anor/melt}$ used (0.5) is too low and instead should be close to unity. Zr contents fit reasonably well, but are in some instances too low. This may indicate a slightly too high proportion of zircon in the fractionating assemblage, rather than too high K_D. Y is controlled by apatite, zircon and cpx and fits the analytical results very well. Nb, on the other hand, shows a calculated increase exceeding the analytical data for all cases, suggesting that some of the K_Ds for apatite (0.1), cpx (0.8), or oxide (2.5) are too low or that the neglected influence of zircon may be important. The results for U are in reasonable agreement, while those for Th show a poorer fit to the analytical data. As discussed for the Rödö rocks, there seems to be some discrepancy in the relative size of the K_Ds for these elements, or alternatively this may be related to different behaviour in relation to a coexisting F-rich fluid (chapter 6.5.1.3. above). The strong increase in these elements in N4a indicates that zircon was not part of the fractionating assemblage. This is supported by the strong increase in Zr and the HREE. The percentage of fractionated apatite is also small in this case. Sc is controlled mainly by cpx (K_D 53) and zircon (K_D 69). The results are consistent except for N4a which, for unknown reasons, is very low in Sc.

Altogether, the trace element modelling is broadly consistent with the results from the major element modelling above. This is thus supporting evidence that the peralkaline rocks can be derived from a syenitic parental magma by 55–70 % fractional crystallization of c. 80 % anorthoclase, 8 % Fe-Ti oxides, 7 % cpx, 4 % fayalite, and 1 % apatite and a little zircon. The phenocryst assemblage of the trachyte dykes also corroborates this, except for fayalite and zircon which, on the other hand, are found in the syenites. Anorthoclasite and magnetite-apatite xenoliths of probable cumulus origin in volcanic rocks (e.g. Upton et al. 1983) provide evidence in support of this model.

The relatively dry nature of the syenitic magmas is indicated by the assemblage of non-hydrous minerals, as well as the hypersolvus character with ternary feldspars (anorthoclase and mesoperthites). Also the peralkaline silicic rocks are hypersolvus with typical striped mesoperthites (although alkali feldspars are totally devoid of Ca; Table 19), indicating relatively low water activities. The change to

Table 26. Summary of closed system fractional crystallization, Jämtland-Ångermanland complexes.

	La	Ce	Nd	Sm	Eu	Tb	Yb	Lu	Rb	Ba	Sr	Y	Nb	Zr	U	Th	Sc
Trachyte N3b -> peralkaline aplite N3a																	
N3b, parental composition	57	110	50	10.5	1.9	1.2	2.9	0.38	120	1140	178	30.5	45	382	1.3	6.6	6.3
N3a, residual, calculated	63	119	51	10.6	1.3	1.2	3.1	0.42	132	548	85.3	30.7	50	438	1.5	7.7	3.8
N3a, residual, analyzed	59	123	50	10.4	0.8	1.1	3.5	0.44	172	n.d	8.3	32.6	68	633	3.0	7.4	3.2
Trachyte N3a -> peralkaline quartz trachyte N10b																	
N3a, parental composition	59	123	50	10.4	0.8	1.1	3.5	0.44	172	n.d.	8.3	32.6	68	633	3.0	7.4	3.2
N10b, residual, calculated	101	208	83	17.1	0.3	2.0	6.1	0.80	236	n.d.	1.6	53.4	107	1089	5.8	14.3	5.3
N10b, residual, analyzed	46	105	60	13.8	0.9	2.1	5.5	0.86	222	n.d.	4.5	52.5	101	907	4.3	17.0	1.7
Trachyte N3b -> peralkaline aplite N4a																	
N3b, parental composition	57	110	50	10.5	1.9	1.2	2.9	0.38	120	1140	178	30.5	45	382	1.3	6.6	6.3
N4a, residual, calculated*	129	233	92	18.0	0.6	2.4	6.0	0.84	205	191	30.0	47.0	90	945	4.0	20.0	2.4
N4a, residual, analyzed	117	232	110	21.2	0.4	3.0	6.2	0.81	243	n.d.	6.0	69.4	64	950	8.6	19.0	0.1
Trachyte N3b -> peralkaline granite S6																	
N3b, parental composition	57	110	50	10.5	1.9	1.2	2.9	0.38	120	1140	178	30.5	45	382	1.3	6.6	6.3
S6, residual, calculated**	74	125	45	8.8	0.7	1.1	2.8	0.35	178	232	36.2	22.9	74	200	1.4	11.4	2.6
S6, residual, analyzed	40	84	40	9.0	0.8	1.1	2.1	0.29	87	139	29.8	23.7	35	235	1.3	3.1	2.5
Trachyte N3b -> peralkaline granite S3																	
N3b, parental composition	57	110	50	10.5	1.9	1.2	2.9	0.38	120	1140	178	30.5	45	382	1.3	6.6	6.3
S3, residual, calculated***	96	166	20	11.8	0.6	1.5	3.8	0.50	195	203	31.6	30.5	83	348	2.2	15.4	2.1
S3, residual, analyzed	80	142	70	13.7	1.2	1.7	3.3	0.48	85	18	9.6	33.6	38	450	1.7	5.8	3.2
Syenite M8 -> peralkaline granite Mu6																	
M8, parental composition	68	134	60	10.2	3.1	1.1	2.2	0.32	110	1350	92.7	23.8	45	309	1.2	4.5	12.8
Mu6, residual, calculated****	118	217	83	13.2	1.2	1.5	1.8	0.23	174	269	18.4	16.6	77	89	0.8	6.8	3.6
Mu6, residual, analyzed	126	233	80	13.3	0.9	1.1	1.6	0.27	104	265	25.1	19.4	26	359	0.5	7.3	1.5

†) 15 % crystallization of 82 % Anor, 10 % Cpx, 7 % Ox, and 1 % Ap.
††) 50 % crystallization of 91 % Anor, 8.9 % Ox, and 0.1 % Ap.
*) 70 % crystallization of 80.75 % Anor, 8 % Ox, 6 % Cpx, 5 % Fay, and 0.25 % Ap.
**) 55 % crystallization of 81 % Anor, 8 % Ox, 6 % Cpx, 3 % Fay, 1.75 % Ap, and 0.25 % Zirc.
***) 65 % crystallization of 81 % Anor, 8 % Ox, 7 % Cpx, 3 % Fay, 0.9 % Ap, and 0.1 % Zirc.
****) 60 % crystallization of 77 % Anor, 9 % Cpx, 8 % Ox, 5 % Fay, 0.5 % Ap, and 0.5 % Zirc.
n.d. = not determined

K_Ds used are from the compilation of Rollinson (1993).
Some values are estimated.

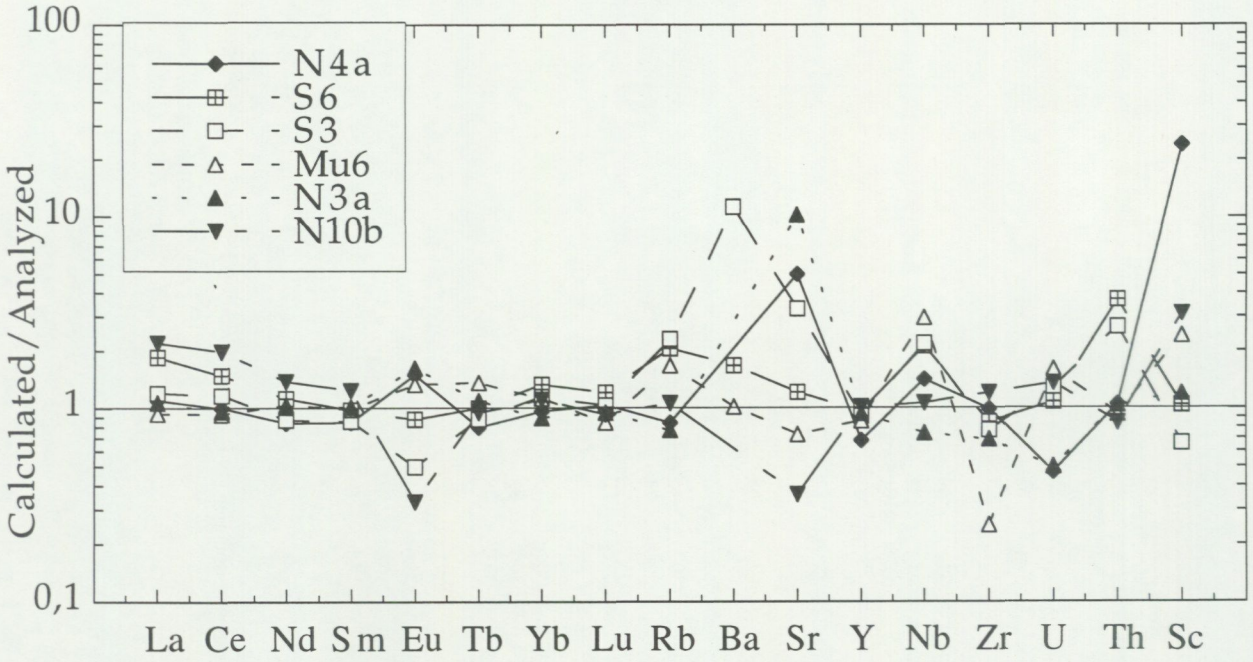

Fig. 66. Graphic representation of the trace element modelling of the syenitic to peralkaline evolution in the Jämtland–Ångermanland complexes summarized in Table 26. Sample numbers refer to the peralkaline modelled rocks (cf. Fig. 55 and Appendix 2b). Calculated results are normalized to the analytical data. A relatively close match is obtained for especially the REEs. The strong depletion in Ba and Sr in the peralkaline rocks was partly difficult to model. Discussion in the text.

alkali amphiboles as the major Fe-Mg silicates in the peralkaline rocks, however, suggests an increase of volatiles in the magma relative to the syenites. This is not unexpected during crystallization, especially if the fractionating assemblage is anhydrous.

8. Discussion on the genesis of the central Swedish rapakivi complexes

Many studies have described differentiation trends for slightly oversaturated syenites (or trachytes) to peralkaline granites (or comendites/pantellerites) resulting from fractionating assemblages similar to those suggested here (e.g. Upton 1960, 1964, Macdonald 1969, 1974, Civetta et al. 1984, Souther & Hickson 1984, Woolley & Jones 1987, Macdonald et al. 1994, Zanvilevich et al. 1995). Such a differentiation sequence finds support also in experimental studies (e.g. Carmichael & MacKenzie 1963, Thompson & MacKenzie 1967). Usually the trachytes themselves have been interpreted as an intermediate stage on a differentiation route from alkali basaltic primary magmas to high silica peralkaline residual melts (e.g. Weaver 1978, Baker et al. 1977, Baker 1987, Thorpe & Tindle 1992). This scenario has, however, been questioned on several grounds (e.g. Bailey & Schairer 1966, Wright 1966, Macdonald & Gibson 1969, Bailey & Macdonald 1970, Williams 1970, Macdonald 1987), including unrealistically low proportions of basic magmas associated with large volumes of silicic continental magmatism, continuous eruption of peralkaline volcanics of the same composition over long geologic periods, and discrepancies with experimental systems. Models involving partial fusion of lower crustal or upper mantle material have been suggested as alternatives (e.g. Bailey & Schairer 1966, Bailey & Macdonald 1970, 1987, Woolley & Jones 1987, Zanvilevich et al. 1995), facilitated by alkalic and carbonic metasomatism (e.g. Bailey 1974, 1987, Bailey & Macdonald 1970, 1987, Black et al. 1997).

On the basis of the literature and evidence provided by the present data set, the following discussion on the origin of the central Swedish rapakivi complexes is offered. The Jämtland–Ångermanland complexes consist of three coeval but not comagmatic units, namely i) a basic unit, ii) a syenitic to peralkaline silicic unit, and iii) a metaluminous (to peraluminous) silicic unit (some units are lacking in

some complexes). Three magmatic units have also been proposed for the Ragunda complex (Persson 1996b). The three magmatic units intruded the upper parts of the crust more or less simultaneously along the same crustal weakness trajectories, and are thus emplaced spatially close. Magmatic interaction between magmas of the three units is very restricted chemically, and hybridization is thus of local nature (in the present data set probably only represented by sample M20). Intense mingling relationships are, however, evident in Ragunda (e.g. Persson 1996a), and Mårdsjö (Plate 3e). As demonstrated above, the syenitic and peralkaline silicic rocks can be related by a process of fractional crystallization of dominantly alkali feldspar (anorthoclase to albitic sanidine). This process probably acted independently in situ in each complex, but along similar evolutionary lines. An intimate spatial relation in the field between syenitic and peralkaline silicic rocks is apparent in Mullnäset and Nordsjö. A close genetic relation between the syenites and granites with peralkaline tendencies in Ragunda was proposed also by Kornfält (1976).

A differentiation relation by fractional crystallization between the basic units and the syenitic units is not favoured on the following arguments. a) There is a compositional jump for several elements between these units (Figs. 59, 62), as well as a relative scarcity of data in the interval 56–58 % SiO_2. b) Field evidence for a suite of intermediate syenodiorites is lacking. When possible to observe, the contact relations between syenite units and basic units are sharp, usually indicating that the syenites are younger (e.g. syenite dykes in gabbro, K.-A. Kornfält unpubl data). c) The FeO*/FeO*+MgO ratios of the syenites and silicic rocks and their constituent minerals jump abruptly up to distinctly higher values, compared with the basic units. d) The transition by fractional crystallization between the basic and syenitic units requires the removal of cpx, most probably coprecipitating with plagioclase and Fe-Ti oxides. This would cause generally higher amounts of the REEs, steeper gradients (higher La_N/Yb_N ratios) in the syenites compared with the gabbros, which is not observed. Most of these arguments also contradict the model where the syenites are generated by a reaction/hybridization between a mantle-derived basic magma and the crust (Barker et al. 1975, Kornfält 1976).

Field relations between the peralkaline granites and metaluminous to peraluminous granites are not exposed in order to allow a close inspection of their relations, but they occur juxtaposed in the Strömsund complex (Fig. 55). In the Ragunda complex they occur close together, without sharp contacts, but the peralkaline ones were nevertheless related to the syenites by Kornfält (1976). Peralkaline and peraluminous granites cannot easily be related by any normal differentiation processes, and if related, this might be due to alkali-rich fluid transfer (Kinnaird and Bowden 1991) or crustal contamination of a peralkaline magma (Bailey & Schairer 1966). The latter is not particularly feasible, since relatively large amounts of peraluminous country rocks would have to be assimilated to achieve the relatively pronounced peraluminousity observed, e.g. in the Ragunda biotite granites (Kornfält 1976), and very little field evidence for such a process is at hand, e.g. xenoliths of sedimentary gneiss in the peraluminous granites (Kornfält 1976). There is also a volume problem associated with this process, because large volumes of peralkaline granites would be needed to generate the large volumes of peraluminous granites in, e.g. Ragunda, and this is not consistent with the relatively smaller volumes of syenite. It is theoretically possible to generate peraluminous granites from syenites by fractionation of feldspars, but such syenites would have to be slightly peraluminous from the beginning (Bailey & Schairer 1964). Since all syenites in Jämtland-Ångermanland are metaluminous with diopside in the norm, this is not an option.

The remaining option is differences in their mode of origin. It is thus suggested that the three units in the Jämtland–Ångermanland complexes were generated penecontemporaneously from three different sources, which provided three chemically distinct magmas. These magmas remained intact during intrusion, and were probably injected in relatively discrete pulses, as is indicated by the aeromagnetic map of the Ragunda complex (Persson 1996a), where the metaluminous to peraluminous granites occupy a central position in most cases. In Mårdsjö, the central gabbro, containing a minor granite body, represents a second injection pulse, intruding a gabbro syenite margin. Recent aeromagnetic data suggest that several additional pulses may be present in the Mårdsjö complex (A. Korja pers. comm. 1997). The other small complexes do not show any evidence of multiple injections.

It is probably not just fortuitous that the gabbros in general occupy a marginal position, which is especially evident in the Ragunda complex. The reason for this may be that the relatively more low-viscous basic magma acted as marginal lubricant in the passageways, and therefore was able to transport the more viscous intermediate and silicic magmas from their source levels to the final emplace-

ment levels. This is consistent with physical conditions considered appropriate for transport of composite dykes in conduits (e.g. Blake & Campbell 1986, Carrigan & Eichelberger 1990, Carrigan 1994). Furthermore, it can also explain the limited amount of mixing of the three magmas, as the more viscous magmas (silicic-intermediate) are relatively passively transported in central parts of the conduit (cf. chapter 6.5.2.). Interaction is also restrained by the physical differences of viscosity, temperature etc. (cf. e.g. Sparks & Marshall 1986, Frost & Mahood 1987, Fernandez & Barbarin 1991), and apparently essentially restricted to intermingling, which is widespread in the Ragunda and Mårdsjö complexes. The Hviddal giant dyke of southwestern Greenland (Upton 1962), with its marginal gabbros and central syenites, may represent an arrested feeder stage in such a scenario.

A model for the generation of the three magma units is as follows. The magmas of the basic units formed in the mantle, and were injected into the lower crust where they provided the heat that induced melting forming the other two magmas. Their quartz tholeiitic alkali-rich character is probably to some extent the result of crustal contamination at this stage (cf. discussion on the isotopes, chapter 6.5.3.2.). Both the syenites and the metaluminous/peraluminous magmas are considered to be generated within the crust, but from different protoliths. The granites can be generated by H_2O-undersaturated melting of undepleted granodioritic to tonalitic sources (e.g. Anderson 1983, Creaser et al. 1991, Skjerlie & Johnston 1993, Johannes & Holtz 1996, and ref. therein), rather than sources depleted after a previous melting event (Collins et al. 1982, Clemens et al. 1986, Whalen et al. 1987), since the latter should be depleted in the granitic constituents and dominantly consist of, e.g. pyroxene, garnet, and plagioclase (Creaser et al. 1991, Skjerlie & Johnston 1993, Singh & Johannes 1996). Such source lithologies are appropriate also for the other metaluminous-peraluminous rapakivi intrusives further east in central Sweden (Nordingrå, Rödön, and Strömsbro), and should contain a mixture of early Svecofennian and Archaean components, as indicated by the Nd isotopes above (chapter 6.5.3.2.). A more alkali-rich source lithology may also be present in lower crustal sections below Jämtlan–Ångermanland. This would be Revsund suite granitoids that failed to intrude to higher levels. Such a source may even easier produce the high alkali contents of the rapakivi granite magmas. Also this source would need an Archaean admixture, according to the isotopic data.

The syenites must be generated from less silicic sources. Such sources may be provided by a mafic lower crust enriched in alkalies due to metasomatism (e.g. Bailey & Schairer 1966, Bailey 1974, Macdonald 1987). It may also include depleted material after a previous melting, containing restitic zircon as indicated by the group of zircons recovered from the Nordsjö syenite having an age of 2.70±0.04 Ga (Claesson et al. 1997). More basic parts of the Revsund suite, e.g. monzodiorites (produced by mixing between basic and crustal melts in the deep crust, cf. chapters 4.5.2.4. and 4.5.3. on Småland–Värmland granitoids), may also be available for remelting, and in such a case metasomatism would not be necessary. This, however, still requires that the syenites can pick up "restitic" Archaean zircons. Thus, at least three "mafic" sources may be available in the lower crust to generate syenites upon renewed basic magma underplating: 1. Mafic essentially undepleted rock emplaced during a previous underplating episode, but metasomatically enriched in alkalies during or just previous to the Subjotnian melting event. 2. Depleted lower crustal material, restitic after a previous melting of essentially undepleted granodioritic-tonalitic source material. 3. Undepleted monzodioritic material, formed by an earlier extensive magmatic hybridization between magmas of mafic magmatic underplating event and crustal melts (presumably the Revsund event, c. 1.8 Ga). No metasomatism would then have to be invoked. Sources type 1 and 3 may be closely related and grade into each other, and the restitic material may be partly mixed into these previous magmas. Xenocrystic zircon may not, however, survive in such hot and presumably zircon-undersaturated basic melts, so at least partly the syenitic magmas should contain a component from the depleted (or even minor undepleted) crustal material.

From the discussion above, the following tentative scenario is proposed. Basic magmas are generated in the upper mantle, due to pressure release, in response to incipient extension of the cratonic Svecofennian lithosphere at c. 1.53 Ga. The mantle magmas intrude the lower crust and induce melting. The intrusions are comparatively minor and underplate discrete areas, as compared, e.g. with the presumably immense and geographically elongated underplating associated with the generation of the Transscandinavian igneous belt (see chapter 4.5.3.). The lower crust is heterogeneous, composed of depleted and undepleted parts. Melting in the lowest regions of K-rich mafic undepleted to restitic material generates the syenitic magmas, whereas undepleted crustal sources slightly higher up give rise to the rapakivi granite magmas. Both these sources contain a significant Archaean component. A

major Archaean component is also assimilated into the basic magmas (see chapter 6.5.3.2. on the Nd isotopes).

All three magma units intrude into the upper crust contemporaneously along crustal conduits produced in the relatively brittle crust during the incipient rifting. The separate identities of the magmas are well preserved as the much less viscous basic magma is able to transport the other two relatively passively while acting as a marginal lubricant. This intrusion mechanism thus restricted the interaction to essentially mingling of some granitic material in the gabbros. In the case of Rödön, evidence for basic magma cointrusion with the granite is lacking. Instead, intense mixing and mingling is observed in the associated dykes. On petrological arguments (see chapter 6.5.1.7. above) it can be inferred that this interaction took place in the dyke conduits or in a mid to upper crustal magma chamber where the basic magma was fractionating mainly cpx and plagioclase, from which the dykes were withdrawn. Similarly, the scatter of the Rödö dykes in a relatively wide area around the intrusion, as well as their strong chemical diversity, can be taken to infer that they have been extracted from a larger fractionating magma chamber at depths of a few kilometres, overlain by a silicic magma. The Rödö granite intrusion may thus be a small isolated high-level expression of a larger system deeper down, and some of the dykes have merely followed the same track to their uppermost crustal emplacement.

Substantial amounts of fluids were present in the Rödö magmas (see chapter 6.5.1.4. above), as indicated by the numerous cavities filled with calcite, quartz, chlorite, fluorite, etc, relatively high F contents, and high values of loss on ignition (LOI, see Appendix 2b). This is an indication that the upper fractionating magma chamber was situated at some depth, perhaps at midcrustal levels, because in a magma chamber at the uppermost crustal level the fluids would exsolve from the melt due to pressure release and dissipate out into the country rocks. The dykes from such a chamber should not contain so abundant exsolved fluids, especially not CO_2 which has lower solubility in silicate melts compared with H_2O (e.g. Holloway & Blank 1994, and ref. therein). A magma at some deeper section in the crust, on the other hand, could keep significantly greater amounts of fluids dissolved, which would be exsolved during dyke intrusion to the uppermost levels.

The abundant, especially calcite-filled, vugs in the basic Rödö dykes provide ample evidence that the mantle derived magmas brought substantial amounts of carbonic fluids into the crust during rapakivi magma formation. This is especially well documented in the mafic enclaves (of relatively primitive composition) chilled in the primitive hybrid porphyries, such that the centres of the enclaves are crowded with bubbles entrapped by the quenched margin (Plate 2g). The relatively high contents of fluorine in the basic rocks (c. 800–1000 ppm; Appendix 2b) also suggest that F was a major component in the mantle magmas. This evidence supports the concept of carbonic input in the lower crust by mafic underplating. No specific evidence at this point, however, indicates that the carbonic fluids brought significant amounts of mantle derived alkalies, but rather some silica since quartz is abundantly precipitated in the vugs.

In the uppermost mantle, in the stability range of amphibole (c. 10–20 kbar, 33–66 km), CO_2 is the dominating fluid since H_2O is partitioned into the amphibole (e.g. Watson et al. 1990). During mantle magma generation and emplacement in the lower crust the fluid phase will contain both CO_2 and H_2O, but CO_2 will exsolve and be released from the melt more readily due to its lower solubility (Holloway & Blank 1994, and ref. therein). Thus, there appears to be no doubt that the mantle supplies the crust with substantial amounts of CO_2. Especially intracontinental rifts usually bear clear evidence of this (e.g. Bailey & Macdonald 1987, and ref. therein). Upper mantle amphibole, phlogopite, and apatite contain F (and Cl) (Watson et al. 1990, and ref. therein), which may also be added to the crust with the underplated magmas. Some workers have also suggested that syenites (trachytes) may be derived from an upper mantle metasomatically enriched in alkali components (Bailey 1987), based, e.g. on the occurrence of ultramafic nodules in such rocks (e.g. Wright 1969). No ultramafic nodules are known from the Jämtland–Ångermanland syenites and a crustal origin is preferred here, as discussed above.

If the carbonic fluids were released to the lower crust they would induce dry F-rich conditions. This promotes the generation of A-type granitic magmas (cf. e.g. Manning 1981, Holtz et al 1992, Johannes & Holtz 1996), as dryer conditions drive the minimum melt compositions towards Or-richer parts of the granite system (Fig. 52). More F-rich conditions also shift the melting point towards more feldspatic compositions (Manning 1981), which may be a contributing factor in syenite formation. Fluorine also stabilizes biotite to higher temperatures (e.g. Peterson et al. 1991, Skjerlie & Johnston 1993). This evidence suggests that elevated temperatures of melting are required for rapakivi granite formation by

biotite dehydration-melting of undepleted granodiorite-tonalite sources at F-rich conditions. Small amounts of melts (<10 %) will be formed up to 950°C, and not more than 25 % up to 1050°C (Skjerlie & Johnston 1993). The experimental results of Skjerlie & Johnston (1993) thus suggest that more than 25 % melting at higher temperatures than 1050°C is required for the formation of A-type melts richer in, e.g. CaO than 1.8 %, MgO than 0.5 %, and TiO_2 than 0.7 %. This is generally not achieved in the Swedish rapakivi granites and therefore strongly suggests that relatively small amounts of basic rocks were underplated in the Subjotnian event which were generally unable to raise the temperatures of the source regions above 1050°C. Only in the largest complexes in the shield, e.g. Wiborg, is the chemical composition of the wiborgites partly "basic" enough (cf. e.g. Hackman 1934, Vorma 1971, Rämö 1991, Rämö & Haapala 1995) to allow the interpretation that 1050°C was exceeded in the source regions. This is, in all probability, linked to a larger volume of basic magma input, which is also evident from the larger volumes of silicic magma production. A component of mixing may also be concealed in the chemistry of the least silicic wiborgites (Eklund et al. 1991, Andersson 1991).

A substantial portion of the carbonic mantle fluids appears in the case of Rödön to have been engulfed in the silicic magmas, perhaps by fluid transfer from the crystallizing underlying basic magma to the immediately overlying crustal rapakivi magma. The solubility of CO_2 in rhyolitic melts may be slightly less than that of basalts, but the experimental data are not unambiguous (cf. Blank & Brooker 1994, and ref. therein). The data suggests that in a Rödö magma chamber in the deepest crust, almost similar amounts of CO_2 can be dissolved in the basic and silicic magmas. Upon entering higher levels in the crust, this high fluid content is released as a separate phase in the silicic magmas. It is contained as bubbles in the relatively viscous silicic magmas and is preserved in this condition in the relatively primitive QFP dykes. Additional fluids may be transferred from the basic to the silicic magma in the upper chamber. Also the basic magmas exsolve their fluid contents at the uppermost levels, preserved in the cavities of the Rödö dolerites.

The Jämtland–Ångermanland rocks seem to be less volatile-rich (generally lower F and LOI contents; Appendix 2b), which may be due to lower amounts originally contained in the basic mantle-derived magmas and the crustal source regions. It may also be an effect of degassing upon plutonic intrusion to high crustal levels. The latter is supported by the somewhat higher volatile contents of the Nordsjö dykes compared with the plutonics. Furthermore, if the syenites are derived partly from depleted sources their volatile contents should be lower, at least with regards to F and H_2O, while the CO_2 is supplied mainly by the underplated magma.

Finally, the fact that syenites and peralkaline rocks occur in Jämtland–Ångermanland in the west (Fig 31) but not in the east along the coast, and further east in Finland (with the exception of minor alkali syenitic dykes in Suomenniemi; Rämö 1991) and Russian Karelia, deserves some comment. This feature seems to be spatially related to the rocks of the Revsund granitoid suite. Thus, it may be related to the substantial reorganization of the lower crust that must have taken place at that time. In the areas of the crust affected by the extraction of the Revsund granitoids, the lower crust is expected to contain more basic underplated material as well as larger proportions of restitic depleted material, compared with the rest of the Svecofennian crust further to the east, where undepleted more felsic sources should be ubiquitous. Such differences in lower crustal lithologies should favour syenite formation in the west, and silica-oversaturated rapakivi granites in the east.

9. Summary of main results

- Småland–Värmland granites with compositions around c. 70 % SiO_2 or slightly more can be derived by 25–40 % melting of tonalitic-granodioritic lower crustal sources. Granitoids with lower SiO_2 contents than c. 70 % have probably experienced some hybridization with a basic component.
- The most primitive basic rocks in the Tjällmo–Vättern zone (TVZ) and Tiveden (associated with the Småland-Värmland granitoids) can be derived by c. 25–30 % melting of spinel-plagioclase lherzolites, similar to those encountered in the area. The phlogopite-rich lherzolites are interpreted as representing an enriched uppermost continental mantle.
- The more evolved rocks in the basic suite in the TVZ and Tiveden can be derived by c. 30–45 %

fractional crystallization of dominantly clinopyroxene, with olivine and/or orthopyroxene and minor plagioclase, from the most primitive magmas in the suite.

- The strongly evolved magmas represented by the mafic enclaves have marked geochemical affinities to lamprophyres. They may be derived by extended fractionation (>80 %) from the evolved gabbro magmas of mainly clinopyroxene and plagioclase.
- Two distinct types of hybrid rocks have been discerned in the Småland–Värmland suite. One with highly evolved basic endmembers, similar to the mafic enclaves (Kårtorp hybrids), and one with less evolved basic endmembers (Tiveden hybrids). The latter seem to contain also a cumulus (mainly feldspar) component. In both cases the silicic endmember is Småland-Värmland granites (Filipstad type) with a composition close to 70 % SiO_2.
- An event of voluminous basic underplating is proposed as being responsible for the lower crustal melt generation forming the Transscandinavian igneous belt. This magmatism may have been activated in response to an extensional collapse along deep crustal listric shear zones of the overthickened orogenic Svecofennian crust. Extensive plutonic magma mixing occurred in the lower crust and during entrainment of the basic magmas in the crustal magmas buoyantly rising to their emplacement levels in the middle crust. The abundant quartz monzonitic to monzodioritic hybrid Småland–Värmland rocks are associated with strong positive magnetic anomalies.
- Nd and Sr isotopic data support the interpretations from geochemistry that the hybrid rocks have formed through mixing of basic and silicic endmembers, as well as a derivation of the Småland-Värmland granites from an early Svecofennian metaigneous crust. Isotopically, the nature of the mantle source for the basic magmatism is generally mildly depleted, but some parts of the magmas derive from more strongly depleted mantle.

- The rapakivi complexes in central Sweden are 1.53–1.50 Ga old (except Nordingrå, 1.58 Ga). This means that the westernmost of the Fennoscandian rapakivi complexes are the youngest, and, excluding the Salmi batholith in east, a general westwards younging of the complexes.
- Strong fractionation has operated in the silicic Rödö rapakivi suite, involving up to 90 % crystallization or more (of K-feldspar, quartz, plagioclase, minor amphibole and Fe-Ti-oxides, and sometimes a little apatite and zircon) to arrive at the most evolved residual liquids, represented by some quartz-feldspar porphyry dykes and aplites. A fluid phase has been an important controlling factor in this evolution, and, e.g. precipitated Ca-LREE-fluorocarbonates.
- Two generations of hybrid porphyries have formed by magma mixing of primitive and evolved endmembers of the basic and silicic Rödö suites.
- The Jämtland-Ångermanland complexes have formed from three coeval but not comagmatic units: a basic unit, a syenitic-peralkaline silicic unit, and a met- to peraluminous silicic unit. These were generated from three different sources: the mantle, a depleted silicic-undepleted basic lower crust, and an undepleted silicic lower crust, respectively. The basic magma intruded the lower crust and induced melting that formed the other two, and they intruded along the same channelways to the upper crust.
- The peralkaline silicic rocks can be derived by crystal fractionation from a syenitic parental magma, by 55–70 % crystallization of dominantly one feldspar (anorthoclase) (c. 80 %), Fe-Ti-oxides, clinopyroxene, fayalite and minor apatite. This fractionating assemblage is supported by the phenocryst assemblage in trachyte dykes associated with the Nordsjö massif. The trachyte dyke is, in itself, evidence that magmas of this composition were present in the complexes. Most of the syenites also show geochemical evidence of a cumulus (mainly feldspar) component.
- Low initial Nd and Pb isotopic values strongly indicate a major Archaean component in the central Swedish rapakivi magmatism. This is verified by a group of zircons recovered from the Nordsjö syenite, all with the age 2.70±0.04 Ga. The conclusion is that a significant part of the lowermost crust in central Sweden is Archaean in age, probably rifted off the Archaean craton in the northeast in an earlier, Presvecofennian stage.

10. Acknowledgements

The person I wish to mention first is my wife Anne, who had to put up with a great deal during these years, especially the last two when I finally got myself together and started to write-up my thesis. I´ve often been an irritated and not particularly tender husband during this time, but she never gave up and helped me see through the dark periods, for which I am deeply grateful. Despite my three-year-old daughter Linn not seeing much of me her first years, she was nevertheless able to develop an intense feeling of affection for her father, which strengthened me during my work.

My parents didn´t really know what I was doing all this time, but they had brought me up in the positive spirit that it mattered to achieve something, which has been inspiring. My grandfather was perhaps the first to inspire me in the natural sciences, especially while helping him with his bee-keeping. My sister left for America early on, but came back to Europe and has been of increasing support during the years. My parents-in-law have also been of great support.

Professor Hans Annersten has perhaps not been a brilliant supervisor, but he let me go my own way and provided valuable scientific freedom. Although the project initially was vague and we had numerous conflicts on adminstrative matters (since I was very active as a student representative), we finally managed to establish a good relationship, which I appreciate. During the final stages, raising funds for covering the printing costs, he provided very valuable support. Anders Wikström at the Geological Survey of Sweden (SGU) was the one who initiated my research and proposed a project in the first place. I was employed as "extra geologist" by the SGU under his leadership during many field seasons, and he was an excellent teacher of field geology. He has been a continuous source of support, although I think he doubted for some time that there would ever be a thesis.

At one stage I decided that my work had to be supplemented with some isotope geological data to support my other results. I wrote to Professor Stefan Claesson and asked if I could come to the Laboratory for Isotope Geology at the Swedish Museum of Natural History (LIG) in Stockholm and conduct some work. He was very positive to the idea and welcomed me to the lab, for which I am most grateful. As it turned out, I spent six years travelling back and forth to the isotope lab, learning the trade with numerous samples, although probably never reaching a proper standard as an isotope geologist. My first and thorough teacher of this trade was Dr Torbjörn Skiöld, who initiated me into the mysteries and showed me how to do it. After this I was rather self-dependant, however, several persons were of invaluable help, partly stopping me from making too many fatal mistakes. These perls were Hans Schöberg, Ann-Marie Kähr, Paula Allart, Åke Johansson, Per-Olof Persson, Joakim Mansfeld, Lars-Gunnar Jarl, Marina Fischerström, and Kjell Billström.

When I started with rapakivi granites and related stuff, I soon come into contact with Olav (Joffi) Eklund in Turku, and we developed a fruitful cooperation, full of intense discussions, that has continued even though Olav took his Ph.D. already in 1993. During the last few years Sören Fröjdö has joined the group in Turku, and with this guy I have had many stimulating discussions and collaborations, especially over the Internet. Lately, also Alex Shebanov (Turku/St.Peterburg) has strongly influnced my thinking, especially concerning fluids. In addition to these collegues, I have benefitted from scientific discussions, especially with Dr. Leonid Neymark (Denver/St.Petersburg), to whom I am very grateful for contributing not only his analytical skills, but also for his keen interest in the problems and for sharing his vast knowledge in isotope geology. I also would like to thank Dr. Kjell Billström for doing analytical work of pure interest, which I have been able to use in this thesis, and for discussions related to Pb isotopes. Other people with whom I have had stimulating scientific discussions are Martin Ahl, Sandy Cruden, Roberto Weinberg, Thomas Lundqvist, and Stefan Claesson. Hans Annersten, Anders Wikström, Sören Fröjdö, Leonid Neymark, Olav Eklund, and Rolf Romer provided valuable comments on earlier versions of the manuscript. The final version, however, remains entirely my responsibility.

Through their professional skill, a number of people have made this thesis possible. I particularly would like to mention the following: Christina Wernström, who skillfully drew most of the figures and put up with my endless changing of them. The late Olle Wallner, who without complaints prepared an endless row of thin sections. Also Majid Hadavi prepared innumerable thin sections. Hans Harrysson operated the different microprobes patiently over a long time in a very professional manner. Anne-Marie Karlsson performed all wet chemical whole-rock analyses reported in Appendix 2a. I would also like to thank Carl-Magnus Backman for giving me access to the sample preparation lab at SGU, and advice concerning chemical analysis. Kersti Gløersen took care of all financial and other problems, and though we´ve had major quarrels, this is all forgotten now.

Finally, would like to mention some friends and collegues, with whom I have had stimulating discussions, though not necessarily scientific. My former room-mates Olof Kruse, Lena Larsson and Sten-Anders Smeds, all achieved their degrees before me. Olof K. was the first, an uncrowned master of bluff languages, who manged to

find a well-paid job in industry. Lena L. actually made her B.Sc.-thesis supervised partly by me, and then suddenly she was a doctor, and I was the eternal student. Sten-Anders S. contributed continuously from his enormous collections of burlesque jokes, and towards his dissertation also an increasing number of sighs. Henrik Skogby and Madis Roots were famous for being nice guys, but with a low profile. This may apply also to Katalin Holenyi, although she is not a guy. In the longstanding group playing badminton in the early mornings, Henrik was the weakest link. He upheld this position until he left and was succeeded by Sandy Cruden. The two other guys, nearly as good as I, were Stefan Bergman and Per Nysten. These two red-bearded gentlemen and I have hit the little featherball continuously for more than ten years. Sandy learned fast, but left for Canada before he reached the advanced level. He was replaced by Roberto Weinberg who played well, but not well enough, and finally by Mariusz Kalinowski, who is still learning.

Leaving sports, Erika Ingvald must be regarded as an important positive social factor at the institute (and for me), always ready to party. This also applies to Sofie Jönsson, not late to be part of social activities. Frequent organizers of our Thank God Its Friday beer parties have been Anders Hallberg, Anna Åberg, Jeanette Bergman-Weihed, Pär Weihed to name a few, and frequent drinkers, e.g. Raymond Munier and Jan Hermansson. Lena Lundqvist never believed she was any good, which was of course not true, and left Uppsala much too early to disprove it (and took a degree in Gothenburg instead). During the field seasons, working for the SGU, I was fortunate to work together with Anna Schytt, who arranged less fashionable, but picturesque and cheap lodgings. Johan Lövgren was also glad spirit in the field, always living in his old caravan. At the Natural History Museum I have, in addition to the isotope geologists, been especially intellectually stimulated by Dan Holtstam, and his knowledge in widely separated fields. In addition to the people named above, I would like to mention also Ala Adin Aldahan, Örjan Amcoff, Ryo Anma, Yngve Cerenius, Tore Ericsson, Patrik Häggkvist, Hemin Koyi, Sadoon Morad, Genene Mulugeta, Peter Rönnlund, Håkan Sjöström, Dimitrios Sokoutis, Varghese Swamy, Chris Talbot, and Ruud Weijermars. Thanks all of you (and those I unwillingly have forgotten) for good companionship over the years.

The work in this thesis was largely financially supported by the Geological Survey of Sweden. Smaller grants came from funds of the Royal Academy of Sciences, Uppsala University, and Geological Section of the Natural Sciences Student Society (Geologiska Sektionen). Printing costs were covered by SGU and Uppsala University. The English was corrected by Nigel Rollinson. All analytical data presented can be obtained from the author in digital form on request. Sampled material including thin sections, specimens, rock powders etc is available for further study by agreement with the author.

11. References

GFF = Geologiska Föreningens i Stockholm Förhandlingar
SGU = Sveriges Geologiska Undersökning (Geological Survey of Sweden)

Åberg, G., 1988: Middle Proterozoic anorogenic magmatism in Sweden and worldwide. Lithos 21, 279–289.

Åberg, G. & Bollmark, B., 1985: Retention of U and Pb in zircons from shocked granite in the Siljan impact structure, Sweden. – Earth Plan. Sci. Lett. 74, 347–349.

Åberg, G. & Charalampides, G., 1986: New lead isotope data from the Långban mineralization, central Sweden. – GFF 108, 243–250.

Ahl, M., 1989: Zn-Pb-Cu-mineraliseringarna vid Ramnebo, sydöstra Sverige, och deras genetiska relation till Smålandsgraniten. – M.Sc.-thesis, Stockholm Univ., 26 pp.

Ahl, M., 1991: Geological and geochemical control of Sn-Pb-Zn-Be-greisen bearing granitoids in the Dala region, central Sweden. – Geol. Survey Finl., Guide 34, 3.

Ahl, M., 1994: Geochemistry, mineralogy and fluid inclusions of Sn-greisen mineralizations in the Siljan/Garberg and Rätan granitoids, central Sweden. – IMA, 16th General Meeting, Pisa, Italy. Abstracts vol. p. 4.

Ahl, M. & Sundblad, K., 1994: Geology and geochemistry of the Rätan batholith, central Sweden. Joint meeting on anorthosites, rapakivi granites and related rocks, IGCP 290 and 315, Montreal, 1–3/8 1994, Program and abstracts, p. 1.

Ahl, M., Sundblad, K., & Schöberg, H., in prep.: Geology, geochemistry, age and geotectonic evolution of the Dala granitoids, central Sweden.

Allen, C.M., 1991: Local equilibrium of mafic enclaves and granitoids of the Turtle pluton, southeast California: mineral, chemical, and isotopic evidence. – Am. Miner. 76, 574–588.

Amelin, Y.V., Larin, A.M. & Tucker, R.D., 1997: Chronology of multiphase emplacement of the Salmi rapakivi granite-anorthosite complex, Baltic shield: implications for magmatic evolution. – Contr. Mineral. Petrol. 127, 353–368.

Anderson, J.L., 1983: Proterozoic anorogenic granite plutonism of North America. – Geol. Soc. Am. Mem. 161, 133–154.
Anderson, J.L. & Cullers, R.L., 1978: Geochemistry and evolution of the Wolf River batholith, a late Precambrian rapakivi massif in north Wisconsin, U.S.A. – Prec. Res. 7, 287–324.
Andersson, U.B., 1989: Evidence of plutonic magma-mixing, southern Sweden. – Rendiconti Soc. Ital. Mineral. Petrol. 43, 831–839.
Andersson, U.B., 1991: Granitoid episodes and mafic-felsic magma interaction in the Svecofennian of the Fennoscandian shield, with main emphasis on the ≈1.8 Ga plutonics. – Prec. Res. 51, 127–149.
Andersson, U.B., 1994: Svenska rapakivigraniter. – Slutrapport, SGU 941107. (Unpubl. report.)
Andersson, U.B., 1997a: The sub-Jotnian Strömsbro granite complex at Gävle, Sweden. – GFF 119, 159–167.
Andersson, U.B., 1997b: The late Svecofennian, high-grade contact and regional metamorphism in southwestern Bergslagen (central southern Sweden). – Final report, SGU. (Unpubl. report.) 36 pp.
Andersson, U.B. & Eklund, O., 1994: Cellular plagioclase intergrowths as a result of crystal-magma mixing in the Proterozoic Åland rapakivi batholith, SW Finland. – Contr. Min. Petr. 117, 124–136.
Andersson, U.B.; Larsson, L. & Wikström, A., 1992: Charnockites, pyroxene granulites and garnet-cordierite gneisses at a boundary between Early Svecofennian rocks and Småland–Värmland granitoids, Karlskoga, southern Sweden. – GFF 114, 1–15.
Andresen, A., 1980: The age of the Precambrian basement in western Troms, Norway. – GFF 101, 291–298.
Arawaka, T. & Shinmura, T., 1995: Nd-Sr isotpic geochemical characteristics of two contrasting types of calc-alkaline plutons in the Hida belt, Japan. – Chem. Geol. 124, 217–232.
Armands, G. & Drake, K.-M., 1978: Litogeokemisk malmprospektering. STU-rapport 77-4170. Innumerable pp.
Armands, G. Xefteris, A., 1987. Swedish granitoids of S- and I-type and their lithophile element distribution. – GFF 109, 177–195.
Arth, J.G., 1976: Behaviour of trace elements during magmatic processes - a summary of theoretical models and their applications. – J. Res. USGS 4, 41–47.
Arzi, A.A., 1978: Critical phenomena in the rheology of partially molten rocks. – Tectonoph. 44, 173–184.
Ashwal, L.D., 1993: Anorthosites. Minerals and rocks 21. – Springer-Verlag, Berlin, 422 pp.
Asklund, B., 1939: Berggrunden. *In* R. Sandegren, B. Asklund och A.H. Westergård: Beskrivning till kartbadet Gävle. – SGU Aa 178, 143 pp.
Ayrton, S.N., 1988: The zonation of granitic plutons: the "failed ring-dyke" hypothesis. Schweiz. – Min. Petr. Mitt. 68, 1–19.
Ayrton, S.N., 1991: Appinites, lamprophyres and mafic microgranular enclaves: three related products of interaction between acid and basic magmas. *In* Didier, J. & Barbarin, B. (eds.) 1991. Enclaves and granite petrology. Developments in petrology 13. – Elsevier, Amsterdam, pp. 465–476.
BABEL working group, 1990: Evidence for early Proterozoic plate tectonics from seismic reflection profiles in the Baltic shield. – Nature 348, 34–38.
Bailey, D.K., 1974: Melting in the deep crust. In, Sörensen, H. (ed.): The alkaline rocks. – Wiley, London, pp. 436–442.
Bailey, D.K., 1987: Mantle metasomatism – perspective and prospect. *In* Fitton, J.G. & Upton, B.G.J. (eds.): Alkaline igneous rocks. – Geol. Soc., Spec. Publ. 30, 1–13.
Bailey, D.K. & Schairer, J.F., 1964: Feldspar-liquid equilibria in peralkaline liquids – the orthoclase effect. – Am. J. Sci. 262, 1198–1206.
Bailey, D.K. & Schairer, J.F., 1966: The system Na_2O-Al_2O_3-Fe_2O_3-SiO_2 at 1 atmosphere, and the petrogenesis of alkaline rocks. – J. Petr. 7, 114–170.
Bailey, D.K. & Macdonald, R., 1970: Petrochemical features of mildly peralkaline (comenditic) rhyolite glasses from the continents and the ocean basins. – Contr. Miner. Petr. 28, 340–351.
Bailey, D.K. & Macdonald, R., 1987: Dry peralkaline felsic liquids and carbon dioxide flux through the Kenya rift zone. *In* Mysen, B.O. (ed.): Magmatic processes: physicochemical principles. – Geochem. Soc., Spec. Publ. 1, 91–105.
Baker, B.H., 1987: Outline of the petrology of the Kenya rift alkaline province. *In* Fitton, J.G. & Upton, B.G.J. (eds.): Alkaline igneous rocks. – Geol. Soc., Spec. Publ. 30, 293–311.
Baker, B.H., Goles, G.G., Leeman, W.P., & Lindstrom, M.M., 1977: Geochemistry and petrogenesis of a basalt-benmoreite-trachyte suite from the southern part of the Gregory Rift, Kenya. – Contr. Miner. Petr. 64, 303–332.
Baker, D.R., 1989: Tracer versus trace element diffusion: diffusional decoupling of Sr concentration from Sr isotopic composition. – Geoch. Cosmoch. Acta 53, 3015–3023.
Baker, J.H., Hellingwerf, R.H., & Oen, I.S., 1988: Structure, stratigraphy, and ore-forming processes in Bergslagen: implications for the development of the Svecofennian of the Baltic shield. – Geol. Mijnb. 67, 121–138.
Banks, D.A., Yardley, B.W.D., Campbell, A.R., & Jarvis, K.E., 1994: REE composition of an aqueous magmatic fluid: a fluid inclusion study from the Capitan Pluton, New Mexico. – Chem. Geol. 113, 259–272.
Barbarin, B., 1989: Importance des différents processus d'hybridation dans les plutons granitiques du batholite de la Sierra Nevada, Californie. – Schw. Min. Petr. Mitt. 69, 303–315
Barbarin, B., 1990a: Plagioclase xenocrysts and mafic magmatic enclaves in some granitoids of the Sierra Nevada batholith, California. – J. Geoph. Res. 95, 17747–17756.
Barbarin, B., 1990b: Granitoids: main petrogenetic classification. – Geol. J. 25, 227–238.
Barbarin, B. & Didier, J., 1992: Genesis and evolution of mafic microgranular enclaves through various types of interaction between coexisting felsic and mafic magmas. – Trans. Roy. Soc. Edinb., Earth Sci. 83, 145–153.
Barker, F., Wones, D.R., Sharp, W.N., & Desborough, G.A., 1975: The Pikes Peak batholith, Colorado Front Range, and a model for the origin of the gabbro-anorthosite-syenite-potassic granite suite. – Prec. Res. 2, 97–160.
Basaltic volcanism study project 1981: Basaltic volcanism on the terrestrial planets. – Pergamon, New York, 1286 pp.

Batchelor, R.A. & Bowden, P., 1985: Petrogenetic interpretation of granitoid rock series using multicationic parameters. – Chem. Geol. 48, 43–55.

Bateman, R., 1995: The interplay between crystallization, replenishment and hybridization in large felsic magma chambers. – Earth-Sci. Rev. 39, 91–106.

Bédard, J., 1990: Enclaves from the A-type granite of the Mégantic complex, White Mountain magma series: clues to granite magmagenesis.– J. Geoph. Res. 95, 17797–17819.

Berg, J.H., 1980: Snowflake troctolite in the Hettasch intrusion, Labrador: evidence for magma-mixing and supercooling in a plutonic environment. – Contr. Miner. Petr. 72, 339–351.

Bergman, L., 1986: Structure and mechanism of intrusion of Postorogenic granites in the archipelago of southwestern Finland. – Acta Academiae Aboensis, Ser. B, Vol. 46, nr 5, 74 pp.

Bergman, S.C., 1987: Lamproites and other potassium-rich igneous rocks: a review of their occurrence, mineralogy and geochemistry. *In* Alkaline igneous rocks, Fitton, J.G. & Upton, B.G.J. (eds.). – Geol. Soc. Spec. Publ. 30, 103–189.

Berthelsen, A. & Marker, M., 1986: 1.9-1.8 Ga old strike-slip megashears in the Baltic shield, and their plate-tectonic implications. – Tectonoph. 128, 163–181.

Beunk, F.F., Page, L.P., Wijbrans, J.R. & Barling, J., 1996: Deformational, metamorphic, and geochronological constraints from the Loftahammar-Linköping deformational zone (LLDZ) in SE Sweden: implications for the development of the Svecofennian orogen. – GFF 118, A9.

Billström, K. 1985: Isotopic studies of two early Proterozoic sulphide ores in the Bergslagen district, south-central Sweden. – Medd. Stockh. Univ. Geol. Inst. N:r 263 (Ph.D.-thesis), 141 pp.

Billström, K., 1989: A model for the lead isotope evolution of early Proterozoic Svecofennian sulphide ores in Sweden and Finland. – Chem. Geol. 79, 307–316.

Billström, K. & Vivallo, W., 1994: Synvolcanic mixing of ore lead and the development of lead isotopic provinces in the Skellefte district, Sweden. – Min. Depos. 29, 111–119.

Billström, K. & Weihed, P., 1996: Age and provenance of host rocks and ores in the Paleoproterozoic Skellefte district, northern Sweden. – Econ. Geol. 91, 1054–1072.

Björk, L., 1985: Beskrivning till berggundskartan Filipstad NV. – SGU Af 147, 110 pp.

Björk, L., 1988: Berggrundskartorna 20 I Björna NO, SO. – SGU Ai 24, 26.

Björk, L., 1995: Berggrunden på kartbladen 22G Vilhelmina NO och SO, 22H Järvsjö och 22I Lycksele. – SGU Rapp. & Medd. 79, 63–67.

Björklund, L. and Claesson, S., 1992: Geochemical character and preliminary Sm-Nd data on basic metavolcanic rocks in the Tiveden area, south Sweden. – GFF 114, 340–341.

Black, S., Macdonald, R. & Kelly, M.R., 1997: Crustal origin for peralkaline rhyolites from Kenya: evidence from U-series disequilibria and Th-isotopes. – J. Petr. 38, 277–297.

Blake, D.H., Elwell, R.W.D., Gibson, I.L., Skelhorn, R.R. & Walker, G.P.L. (1965): Some relationships resulting from the intimate association of acid and basic magmas. – Quart. J. Geol. Soc. Lond. 121, 31–49

Blake, S. & Campbell, I.H., 1986: The dynamics of magma-mixing during flow in volcanic conduits. – Contr. Miner. Petr. 94, 72–81.

Blank, J.G. & Brooker, R.A., 1994: Experimental studies of carbon dioxide in silicate melts: solubility, speciation, and stable carbon isotope behaviour. *In* Carroll, M.R. & Holloway, J.R. (eds.): Volatiles in magmas. – Rev. in Mineral. Vol. 30. Mineral. Soc. of America, pp. 157-186.

Blank, J.G., Stolper, E.M. & Carroll, M.R., 1993: Solubilities of carbon dioxide and water in rhyolitic melt at 850°C and 750 bars. – Earth Plan. Sci. Lett. 119, 27–36.

Blomberg, A., 1895: Praktiskt geologiska undersökningar inom Gefleborgs län. – SGU C 152, 209 pp.

Blundy, J.D. & Sparks, R.S.J., 1992: Petrogenesis of mafic inclusions in granitoids of the Adamello massif, Italy. – J. Petr. 33, 1039–1104.

Bowen, N.L., 1945: Phase equilibria bearing on the origin and differentiation of alkline rocks. – Am. J. Sci. 243A, 75–89.

Boyd, W.W., Jr., 1972: Diabase variation and genesis. – Bull. Geol. Soc. Finl. 44, 21–34.

Branigan, N.P., 1989: Hybridization in middle Proterozoic high-level ring complexes, Åland, SW Finland. – Prec. Res. 45, 83–85

Brown, P.E. & Becker, S.M., 1986: Fractionation, hybridisation and magma mixing in the Kialineq centre, east Greenland. – Contr. Min. Petr. 92, 57–70.

Burt, D.M., 1989: Compositional and phase relations among rare earth element minerals. *In* Lipin, B.R. & Mckay, G.A. (eds.): Geochemistry and mineralogy of rare earth elements. – Rev. in Miner. Vol. 21. Mineral. Soc. America, pp. 259–307.

Bussy, F., 1987. Interactions physico-chimique entre le granite du Mont-Blanc et ses enclaves. – Schw. Miner. Petr. Mitt. 67, 380–384.

Bussy, F., 1990: The rapakivi texture of feldspars in a plutonic mixing environment: a dissolution-recrystallization process? – Geol. Jour. 25, 319–324.

Bussy, F. & Ayrton, S., 1990. Quartz textures in dioritic rocks of hybrid origin. –Schweiz. Min. Petr. Mitt. 70, 223–235.

Cabanis, B. & Lecolle, M., 1989: Le diagramme La/10-Y/15-Nb/8: un outil pour la discrimination des series volcaniques et la mise en evidence des processus de melange et/ou de contamination crustale. – C.R. Acad. Sci. Ser. II 309, 2023–2029.

Carlsson, G.A., 1880: Beskrifning till kartbladet "Norsholm". – SGU Aa 79, 35 pp.

Carmichael, I.S.E. & MacKenzie, W.S., 1963: Feldspar-liquid equilibria in pantellerites: an experimental study. – Am. J. Sci. 261, 382–396.

Carrigan, C.R., 1994: Two-component magma transport and the origin of composite intrusions and lava flows. *In* Ryan, M.P. (ed.): Magmatic systems. – Academic Press, pp. 319–354.

Carrigan, C.R. & Eichelberger, J.C., 1990: Zoning of magmas by viscosity in volcanic conduits. – Nature 343. 248–251.

Carroll, M.R. & Webster, J.D., 1994: Solubilities of sulfur, noble gases, nitrogen, chlorine, and fluorine in magmas. *In* Carroll, M.R. & Holloway, J.R. (eds.): Volatiles in magmas. – Rev. in Mineral. Vol. 30. Mineral. Soc. of America, pp. 231–279.

Castro, A., Moreno-Ventas, I., & De la Rosa, J.D., 1991: H-type (hybrid) granitoids: a proposed revision of the granite type classification and nomenclature. – Earth-Sci. Rev. 31, 237–253.

Castro, A., De la Rosa, J.D., Fernández, C, & Moreno-Ventas, I., 1995: Unstable flow, magma mixing and magma-rock deformation in a deep-seated conduit: the Gil-Márquez complex, south-west Spain. – Geol. Rundsch. 84, 359–374.

Chappell, B.W., 1996: Magma mixing and the production of compositional variation within granite suites: evidence from the granites of southeastern Australia. – J. Petr. 37, 449–470.

Chappell, B.W. and White, A.J.R., 1974: Two contrasting granite types. – Pac. Geol. 8, 173–174.

Christiansen, E.H., 1996: Are Cenozoic topaz rhyolites of western North America the erupted equivalents of rapakivi granites? Seventh international symposium on rapakivi granites and related rocks. – Helsingfors, 24-26/7 1996. Abstract Vol., p. 15.

Christiansen, E.H., Burt, D.M., Sheridan, M.F. & Wilson, R.T., 1983: The petrogenesis of topaz rhyolites from western United States. – Contr. Min. Petr. 83, 16–30.

Christiansen, E.H., Bikun, J.V., Sheridan, M.F. Burt, D.M., 1984: Geochemical evolution of topaz rhyolites from the Thomas Range and Spor Mountain, Utah. – Am. Min. 69, 223–236.

Christiansen, E.H., Sheridan, M.F. & Burt, D.M., 1986: The geology and geochemistry of Cenozoic topaz rhyolites from the western United States. – Geol. Soc. Am., Spec. Paper 205, 82 pp.

Christiansen, E.H. & Venchiarutti, D.A., 1990: Magmatic inclusions in rhyolites of the Spor Mountain formation, western Utah: limitations on compositional inferences from inclusions in granitic rocks. – J. Geopys. Res. 95, 17717–17728.

Civetta, L., Cornette, Y., Crisci, G., Gillot, P.Y., Orsi, G., & Requejo, C.S., 1984: Geology, geochronology and chemical evolution of the island of Pantelleria. – Geol. Mag. 121, 541–668.

Claesson, L-Å., 1985: The geochemistry of early Proterozoic metavolcanic rocks hosting massive sulphide deposits in the Skellefte district, northern Sweden. – J. Geol. Soc., Lond. 142, 899–909.

Claesson, S., 1987: Nd isotope data on 1.9–1.2 Ga old basic rocks and metasediments from the Bothnian basin, central Sweden. – Prec. Res. 35, 115–126.

Claesson, S. and Lundqvist, Th., 1995: Origins and ages of Proterozoic granitoids in the Bothnian basin, central Sweden: isotopic and geochemical constraints. – Lithos 36, 115–140.

Claesson, S. & Kresten, P., 1997: The anorogenic Noran granite – a Mesoproterozoic rapakivi intrusion in south-central Sweden. – GFF 119, 115–122.

Claesson, S., Huhma, H., Kinny, P.D. & Williams, I.S., 1993: Svecofennian detrital zircon ages – implications for the Precambrian evolution of the Baltic shield. – Prec. Res. 64, 109–130.

Claesson, S., Andersson, U.B., Schuhmacher, M., Sunde, T., Whitehouse, M. & Vestin, J., 1997: Inherited Archaean components in a Mesoproterozoic rapakivi complex from Central Sweden: implications from SIMS U-Pb imaging and spot analysis of zircon. EUG 9 meeting (European Union of Geosciences), Strasbourg, 23–27/3 1997. – Abstract Supplement No 1, Terra Nova Vol. 9, p. 356.

Clarke, D., Mengel, F., Coish, R.A., & Kosinowski, M.H.F., 1994: Program Newpet, Version 94.01.07.

Clemens, J.D., 1992: Partial melting and granulite genesis: a partisan overview. – Prec. Res. 55, 297–301.

Clemens, J.D., Holloway, J.R. & White, A.J.R., 1986: Origin of an A-type granite: Experimental constraints. – Am Mineral 71, 317–324.

Collins, W.J., 1996: Lachlan fold belt granitoids: products of three-component mixing. – Trans. Roy. Soc. Edinb., Earth Sci. 87, 171–181.

Collins, W.J., Beams, S.D., White, A.J.R. & Chappell, B.W., 1982: Nature and origin of A-type granites with particular reference to southeastern Australia. – Contr. Min. Petr. 80,189–200.

Congdon, R.D. & Nash, W.P., 1991: Eruptive pegmatite magma: rhyolite of the Honeycomb Hills, Utah. – Am. Min. 76, 1261–1278.

Connelly, J.N. & Åhäll, K.-I., 1996: The Mesoproterozoic cratonization of Baltica – new age constraints from SW Sweden. *In* Brewer, T.S. (ed.): Precambrian crustal evolution in the north Atlantic Region. – Geol. Soc., Spec. Publ. 112, 261–273.

Connelly, J.N., Berglund, J., & Larson, S.Å., 1996: Thermotectonic evolution of the eastern segment of southwestern Sweden: tectonic constraints from U-Pb geochronology. *In* Brewer, T.S. (ed.): Precambrian crustal evolution in the north Atlantic Region. – Geol. Soc., Spec. Publ. 112, 297–313.

Conrad, W.K., Nicholls, I.A., & Wall, V.J., 1988: Water-saturated and -undersaturated melting of metaluminous and peraluminous crustal compositions at 10 kb: evidence for the origin of silicic magmas in the Taupo volcanic zone, New Zealand, and other occurrences. – J. Petr. 29, 765–803.

Cox, K.G., 1980: A model for flood basalt vulcanism. – J. Petr. 21, 629–650.

Creaser, R.A., Price, R.C. & Wormald, R.J., 1991: A-type granites revisited: assessment of a residual-source model. – Geology 19, 163–166.

Cruden, A.R., Koyi, H., & Schmeling, H., 1995: Diapiric basal entrainment of mafic into felsic magma. – Earth Plan. Sci. Lett. 131, 321–340.

Czamanske, G.K. & Wones, D.R., 1973: Oxidation during magmatic differentiation, Finnmarka complex, Oslo area, Norway: Part 2, the mafic silicates. – J. Petr. 14, 349–380.

Czamanske, G.K., Ishihara, S., & Atkin, S.A., 1981: Chemistry of rock-forming minerals of the Cretaceous batholith in southwestern Japan and implications for magma genesis. – J. Geoph. Res. 86, 10431–10469.

Davidson, J.P., De Silva, S.L., Holden, P. & Halliday, A.N., 1990: Small-scale disequilibrium in a magmatic inclusion and its more silicic host. – J. Geophys. Res. 95, 17661–17675.

Debon, F. 1991: Comparative major element chemistry in various "microgranular enclave-plutonic host" pairs. *In* Didier, J. & Barbarin, B. (eds.) 1991. Enclaves and granite petrology. – Developments in petrology 13, Elsevier, Amsterdam, pp. 293-312.

Debon, F. & Le Fort, P., 1982: A chemical-mineralogical classification of common plutonic rocks and associations. – Transactions of the Royal Society of Edinburgh. – Earth Sciences 73, 135–149.

Deer, W.A., Howie, R.A. & Zussman, M.A., 1963: Rock-forming minerals. Vol. 2, chain silicates. – Longmans, London, 379 pp.

Deer, W.A., Howie, R.A. & Zussman, M.A., 1992: An introduction to rock-foming minerals. 2nd ed. – Longman, Harlow, 696 pp.

De la Roche, H., LeTerrier, J., Grand Claude, P. & Marchal, M., 1980: A classification of volcanic and plutonic rocks using R1-R2 diagrams and major element analyses – its relationship with current nomenclature. – Chem. Geol. 29: 183-210.

Delin, H., 1996: U-Pb zircon ages of granitoids in the Kårböle region, central Sweden. – SGU C828, 6–14.

Delin, H. & Aaro, S., 1992: Berggrundskartorna Kårböle NV, SV, NO, SO. – SGU Ai 56, 57, 58, 59.

DePaolo, D.J., 1981: Neodymium isotopes in the Colorado front range and crust-mantle evolution in the Proterozoic. – Nature 291, 193–196.

DePaolo, D.J., 1988: Neodymium isotope geochemistry. An introduction. – Springer-Verlag, Berlin. 187 pp.

DePaolo, D.J., Perry, F.V. & Baldridge, W.S., 1992: Crustal versus mantle sources of granitic magmas: a two-parameter model based on Nd isotopic studies. – Trans. Roy. Soc. Edinb., Earth Sci. 83, 439–446.

Didier, J., 1973: Granites and their enclaves. – Developments in petrology 3. Elsevier, Amsterdam. 393 pp.

Didier, J., 1987: Contribution of enclave studies to the understanding of origin and evolution of granitic magmas. – Geol. Rundschau 76, 41–50.

Didier, J. & Barbarin, B. (eds.), 1991: Enclaves and granite petrology. – Developments in petrology 13. Elsevier, Amsterdam. 625 pp.

Dingwell, D.B., Scarfe, C.S. & Cronin, D.J., 1985: The effect of fluorine on viscosities in the system Na_2O-Al_2O_3-SiO_2: implications for phonolites, trachytes and rhyolites. – Am. Min. 70, 80–87.

Dingwell, D.B., Knoche, R. & Webb, S.L., 1993: The effect of P_2O_5 on the viscosity of haplogranitic liquid. – Eur. J. Min. 5, 133–140.

von Eckermann, H., 1938: The anorthosite and kenningite of the Nordingrå–Rödö region. A contribution to the problem of the anorthosites. –Geol. För. Stockh. Förh. 60, 243–284.

Ehlers, C. & Lindroos, A., 1990: Tonalite and granodiorite formation and evolution of early Svecofennian Proterozoic crust in SW Finland. – Geonytt 17, 40–41.

Ekambaram, V., Brookins, D.G., Rosenberg, P.E. & Emanuel, K.M., 1986: Rare-earth element geochemistry of fluorite-carbonate deposits in western Montana, U.S.A. – Chem. Geol. 54, 319–331.

Eklund, O., 1993: Coeval contrasting magmatism and magma mixing in Proterozoic post- and anorogenic granites, Åland, SW Finland. – Ph.D.-thesis, Åbo Academy University, 154 pp.

Eklund, O. & Lindberg, B., 1992: Interaction between basaltic melts and their wallrock in dykes and sills in Åland, southwestern Finland. – GFF 114, 93–102.

Eklund, O., Fröjdö, S., Lindberg, B. & Andersson, U.B., 1991: The link between anorthositic suites and rapakivi granites. – Geol. Survey Finl., Guide 34, 14.

Eklund, O., Fröjdö, S. & Lindberg, B., 1994: Magma mixing, the petrogenetic link between anorthositic suites and rapakivi granites, Åland, SW Finland. – Min & Petr. 50, 3–19.

Eklund, O., Shebanov, A. & Andersson, U.B., 1996a: Origin of the rapakivi texture by subisothermal decompression. – Seventh international symposium on rapakivi granites and related rocks. Helsingfors, 24.26/7 1996. Abstract Vol., p. 19.

Eklund, O., Kolker, A., Fröjdö, S., Rutanen, H., 1996b: Tracing crust – mantle interaction of the Svecofennian orogen using early Postorogenic intrusions. – Abstract, The 22nd Nordic Geological Winter Meeting, Turku. Abstracts vol. p. 42.

Eklund, O., Fröjdö, S. & Shebanov, A.D., 1996c: Dynamic evolution of the 1.57 Ga anorogenic magmatism in SW Finland. – Abstract, The 22nd Nordic Geological Winter Meeting, Turku. Abstracts vol. p. 41.

Eklund, O., Shebanov, A., Fröjdö, S., Yli-Kyyny, K. & Andersson, U.B., 1996d: A flow-foliated ignimbrite related to the Åland rapakivi granite in SW Finland. – Terra Nova 8, 548–557.

Elburg, M.A., 1996a: Evidence of isotopic equilibration between microgranitoid enclaves and host granodiorite, Warburton granodiorite, Lachlan fold belt, Australia. – Lithos 38, 1–22.

Elburg, M.A., 1996b: Genetic significance of multiple enclave types in a peraluminous ignimbrite suite, Lachlan fold belt, Australia. – J. Petr. 37, 1385–1408.

Elburg, M.A. & Nicholls, I.A., 1995: Origin of microgranitoid enclaves in the S-type Wilson´s Promontory batholith, Victoria: evidence for magma mingling. – Austr. J. Earth Sci. 42, 423–435.

Elo, S. & Korja, A., 1993: Geophysical interpretation of the crustal and upper mantle structure in the Wiborg rapakivi granitoid area, southeastern Finland. – Prec. Res. 64, 273–288.

Emslie, R.F., 1975: Pyroxene megacrysts from anorthositic rocks: new clues to the sources and evolution of the parent magmas. – Can. Min. 13, 138–145.

Emslie, R.F., 1978: Anorthosite massifs, rapakivi granites and late Proterozoic rifting in North America. – Precambrian. Res. 7, 61–98.

Emslie, R.F., 1980: Geology and petrology of the Harp Lake complex, central Labrador: an example of Elsonian magmatism. – Geol. Surv. Canada, Bull. 293, 136 pp.

Emslie, R.F., 1985: Proterozoic anorthosite massifs. *In* Tobi, A.C. & Touret, J.L.R. (eds.): The deep Proterozoic crust in the North Atlantic provinces, pp. 39-60.

Emslie, R.F., 1991: Granitoids of rapakivi granite-anorthosite and related associations. – Prec. Res. 51, 173–192.

Emslie, R.F. & Hegner, E., 1993: Reconnaissance isotopic geochemistry of anorthosite-mangerite-charnockite-granite (AMCG) complexes, Grenville province, Canada. – Chem. Geol. 106, 279–298.

Emslie, R.F. & Stirling, J.A.R., 1993: Rapakivi and related granitoids of the Nain plutonic suite: Geochemistry, mineral assemblages and fluid equilibria. – Can. Min. 31, 821–847.

Emslie, R.F., Hamilton, M.A. & Thériault, R.J., 1994: Petrogenesis of a Mid-Proterozoic Anorthosite-Mangerite-Charnockite-Granite (AMCG) Complex: Isotopic and Chemical Evidence from the Nain Plutonic Suite. – J. Geol. 102, 539–558.

Erdmann, A., 1847: Gångar av granit, genomsättande hyperstenfels. – Öfv. af K. Vet. Ak. förhandl.

Erdmann, E., 1889: Beskrifning till kartbladet Askersund. – SGU Aa 84, 100 pp.

Eriksson, L. & Henkel, H., 1994: Geofysik. – *In* Berg och Jord, Sveriges nationalatlas (Fredén, C., ed.), pp. 76– 101.

Evensen, N.M., Hamilton, P.J. & O´Nions, R.K., 1978: Rare earth abundances in chondritic meteorites. – Geoch. Cosmoch. Acta 42, 1199–1212.

Faure, G., 1986: Principles of isotope geology, 2nd ed. – Wiley, New York. 589 pp.

Fernandez, A.N. & Barbarin, B., 1991: Relative rheology of coeval mafic and felsic magmas: nature of resulting interaction processes. Shape and mineral fabrics of mafic microgranular enclaves. *In* Didier, J. & Barbarin, B. (eds.): Enclaves and granite petrology. – Developments in petrology 13, Elsevier, Amsterdam, pp. 263-276.

Fleck, R.J., 1990: Neodymium, strontium, and trace element evidence of crustal anatexis and magma mixing in the Idaho batholith. – Geol. soc. Am., Mem. 174, 359–373.

Floyd, P.A. & Winchester, J.A., 1975: Magma-type and tectonic setting discrimination using immobile elements. – Earth Plan. Sci. Lett. 27, 211–218.

Fogel, R.A. & Rutherford, M.J., 1990: The solubility of carbon dioxide in rhyolitic melts: a quantitative FTIR study. – Am. Min. 75, 1311–1326.

Fourcade, S. & Javoy, M., 1991: Sr-Nd-O isotopic features of mafic microgranular enclaves and host granitoids from the Pyrenees, France: evidence for their hybrid nature and inference on their origin. *In* Didier, J. & Barbarin, B. (eds.): Enclaves and granite petrology. – Developments in petrology 13, Elsevier, Amsterdam, pp. 345–364.

Fram, M.S. & Longhi, J., 1992: Phase equilibria of dikes associated with Proterozoic anorthosite complexes. – Am. Min. 77, 605–616.

Freundt, A. & Tait, S.R., 1986: The entrainment of high-viscosity magma into low-viscosity magma eruption conduits. – Bull. Volc. 48, 325–339.

Frödin, G., 1918: Om en förekomst av Ragundabergarter i trakten av Strömsund i norra Jämtland. – SGU C 290, 26 pp.

Fröjdö, S., 1994: Spår av ett polybariskt intrusionsförlopp i en proterozoisk massiv anortosit, Åland, sydvästra Finland. – Fil.Lic.-thesis, Åbo Academy University, 50 pp.

Fröjdö, S., Andersson, U.B. & Claesson, S., 1996: Nd isotope geochemistry of some mafic rocks and minerals associated with the Mesoproterozoic Åland and Nordingrå rapakivi batholiths, Fennoscandian shield. – Abstract. International Conference on Proterozoic evolution in the North Atlantic Realm. Goose Bay, Labrador, 29/7–2/8 1996. Abstract Vol. pp. 62–63.

Front, K. & Nurmi, P.A., 1987: Characteristics and geological setting of synkinematic Svecokarelian granitoids in southern Finland. – Prec. Res. 35, 207–224.

Frost, B.R., 1991: Magnetic petrology: factors that control the occurrence of magnetite in crustal rocks. *In* Oxide minerals: petrologic and magnetic significance (Lindsley, D.H., ed.). – Miner. Soc. America, Rev. in Min. Vol. 25, 489–509.

Frost, B.R. & Lindsley, D.H., 1991: Occurrence of iron-titanium oxides in igneous rocks. *In* Oxide minerals: petrologic and magnetic significance (Lindsley, D.H., ed.). – Miner. Soc. America, Rev. in Min. Vol. 25, 433– 468.

Frost, T.P. & Mahood, G.A., 1987: Field, chemical, and physical constraints on mafic-felsic magma interaction in the Lamarck granodiorite, Sierra Nevada, California. – Geol Soc Am Bull 99, 272–291.

Gaál, G., 1986: 2200 million years of crustal evolution: the Baltic shield. – Bull. Geol. Soc. Finl. 58, 149–168.

Gaál, G., 1990: Tectonic styles of early Proterozoic ore deposition in the Fennoscandian shield Prec. – Res. 46, 83–114.

Gaál, G. & Gorbatschev, R., 1987: An outline of the Precambrian evolution of the Baltic shield. – Precambrian Res. 35, 15–52.

Gamble, J.A., 1979: Some relationships between coexisting granitic and basaltic magmas and the genesis of hybrid rocks in the tertiary central complex of Slieve Gullion, northeast Ireland. – J. Volc. Geotherm. Res. 5, 297–316.

Gavelin, S., 1955: Urbergsområdet inom Västerbottens län. *In* Gavelin, S. & Kulling, O.: Beskrivning till berggrundskarta över Västerbottens län. – SGU Ca 37, 5–99.

Gieré, R., 1996: Formation of rare earth minerals in hydrothermal systems. *In* Jones, A.P., Wall, F. & Williams, C.T. (eds.): Rare earth minerals. Chemistry, origin and ore deposits. – The Min. Soc. Series, vol. 7, 105–150.

Gittins, J., 1979: The feldspatoidal alkaline rocks. *In* The evolution of igneous rocks. – Fiftieth anniversary perspectives, H.S. Yoder, jr (ed.). Princeton Univ. Press, Princeton, pp. 351–390.

Gladney, E.S., Jones, E.A. & Nickell, E.J., 1990: 1988 compilation of elemental concentration data for USGS basalt BCR-1. – Geostand. Newslett. 14, 209–359.

Goldie, R. (1978): Magma mixing in the Flavarian pluton, Naranda area, Quebec. – Can. J. Earth Sci. 15, 132– 144

Gorbatschev, R., 1967: Petrology of the Jotnian rocks in the Gävle area. – SGU C 621, 50 pp.

Gorbatschev, R., 1971: Age relations and the rocks of the Svecofennian–Gothian boundary, Linköping, south central Sweden. – SGU C 664, 1–62.

Gorbatschev, R., 1975: Beskrivning till berggrundskartan Linköping SO. – SGU Af 113, 76 pp.

Gorbatschev, R., 1980: The Precambrian development of southern Sweden. – GFF 102, 129–136.

Gorbatschev, R., 1985: Precambrian basement of the Scandinavian Caledonides. *In* D.G. Gee & B.A. Sturt (eds.), The Cale-

donide orogen – Scandinavia and related areas. – J. Wiley, New York.
Gorbatschev, R., 1990: Granitic magmatism in the western part of the central Svecofennian province. – Abstract. Second symposium on the Baltic shield, Lund, 5–7/6 1990. Abstracts vol., 39–40.
Gorbatschev, R. & Gaál, G., 1987: The Precambrian history of the Baltic shield. *In* Kröner, A (ed.): Proterozoic lithospheric evolution. – Am. Geophys. Union, Geodynamics Series Vol. 17, 149–159.
Gorbatschev, R. & Bogdanova, S., 1993: Frontiers in the Baltic shield. – Prec. Res. 64, 3–21.
Gorbatschev, R., Fromm, E. & Kjellström, G., 1976: Beskrivning till berggrundskartan Linköping NO. – SGU Af 107, 111 pp.
Gorbatschev, R., Solyom, Z. & Johansson, I., 1979: The Central Scandinavian Dolerite Group in Jämtland, central Sweden. – Geologiska Föreningens i Stockholm Förhandlingar 101, 177–190.
Gorbatschev, R., Lindh, A., Solyom, Z., Laitakari, I., Aro, K., Lobach-Zhuchenko, S.B., Markov, M.S., Ivliev, A.I. & Bryhni, I., 1987: Mafic dyke swarms of the Baltic shield. *In* Halls, H.C. & Fahrig, W.F. (eds.): Mafic dyke swarms. – Geol. Assoc. of Canada, Spec. Paper 34, 361–372.
Grauch, R.I., 1989: Rare earth elements in metamorphic rocks. *In* Lipin, B.R. & Mckay, G.A. (eds.): Geochemistry and mineralogy of rare earth elements. – Rev. in Miner. Vol. 21. Mineral. Soc. America, pp. 147–167.
Gray, C.M., 1984: An isotopic mixing model for the origin of granitic rocks in southeastern Australia. – Earth Plan. Sci. Lett. 70, 47–60.
Green, T.H., Green, D.H. & Ringwood, A.E., 1967: The origin of high-alumina basalts and their relationships to quartz tholeiites and alkali basalts. – Earth Plan. Sci. Lett. 2, 41–51.
Guggisberg, B. & Berthelsen, A., 1987: A two-dimensional velocity model for the lithosphere beneath the Baltic shield and its possible tectonic significance. – Terra Cognita 7, 631–638.
Guggisberg, B., Kaminski, W. & Prodehl, C., 1991: Crustal structure of the Fennoscandian shield: a traveltime interpretation of the long-range FENNOLORA seismic refraction profile. – Tectonoph. 195, 105–137.
Haapala, I., 1977: Petrography and geochemistry of the Eurajoki stock, a rapakivi-granite complex with greisen-type mineralization in southwestern Finland. – Geol. Survey Finl., Bull. 286, 128 pp.
Haapala, I., 1988: Metallogeny of the Proterozoic rapakivi granites of Finland. *In* Taylor, R.P. & Strong, D.F. (eds.): Recent advances in the geology of granite-related mineral deposits. – Can. Inst. Mining Metallurgy, Spec. Vol. 39, 124–132.
Haapala, I. & Rämö, O.T., 1992: Tectonic setting and origin of the Proterozoic rapakivi granites of southeastern Fennoscandia. – Trans. Roy. Soc. Edinb.: Earth Sci. 83, 165–171.
Haas, J.R., Shock, E.L. & Sassani, D.C., 1995: Rare earth elements in hydrothermal systems: estimates of standard partial molal thermodynamic properties of aqueous complexes of the rare earth elements at high pressures and temperatures. – Geoch. Cosmoch. Acta. 59, 4329–4350.
Hackman, V., 1934: Das Rapakiwirandgebiet der gegend von Lappeenranta (Willmanstrand). – Bull. Comm. Geol. Finl. 106, 1–82.
Haggerty, S.E., 1979: The aeromagnetic mineralogy of igneous rocks. – Can. J. Earth Sci. 16, 1281–1293.
Hallberg, A., 1989: Metal sources in the early Proterozoic Svecofennian terrain of central Sweden: Pb isotope evidence. – Miner. Depos. 24, 250–257.
Hammarstrom, J.M. & Zen, E.-an, 1986: Aluminium in hornblende: An empirical igneous geobarometer. – Am. Min. 71, 1297–1313.
Hanson, G.N., 1978: The application of trace elements to the petrogenesis of igneous rocks of granitic composition. – Earth Plan. Sci. Lett. 38, 26–43.
Harte, B., 1987: Metasomatic events recorded in mantle xenoliths: an overview. *In* Nixon, P.H. (ed.): Mantle xenoliths. – Wiley, Chichester, pp. 625–640.
Hawthorne, F.C., 1981: Crystal chemistry of the amphiboles. *In* Veblen, D.R. (ed.): Amphiboles and other hydrous pyriboles – mineralogy. – Min. Soc. America, Rev. in Miner. vol. 9A, 1–102.
Heim, M., Skiöld, T. & Wolff, F. Chr., 1996: Geology, geochemistry and age of the "Tricolor" granite and some other Proterozoic (TIB) granitoids at Trysil, southeast Norway. – Norsk Geologisk Tidsskrift 76, 45–54.
Hibbard, M.J., 1981: The magma mixing origin of mantled feldspars. – Contrib Mineral Petrol 76, 158–170
Hibbard, M.J., 1991: Textural anatomy of twelwe magma-mixed granitoid systems. *In* Didier, J. & Barbarin, B. (eds.), 1991: Enclaves and granite petrology. – Developments in petrology 13, Elsevier, Amsterdam, pp. 431– 444.
Hibbard, M.J., 1995: Petrography to petrogenesis. Prentice-Hall, Englewood Cliffs, 587 pp.
Hietanen, A., 1975: Generation of potassium-poor magmas in the northern Sierra Nevada and the Svecofennian of Finland. – J. Res. U.S. G. S. 3, 631–645.
Hjelmqvist, S., 1966: Beskrivning till berggrundskarta över Kopparbergs län. – SGU Ca 40, 217 pp.
Högbom, A.G., 1910: Precambrian geology of Sweden. – Bull. Geol. Inst. Upsala 10, 1–80.
Holden, P., Halliday, A.N. & Stephens, W.E., 1987: Neodymium and strontium isotope content of microdiorite enclaves points to mantle input to granitoid production. – Nature 330, 53–56.
Holden, P, Halliday, A.N., Stephens, W.E. & Henny, P.J., 1991: Chemical and isotopic evidence for mass transfer between mafic enclaves and felsic magma. – Chem. Geol. 92, 135–152.
Hollister, L.S., Grissom, G.C., Peters, E.K., Stowell, H.H. & Sisson, V.B., 1987: Confirmation of the empirical correlation of Al in hornblende with pressure of solidification of calc-alkaline plutons. – Am. Min. 72, 231– 239.
Holloway, J.R. & Blank, J.G., 1994: Application of experimental results to C-O-H species in natural melts. *In* Carroll, M.R. & Holloway, J.R. (eds.): Volatiles in magmas. – Rev. in Mineral. Vol. 30. Mineral. Soc. of America, 187–230.
Holmquist, P.J., 1899: Om Rödöområdets rapakivi och gångbergarter. – SGU C 181, 1–118.
Hölttä, P., 1988: Metamorphic zones and the evolution of granulite grade metamorphism in the early Proterozoic Pielavesi

area, central Finland. – Geol. Surv. Finl., Bull. 344, 1–49.
Hölttä, P., 1995: Contact metamorphism of the Vaaraslahti pyroxene granitoid intrusion in Pielavesi, central Finland. – Geol. Surv. Finl., Bull. 382, 27–79.
Holtz, F., Pichavant, M., Barbey, P. & Johannes, W., 1992a: Effects of H_2O on liquidus phase relations in the haplogranite system at 2 and 5 kbar. – Am. Min. 77, 1223–1241.
Holtz, F, Johannes, W. & Pichavant, M., 1992b: Effects of excess aluminium on phase relations in the system Qz-Ab-Or. Experimental investigation at 2 kbar and reduced H_2O-activity. – Eur. J. Mier. 4, 137–152.
Hopgood, A.M., Bowes, D.R., Kouvo, O. & Halliday, A.N., 1983: U-Pb and Rb-Sr isotopic study of polyphase deformed migmatites in the Svecokarelides, southern Finland. *In* Atherton, M.P. & Gribble, C.D. (eds.): Migmatites, melting, and metamorphism. – Shiva Publ., Nantwich, 80–92.
Hsu, L.C., 1992: Synthesis and stability of bastnaesites in a part of the system (Ce, La)-F-H-C-O. – Miner. & Petr. 47, 87–101.
Hubbard, F. & Branigan, N., 1987: Late Svecofennian magmatism and tectonism, Åland, southwest Finland. – Prec. Res. 35, 241–256.
Huhma H., 1986: Sm-Nd, U-Pb and Pb-Pb isotopic evidence for the origin of the early Proterozoic Svecokarelian crust in Finland. – Geol. Surv. Finl., Bull. 337, 1–48.
Huhma, H., 1987: Provenance of early Proterozoic and Archean metasediments in Finland: a Sm-Nd isotopic study. – Prec. Res. 35, 127–143.
Huppert, H.E. & Sparks, R.S.J., 1988: The generation of granitic magmas by intrusion of basalt into continental crust. – J. Petrol. 29, 599–624.
Hyndman, D.W. & Foster, D.A., 1988: The role of tonalites and mafic dikes in the generation of the Idaho batholith. – J. Geol. 96, 31–46
Idman, H., 1989: The Siipyy granite – a new rapakivi occurrence in Finland. – Bull. Geol. Soc. Finl. 61, 123–127.
Ishihara, S., 1984: Granitoid series and Mo/W-Sn mineralization in east Asia. – Geol. Surv. of Japan, Report 263, 173–208.
Jacobsen, S.B. & Wasserburg, G.J., 1980: Sm-Nd evolution of chondrites. – Earth Plan. Sci. Lett. 50, 139–155.
James, R.S. & Hamilton, D.L., 1969: Phase relations in the system $NaAlSi_3O_8$-$KAlSi_3O_8$-$CaAl_2Si_2O_8$-SiO_2 at 1 kilobar water pressure. – Contr. Miner. Petr. 21, 111–141.
Jahn, B.-M., Vidal, P. & Kröner, A., 1984: Multi-chronometric ages and origin of Archaean tonalitic gneisses in Finnish Lapland: a case for long crustal residence time. – Contr. Min. Petr. 86, 398–408.
Jarl, L.-G., 1992: New isotope data from the Protogine zone and southwestern Sweden. – GFF 114, 349–350.
Jarl, L.-G. & Johansson, Å., 1988: U-Pb zircon ages of granitoids from the Småland–Värmland granite-porphyry belt, southern and central Sweden. – GFF 110, 22–28.
Jarl, L.-G., Stephens, M.B. & Wahlgren, C.-H., 1993: U-Pb titanite ages from ductile deformation zones in the eastern part of the Sveconorwegian orogen, Karlskoga-Kristinehamn are, south-central Sweden. – SGU Rapp. & Medd. 76, 11–12.
Johannes, W. & Holtz, F., 1996: Petrogenesis and experimental petrology of granitic rocks. – Springer, Berlin. 335 pp.
Johansson, Å., 1988: The age and geotectonic setting of the Småland–Värmland granite-porphyry belt. – Geologiska Föreningens i Stockholm Förhandlingar 110, 105–110.
Johansson, Å., 1990: Age of the Önnestad syenite and some gneissic granites along the southern part of the Protogine zone, southern Sweden. *In* Gower, C.F., Rivers, T. & Ryan, A.B. (eds.): Mid-Proterozoic Laurentia-Baltica. – Geol. Assoc. of Canada, Spec. Paper 38, 131–148.
Johansson, Å. & Rickard, D., 1985: Some new lead isotope determinations from the Proterozoic sulfide ores of central Sweden. Miner. Dep. 20, 1–7.
Johansson, L. & Johansson, Å., 1990: Isotope geochemistry and age relationships of mafic intrusions along the Protogine zone, southern Sweden. – Prec. Res. 48, 395–414.
Johansson, L., Lindh, A. & Möller, Ch., 1991: Late Sveconorwegian (Grenville) high-pressure granulite facies metamorphism in southwestern Sweden. – J. Metam. Geol. 9, 283–292.
Johnson, M.C. & Rutherford, M.J., 1989: Experimental calibration of the aluminium-in-hornblende barometer with application to the Long Valley caldera (California) volcanic rocks. – Geology 17, 837–841.
Jönsson, J., 1887: Beskrifning till kartbladet Motala. – SGU Aa 102, 43 pp.
Joyce, D.B. & Voigt, D.E., 1994: A phase equilibrium study in the system $KAlSi_3O_8$-$NaAlSi_3O_8$-SiO_2-Al_2SiO_5-H_2O and petrogenetic interpretations. – Am. Min. 79, 504–512.
Karlsson, V., 1877: Beskrifning till Kartbladet "Claestorp". – SGU Aa 62, 41 pp.
Keppler, H., 1993: Influence of fluorine on the enrichment of high field strength trace elements in granitic rocks. – Contr. Min. Petr. 114, 479–488.
Keppler, H. & Wyllie, P.J., 1991: Partitioning of Cu, Sn, Mo, W, U, and Th between melt and aqueous fluid in the systems haplogranite-H_2O-HCl and haplogranite-H_2O-HF. – Contr. Min. Petr. 109, 139–150.
Keppler, H. & Wyllie, P.J., 1990: Role of fluids in transport and fractionation of uranium and thorium in mag-matic processes. – Nature 348, 531–533.
Kerr, A. & Fryer, B.F., 1993: Nd isotope evidence for crust-mantle interaction in the generation of A-type granitoid suites in Labrador, Canada. – Chem. Geol. 104, 39–60
Kinnaird, J.A. & Bowden, P., 1991: Magmatism and mineralization associated with Phanerozoic anorogenic plutonic complexes of the Afrcan plate. *In* Kampunzu, A.B. & Lubala, R.T. (ed.): Magmatism in extensional structural settings. – Springer-Verlag, Berlin, pp. 410–485.
Kirs, J., Huhma, H. & Haapala, I., 1991: Petrological-chemical features and age of estonian anorogenic potassium granites. – Geol. Survey of Finl. Opas-Guide 34, 28–29.
Koistinen, T. (ed.), 1994: Precambrian basement of the Gulf of Finland and surrounding area. Map sheet, 1:1 million. – Geol.

Surv. Finl., Espoo.
Konopelko, D.L. & Ivanikov, V.V., 1996: Postorogenic intrusions in the NW Ladoga region. Seventh international symposium on rapakivi granites and related rocks. – Helsingfors, 24–26/7 1996. Abstract Vol., p. 37.
Korja, A., 1995: Structure of the Svecofennian crust – growth and destruction of the Svecofennian orogen. – Inst. of Seismology, Univ. of Helsinki, Report S-31, 36 pp.
Korja, A. & Heikkinen, P., 1995: Proterozoic extensional tectonics of the central Fennoscandian shield: results from the Baltic and Bothnian echoes from the lithosphere experiment. – Tectonics 14, 504–517.
Korja, A., Korja, T., Luosto, U. & Heikkinen, P., 1993: Seismic and geoelectric evidence for collisional and extensional events in the Fennoscandian shield-implications for Precambrian crustal evolution. Tectonophysics 219, 129–152.
Korja, T., Luosto, U., Korsman, K, & Pajunen, M., 1994: Geophysical and metamorphic features of Palaeoproterozoic Svecofennian orogeny and Palaeoproterozoic overprinting on Archaean crust. *In* Pajunen, M. (ed.): High temperature-low pressure metamorphism and deep crustal structures. – Geol. Surv. Finl., Guide 37, 11–20.
Kornfält, K.-A., 1969: X-ray and optical observations on the K-feldspars from the Ragunda area, central Sweden. – SGU C 636, 33 pp.
Kornfält, K.-A., 1975: Beskrivning till berggrundskartan Norrköping NV. – SGU Af 108, 54 pp.
Kornfält, K.-A., 1976: Petrology of the Ragunda rapakivi massif, central Sweden. –SGU C725, 1–111.
Korsman, K., Hölttä, P., Hautala, T. & Wasenius, P., 1984: Metamorphism as an indicator of evolution and structure of the crust in eastern Finland. – Geol. Surv. Finl., Bull. 328, 40 pp.
Kosterin, A.V., 1959: The possible modes of transport of rare earths by hydrothermal solutions. – Geochemistry 4, 381–387.
Kresten, P., 1990: Alnöområdet. *In* Lundqvist, Th., Gee, D.G., Kumpulainen, R., Karis, L. & Kresten, P., 1990: Beskrivning till karta över berggrunden i Västernorrlands län. – SGU Ba 31, 238–278.
Krogh, T.E., 1973: A low-contamination method for hydrothermal decomposition of zircon and extraction of U and Pb for isotopic age determinations. – Geoch. Cosmoch. Acta 37, 485–494.
Krogh, T.E., 1982: Improved accuracy of U-Pb zircon ages by the creation of more concordant systems using an air-abrasion technique. – Geoch. Cosmoch. Acta 46, 637–649.
Kumpulainen, R.A., Mansfeld, J., Sundblad, K., Neymark, L.A. & Bergman, T., 1996: Stratigraphy, age, and Sm-Nd isotope systematics of the country rocks to Zn-Pb sulfide deposits, Åmmeberg district, Sweden. – Econ. Geol. 91, 1009–1021.
Lagerblad, B., 1988: Evolution and tectonic history of the Bergslagen vulcano-plutonic complex, central Sweden. – Geol. Mijnb. 67, 165–176.
Lahti, S.I. & Suominen, V., 1988: Occurrence, crystallography and chemistry of the fluocerite-bastnäsite-cerianite intergrowth from the Fjälskär granite, southwestern Finland. – Bull. Geol. Soc. Finl. 60, 45–53.
Laitakari, I., 1991: Overview of the Häme diabase dyke swarm. *In* Fennoscandian meeting and excursion on Precambrian dyke swarms, june 1991, Finland, Laitakari, I. (ed.). – IGCP-257 Tech. Rep. No. 4, 13–15.
Landenberger, B. & Collins, W.J., 1996: Derivation of A-type granites from a dehydrated charnockitic lower crust: evidence from the Chaelundi complex, eastern Australia. – J. Petr. 37, 145–170.
Larin, A.M., Neymark, L.A., Gorokhovsky, B.M. & Ovchinnikova, G.V., 1990: Connection of the complex skarn mineralization of the Pitkäranta district with the rapakivi granites of the Salmi massif according to Pb isotope data. – Izvestiya Acad. Nauk. Ser. Geol. 5, 47–57. (In Russian.)
Larsen, L.L. & Smith, E.I., 1990: Mafic enclaves in the Wilson Range pluton, northwestern Arizona: implications for the generation of a calc-alkaline intermediate pluton in an extensional environment. – J. Geoph. Res. 95, 17693–17716.
Larson, S.Å., 1973: Igneous layering in the Ulvö Dolerite, Ångermanland, Central Sweden. – GFF 95, 407–409.
Larson, S.Å., 1980: Layered intrusions of the Ulvö Dolerite Complex, Ångermanland, Central Sweden. – Dissertation, Chalmers University of Technology/University of Gothenburg, Department of Geology, Publication A36, 213 pp.
Larson, S.Å. & Magnusson, K.-Å., 1979: A gravity investigation of the dolerite area on the coast of Ångermanland, Sweden. – GFF 101, 1–16.
Larson, S.Å. & Berglund, J., 1992: A chronological subdivision of the Transscandinavian Igneous Belt – three magmatic episodes? – GFF 114, 459–461.
Larson, S.-Å., Stigh, J. & Tullborg, E.-L., 1986: The deformation history of the eastern part of the southwest Swedish gneiss belt. – Prec. Res. 31, 237–257.
Laurén, L., 1970: An interpretation of the negative gravity anomalies associated with the rapakivi granites and the Jotnian sandstone in southern Finland. – GFF 92, 21–34.
Leake, B.E., 1978: Nomenclature of amphiboles. – Can. Min. 16, 501–520.
Lee, J.K.W., Onstott, T.C. & Henne, R., 1988: $^{40}Ar/^{39}Ar$ laser microprobe and U-Pb geochronology of Siljan ring samples. – Abstract. GSA Abstracts with Programs 1988, p. A24.
Lejeune, A.M. & Richet, P., 1995: Rheology of crystal-bearing silicate melts: an experimental study at high viscosities. – J. Geophys. Res. 100, 4215–4229.
Lesher, C.E., 1990: Decoupling of chemical and isotopic exchange during magma mixing. – Nature 344, 235– 237.
Lesher, C.E., 1994: Kinetics of Sr and Nd exchange in silicate liquids: theory, experiments, and applications to uphill diffuson, isotopic equilibrium, and irreversible mixing of magmas. – J. Geophys. Res. 99, 9585–9604.
Lindberg, B. & Eklund, O., 1988: Interactions between basaltic and granitic magmas in a Svecofennian postorogenic granitoid intrusion, Åland, southwest Finland. – Lithos 22, 13–23.
Lindberg, B., Eklund, O. & Suominen, V., 1991: Middle Proterozoic, Subjotnian diabases and related mafic rocks in the archipelago of southwestern Finland. *In* Fennoscandian meeting and excursion on Precambrian dyke swarms, june 1991, Finland, Laitakari, I. (ed.). – IGCP-257 Tech. Rep. No. 4, 18–30.

Lindh, A. & Gorbatschev R., 1984: Chemical variation in a Proterozoic suite of granitoids extending across a mobile belt craton boundary. – Geol. Rundsch. 73, 881–893.

Lindh, A. & Persson, P.-O., 1990: Proterozoic granitoid rocks of the Baltic shield – trends of development. *In* Gower, C.F., Rivers, T. & Ryan, A.B. (eds.): Mid-Proterozoic Laurentia-Baltica. – Geol. Assoc. of Canada, Spec. Paper 38, 23–40.

Lindh, A. & Johansson, I., 1996: Rapakivi granites of the Baltic Shield: The Nordingrå granite, it chemical variation and Sm-Nd isotope composition. – Neues Jahrbuch für Mineralogie, Abhandlungen 170, 291–312.

Lindroos, A., Romer, R.L., Ehlers, C. & Alviola, R., 1996: Late-orogenic Svecofennian deformation in SW Finland constrained by pegmatite emplacement ages. – Terra Nova 8, 567–574.

Linnarsson, G. & Tullberg, S.A., 1882: Beskrifning till kartbladet "Vreta Kloster". – SGU Aa 83, 45 pp.

London, D., 1995: Geochemical features of peraluminous granites, pegmatites, and rhyolites as sources of lithophile metal deposits. *In* Thompson, J.F.H. (ed.): Magmas, fluids, and ore deposits. – Min. Assoc.of Canada, Short Course Vol. 23, 175–202.

Longhi, J., Fram, M.S., Van der Auwera, J. & Montieth, J.N., 1993: Pressure effects, kinetics, and rheology of anorthositic and related magmas. – Am. Min. 78, 1016–1030.

Ludwig, K.R., 1993: PBDAT. A computer program for processing Pb-U-Th isotope data. Version 1.24. – USGS Open-file report 88-542, 23 pp.

Ludwig, K.R., 1995: ISOPLOT. A plotting and regression program for radiogenic isotope data. Version 2.82. – USGS Open-file report 91-445, 45 pp.

Ludwig, K.R., Halley, R.B., Simmons, K.R. & Peterman, Z.E. ,1988: Strontium-isotope stratigraphy of Enewetak atoll. – Geology 16, 173–177.

Lundberg, B., 1980: Aspects of the geology of the Skellefte field, northern Sweden. – GFF 102, 156–166.

Lundegårdh, P.H., 1967: Berggrunden i Gävleborgs län. – SGU Ba 22, 303 pp.

Lundegårdh, P.H., 1980: The gneissic granites and allied rocks in central and northwestern Värmland, western Sweden. – SGU C 777, 3–23.

Lundegårdh, P.H., 1987: Beskrivning till berggrundskartan Filipstad SV. – SGU Af 157, 77 pp.

Lundegårdh, P.H., Gorbatschev, R. & Kornfält, K.-A., 1984: Karta över berggrunden i Jämtlands län (Precambrian). – SGU Ca 53.

Lundqvist, L. & Korja, A., 1997: Kartbladen 18F Bräcke NV, NO och 19F Häggensås SV, SO. – SGU Rapp. & Medd. 89, 27–34.

Lundqvist, Th., 1975: The "kenningite" found near Sundsvall, central Sweden. –GFF 97, 189–192.

Lundqvist, Th., 1979: The Precambrian of Sweden. – SGU C 768, 87 pp.

Lundqvist, Th., 1987: Early Svecofennian stratigraphy of southern and central Norrland, Sweden, and possible existence of an Archaean basement west of the Svecokarelides. – Prec. Res. 35, 343–352.

Lundqvist, Th. & Samuelsson, L., 1973: The differentiation of a dolerite at Nordingrå, central Sweden. – SGU C 692, 62 pp.

Lundqvist, Th. & Persson, P.-O., 1996: U-Pb ages of porphyries and related rocks in northern Dalarna, south-central Sweden. – Abstract, GFF 118, A17–A18

Lundqvist, Th., Gee, D.G., Kumpulainen, R., Karis, L. & Kresten, P., 1990: Beskrivning till karta över berggrunden i Västernorrlands län. – SGU Ba 31, 429 pp.

Lundqvist, Th., Bygghammar, B., Stephens, M.B., Beckholmen, M., Zachrisson, E., Norling, E., Lidmar-Bergström, K., Åkerman, Ch. & Wik, N.-G., 1994: Berggrunden. *In* Berg och Jord, Sveriges nationalatlas (Fredén, C., ed.), 14–75.

Lundqvist, Th., Vaasjoki, M. & Skiöld, T., 1996: Preliminary note on the occurrence of Archaean rocks in the Vallen–Alhamn area, northern Sweden. – SGU C 828, 32–33.

Macdonald, R., 1969: The petrology of alkaline dykes from the Tugtutôq area, south Greenland. – Bull Geol. Soc. Denmark 19, 257–282.

Macdonald, R., 1974: The rôle of fractional crystallization in the formation of the alkaline rocks. *In* Sörensen, H. (ed.): The alkaline rocks. – Wiley, London, pp. 442–459.

Macdonald, R., 1987: Quarternary peralkaline silicic rocks and caldera volcanoes of Kenya. *In* Fitton, J.G. & Upton, B.G.J. (eds.): Alkaline igneous rocks. – Geol. Soc., Spec. Publ. 30, 313–333.

Macdonald, R. & Gibson, I.L., 1969: Pantelleritic obsidians from the volcano Chabbi (Ethiopia). – Contr. Miner. Petr. 24, 239–244.

Macdonald, R., Navarro, J.M., Upton, B.G.J. & Davies, G.R., 1994: Strong compositional zoning in peralkaline magma: Menengai, Kenya Rift Valley. – J. Volc. Geoth. Res. 60, 301–325.

Magnusson, N.H., 1940: Herrängsfältet och dess järnmalmer. – SGU C 431, 78 pp.

Magnusson, N.H., 1962: De prekambriska bergarterna utanför fjällkedjan. *In* Magnusson, N.H., Thorslund, P., Brotzen, F., Asklund, B. & Kulling, O.: Beskrivning till karta över Sveriges berggrund. – SGU Ba 16, 5–110.

Magnusson, N.H., Lundqvist, G. & Regnéll, G., 1963: Sveriges geologi. – Norstedts, 4th ed., 698 pp.

Mahood, G.A. & Hildreth, W., 1983: Large partition coefficients for trace elements in high-silica rhyolites. – Geoch. Cosmoch. Acta 47, 11–30.

Mahood, G.A. & Stimac, J.A., 1990: Trace-element partitioning in pantellerites and trachytes. – Geoch. Cosmoch. Acta 54, 2257–2276.

Manhes, G., Minster, I.F., Allegre, C.J., 1978: Comparative uranium-thorium-lead and rubidium-strontium study of the Saint Severin amphoterite: consequenses for early solar system chronology. – Earth Plan. Sci. Lett. 39, 14–24.

Manning, D.A.C., 1981: The effect iof fluorine on liquidus phase relationships in the system Qz-Ab-Or with excess water at 1 kbar. – Contr. Miner. Petr. 76, 206–215.

Manning, D.A.C., Hamilton, D.L., Henderson, C.M.B., & Bempsey, M.J., 1980: The probable occurrence of interstitial Al in

hydrous, F-bearing and F-free aluminosilicate melts. – Contr. Miner. Petr. 75, 257–262.
Mansfeld, J., 1995: Crustal evolution in the southestern part of the Fennoscandian shield. – Medd. Stockh. Univ. Inst. Geol. Geokemi. Nr. 289 (Ph.D.-thesis).
Martin, H., 1987: Evolution in composition of grantic rocks controlled by time-dependent changes in petrogenetic processes: examples from the Archaean of eastern Finland. – Prec. Res. 35, 257–276.
Martin, H., Chauvel, C., Jahn, B.-M. & Vidal, P., 1983: Rb-Sr and Sm-Nd ages and isotopic geochemistry of Archaean granodioritic gneisses from eastern Finland. – Prec. Res. 20, 79–91.
Matielli, N., Weis, D., Grégoire, M., Mennessier, J.P., Cottin, J.Y. & Giret, A., 1996: Kerguelen basic and ultrabasic xenoliths: evidence for long-lived Kerguelen hotspot activity. – Lithos 37, 261–280.
McDonough, W.F., 1990: Constraints on the compsition of the subcontinental mantle. – Earth Plan. Sci. Lett. 101, 1–18.
McDonough, W.F., Sun, S.-S., Ringwood, A.E., Jagoutz, E. & Hofmann, A.W., 1992: Potassium rubidium, and cesium in the earth and moon and the evolution of the mantle of the earth. – Geoch. Cosmoch. Acta 56, 1001– 1012.
McLennan, S.M. & Taylor, S.R., 1979: Rare earth element mobility associated with uranium mineralisation. Nature 282, 247–250.
Mellqvist, C., 1996: Using Sm-Nd isotopes and the occurrence of Archaean megaxenoliths as tracers when delineating the Archaean-proterozoic palaeoboundary in the Luleå area. – GFF 118, A20.
Menzies, M.A. & Hawkesworth, C.J., 1987: Upper mantle processes and composition. *In* Nixon, P.H. (ed.): Mantle xenoliths. Wiley, Chichester, pp. 725–738.
Meschede, M., 1986: A method of discriminating between different types of mid-ocean ridge basalts and continental tholeiities with the Nb-Zr-Y diagram. – Chem. Geol. 56, 207–218.
Metcalf, R.V., Smith, E.I., Walker, J.D., Reed, R.C. & Gonzales, D.A., 1995: Isotopic disequilibrium among commingled hybrid magmas: evidence for a two-stage magma mixing-commingling process in the Mt. Perkins pluton, Arizona. – J. Geol. 103, 509–527.
Middlemost, E.A.K., 1985: Magmas and magmatic rocks. – Longman, London, 266 pp.
Miller, C.F., Watson, E.B. & Harrison, T.M., 1988: Perspectives on the source, segregation and transport of granitoid magmas. – Trans. Roy. Soc. Edinb.: Earth Sci. 79, 135–156.
Miller, R.G., O'Nions, R.K., Hamilton, P.J. & Welin, E., 1986: Crustal residence ages of clastic sediments, orogeny and continental evolution. – Chem. Geol. 57, 87–99.
Mitchell, J.N., Scoates, J.S. & Frost, C.D., 1995: High-Al gabbros in the Laramie anorthosite complex, Wyoming: implications for the composition of melts parental to Proterozoic anorthosite. – Contr. Min. Petr. 119, 166– 180.
Mitchell, J.N., Scoates, J.S., Frost, C.D. & Kolker, A., 1996: The geochemical evolution of anorthosite residual magmas in the Laramie anorthosite complex, Wyoming. – J. Petr. 37, 637–660.
Miyashiro, A., 1974: Volcanic rock series in island arcs and active continental margins. – Am. J. Sci. 274, 321– 355.
Moreno-Ventas, I., Rogers, G. & Castro, A., 1995: The role of hybridization in the genesis of Hercynian granitoids in the Gredos massif, Spain: inferences from Sr-Nd isotopes. – Contr. Min. Petr. 120, 137–149.
Murase, T, & McBirney, A.R., 1973: Properties of some common igneous rocks and their melts at high temperatures. – GSA Bull. 84, 3563–3592.
Nash, W.P. & Crecraft, H.R., 1985: Partition coefficients for trace elements in silicic magmas. – Geoch. Cosmoch. Acta 49, 2309–2322.
Nekvasil, H., 1991: Ascent of felsic magmas and formation of rapakivi. – Am. Min. 76, 1279–1290.
Neymark, L.A., Amelin, J.V. & Larin, A.M., 1994: Pb-Nd-Sr isotopic and geochemical constraints on the origin of the 1.54–1.56 Ga Salmi rapakivi granite-anorthosite batholith (Karelia, Russia). – Min. Petr. 50, 173–193.
Ngwenya, B.T., 1994: Hydrothermal rare earth mineralisation in carbonatites of the Tundulu complex, Malawi: processes at the fluid/rock interface. – Geoch. Cosmoch. Acta 58, 2061–2072.
Nielsen, F.M., Campbell, I.H., McCulloch, M. & Wilson, J.R., 1996: A strontium isotopic investigation of the Bjerkreim-Sokndal layered intrusion, southwest Norway. – J. Petr. 37, 171–193.
Nironen, M., 1989: Emplacement and structural setting of granitoids in the early Proterozoic Tampere and Savo schist belts, Finland – implications for contrasting crustal evolution. – Geol. Surv. Finl., Bull. 346, 83 pp.
Nurmi, P.A. & Haapala, I., 1986: The Proterozoic granitoids of Finland: granite types, metallogeny and relation to crustal evolution. – Bull. Geol. Soc. Finl. 58, 203–233.
Nyström, J.O., 1982: Post-Svecokarelian Andinotype evolution in central Sweden. – Geol. Rundschau 71, 141– 157
Öhlander, B. & Zuber, J., 1988a: Geochemistry of the Fellingsbro type granites, south central Sweden. – Geol. Mijnb. 67, 213–225.
Öhlander, B. & Zuber, J., 1988b: Genesis of the Fellingsbro-type granites: evidence from gravity measurements and geochemistry. – GFF 110, 39–54.
Öhlander, B. & Romer, R.L., 1996: Zircon ages of granites occurring along the central Swedish gravity low. – GFF 118, 217–225.
Öhlander, B., Skiöld, T., Hamilton, P.J. and Claesson L.-Å., 1987: The western border of the Archean province of the Baltic shield: evidence from northern Sweden. – Contr. Miner. Petr. 95, 437–450.
Öhlander, B., Skiöld, T., BABELworking group, Claesson, S. & Nisca, D.H., 1993: Delineation and character of the Archaean–Proterozoic boundary in northern Sweden. – Prec. Res. 64, 67–84.
Olson, K.E. & Morse, S.A., 1990: Regional Al-Fe mafic magmas associated with anorthosite-bearing terranes. – Nature 344, 760–762.
Orsini, J.-B., Cocirta, C. & Zorpi, M.-J., 1991: Genesis of mafic microgranular enclaves through differentiation of basic magmas, mingling and chemical exchanges with their host granitoid magmas. *In* Didier, J. & Barbarin, B. (eds.) 1991:

Enclaves and granite petrology. – Developments in petrology 13, Elsevier, Amsterdam, pp. 445–464.
Page, L.M., Stephens, M.B. & Wahlgren, C.-H., 1996: $^{40}Ar/^{39}Ar$ geochronological constraints on the tectonothermal evolution of the eastern segment of the Sveconorwegian orogen, south-central Sweden. *In* Brewer, T.S. (ed.): Precambrian crustal evolution in the north Atlantic Region. – Geol. Soc., Spec. Publ. 112, 315–330.
Papanastassiou, D.A. & Wasserburg, G.J., 1969: Initial strontium isotopic abundances and the resolution of small time differences in the formation of planetary objects. – Earth Plan. Sci. Lett. 5, 361–376.
Parák, T., 1975: The origin of the Kiruna iron ores. – SGU C 709, 209 pp.
Parrish, R.R., 1987: An improved micro-capsule for zircon dissolution in U-Pb geochronology. – Chem. Geol. 66, 99–102.
Patchett, P.J. & Arndt, N.T., 1986: Nd isotopes and tectonics of 1.9–1.7 Ga crustal genesis. – Earth Planet. Sci. Lett. 78, 329–338.
Patchett P.J. & Kouvo O., 1986: Origin of Continental crust of 1.9–1.7 Ga age: Nd isotopes and U-Pb zircon ages in the Svecokarelian terrain of south Finland. – Contr. Miner. Petr. 92, 1–12.
Patchett, P.J., Todt, W. & Gorbatschev, R., 1987: Origin of continental crust of 1.9–1.7 Ga age: Nd isotopes in the Svecofennian orogenic terrains of Sweden. – Prec. Res. 35, 145–160.
Patchett, P.J., Lehnert, K., Rehkämper, M. & Sieber, G., 1994: Mantle and crustal effects on the geochemistry of Proterozoic dikes and sills in Sweden. – J. Petr. 35, 1095–1125.
Pearce, J.A. & Cann, J.R., 1973: Tectonic setting of basic volcanic rocks determined by using trace element analyses. – Earth Plan. Sci. Lett. 19, 290–300.
Pearce, J.A. & Norry, M.J., 1979: Petrogenetic implications of Ti, Zr, Y and Nb variations in volcanic rocks. – Contr. Miner. Petr. 69, 33–47.
Pearce, J.A., Harris, N.B.W. & Tindle, A.G., 1984: Trace element discrimination diagrams for the tectonic interpretation of granitic rocks. – J. Petr. 25, 956–983.
Perdahl, J.-A., 1995: Svecofennian volcanism in northernmost Sweden. – Doctoral thesis (Luleå), 1995, 169 D.
Perry, F.V., DePaolo, D.J. & Baldridge, W.S., 1993: Neodymium isotopic evidence for decreasing crustal contributions to Cenozoic ignimbrites in the western United States: implications for the thermal evolution of the Cordilleran crust. – GSA Bull. 105, 872–882.
Persson, A.I., 1995: Geochemistry, petrology and geochronology of the Ragunda rapakivi complex, central Sweden. Symposium on Rapakivi granites and related rocks. – Belém, Brazil. Abstracts vol., 62–63.
Persson, A.I., 1996a: The Ragunda rapakivi complex. *In* Ahl, M., Andersson, U.B., Bergman, T. Claesson, S., Fröjdö, S., Lindh, A., Lundqvist, T., Persson, A.I. & Sundblad, K.: Rapakivi granites and related rocks in central Sweden. – Excursion guide. 7:th International Symposium on Rapakivi Granites. IGCP 315, 62–75.
Persson, A.I., 1996b: Petrogenesis of the Ragunda rapakivi complex, central Sweden. – Seventh international symposium on rapakivi granites and related rocks. Helsingfors, 24-26/7 1996. Abstract Vol., p. 57.
Persson, L., 1974: Precambrian rocks and tectonic structures of an area in northeastern Småland, southern Sweden. – SGU C 703, 55 pp.
Persson, L., 1978: The Revsund–Sörvik granites in the western parts of the province of Ångermanland, central Sweden. – SGU C 741, 59 spp.
Persson, L., 1985: Beskrivning till berggrundskartorna Vetlanda NV och NO. (English summary.) – SGU Af 150 & 151, 138 pp.
Persson, L., 1989: Beskrivning till berggrundskartorna Vetlanda SV och SO. (English summary.) – SGU Af 170 & 171, 130 pp.
Persson, L. & Wikman, H., 1986: Beskrivning till provisoriska översiktliga berggrundskartan Jönköping. – SGU Ba 39, 25 pp.
Persson, L., Bruun, Å. & Dahlman, B., 1981: Beskrivning till berggrundskartan Linköping SV. – SGU Af 132, 150 pp.
Persson, L., Bruun, Å. & Vidal, G., 1985: Beskrivning till berggrundskartan Hjo SO. – SGU Af 134, 143 pp.
Persson, P.-O., 1995: "Radiometric age determinations of three rock samples from the access ramp to the Äspö Hard Rock Laboratory." Appendix 3. *In* Wikman, H. & Kornfält, K.-A.: Updating of a lithological model of the bedrock of the Äspö area. – SKB Progress report 25-95-04.
Persson, P-O. & Ripa, M., 1993: U-Pb zircon dating of a Järna-type granite in western Bergslagen, south-central Sweden. *In* Lundqvist, T. (ed.): Radiometric dating results. – SGU C 823, 41–45.
Persson, P.-O. & Wikström, A., 1993: A U-Pb dating of the Askersund granite and its marginal augen gneiss. – GFF 115, 321–329.
Peterson, J.W., Chacko, T. & Kuehner, S.M., 1991: The effects of fluorine on the vapor-absent melting of phlogopite+quartz: implications for deep crustal processes. – Am. Min. 76, 470–476.
Petrík, I. & Broska, I., 1989: Mafic enclaves in granitoid rocks of the Tribec Mountains, western Carpathians: geochemistry and petrology. – Geologicky Zborník-Geologica Carpathica 40, 667–696.
Pin, C., Binon, M., Belin, J.M., Barbarin, B. & Clemens, J.D., 1990: Origin of microgranular enclaves in granitoids: equivocal Sr-Nd evidence from Hercynian rocks of the Massif Central (France). – J. Geophys. Res. 95, 17821–17828.
Pitcher, W.S., 1993: The nature and origin of granite. – Blackie (Chapman-Hall), London, 321 pp.
Poli, G., Tommasini, S. & Halliday, A.N., 1996: Trace element and isotopic exchange during acid-basic magma interaction processes. – Trans. Roy. Soc. Edinb., Earth Sci,. 87, 225–232.
Presnall, D.C., Dixon, S.A., Dixon, J.R., O'Donnell, T.H., Brenner, N.L., Schrock, R.L. & Dycus, D.W. 1978: Liquidus phase relations on the join diopside-forsterite-anorthite from 1 atm to 20 kbar: their bearing on the generation and crystallization of basaltic magma. – Contr. Miner. Petr. 66, 20–220.
Presnall, D.C., Dixon, J.R., O'Donnell, T.H. & Dixon, S.A., 1979: Generation of mid-ocean ridge tholeiites. – J. Petr. 20,

3–35.
Provost, A., 1990: An improved diagram for isochron data. – Chem. Geol. 80, 85–99.
Rämö, O.T., 1990: Diabase dyke swarms and silicic magmatism – evidence from the Proterozoic of Finland. *In* Parker, A.J., Rickwood, P.C. & Tucker, D.H. (eds.): Mafic dykes and emplacement mechanisms. – Balkema, Rotterdam, pp. 185–199.
Rämö, O.T., 1991: Petrogenesis of the Proterozoic rapakivi granites and related basic rocks of southeastern Fennoscandia: Nd and Pb isotopic and general geochemic constraints. – Geol. Survey of Finl. Bull. 355, 161 pp.
Rämö, O.T. & Haapala, I., 1995: One hundred years of rapakivi granite. – Min. & Petr. 52, 129–185.
Rämö, O.T., Huhma, H. & Kirs, J., 1996: Radiogenic isotopes of the Estonian and Latvian rapakivi granite suites: new data from the concealed Precambrian of the east European craton. – Prec. Res. 79, 209–226.
Reid jr, J.B., Evans, O.C. & Fates, D.G., 1983: Magma mixing in granitic rocks of the central Sierra Nevada, California. – Earth Plan. Sci. Lett. 66, 243–261.
Reid jr, J.B. & Hamilton, M.A., (1987): Origin of Sierra Nevadan granite: evidence from small-scale composite dikes. – Contr. Min. Petr. 96, 441–454.
Rickard, D., 1986: Geology and metallogeny of the Skellefte field. *In* Rickard, D. (ed.): The Skellefte field. – SGU Ca 62, 5–20.
Rickard, D. & Svensson, S.-Å., 1984: Ore lead isotope variations in the Proterozoic massive pyrite deposit at Näsliden, Skellefte district, Sweden. – Miner. Dep. 19, 145–151.
Rickard, P., Shimizu, N. & Allegre, C.J., 1976: $^{143}Nd/^{146}Nd$, a natural tracer: an application to oceanic basalts. – Earth Plan. Sci. Lett. 31, 269–273.
Rodhe, A., 1992: Terminology and ideas regarding the Protogine zone in southern Sweden. – GFF 114, 360–365.
Rollinson, H.R., 1993: Using geochemical data. Evaluation, presentation, interpretation. – Longman, Harlow, 352 pp.
Romer, R.L., 1994: Rb-Sr data structure – a possible cause for differences in Rb-Sr whole-rock and U-Pb zircon ages. – GFF 116, 93–103.
Romer, R.L. & Smeds, S.-A., 1994: Implications of U-Pb ages of columbite-tantalites from granitic pegmatites for the Palaeoproterozoic accretion of 1.90–1.85 Ga magmatic arcs to the Baltic Shield. – Prec. Res. 67, 141–158.
Romer, R.L. & Öhlander, B., 1995: Tectonic implications of an 1846±1 Ma old migmatitic granite in south-central Sweden. – GFF 117, 69–74.
Romer, R.L. & Smeds, S.-A., 1996: U-Pb columbite ages of pegmatites from Sveconorwegian terranes in southwestern Sweden. – Prec. Res. 76, 15–30.
Romer, R.L., Kjösnes, B., Korneliussen, A., Lindahl, I., Skyseth, T., Stendal, M. & Sundvoll, B., 1992: The Archaean–Proterozoic boundary beneath the Caledonides of northern Norway and Sweden: U-Pb, Rb-Sr, and e_{Nd} isotope data from the Rombak–Tysfjord area. – NGU rapport 91.225, 66 pp.
Ruotoistenmäki, T., 1996: A schematic model of the plate tectonic evolution of Finnish bedrock. – Geol. Surv. Finl., Report of Invest. 133, 23 pp.
Rutter, M.J. & Wyllie, P.J., 1988: Melting of vapour-absent tonalite at 10 kbar to simulate dehydration-melting in the deep crust. – Nature 331, 159–160.
Ryan, B., 1991: Makhavinekh Lake pluton, Labrador, Canada: geological setting, subdivisions, mode of emplacement, and a comparison with Finnish rapakivi granites. – Prec. Res. 51, 193–225.
Sabatier, H., 1991: Vaugnerites: special lamprophyre-derived mafic enclaves in some Hercynian granites from western and central Europe. *In* Didier, J. & Barbarin, B. (eds.): Enclaves and granite petrology. – Developments in petrology 13, Elsevier, Amsterdam, pp. 63–81.
Sahama, Th.G., 1945: On the geochemistry of the east Fennoscandian rapakivi granites. – Bull. Comm. Geol. Finl. 136, 15–67.
Salonsaari, P.T., 1995: Hybridization in the subvolcanic Jaala-Iitti complex and its petrogenetic relation to rapakivi granites and associated mafic rocks of southeastern Finland. – Bull. Geol. Soc. Finl. 67, part 1b, 1–104.
Salvi, S. & Williams-Jones, A.E., 1990: The role of hydrothermal processes in the granite-hosted Zr, Y, REE deposit at Strange Lake, Quebéc/Labrador: evidence from fluid inclusions. – Geoch. Cosmoch. Acta 54, 2403–2418.
Sandiford, M., Foden, J., Zhou, S. & Turner, S., 1992: Granite genesis and the mechanics of convergent orogenic belts with application to the southern Adelaide fold belt. – Trans. Roy. Soc. Edinb., Earth Sci. 83, 83–93.
Savolahti, A., 1956: The Ahvenisto massif in Finland. – Bull. Comm. Geol. Finl. 174, 1–96.
Schaller, T., Dingwell, D.B., Keppler, H., Knöller, W., Merwin, L. & Sebald, A., 1992: Fluorine in silicate glasses: a multinuclear nuclear magnetic resonance study. – Geoch. Cosmoch. Acta. 56, 701–707.
Schmidt, M.W., 1992: Amphibole compostition in tonalite as a function of pressure: an experimental calibration of the Al-in-hornblende barometer. – Contr. Miner. Petrol. 110, 304–310.
Sederholm, J.J., 1926: On migmatites and associated Pre-Cambrian rocks of southwestern Finland. Part II. The region around the Barösundsfjärd w. of Helsingfors and neighbouring areas. – Bull. Comm. Geol. Finl. 77, 143 pp.
Shebanov, A.D., Belyaev, A.M. & Savatenkov, V.M., 1996: The significance of residual source material (restite) in rapakivi granite petrogenesis: an example from the Salmi batholith, Russian Karelia. – Seventh international symposium on rapakivi granites and related rocks. Helsingfors, 24.26/7 1996. Abstract Vol., p. 65.
Shirey, S.B., 1991: The Rb-Sr, Sm-Nd and Re-Os isotope systems: a summary and compilation of their applications to the cosmochronology and geochronology of igneous rocks. *In* Short course handbook on applications of radiogenic isotope systems to problems in geology (Heaman, L. & Ludden, J.N. eds.). – Min. Ass. Canada, Short course handbook Vol. 19, 103–166.
Siebel, W., Höhndorf, A. & Wendt, I., 1995: Origin of Variscan granitoids from NE Bavaria, Germany, exemplified by REE

and Nd isotope systematics. – Chem. Geol. 125, 249–270.
Simonen, A., 1980: The Precambrian in Finland. – Geol. Survey of Finl., Bull. 304, 58 pp.
Simonen, A. & Vorma, A., 1969: Amphibole and biotite from rapakivi. – Bull. Comm. Géol. Finl. 238, 28 pp.
Singh, J. & Johannes, W., 1996: Dehydration melting of tonalites. Part II. Composition of melts and solids. Contr. Miner. Petr. 125, 26–44.
Sisson, D.H., Mode, V.A. & Campbell, D.O., 1972: High-speed separation of the rare earths by ion exchange, part II. – J. Chromatogr. 66, 129–135.
Sisson, T.W., Grove, T.L. & Coleman, D.S., 1996: Hornblende gabbro sill complex at Onion Valley, California, and a mixing origin for the Sierra Nevada batholith. – Contr. Min. Petr. 126, 81–108.
Sjöström, H. & Bergman, S. ,1996: Deformation zones in central Sweden - relation to the Svecokarelian orogeny. – Abstract, The 22nd Nordic Geological Winter Meeting, Turku. Abstracts vol. p.194.
Skiöld, T., 1988: Implications of new U-Pb chronology to the early Proterozoic crustal accretion in northern Sweden. – Precambrian Res. 38, 147–164.
Skiöld, T., Öhlander, B., Markkula, H., Widenfalk, L. & Claesson, L.-Å., 1993: Chronology of Proterozoic orogenic processes at the Archaean continental margin in northern Sweden. – Prec. Res. 64, 225–238.
Skjerlie, K.P. & Johnston, A.D., 1993: Fluid-absent melting behavior of an F-rich tonalitic gneiss at mid-crustal pressures: implications for the generations of anorogenic granites. – J. Petr. 34, 785–815.
Smeds, S.-A., 1994: The Räggen Sn-deposit and the two types of granitic rare-mineral pegmatites of the Räggen area, Bräcke, Jämtland county, Sweden. – Abstract, 21.a Nordiska Geologiska Vintermötet, Luleå, p. 192.
Smith, E.I., Feuerbach, D.L., Naumann, T.R. & Mills, J.G., 1990: Mid-Miocene volcanic and plutonic rocks in the Lake Mead area of Nevada and Arizona: production of intermediate igneous rocks in an extensional en-vironment. – Geol. Soc. Am., Mem. 174, 169–194.
Sobral, J.M., 1913: Contributions to the geology of the Nordingrå region. – Ph.D.-thesis (unpubl.), Uppsala Univ. 177 pp.
Souther, J.G. & Hickson, C.J., 1984: Crystal fractionation of the basalt comendite series of the Mount Edziza volcanic complex, British Columbia: major and trace elements. – J. Volc. Geoth. Res. 21, 79–106.
Sparks, R.S.J. & Marshall, L.A., 1986: Thermal and mechanical constraints on mixing between mafic and silicic magmas. – J. Volc. Geoth. Res. 29, 99–124.
Spera, F.J., Borgia, A. & Strimple, J., 1988: Rheology of melts and magmatic suspensions. 1. Design and calibration of concentric cylinder viscosimeter with applications to rhyolite magma. – J. Geoph. Res. 93, 10273– 10294.
Stacey, J.S. & Kramers, J.D., 1975: Approximation of the terrestrial lead isotope evolution by a two-stage model. – Earth Plan. Sci. Lett. 26, 207–221.
Stålhös, G., 1991: Beskrivning till berggrundskartorna Östhammar NV, NO, SV, SO. – SGU Af 161, 166, 169, & 172. 249 pp.
Steiger, R.H. & Jäger, E., 1977: Subcommission on geochronology: Convention on the use of decay constants in geo- and cosmochronology. – Eart Plan. Sci. Lett. 36, 359–362.
Stephens, M.B. & Wahlgren, C.-W., 1996: Post-1.85 Ga tectonic evolution of the Svecokarelian orogen with special reference to central and SE Sweden. – GFF 118, A26–A27.
Stephens, M.B., Wahlgren, C.-H. & Annertz, K., 1993: U-Pb zircon dates in two younger suites of Palaeoprotrozoic intrusions, Karlskoga area, south-central Sweden. – SGU C 823, 46–58.
Stephens, M.B., Wahlgren, C.-H., Weijermars, R. & Cruden, A.R., 1996: Left-lateral transpressive deformation and its tectonic implications, Sveconorwegian orogen, Baltic shield, southwestern Sweden. – Prec. Res. 79, 261–279.
Stimac, J.A. & Wark, D.A., 1992: Plagioclase mantles on sanidine in silicic lavas, Clear Lake, California: Implications for the origin of rapakivi texture. – Geol Soc Am Bull 104, 728–744.
Stimac, J.A., Clark, A.H., Chen, Y. & Garcia, S., 1995: Enclaves and their bearing on the origin of the Cornubian batholith, southwest England. – Min. Mag. 59, 273–296.
Stolpe, M., 1881a: Beskrifning till kartbladet "Tjällmo". – SGU Aa 70, 22 pp.
Stolpe, M., 1881b: Beskrifning till kartbladet "Finspång". – SGU Aa 82, 20 pp.
Stormer, J.C. & Nicholls, J., 1978: XLFRAC: a program for the interactive testing of magmatic differentiation models. – Comp. & Geosci. 4, 143–159.
Sundblad, K., 1991: Lead isotopic evidence for the origin of 1.8–1.4 Ga ores, and granitoids in the southeastern part of the Fennoscandian shield. – Prec. Res. 51, 265–281.
Sundblad, K., Särkinen, M. & Mansfeld, J., 1988: Origin of precious and base metal deposits in the Fröderyd area, southern Sweden. – Abstract. 18:de Nordiska Geologiska Vintermötet, Köpenhamn, 12-14/1 1988. Absracts Vol., 397–398.
Sundblad, K., Weihed, P., Billström, K., Markkula, H. & Mäkelä, M., 1993: Source of metals and age constraints for epigenetic gold deposits in the Skellefte and Pohjanmaa districts, central part of the Fennoscandian shield. – Miner. Dep. 28, 181–190.
Suominen, V., 1991: The chronostratigraphy of SW Finland with special reference to the Postjotnian and Subjotnian diabases. – Geol. Survey of Finl. Bull. 356, 100 pp.
Sviridenko, L.P., 1968: Petrology of the Salmi rapakivi granite massif. (In Russian.) 115 pp.
Taylor, R.P. & Pollard, P.J., 1996: Rare earth element mineralization in peralkaline systems: the T-zone REE-Y-Be deposit, Thor Lake, Northwest Territories, Canada. *In* Jones, A.P., Wall, F. & Williams, C.T. (eds.): Rare earth minerals. Chemistry, origin and ore deposits. – The Min. Soc. Series, vol. 7, 167–192.
Taylor, S.R. & McLennan, S.M., 1985: The continental crust: its composition and evolution. – Blackwell, Oxford. 312 pp.
Taylor, T.R., Vogel, T.A. & Wilband, J.T., 1980: The composite dikes at Mount Desert Island, Maine: an example of coexisting acidic and basic magmas. – J. Geol. 88, 433–444.
Thompson, R.N. & MacKenzie W.S., 1967: Feldspar-liquid equilibria in peralkaline acid liquids: an experimental study. – Am.

J. Sci. 265, 714–734.
Thompson, R.N., Morrison, M.A., Dickin, A.P. & Hendry, G.L., 1983: Continental flood basalts...arachnids rule OK? *In* C.J. & Norry, M.J. (eds.): Continental basalts and mantle xenoliths, Hawkesworth. – Shiva Publ., Nantwich, pp. 158–185.
Thompson, R.N., Morrison, M.A., Hendry, G.L. & Parry, S.J., 1984: An assessment of the relative roles of crust and mantle in magma genesis: an elemental approach. – Phil. Trans. R. Soc. Lond. A310, 549–590.
Thorpe, R.S. & Tindle, A.G., 1992: Petrology and petrogenesis of a Tertiary bimodal dolerite-peralkaline/subalkaline trachyte/rhyolite dyke association from Lundy, Bristol Channel, UK. – Geol. J. 27, 101–117.
Törnebohm, A.E., 1877: Om sandstens bäckenet i Gästrikland. – GFF 3, 412–420.
Upton, B.G.J., 1960: The alkaline igneous complex of Kûngnât Fjeld, south Greenland. – Medd. om Grønland Bd. 123, Nr. 4, 145 pp.
Upton, B.G.J., 1962: Geology of Tugtutôq and neighbouring islands, south Greenland. Part I. – Grønlands Geol. Unders., Bull. 34, 60 pp.
Upton, B.G.J., 1964: The geology of Tugtutôq and neighbouring islands, south Greenland. Part II. Nordmarkitic syenites and related alkaline rocks. – Medd. om Grønland. Bd. 169, Nr. 2, 62 pp.
Upton, B.G.J., Aspen, P. & Chapman, N.A., 1983: The upper mantle and deep crust beneath the British Isles: evidence from inclusions in volcanic rocks. – J. Gel. Soc. Lond. 140, 105–121.
Vaasjoki, M., 1977. Rapakivi granites and other postorogenic rocks in Finland: Their age and the lead isotopic composition of certain associated galena mineralizations. – Geol. Surv. Finl., Bull. 294, 1–64.
Vaasjoki, M., 1981: The lead isotopic composition of some Finnish galenas. – Geol. Surv. of Finl., Bull. 316, 30 pp.
Vaasjoki, M. & Sakko, M., 1988: Evolution of the Raahe-Ladoga zone in Finland: isotopic constraints. *In* Korsman, K. (ed.): Tectono-metamorphic evolution of the Raahe-Ladoga zone. – Geol. Surv. of Finl., Bull. 343, 7–32.
Vaasjoki, M. & Vivallo, W., 1990: New lead isotope determination from five Proterozoic sulfide deposits, Skellefte district, Sweden. – Miner. Dep. 25, 50–56.
Vaasjoki, M., Pihlaja, P. & Sakko, M., 1988: The radiometric age of the Reposaari granite and its bearing on the extent of the Laitila rapakivi batholith in western Finland. – Bull. Geol. Soc. Finl. 60, 129–134.
Vaasjoki, M., Rämö, O.T. & Sakko, M., 1991: New U-Pb ages from the Wiborg rapakivi area: Constraints on the temporal evolution of the rapakivi granite – anorthosite – diabase dyke association of southeastern Finland. – Prec. Res. 51, 227–243.
Vaasjoki, M., Rämö, O.T., Alviola, R. & Johanson, B.S., 1993: Petrography and new U-Pb age data on the Ahvenisto rapakivi granite complex, southeastern Finland. – Geological Society of America, Abstracts with Programs. 25, p. 86.
Väisänen, M. & Hölttä, P., 1996: Evolution of the crust in the high T-low P belt in SW Finland. – Abstract, The 22nd Nordic Geological Winter Meeting, Turku. Abstracts vol. p. 227.
Väisänen, M., Hölttä, P., Rastas, J., Korja, A. & Heikkinen, P., 1994: Deformation, metamorphism and the deep structure of the crust in the Turku area, southwestern Finland. – Geol. Surv. Finl., Guide 37, 35–41.
Valbracht, P.J., 1991: The origin of the continental crust of the Baltic shield, as seen through Nd and Sr isotopic variations in 1.89–1.85 Ga old rocks from western Bergslagen, Sweden. – Ph.D.-thesis, Amsterdam, GUA Papers of Geology, Series 1, No 29, 222 pp.
Van der Laan, S.R. & Wyllie, P.J., 1993: Experimental interaction of granitic and basaltic magmas and implications for mafic enclaves. – J. Petr. 34, 491–517.
Van der Molen, I. & Paterson, M.S., 1979: Experimental deformation of partially melted granite. – Contr. Miner. Petr. 70, 218–229.
Vernon, R.H., (1983): Restite, xenoliths and microgranitoid enclaves in granites. – J. Proc. Roy. Soc. NS Wales 116, 77–103.
Vernon, R.H., 1990: Crystallization and hybridism in microgranitoid enclave magmas: microstructural evidence. – J. Geophys. Res. 95, 17849–17859.
Vielzeuf, D. & Holloway, J.R., 1988: Experimental determination of the fluid-absent melting reactions in the pelitic system. Consequences for crustal differentiation. – Contr. Miner. Petr. 98, 257–276.
Vinnefors, A., 1985: Post-Svecokarelian basic plutonics and bronzite diabases in eastern Värmland, Sweden. – Univ. of Gothenburg, Geol. Inst. Publ. A 50, 228 pp (Ph.D.-thesis).
Vivallo, W., 1987: Early Proterozoic bimodal volcanism, hydrothermal activity, and massive sulphide deposition in the Boliden–Långdal area, Skellefte district, Sweden. – Econ. Geol. 82, 440–456.
Vivallo, W. & Claesson, L-Å., 1987: Intra-arc rifting and massive sulphide mineralization in an early Proterozoic volcanic arc, Skellefte district, northern Sweden. *In* Pharaoh, T.C., Beckinsale, R.D. & Rickard, D. (eds.): Geochemistry and mineralization of Proterozoic volcanic suites. – Geol. Soc., Spec. Publ. 33, 69–79.
Vivallo, W. & Willdén, M., 1988: Geology and geochemistry of an early Proterozoic volcanic arc sequence at Kristineberg, Skellefte district, Sweden. – GFF 110, 1–12.
Vorma, A., 1971: Alkali feldspars of the Wiborg rapakivi massif in southeastern Finland. – Bull. Comm. Geol. Finl. 246, 72 pp.
Vorma, A., 1972: On te contact aureole of the Wiborg rapakivi granite massif in southeastern Finland. – Geol. Survey Finl., Bull. 255, 28 pp.
Vorma, A., 1975: On two roof pendants in the Wiborg rapakivi massif, southeastern Finland. – Gel. Survey Finl., Bull. 272, 86 pp.
Vorma, A., 1976: On the petrochemistry of rapakivi granites with special reference to the Laitila massif, southwestern Finland. – Geol. Surv. Finl., Bull. 285, 1–98.
Voshage, H, Hofmann, A.W., Mazzuchelli, M., Rivalenti, G., Sinigoi, S., Raczek, I. & Demarchi, G., 1990: Isotopic evidence from the Ivrea zone for a hybrid lower crust formed by magmatic underplating. – Nature 347, 731–736.

Wager, L.R., Vincent, E.A., Brown, G.M. & Bell, J.D. (1965): Marscoite and related rocks of the western Red Hills complex, Isle of Skye. – Phil. Trans. Roy. Soc. Lond. A257, 273–307.

Wahlgren, C.-H., in prep: Beskrivning till berggrundskartan Askersund NV.

Wahlgren, C.-H., Cruden, A.R. & Stephens, M.B., 1994: Kinematics of a major fan-like structure in the eastern part of the Sweconorwegian orogen, Baltic shield, south-central Sweden. – Prec. Res. 70, 67–91.

Walker, G.P.L. & Skelhorn, R.R., 1966: Some associations of acid and basic igneous rocks. – Earth-Sci. Rev. 2, 93–109.

Watson, E.B., Brenan, J.M. & Baker, D.R., 1990: Distribution of fluids in the continental mantle. *In* Menzies, M.A. (ed.): Continental mantle. – Oxford Sci. Publ., Oxford, pp. 111–125.

Weaver, S.D., 1978: The Quarternary caldera volcano Emuruangogolak, Kenya rift, and the petrology of bimodal ferrobasalt-pantelleritic trachyte association. – Bull. Volc. 40, 209–230.

Webster, J.D., 1990: Partitioning of F between H_2O and CO_2 fluids and topaz rhyolite melt. – Contr. Miner. Petr. 104, 424–438.

Weihed, P., Bergman, J. & Bergström, U., 1992: Metallogeny and tectonic evolution of the early Proterozoic Skellefte district, northern Sweden. – Prec. Res. 58, 143–167.

Weinberg, R.F., 1992: Internal circulation in a buoyant two-fluid Newtonian sphere: implications for composed magmatic diapirs. – Earth Plan. Sci. Lett. 110, 77–94.

Welin, E., 1994: The U-Pb zircon age of the Rödön rapakivi granite, central Sweden. – GFF 116, 113–114.

Welin, E. & Lundqvist, Th., 1984: Isotopic investigations of the Nordingrå rapakivi massif, north-central Sweden. – GFF 106, 41–49.

Welin, E., Christiansson, K. & Kähr, A.-M., 1993: Isotopic investigations of metasedimentary and igneous rocks in the Palaeoproterozoic Bothnian basin, central Sweden. – GFF 115, 285–296.

Wendlandt, R.F. & Harrison, W.J., 1979: Rare earth partitioning between immiscible carbonate and silicate liquids and CO_2 vapor: results and implications for the formation of light rare earth-enriched rocks. – Contr. Mineral. Petr. 69, 409–419.

Wendt, I., 1993: Isochron or mixing line. – Chem. Geol. 104, 301–305.

Westergård, A.H., Johansson, H.E. & Willén, N., 1926: Beskrivning till kartbladet Karlsborg. – SGU Aa 162, 94 pp.

Whalen, J.B. & Currie, K.L. (1984): The Topsails igneous terrane, western New Foundland: Evidence for magma-mixing. – Contr. Min. Petr. 87, 319–327.

Whalen, J.B., Currie, K.L. & Chappell, B.W., 1987: A-type granites: geochemical characteristics, discrimination, and petrogenesis. – Contr. Min. Petr. 95, 407–419.

Whitney, J.A., 1975: The effects of pressure, temperature, and X_{H2O} on phase asemblages in four synthetic rock compositions. – J. Geol. 83,1–30.

Wiebe, R.A., 1974: Coexisting intermediate and basic magmas, Ingonish, Cape Breton Island. – J. Geol. 82, 74–87.

Wiebe, R.A., 1980: Commingling of contrasted magmas in the plutonic environment: examples from the Nain anorthosite complex. – J. Geol. 88, 197–209.

Wiebe, R.A., 1988: Structural and magmatic evolution of a magma chamber: The Newark Island layered intrusion, Nain, Labrador. – J. Petr. 29, 383–411.

Wiebe, R.A., 1991: Commingling of contrasted magmas and generation of mafic enclaves in granitic rocks. *In* Didier, J. & Barbarin, B. (eds.), 1991: Enclaves and granite petrology. Developments in petrology 13, Else-vier, Amsterdam, pp. 393–402.

Wiebe, R.A., 1993: The Pleasant Bay layered gabbro-diorite, coastal Maine: ponding and crystallization of basaltic injections into a silicic magma chamber. – J. Petr. 34, 461–489.

Wiebe, R.A., 1994: Silicic magma chambers as traps for basaltic magmas: the Cadillac Mountain intrusive complex, Mount Desert Island, Maine. – J. Geol. 102, 423–437.

Wiebe, R.A., 1996: Mafic-silicic layered intrusions: the role of basaltic injections on magmatic processes and the evolution of silicic magma chambers. – Trans. Roy. Soc. Edinb., Earth Sci. 87, 233–242.

Wiebe, R.A., Smith, D., Sturm, M., King, E.M. & Seckler, M.S., 1997: Enclaves in the Cadillac Mountain granite (coastal Maine): samples of hybrid magma from the base of the chamber. – J. Petr. 38, 393–423.

Wiechert, U., Ionov, D.A. & Wedepohl, K.H., 1997: Spinel peridotite xenoliths from the Atsagin-Dush volcano, Dariganga lava plateau, Mongolia: a record of partial melting and cryptic metasomatism in the upper mantle. – Contr. Min. Petr. 126, 345–364.

Wikman, H., 1993: U-Pb ages of Småland granites and a Småland volcanite from the Växjö region, southern Sweden. – SGU C 823, 64–71.

Wikman, H. & Kornfält, K.-A., 1995: Updating of a lithological model of the bedrock of the Äspä area. – SKB Progress Report 25-95-04.

Wikman, H., Bruun, Å. & Dahlman, B., 1980: Beskrivning till berggrundskartan Linköping NV. – SGU Af 119, 105 pp.

Wikman, H., Bruun, Å, Dahlman, B. & Vidal, G., 1982: Beskrivning till berggrundskartan Hjo NO. – SGU Af 120, 112 pp.

Wikström, A., 1976: Beskrivning till berggrundskartan Katrineholm SV. – SGU Af 116, 88 pp.

Wikström, A., 1984: A possible relationship between augen-gneisses and post-orogenic granites in SE Sweden. – J. Struct. Geol. 6, 409–415.

Wikström, A., 1987: Magmatic diapirism of granites in south-eastern Sweden. – Revista Brasil. Geociencias 17, 456–458.

Wikström, A., 1991: Structural features of some younger granitoids in central Sweden, and implications for the tectonic subdivision of granitoids. – Prec. Res. 51, 151–159.

Wikström, A., 1992: Some composite dikes in Sweden. – GFF 114, 385–394.

Wikström, A., 1993: U-Pb dating of the Stormandebo rhyolite in the Västervik area, southeastern Sweden. – SGU C 823,

72–76.
Wikström, A., 1995: Berggrunden på kartbladet 9E Askersund SO. *In* Wahlgren, C.-H.(ed.): Regional berggrundsgeologisk underökning. Sammanfattning av pågående undersökningar 1994. – SGU Rapp. & Medd. 79, 17–20.
Wikström, A., 1996: U-Pb zircon dating of a coarse porphyritic quartz monzonite and an even grained, grey tonalitic gneiss from the Tiveden area, south central Sweden. – SGU C 828, 41–47.
Wikström, A., in prep.: Beskrivning till berggrundskartorna Askersund NO, SO.
Wikström, A. & Aaro, S., 1986: The Finspång augen-gneiss massif – geology, geophysics and relationships to post-orogenic granites. – SGU C 813, 39 pp.
Wikström, A. & Karis, L., 1991: Beskrivning till berggrundskartorna Finspång NO, SO, NV, SV. – SGU Af 162, 163, 164, 165, 216 pp.
Wikström, A. & Larsson, L., 1993: Geothermometry of garnet-cordierite rocks in Kilsbergen and northern Tiveden, southern Sweden. – GFF 115, 339–344.
Wikström, A., Aaro, S. & Lagmansson, M., 1980: The Graversfors and Stavsjö granites and some problems connected with the magmatism in the final stages of the Svecokarelian orogeny. – SGU C 773, 48 pp.
Wikström, A., Annertz, K. & Wahlgren, C.-H.,1985: Post-granitoid basic plutonics in the Småland–Värmland belt. – GFF 107, 183–184.
Wikström, A., Mellqvist, C. & Persson, P.-O., 1996: An Archaean megaxenolith and a Proterozoic fragment within the Bälinge magmatic breccia, Luleå, northern Sweden. – SGU C828, 48–56.
Williams, L.A.J., 1970: The volcanics of the Gregory Rift Valley, East Africa. – Bull. Volc. 34, 439–465.
Williams-Jones, A.E. & Wood, S.A., 1992: A preliminary petrogenetic grid for REE fluorocarbonates and associated minerals. – Geoch. Cosmoch. Acta 56, 725–738.
Wilson, M., 1989: Igneous petrogenesis. A global tectonic approach. – Unwin-Hyndman, London, 466 pp.
Wilson, M.R., 1980: Granite types in Sweden. – GFF 102, 167–176.
Wilson, M.R., 1982: Magma types and the tectonic evolution of the Swedish Proterozoic. – Geol. Rundsch. 71, 120–129.
Wilson, M.R., Hamilton, P.J., Fallick, A.E., Aftalion, M. & Michard, A., 1985: Granites and early Proterozoic crustal evolution in Sweden: evidence from Sm-Nd, U-Pb and O isotope systematics. – Earth Plan. Sci. Lett. 72, 376–388.
Wilson, M.R., Fallick, A.E., Hamilton, P.J. & Persson, L., 1986: Magma sources for some mid-Proterozoic granitoids in SE Sweden: geochemical and isotopic constraints. – GFF 108, 79–91.
Wilson, M.R., Öhlander, B., Cuney, M. & Hamilton, P.J., 1987a: Geodynamic significance of contrasting granitoid types in Northern Sweden. *In* A. Kröner (ed.): Proterozoic lithospheric evolution. – Am. Geophys. Union, Geodyn. Ser. 17, 161–173.
Wilson, M.R., Sehlstedt, S., Claesson, L.-Å., Smellie, J.A.T., Aftalion, M., Hamilton, P.J. & Fallick, A.E., 1987b: Jörn: an early Proterozoic intrusive complex in a volcanic-arc environment, north Sweden. – Prec. Res. 36, 201–225.
Wood, S.A., 1990: The aqueous geochemistry of rare earth elements and yttrium. 2. Theoretical predictions of speciation in hydrothermal solutions to 350°C at saturation water vapour pressure. – Chem. Geol. 89, 99–125.
Woolley, A.R. & Jones, C.G., 1987: The petrochemistry of the northern part of the Chilwa alkaline province, Malawi. *In* Fitton, J.G. & Upton, B.G.J. (eds.): Alkaline igneous rocks. – Geol. Soc., Spec. Publ. 30, 335–355.
Wright, J.B., 1966: Olivine nodules in a phonolite of the east Otago alkaline province, New Zealand. – Nature 210, 519.
Wyllie, P.J., 1979: Magmas and volatile components. – Am. Min. 64, 469–500.
Wyllie, P.J., Cox, K.G. & Biggar, G.M., 1962: The habit of apatite in synthetic systems and igneous rocks. – J. Petrol. 3, 238–243.
Yoder jr, H.S., 1973: Contemporaneous basaltic and rhyolitic magmas. – Am. Min. 58, 153–171.
Zanvilevich, A.N., Litvinovsky, B.A., Wickham, S.M. & Bea, F., 1995: Genesis of alkaline and peralkaline syenite-granite series: the Kharitonovo pluton (Transbaikalia, Russia). – J. Geol. 103, 127–145.
Zartman, R.E. & Doe, B.R., 1981: Plumbotectonics – the model. – Tectonophys. 75, 135–162.
Zindler, A. & Hart, S.R., 1986: Chemical geodynamics. – Ann. Rev. Earth Plan. Sci. 14, 493–571.
Zorpi, M.J., Coulon, C., Orsini, J.B. & Cocirta, C., 1989: Magma mingling, zoning and emplacement in calcalkaline granitoid plutons. – Tectonophys. 157, 315–329.
Zorpi, M.J., Coulon, C. & Orsini, J.B., 1991: Hybridization between felsic and mafic magmas in calc-alkaline granitoids – a case study in northern Sardinia, Italy. – Chem. Geol. 92, 45–86.
Zuber, J.A. & Öhlander, B., 1990: Geophysical and geochemical evidence of Proterozoic collision in the western marginal zone of the Baltic shield. – Geol. Rundsch. 79, 1–11.
Zuber, J.A. & Öhlander, B., 1991: Gravimetrical and geochemical studies of 1.8 Ga old granites in the Strängnäs–Enköping area, south central Sweden. – GFF 113, 309–318.

Appendices:

APPENDIX 1. ANALYTICAL TECHNIQUES

All samples in Appendix 2b and most of the samples in Appendix 2a (indicated) have been analysed for *whole rock (WR) geochemistry* by X-ray Assay Laboratories, Don Mills, Ontario, Canada (XRAL). Three different analytical methods were utilized: 1) X-ray fluorescence spectrometry (XRF), 2) neutron activation analysis (NA), and 3) inductively coupled plasma-atomic emission (ICP-AES) spectrometry. Of the listed elements, the following are reported from a) XRF: all major element oxides, Rb, Ba, Zr, and Nb, b) NA: Cs, Th, U, Hf, Ta, Sc, Co, Sb, and the rare earth elements (REEs), ICP: Sr, Li, Be, Y, Pb, Sn, Zn, V, Cr, Ni, Cu, Ag, and Bi. F was analysed separately using specific ion wet chemical methods. Certain elements were analysed by several of the methods. The choice of analysis in these cases was decided based on i. precision of the analysis (reproducibility, closeness to detection limits), ii. accuracy (closeness to a "correct" value), iii. uniformity (e.g. all major oxides by XRF). This means that an element which is close to its detection limit with one method generally will have worse reproducibility compared with a method with a lower detection limit. This, however, does not mean that the accuracy of the first method is lower than the other. Generally, the ICP method has lower detection limits compared with XRF (and for certain elements compared with NA), but due to the chemical dissolution step necessary in this method some elements bound in very resistant minerals, such as e.g. zircon, may not be fully digested and therefore be lost. This means that the accuracy in the ICP analyses of these elements is lower (in this case giving too low abundances). Such effects are clearly seen for elements like Zr, Nb, Sr, Y, and Zn. The methods not involving a chemical preparation step (XRF and NA) are clearly indicated to have better accuracy (also seen in the closeness to the "literature" value for an analysed rock standard (AGV-1, USGS andesite standard)). When possible, XRF or NA were therefore preferred to ICP. However, ICP was still selected for, e.g. Sr, Y, and Zn due to its lower detection limits since the contents of many samples were not detected by the other methods. This may have led to somewhat too low reported abundances. Certain analysed elements are not reported here due to 1) generally too low concentrations (Mo), 2) contamination during sample preparation (W, may also apply to the reported Co), or 3) little petrogenetic interest (Au, As, Se, Br, Cd, and Ir).

XRAL reports precision (reproducibilities) for duplicate samples (as relative standard deviations) according to method and concentration for each element as follows (for the concentration ranges applicable in this study). The highest standard deviations are usually for the samples with the lowest concentration of each element.

XRF: SiO_2 (0.56%), TiO_2 (1.18–6.04%), Al_2O_3 (0.47%), Fe_2O_{3*} (1.39%), MnO (0.74–1.04%), MgO (0.78%), CaO (0.75%), Na_2O (1.30%), K_2O (1.10%), P_2O_5 (0.05–1.48%), Ba (1.65–4.79%), Rb (4.23–15.16%), Zr (4.23–12.96%).

ICP-AES: Sr (3.19–4.32%), Li (8.60–12.00%), Be (8.49–22.10%), Y (3.91–4.82%), Pb (8.23–16.93%), Sn (2.71–20.66%), Zn (4.13–7.17%), V (6.04–32.30%), Cr (6.43–49.46%), Ni (3.79–20.44%), Cu (5.52–18.99%), Ag (12.27–36.95%), Bi (17.37–19.05%). Ga not reported.

XRAL also reports reproducibility for the XRF method on 42 different sample preparations of one single sample (the material is not stated) as follows: SiO_2 65.9±0.25% (1 std.dev.), TiO_2 0.33±0.005%, Al_2O_3 13.0±0.06%, Fe_2O_3 7.14±0.03%, MnO 0.14±0.005%, MgO 6.08±0.06%, CaO 0.72±0.005%, Na_2O 0.60±0.02%, K_2O 2.51±0.01%, P_2O_5 0.10±0.00x%, Rb 220±20 ppm, Ba 1200±40 ppm, Zr 280±10 ppm, Nb 870±20 ppm.

Reproducibility of the NA analyses is reported as 10 duplicate analyses of the NBS standard number 1632a as follows: Cs 2.3±0.1 ppm, Th 4.39±0.08 ppm, Hf 1.35±0.05 ppm, Sc 6.05±0.04 ppm, Co 6.2±0.2 ppm, La 15.5±0.4 ppm, Ce 29.4±0.7 ppm, Nd 11.5±0.8 ppm, Sm 2.23±0.03 ppm, Eu 0.53±0.04 ppm, Tb 0.31±0.03 ppm, Yb 1.10±0.08 ppm, Lu 0.186±0.007 ppm.

The present author has made a similar test of reproducibility by supplying one specific sample repeated times for analysis (S8, Strömsund granite; Appendix 1a). 5 analyses gave the following reproducibilities (method; average± 1s %):

SiO_2 (XRF; 72.28±0.5 %), TiO_2 (XRF; 0.48±2.8 %), Al_2O_3 (XRF; 13.16±0.8 %), Fe_2O_3 (XRF; 2.80±2.5 %), MnO (XRF; 0.05±8.4 %), MgO (XRF; 0.44±1.5 %), CaO (XRF; 1.14±9.7 %), Na_2O (XRF; 3.80±0.6 %), K_2O (XRF; 5.10±2.1 %), P_2O_5 (XRF; 0.10±3.9 %), F (WET; 1313±3.0 %), Ba (XRF; 485±17 %), Rb (XRF; 146±7 %), Sr (ICP; 143±2.9 %), Th (NA; 9.0±6.5 %), U (NA; 2.5±30 %), Li (ICP; 16.2±16 %), Be (ICP; 2.8±5.5 %), Ga (ICP; 22±8 %), Y (ICP; 18.0±2.4 %), Zr (XRF; 260±5 %), Hf (NA; 6.5±7.5 %), Nb (XRF; 27±17 %), Zn (ICP; 47.3±3.0 %), Sc (NA; 2.6±5.0 %), Co (NA; 67±4.0 %), V (ICP; 14.4±11 %), Cr (ICP; 2.25±37 %), Ni (ICP; 2.2±34 %), Cu (ICP; 4.7±55 %), Ag (ICP; 0.43±11 %), La (NA; 43.8±4.2 %), Ce (NA; 85.2±4.6 %), Nd (NA; 36±14 %), Sm (NA; 6.6±4.5 %), Eu (NA; 1.0±28 %), Tb (NA; 0.8±20 %), Yb (NA; 1.7±4.5 %), and Lu (NA; 0.25±7.5 %).

Due to the low contents and closeness to the detection limits, the errors in analyses are exceptionally large for Cr, Ni, and Cu in this granite. Nevertheless, a qualitative picture of the reproducibilities associated with granite analyses at this lab (XRAL) emerges.

The precision is monitored by XRAL by analyzing a number of reference materials. The XRF measurements of these standards are reported to be close to the values in the literature, but the number of analyses used is not stated.

A number of analyses in Appendix 2a were performed at other labs as indicated. No statistics concerning reproducibility are available for these analyses. The wet chemical analyses of major elements performed at the Institute of Geology in Uppsala (Anne-Marie Karlsson) and Geological Survey of Sweden (SGU) (Carl-Magnus Backman) are believed to be of very good quality. The atomic absorption analyses (SGU) of Rb, Sr, Y, Zr have been rounded off to tenths of ppm, according to estimated errors in reproducibility. NA analyses were performed at Studsvik Energiteknik AB and measured 15 days after irradiation. A few analyses were selected from Armands & Drake (1978), the qualities of which are stated there.

The *isotopic analyses* presented in Tables 2, 3, 12, 13, and 21, were performed by the present author at the Laboratory of Isotope Geology (LIG) at the Swedish Museum of Natural History, in Stockholm, while the Nd isotopic analyses in Table 22, were performed by Dr. Leonid Neymark at the Institute of Precambrian Geology and Geochronology in St. Petersburg. Dr. Neymark also made the U-Pb, Pb-fsp, and Sr isotopic analyses reported in Tables 20, 22, and 23, while working at United States Geological Survey in Denver. The Pb-WR analyses in Table 14 were performed by Dr. Kjell Billström at LIG, Stockholm.

For the WR analyses performed at LIG, 100–200 mg rock powder was weighed in and added to teflon capsules, so-called Krogh capsules. The method essentially follows Krogh (1973). The samples were dissolved in a mixture of concentrated HF and HNO_3 for at least five days at 205°C, and thereafter in 6N HCl for at least one day. After this treatment a clear solution was obtained which was evaporated and dissolved in 1 ml 2.5N HCl. The solutions were then added to 3.5 ml ion exchange columns, filled with Biorad AG 50W-X8 200–400 mesh resin, for the separation of Sr and the REEs (and in some samples Pb). Sr was eluated with 2.5N HCl and the REEs with 6N HNO_3. The Sr fraction was then further purified in a second ion exchange step by the same procedure. The REE fractions were evaporated, and then dissolved in 0.22N (pH ca 4.5) α-Hiba (α-hydroxyisobutyric acid, $C_4H_8O_3$) solution and added to another set of ion exchange columns for the separation of Sm and Nd. These c. 0.9 ml columns were filled with Biorad AG 50W-X12 200–400 mesh resin. Eluation was performed in a closed pressure-driven system with α-Hiba pH- adjusted to c. 4.5, where Sm was extracted before Nd (e.g. Sisson et al. 1972) The evaporated fractions of Sm and Nd were dissolved in 2.5N HNO_3 and loaded onto Re filaments together with 0.75N H_3PO_4. Sr was dissolved in 2.5N HCl and evaporated om Re filaments without additional H_3PO_4. The analyses were performed on a Finnegan MAT 261 multicollector mass spectrometer in a static mode.

The samples were spiked with a mixed $^{150}Nd/^{147}Sm$ spike initially during weighing (totally spiked). The measurements were normalized to $^{146}Nd/^{144}Nd=0.7219$. During the course of this study (900613-951122) the analytical stability of the instrument has been monitored by repeated measurements of the La Jolla Nd standard. During measurements of the variable detector cup sensitivities and calculation of relative Faraday cup efficiencies according to Makishima & Nakamura (1991), a value of the La Jolla standard of 0.511854 was obtained (H. Schöberg pers. comm. 1996). This value is considered as the best estimate of the actual value. Considerable fluctuations of the measured standard value have, however, been documented, and generally these values have been below the "best estimate" above. During different time periods with relatively uniform standard values average $^{143}Nd/^{144}Nd$ have been calculated, and used to correct the measurements of the samples. The average measured $^{143}Nd/^{144}Nd$ values of the La Jolla standard during the different periods and the used correction factor were as follows, 900101-910930: 0.511817±16 (1s; n=29; corr.fact.= +0.000037), 911001-920930: 0.511783±9 (n=10; c.f.= +0.000071, no measurements in this study), 921001-931231: An RFCE (relative Faraday cup efficiency; Makishima & Nakamura 1991) calibration of about +0.000100 was included in the program, automatically calibrating the data output. This procedure gave an average $^{143}Nd/^{144}Nd$ of 0.511875±42 (n=101), which is 0.000021 above the "best estimate". This was considered sufficiently close and no further correction was applied. After this period the RFCE calibration was abandoned, and regular measurements and corrections utilized again. 940101-940331: 0.511741±12 (n=28; c.f.= +0.000113; no measurements in this study), 940401-940715: 0.511766±33 (n=26; c.f. = +0.000088), 940716-941102: no measurements, 941103-941231: 0.511782±13 (n=24; c.f.= +0.000072), 950101-950516: 0.511766±16 (n=17; c.f. +0.000088), 950517-950711: no measurements, 950712-951231: a very unstable period, which has been subdivided into short periods with relatively stable La Jolla measurements. Just a few measurements in this study were made during 951121-951123.

950712-950717: 0.511842±14 (n=8; c.f. +0.000012), 950815-950912: 0.511797±19 (n=13; c.f. = +0.000057), 951016-951108: very disparate measurements, 0.511795±39 (n=10, c.f. = 0.000059), 951121-951129: 0.511755±17 (n=10; c.f. = +0.000099).

Repeated measurements (n=6) of the USGS basalt standard BCR-1 during the period 940402-941221 (corrected in the manner discussed above), which are included in Table 22 gave an average of 0.512636±40. This is close to the literature value 0.512640 (Gladney et al. 1990). The calculated averages for the Sm and Nd contents were 28.82 and 6.59, respectively, which is very close to the literature values (6.59 ppm and 28.8 ppm, respectively). The average $^{147}Sm/^{144}Nd$ value of BCR-1 was 0.1383±14 (=1 % 2σ; lit.val.= 0.1371). The error in the measured $^{147}Sm/^{144}Nd$ values are, however, generally estimated to be lower than 0.5 % (2σ), based on measurements of the BCR-1 rock standard (H. Schöberg pers. comm. 1996). Duplicate analyses of the same rock samples (different dissolutions or ion exchanges) in this study gave differences (reproducibilities) in the range $0.2\text{-}19.5*10^{-3}$ % for the $^{143}Nd/^{144}Nd$ ratios, and 0-4.8 % for the ratios $^{147}Sm/^{144}Nd$ (except in two cases where the difference were over 30 %).

The Sr samples were unspiked, and the mass spectrometric measurements were normalized to $^{88}Sr/^{86}Sr = 8.375209$. The Sr standard SRM987 has been analysed continuously to monitor the long-term stability of the spectrometer with respect to Sr. The accepted "literature" value of $^{87}Sr/^{86}Sr$ of SRM987 is 0.710240 (Gladney et al. 1990). The standard measurements of Sr show much better long-term homogeneity, compared with the Nd standard. During the period 900101- 931231, the average $^{87}Sr/^{86}Sr$ was 0.710227±32 (1s, n=41), which is 0.000013 units lower than the accepted value, and the sample measurements were corrected accordingly. During the period 940101-950630 the average was 0.710172±28 (n=61), and a correction factor of +0.000068 has thus been applied for these measurements. Sr measurements on unspiked BCR-1 have also been performed (Table 22). The average during the period 930906-950614 was 0.705066±55 (1s, n=6, including the correction factor), which is 0.000056 above the accepted "literature" value, 0.70501 (Gladney et al. 1990).

The Rb/Sr ratios were obtained from XRF measurements, and the $^{87}Rb/^{86}Sr$ ratio calculated from the isotopic abundances of Rb and the mass spectrometric measurements of Sr. Generally two pressed rock powder briquettes were prepared for each sample, and two measurements performed on each briquette, with exceptions in a few samples. The reproducibility in % (1 std. dev.) was thus usually calculated from four measurements on each sample. These range from 0.12 to 6.29 % with an average of 0.75 % and a great majority of the samples having reproducibility errors in the range 0–1 %. The number of significant figures given in Tables 3, and 13 is indicative of the calculated errors for each sample. The reproducibility in the Rb/Sr ratio is related to this ratio itself. If this ratio is very small or large the errors increase, due to poorer reproducibilities at lower contents of the elements. The lowest errors are obtained in rock samples with Rb/Sr ratios of ca 1–8.

The Pb fraction obtained from the first ion exchange procedure used for whole rock samples, was further purified in a second ion exchange step using HBr. The samples were dissolved in 0.4N HBr and added to 0.2 ml columns filled with Biorad AG 1-X8 100-200 mesh resin, which had been previously washed with 0.5N HNO_3 and DB H_2O. The samples were stripped from other ions by repeated washings with 0.4N HBr, and the Pb fraction was eluated with DB H_2O. The evaporated fractions were dissolved in a mixture of Si-gel and 0.25N H_3PO_4 and loaded onto Re single filaments. Isotopic measurements were made with a Finnegan MAT-261 mass spectrometer in static mode. The Pb content of the WR fractions were considered high enough to render corrections for blanks unnecessary. Corrections for mass fractionation were done relative to the NBS standard SRM981 measured at different temperatures and amounts according to a specific scheme worked out by Hans Schöberg (H. Schöberg pers. comm. 1995). The Pb analyses were performed by Dr. Billström and are presented in Table 14.

The procedure followed by Dr. Neymark in St. Petersburg to obtain the Nd analyses in Table 22, was similar to that in use at LIG. Differences include the use of HDEHP-covered teflon powder during the ion exchange separation of Sm and Nd according to the method of Richard et al. (1976), instead of Biorad AG 50W-X12 200-400 mesh at LIG. The samples were totally spiked with a mixed $^{149}Sm/^{146}Nd$ spike solution. Also here the measurements were performed with a Finnegan MAT 261 in a multicollector static mode, and normalized to $^{148}Nd/^{144}Nd = 0.24157$. Analysed blanks are between 0.1 and 0.4 ng for Sm and from 0.1 to 0.5 ng for Nd. 18 measurements on the La Jolla Nd standard during the same period as the samples gave 0.511860±9, and were corrected accordingly. This is very close to the "literature" value of 0.511854. Three measurements of the basalt standard BCR-1 are also reported in Table 22, and are close to the accepted value (Gladney et al. 1990). The duplicate runs reported in Table 22 have reproducibilities between $7.8*10^{-6}$ and $1.1*10^{-4}$ for $^{143}Nd/^{144}Nd$.

The Rb-Sr analytical data in Table 22 was obtained by Dr. Neymark while working at the USGS in Denver. Rb and Sr were determined on separate aliquots of the samples by conventional isotope dilution methods (^{87}Rb and ^{84}Sr spikes), using HF and H_2SO_4 dissolution. Sr isotopic composition was measured using a fully

automated multi-collector MAT-262 mass-spectrometer in a static mode. Data collected on the USGS Sr standard EN-1 during course of this study give 0.70906±0.0000075. Ludwig et al. (1988) reported a value of 0.7092494±35 for EN-1. Replicate analyses for granitic rocks performed in the laboratory indicate an uncertainty of 1.5 % in the $^{87}Rb/^{86}Sr$ ratios. Rb and Sr total chemistry blanks were lower than 5 ng.

Pb isotopic analyses were also performed by Dr. Neymark in Denver on separated feldspar fractions from the four northernmost studied complexes and selected country rocks. The fractions consisted of plagioclase for the mafic rocks and the metasediment, mesoperthite for the intermediate rocks, perthitic K-feldspar for the rapakivi granites, and probably a mixture of plagioclase and K-feldspar for the country rock granites. 50 to 100 mg of the cleanest grains were picked out by hand from each fraction. The fractions were leached on a hot plate for half an hour in 7N HNO_3 and 6.5N HCl each, followed by rinsing in hot H_2O. The samples pretreated in this way were digested overnight also on a hot plate in a mixture of HF and HNO_3 in tightly capped PFA (perfluoralkoxy) teflon vials. Pb was separated using HBr techniques modified from Manhes et al. (1978). The measured Pb blank for the total procedure during this study was 100 pg. Therefore, assuming that the Pb content of the feldspars is higher than 1 ppm, no correction for lead blanks was necessary. The isotopic analyses were performed on the MAT-262 seven collector mass-spectrometer in a static mode using silica-gel emitter. Mass discrimination of 0.0005±0.0002 per amu, determined by 30 runs of the NBS Pb standard SRM982, was used to correct the data. Average ratios for SRM982 measured during the course of these analyses were: $^{206}Pb/^{204}Pb$= 36.720±0.024 (2σ), $^{207}Pb/^{204}Pb$= 17.143±0.018, and $^{208}Pb/^{204}Pb$= 36.692±0.047. Within-run errors for all the sample measurements were better than 0.005 % (2σ). An external 2σ error of 0.05 % per amu was accepted for the samples, based on the SRM982 measurements.

The U-Pb zircon analyses presented in Table 20 were performed by Dr. Neymark in Denver. The separated zircon fractions were recovered using standard Wilfrey table, magnetic, and heavy liquid separation techniques. Based on selection criteria such as crystallinity, surface reflectance, colour, and freedom from inclusions and cracks, approximately 100 of the best crystals were chosen from the 75–150 μm fraction of each sample and loaded together with pyrite into a pneumatic stainless steel abrader (Krogh 1982). The abrasion process was carefully monitored and halted when the last 20–30 of the largest remaining zircon grains had been reduced to about 3/4 of their original volume. The cleanest three of these rounded and polished crystals from each of the two samples were chosen for analysis.

In order to minimize laboratory contamination of the small (1.7–4.6 μg) zircon grains being analysed, an abbreviative chemistry was employed. Individual grains were leached in 1N HNO_3 and rinsed in H_2O on a hot plate. Next, each crystal was transferred by micropipette onto a microbalance for weighing, and finally into a PFA teflon capsule where c. 300 μl HF, c. 50 μl HNO_3, and 4 μl of weighed ^{205}Pb-^{235}U-^{230}Th spike were added. Six samples and one blank capsules were loaded for simultaneous digestion into a steel jacketed FTE (fluortetraethylene) teflon bomb containing an additional reservoir of HF. Complete digestion was accomplished in a week in an oven maintained at 210°C, after which the solutions were evaporated to dryness, refilled with HNO_3, and reevaporated to dryness to ensure equilibration with the spike. Without further chemistry the sample was picked up in a drop of silica gel-H_3PO_4 and loaded onto the source filament of a VG Isomass 54E mass spectrometer equipped with Daly multiplier. Pb, U, and Th blanks for the total technique over duration of this study averaged 4±1 pg, 1 pg and 2 pg, respectively. All reported element and isotope concentrations, ages and 2 sigma uncertainties were calculated using the PBDAT and ISOPLOT computer programs of Ludwig (1993, 1995).

The U-Pb zircon analyses presented in Tables 2, 12, 21, and 27, were performed by the present author at LIG. The zircons were separated using standard wet shaking table, magnetic and heavy liquid techniques. No magnetic zircons were used. The zircon grains were sieved into fractions of -45, 45–74, 74–100, 100–150, 150–210, and 210– μm. From the size fractions, generally the clearest zircons, with least (or no visible) inclusions or cracks were picked out for analysis, in amounts proportional to their sizes (>210 μm 2–13 grains, 150–210 μm 5–15, 100–150 μm 7–56, 74–100 μm 50–145, and 45–74 μm 84–205). Two fractions from three of the samples (>100 mm) were air abraded together with pyrite in stainless steel abraders, for several hours. The abrasion was halted when the crystals were significantly rounded and reduced in size. The clearest and still unbroken crystals were picked out for analysis. The fractions were washed on a hot plate successively in 6N HCl, 7N HNO_3, Elga H_2O, and DB (double bottled) H_2O. The fractions were weighed on a microbalance and transferred into 0.2 ml teflon micro capsules (Parrish 1987). A mixture of DB HF:HNO_3 10:1 was added to each capsule, and four micro capsules were loaded into a larger Krogh-type teflon capsule (Krogh 1973) containing an additional reservoir of HF. The Krogh capsule was steel jacketed and put into an oven at 205°C for about a week. The solutions were evaporated, and a mixed ^{233}U–^{235}U spike was added, as well as 3.1N HCl, and the capsules were left for at least one day in a warming cupboard at 70°C. The solutions were then aliquotted and transferred into

Savillex teflon beakers, with about 3/4 in the IC (isotope composition=unspiked) beaker, and 1/4 in the ID (isotope dilution=spiked) beaker. To the solution in the ID beaker a few drops of ^{208}Pb spike was added, and all solutions were evaporated.

The samples were passed through ion exchange procedures either in HBr (Nordsjö and Strömsbro samples) or HCl (Rödön and Kårtorp samples) to extract U and Pb. In the HBr method the evaporated samples were dissolved in 200 µl 0.4M HBr and loaded onto 45 µl columns with Biorad AG 1-X8 100-200 mesh resin. The U fraction was eluated with the HBr and the Pb fraction with DB H_2O. The U fraction was further purified in a second ion exchange using HCl, in 0.5 ml columns using Biorad AG 1-X8 200-400 mesh resin. It was dissolved in 0.5 ml 3.1N HCl, stripped from other ions in HCl, and eluated in DB H_2O. In the HCl method the evaporated samples were dissolved in 100 µl 3.1N HCl and loaded onto 45 µl columns with Biorad AG 1-X8 200-400 mesh resin. The fractions were washed with 3.1N HCl and Pb eluated using 6.2N HCl and U using DB H_2O. No further purification was needed.

The fractions from the ion exchange were evaporated, and dissolved in a mixture of silica gel and 0.25 N H_3PO_4 and evaporated on Re single filaments. The analyses were performed on a Finnegan MAT-261 mass spectrometer with a multicollector in a static mode. Measured U and Pb blanks during course of this study were in the ranges 0.01–2.3 ng and 0.04–0.12 ng, respectively. In two cases the U-blank was thus very high (1.116–2.3 ng) which remains unexplained. In the data reduction, a U-blank level normal for the laboratory was used (0.01 ng). The isotopic composition used for common lead in the case of the rapakivi age calculations was taken from the Pb determination on the feldspars from the Nordsjö monzonite (N12; Table 23; $^{206}Pb/^{204}Pb$=15.8, $^{207}Pb/^{204}Pb$=15.2, $^{208}Pb/^{204}Pb$=35.3), which was considered to be the best estimate of initial lead composition. The isotopic composition of present day contamination lead used was: $^{206}Pb/^{204}Pb$=18.5±2, $^{207}Pb/^{204}Pb$= 15.6±0.2, $^{208}Pb/^{204}Pb$= 38.5±1.5. A mass discrimination of 0.1±0.4 per atomic mass unit was used, based on repeated measurements on the SRM981 lead standard. Average measured values of the SRM981 Pb standard during the time of MS data collection was (n=24):$^{206}Pb/^{204}Pb$=16.893±0.015 (2σ), $^{207}Pb/^{204}Pb$=15.434±0.016, $^{208}Pb/^{204}Pb$=36.519±0.054. The calculation of the corrected isotopic ratios, intercept ages, and error propagation was performed using the programs by Ludwig (1993, 1995), applying the decay constants recommended by Steiger & Jäger (1977). Stated errors are 2 sigma.

The *microprobe analyses* in Table 1 were collected with a Cambridge Geoscan. Accelerating voltage was 20 kV, beam current was in the order of 50–100 nA, and beam diameter 1–5 µm (H. Harrysson pers. comm. 1996). Correction of measured intensities was made for atomic number, absorption, and fluorescence (ZAF-correction) according to the program MK13. This program originates from the National Physical Laboratory, Teddington, Middlesex, England as MK1 (Mason, Frost, & Reed 1969?). It was modified to version MK13 at the SGU (Ålinder, Röhr, Larkin, & Sturesson 1974).

The microprobe analyses in Tables 11 and 19 were obtained with a Cameca Camebax SX50. Accelerating voltage was 20 kV and the beam current 12 nA, and the beam diameter approximately 1–2 µm. Correction of measured intensities was performed according to the Cameca ZAF-PAP-correction software.

The internal analytical precision in the microprobe measurements is related to a number of factors, eg. atomic number, concentration of the element in the sample and standard, counting time, interference with other elements, selected line (wave length) or analysis crystal, and nature of the mineral. The external analytical precision is related to these same parameters, but includes in addition also the reproducibility from repeated measurements of the same homogeneous material. The errors in the external precision is expected to be considerably larger, compared with the internal. A rough idea of external precision is obtained from repeated measurements on the same homogeneous mineral, although it varies according to the abundance of each element in different minerals. If an element occurs with an abundance of 10 to >50 wt% in the mineral, the reproducibility is roughly between 1 and 5 %, for 1–10 wt% between 5 and 10 %, and below 1 wt% it is more than 10 %. As an example, analyses (50 measurements) of an apparently homogeneous clinopyroxene from a Postjotnian dolerite are given here (sample R120a): Na_2O 0.41 (wt% average) (±13.45 %, 1s), MgO 12.68 (±3.57 %), Al_2O_3 2.17 (±34.77 %), SiO_2 51.48 (±1.02 %), CaO 20.21 (±2.20 %), TiO_2 1.08 (±7.92 %), MnO 0.25 (±22.12 %), and FeO 11.91 (±5.55 %).

Appendix 2a. Whole rock geochemistry of rocks from the Transscandinavian Igneous Belt and related rocks in northern Östergötland and southern Närke, central southern Sweden.

Appendix 2b. Whole rock geochemistry of rocks from the central Swedish rapakivi complexes and related rocks.

Appendix 2a. Chemical composition of the Småland-Värmland and related rocks

Tiveden samples

SAMPLE	Rocktype	Coordinates. National grid.	SiO2 % (XRF)	TiO2 % (XRF)	AL2O3 % (XRF)	FE2O3 % (XRF)	MNO % (XRF)	MgO % (XRF)	CAO % (XRF)	NA2O % (XRF)	K2O % (XRF)	P2O5 % (XRF)
103/89	Silicic Filipstad granite	652361/144323	75.7	0.181	12	1.43	0.02	0.25	0.86	2.51	5.59	0.04
XA	Filipstad granite	652329/144347	67	0.555	14.7	4.58	0.06	1.02	2.09	2.95	4.94	0.17
XE*	Rel. dark Filipstad-type granitoid	651332/143233	59.00	1.04	17.20	8.09	0.13	2.08	4.11	3.58	3.56	0.31
XF	Rel. dark Filipstad-type granitoid	651509/143769	58.80	0.98	17.40	8.01	0.13	2.00	4.40	3.63	3.14	0.33
XD	Rel. dark Filipstad-type granitoid	651350/143197	58.9	0.888	17.1	6.98	0.11	1.65	3.84	3.42	4.28	0.31
XG	Rel. dark Filipstad-type granitoid	652098/143273	58.1	0.957	17.1	7.98	0.12	1.95	4.02	3.37	3.81	0.32
143/89*	Rel. dark Filipstad-type granitoid	651123/143902	59.60	0.99	17.70	7.77	0.12	2.10	4.12	3.28	3.21	0.33
8859A	Rel. dark Filipstad-type granitoid	651561/144143	57.30	1.15	16.40	8.80	0.15	2.30	4.08	3.40	3.34	0.34
8859B*	Rel. dark Filipstad-type granitoid	651315/144045	56.80	1.08	17.50	8.50	0.13	2.44	4.01	2.95	3.50	0.38
119/89*	Black Filipstad-type rock	651702/143540	57.50	1.23	17.20	9.66	0.14	2.39	4.93	3.31	2.67	0.37
8859C	Dark Filipstad-type rock	651498/144132	56.30	1.12	17.10	8.53	0.11	2.08	4.49	3.47	3.58	0.34
110/89	Black Filipstad-type rock	652125/144057	55	1.48	16.4	10.9	0.15	2.74	5.08	3.19	2.36	0.45
105/89	TIB-gabbro	652381/144305	45.9	2.02	13.6	17.2	0.17	4.97	9.05	2.3	1.44	1.26
8859D1*	Mediumgrained TIB-gabbro (High-Al)	651370/144060	47.20	0.50	18.50	10.50	0.15	5.13	11.30	2.57	1.40	0.18
139b/89	Basic dyke	651500/144133	48.7	0.765	14.8	11.2	0.2	8.49	9.71	2.88	0.94	0.19
101/89	Basic dyke	652476/144365	51.7	1.75	15.1	12.2	0.17	5	7.59	2.6	2.11	0.58
124/89(1)*	Older "metasediment"	651465/143159	60.80	0.68	21.40	8.44	0.12	3.57	2.28	2.07	0.22	0.06
124/89(2)	Older "metasediment"	651465/143159	48.2	0.965	26.4	12.1	0.16	4.22	2.66	2.73	0.42	0.07
XC	Older grante, granitic	651609/143486	69.5	0.298	15.2	3.01	0.03	0.93	2.57	3.99	2.87	0.15
XB	Silicic older granite	652356/144355	72.7	0.132	14.5	1.22	0.02	0.35	0.79	3.33	5.61	0.31
XH	Older tonalite	652204/143111	68.5	0.242	16.1	2.83	0.05	1.07	3.38	4.8	1.4	0.08

All analyses peformed at XRAL according to the stated methods. Details in Appendix 1. (1) and (2) are replicate analyses.

Tjällmo-Vättern zone samples

Sample	Rocktype	Coordinates. National grid.	SiO2 (%)	TiO2 (%)	Al2O3 (%)	Fe2O3 (%)	FeO (%)	Fe2O3tot (%)	MnO (%)	MgO (%)	CaO (%)	Na2O (%)
8815*	Silicic Filipstad granite	650127/147592	71.50	0.33	13.40			2.57	0.04	0.43	1.26	2.94
8820	Silicic Filipstad granite	650296/147683	72.00	0.33	13.60			2.64	0.03	0.47	1.27	3.19
8828A	Silicic Filipstad granite	650694/146680	73.60	0.33	12.60			2.53	0.04	0.47	1.17	2.80
8843A	Silicic Filipstad granite	650345/145495	74.50	0.24	12.90			1.89	0.03	0.29	0.77	2.94
8845*	Silicic Filipstad granite	650541/145145	73.00	0.22	13.60			1.70	0.04	0.50	1.57	3.83
8824B	Silicic net-vein host	650561/146716	70.40	0.24	14.80			2.65	0.06	0.52	0.90	3.96
8823*	Filipstad granite	650555/146820	68.10	0.52	14.60			3.91	0.07	0.76	1.93	3.23
8827	Filipstad granite	650896/146006	66.20	0.64	14.90			4.90	0.07	0.88	2.34	3.65
8872(2)	Filipstad granite (same as 8827)	650896/146006	66.00	0.64	14.80			4.79	0.07	0.88	2.35	3.60
8843C*	Filipstad granite	650345/145495	69.10	0.52	14.20			3.81	0.05	0.86	1.93	3.26
8844A*	Filipstad granite	650630/145178	66.60	0.71	13.90			4.58	0.06	1.20	2.27	3.19
8847	Filipstad granite	650972/145169	70.10	0.39	14.00			2.87	0.06	0.76	1.44	2.89
8853A*	Filipstad granite	650490/145823	66.60	0.65	14.00			4.53	0.07	0.82	2.31	3.02
8857A	Filipstad granite	653034/144922	63.90	0.69	15.70			5.33	0.09	1.15	2.65	3.45
8841	Rel. dark Filipstad-type granitoid	650077/146049	60.60	0.81	17.50			7.53	0.16	1.06	3.61	3.27
8821	Medium-grained hybrid type	650388/147427	66.70	0.63	14.50			4.59	0.07	1.23	2.51	3.02
XG15A	Intermediate dyke, with xenoliths	650409/145727	63.30	0.51	17.60			4.58	0.08	1.02	3.16	4.33
8816A+B	Medium-grained hybrid type	650457/147601	67.10	0.51	15.20			3.78	0.04	0.91	2.20	3.54
8853C*	Mediumgr. hybrid magmatic enclave	650490/145823	60.90	1.02	15.30			7.39	0.12	1.25	3.28	3.31
8814*	Hybrid magmatic enclave	649995/147693	58.40	1.83	13.60			10.30	0.19	2.52	4.66	3.28
8811A*	Mafic magmatic enclave, xenocrystic	649920/148070	47.60	3.20	10.40			19.00	0.34	4.70	6.70	1.36
8812M	Mafic magmatic enclave, dark rim	650061/147982	50.90	2.38	15.10			12.60	0.23	2.91	6.17	3.15
8812L	Mafic magmatic enclave, lighter center	650061/147982	52.60	2.22	14.90			11.80	0.22	2.73	5.88	3.10
8843B	Finegrained basic magmatic enclave	650345/145495	49.00	1.93	14.60			13.00	0.18	6.81	8.24	2.31
8824A	Basic net-vein pillow	650561/146716	59.30	0.81	16.60			7.34	0.14	2.39	4.94	3.54
9M*	Hornblende diorite dyke, TIB	650479/145818	50.50	1.23	17.60	3.37	7.06	11.21	0.18	3.93	7.93	3.57
8828B	Basic TIB-dyke	650694/146680	50.00	1.53	15.50			12.20	0.18	5.54	8.02	2.24
15D	Hornblende diorite dyke, TIB	650409/145727	46.30	2.04	16.90	5.34	8.38	14.65	0.20	5.50	8.14	2.56
8850	Fine-grained basic dyke (primitive)	650581/145876	50.70	0.71	11.70			10.70	0.18	9.73	10.10	2.55
N86OC	Pyroxene hbl gabbro, TIB	650332/146386	51.30	0.94	16.20	3.14	6.39	10.24	0.15	6.17	10.30	2.12
8822*	Finegrained TIB-basite	650365/147335	47.00	1.62	15.80			13.50	0.21	6.88	8.38	2.58
8802	TIB-gabbro	650715/148102	46.10	1.13	14.30			13.70	0.17	7.17	10.60	2.08
11*	Pyroxene hbl gabbro, TIB	650449/145770	46.20	1.59	13.50	6.29	8.72	15.98	0.14	5.55	11.30	1.43
8829	Mediumgrained TIB-gabbro	650598/147310	51.50	0.92	16.90			10.60	0.14	4.71	8.73	2.12
8830	Finegrained TIB-basite	650692/147328	60.30	0.78	16.80			6.56	0.10	2.30	4.85	3.94
8839	Coarse TIB-gabbro	650354/146551	48.40	1.37	15.40			13.10	0.18	5.87	9.35	2.21
8840*	TIB-gabbro, slightly xenocrystic	650367/146597	51.60	0.88	16.40			9.66	0.16	5.11	8.39	2.34
8846	Coarse hornblende TIB-gabbro	650384/145082	44.30	1.18	16.00			14.80	0.15	6.72	12.10	1.35
8842A	Mediumgrained TIB-gabbro	650207/147335	52.20	1.14	15.80			11.00	0.18	5.05	7.78	2.95
8860	Mediumgrained TIB-gabbro	650301/146425	49.50	0.99	15.90			10.80	0.17	5.82	9.38	2.47
8848	Ultrabasite, TIB	650372/145958	44.90	0.27	18.40			9.49	0.14	10.40	9.59	1.45
200*	Spinel-plagioclase lherzolite, TIB	650560/145864	43.40	0.47	10.10	4.56	8.08	0.00	0.18	19.30	7.26	1.15
203*	Spinel-plagioclase lherzolite, TIB	650346/146610	38.30	0.26	3.92	7.39	6.82	14.97	0.18	28.20	1.99	0.50
8838A	Spinel-plagioclase lherzolite, TIB	650355/146535	40.90	0.21	6.62			12.80	0.18	24.90	4.65	0.76
8819*	Older tonalite	650200/147493	67.90	0.36	15.90			3.39	0.06	1.37	3.17	4.26
8832*	Older granite	650189/146647	69.30	0.37	15.10			3.12	0.05	0.86	1.98	3.77
8857E*	Finegrained dark enclave	653034/144922	56.40	0.60	18.60			6.83	0.07	2.07	1.45	3.05

Analyses performed at XRAL according to the stated methods, except samples 11, 9M, 15D, 200, 203, and N86OC, which were analysed at SGU according to the methods indicated in the table for the Kårtorp area samples below.
Details in Appendix 1.

Kårtorp area samples

PROVNR.	Rocktype	Coordinates. National grid.	SiO2 (%)	Al2O3 (%)	TiO2 (%)	Fe2O3 (%)	FeO (%)	Fe2O3tot (%)	MnO (%)	MgO (%)	CaO (%)	Na2O (%)
8504*	Vitxjö type granite (*)	650756/148023	73.21	12.86	0.50	1.44	1.47	3.07	0.01	0.43	1.28	2.78
N86A	Vitxjö type granite (+)	650837/148146	75.60	12.30	0.27	0.73	1.10	1.95	0.03	0.26	1.01	2.97
24	Filipstad type granite	650860/147692	74.70	13.20	0.28	0.54	1.50	2.21	0.02	0.39	0.64	2.15
20	Filipstad type granite, red	650975/147929	70.60	14.00	0.49	0.66	2.84	3.82	0.05	0.75	1.88	2.70
22	Filipstad type granite, red (+)	651009/147847	70.43	13.83	0.34	0.85	1.65	2.68	0.03	0.52	1.34	3.29
19	Filipstad type granite (+)	650908/147978	67.23	14.75	0.51	1.76	2.33	4.35	0.05	0.88	1.98	3.00
18	Filipstad type granite (+)	651036/147996	66.41	15.45	0.55	1.48	2.70	4.48	0.06	0.94	2.19	3.39
39*	Filipstad type granite (*)	650794/148216	66.83	15.65	0.67	1.59	2.92	4.83	0.04	1.03	2.39	3.02
1z	Filipstad type granite, red (+)	650632/147610	66.60	13.30	1.08	1.63	3.75	1.95	0.10	1.29	2.59	2.90
26	Filipstad type granite (*)	650602/147775	64.46	15.12	1.16	1.73	4.21	6.41	0.07	1.28	2.93	3.12
17	Filipstad type granite, grey	651117/147681	63.30	15.80	0.85	1.35	6.20	8.24	0.13	1.14	3.29	3.46
1bb*	Filipstad type granite (+)	650285/147895	63.30	13.60	1.41	2.14	4.98	3.07	0.13	1.55	3.71	3.21
21	Filipstad type granite, red (+)	650984/147882	63.88	15.24	0.74	1.96	3.48	5.83	0.09	1.41	2.22	3.09
32	Filipstad type granite, red (*)	650720/147911	63.33	15.67	1.32	2.54	3.81	6.77	0.07	1.84	2.73	3.10
8514l	Filipstad type granitoid (*)	650726/148081	63.48	15.93	1.33	2.14	4.20	6.81	0.03	1.57	3.42	3.44
34	Filipstad type granitoid (*)	650626/148020	63.37	15.57	1.18	2.06	4.56	7.13	0.08	1.72	3.22	2.90
23	Filipstad type granite	650897/147675	62.70	16.30	0.85	2.21	5.10	7.88	0.13	1.30	3.33	3.32
38V	Filipstad type granitoid (*)	650916/148223	62.01	15.32	1.32	2.33	5.32	8.24	0.09	1.92	3.67	2.79
29	Filipstad type granitoid, red (*)	650522/147962	62.03	15.48	1.51	3.26	3.78	7.46	0.09	2.15	2.38	3.22
127	Filipstad type hybrid (+)	650691/147982	62.10	14.20	1.61	2.80	4.68	8.00	0.12	1.90	4.44	3.19
35(aa)	Filipstad type granitoid (*)	650590/148045	61.11	15.47	1.57	2.87	5.05	8.48	0.11	1.81	3.67	2.96
8510	Filipstad type granitoid (*)	650678/148056	61.28	15.64	1.59	2.93	4.92	8.40	0.07	1.92	3.88	3.07
28	Filipstad type granitoid (+)	650783/147980	61.34	15.37	1.40	3.18	4.17	7.81	0.11	1.84	3.98	4.04
115c	Filipstad type hybrid (+)	650906/148187	61.80	14.00	1.64	2.88	4.90	8.32	0.13	1.98	4.37	2.95
8501	Dark, red Filipstad type granitoid (*)	650701/147929	61.25	14.32	1.52	3.68	4.44	8.61	0.08	2.15	3.93	2.67
129d*	Filipstad type hybrid (+)	650865/148086	61.10	14.90	1.67	2.83	4.96	8.34	0.11	2.01	4.18	2.85
38ö	Filipstad type granitoid (*)	650922/148237	60.96	16.12	1.40	2.36	4.88	7.78	0.10	1.63	3.78	3.06
8505	Dark Filipstad type granitoid (*)	650736/148005	60.64	15.84	1.58	2.66	4.98	8.19	0.08	2.03	4.39	2.98
30	Dark Filipstad type granitoid (*)	650495/148002	60.65	15.62	1.61	2.22	5.59	8.43	0.11	1.98	4.05	3.12
118	Hybrid dyke (+)	650689/147510	60.50	16.90	0.50	1.68	3.54	5.61	0.11	1.15	4.34	4.49
1gg	Dark Filipstad type granitoid (+)	650383/147884	59.20	15.40	1.11	2.47	5.73	8.84	0.14	1.25	4.20	3.42
8507	Filipstad type hybrid (*)	650788/148052	59.93	15.45	1.56	3.08	5.25	8.91	0.10	2.19	4.53	2.99
132b*	Filipstad type hybrid	650654/147914	58.80	14.80	1.73			9.20	0.16	2.29	5.25	2.96
8514m	Filipstad type hybrid (*)	650719/148079	58.72	16.09	1.98	2.93	5.67	9.23	0.08	2.38	4.65	2.86
27	Dark Filipstad type granitoid (+)	650451/148001	58.28	14.48	1.36	1.29	7.42	9.53	0.13	1.90	3.64	3.13
33	Filipstad type hybrid (*)	650687/147948	58.31	16.37	1.88	2.55	6.10	9.33	0.11	2.38	4.77	2.92
131a	Dark Filipstad type hybrid (+)	650669/147949	57.50	14.40	2.31	3.42	6.69	10.85	0.16	2.53	5.85	2.75
128	Dark Filipstad type hybrid (+)	650670/147999	57.60	13.70	2.31	3.43	6.60	10.76	0.15	2.68	5.92	2.76
N86B	monzodiorite" (+)	650684/148004	57.60	14.60	2.12	3.24	6.01	9.92	0.16	2.74	5.67	2.92
35B2	Basic-hybrid magmatic enclave (+)	650613/148023	57.30	14.90	2.12	3.00	6.60	10.33	0.17	2.08	5.21	3.21
8508*	Dark Filipstad type hybrid (*)	650704/148058	56.30	16.64	1.89	3.44	6.07	10.18	0.11	2.58	5.45	3.10
8514n	monzodiorite" (*)	650708/148077	55.79	16.41	2.26	3.90	6.22	11.69	0.10	2.89	5.94	2.48
8502	Diorit" (*)	650715/148102	55.96	16.14	2.06	3.40	6.21	10.30	0.11	2.76	6.03	2.89
36V	monzodiorite" (*)	650694/148066	54.48	16.92	2.32	3.87	6.87	11.50	0.14	3.19	6.10	2.65
36Ö	monzodiorite" (*)	650694/148066	54.42	16.97	2.13	4.23	6.26	10.76	0.13	2.81	5.82	2.98
8511*§	monzodiorite" (*)	650682/148057	54.08	17.24	2.29	3.23	7.21	10.33	0.12	2.90	6.59	2.90
8512	monzodiorite" (*)	650691/148060	52.99	16.10	2.50	4.86	6.85	9.92	0.11	4.09	6.42	2.46
35B1	Basic magmatic enclave (+)	650613/148023	51.60	15.20	2.65	2.64	8.15	11.69	0.20	2.90	6.62	3.14
1t	Basic dyke (+)	650824/147866	49.60	14.20	0.71	2.18	7.67	10.70	0.16	10.20	7.60	2.04

Major elements were analyzed by wet chemical methods at the Department of Geology, Uppsala University (*), at SGU (+), and at XRAL by XRF (only 132b).
The NA analyses were performed by Studsvik energiteknik AB, whereas P2O5, Sr, and Y were analyzed at SGU by wet chemical methods (P2O5) and XRF (Sr and Y). Details in Appendix 1.
*=samples selected for Nd and Sr isotopic analysis; §=sample selected for U-Pb zircon analysis

	N	O	P	Q	R	S	T	U	V	W	X	Y	Z	AA
1														
2														
3														
4	LOI	SUM	BA	RB	SR	CS	TH	U	LI	BE	GA	Y	ZR	HF
5	%	%	PPM (XRF)	PPM (XRF)	PPM (ICP)	PPM (NA)	PPM (NA)	PPM (NA)	PPM (ICP)	PPM (ICP)	PPM (ICP)	PPM (ICP)	PPM (XRF)	PPM (NA)
6	0.55	99.2	267	199	58.8	4	45	4.6	7	1.9	18	26.6	154	6
7	1	99.2	835	159	133	3	13	2.2	28	2	22	29.5	288	8
8	0.77	100.20	1530.00	108.00	271.00	2.00	9.00	1.80	24.00	10.70	26.50	33.80	476.00	13.00
9	0.93	100.00	1360.00	90.00	233.00	4.00	2.00	3.90	37.00	10.40	22.80	17.70	379.00	9.10
10	0.95	98.7	1900	103	275		7.4	2.3	21	1.7	29	25.7	401	11
11	0.4	98.4	1740	85	272	3	6.6	2.5	18	1.7	28	21.6	464	12
12	0.85	100.40	1800.00	95.00	257.00	3.00	2.00	2.30	43.00	8.40	23.80	21.90	425.00	11.00
13	0.70	98.26	1510.00	100.00	265.00	3.00	7.00	2.30	40.00	10.90	25.90	40.80	549.00	14.00
14	1.08	98.68	1740.00	91.00	280.00	5.00	4.00	1.80	44.00	9.80	27.90	34.90	406.00	12.00
15	0.77	100.50	1440.00	97.00	263.00	3.00	2.00	2.10	24.00	10.60	27.90	29.00	465.00	12.00
16	0.93	98.39	1910.00	88.00	297.00	2.00	9.00	2.20	26.00	11.30	28.50	35.20	481.00	13.00
17	0.78	98.8	1220	61	311	4	3.3	3	20	2	28	29.3	527	14
18	0.95	99	721	40	705	3	4.1	1.8	19	1.1	31	31.5	150	3
19	0.77	98.32	290.00	63.00	553.00	3.00	1.00		28.00	2.40	22.10	9.10		0.50
20	0.7	98.7	248	24	461		1.9	1.8	14	1	23	15	78	1
21	0.95	99.9	446	70	281	3	4.7	1.7	25	1.6	27	31.9	208	4
22	0.77	100.50	65.00	15.00	162.00	3.00	22.00	2.50	57.00	7.00	30.20	12.00	117.00	4.20
23	1	99			189	7	25	6.5	64	5.3	44	12.5	203	5
24	0.5	99.1	368	123	171	3	7.3	3.8	27	1	21	7.4	115	
25	0.9	100	284	314	56	6	13	3.1	8	1.9	18	24.3	76	3
26	0.5	99.1	316	47	346	3	7.9	2.2	34	1	22	7.3	113	3
27														
28														
29														
30	K2O (%)	P2O5 %	Ba (XRF)	Rb (XRF)	Sr (ICP)	Cs (NA)	Th (NA)	U (NA)	Li (ICP)	Be (ICP)	Ga (ICP)	Y (ICP)	Zr (XRF)	Hf (NA)
31	5.43	0.08	745.00	204.00	68.20	4.00	25.00	5.40	43.00	5.30	18.20	33.90	224.00	7.00
32	5.11	0.08	659.00	223.00	63.80	3.00	22.00	9.50	42.00	5.00	19.10	34.90	239.00	8.20
33	5.22	0.07	737.00	166.00	74.50	2.00	14.00	3.90	26.00	5.20	17.90	28.60	238.00	8.40
34	5.51	0.05	435.00	201.00	54.30	2.00	28.00	3.20	21.00	5.30	15.90	21.70	164.00	5.90
35	4.21	0.07	689.00	189.00	129.00	6.00	25.00	6.50	36.00	6.70	16.50	28.00	126.00	5.70
36	4.60	0.08	1010.00	158.00	170.00	3.00	14.00	5.80	39.00	5.10	18.00	16.20	192.00	5.60
37	5.27	0.14	1210.00	245.00	139.00	4.00	16.00	6.60	42.00	9.10	22.70	62.30	338.00	9.50
38	4.87	0.18	1210.00	165.00	113.00	3.00	8.00	3.20	36.00	8.80	23.40	51.90	417.00	11.00
39	4.80	0.18	1170.00	163.00	129.00	3.00	9.00	3.20	39.00	8.20	24.30	62.30	423.00	12.00
40	4.34	0.14	1200.00	193.00	167.00	2.00	25.00	3.70	40.00	8.40	17.20	27.40	306.00	9.20
41	4.65	0.21	852.00	196.00	139.00	9.00	25.00	6.30	51.00	10.90	19.90	35.60	247.00	7.20
42	5.16	0.10	766.00	177.00	135.00	3.00	23.00	5.50	30.00	8.10	17.80	25.80	196.00	7.30
43	5.08	0.20	1150.00	128.00	145.00	1.00	13.00	3.90	21.00	7.60	21.60	26.00	416.00	12.00
44	4.86	0.20	1290.00	123.00	178.00	2.00	8.00	2.80	31.00	7.50	21.50	28.40	408.00	12.00
45	3.92	0.23	2870.00	90.00	244.00	4.00	1.00	3.90	89.00	11.70	25.20	14.40	712.00	19.00
46	5.06	0.21	1340.00	173.00	176.00	2.00	23.00	3.00	29.00	7.70	22.70	26.60	340.00	10.00
47	4.12	0.17	1430.00	181.00	372.00	3.00	14.00	5.80	54.00	7.80	25.10	23.30	379.00	8.40
48	5.06	0.18	1430.00	185.00	147.00	2.00	4.00	1.50	38.00	5.90	22.30	24.60	292.00	8.30
49	4.69	0.27	939.00	182.00	156.00	2.00	17.00	3.20	30.00	11.50	25.60	65.20	291.00	7.50
50	2.66	0.78	810.00	83.00	216.00	1.00	2.00	0.70	34.00	17.00	27.00	66.00	336.00	7.40
51	2.13	1.12	366.00	97.00	152.00	2.00	5.00	2.40	58.00	27.30	32.00	112.00	1430.00	33.00
52	3.43	0.86	1080.00	128.00	242.00	4.00	3.00	1.70	60.00	20.40	30.90	84.80	937.00	22.00
53	4.04	0.79	1630.00	148.00	245.00	4.00	2.00	1.80	53.00	20.00	28.90	81.70	892.00	19.00
54	2.22	0.47	409.00	92.00	231.00	3.00	4.00	1.20	40.00	20.20	21.30	30.80	137.00	3.80
55	3.01	0.26	875.00	103.00	434.00	4.00	7.00	3.40	51.00	9.40	23.00	21.20	172.00	5.30
56	1.54	0.36	800.00	50.00	720.00		1.00					20.00	160.00	3.30
57	2.49	0.57	581.00	108.00	270.00	4.00	3.00	0.80	49.00	14.50	25.10	27.50	178.00	3.90
58	0.85	0.23		60.00	250.00	2.50	0.60					30.00	140.00	3.40
59	1.09	0.17	171.00	80.00	332.00	2.00	3.00		32.00	7.40	21.10	15.80	76.00	2.00
60	1.37	0.14	310.00	50.00	460.00	2.20	2.70					20.00	110.00	3.00
61	1.30	0.15	221.00	55.00	258.00	4.00	2.00	0.70	32.00	11.10	28.80	24.60	114.00	3.60
62	1.36	0.13	308.00	38.00	336.00	2.00	1.00	0.80	26.00	4.70	24.60	16.10	90.00	1.90
63	1.18	0.06		60.00	380.00		3.50					10.00	100.00	2.60
64	1.70	0.13	522.00	55.00	367.00	3.00	5.00	1.90	28.00	6.40	24.40	16.80	65.00	2.60
65	2.72	0.24	816.00	104.00	573.00	3.00	7.00	3.40	48.00	10.90	21.90	12.60	105.00	3.40
66	1.41	0.49	426.00	52.00	393.00	1.00	2.00	1.50	17.00	13.80	25.50	27.10	162.00	4.10
67	2.42	0.22	897.00	86.00	369.00	2.00	3.00	1.50	29.00	10.60	24.90	29.00	131.00	4.60
68	0.71	0.14	185.00	32.00	439.00	2.00	2.00	1.00	9.00	7.20	26.90	14.80	42.00	2.20
69	1.48	0.27	458.00	60.00	231.00	3.00	2.00	0.80	39.00	13.00	25.20	34.60	169.00	4.50
70	1.46	0.26	332.00	33.00	452.00	3.00	3.00	1.50	26.00	7.40	23.90	26.50	85.00	3.80
71	0.84	0.07	191.00	21.00	490.00	4.00	2.00	0.90	20.00	4.30	17.40	7.00	22.00	1.10
72	0.60	0.60		40.00	310.00	1.70	0.40						40.00	0.60
73	0.39	0.03		30.00	70.00	0.90	0.72						30.00	0.72
74	0.52	0.07	251.00	21.00	167.00	1.00	1.00	0.50	19.00	2.00	14.30	4.50	81.00	1.30
75	2.38	0.10	631.00	93.00	257.00	4.00	7.00	3.10	50.00	3.90	21.70	10.30	100.00	3.40
76	3.98	0.18	1100.00	150.00	161.00	3.00	20.00	2.90	82.00	6.80	18.30	10.40	299.00	6.60
77	8.61	0.14	911.00	204.00	188.00	5.00	16.00	6.70	53.00	6.20	26.10	25.20	146.00	4.50
78														
79														
80														
81														
82	K2O (%)	P2O5 (wet)	Ba (NA)	Rb (NA)	Sr (XRF)	Cs (NA)	Th (NA)	U (NA)	Y (XRF)	Zr (NA)	Hf (NA)	Nb (XRF)	Ta (NA)	Zn (NA)
83	5.03		470.00	309.00	90.00	3.00	29.90		40.00		6.40		1.84	48.00
84	5.80	0.05	330.00	308.00	70.00	2.50	21.20		30.00	190.00	5.90		1.16	
85	6.00													
86	5.20		1000.00	198.00	130.00	3.70	26.30		20.00	210.00	8.10		0.92	76.00
87	4.49													
88	4.76													
89	4.78													
90	5.15		1000.00	158.00	180.00	2.60	4.50		20.00	350.00	11.10		1.06	80.00
91	4.85	0.30	1100.00	195.00	220.00	2.60	17.70		40.00	570.00	13.60		1.38	114.00
92	5.12													
93	3.74													
94	4.25	0.42	1300.00	113.00	270.00	2.10	8.70		50.00	620.00	14.10		1.70	147.00
95	4.42		1000.00	123.00	190.00	2.70	5.80		20.00		6.40		1.61	103.00
96	4.39													
97	3.40		1300.00	135.00	330.00	2.50	11.50		60.00	600.00	14.70		2.02	138.00
98	4.67													
99	3.70													
100	4.19		1200.00	111.00	290.00	1.80	7.40		60.00	510.00	15.90		2.50	171.00
101	4.26		1100.00	108.00	300.00	2.30	7.60		50.00	330.00	13.60		1.80	138.00
102	4.15	0.51	1100.00	132.00	320.00	1.30	6.50		50.00	580.00	13.70		2.80	150.00
103	4.66		1200.00	148.00	290.00	3.10	8.80		50.00	540.00	13.20		1.61	142.00
104	4.48													
105	3.98		1100.00	167.00	300.00	2.20	7.60		50.00	410.00	14.30		1.70	144.00
106	4.15	0.51	1300.00	136.00	310.00	2.20	9.40		60.00	490.00	15.50		1.40	143.00
107	3.71													
108	3.77	0.54	1300.00	120.00	310.00	3.80	6.30		60.00	350.00	14.50		1.70	153.00
109	4.73													
110	3.76													
111	4.45		1400.00	131.00	320.00	2.40	8.70		50.00	810.00	13.70		1.70	134.00
112	2.48	0.19	800.00	83.00	630.00	1.50	8.60		10.00	260.00	6.80		0.68	97.00
113	3.55	0.26	1800.00	102.00	300.00	2.40	11.50		40.00	390.00	13.80		1.24	169.00
114	3.78													
115	3.58	0.65	1350.00	112.00		2.00	4.00	1.80		611.00	14.00	54.00	2.00	
116	3.98													
117	3.64		1400.00	108.00	290.00	1.50	4.60		50.00	760.00	14.80		1.59	144.00
118	3.76		1400.00	123.00	350.00	1.60	7.20		60.00	430.00	14.90		2.20	165.00
119	3.64	0.91	1200.00	120.00	380.00	0.90	4.50		70.00		13.10		2.20	175.00
120	2.64	0.99	1100.00	116.00	410.00	1.60	6.00		70.00		9.10		2.30	182.00
121	3.64	0.68	1300.00	103.00	390.00	2.60	4.60		70.00	310.00	13.90		1.61	174.00
122	4.13	0.52	1400.00	88.00	320.00		3.90		50.00	750.00	22.20		2.20	195.00
123	2.91		1500.00	118.00	420.00	1.50	5.80		70.00	670.00	14.60		2.20	174.00
124	3.13													
125	3.36													
126	2.34													
127	3.05													
128	2.93		1400.00	80.00	510.00	2.10	3.20		60.00	510.00	13.50		1.70	186.00
129	2.69													
130	3.79	0.73	1400.00	94.00	340.00		3.70		80.00	1000.00	26.10		2.90	210.00
131	2.60	0.14	470.00	120.00	330.00	3.70	2.90		10.00		1.90			132.00
132														
133														
134														

	AB	AC	AD	AE	AF	AG	AH	AI	AJ	AK	AL	AM	AN	AO
1														
2														
3														
4	NB	TA	PB	SN	ZN	SC	CO	V	CR	NI	CU	AG	SB	BI
5	PPM (XRF)	PPM (NA)	PPM (ICP)	PPM (ICP)	PPM (ICP)	PPM (NA)	PPM (NA)	PPM (ICP)	PPM (ICP)	PPM (ICP)	PPM (ICP)	PPM (ICP)	PPM (NA)	PPM (ICP)
6	11	2	6		20.7	4.4	52	8	9		2.8	0.2		
7	18	3	5		66	12	31	35	6	4	7.4	0.2		
8	15.00	1.00	18.00		108.00	20.20	23.00	69.80	20.00		18.60	0.10	0.30	
9	16.00	1.00	3.00		98.40	20.70	24.00	63.80	21.00		19.40	0.60		
10	15		6		92	18.6	34	61	10	9	17			
11	11				107	19.8	32	67	15	11	20.4	0.2		
12	18.00	1.00	6.00		91.30	19.70	27.00	55.70	16.00		22.90		0.20	
13	21.00	1.00	9.00		122.00	23.70	37.00	73.50	22.00		20.50	0.20	0.40	
14	36.00	1.00	9.00		114.00	21.50	32.00	81.00	21.00		18.00	0.20	0.30	
15	52.00	1.00			106.00	22.20	31.00	76.80	25.00		21.80			
16	37.00	1.00	9.00		119.00	22.10	28.00	75.50	20.00		20.00	0.30		
17	18		2		139	31.5	40	133	21	17	29	0.2	0.5	
18					126	32.2	60	480	8	3	25.6		0.2	
19	17.00				57.40	30.80	43.00	286.00	54.00	24.00	19.80	0.20	1.90	
20					93.8	33.7	59	203	140	91	35.5			
21	15				117	29.7	52	218	56	24	26.6	0.3	0.2	
22	31.00	1.00			76.60	17.30	51.00	100.00	86.00	41.00	2.10			
23	15				119	10.4	47	171	95	71	52.9	0.1	0.4	
24	15		9		45.4	10.3	34	33	3	1	15.2			
25	19	2	8		19.7	5.9	42	8	9	2	1.7			
26					48.5	6	41	29	13	4	2.5			
27														
28														
29														
30	Nb (XRF)	Ta (NA)	Pb (ICP)	Sn (ICP)	Zn (ICP)	Sc (NA)	Co (NA)	V (ICP)	Cr (ICP)	Ni (ICP)	Cu (ICP)	Ag (ICP)	Sb (ICP)	La (NA)
31	11.00	2.00	18.00		43.20	6.80	27.00	7.60	3.00		0.60		0.20	65.70
32		1.00			49.80	8.10	26.00	13.50	2.00		0.70	0.20	0.20	58.40
33	18.00	1.00	15.00		43.50	8.10	44.00	6.10	1.00	2.00	2.20	0.70	0.20	56.50
34		1.00	25.00		32.30	5.20	29.00	9.10			2.10			60.10
35	24.00	2.00	8.00	11.00	51.00	2.80	26.00	19.90	1.00				0.30	39.70
36	23.00	1.00	6.00		45.80	3.40	24.00	5.70				0.60		36.90
37	25.00	4.00	18.00		64.90	9.40	25.00	20.90	4.00		7.60	1.00	0.30	49.80
38	30.00	1.00	12.00		67.80	22.80	26.00	21.70	2.00		7.00	0.20	0.20	46.70
39	35.00	1.00	16.00		75.60	23.30	28.00	26.30	3.00		7.70	0.70		48.60
40	16.00	1.00	20.00		66.20	7.00	24.00	29.80	11.00		7.20	0.20		78.30
41	17.00	1.00	21.00		66.80	10.80	26.00	50.50	7.00		5.90	0.40	0.40	69.30
42		1.00	15.00		50.70	8.00	27.00	26.00	6.00		6.20	0.40	0.30	59.90
43	27.00	1.00	18.00		73.10	11.90	42.00	22.50	2.00		5.80	0.60		53.00
44	19.00	1.00	15.00		80.10	13.70	28.00	30.90	9.00		12.10	0.20	0.20	50.50
45	15.00	1.00	13.00		116.00	22.40	20.00	17.20	6.00		35.10	0.40	0.20	19.80
46	31.00	1.00	17.00		73.10	10.40	26.00	50.10	11.00		11.90	0.30	0.30	83.00
47	29.00	1.00	15.00		88.80	5.50	23.00	21.50	3.00		3.70	1.00		84.10
48	18.00		8.00		61.20	10.40	21.00	29.80	8.00		8.90	0.80		29.90
49	39.00	3.00	14.00		106.00	22.10	32.00	40.10	1.00		6.90	0.20		75.20
50	58.00	2.00	9.00		126.00	27.60	31.00	115.00	3.00		16.60	0.30		91.50
51	77.00	3.00	16.00	10.00	261.00	50.40	36.00	155.00	17.00	8.00	17.80	0.30		116.00
52	61.00	2.00	6.00		150.00	28.00	28.00	112.00	3.00		15.10	0.70		113.00
53	52.00	2.00	3.00		151.00	27.90	32.00	110.00	3.00		13.20	0.70		112.00
54	24.00	1.00	6.00		114.00	30.60	51.00	204.00	213.00	85.00	38.40		0.20	28.80
55	19.00	1.00	3.00		92.40	13.00	27.00	80.80			0.80	0.70	0.20	36.80
56					154.00	21.00	29.80		6.80					20.60
57	25.00	1.00			101.00	29.10	41.00	172.00	112.00	48.00	41.00	0.20		36.40
58					173.00	28.50	56.00		91.00					10.90
59			4.00		93.30	33.90	59.00	209.00	654.00	156.00	46.50		0.20	18.40
60					132.00	33.50	40.90		155.00					15.30
61	20.00				93.40	31.70	63.00	220.00	55.00	62.00	50.60		0.20	10.10
62	18.00				88.00	41.50	60.00	353.00	63.00	8.00	73.30	0.10		15.30
63					150.00	39.00	61.10		12.00					13.80
64	15.00				76.70	37.50	51.00	247.00	22.00	5.00	166.00		0.20	17.10
65	17.00	1.00	3.00		93.40	5.90	41.00	79.50			4.70			29.30
66		1.00			120.00	35.00	50.00	215.00	74.00	30.00	59.70			29.00
67	22.00		3.00		93.00	30.80	42.00	144.00	58.00	10.00	48.90			28.60
68	14.00				98.60	44.10	68.00	465.00	70.00	19.00	114.00			14.30
69	34.00	1.00	6.00		108.00	32.60	45.00	187.00	69.00	35.00	43.70		0.20	34.20
70		1.00			97.40	38.80	44.00	235.00	54.00	10.00	38.70	0.20	0.30	24.20
71					76.20	11.90	69.00	59.00	33.00	109.00	65.90		0.20	7.90
72					99.00	22.30	101.00		138.00					4.50
73					97.00	10.20	138.00		1500.00					4.00
74	16.00		6.00		70.80	16.50	120.00	55.40	1310.00	519.00	42.80			7.60
75			6.00		53.00	8.40	27.00	42.30	14.00	3.00	10.70		0.20	25.10
76	23.00	1.00	24.00		61.80	7.60	30.00	25.40	7.00		4.00	0.30		59.20
77	19.00	1.00	31.00		99.20	16.90	38.00	89.50	93.00	28.00	1.40	0.50		53.60
78														
79														
80														
81														
82	Sc (NA)	Co (NA)	Cr (NA)	Sb(NA)	La NA)	Ce (NA)	Nd (NA)	Sm (NA)	Eu (NA)	Tb (NA)	Yb (NA)	Lu (NA)	Outcrop suscept.	
83	3.88	28.30	1.70		60.00	124.00	51.00	11.40	0.94	1.02	3.20	0.62	215.00	
84	3.08	25.60			47.00	107.00	32.00	10.00	0.85	0.76	2.60	0.50		
85													99.00	
86	8.20	20.30	7.70		68.00	144.00	60.00	11.70	1.57	0.85	2.60	0.47	1008.00	
87													1440.00	
88													1011.00	
89													1019.00	
90	9.90	25.20	7.10		33.00	69.00	54.00	9.30	1.54	0.96	2.10	0.39	1980.00	
91	12.30	21.50	7.50		73.00	170.00	79.00	17.90	2.24	1.50	4.50	0.81	666.00	
92													1321.00	
93													82.00	
94	17.00	24.40	7.80		66.00	151.00	79.00	15.90	2.87	1.90	4.70	0.88	1610.00	
95	10.50	19.50	8.30		31.00	65.00	49.00	6.30	1.67	0.60	2.10	0.39	681.00	
96													1843.00	
97	17.90	26.30	12.50		73.00	171.00	84.00	21.20	3.04	1.90	4.30	0.82	3447.00	
98													2528.00	
99													1830.00	
100	21.60	24.50	10.30		74.00	180.00	94.00	16.80	3.05	2.10	5.60	0.94	2616.00	
101	15.60	23.80	6.20		65.00	155.00	74.00	19.30	2.91	1.80	4.30	0.81	2760.00	
102	18.70	25.50	15.00		70.00	161.00	69.00	15.40	2.92	1.70	4.60	0.85		
103	15.00	21.20	6.20		64.00	152.00	96.00	19.20	2.79	1.50	4.60	0.81	2787.00	
104													3868.00	
105	17.20	23.70	15.00		70.00	168.00	85.00	16.30	3.04	2.00	4.90	0.80	2903.00	
106	16.80	21.00	15.00		74.00	171.00	105.00	19.80	3.06	2.40	4.90	0.86		
107														
108	18.80	21.50	7.50		74.00	176.00	104.00	17.70	3.23	1.90	5.10	0.89		
109													2802.00	
110													(2708)	
111	16.10	26.30	6.10		63.00	149.00	100.00	15.60	2.86	1.70	4.30	0.83	3242.00	
112	4.09	15.40	2.00		40.00	79.00	21.00	6.20	1.40	0.38	1.39	0.32		
113	24.30	17.40	10.00		33.00	73.00	32.00	11.80	3.70	1.30	4.00	0.81	1253.00	
114													3689.00	
115	23.10	27.00		0.20	81.80	167.00	78.00	15.40	3.30	2.00	6.00	0.87		
116													4871.00	
117	16.60	19.90	5.50		62.00	148.00	74.00	14.40	3.10	1.80	4.30	0.78	3113.00	
118	20.30	24.20	10.10		76.00	183.00	101.00	16.30	3.25	2.30	5.60	0.97	3485.00	
119	23.30	28.90	9.00		84.00	197.00	96.00	19.10	3.60	1.70	5.90	0.99		
120	23.20	28.60	7.00		78.00	189.00	99.00	18.20	3.40	2.40	5.90	1.04		
121	22.80	27.30	15.00		75.00	185.00	79.00	18.40	3.60	2.20	5.60	0.96		
122	21.90	22.40			68.00	161.00	93.00	15.40	3.02	1.80	5.10	0.96		
123	23.30	27.90	8.30		82.00	192.00	102.00	18.60	3.80	2.70	5.20	1.02	5974.00	
124														
125													4106.00	
126													9250.00	
127													9250.00	
128	23.90	30.90	10.00		77.00	184.00	124.00	18.40	3.90	2.10	5.00	0.93	8729.00	
129														
130	34.90	25.00			84.00	213.00	148.00	26.00	3.50	2.70	7.40	1.33		
131	22.80	54.10	427.00		12.40	32.20		4.10	1.06	0.70	1.50	0.27		
132														
133														
134														

	AP	AQ	AR	AS	AT	AU	AV	AW	AX
1									
2									
3									
4	MO	LA	CE	ND	SM	EU	TB	YB	LU
5	PPM (ICP)	PPM	PPM	PPM	PPM	PPM	PPM	PPM	PPM
6		76	145	60	10.9	1	1.4	3.2	0.47
7		57	113	50	9	2.6	1.4	2.9	0.46
8		59.10	104.00	48.00	8.80	2.50	1.10	3.50	0.51
9		36.60	64.00	29.00	5.40	2.10	0.80	1.90	0.31
10	2	48	100	40	8.6	3.5	1.2	3	0.45
11		38	74	30	6.6	3.3	0.9	3	0.42
12		33.90	59.00	30.00	5.80	2.70		2.00	0.34
13		52.90	96.00	46.00	9.80	2.40	1.20	4.30	0.64
14		40.30	74.00	33.00	6.70	2.40	1.10	4.40	0.68
15		38.00	75.00	35.00	7.10	2.50	0.80	3.10	0.47
16		65.20	122.00	52.00	9.90	2.60	1.20	3.40	0.52
17		43	90	40	8.2	3.5	0.8	3.5	0.57
18		61	120	50	9.1	1.7	1	2.6	0.38
19		8.60	18.00	8.00	1.80	0.70		1.00	0.15
20	3	19	42	20	4.1	1.2	0.6	1.6	0.27
21	1	38	78	40	7.4	2.9	1	2.9	0.46
22		65.50	118.00	47.00	7.90	1.30	0.80	2.50	0.38
23	1	81	156	60	10.4	2.1	1.4	1.7	0.24
24	3	21	42	20	3.7	1.8		1.5	0.15
25		23	51	20	5.9	0.2	1.1	3.1	0.41
26	1	26	48	20	3.7	1.1	0.5	1.2	0.19
27									
28									
29									
30	Ce (NA)	Nd (NA)	Sm (NA)	Eu (NA)	Tb (NA)	Yb (NA)	Lu (NA)		
31	119.00	48.00	8.50	1.40	1.50	4.20	0.60		
32	103.00	43.00	8.10	1.10	1.50	3.40	0.50		
33	106.00	44.00	7.80	1.30	1.10	2.90	0.41		
34	107.00	43.00	7.70	0.70	1.00	1.70	0.22		
35	72.00	27.00	5.00	0.70	1.00	3.00	0.43		
36	63.00	23.00	3.70	0.90	0.50	1.80	0.27		
37	97.00	38.00	6.90	1.40	1.60	8.40	1.39		
38	101.00	56.00	13.40	1.80	2.20	5.00	0.71		
39	98.00	60.00	13.60	1.60	2.10	5.20	0.73		
40	146.00	54.00	8.80	1.20	1.10	2.40	0.32		
41	120.00	48.00	8.40	1.30	1.30	4.20	0.59		
42	104.00	40.00	7.60	1.30	1.10	2.50	0.34		
43	90.00	36.00	6.60	1.70	1.00	2.40	0.34		
44	88.00	40.00	8.00	2.10	1.00	3.00	0.45		
45	35.00	18.00	3.80	4.00		1.50	0.23		
46	157.00	59.00	10.10	1.50	1.10	2.70	0.37		
47	134.00	46.00	6.50	1.70	0.90	2.50	0.41		
48	59.00	28.00	5.80	1.80	0.80	2.20	0.31		
49	152.00	71.00	14.30	2.30	2.20	6.40	0.93		
50	179.00	85.00	17.40	2.70	2.40	6.30	0.91		
51	240.00	115.00	24.40	3.30	3.90	8.80	1.29		
52	237.00	107.00	22.00	3.40	2.70	7.60	1.13		
53	230.00	103.00	21.80	3.60	2.90	7.80	1.18		
54	53.00	27.00	6.00	1.80	0.90	3.20	0.46		
55	68.00	31.00	6.30	1.80	0.80	2.60	0.39		
56	52.00	46.00	6.00	1.97		1.80	0.37		
57	76.00	33.00	6.50	1.90	0.80	2.90	0.44		
58	28.40		4.50	1.58	0.90	3.10	0.56		
59	38.00	17.00	3.60	1.10	0.50	1.40	0.22		
60	40.40		4.90	1.23		2.10	0.41		
61	25.00	15.00	4.10	1.50	0.80	2.40	0.35		
62	33.00	16.00	3.70	1.00	0.50	1.60	0.24		
63	32.80		3.30	0.92		2.10	0.32		
64	37.00	19.00	4.30	1.30	0.60	1.60	0.25		
65	55.00	22.00	3.80	1.40		1.10	0.16		
66	58.00	31.00	7.10	2.00	0.70	2.70	0.40		
67	62.00	31.00	6.70	1.70	0.90	3.00	0.44		
68	28.00	15.00	3.10	0.90		1.40	0.21		
69	68.00	33.00	6.90	1.40	0.90	3.60	0.54		
70	50.00	23.00	5.50	1.50		2.40	0.36		
71	16.00	8.00	1.50	0.40		0.70	0.10		
72	12.60		1.60	0.56		1.20	0.12		
73			1.14	0.31			0.11		
74	15.00	6.00	1.20	0.40		0.50	0.07		
75	51.00	20.00	3.60	0.90		1.20	0.18		
76	110.00	39.00	6.50	1.20	0.70	1.10	0.15		
77	93.00	39.00	7.10	1.80	0.70	2.50	0.37		
78									
79									
80									
81									
82									
83									
84									
85									
86									
87									
88									
89									
90									
91									
92									
93									
94									
95									
96									
97									
98									
99									
100									
101									
102									
103									
104									
105									
106									
107									
108									
109									
110									
111									
112									
113									
114									
115									
116									
117									
118									
119									
120									
121									
122									
123									
124									
125									
126									
127									
128									
129									
130									
131									
132									
133									
134									

	A	B	C	D	E	F	G	H	I	J	K	L	M	N	O	P
1	Appendix 2b. Chemical composition of the Subjotnian and related rocks															
2																
3	SAMPLE	Description	Coordinates	SiO2	TiO2	Al2O3	Fe2O3	MnO	MgO	CaO	Na2O	K2O	P2O5	F	LOI	SUM
4			Rikets nät	% (XRF)	% (XRF)	% (XRF)	% (XRF)	% (XRF)	% (XRF)	% (XRF)	% (XRF)	% (XRF)	% (XRF)	PPM (WET)	%	%
5	**STRÖMSBRO ROCKS**															
6	Sbro1	Strömsbro granite	673204/157391	70	0.437	13.1	2.83	0.04	0.6	0.6	4.44	4.52	0.07	1400	0.9	97.676
7	Sbro5	Strömsbro granite*+	673198/157378	72.4	0.414	13.1	3.29	0.02	0.6	0.73	4.05	4.98	0.07	1800	0.8	100.606
8	Sbro7	Strömsbro granite*+§	673225/157457	70.7	0.435	13	2.82	0.04	0.42	1.15	3.28	5.62	0.07	1400	1.05	98.755
9	Sbro10	Strömsbro granite*+	673261/157688	76.2	0.199	11.9	1.79	0.03	0.22	0.97	3.25	5	0.03	3200	0.7	100.423
10	Sbro9	Strömsbro granite porphyry	673199/157403	73.7	0.227	12.1	1.37	0.02	0.41	0.8	3.84	4.5	0.03	2900	1.05	98.141
11	Sbro13	Bäcksbro granite	673035/157178	65.7	0.664	13.5	5.43	0.08	0.59	1.71	3.56	4.96	0.12	400	1.95	98.482
12	Sbro16a+b	Strömsbro dolerite*+	673845/158445	48	2.52	15.2	15.4	0.21	5.03	4.34	2.4	1.99	0.42	1100	4.9	100.576
13	Sbro22	Strömsbro dolerite	672755/158410	50.6	1.69	14.7	12.1	0.18	4.41	7.72	2.29	2.28	0.41	818	2.05	98.6
14	Sbro23d	Strömsbro dolerite	672845/158180	47.6	1.92	15.4	12.6	0.2	5.09	4.59	1.03	4.2	0.42		5.95	99.2
15	Sbro24	Strömsbro dolerite	673695/158210	49.3	1.78	15.3	12.9	0.17	5.17	6.2	2.25	2.24	0.29		4.05	99.8
16	Sbro17a+b	Postjotnian dolerite	672989/157532	46.2	2.64	14.1	15.3	0.15	5.16	7.66	2	0.69	0.64	720	4.15	98.825
17	Sbro6P	Postjotnian dolerite	673357/157488	50.1	1.17	15.8	10.8	0.14	6	7.49	2.43	1.86	0.22	810	3.75	99.883
18	Sbro21a	Postjotnian dolerite	672734/158633	46.50	1.58	16.60	13.40	0.18	7.85	9.81	2.44	0.51	0.20		0.90	100.10
19	Sbro21a(2)	Postjotnian dolerite	672734/158633	46.10	1.62	16.70	13.10	0.18	7.94	9.80	2.36	0.54	0.19		0.85	99.50
20	Sbro6G1+2	Paragneiss, sed.*+	673357/157488	58.4	0.907	18.7	8.9	0.1	3.17	1.08	1.71	4.44	0.08	1100	2.4	100.052
21	Sbro6M	Mesosome, migm. paragneiss	673357/157488	62.4	0.795	16.6	6.9	0.06	2.92	1.25	1.63	3.2	0.06	720	2.95	98.905
22	Sbro6L1	Leucosome, migm. paragneiss	673357/157488	72.2	0.044	16	0.49	0.02	0.21	1.67	3.73	5.14	0.15	72	0.65	100.481
23	Sbro14a+b	Orthogneiss, grey*+	673169/157127	68.6	0.292	15.5	2.67	0.05	1.16	2.8	3.47	3.72	0.09	350	1.65	100.256
24	Sbro15a+b	Orthogneiss, red	673240/157057	74.8	0.24	11.9	2.78	0.07	0.42	0.59	3.64	3.38	0.04	88	0.8	98.822
25	Sbro8	Gneiss, unknown origin	673180/157392	49.4	0.74	14.8	7.05	0.13	2.74	9.13	4.48	2.9	0.24	330	8.02	99.81
26																
27	**GRÖTINGEN ROCKS**															
28	Gr1	Grötingen granite	696500/148515	72.9	0.224	13.4	2.6	0.04	0.19	1.21	3.71	4.96	0.05	3930	0.65	100.1
29	Gr3b	Grötingen granite	696890/149825	77.8	0.14	10.7	2.08	0.04	0.12	1.07	3.07	3.96	0.02	3690	0.65	99.8
30	A5	Abborrselet granite, yellow	697195/150140	75.2	0.105	12.5	1.5	0.03	0.17	0.67	3.59	4.61	0.02	1750	0.65	99.2
31	Gr2c	Revsund granite, red	696890/149700	65	0.596	13.9	6.67	0.12	0.34	2.41	3.27	5.47	0.17	1680	0.25	98.5
32	Gr2a	Dark green Revsund granite	696950/149750	64.5	0.622	14.8	7.08	0.13	0.35	2.73	3.69	5.34	0.2	1690	0.4	100.2
33	PJ1a	Postjotnian dolerite	697795/150217	47.90	1.62	17.30	13.60	0.19	6.60	9.44	2.90	0.57	0.21			100.10
34	PJ1a(2)	Postjotnian dolerite	697795/150217	47.30	1.64	17.40	13.40	0.18	6.76	9.63	2.88	0.58	0.20			99.80
35																
36	AGV-1	USGS Andesite standard		59.20	1.05	17.10	6.77	0.10	1.52	4.91	4.13	2.95	0.49	368.00	1.60	100.10
37	**MÅRDSJÖ ROCKS**															
38	M14a	Mårdsjö granite*+§	702589/149466	65.5	0.729	15.4	4.91	0.07	0.69	1.77	4	6.02	0.16	1610	0.55	100
39	M15b	Small porh. Mårdsjö granite*	702248/149593	67.7	0.443	14.8	2.9	0.04	0.48	0.95	3.66	6.62	0.09	740	0.55	98.4
40	M14b	Granite porphyry inclusion	702589/149466	65.4	0.742	15.2	4.36	0.06	0.65	1.61	4.02	6.28	0.15	1370	0.45	99.2
41	M19a apl.	Finer-grained pegmatite	702330/149452	75.3	0.127	11.9	0.73	0.03	0.11	0.18	3.58	5.37	0.02	69	0.5	97.9
42	M19c peg.	Pegmatitic material	702330/149452	74.8	0.198	12.6	1.23	0.02	0.24	0.62	3.55	5.39	0.02	90	0.25	99
43	M8	Red-brown Mårdsjö syenite	702621/149692	61.8	0.777	15.5	7.63	0.16	0.43	2.44	4.62	5.94	0.15	675		99.5
44	M11	Dark green Mårdsjö syenite*+	702265/149736	59.7	0.885	16.1	7.85	0.18	0.51	2.65	4.69	5.88	0.21	640	0.35	99.4
45	M12a	Red-brown Mårdsjö syenite	702192/149683	58.7	0.829	18.7	4.86	0.09	0.75	4.25	5.78	3.58	0.3	310	0.25	98.6
46	M13	Red-green Mårdsjö syenite	702688/149490	61.5	0.689	16.3	6.98	0.15	0.46	2.31	4.57	6.26	0.15	462		99.5
47	M20	Monzodiorite*	702292/149404	58.4	1.13	15.6	7.24	0.1	3.2	5.26	3.62	3.43	0.27	1230	1.2	99.7
48	M9	Mårdsjö monzogabbro	702754/149697	53.9	1.83	15.1	11.1	0.14	3.85	6.6	3.5	2.81	0.43	946	0.3	99.8
49	M17	Mårdsjö gabbro	702422/149138	54.3	1.36	15.2	9.23	0.12	4.87	7.89	3.34	2.15	0.31	780	1.2	100.2
50	M18	Mårdsjö gabbro*	702300/149462	55.2	1.2	15.6	8.26	0.11	4.63	7.8	3.31	2.17	0.27	750	1.1	99.8
51	M15a	Mårdsjö gabbro, fine-grained*+	702248/149593	55	1.5	15.2	9.2	0.13	4.5	7.01	3.74	2.41	0.34	960	0.85	100.1
52	M2a	Mårdsjö gabbro, fine-grained	702112/149540	54	1.26	15.4	9.21	0.12	5.29	8.36	3.29	1.92	0.27	648	0.65	100
53	M3	Coarse Mårdsjö leucogabbro	702098/149350	50.2	0.592	18.4	5.14	0.09	6.19	10.3	3.01	1.78	0.1	500	2.35	98.4
54	M5	Small porph. older granite*+	703407/148803	69.6	0.324	14.3	2.7	0.05	0.74	0.73	3.22	5.34	0.13	370	0.95	98.2
55	M6	Grey-white older granite	703560/148495	73.8	0.162	14.2	1.58	0.03	0.43	0.95	3.8	4.25	0.2	317	0.35	99.8
56	M7	Tonalite, early Svecofeanian	704115/148207	63.2	0.637	15	6.45	0.1	2.75	3.66	2.7	3.75	0.16	1120	1.2	99.8
57	M1	Sedimentary gneiss*+	700580/149005	66.3	0.745	14.5	5.68	0.07	2.61	1.79	2.7	3.41	0.08	750	0.7	98.8
58	M21	White leucogranite	701830/149475	72.8	0.059	14.8	1.08	0.04	0.21	0.53	5.08	3.3	0.23	461	0.6	98.8
59	M22	Metased. restitic enclave	701840/149365	69.3	0.607	13.9	4.68	0.05	1.92	1.82	3.88	2.44	0.13	660	0.85	99.7
60																
61	**NORDSJÖ ROCKS**															
62	RevI	Revsund granite	707100/149625	65.40	0.83	15.20	6.29	0.08	0.95	2.89	2.99	4.76	0.27	1220.00	0.45	100.30
63	N2	Revsund granite*	706375/151745	67.60	0.64	14.90	4.66	0.04	0.65	2.18	3.49	5.21	0.20	1340.00	0.55	100.30
64	N6	Revsund granite	706485/151854	63.60	0.93	15.30	6.60	0.08	1.00	2.81	3.02	5.90	0.28	788.00	0.40	100.20
65	N13	Revsund granite	706090/151950	64.10	0.82	15.50	5.80	0.07	0.91	2.68	2.99	6.13	0.25	772.00	0.45	100.00
66	N8	Pink Revsund granite*	706240/151415	64.60	0.69	16.20	4.65	0.06	0.80	2.59	3.29	6.27	0.21	636.00	0.65	100.30
67	N5	Nordsjö syenite, coarse	706385/151850	59.80	0.68	16.80	6.03	0.13	0.55	1.81	5.17	6.52	0.13	475.00	0.50	98.40
68	N9	Nordsjö syenite*	706320/151810	61.20	0.78	16.90	5.98	0.12	0.62	2.32	5.68	5.85	0.22	1070.00	0.35	100.30
69	N11	Nordsjö syenite*	706260/151648	58.90	1.24	15.30	8.26	0.16	0.91	3.16	4.93	5.01	0.45	863.00	0.40	99.10
70	N12	Nordsjö syenite§	706214/151693	59.30	1.18	15.90	8.71	0.16	0.70	2.93	4.90	5.36	0.30	456.00	0.30	100.00
71	N3a	Nordsjö trachyte dyke	706387/151780	60.80	0.37	17.10	6.61	0.17	0.22	1.43	6.55	5.50	0.07	1640.00	1.45	100.40
72	N4a	Green Nordsjö aplite (peralk)	706394/151784	73.50	0.25	12.80	2.45	0.03	0.06	0.37	4.87	4.81	0.02	1700.00	0.90	100.30
73	N10b	Nordsjö quartz trachyte dyke (peralk)	706300/151640	66.40	0.41	14.50	6.00	0.14	0.11	0.79	6.17	5.04	0.04	788.00	0.55	100.30
74	N7	Nordsjö dolerite, plag.phyric*	706270/152128	52.10	1.78	15.90	10.80	0.16	4.00	6.59	4.25	2.36	0.63	801.00	1.65	100.40
75	N3b	Nordsjö trachyte dyke	706387/151780	58.40	0.90	16.90	6.21	0.13	0.87	1.92	5.76	5.29	0.26	877.00	1.25	98.10
76	N10a	Postjotnian dolerite	706300/151640	45.40	1.01	17.30	13.60	0.19	7.93	10.30	2.37	0.98	0.06	1270.00	1.25	100.50
77																
78	**STRÖMSUND ROCKS**															
79	S2b	Postjotnian dolerite	707940/149079	46.30	1.55	16.30	13.30	0.19	6.90	8.83	1.94	1.73	0.26	336.00	2.60	100.00
80	S1	Revsund granite	707575/149072	60.00	1.38	14.90	10.50	0.13	1.65	3.81	3.08	4.15	0.46	778.00	0.25	100.60
81	S2a	Revsund granite	707937/149089	62.90	0.92	15.40	6.67	0.08	1.13	2.81	2.97	5.26	0.29	719.00	1.20	99.90
82	S3	Browned Strömsund granite (peralk)	708855/149493	71.50	0.41	12.50	4.34	0.09	0.13	0.50	4.49	5.33	0.04	694.00	0.60	100.00
83	S4	Greenbrown Strömsund granite*(peralk)	708740/149535	71.80	0.44	12.50	4.09	0.10	0.16	0.48	4.48	5.47	0.04	264.00	0.45	100.10
84	S6	Green Strömsund granite* (peralk.)	708580/149476	70.30	0.39	13.00	3.32	0.06	0.15	0.66	4.55	5.52	0.05	726.00	0.65	98.70
85	S10	Red Strömsund quartz syenite	708376/149320	67.20	0.53	14.90	4.18	0.07	0.28	0.98	4.55	6.06	0.08	300.00	1.20	100.10
86	S7	Strömsund granite*§	708708/149449	73.40	0.47	12.80	2.38	0.04	0.38	0.96	3.71	5.37	0.08	1220.00	0.70	100.40
87	S8(2)	Strömsund granite	708610/149437	71.90	0.49	13.00	2.78	0.05	0.45	1.10	3.84	5.24	0.10	1290.00	0.65	99.70
88	S8(2)	Strömsund granite	708610/149437	72.40	0.49	13.20	2.72	0.05	0.43	1.07	3.81	5.06	0.10	1280.00	0.70	100.20
89	S8(2)	Strömsund granite	708610/149437	72.70	0.46	13.30	2.74	0.04	0.44	1.08	3.77	5.13	0.10	1370.00	0.70	100.60
90	S8(2)	Strömsund granite	708610/149437	71.8	0.49	13.2	2.90	0.05	0.44	1.10	3.8	5.16	0.1		0.45	99.6
91	S8(2)	Strömsund granite	708610/149437	72.60	0.46	13.10	2.87	0.05	0.44	1.35	3.79	4.92	0.11		0.45	100.30
92	S5	Fine-grained grey older granite	708360/149020	72.90	0.30	12.60	1.90	0.03	0.29	0.67	2.91	6.29	0.05	457.00	0.95	99.00
93																
94	**MULLNÄSET ROCKS**															
95	Mu7	Mullnäset granite+§	707200/149208	70.40	0.48	13.50	3.54	0.06	0.33	1.17	4.30	5.49	0.07	925.00	0.55	100.00
96	Mu8	Mullnäset granite*+	707144/149270	69.90	0.50	14.00	3.75	0.06	0.41	1.25	4.44	5.53	0.08	1000.00	0.60	100.70
97	Mu1	Browngreen Mullnäset syenite	707191/148975	58.40	1.15	15.00	9.67	0.19	0.73	3.18	4.62	5.41	0.42	647.00	0.35	99.30
98	Mu5	Green Mullnäset syenite*	707197/148955	63.00	0.86	14.50	8.33	0.16	0.42	2.67	4.49	5.50	0.23	391.00	0.15	100.60
99	Mu6	Brown Mullnäset granite (peralk)	707296/149063	75.10	0.33	11.60	2.72	0.05	0.14	0.39	3.58	5.55	0.03	348.00	0.60	100.20
100	Mu12	Dark green Mullnäset syenite*+	706974/149315	60.80	1.01	15.50	7.42	0.13	0.64	2.51	4.72	5.59	0.27	388.00	0.90	99.70
101	Mu9	Mullnäset gabbro	706907/149278	53.60	1.09	15.90	10.30	0.14	4.84	8.04	3.79	1.55	0.30	496.00	0.45	100.10
102	Mu11a	Mullnäset gabbro*+	706800/149205	57.10	1.15	14.70	8.77	0.12	3.93	6.46	3.35	2.11	0.21	376.00	0.70	98.80
103	Mu2	Revsund granite*+	707309/149000	64.90	0.84	15.10	6.29	0.08	0.96	2.72	3.08	5.41	0.26	955.00	0.55	100.50
104	Mu4	Dark Revsund monzonite*	706812/148752	57.30	1.36	15.40	10.90	0.15	1.87	3.91	3.08	3.64	0.45	726.00	0.55	98.90
105	Mu10	Dark Revsund quartz monzonite	706650/149280	59.20	1.29	15.10	10.10	0.14	1.72	4.51	3.21	3.11	0.42	904.00	1.05	100.10
106	Mu3	White Sörvik granite?	706705/148750	76.00	0.10	12.50	1.23	0.02	0.08	0.81	3.42	5.32	0.02	4100.00	0.80	100.40
107																
108	**RÖDÖ ROCKS**															
109	R126a	Rödö granite*+(+§)	692031/159275	73.40	0.38	12.30	2.65	0.04	0.36	0.70	3.25	5.41	0.07	1430.00	1.00	99.70
110	R127:1+2	Rödö granite*+(+§)	692077/159238	73.20	0.42	12.40	2.80	0.04	0.38	0.89	3.29	5.61	0.08	1770.00	1.00	100.30
111	R133:2	Rödö granite*+(+§)	692130/159243	72.20	0.46	12.80	2.84	0.03	0.36	0.90	3.08	5.84	0.08	1180.00	1.25	100.00
112	R138	Rödö granite*+(+§)	692222/159610	70.7	0.375	13.3	2.82	0.04	0.37	1.02	3.1	5.96	0.08	1640	0.85	98.8
113	R139b	Rödö granite(+§)	692210/159204	74.7	0.278	12.1	2.29	0.02	0.25	0.21	2.78	5.89	0.05	285	0.65	99.3
114	R115:II	Rödö granite(+§)	691990/159154	71.1	0.347	13.6	2.65	0.03	0.32	0.92	3.21	6.13	0.07	1360	1.3	99.8
115	R13	Rödö granite(+§)	692031/159095	73.4	0.325	12.5	2.32	0.03	0.39	1.01	3.17	5.34	0.06	1300	0.9	99.574
116	R115R:II	Dark brickred Rödö granite	691990/159154	68.2	0.45	14.6	3.4	0.04	0.38	0.76	3.64	6.35	0.1	413	1.2	99.3
117	R115R:III	Dark brickred Rödö granite	691990/159154	71.4	0.339	12.2	2.43	0.03	0.25	1.03	3.24	5.34	0.06	2340	1.8	98.2
118	R133:1	Granite porphyry	692123/159243	75.60	0.17	12.20	1.74	0.02	0.16	0.55	2.55	6.12	0.02	2560.00	1.00	100.30
119	R133d	Granite porphyry	692156/159230	75.00	0.20	12.30	1.70	0.02	0.13	0.60	3.17	5.70	0.03	2200.00	0.75	99.70
120	R138a1	Granite porphyry	692222/159610	73.9	0.285	12.2	2.3	0.02	0.22	0.35	2.93	6	0.05	1950	1.05	99.4
121	R113Gr.porf.	Granite porphyry enclave	691980/159191	74.20	0.29	12.00	2.23	0.03	0.23	0.60	3.22	5.70	0.05	2160.00	1.00	99.70
122	R127a1	Granite porphyry enclave	692081/159235	69.70	0.46	13.30	3.04	0.03	0.39	0.99	3.36	5.93	0.08	2180.00	1.00	98.40
123	R138c	Aplite	692221/159624	74.7	0.041	13.2	0.84	0.02	0.04	0.43	5.08	4.24	0.03	3570	0.5	99.2
124	R126f	Aplite*+	692039/159286	75.90	0.04	13.10	0.72	0.03	0.08	0.50	4.78	4.28	0.02	3460.00	0.70	100.30
125	R113ap.	Aplite	691980/159191	75.80	0.03	13.50	0.35	0.02	0.06	0.37	4.91	4.65	0.02	2080.00	0.55	100.40
126	R126b	Aplite	692028/159274	76.20	0.06	13.00	0.81	0.02	0.08	0.64	4.61	4.31	0.03	3820.00	0.60	100.50
127	R113sch	Dark rapakivi schlieren	691980/159191	62.7	2.06	9.78	11.4	0.12	1.73	3.16	1.34	2.94	0.46	1240	4.05	100
128	R115s1	Dark rapakivi schlieren	691990/159154	58.4	2.88	9.07	17.7	0.16	2.26	2.25	0.41	0.88	0.58	1220	4.4	99.4
129	R115s3	Dark rapakivi schlieren	691990/159154	58.5	2.86	9.21	17.8	0.16	2.28	1.77	0.35	0.88	0.58	1120	4.35	99.1
130	R58eur	Quartz-feldspar porphyry	691822/158932	68.4	0.455	13.4	3.34	0.04	1.09	1.8	3.22	5.58	0.1	1370	1.9	99.5
131	R55	Quartz-feldspar porphyry	691825/158963	71.1	0.393	13.3	3.08	0.04	0.47	0.8	2.97	6.28	0.08	191	1.6	100.3
132	R117h	Porphyry	691511/159031	73.1	0.213	12.7	2.98	0.03	0.14	0.76	3.34	5.81	0.03	2400	0.85	100.1
133	R96a+b	Porphyry*+	691838/158520	69.9	0.332	13.5	3.79	0.05	0.2	1.31	2.83	6.11	0.06	180	2.05	100.334
134	R73a	Quartz-feldspar porphyry*+	692458/159520	74.40	0.22	12.00	1.76	0.03	0.12	0.54	3.16	5.64	0.03	2220.00	1.00	99.00
135	R107a	Quartz-feldspar porphyry	691668/159008	73.00	0.24	12.50	1.87	0.02	0.11	0.27	2.55	6.96	0.03	85.00	1.10	98.80
136	R47a+c	Quartz-feldspar porphyry	691819/158891	71	0.243	13.4	3.27	0.04	0.13	0.82	3.4	6.01	0.04	110	1.2	99.7
137	R52	Quartz-feldspar porphyry	691900/158961	72.1	0.243	13.3	3.11	0.04	0.15	0.73	3.24	5.93	0.04	135	0.85	99.9
138	R171a	Quartz-feldspar porphyry	691566/159082	73.3	0.259	13	2.91	0.03	0.24	0.47	3.06	6.2	0.03	463	0.85	100.5
139	R175	Quartz-feldspar porphyry	691590/159074	72.5	0.217	12.7	2.91	0.04	0.2	0.4	2.85	6.23	0.03	263	0.85	99.1
140	R122b+c	Quartz-feldspar porphyry	691626/159062	74.3	0.189	12.4	1.31	0.02	0.11	0.05	3.11	6.24	0.03	133	0.7	98.6

	AH	AI	AJ	AK	AL	AM	AN	AO	AP	AQ	AR	AS	AT	AU	AV	AW	AX
141	1	26				4.3	0.4			104	200	80	14.2	0.9	1.5	3.1	0.34
142	1	39		1		4.8	0.7			117	225	90	16	0.7	1.8	3.9	0.57
143	0.9	44			1	1.9	0.5			98	195	80	14.5	0.6	1.7	3.4	0.47
144	0.4	28				2	0.2			36	98	60	21.3	0.4	3.9	10	1.18
145	0.9	32			2	6.1	0.4			37	84	40	10.7	0.2	1.6	19.1	2.67
146	0.3	62	3			4		0.4		66	129	50	11.1		1.2	5.2	0.84
147	0.5	38				5.9				139	278	120	21.7	0.3	2.2	6	0.83
148	0.3	41			2	4.6				18	48	30	11.4		2.1	9.4	1.4
149	1.8	25	10		5	3.2		1		16	36	20	3.9		0.6	4	0.53
150	1	33	7	2	3	6.7	0.4	0.2		10.9	25	11	2.6	0.2		1.7	0.29
151	2.30	25.00	3.00	2.00		16.00	1.80	0.80		8.00	21.00	10.00	4.30	0.30	1.40	14.00	2.47
152	3.10	30.00			2.00	13.50	2.60	0.90		9.00	26.00	20.00	5.60		1.70	21.40	3.74
153	1.80	48.00	5.00	1.00		7.40	0.30	0.20		127.00	242.00	90.00	15.70	0.70	1.50	2.40	0.31
154	0.60	24.00				15.30	0.40			137.00	269.00	120.00	23.50		2.60	6.70	0.87
155	0.70	44.00	4.00	1.00		9.60	0.20			21.00	60.00	40.00	13.20		4.40	18.50	2.74
156	0.60	43.00	3.00	1.00		9.20	0.20	0.40		15.00	39.00	20.00	6.90	0.30	1.50	8.00	1.03
157	1.00	26.00				6.10	0.10			100.00	211.00	90.00	19.90	0.40	2.40	5.20	0.65
158	1.00	32.00	3.00	2.00		9.40	0.70	1.00		110.00	232.00	110.00	21.80	0.50	2.80	5.70	0.76
159	2.5	21	4		3	4.7	0.6			92	180	80	15.4	2.3	1.8	3.4	0.38
160	1.00	34.00		1.00		12.10	0.90			104.00	205.00	90.00	16.10	0.60	1.80	5.00	0.71
161	1.4	20		2		9.4	1.5			144	290	130	24.8	1.4	3	8.4	1.17
162	2.9	23	13		2	2				93	179	70	11.7	0.7	1.4	2.6	0.28
163	2.4	38	12		2	3.7				18	43	30	7.2	0.5	1.5	1.9	0.25
164	0.7	21				8.3	0.6	0.3		166	330	140	27.2	0.6	2.8	6.9	0.79
165	0.60	19.00	7.00	2.00	4.00	10.30	0.90			1.00			0.50			1.10	0.25
166	1.5	41	14	3	3	2.4	0.2	0.5		13	24	9	1.6	0.3		1.1	0.16
167	12.7	37	125	55	51	24.9	0.4		19	29	60	30	5.3	1.4	0.6	1	0.18
168	10.00	32.00	84.00	27.00	31.00	19.30	0.80		3.00	40.00	83.00	40.00	7.80	1.80	1.00	1.40	0.19
169	11.60	31.00	111.00	4.00	15.00	25.20	1.10		7.00	46.00	99.00	50.00	10.00	2.20	1.50	1.70	0.25
170	10.1	36	96	11	22	11.6			10	47	88	40	7.6	1.5	0.5	1.3	0.22
171	11	40	91	92	67	21.5			13	37	78	30	6	1.3	0.6	1.2	0.2
172	6.1	30	47	16	24	13.4	0.3	0.2		61	118	50	8.6	0.5	1.1	1.9	0.24
173	8.8	23	70	19	36	14.6	0.2	0.3	11	70	137	60	10.6	1.4	1.1	2	0.26
174	5	19	41	8	21	8.1	0.1	0.4		72	133	50	9.4	0.6	1	1.7	0.23
175	5	20	37	5	6	6.8	0.8			80	154	60	10.8	0.5	1.2	1.8	0.24
176	5.1	19	42	10	35	13.2	0.1		6	79	154	60	10.9	1.2	1.1	1.9	0.28
177	4.1	17	30	9	17	7.8		0.2		81	158	60	11.2	0.6	1.1	2.2	0.31
178	3.6	29	25	9	15	9.5				65	129	50	10.1	0.8	1.3	1.9	0.24
179	4.2	17	28	4	17	9.7	0.2	0.2		89	176	70	12	0.5	1.2	1.9	0.28
180	2.3	17	4	3	2	5.9	0.5			80.8	156	67	12.5	1.9	1.6	3.7	0.48
181	9.6	27	88	48	83	15.7		0.2	8	49	84	40	7.5	0.7	0.8	1.4	0.18
182	10.60	37	98.00	44.00	94	34.1	0.2		9	45	91	40	7.2	1.4	0.7	1.4	0.19
183	6	15	43	9	17	6.8	0.3		4	43	91	40	8.4	1.1	1.2	3	0.44
184	8.1	30	113	8	22	5.7	0.7	0.5		42.2	82	36	7.3	0.6	1.5	8.5	1.32
185	7.7	12	4			6	0.5	0.3	11	52	110	50	10.2	3	1.2	1.8	0.25
186	4.9	10	4			7.5	1	0.4	3	89	176	70	14	1.4	1.4	3.1	0.44
187	5.9	10		1		7.3	1.4	0.2		78	158	70	12.1	1	1.3	2.9	0.43
188	1.50	16	3.00		1	8.6	1.5			132	249	100	17.2	1.3	1.6	4.6	0.69
189	11.1	27	99	11	19	19.4	0.9		8	50	106	50	9.1	2.2	1	1.8	0.25
190	5.70	21	41.00	31.00	58	19.6				57	110	50	8.1	0.8	0.7	1.5	0.27
191	10.1	36	99	5	3	16.2	1.1			48.1	100	47	9.5	2.3	1.3	1.7	0.21
192	10.20	22	89.00	4.00	4	13.1			6	48	100	50	9.8	1.9	1.2	1.8	0.23
193	12.70	30	117.00	41.00	48	17.6			11	31	62	30	5.6	1.5	0.5	1.3	0.16
194	10.40	27	92.00	3.00	1	14.6	0.4		16	49	100	50	9.9	2.6	1.1	1.8	0.25
195	12.00	34.00	105.00	104.00	63.00	22.80	0.50			34.00	70.00	30.00	6.30	1.10	0.70	0.90	0.13
196	11.90	38.00	94.00	54.00	60.00	20.40	0.30		12.00	34.00	68.00	30.00	5.60	1.30	0.50	1.20	0.15
197	10.30	28	78.00	26.00	50	19	0.1		9	42	84	40	6.6	0.9	0.9	1.4	0.2
198	6.90	10	4.00		1	7.2	0.6		7	104	204	80	14.4	1.9	1.4	3.3	0.46
199	6.40	12	3.00			16.3	0.6		9	94	185	70	12.8	1.2	1.3	3.3	0.44
200	11.00	41	94.00	2.00	25	487	1.1	0.7	13	40	85	40	7.3	1.7	0.8	1.4	0.22
201	10.80	39.00	116.00	18.00	25.00	556.00	1.90	0.50		40.00	86.00	40.00	8.30	1.40	0.90	1.60	0.23
202	12.00	16	7.00	1.00		28.5	0.6		16	60	125	60	12.1	3.3	1.4	2.1	0.31
203	8.6	9	3	2		8.5	1.7	0.2		81	165	70	13.5	2.1	1.5	3	0.42
204	8.40	10.00	4.00			8.80	1.00	0.20		81.00	162.00	70.00	14.30	2.10	1.60	3.00	0.49
205	14.5	15	15	6		11.3	0.8			55	120	50	10.7	3.2	1.2	2	0.3
206	25.1	60	142	197	155	122	0.8			7	18	10	3.5	1.2		1.4	0.23
207	13.8	12	7	3		10.2	1.4			62	125	60	11.3	3.4	1.4	2.4	0.34
208	11.4	26	47	55	40	18.6	0.7	0.2		54	110	50	9.2	2.7	1	1.6	0.25
209	15.7	41	137	9	22	23.4	1.1	0.2		36	78	40	8.6	2.9	1.3	1.7	0.24
210	10.3	29	60	32	40	17.4	0.4		9	44	91	40	8.8	2.5	1	1.6	0.21
211	0.1	7	2			5	3.2	0.9	6	158	328	150	31.1	0.3	4.1	10.8	1.48
212	0.20	7.00	2.00	1.00		6.50	4.30	0.80		159.00	343.00	160.00	33.00		4.30	11.20	1.54
213	13.7	51	124	115	128	29.4	0.2		13	28	58	30	5.3	1.5	0.6	1	0.12
214	11.8	33	123	15	24	19.3			14	42	83	40	8.2	2.1	0.9	1.5	0.22
215	11.9	29	111	31	47	19.5	0.3		16	32	66	30	5.9	1.4	0.6	1.2	0.18
216	15.90	48	139.00	158.00	156	30.2			18	17	38	20	3.4	0.7		0.9	0.12
217	11.60	19	9.00			162	0.9		7	59	125	60	11.9	3.2	1.5	2	0.31
218	8.60	26	82.00	3.00	3	14.1	0.2		10	40	84	40	8.2	2.4		1.4	0.27
219	11.50	35	125.00	11.00	50	23.6		1.5	8	34	70	30	6.7	1.4		1.2	0.21
220	8.50	34	77.00	22.00	46	19.3			10	45	91	40	6.7	1.1		1.2	0.17
221	11.20	34	119.00	10.00	25	19.1	0.3	0.2	19	37	77	40	7.2	1.6	0.8	1.6	0.22
222	11.20	30	116.00	23.00	36	16.7			16	33	69	30	6.6	1.7	0.8	1.3	0.2
223	12.90	31	130.00	14.00	25	14.6			18	36	74	40	6.8	1.9	0.9	1.2	0.19
224	11.20	30	97.00	46.00	77	27.4		0.2	19	23	50	20	4.8	1.2	0.5	1	0.16
225	13.3	28	132	17	27	16	0.1		6	33	67	30	6.3	1.4	0.8	1.2	0.22
226	33.5	61	321	95	70	57.3	0.6			16	37	20	5	1.2	0.7	1.6	0.3
227	10.8	33	98	73	113	27.3	0.6	0.2	16	26	56	30	5.4	1	0.7	0.9	0.12
228	14.3	49	134	158	144	30.7		0.2	11	18	37	20	3.2	1.1		1.2	0.13
229	10.7	30	112	47	113	39.2	0.2	0.2	9	26	58	30	6.1	1.2	0.8	0.9	0.13
230	29.1	58	274	52	81	64.6			13	9	22	10	3.6	0.8	0.7	2	0.29
231	34.5	64	276	45	77	60.7	0.4		11	10	24	10	3.8	1.1	0.7	2	0.31
232	23.30	58.00	238.00	54.00	43.00	72.20	0.50			13.00	31.00	20.00	4.80	1.30	0.90	2.20	0.33
233	25.00	65.00	218.00	25.00	42.00	66.10			10.00	13.00	31.00	20.00	4.50	1.40	0.70	2.30	0.36
234	27.5	37	248	42	19	69.6			5	15	36	20	5.5	1.4	1	3.1	0.4
235	68.40	45.00	435.00	241.00	35.00	62.50	0.40			10.00	25.00	20.00	4.90	1.50	1.00	2.20	0.43
236	78.40	57.00	414.00	171.00	35.00	58.90			14.00	12.00	31.00	20.00	5.20	1.60	1.00	2.60	0.39
237	25.50	56.00	223.00	47.00	101.00	64.90	0.70			11.00	29.00	10.00	4.20	1.10	0.80	2.10	0.29
238	28.60	68.00	201.00	25.00	97.00	58.50			18.00	12.00	28.00	20.00	4.30	1.50	0.80	2.00	0.33
239	20.40	37.00	132.00	140.00	83.00	61.10	0.40	0.20		5.00	15.00	10.00	3.70	1.80	0.70	2.20	0.35
240	20.10	42.00	117.00	26.00	79.00	53.90			13.00	5.00	13.00	10.00	3.30	1.80	0.80	2.20	0.37
241	22	45	177	158	158	130	0.2		23	5	13	10	3.7	1.2	0.5	1.7	0.2
242	21.20	35	177.00	17.00	12	31.3			10	12	28	10	2.7	0.8		1.6	0.22
243	21.2	34	188	21	15	58.2	0.4	0.2		11.9	25	12	2.6	0.9		1.3	0.21
244	35.8	59	225	70	44	83.7	0.6	0.4		15	36	20	5.7	1.7	1	3.2	0.5
245	30.2	46	130	206	38	45.1	0.5	1.4		7	18	10	2.3	0.9		1.4	0.19
246	29.1	64	252	61	101	64.2	0.7			12	30	10	4.4	1.8	0.6	2.1	0.35
247	34.9	77	195	409	321	117	0.8			7	17	10	2.7	0.8	0.5	1	0.18
248	12.70	41.00	66.00	113.00	38.00	22.30				33.00	62.00	30.00	5.00	0.70	0.70	1.90	0.34
249	12.3	43	77	75	35	8.8	1			40	79	30	5.5	1	0.6	1.6	0.29
250	11	44	44	50	27	4.8	0.8			46	84	30	6.1	1.3	0.8	2.1	0.3
251	9.60	39.00	49.00	42.00	26.00	29.90	0.20	0.20		25.00	51.00	20.00	3.70	0.70		1.00	0.16
252	11.70	39.00	61.00	74.00	29.00	24.80	0.30			34.00	62.00	30.00	5.30	1.20	0.70	1.80	0.26
253	9.8	38	46	60	21	7.9	0.6			40	80	30	6.2	1.1	0.7	0.5	0.1
254	8.7	40	49	15	16	9.3	0.2			29	53	20	3.5	0.9		1.3	0.23
255	11.3	46	74	31	22	18.4			8	34	65	30	5.3	0.7	0.8	2	0.35
256	12.40	46.00	76.00	31.00	35.00	31.10	0.20			41.00	80.00	30.00	6.00	0.80	0.70	1.00	0.19
257	10.60	35.00	37.00	36.00	15.00	17.00	0.90	0.20		59.00	111.00	50.00	9.90	0.80	1.30	1.40	0.24
258	12	36	69	60	25	24.4	0.8			29	56	20	4.6	1.1	0.5	1.6	0.27
259	6.2	56	23	25	3	2.1	0.8			30	55	20	3.5	0.8		0.8	0.18
260																	
261																	
262																	
263																	
264																	

	AH	AI	AJ	AK	AL	AM	AN	AO	AP	AQ	AR	AS	AT	AU	AV	AW	AX
1																	
2																	
3	Sc	Co	V	Cr	Ni	Cu	Ag	Sb	Bi	La	Ce	Nd	Sm	Eu	Tb	Yb	Lu
4	PPM (NA)	PPM (NA)	PPM (ICP)	PPM (ICP)	PPM (ICP)	PPM (ICP)	PPM (ICP)	PPM (NA)	PPM (ICP)	PPM (NA)	PPM (NA)	PPM (NA)	PPM (NA)	PPM (NA)	PPM (NA)	PPM (NA)	PPM (NA)
5																	
6	3.8	35	12	2	1	1.6	0.2	0.2		65	124	48	8.7	0.9	1.2	4.5	0.64
7	3.6	59	12	2	3	3.5	0.6			67.3	123	47	8.2	0.8	1	4.3	0.62
8	3.9	37	12	2	2	6.8	0.6			65.6	125	49	8.9	0.5	1.3	4.7	0.71
9	1.4	47	3	1		3.5	0.3	0.2		98.9	176	65	10.9	0.6	1.2	8.6	1.3
10	1.7	73	5	2		1.5	0.4			54.4	105	41	7.4	0.5	1.1	4.9	0.76
11	9.1	18	13	3	1	2.5	0.7			68	136	60	11.1	1	1.5	5.8	0.93
12	31.4	46	213	34	25	18.9	1.3			32	71	40	8.5	2	1.3	4.3	0.66
13	28.3	43	204	19	26	16.5			6	33	68	30	7	2	0.9	3.5	0.51
14	24.9	43	190	22	48	19.9			17	26	60	30	7.5	1.9	1	3.4	0.52
15	25.7	48	209	21	42	17.6			24	22	48	30	5.7	1.6	0.8	2.8	0.43
16	28.6	56	223	14	45	41	1.1			37	81	40	9.1	2.3	1.3	4.6	0.65
17	25.5	48	154	55	31	27.6	1			20	44	20	5	1	0.7	2.2	0.31
18	28.00	66.00	249.00	76.00	119.00	63.10	0.70			9.00	22.00	10.00	3.50	1.10	0.60	1.70	0.25
19	30.00	72.00	199.00	30.00	107.00	51.20			14.00	9.00	22.00	10.00	3.40	1.40	0.60	1.90	0.26
20	21.3	26	91	119	46	26	0.8			65	130	50	10.1	1.1	1.2	3.8	0.56
21	18.1	35	71	78	47	1.4	0.6			48	95	40	6.9	0.7	1.1	2.8	0.4
22	2.2	42	3	5	3	4.9	0.5			98	180	70	15.6	2.3	1.7	0.8	
23	4.2	28	29	13	4	9.9	0.8			73	120	40	6	0.7	0.7	0.6	0.06
24	5.3	24		1		8.9	1.3			50	102	50	9.9	1.5	1.4	6.8	1.11
25	28.3	27	156	249	65	93.8		0.2		7	17	10	2.5	0.9	0.5	1.9	0.34
26																	
27																	
28	3.2	47	4			0.8		0.2		89	170	70	13.4	0.9	1.6	5.8	0.83
29	1.7	66			2	1.1				70	151	70	17.3	0.7	2.6	8.6	1.26
30	1.7	55		7	3	3	0.1	0.2		47	89	40	6.8	1.6	1	3.9	0.51
31	15.2	33	7			8.7			4	88	186	80	18.2	3	2.3	7.1	1.02
32	16.3	36	8	2	1	21.2				71	157	80	17.1	3.1	2.8	7.5	1.12
33	23.10	63.00	191.00	39.00	62.00	60.30	0.60			10.00	25.00	10.00	3.80	2.00	0.60	1.80	0.29
34	23.80	69.00	174.00	30.00	58.00	52.10		0.30	18.00	10.00	24.00	20.00	3.50	1.50	0.60	2.20	0.31
35																	
36	11.80	20.00	95.00	9.00	14.00	61.20	0.70	5.40	5.00	41.00	75.00	30.00	5.50	1.20	0.50	1.70	0.27
37																	
38	5.4	29	20		3	2				65	124	50	8	1.2	0.8	2	0.3
39	3.7	28	14		2	2.9	0.5		11	73	141	50	8.7	0.6	0.7	1.9	0.2
40	4.3	37	17	1	1	3			4	64	123	50	7.9	0.9	0.9	2.5	0.35
41	1.3	73	2		3	3.4	0.2			35	70	30	4.4	0.5	0.7	2.4	0.33
42	2.4	64	5		2	4.7				79	148	50	7.4	0.9	0.7	2	0.3
43	12.8	18	4		2	2.4			5	68	134	60	10.2	3.1	1	2.2	0.32
44	13.5	26	4			2.6	0.1			53	108	50	9.1	3.7	1	1.9	0.28
45	11.5	28	12	2		4.1				33	65	30	5.2	5.6	0.5	0.8	0.11
46	12.6	28	5	2		4.8				38	77	30	6.7	2.7	0.7	1.7	0.26
47	10.7	42	110	4	16	12.7		0.2	11	48	91	30	6.1	1.6	0.5	1.5	0.13
48	16.4	39	162	14	26	11.9			7	49	98	40	8.1	2	0.9	1.5	0.22
49	15.5	47	140	92	25	22.4			16	35	69	30	5.7	1.6	0.5	0.9	0.22
50	15	44	120	96	28	21.9				33	67	30	5.2	1.5	0.5	1.2	0.13
51	14.7	36	137	41	22	20.7			12	39	78	30	6	1.3	0.6	1.2	0.17
52	17.2	40	138	48	38	26.6		0.3	7	32	64	30	5.4	1.6	0.6	1.1	0.14
53	12.2	32	68	225	105	20.3			4	12	22	10	2.2	0.8		0.6	0.09
54	5.5	25	25	11	11	9.2			4	31	55	20	4.5	1	0.6	2.2	0.33
55	4.7	33	10	26	5	0.7				13	26	10	2.6	0.5		1.8	0.24
56	17.3	40	75	79	21	28.9	0.2	0.6		43	83	30	5.8	1	0.7	2	0.29
57	13.8	29	95	76	40	10.1	0.1	0.2	3	47	88	30	6.3	1.3	0.7	1.9	0.31
58	4.5	58	3		3	1.3				6	12		1.6			0.8	0.18
59	12.2	30	85	32	24	49.7		0.5		39	74	30	5.6	1.2	0.6	2.2	0.32
60																	
61																	
62	12.60	29.00	32.00	17.00	6.00	17.20	0.60	1.30		42.00	84.00	40.00	9.10	1.30	1.20	3.80	0.53
63	4.30	21.00	23.00	8.00	3.00	12.70	0.70	0.70		43.00	85.00	40.00	7.50	0.70	0.90	2.00	0.26
64	13.00	29.00	31.00	12.00	4.00	18.30	0.30	0.70		46.00	95.00	50.00	9.70	1.50	1.30	3.60	0.53
65	10.90	32.00	30.00	10.00	3.00	18.40	0.10	1.20		50.00	95.00	40.00	8.30	1.70	1.10	3.20	0.45
66	8.80	27.00	27.00	9.00	3.00	12.30	0.20	0.90		37.00	75.00	40.00	6.80	1.60	0.80	2.70	0.44
67	5.90	26.00		2.00		6.00				25.00	53.00	20.00	5.20	2.70	0.60	1.50	0.20
68	8.10	19.00	3.00			9.10	0.40			92.00	173.00	70.00	11.50	3.00	1.10	2.40	0.33
69	12.20	28.00	5.00	2.00		8.80	0.50			50.00	109.00	50.00	10.30	4.20	1.40	2.30	0.32
70	12.10	30.00	4.00	2.00		10.90	0.50		8.00	31.00	69.00	40.00	8.40	3.80	1.20	2.10	0.34
71	3.20	20.00		1.00		9.90	0.70			59.00	123.00	50.00	10.40	0.80	1.10	3.50	0.44
72	0.10	53.00		2.00		13.20	2.40			117.00	232.00	110.00	21.20	0.40	2.40	6.20	0.81
73	1.70	26.00				6.70	1.60			46.00	105.00	60.00	13.80	0.90	2.10	5.50	0.86
74	13.90	36.00	92.00	68.00	40.00	26.00	0.60	1.00	9.00	27.00	62.00	30.00	7.70	2.20	1.00	1.60	0.26
75	6.30	19.00	9.00	2.00		9.90	0.90		4.00	57.00	110.00	50.00	10.00	1.90	1.20	2.90	0.38
76	35.30	69.00	137.00	71.00	89.00	24.40	0.30		7.00	3.00	9.00		2.50	1.00	0.60	2.50	0.33
77																	
78																	
79	26.80	65.00	132.00	105.00	87.00	46.70	0.30	0.30	9.00	7.00	18.00	10.00	3.30	1.00	0.70	2.30	0.34
80	22.00	37.00	56.00	30.00	9.00	28.80	0.80	0.70		55.00	108.00	50.00	10.70	1.60	1.20	4.50	0.66
81	14.00	31.00	36.00	18.00	8.00	20.70	0.40	0.90		50.00	99.00	50.00	9.00	1.40	1.00	3.20	0.48
82	3.20	55.00		1.00		5.70	0.70			67.00	142.00	70.00	13.70	1.20	1.70	3.30	0.48
83	2.90	69.00		1.00		5.00	0.20			39.00	80.00	40.00	9.90	0.80	1.40	2.10	0.31
84	2.50	64.00		2.00	1.00	6.10	0.40			40.00	84.00	40.00	9.00	0.80	1.10	2.10	0.29
85	5.40	40.00	2.00	1.00		9.00		0.20		46.00	101.00	50.00	9.80	0.80	1.00	2.10	0.30
86	2.40	63.00	11.00	5.00	2.00	6.70				42.00	82.00	30.00	5.80	0.70	0.50	1.30	0.21
87	2.50	70.00	14.00	2.00	1.00	7.30	0.50			43.00	80.00	30.00	6.60	1.20	1.00	1.60	0.25
88	2.50	67.00	14.00	3.00	3.00	7.70	0.40			42.00	82.00	30.00	6.60	1.00	0.80	1.60	0.26
89	2.60	68.00	12.00	3.00	3.00	4.70				42.00	85.00	40.00	6.50	0.50	0.60	1.70	0.23
90	2.80	62	15.00		2	1.7				46	88	40	6.3	0.9	0.6	1.7	0.28
91	2.80	68.00	17.00	1.00	2.00	1.90	0.40			46.00	91.00	40.00	7.20	1.30	0.80	1.80	0.23
92	4.00	59.00	9.00	2.00	3.00	4.50	0.80			66.00	124.00	50.00	8.40	0.60	1.00	3.50	0.47
93																	
94																	
95	2.40	59.00	7.00	3.00	2.00	5.50		0.30		29.00	63.00	30.00	7.60	0.90	1.00	1.90	0.24
96	2.70	48.00	8.00	3.00	3.00	5.10				35.00	75.00	40.00	8.10	1.20	1.20	1.90	0.26
97	13.10	27.00	5.00	3.00		8.20		0.20		15.00	35.00	20.00	6.00	3.80	1.20	1.40	0.22
98	11.70	26.00	3.00	2.00		6.20	0.20			31.00	68.00	40.00	8.30	4.10	1.20	2.00	0.26
99	1.50	55.00		2.00		4.10				126.00	233.00	80.00	13.30	0.90	1.10	1.60	0.27
100	7.60	23.00	3.00	2.00		10.70	0.40	0.30		17.00	40.00	20.00	5.60	2.90	0.90	1.30	0.20
101	16.50	60.00	128.00	12.00	47.00	26.40	0.20		3.00	20.00	46.00	30.00	6.50	1.30	1.20	1.60	0.25
102	17.20	48.00	90.00	48.00	46.00	19.50	0.20			22.00	50.00	30.00	6.60	1.50	1.10	2.20	0.29
103	13.00	30.00	34.00	17.00	5.00	16.50	0.60	0.90		46.00	95.00	40.00	8.80	1.40	1.10	3.10	0.39
104	25.70	32.00	60.00	39.00	14.00	35.30	0.60	1.20		49.00	100.00	50.00	10.70	1.70	1.50	4.10	0.61
105	22.40	36.00	63.00	37.00	13.00	17.40	0.70	0.70		49.00	101.00	50.00	10.20	2.20	1.40	3.80	0.64
106	0.90	63.00			2.00	6.80		0.20		50.00	117.00	60.00	17.70	0.40	3.30	12.20	1.63
107																	
108																	
109	2.40	32.00	8.00	4.00		7.30	0.80			99.00	185.00	80.00	13.20	0.50	1.30	1.70	0.31
110	2.40	32.00	9.00	2.00	3.00	6.90	0.60			87.00	165.00	70.00	11.80	0.60	1.40	2.30	0.28
111	2.50	30.00	9.00	2.00	1.00	7.50	0.50			88.00	169.00	70.00	11.60	0.60	1.20	1.80	0.25
112	2.5	40	11		1	2.8				87	163	60	10.8	0.9	1.2	2	0.28
113	1.7	43	7		1	4.2			4	103	193	70	11.5	0.4	1.3	1.9	0.27
114	2.3	29	11			9.8	0.2		6	74	141	60	9.7	0.8	0.9	1.6	0.18
115	1.9	69	11	3	2	2.9	0.4			72.9	140	54	9.4	0.7	1	1.7	0.21
116	2.8	31	15	4	2	150	0.3	0.2		90	172	70	11.7	0.9	1.1	2	0.3
117	2	28	9			3.7	0.1		3	84	166	60	10.9	0.9	1	1.9	0.28
118	1.50	51.00				12.30	0.30			115.00	219.00	80.00	13.80		1.60	2.90	0.52
119	1.20	57.00			1.00	10.00				125.00	233.00	80.00	13.00		1.50	2.70	0.42
120	2.3	44	6		1	3		0.3		106	209	80	14	0.5	1.5	2.2	0.26
121	2.10	41.00	6.00	2.00	1.00	7.70	0.90			125.00	234.00	100.00	15.50		1.60	2.80	0.49
122	2.70	44.00	11.00	2.00		5.60	0.90			65.00	129.00	50.00	9.20	0.60	1.00	1.60	0.20
123	1.5	53		2	1	1.5		0.7		13	40	30	10.5		2.3	6.5	0.91
124	1.10	53.00			2.00	7.40				19.00	50.00	30.00	11.50	0.40	2.30	6.20	0.85
125	1.10	47.00		1.00	1.00	5.10	0.20			17.00	49.00	40.00	14.90		3.00	7.30	0.91
126	0.60	49.00			1.00	5.90	0.20	0.30		23.00	53.00	30.00	6.70	0.40	1.30	4.90	0.67
127	13.6	28	80	6	7	8.3	0.3		7	154	325	150	30.2	0.5	3.3	5.5	0.79
128	13.9	33	108	12	9	18.4	2		23	208	431	200	42.4	0.6	4	6.9	0.95
129	14.4	34	115	7	9	17.3			17	217	435	210	43.1	0.7	3.9	7.3	0.97
130	3.3	31	21	2	14	8.8	0.3		7	83	158	60	10	1	1.2	2	0.27
131	2.5	22	15		5	7.1		0.2		88	165	70	11.4	0.7	1.1	2.2	0.32
132	0.9	27			1	7.4	0.2			126	255	110	21.2	0.8	2.4	4.6	0.65
133	2.4	19		2		6.1	0.9	0.5		76	157	70	13.4	1.8	1.8	3.4	0.45
134	1.10	39.00	3.00			6.80	0.30			96.00	184.00	70.00	12.80	0.40	1.60	3.10	0.43
135	0.90	29.00	3.00			19.50	0.60	0.50		99.00	205.00	90.00	17.70	1.20	2.20	4.50	0.57
136	1.8	14				5.7				105	210	90	16.3	1.7	1.6	4	0.54
137	1.8	22	5		2	6.5	0.7			100	211	90	16.3	1.4	1.7	4.2	0.55
138	1.2	28	2		2	14.8	0.1	0.2		92	190	80	15.3	1.1	1.7	3.9	0.51
139	1.1	25	3	3	20	54.7	0.4			110	222	90	17.3	1.1	1.9	4.2	0.55
140	0.7	28	5			10.7		0.4		99	198	80	16	1	1.8	2.9	0.4

	Q	R	S	T	U	V	W	X	Y	Z	AA	AB	AC	AD	AE	AF	AG
141	98	312	13.5		24	5.3	12	5.1	23	32.7	243	7	42	3	10		54.6
142	119	324	20.3	3	33	6.7	5	3.2	23	38.4	211	7	46	4	26		88.2
143	39	334	14.3		29	6.1	8	2.3	23	27.7	206	7	30	3	10		40.1
144	60	528	12.3		45	8.7	56	1.1	34	99.4	158	10	101	8			39
145	488	397	45.3		93	23.5	6	1.8	31	76.1	512	29	317	19	50	19	36.1
146	316	251	23.3		14	10.4	5	1.5	33	64.3	104	4	81	9			24.9
147	299	237	15.5		17	4.6	17	4.4	31	73.6	351	9	61	2	10		156
148	340	451	31	4	15	10	8	3.4	41	95.5	118	6	44	6			75
149	251	1100	36.7	15	17	7	100	8.2	42	13.2	50	4	82	18			32.9
150	331	797	40.4	9	8.3	6.3	94	3.5	39	7.8	18	2.4	86	20	43	35	99
151	243.00	1870.00	35.10	10.00	160.00	52.80	18.00	5.50	66.00	24.80	709.00	62.00	499.00	82.00	8.00	118.00	27.00
152	216.00	2080.00	42.30	14.00	240.00	75.20	28.00	9.00	79.00	36.50	1020.00	85.00	659.00	86.00	55.00	123.00	86.50
153	112.00	288.00	32.70	5.00	28.00	2.60	13.00	3.30	23.00	29.70	214.00	6.00	13.00	2.00			59.10
154	58.00	204.00	17.80	3.00	22.00	5.60	12.00	7.70	35.00	67.50	360.00	11.00	58.00	5.00			130.00
155	159.00	356.00	23.30	3.00	44.00	16.20	14.00	2.70	34.00	193.00	333.00	15.00	200.00	10.00		11.00	129.00
156	80.00	385.00	18.40	9.00	24.00	6.10	12.00	3.60	43.00	62.70	169.00	9.00	115.00	10.00			63.00
157	97.00	264.00	21.60	5.00	21.00	6.00	10.00	5.90	30.00	59.90	267.00	12.00	43.00	3.00			73.30
158	153.00	344.00	33.60	8.00	26.00	7.10	20.00	5.60	38.00	64.10	255.00	11.00	35.00	3.00			110.00
159	661	217	43.4	3	11	3.2	22	3.3	25	37.3	512	11	45	2			112
160	121.00	184.00	24.70		18.00	7.20	8.00	3.00	28.00	48.40	717.00	16.00	46.00	2.00			68.30
161	151	194	72.3		9	2.9	9	5.7	31	89.9	547	15	75	4			188
162	403	230	51.9		22	4.2	13	2.1	18	24.1	366	11	37	2			50.6
163	362	233	41.4	3	22	4.9	14	2.3	16	21.5	310		22	1			31.6
164	99	266	10.9	3	17	3.7	25	6.3	32	95.5	443	11	74	4	4		155
165			18.90		6.70	3.30	5.00	1.50	18.00	6.40	224.00	8.00					92.80
166	310	1140	52.5	21	6.9	2.2	57	4.7	43	6.1	31	2	55	21		34	15.9
167	473	57	571	7	3.7	0.8	73	2.8	19	15.2	151	4	33				90.2
168	513.00	129.00	400.00	4.00	5.80	1.50	57.00	3.00	26.00	18.20	203.00	5.00					83.30
169	736.00	98.00	287.00	3.00	3.40	1.20	63.00	3.70	30.00	23.90	263.00	7.00	23.00				130.00
170	783	147	374	3	6.2	1.1	31	2.4	17	17.1	238	7	42				84.8
171	674	111	523	4	6.2	1.1	54	2.2	16	14.5	172	4	35				80.7
172	444	172	184	3	13	2.2	40	2.4	17	19.6	285	7	39				66
173	362	131	234	3	12	3.2	49	3.4	24	21.5	304	8	22	1			93.2
174	431	197	75		17	5.7	33	2.8	23	23.8	292	8	31	1			68.5
175	449	224	136	3	16	3.8	20	2.2	20	22.1	327	9	26	2			63.8
176	519	212	158		15	3.5	25	2.5	19	24.1	309	9	31	1			68.5
177	700	244	111		15	3.6	27	1.7	19	24.7	325	9	18	1	8		57.8
178	593	263	114	3	18	3.4	23	2	20	24.2	308	10	24				61.7
179	555	172	181		16	3.5	12	2.8	19	22.9	326	10	40	1			60.8
180	655	232	42.6	3	10	2.5	52	3.5	28	39.1	476	11	68	2	13		114
181	362	128	141		7.4	2.5	52	3.3	22	19.4	225	6	28	1			100
182	421	150	315	3	7.3	1.3	44	3.5	19	17.6	201	5	25	1			89.7
183	494	143	61.3		6.1	2.4	24	3.1	30	41.7	496	11	46	2		10	163
184	221	538	76.4	4	13	9.8	83	5.7	49	61.4	230	7.3	105	6	3	19	56.2
185	1210	225	221	7	3.4	1.3	11	2.5	24	23.7	313	8	39	1			127
186	542	186	50	8	7.4	1.8	6	4.3	30	39.1	533	12	68	3			171
187	641	178	53.7	10	6.9	1.6	8	4	29	33.4	457	11	61	3			151
188	505	393	200	5	14	2.6	22	5.4	26	52	880	18	85	3			93.1
189	699	117	231		5.8	1.8	36	2.8	23	24.1	277	7	35	1			116
190	377	186	138		14	2.5	41	2.5	17	19.6	264	7	17	1			69.2
191	1050	130	411	2	3.1	0.8	31	3	28	24.5	282	6.5	43	1			145
192	1010	109	330		3.9	1.3	25	2.7	19	22.9	276	6	46			11	128
193	552	49	567	5	3.8	0.8	33	2.1	16	14.6	156	3	43				95.4
194	955	70	405	3	3.3	1.1	37	3.4	22	23.3	253	6	39	1			134
195	696.00	148.00	573.00	3.00	5.20	1.40	67.00	1.90	21.00	14.00	146.00	5.00	27.00	1.00			90.10
196	645.00	151.00	557.00	4.00	5.20	0.90	58.00	1.90	16.00	13.60	137.00	4.00	20.00	1.00			82.70
197	547	93	435	3	7.7	1.5	60	2.4	18	16	195	5	27				82.8
198	555	285	93.6	3	7.5	2.3	12	4.3	32	35.6	600	13	70	2			86
199	551	266	112	3	7	1.7	7	3.9	31	31	508	13	43	2			88.8
200	607	208	429	32	4.3	0.8	36	3.1	18	18	215	5	22	1			98.5
201	620.00	201.00	459.00	30.00	3.70	1.20	47.00	3.20	27.00	19.50	230.00	5.00	26.00	1.00			104.00
202	1280	100	367	10	4.9	1.6	28	3.4	24	29.8	334	8	48				104
203	188	237	104	6	5.6	2	16	4.2	34	34.1	442	10	44	2			180
204	275.00	260.00	104.00	7.00	6.10	1.90	20.00	3.70	35.00	34.20	473.00	10.00	59.00	2.00			178.00
205	736	109	93.2	5	3.3	0.8	16	2.9	29	23.5	231	6	25	2			140
206	119	50	252	5			38	2	25	17.1	106	3	27				110
207	466	121	61.2	8	3.8	1.4	8	2.9	28	25.9	299	6	29	1			150
208	758	76	334		2.7		20	3	25	20	243	7	39	2			125
209	548	47	501	9	1.6		53	2.5	28	20.4	183	4	19	1			133
210	886	185	250	4	3.5	0.8	94	4	19	21.9	250	6	26	1			123
211	167	430	20.6	11	31	11	42	8.1	51	130	1940	47	158	9	26	22	609
212	151.00	464.00	21.20	12.00	34.00	11.90	50.00	8.10	54.00	117.00	2150.00	46.00	175.00	10.00	3.00	22.00	621.00
213	484	41	532	5	2.7	0.5	39	2	15	13.9	130	3	18				102
214	707	83	409		4.2	1.4	40	2.6	22	21.6	211	6	30	1			116
215	644	66	573	3	3	1	27	2.1	20	15.3	163	4	32	1			97
216	441	72	167	6	2.1	0.5	157	4.4	10	10.7	98	2	31				81
217	1270	115	210	3	4.6	1.8	29	6	25	29.6	341	8	55	1			119
218	832	180	187	3	3.1	0.8	27	2.8	23	22.1	249	5	37	1			146
219	677	215	558	89	2.7	0.5	26	2.5	19	17.9	198	4	38		2		137
220	486	159	172		8.3	2.1	29	2.3	18	17.2	202	6	37	2			85.3
221	725	121	416		3.6	0.8	34	2.8	20	20.3	217	5	50	1			91.9
222	786	201	341	3	2.5	0.8	35	2.1	17	15.9	175	4	22				96
223	589	48	522	3	3.6	0.8	47	3.4	20	16.6	169	5	38				106
224	646	115	353	7	1.9		68	2.1	16	12.7	131	3	29				86.6
225	575	98	475	3	4.5	1.2	44	2.3	20	17.1	162	4	34				109
226	135	139	238	4	0.8	0.5	55	3.6	29	18.7	134	4	32				171
227	88	11	142		3.1	0.9	50	3.3	29	14.7	133	3	21				126
228	763	236	131	6	1.9		154	4.1	17	12.6	85	2	18				102
229	129	34	150		2.9	0.8	83	2.5	22	15.6	155	3	36				87.1
230	293	14	346		0.8	0.5	6	2.1	15	19.9	95		10	1			96.3
231	267	22	373		0.8		6	1.9	15	19.7	86	2	19				85.1
232	353.00		338.00		0.80		9.00	2.00	26.00	23.50	126.00	3.00	37.00				98.30
233	352.00	23.00	335.00		1.10		6.00	2.20	15.00	23.00	120.00	3.00	19.00	1.00			101.00
234	566	32	395	3			12	2.3	17	30.8	161	3	41				124
235	341.00	17.00	244.00		0.80	1.00	23.00	1.70	23.00	26.10	118.00	3.00	51.00				83.40
236	345.00	25.00	250.00	4.00			16.00	2.00	15.00	26.10	117.00	3.00	34.00				86.30
237	188.00	61.00	292.00	6.00			45.00	2.30	22.00	20.80	108.00	3.00	14.00				119.00
238	170.00	59.00	282.00	6.00	0.80		38.00	2.40	12.00	19.50	100.00	2.00					119.00
239	236.00	71.00	260.00	5.00		0.60	63.00	5.20	25.00	24.00	114.00	4.00	23.00				72.30
240	236.00	60.00	250.00	5.00	0.50		54.00	4.90	17.00	22.40	125.00	3.00					72.20
241	114	38	193	6	0.5		40	3	20	17.8	122	3	20	1			48.6
242	463	137	490	5	3.2	0.9	53	2.3	12	13.4	65		20				61.7
243	368	114	512	8	2.8	1.1	94	3.5	21	11.5	58	1.7	31				49.8
244	273	62	381	12	1.3		25	2.8	27	26.5	165	4	18	1			122
245	323	81	445		1.3	0.7	28	2	19	11.5	53		11				85.6
246	206	17	318	8	0.9		17	2	28	21.4	114	3	19				93.9
247	205	90	135		1		108	2.3	19	10.6	37	1					56.5
248	426.00	105.00	219.00	8.00	12.00	2.80	31.00	1.40	20.00	11.70	170.00	3.00		1.00			67.90
249	751	142	190	5	11	3.3	29	2.1	20	8.5	180	4	19	1	7		66.2
250	900	131	193	5	12	2.2	28	0.8	15	9.9	215	6	21	1	5		61.2
251	539.00	130.00	192.00	11.00	8.90	4.20	51.00	1.50	19.00	8.00	118.00	3.00	12.00	1.00	13.00		78.00
252	939.00	130.00	216.00	4.00	12.00	2.70	53.00	2.30	20.00	16.70	161.00	4.00	22.00	1.00	11.00		80.80
253	359	146	176	8	13	3.8	58	1.8	20	6.4	198	5	30	1	4		92.5
254	694	165	198	5	10	3.7	33	1.9	16	11.5	133		17	1	12		57.4
255	758	169	200	8	11	5.8	45	2	15	13.2	153		23	1	8		61.9
256	552.00	177.00	189.00	14.00	16.00	5.40	56.00	1.70	24.00	9.50	186.00	6.00	12.00	1.00	6.00		90.60
257	731.00	164.00	168.00	6.00	33.00	11.70	39.00	0.80	17.00	17.90	214.00	7.00		1.00	20.00		54.60
258	654	188	165	11	8.6	8.3	53	2	19	13.3	126	4	18	1	10		67.4
259	372	101	217	4	7	3.8	68	4.2	20	8	195		33	2			61.4
260																	
261																	
262																	
263																	
264																	

	Q	R	S	T	U	V	W	X	Y	Z	AA	AB	AC	AD	AE	AF	AG
1																	
2																	
3	Ba	Rb	Sr	Cs	Th	U	Li	Be	Ga	Y	Zr	Hf	Nb	Ta	Pb	Sn	Zn
4	PPM (XRF)	PPM (XRF)	PPM (ICP)	PPM (NA)	PPM (NA)	PPM (NA)	PPM (ICP)	PPM (ICP)	PPM (ICP)	PPM (ICP)	PPM (XRF)	PPM (NA)	PPM (XRF)	PPM (NA)	PPM (ICP)	PPM (ICP)	PPM (ICP)
5																	
6	460	178	41	1	26	2.8	6	2.4	14	30.2	362	9.7	30	1	2		63.6
7	509	217	38.4	1	28	3.7	6	3.5	17	22.8	371	9.7	51	2	9	21	47.6
8	650	221	56.9	1	26	6.5	2	3.9	20	47.5	382	10	47	2	26		62
9	362	245	25.5	1	50	9.6	2	6	23	84	251	8.7	77	4	28		25.4
10	197	244	20.1	1	31	8.7	4	3.3	19	37.1	191	5.3	38	1	4		36.2
11	986	195	81.3		24	5.7	8	3.9	20	51.1	415	11	42	1			102
12	644	98	240		1.8	0.6	41	3.6	29	42.1	269	6	34	2			150
13	671	65	310		2.3		17	2.3	16	35	165	4					125
14	962	235	81.2	5	2		63	5.3	16	35.9	215	4	89	1			132
15	488	125	425		1.9	0.6	26	2.7	18	29.3	151	3	17				140
16	533	21	265		2.4	0.8	12	2.8	28	46.6	256	5	20				144
17	338	79	345		2.7	0.8	30	2.9	24	21.7	134	3	30	1			96.8
18	267.00		379.00		0.50		19.00	1.80	26.00	19.80	85.00		39.00				95.70
19	268.00		334.00				9.00	1.80	13.00	17.20	77.00	2.00	15.00				86.80
20	629	263	123	6	26	3.6	40	6.1	28	21	179	5	31	1	14		147
21	539	171	115	3	14	2.1	37	3.3	25	23.8	173	5	22	1			120
22	936	146	250	3	53	5.9	5		14	16.7	72				36		10.2
23	1580	134	207		28	2.2	18	1.7	15	7	192	5					45.4
24	661	106	55.3		18	9.4	11	1.9	17	38.2	387	11	24	1	11		78
25	865	71	200		1.1	5.3	16	1.7	17	17.5	59		11	1			57.4
26																	
27																	
28	422	318	61	6	33	5.2	58	5.3	19	47	221	7	46	3	21		51.9
29	204	199	26.6		34	11.4	41	3.1	21	88.2	229	8	41	3	17		64.7
30	671	207	99.1		14	8	18	4.9	18	29.8	198	7	33	3	33		29.1
31	1700	173	165		11	3.2	33	4	22	79.7	575	13	87	2	6		164
32	1800	191	171		9.3	4.1	40	4.8	19	79.3	570	14	105	4			159
33	234.00	40.00	326.00		0.90	0.70	12.00	1.90	25.00	20.80	103.00	4.00	32.00				95.30
34	222.00		308.00				8.00	2.00	16.00	19.40	93.00	2.00	11.00				87.70
35																	
36	1100.00	57.00	614.00		6.20	1.90	11.00	2.60	25.00	17.20	209.00	4.00			27.00		89.60
37																	
38	1120	148	181	3	11	1.2	16	2.7	19	22.6	495	10	30	1			77.7
39	533	160	132	4	11	2.3	8	2.1	19	21.8	486	10	35	2			43.5
40	1290	180	176		11	1.6	20	2.5	20	23.6	580	11	41	2			68.5
41	307	105	72.3		20	2	1	2.6	12	18.6	111		35	2			7.7
42	366	116	155		26	3.8	2	2.1	8	21.7	189		27	2			18.2
43	1350	110	92.7		4.5	1.2	2	2.2	19	23.8	309	7	45	2			138
44	2710	82	195		3.3	0.6	2	1.9	19	21.6	235	4	46	1			138
45	3260	57	728		1.5		3	1.5	21	12.4	45		21				68.2
46	1050	126	99.4		3.4	1.4	5	1.7	19	16	182	4	50	1			127
47	853	112	674	3	6.4	1.1	17	2.3	16	16	216		47	2			86.3
48	1120	69	674		3	1.1	26	2.2	18	19.1	225	6	18	1			116
49	758	50	722	3	2.7		16	1.9	16	14.2	120	3	28				93.1
50	666	66	746	3	2.7	1.3	15	1.8	16	13.2	126		17				85
51	847	68	671	3	3	0.6	26	2.1	17	15.9	148	3	28				101
52	687	37	737		2	0.7	15	1.8	17	14.1	136	4	29				94.2
53	383	78	1030	3	0.8	0.5	21	1	11	6.6	15						55.6
54	453	294	95.5	4	14	2.2	23	1.7	16	18.5	111		26	3			55.3
55	295	190	66.5	4	6.5	6.4	38	1.2	10	8.3	66	2	15	1	15		28.4
56	695	203	243	10	14	4.3	45	2.9	15	20	220	6	44	1	6		71.5
57	932	151	228	6	13	2.8	38	2.6	15	7.9	208	5	54	1			91.5
58	106	223	20.8	12	2.9	4.1	50	0.6	12	5.2	35		35		2		38.6
59	729	125	252	18	11	3.9	81	1.8	10	10.9	209	5	28	1	6		60.6
60																	
61																	
62	957.00	185.00	165.00	11.00	10.00	4.50	63.00	3.60	23.00	40.20	410.00	9.00	20.00	2.00	23.00		108.00
63	816.00	241.00	121.00	7.00	8.20	3.40	51.00	3.00	27.00	23.10	361.00	7.00	13.00	1.00	22.00		76.70
64	1200.00	200.00	196.00	7.00	8.30	3.40	41.00	3.20	26.00	37.00	465.00	12.00	16.00	1.00	14.00		110.00
65	1290.00	184.00	216.00	9.00	17.00	4.40	50.00	3.30	28.00	32.90	400.00	8.00	13.00	2.00	17.00		101.00
66	1370.00	190.00	230.00	8.00	14.00	1.80	31.00	3.00	27.00	26.50	304.00	6.00	13.00	1.00	12.00		78.60
67	1450.00	113.00	185.00	3.00	2.00	0.60	6.00	1.50	30.00	15.10	151.00						94.90
68	1540.00	110.00	191.00		6.90	1.30	14.00	2.30	31.00	26.40	320.00	9.00	27.00	2.00			110.00
69	2500.00	82.00	197.00		4.70	1.30	15.00	2.10	31.00	26.80	219.00	5.00	36.00	1.00			123.00
70	1670.00	86.00	241.00		2.80		11.00	1.90	31.00	22.10	385.00		24.00				159.00
71		172.00	8.30	6.00	7.40	3.00	38.00	4.30	45.00	32.60	633.00	13.00	68.00	3.00			183.00
72		243.00	6.00	3.00	19.00	8.60	4.00	2.60	43.00	69.40	950.00	23.00	64.00	2.00			207.00
73		222.00	4.50	3.00	17.00	4.30	37.00	7.00	42.00	52.50	907.00	21.00	101.00	4.00			161.00
74	789.00	71.00	507.00	5.00	2.30	0.80	65.00	2.20	32.00	22.50	159.00	4.00	23.00				133.00
75	1140.00	120.00	178.00	15.00	6.60	1.00	35.00	3.60	35.00	30.50	382.00	9.00	45.00	2.00			120.00
76	107.00	24.00	259.00	5.00			46.00	1.60	27.00	21.80	33.00						157.00
77																	
78																	
79	399.00	109.00	258.00	16.00			51.00	1.70	23.00	23.30	58.00		15.00				105.00
80	986.00	142.00	214.00	7.00	9.60	3.90	37.00	3.50	29.00	38.80	560.00	13.00	15.00	1.00	6.00		153.00
81	1330.00	153.00	213.00	5.00	11.00	4.20	34.00	3.30	28.00	34.20	415.00	12.00	28.00	1.00	14.00		112.00
82	18.00	85.00	9.60	3.00	5.80	1.70	18.00	3.00	35.00	33.60	450.00		38.00	1.00			153.00
83		84.00	9.20	3.00	3.30	1.30	10.00	2.10	31.00	23.90	234.00		31.00	1.00			143.00
84	139.00	87.00	29.80		3.10	1.30	8.00	2.20	30.00	23.70	235.00			1.00			150.00
85	207.00	110.00	46.00	3.00	4.00	1.10	5.00	2.30	26.00	22.10	225.00		25.00	2.00			55.10
86	429.00	147.00	119.00	3.00	9.10	2.30	16.00	2.30	25.00	16.10	247.00		21.00				41.70
87	417.00	141.00	143.00		8.70	2.30	15.00	2.90	25.00	18.10	262.00			2.00			48.00
88	416.00	151.00	140.00		9.80	3.30	15.00	2.90	21.00	18.20	257.00	6.00		2.00			48.10
89	412.00	145.00	147.00		9.60	1.70	16.00	2.90	23.00	18.50	236.00		21.00	1.00			48.70
90	585	162	138		8.3	1.8	14	2.5	20	17.2	269		27	1			44.8
91	594.00	131.00	149.00		8.70	3.50	21.00	2.80	21.00	17.90	274.00	7.00	32.00				46.70
92	484.00	280.00	79.10		33.00	3.40	14.00	2.20	17.00	28.20	232.00			1.00	5.00		27.80
93																	
94																	
95	311.00	129.00	101.00		5.40	1.60	10.00	2.40	27.00	23.20	331.00		30.00	2.00			72.30
96	348.00	134.00	113.00	3.00	6.60	1.80	11.00	2.70	28.00	23.60	330.00		13.00	2.00			89.30
97	1200.00	64.00	129.00	4.00	2.50	0.80	5.00	1.80	27.00	16.00	31.00		11.00				141.00
98	1490.00	83.00	117.00		2.30	0.50	6.00	1.90	26.00	22.60	243.00		20.00	1.00			123.00
99	265.00	104.00	25.10		7.30		5.00	1.70	25.00	19.40	359.00		26.00	1.00			67.70
100	894.00	49.00	149.00	3.00	1.40	0.50	10.00	1.60	28.00	16.00	287.00	6.00	26.00		40.00		222.00
101	177.00	36.00	577.00		1.50	0.70	14.00	1.90	25.00	19.50	98.00	2.00					102.00
102	536.00	36.00	412.00		2.00	0.60	13.00	1.90	24.00	24.00	291.00	7.00	28.00	1.00			108.00
103	1190.00	186.00	186.00	9.00	12.00	5.30	41.00	3.30	26.00	33.40	409.00	10.00	26.00		11.00		102.00
104	1180.00	122.00	275.00	8.00	7.30	2.70	52.00	4.00	29.00	43.00	315.00	8.00	27.00	1.00	27.00		244.00
105	1010.00	117.00	253.00	6.00	12.00	4.00	52.00	4.00	29.00	42.40	347.00	9.00	19.00	2.00	6.00		156.00
106		455.00	11.10	6.00	39.00	10.50	34.00	8.30	24.00	139.00	208.00		49.00	3.00	32.00		55.60
107																	
108																	
109	213.00	223.00	62.60		25.00	3.70	21.00	3.50	26.00	28.10	345.00	11.00		2.00	100.00		72.80
110	316.00	226.00	76.80	4.00	21.00	4.30	22.00	3.90	23.00	26.80	345.00	8.00	14.00	2.00			50.40
111	377.00	208.00	102.00	3.00	17.00	2.80	14.00	3.00	23.00	22.50	358.00	10.00		1.00	8.00		61.20
112	617	227	112	3	18	3	14	2.9	20	22.7	347	7	27	1			45.5
113	388	240	68	5	20	1.9	11	3	20	23	286	7		2	6		54.4
114	602	254	92.6		16	3	11	2.6	20	20.8	325	8	23	1			55.6
115	406	238	86.8	2	17	2.9	14	3.5	20	24	263	6.8	31	1	9		51.5
116	639	227	54		14	3.4	14	2.4	21	22.8	390	9	22	1			223
117	344	225	41.5		24	3.3	9	2.5	18	21.7	287	7	24	1			38.6
118	339.00	251.00	27.30	3.00	23.00	7.00	10.00	3.00	24.00	29.60	229.00	10.00	31.00	1.00			41.10
119		313.00	21.00	4.00	39.00	8.40	29.00	3.80	25.00	28.70	223.00		22.00	2.00	10.00		34.70
120	417	259	37.1		28	4.5	8	2.2	18	25.5	257		25	2			43.9
121	81.00	296.00	37.50	3.00	32.00	5.10	24.00	4.80	25.00	33.30	319.00	12.00	20.00	4.00	2.00		42.80
122	379.00	271.00	92.80	4.00	16.00	4.60	25.00	6.10	23.00	20.90	407.00	9.00	22.00	1.00			58.30
123	83	519	14	17	49	9	151	5.8	29	69.1	144	9	49	9	16		23.8
124		540.00	9.10	13.00	71.00	19.10	163.00	6.40	31.00	76.70	240.00	14.00	43.00	7.00	18.00		17.90
125		400.00	10.70	7.00	38.00	14.40	34.00	8.40	38.00	71.10	134.00	11.00	37.00	11.00	29.00		15.60
126		461.00	10.50	11.00	46.00	7.60	226.00	10.20	31.00	49.70	169.00	10.00	23.00	5.00	19.00		15.20
127	209	126	58.2	4	20	4.6	74	4.2	25	60.3	1750	35	98	3			210
128	155	50	51.6		24	4.7	106	5.3	37	84.6	2500	47	124	4			360
129	238	42	41.3		26	4.1	109	5.6	36	85	2520	51	112	3			376
130	643	190	164		17	3.3	15	2	19	21.3	305	12	26	1			52.8
131	610	260	79.8		19	4	9	2.2	21	25.5	350	8	19	1			43.3
132	214	260	28.8		15	3.8	6	4.2	30	55.2	498	15	55	3			97.4
133	823	208	41.4		9.4	3.5	12	2.7	25	36.9	486	14	53	2			107
134	175.00	281.00	27.00	3.00	30.00	8.00	9.00	3.10	23.00	36.30	221.00		17.00	2.00	5.00		67.60
135	224.00	325.00	35.50	4.00	25.00	7.00	11.00	2.50	29.00	46.10	418.00	12.00	42.00	3.00	4.00		124.00
136	565	217	32.6		11	2.8	5	3.1	25	42.6	496	11	53	2			109
137	665	210	40.6		11	3.7	10	2.8	24	44.7	506	12	47	2			85
138	535	241	41.9		12	3.5	7	3.5	27	44.2	557	12	56	2	34		139
139	533	281	46		13	3.1	11	3.4	21	46	478	12	51	3			85.6
140	366	210	32.1		20	7.1	6	2.3	25	32.1	329	9	53	3			15

	A	B	C	D	E	F	G	H	I	J	K	L	M	N	O	P
141	R77a+b	Sundsvall porphyry	691910/157923	75.7	0.161	11.8	1.8	0.03	0.13	0.65	3	5.06	0.02	3000	0.75	99.191
142	R88	Sundsvall porphyry	691739/157949	74.7	0.163	11.8	0.99	0.03	0.12	0.61	3.2	5.41	0.02	2400	0.95	98.089
143	R90b	Sundsvall porphyry	692221/157974	74.7	0.183	12.1	1.63	0.03	0.1	0.65	3.57	5.01	0.02	3100	1.05	99.126
144	R94c	Quartz-feldspar porphyry (QFP)	692372/158038	73.3	0.095	13.6	1.73	0.02	0.09	0.67	4.42	4.83	0.02	3600	0.7	99.599
145	R118b	Quartz-feldspar porphyry	691533/159062	76.5	0.064	12.4	1.27	0.02	0.07	0.02	3.91	5.24	0.02	104	0.35	100.1
146	R144a+b	Quartz-feldspar porphyry*+	692026/159122	77.2	0.073	11.7	0.94	0.01	0.04	0.16	4.24	4.28	0.03	1170	0.4	99.2
147	R160	Quartz-feldspar porphyry*+	692178/159114	75.9	0.167	11.7	2.44	0.04	0.08	0.4	2.8	4.58	0.02	1270	0.95	99.2
148	R167:2	Quartz-feldspar porphyry*+	692168/158953	73.7	0.065	14.1	1.13	0.02	0.17	0.03	3.72	5.46	0.04	325	0.95	99.5
149	R45	Quartz-feldspar porphyry	691786/158873	71.1	0.184	15.2	1.27	0.04	0.34	0.04	4.72	4.18	0.04	2510	1.3	98.6
150	R18QFP	Quartz-feldspar porphyry (QFP)	691772/158958	73.3	0.132	13.7	0.84	0.03	0.28	0.26	4.25	4.33	0.03	640	0.95	98.251
151	R117g1	Quartz-feldspar porphyry*+	691511/159039	72.80	0.03	15.40	0.74	0.02	0.17	0.03	4.28	5.35	0.03	370.00	0.95	100.20
152	R117f2	Quartz-feldspar porphyry	691517/159035	73.90	0.02	15.20	0.47	0.02	0.17	0.03	3.20	5.64	0.03	440.00	1.10	100.30
153	R127b	Quartz-feldspar porphyry	692086/159232	75.10	0.28	12.10	2.07	0.02	0.21	0.35	2.99	5.91	0.04	1900.00	0.80	100.00
154	R133c1	Quartz-feldspar porphyry	692140/159241	75.50	0.18	11.70	2.01	0.03	0.12	0.63	2.51	4.82	0.02	2550.00	1.35	99.00
155	R130a+b+e	Quartz-feldspar porphyry	692022/159217	75.40	0.15	12.00	1.92	0.02	0.13		2.49	5.64	0.03	130.00	0.75	98.70
156	R126c1+c2	Quartz-feldspar porphyry	692023/159281	75.60	0.12	12.40	1.91	0.02	0.20	0.05	2.92	4.61	0.04	260.00	1.00	99.00
157	R128a	Qz-fsp porphyry, altered	692053/159242	76.60	0.17	11.70	1.79	0.03	0.15	0.61	2.71	4.81	0.02	1700.00	1.40	100.10
158	R128b+c	Qz-fsp porphyry, less altered	692053/159242	75.50	0.17	12.30	2.15	0.03	0.19	0.23	2.08	5.92	0.02	428.00	1.40	100.10
159	R140a1+a2	Quartz-feldspar porphyry	692198/159198	69.5	0.289	13.4	3.88	0.04	0.18	1.13	2.92	5.63	0.05	1130	2	99.2
160	R114a1	Quartz-feldspar porphyry	691989/159171	74.50	0.26	12.20	2.51	0.05	0.09	0.22	3.74	5.09	0.03	591.00	1.05	99.90
161	R74a+b	Central QFP, comp. Rödö dike	693443/159902	71	0.274	12.5	3.88	0.05	0.4	1.02	2.79	5.55	0.04	2100	0.65	98.301
162	R12QFP	Central qz-fsp porphyry	692035/159078	73.2	0.397	12.2	2.94	0.03	0.39	0.87	2.85	5.57	0.08	1130	1.45	100.1
163	R135a+b	Central qz-fsp porphyry	692104/159985	74.4	0.359	12.3	2.4	0.03	0.48	0.43	2.88	5.91	0.07	108	1.25	100.6
164	R87a	Porphyry	691085/158092	74.8	0.227	13	2.82	0.04	0.24	0.81	0.64	5.36	0.02	2500	2.15	100.235
165	R103d	Postjotnian aplite	691661/159186	65.70	0.12	18.60	1.64	0.04	0.82	0.79	11.60	0.08	0.02	46.00	0.95	100.40
166	R18MQFP	Dark QFP	691772/158960	71.2	0.213	14.9	1.02	0.03	0.41	0.25	4.34	4.59	0.04	870	1.15	98.322
167	R140b1	Rödö dolerite, xenocrystic	692192/159206	51.8	1.21	15.5	8.93	0.12	4.51	7.11	2.78	1.76	0.23	818	5.55	99.7
168	R133b1	Rödö dolerite, xenocrystic	692129/159244	56.20	1.44	15.20	7.44	0.09	2.43	4.25	4.43	3.50	0.31	1140.00	4.70	100.20
169	R114b	Rödö dolerite, xenocrystic	691986/159169	54.90	2.02	14.00	10.40	0.11	1.84	4.44	3.53	3.68	0.48	717.00	4.25	99.80
170	R115a1	Brown marginal xenocrystic dolerite*+	691989/159153	59.1	1.37	14.7	7.82	0.1	3.12	3.67	4	3.94	0.29	930	2.2	100.5
171	R115a4	Grey-green central xenocrysti dolerite	691989/159153	56.6	1.02	14.8	7.31	0.1	4.56	4.84	3.41	2.98	0.2	921	2.7	98.7
172	R115b1+b2	Brown central hybrid porphyry	691988/159147	66.4	0.803	13.2	5.19	0.06	2.02	1.87	3.61	4.31	0.17	1480	2.3	100.1
173	R115b5+b6	Marginal dolerite	691988/159147	55.8	1.09	15.9	6.85	0.08	2.87	3.98	5.02	3.22	0.23	1240	4.15	99.3
174	R135h	Dark marginal hybrid porphyry	692104/159985	67.9	0.66	13.6	4.58	0.05	1.17	1.2	3.75	4.62	0.13	238	2.3	100.1
175	R12HPF	Transitional hybrid porphyry	692035/159078	68.3	0.62	12.9	4.36	0.05	1.1	2.02	3.2	4.95	0.12	1510	2.6	100.4
176	R3	Dark coarse hybrid porphyry	691801/158944	66.5	0.616	13.3	4.48	0.05	1.67	2.26	3.06	5.06	0.13	1170	2.8	100.1
177	R53	Dark coarse hybrid porphyry	691846/158959	69.3	0.535	13.7	3.89	0.04	1.15	1.1	2.86	6.05	0.12	280	1.55	100.5
178	R58	Dark coarse hybrid porphyry	691822/158932	68.4	0.475	13.1	3.56	0.04	0.96	1.48	2.62	6.15	0.1	230	2	99
179	R68	Dark coarse hybrid porphyry*+	691882/159037	68.8	0.546	13.5	3.83	0.05	1.23	1.49	3.24	5.37	0.11	1540	1.35	99.7
180	R33	Hybrid porphyry	692093/159021	64.3	0.313	14.7	5.35	0.06	0.42	1.86	3.83	4.9	0.06	280	2.4	98.377
181	R55Enkl.	Hybrid enclave	691825/158963	59.1	1.01	14.7	7.33	0.08	3.28	3.08	4.04	2.69	0.2	700	4.6	100.2
182	R58Enkl.	Hybrid enclave	691822/158932	56.6	1.06	14.5	7.22	0.09	3.69	3.61	3.36	3.34	0.22		4.45	98.3
183	R46c+fEnkl	Vesicular hybrid enclave	691792/158867	63.6	0.797	14.2	6.33	0.08	1.14	2.34	4.21	3.76	0.21	335	3.35	100.2
184	R18Enkl	Dark enclave in QFP, xenocr.*+	691772/158958	57.6	1.59	15.4	7.82	0.12	1.64	3.74	2.97	4.08	0.56	960	4.68	100.346
185	R151h	Dark brown hybrid porphyry*+	692102/159153	62.3	0.694	14.9	7.41	0.11	0.78	1.27	3.84	6.07	0.14	875	2.55	100.3
186	R82a+b	Dark brown-green hybrid porphyry	691758/158743	61.8	0.548	15.1	7.62	0.13	0.26	2.2	4.72	6.07	0.09	2080	1.45	100.2
187	R86a	Dark brown-green hybrid porphyry *+	691780/158667	61.5	0.597	15.7	7.17	0.15	0.45	1.81	5.3	5.34	0.1	510	1.4	99.692
188	R169	Hybrid porphyry	691569/159077	63.4	0.35	15.2	5.72	0.08	0.73	1.70	1.26	9.12	0.05		1.35	99.2
189	R62rödbr.	Monzodolerite	691845/158932	59	1.49	14.2	8.68	0.1	2.64	2.84	3.68	3.71	0.35	1180	2.45	99.3
190	R60	Small porphyritic hybrid porphyry	691831/158936	64.9	0.62	12.6	4.67	0.06	2.38	2.41	3.08	3.94	0.12		3.35	98.3
191	R50	Xenocrystic reddish Rödö dolerite	692077/159099	56.2	2.05	13.8	10.9	0.12	2.31	4.28	3.52	3.73	0.59	970	2.05	99.779
192	R31	Rödö dolerite, xenocrystic	692095/159104	56.1	1.99	14	10.50	0.13	2.22	3.91	3.7	3.67	0.56		1.95	98.9
193	R151i:2+3	Rödö dolerite, xenocrystic	692110/159146	54.4	1.38	15.2	8.64	0.11	4.28	6.77	3.02	2.23	0.28		2.3	98.8
194	R151c	Rödö dolerite, xenocrystic	692157/159148	55.8	1.94	13.9	10.30	0.12	1.82	4.68	3.65	3.21	0.57		3.15	99.3
195	R150	Xenocrystic Rödö dolerite	692069/159111	55.70	1.13	15.00	8.34	0.11	4.70	5.85	2.94	2.94	0.23		2.90	100.00
196	R150(2)	Xenocrystic Rödö dolerite	692069/159111	54.70	1.17	15.00	7.81	0.10	4.64	5.63	2.92	3.09	0.22		3.00	98.50
197	R14a	Rödö dolerite, xenocrystic	692015/159123	57.2	1.03	14.3	7.30	0.09	3.67	5.80	2.71	2.74	0.21		4.35	99.6
198	R123a	Brown central hybrid dolerite	691608/159081	59.3	0.63	16.7	7.78	0.11	0.65	1.75	3.47	7.77	0.14		1.05	99.5
199	R123c	Black marginal hybrid dolerite	691608/159081	61.1	0.56	15.3	5.81	0.10	0.58	2.33	2.5	8.41	0.12		1.35	98.3
200	R124a	Rödö dolerite, xenocrystic	691605/159079	56.8	1.77	15.3	9.96	0.09	3.08	4.33	2.93	3.08	0.38		1.05	98.9
201	R124a(2)	Xenocrystic Rödö dolerite	691605/159079	57.80	1.76	15.20	10.30	0.10	3.12	4.51	3.08	3.06	0.40		0.85	100.40
202	R172b	Rödö dolerite, Kfsp xenocrysts	691574/159078	59.1	1.37	14.2	9.93	0.12	1.43	3.37	3.25	3.7	0.49		1.55	98.8
203	R101a+b	Rödö hybrid dolerite*+	691667/158441	59.6	0.782	14.9	8.76	0.15	0.61	2.23	4.18	5.66	0.19	1300	1.7	98.892
204	R101a+b(2)	Rödö hybrid dolerite	691667/158441	60.30	0.76	14.70	9.11	0.16	0.63	2.46	4.08	5.75	0.20		1.75	100.00
205	R81b	Rödö dolerite	691625/158122	56.3	1.35	14.8	9.97	0.15	1.27	3.51	4.26	5.23	0.48	950	1.5	98.964
206	R94f	Rödö dolerite?	692390/158031	50.4	1.76	14.2	13	0.17	6.39	8.55	2.47	0.69	0.14	310	1.6	99.471
207	R92a	Rödö dolerite	691723/157767	58	1.14	14.7	10.3	0.17	0.8	3.53	4.64	5.03	0.37	980	1.35	100.15
208	R99	Rödö dolerite	691757/158381	54.6	1.25	16.5	7.33	0.1	2.52	5.66	3.95	3.78	0.38	970	2.6	98.857
209	R98	Rödö dolerite	691739/158465	49.2	2.78	13.2	13.3	0.14	3.23	6.79	2.6	1.85	0.62	800	5	98.867
210	R134a	Rapakivi dolerite*+	691700/158385	51.7	1.18	16	8.12	0.12	2.69	5.53	3.33	4.94	0.37	837	5.6	99.8
211	R117b1+b2	Black silicic porphyry	691529/159025	76.6	0.232	11.7	4	0.05	0.27	0.15	0.14	3.9	0.02	180	1.95	99.4
212	R117b1+b2(2)	Black silicic porphyry	691529/159025	77.00	0.16	11.40	4.38	0.06	0.32	0.45	0.19	3.90	0.03		1.90	100.20
213	R111	Rödö dolerite*+	691862/159039	53.4	1.41	14.8	9.33	0.11	6.91	6.9	2.43	1.9	0.27	840	2.85	100.5
214	R62	Rödö dolerite	691845/158932	56.6	1.75	14.5	9.41	0.1	3.11	4.11	3.55	3.17	0.39	1070	2.85	99.7
215	R65	Rödö dolerite	691827/159030	55.3	1.53	16.4	8.13	0.08	4.13	5.32	3.1	2.66	0.32	938	2.75	99.9
216	R54	Rödö dolerite	691841/158961	50	1.11	15.3	10.80	0.13	7.79	3.12	1.39	2.99	0.19		7	100
217	R168a	Rödö dolerite	691561/159068	58.9	1.39	14.3	10.50	0.12	1.55	2.80	3.19	4.07	0.49		2	99.5
218	R141a2	Rödö dolerite	692244/159187	56.2	1.75	13	10.10	0.10	2.32	4.84	2.7	3.4	0.52		4.9	100
219	R122e	Rödö dolerite	691626/159062	54.3	1.75	15.1	9.66	0.11	3.42	6.11	2.67	3.45	0.39		1.1	98.3
220	R137c1+c4	Rödö hybrid dolerite	692166/159905	60.9	1.04	14.2	6.95	0.09	3.46	2.76	3.96	3.77	0.21		2.65	100.1
221	R61	Rödö dolerite	691838/158935	55.5	1.78	14.5	9.53	0.10	2.99	3.60	3.44	3.5	0.39		2.9	98.4
222	R70	Rödö dolerite	691813/158916	54.4	1.65	15.8	8.46	0.10	3.76	4.16	3.06	4.71	0.36		2.85	99.5
223	R14c	Rödö dolerite*+	692015/159123	53.5	1.74	14.9	9.49	0.10	3.32	6.52	3.71	1.57	0.36		3.2	98.6
224	R59D	Rödö dolerite	691828/158935	53.3	1.36	15.5	8.02	0.10	4.48	5.15	1.82	3.39	0.28		5.55	99.1
225	R12DIAB	Marginal rapakivi dolerite	692035/159078	55	1.52	14.9	9.47	0.13	3.9	6.21	3	2.42	0.3	886	2.9	99.9
226	R74c	Marginal Rödö dol.?, comp. dike	693443/159902	45	2.25	15.8	15.1	0.27	5.75	9.54	2.1	1.73	0.22	570	2.35	100.204
227	R3Enkl.	Mafic enclave	691801/158944	52.6	1.13	15.1	8.76	0.12	4.13	5.63	5.4	0.34	0.23	1060	6.35	99.8
228	R53E	Mafic enclave	691846/158959	50.8	1.13	14.6	9.49	0.12	6.57	3.56	1.36	4.65	0.19	1340	6.25	98.9
229	R53Ehål	Vesicular mafic enclave	691846/158959	52.2	1.16	14.1	8.06	0.11	4.12	7.04	4.34	0.91	0.23	952	7.6	99.9
230	R103a	Medium-grained Postjotnian dolerite	691666/159178	46.2	1.95	15.9	14.5	0.19	7.39	9.47	2.68	0.6	0.22	298		99.1
231	R120a	Medium-grained Postjotnian dolerite*+	691450/159055	47	1.95	17.2	12.9	0.17	6.75	10.8	2.64	0.56	0.2	280	0.1	100.4
232	R121	Coarse Postjotnian dolerite	691556/159128	47.20	2.07	16.30	15.80	0.22	5.67	8.91	3.03	0.78	0.28			100.00
233	R121(2)	Coarse Postjotnian dolerite	691556/159128	46.50	2.08	16.40	15.10	0.21	5.67	8.84	3.00	0.78	0.27			98.60
234	R120p1+p2	Pegmatitic Postjotnian dolerite	691450/159055	48.8	2.28	17.2	13.3	0.19	3.53	8.95	3.59	1.25	0.34	455	0.6	100.2
235	R103c	Pegmatitic Postjotnian dolerite	691666/159175	48.10	2.28	12.00	13.90	0.22	6.81	12.20	2.47	0.75	0.27		1.10	100.20
236	R103c(2)	Pegmatitic Postjotnian dolerite	691666/159175	47.80	2.31	12.10	13.90	0.21	6.94	12.40	2.38	0.75	0.25		1.00	100.20
237	R117e	Postjotnian dolerite	691520/159033	46.00	1.83	16.20	14.50	0.23	7.40	8.87	2.09	0.79	0.25		2.35	100.60
238	R117e(2)	Postjotnian dolerite	691520/159033	45.70	1.84	16.50	14.20	0.23	7.50	8.99	2.18	0.83	0.24		2.25	100.50
239	R119a+c	Postjotnian dolerite	691507/159060	55.40	1.75	15.60	10.80	0.15	3.97	4.84	4.41	0.99	0.12		2.15	100.30
240	R119a+c(2)	Postjotnian dolerite	691507/159060	54.60	1.78	15.70	10.30	0.14	3.95	4.67	4.34	0.99	0.11		2.00	98.70
241	R136a2	Postjotnian dolerite	692139/159941	48.3	2.33	14.8	13.5	0.15	6.14	5.83	2.68	0.45	0.16	671	5.55	100
242	R56	Postjotnian dolerite	691825/158957	54.2	0.72	16.8	8.74	0.12	4.46	6.29	2.77	2.28	0.16		2.7	99.4
243	R18PJD	Postjotnian dolerite	691772/158959	53.6	0.786	17.2	8.44	0.13	3.7	6.46	2.56	1.65	0.16	660	4.25	99.075
244	R75a	Postjotnian dolerite	693495/158270	44.6	2.46	15.3	15.3	0.22	7.18	7.23	2.57	1.05	0.31	650	3.35	99.691
245	R76	Postjotnian dolerite	691970/158909	52	0.694	14.5	9.3	0.16	6.49	9.1	2.81	1.85	0.15	420	2.95	100.147
246	R72b	Postjotnian dolerite*+	692503/159537	45.5	1.92	16.2	14.1	0.2	7.19	9.64	2.26	0.62	0.25	290	1.2	99.168
247	R102	Postjotnian dolerite	691683/158413	45.7	0.577	11.1	10.8	0.19	15.6	8.63	0.79	1.59	0.17	970	3.8	99.149
248	R89	Metasedimentary gneiss*+	691829/157824	68.00	0.58	14.50	5.19	0.07	2.29	2.48	3.22	2.89	0.16	574.00	0.90	100.40
249	R91	Migmatitic paragneiss*+	692224/158190	68.7	0.636	14.3	4.86	0.06	2.15	1.77	2.71	3.11	0.14	580	1.25	99.86
250	R93b	Mesosome, paragneiss	691824/157761	72.3	0.606	12.6	4.47	0.05	1.85	1.57	2.51	3.3	0.14	560	0.8	100.391
251	R125	Palingenic granite	691603/159040	67.90	0.42	14.60	3.99	0.05	1.62	1.57	2.93	3.83	0.12	545.00	1.50	98.70
252	R22	Palingenic granite*+	692032/159035	67.30	0.59	15.40	4.85	0.05	1.95	0.86	2.75	3.80	0.13	433.00	2.20	100.10
253	R38b	Palingenic granite, gneissic*+	692017/158864	69.4	0.565	14.2	4.36	0.04	1.86	2.09	3.39	2.65	0.1	520	0.8	99.581
254	R134	Palingenic granite	691700/158385	68.6	0.395	14.7	3.48	0.05	1.45	1.47	3.22	4.11	0.09	493	1.45	99.2
255	R135	Palingenic granite	692104/159985	68.3	0.499	15	4.95	0.07	2	2.04	2.96	3.83	0.17	565	0.8	100.8
256	R48	Palingenic granite?	691797/158889	67.00	0.66	14.90	5.25	0.06	2.17	2.24	3.20	3.02	0.12	721.00	1.10	99.90
257	R15	Orthogneiss*+	691756/158930	70.00	0.54	14.40	3.73	0.06	1.23	1.41	2.83	5.07	0.16	393.00	0.65	100.30
258	R87	Orthogneiss	691084/158086	68.2	0.509	15.2	4.55	0.06	1.8	1.91	2.98	4.1	0.23	590	0.8	100.493
259	R94a+b	Gneissic granodiorite*+	692412/158001	69.1	0.447	15.6	3.27	0.06	1.14	3.34	4.15	1.97	0.12	540	0.7	100.023
260																
261	All analyses performed by X-Ray Assay Labs (XRAL), Don Mills, Ontario. Method as stated for each element.															
262	* = selected for Nd isotope analysis, + = selected for Sr isotope analysis															
263	• = selected for Pb feldspar isotope analysis, § = selected for U-Pb zircon geochronology															
264	(2) denotes duplicate analyses															

Lillkalven
Storkalven
Lusholmen
Rödön
Rödhällan
Yxskäret
Hartungviken
Bredsandsviken
Alnön
Skatudden
Rödögubben
Norrklubben
Lergrundet
Känningen
Långfläsjan
Gråfläsjan
Storgrundet
Klubbåsen
SPIKARNA
Spikarö
Skorven
Snöskäret
Gubben
aplites
medium to coarse grained
Storholmen
QFP-rubble
Österåsen
Norrklacken
Storholmsfläsjan
Sörklacken
Draget

- Rödö granite / granite porphyry
- Quartz-feldspar porphyry (QFP) dykes, with mafic/hybrid magmatic enclaves (right)
- Rödö dolerite, xenocryst-bearing (right)
- Hybrid porphyry, *silicic* (left), intermediate (right)
- Postjotnian dolerite, with pegmatitic pods (middle), as dykes (right)
- Dykes associated with the alkaline Alnö intrusion, carbonatites, alnöites etc
- Sedimentary gneiss, (metagreywacke), strongly migmatized with pegmatites
- Ortogneiss, with pegmatites and palingenic granite
- Palingenic granite, coarse porphyritic, grey (left), greyish red, finely medium-grained (right). (Occupying > 50% of the rock volyme)
- Restitic (above) and xenolithic enclaves (below) of granitic gneiss (left) and sedimentary gneiss (right)
- 100 Locality numbers
- 10 Dips
- Penetrative foliation (left), lineation (right)
- Brittle zones
- Dyke orientation

N

0 500 m



Distribution

SGU
Box 670
751 28 UPPSALA
Tel 018-17 90 00
Fax 018-17 93 70

Wikströms Tryckeri AB, Uppsala 1997

ISSN 0349-2176
ISBN 91-7158-596-6